

May 2021

Past Ice-Ocean Interactions on the Sabrina Coast shelf, East Antarctica: Deglacial to Recent Paleoenvironmental Insights from Marine Sediments

Kara J. Vadman
University of South Florida

Follow this and additional works at: <https://digitalcommons.usf.edu/etd>

 Part of the [Climate Commons](#), [Geochemistry Commons](#), and the [Geology Commons](#)

Scholar Commons Citation

Vadman, Kara J., "Past Ice-Ocean Interactions on the Sabrina Coast shelf, East Antarctica: Deglacial to Recent Paleoenvironmental Insights from Marine Sediments" (2021). *USF Tampa Graduate Theses and Dissertations*.

<https://digitalcommons.usf.edu/etd/9621>

This Dissertation is brought to you for free and open access by the USF Graduate Theses and Dissertations at Digital Commons @ University of South Florida. It has been accepted for inclusion in USF Tampa Graduate Theses and Dissertations by an authorized administrator of Digital Commons @ University of South Florida. For more information, please contact scholarcommons@usf.edu.

Past Ice-Ocean Interactions on the Sabrina Coast shelf, East Antarctica: Deglacial to Recent
Paleoenvironmental Insights from Marine Sediments

by

Kara J. Vadman

A dissertation submitted in partial fulfillment
of the requirements of the degree of
Doctor of Philosophy
with a concentration in Geological Oceanography
College of Marine Science
University of South Florida

Major Advisor: Amelia E. Shevenell, Ph.D.
Brad E. Rosenheim, Ph.D.
Timothy M. Conway, Ph.D.
John M. Jaeger, Ph.D.
Leanne K. Armand, Ph.D.

Date of approval:
May 10, 2021

Keywords: Holocene, paleoceanography, sediments, geochemistry

Copyright © 2021, Kara J. Vadman

ACKNOWLEDGEMENTS

I would like to thank my advisor, Dr. Amelia Shevenell, for mentorship throughout graduate school and the opportunity to conduct Antarctic research. Thank you to my committee members Drs. Brad Rosenheim, Tim Conway, Leanne Armand, and John Jaeger for research guidance and support. Thank you also to Dr. Amy Leventer and Dr. Peggy Delaney for mentorship and feedback over the years.

Thank you to Ethan Goddard for continuous guidance with method development, data generation, and analyses. For their support, encouragement, and friendship, I thank Shevenell Lab members: Michelle Guitard, Imogen Browne, Catherine Prunella, and Rosenheim Lab members: Ryan Venturelli, Carey Schafer, and Theresa King.

Thank you to the people who made my Antarctic fieldwork possible, including the NBP14-02 Shipboard Scientific Party, RV/IB *Nathaniel B. Palmer* marine projects coordinator, marine technicians, and vessel crew. Thank you to the staff at Florida State University Antarctic Marine Geology Research Facility (formerly) and Oregon State University Marine and Geology Repository (currently) for assistance with core curation and sampling.

This project would not have been possible without funding from: the National Science Foundation Graduate Research Fellowship Program; National Science Foundation (NSF) grants, including: Antarctic Integrated Systems Science Program #1143834, 1143836, 1143837, 1143843, 1313826 to A. Leventer, S. Gulick, B. Huber, A. Orsi, and A. Shevenell, NSF Antarctic Earth Sciences #1744970 to A. Shevenell; USF internal fellowships, including: the Von Rosenstiel Fellowship, Southern Kingfish Association Fellowship, Thomas Pyle

Fellowship, and the Dissertation Completion Fellowship; and student research grants from: the Cushman Foundation and the North American Micropaleontology Section of the Society for Sedimentary Geology.

I gratefully acknowledge the staff at the USF Saint Petersburg Wellness Center for mental health support. Thank you to College of Marine Science Academic Director Dr. David Naar and Assistant Director Sami Francis for guidance throughout the dissertation process. I would also like to recognize the many dogs I have cared for over the years in St. Petersburg for their companionship, and my other favorite pastime, climbing at Vertical Ventures gym.

Finally, thank you to my friends and family outside of Florida for their support and understanding throughout my graduate studies.

TABLE OF CONTENTS

List of Tables	iv
List of Figures.....	vi
Abstract.....	ix
Chapter 1: Introduction.....	1
1.1 Research Context	1
1.2 Research Aims and Objectives	3
1.3 Cenozoic Antarctic Cryosphere Evolution	4
1.4 Development and importance of the East Antarctic Ice Sheet	6
1.4.1 The Aurora Subglacial Basin.....	8
1.4.2 Climate-driven ice sheet instabilities.....	8
1.4.3 Aurora Subglacial Basin vulnerability to ice sheet instabilities	10
1.5 Physical Setting.....	11
1.5.1 Totten Glacier and the Sabrina Coast	11
1.5.2 Sabrina Coast physical oceanographic setting.....	14
1.5.3 Sabrina Coast atmospheric processes	19
1.5.4 Atmospheric and oceanic teleconnections.....	20
1.6 East Antarctic Deglacial to Recent Climate.....	22
1.7 Marine Sediments and Paleoceanographic Proxies	24
1.7.1 Lithology and physical properties.....	24
1.7.2 Radiocarbon dating	26
1.7.3 ²¹⁰ Pb dating	28
1.7.4 Foraminifer assemblages	29
1.7.5 Foraminifer stable isotopes.....	30
1.7.6 Foraminifer trace elements	31
1.7.6 Archaeal lipids	32
Chapter 2: Deglacial to Holocene evolution of ice-ocean interactions on the Sabrina Coast shelf, East Antarctica	34
2.1 Author Contributions	34
2.2 Abstract.....	34
2.3 Introduction.....	36
2.4 Study Location: the Sabrina Coast, East Antarctica	39
2.4.1 Continental shelf morphology and glacial history.....	39
2.4.2 Sabrina Coast physical oceanography	40
2.5 Methods.....	41

2.5.1 Sediment sampling, lithology, physical properties, and composite depths	41
2.5.2 Diatom assemblages.....	46
2.5.3 Foraminifer assemblages and stable isotope analyses	47
2.5.4 Radiocarbon sample and age model preparation	48
2.6 Results.....	50
2.6.1 Lithology.....	50
2.6.2 Diatom assemblages.....	51
2.6.3 Foraminifer assemblages and stable isotopes	54
2.6.4 Downcore radiocarbon chronology.....	55
2.7 Discussion.....	57
2.7.1 Sabrina Coast deglaciation (16.2 to ~14.4 ka).....	58
2.7.2 The Antarctic Cold Reversal (~14.4 to 11.2 ka).....	63
2.7.3 Early Holocene (11.2 to 9 ka).....	64
2.7.4 Early to middle Holocene (9 to 5.2 ka).....	68
2.7.5 Middle to late Holocene (5.2 to 0 ka)	69
2.7.6 Regional to global forcings of Sabrina Coast paleoceanography	72
2.8 Conclusion	74
Chapter 3: Upper ocean warming near the Sabrina Coast shelf since 1000 CE.....	76
3.1 Author Contributions	76
3.2 Abstract.....	76
3.3 Introduction.....	77
3.4 Materials and Methods.....	80
3.4.1 Lithology, magnetic susceptibility, and composite depth scale.....	80
3.4.2 Radiometric dating methods and age model.....	83
3.4.3 Archaeal lipid preparation, analysis, and calibration.....	86
3.4.4 Stable isotopes of foraminifer calcite	87
3.4.5 Trace metal/calcium analysis.....	88
3.4.5 Diatom assemblages.....	91
3.5 Results.....	92
3.5.1 Chronology	92
3.5.2 TEX ₈₆ -derived upper ocean temperatures.....	96
3.5.3 <i>N. pachyderma</i> (s) stable isotopes metals	99
3.5.4 <i>N. pachyderma</i> (s) trace metals.....	100
3.5.5 Diatom assemblages.....	101
3.6 Discussion.....	102
3.6.1 Proxy validation over the 20 th -21 st centuries	102
3.6.2 Late Holocene paleoceanographic variability.....	105
Chapter 4: Holocene surface to deep water temperature variability on the Sabrina Coast, East Antarctica.....	112
4.1 Author Contributions	112
4.2 Abstract.....	112
4.3 Introduction.....	113
4.3.1 Sabrina Coast study area.....	116

4.4 Methods.....	116
4.4.1 Lithology, physical properties, and composite depths.....	116
4.4.2 ²¹⁰ Pb and ¹⁴ C sample preparation and age model	118
4.4.3 Lipid biomarker extraction and analysis.....	121
4.4.4 Foraminifer assemblages and stable isotopes	122
4.4.5 Foraminifer trace element/calcium ratios	123
4.4.6 Grain size	125
4.5 Results.....	126
4.5.1 Lithology and chronology.....	126
4.5.2 TEX ₈₆ paleothermometry.....	128
4.5.3 <i>T. angulosa</i> stable isotopes	130
4.5.4 <i>T. angulosa</i> trace metals	130
4.5.5 Sortable silt	132
4.6 Discussion.....	133
4.6.1 Paleotemperature proxy validation	133
4.6.2 Deglacial paleotemperature conditions.....	134
4.6.3 Holocene paleotemperature variations.....	136
4.6.4 Global importance.....	138
Chapter 5: Conclusion.....	140
References.....	143
Appendix A: Chapter 2 Supplementary Material	167
Appendix B: Chapter 3 Supplementary Material.....	171
Appendix C: Chapter 4 Supplementary Material.....	173
Appendix D: Additional Data Tables and Figures.....	175
Appendix E: Permissions and Copyright Information.....	266

LIST OF TABLES

Table 2.1: NBP14-02 sediment core locations, water depths, and core lengths	42
Table 2.2: Summary of relationship between diatoms species and environmental conditions	47
Table 2.3: NBP14-02 radiocarbon results from CaCO ₃ and the first aliquot of bulk sediment acid insoluble organic matter (AIOM) prepared via Ramped PyrOx.....	49
Table 2.4: Sabrina Coast deglacial to Holocene lithologic and micropaleontologic summary.....	52
Table 3.1: NBP14-02 sediment core locations.....	82
Table 3.2: Modeled ²¹⁰ Pb chronology for NBP1402 MC-45.....	84
Table 3.3: Modeled ²¹⁰ Pb chronology for NBP1402 MC-61	84
Table 3.4: Radiocarbon measurements	84
Table 3.5: Summary of relationship between diatoms species and environmental conditions.....	92
Table 4.1: NBP14-02 sediment core locations, water depths, and core lengths	117
Table 4.2: NBP14-02 R-code inputs for the Bacon-generated age model.....	120
Table 4.3: TEX ₈₆ temperature t-table significance tests	129
Table A1: JPC-27 and JPC-57 deglacial radiocarbon dates	167
Table B1: NBP14-02 R-code inputs for the MC-45 Bacon-generated age model	171
Table B2: NBP14-02 R-code inputs for the MC-61 Bacon-generated age model	172
Table D1: NBP14-02 magnetic susceptibility tie points.....	183
Table D2: NBP14-02 sediment cores with Magnetic Susceptibility (Mag Susc) in cgs	184
Table D3: Calcium carbonate (CaCO ₃) radiocarbon data.....	212

Table D4: Ramped PyrOx radiocarbon data	213
Table D5: NBP14-02 MC-45 ²¹⁰ Pb activity data	214
Table D6: NBP14-02 MC-61 ²¹⁰ Pb activity data	215
Table D7: NBP14-02 MC-45 ²¹⁰ Pb age model results.....	216
Table D8: NBP14-02 MC-61 ²¹⁰ Pb age model results.....	217
Table D9: Foraminifer assemblages (raw test counts).....	218
Table D10: Foraminifer assemblages (percent abundance; # tests/cc sediment)	225
Table D11: MC-45 foraminifer stable isotopes	232
Table D12: MC-61 foraminifer stable isotopes	233
Table D13: KC-27B foraminifer stable isotopes	234
Table D14: JKC-53 foraminifer stable isotopes	236
Table D15: Processed Trace metals data for <i>T. angulosa</i> in μmol/mol.....	237
Table D16: Raw trace metals data for <i>T. angulosa</i> in counts per second.....	239
Table D17: Processed trace metals data for <i>N. pachyderma</i> (s) in μmol/mol.	240
Table D18: Raw Trace metals data for <i>N. pachyderma</i> (s) in counts per second.....	244
Table D19: TEX ₈₆ values and calibrated temperatures.....	245
Table D20: NBP14-02 Grain Size data by bin (wt%).....	250
Table D21: NBP14-02 sortable silt data	262

LIST OF FIGURES

Figure 1.1: Antarctic regional ice surface lowering and ice mass loss	2
Figure 1.2: Global temperature and ice volume changes over the Cenozoic and future projections.....	5
Figure 1.3: Antarctica with Bedmap2 elevations, annotated with key East Antarctic locations mentioned herein.....	7
Figure 1.4: Aurora Subglacial Basin structure.....	9
Figure 1.5: Illustration of processes impacting growth and loss of an ice shelf.....	10
Figure 1.6: Bathymetric map of the Sabrina Coast continental shelf	13
Figure 1.7: Primary Southern Ocean physical oceanographic features	15
Figure 1.8: Dalton Polynya physical oceanography	16
Figure 1.9: Satellite image of the Dalton Polynya from February 2014.....	18
Figure 1.10: Schematic of Sabrina Coast continental shelf physical oceanography	18
Figure 1.11: Antarctic wind trend vectors overlaid on trend in sea-level pressure	20
Figure 1.12: Schematic of ACC and SAM relationship in the Southern Ocean.....	22
Figure 1.13: Depiction of SAM influence on the Antarctic Circumpolar Current and Southern Ocean.....	26
Figure 2.1: Sabrina Coast study location	38
Figure 2.2: Sabrina Coast lithology, magnetic susceptibility, composite depth, and radiocarbon ages	44
Figure 2.3: Sabrina Coast deglacial lithologies	45
Figure 2.4: Sabrina Coast multiproxy record plotted against composite depth.....	54
Figure 2.5: Calibrated ¹⁴ C ages versus depth in centimeters composite depth.....	56

Figure 2.6: Regional proxy records of oceanic and atmospheric variability related to deglaciation and Holocene climate	61
Figure 2.7: Sabrina Coast multiproxy environmental reconstruction plotted versus age	65
Figure 2.8: Sabrina Coast diatom assemblages plotted versus regional proxy records of oceanic and atmospheric variability related to Holocene climate.	67
Figure 2.9: Conceptual model of deglacial to Holocene water column conditions	71
Figure 3.1: Bathymetry of the Dalton Polynya on the Sabrina Coast continental shelf, East Antarctica, offshore Moscow University Ice Shelf (MUIS).....	80
Figure 3.2: Sabrina Coast lithology and composite depth scale	82
Figure 3.3: <i>N. pachyderma</i> (s) sample results for trace metals cleaning indicators	90
Figure 3.4: ²¹⁰ Pb chronology and age-depth model for NBP14-02 MC-45 (left) and MC-61 (right).	93
Figure 3.5: Calendar age-depth model derived using Bacon 2.3 software	95
Figure 3.6: Proxy ghost plots with MC-45 and MC-61 TEX ₈₆ data	96
Figure 3.7: NBP14-02 cores MC-45 and MC-61 multiproxy record vs. depth	98
Figure 3.8: Comparison of global and Antarctic TEX ₈₆ calibrations.	99
Figure 3.9: <i>N. pachyderma</i> (s) Mg/Ca calibration lines.....	101
Figure 3.10: MC-45 and MC-61 data for the past 120 years	103
Figure 3.11: MC-45 and MC-61 multiproxy records vs. age	106
Figure 3.12: Sabrina Coast TEX ₈₆ records vs. regional proxy records.....	108
Figure 4.1: Sabrina Coast study location and oceanography	115
Figure 4.2: Lithology, radiocarbon ages, and composite depth scale.....	118
Figure 4.3: Trace metals cleaning indicators for <i>Trifarina angulosa</i>	124
Figure 4.4: Unit lithology, composite magnetic susceptibility (MS), and age model plotted versus centimeters composite depth	127

Figure 4.5: Sabrina Coast Holocene reconstruction of surface and bottom water conditions.....	129
Figure 4.6: Mg/Ca-temperature calibrations from Mawbey et al., 2020	131
Figure 4.7: The log of calculated mean sortable silt (\overline{SS}) plotted against the log of present sortable silt (%SS).....	133
Figure 4.8: Sabrina Coast and regional Antarctic records of Holocene climate variability	135
Figure A1: Determinations of modern and dead contributions of carbon	168
Figure A2: Alternative chronology for JPC-27 and JPC-57.....	169
Figure A3: Core photos and x-radiographs of representative lithologic units.....	170
Figure C1: Relative abundance (%) of individual bins in the sortable silt size range (10-31 μm) plotted against centimeters composite depth (cmcd).....	173
Figure D1: NBP14-02 JPC-27 core photos and x-rays.....	176
Figure D2: NBP14-02 JPC27 CT scan (861-1004 cmbsf).....	178
Figure D3: NBP14-02 JKC-53 core photos	179
Figure D4: NBP14-02 KC-27B core photos.....	180
Figure D5: NBP14-02 JPC-57 core photos and x-rays.....	181

ABSTRACT

The East Antarctic Ice Sheet (EAIS) contains ~53 meters of sea level equivalent (SLE) ice, and observations suggest it is sensitive to ongoing and past climate change. The EAIS has traditionally been considered insensitive to climate perturbations because it is largely grounded above sea level. However, aerogeophysical surveys, oceanographic observations, and models indicate that large areas of the EAIS are grounded below sea level and contain 19.2 m SLE. Marine-based parts of the EAIS are thought to be located on inland-sloping beds that drain through marine terminating outlet glaciers, indicating large areas of the EAIS may be more sensitive to ongoing climate change than previously thought. Many of Antarctica's marine outlet glaciers and fringing ice shelves are losing mass as warm ocean waters move across continental shelves toward deep glacial grounding lines. Predictions of future ice sheet response to climate change are limited by the short time-series of observations and the complexity of associated forcings and feedbacks. To accurately predict future Antarctic cryosphere response to ongoing ocean warming, it is critical to understand how Antarctica's ice sheets responded to past climate variations. Antarctic margin marine geological records provide a longer-term perspective (up to millions of years) on current Antarctic ice retreat than instrumental and ice core records. Ice-proximal geologic records are crucial for understanding past regional ice dynamics near sensitive Antarctic outlet glacier systems.

The Totten Glacier and Moscow University Ice Shelf systems on the Sabrina Coast, East Antarctica, drains a large, marine-based catchment system called the Aurora Subglacial Basin

(ASB), which contains one eighth of the ice in East Antarctica. Oceanographic observations indicate that warm modified Circumpolar Deep Water (mCDW) flows across the continental shelf to access regional grounding lines, thus the ASB catchment might be susceptible to ice mass loss via ocean thermal forcing. Present estimates show lowering of Totten Glacier's ice surface (1 m/yr) and the regional transfer of grounded ice to the Southern Ocean (100 G tons/yr). There is a significant amount of ice in the ASB catchment, so continued ocean and atmospheric warming could lead to contributions to global eustatic sea level rise from the ASB.

In order to put the present day oceanographic and glacial changes on the Sabrina Coast, East Antarctica into the context of natural variability, this dissertation establishes the region's deglacial (16,500 years before present) to recent paleoceanographic history. All data included in this dissertation are from a suite of seven marine sediment cores collected from ~600 m water depth on the middle continental shelf, seaward of the Moscow University Ice Shelf system, where the Antarctic Coastal Current flows onshore and relatively warm deep water (0.3-0.5 °C) was observed.

To develop palaeoceanographic reconstructions, seven sediment cores were studied to determine their lithologic composition, geochemistry, micropaleontology, and chronology (Chapter 2). Microfossil assemblages (foraminifer and diatom), benthic and planktic foraminifer stable isotopes ($\delta^{18}\text{O}$, $\delta^{13}\text{C}$), and diatom assemblages were analyzed (Chapter 2). To address the deglacial to Holocene paleotemperature history of the Sabrina Coast, ocean temperature estimates were made by analyzing foraminifer Mg/Ca and archaeal membrane lipids from surface sediment samples, compared to regional upper ocean temperatures, and added to existing TEX_{86} and Mg/Ca to temperature calibrations (Chapter 3). To reconstruct Holocene upper ocean temperatures, TEX_{86} and foraminifer Mg/Ca were generated (Chapter 4).

Deglaciation of the middle continental shelf occurred ~16.5 ka, coincident with circum-Antarctic atmospheric warming, increasing concentrations of atmospheric CO₂, and enhanced Southern Ocean upwelling after the end of the Last Glacial Maximum. Upper ocean paleotemperatures reconstructed using TEX₈₆ are the first from the Sabrina Coast sector of the East Antarctic margin, and reveal that upper ocean temperatures were relatively warm immediately following deglaciation. Diatom and foraminifer assemblages indicate shelf water formation and seasonally open water conditions existed in the early to middle Holocene, coincident with relatively warm upper ocean temperatures. Early to middle Holocene conditions are inferred to be associated with local polynya dynamics and ocean current influence, which are driven by regional atmospheric forcing. Late Holocene sediments contain diatom assemblages that suggest increased offshore water mass influence, similar in timing and character to other Antarctic marine, terrestrial, and ice core records, suggesting that regional oceanography was influenced by forcings from lower latitudes. Upper ocean temperatures based on TEX₈₆ and foraminifer Mg/Ca reveal confirm that the paleotemperature proxies produce upper ocean temperatures realistic for the Antarctic shelf setting, and warming of 2°C occurred over the last 1000 years.

The first deglacial to Holocene paleoenvironmental reconstruction for the Sabrina Coast, East Antarctica provides crucial information about timing of ice sheet retreat during the last deglaciation. Although present ocean temperatures do not exceed the range of reconstructed ocean temperatures since deglaciation, data suggest that present temperatures are approaching those of the middle Holocene, when Antarctic climate was generally warmer and ice extent was reduced. As such, this region likely contributed to global eustatic sea level in the past, and will likely under future warming scenarios.

CHAPTER ONE: INTRODUCTION

1.1 Research Context

Over the past 60 years, satellite observations and remote geophysical surveys have documented ice mass loss from Antarctic glaciers and buttressing ice shelves, associated with warm atmospheric and oceanic temperatures (Rignot et al., 2013; 2019; Shepherd et al., 2004). As the atmosphere has warmed, both surface and deep ocean waters have accommodated the warming, particularly in the Southern Ocean (Purkey & Johnson 2010, Jun et al., 2020). Warming oceanic and atmospheric temperatures are important because the Antarctic cryosphere is susceptible to basal melting and grounding line retreat, which threaten the stability of marine-terminating ice (DeConto and Pollard, 2016; Pritchard et al., 2009; Rignot et al., 2013; Shepherd et al., 2018). In particular, the East Antarctic Ice Sheet (EAIS) represents ~53 m of sea level change equivalent, and ice sheet models demonstrate that with unchecked CO₂ emissions, EAIS ice mass loss will commit ~0.4 m of sea level rise by 2100 (DeConto and Pollard. 2016; Golledge et al., 2015; 2017). Within the EAIS, 19.2 m of sea level equivalent ice is contained in glacier systems grounded on bedrock that is below sea level, making these systems vulnerable to warming ocean temperatures (DeConto & Pollard, 2016; Fretwell et al., 2013; Golledge et al., 2015; 2017; Morlighem et al., 2020).

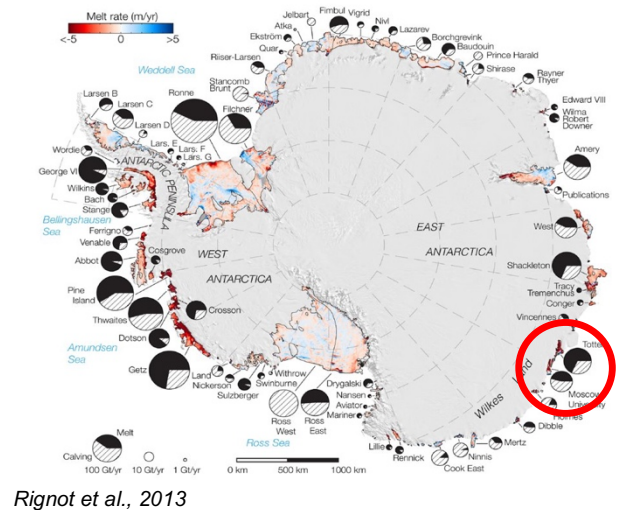
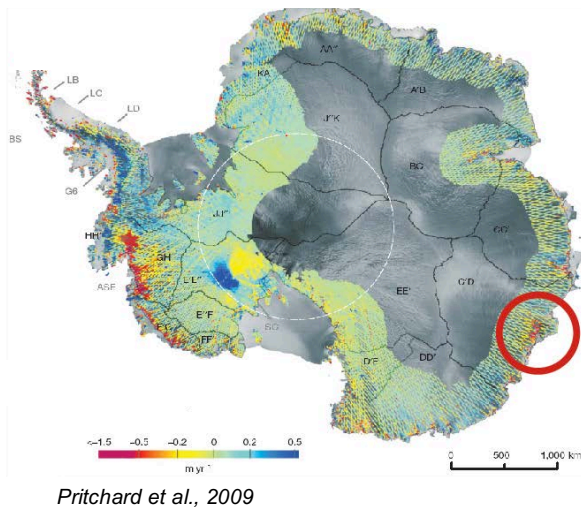


Figure 1.1 Antarctic regional ice surface lowering and ice mass loss. One region of East Antarctica that is losing ice is the Sabrina Coast, where the Totten Glacier drains 1/8th of the interior of the East Antarctic Ice Sheet. The ice in this catchment, called the Aurora Subglacial Basin, is equivalent to ~5 m of sea level rise – this is the same for all of West Antarctica (Morlighem et al., 2020). The ice surface lowering (1 m/yr; Pritchard et al., 2009) and ice mass loss (100 G tons/yr; Rignot et al., 2013) are attributed the presence of warm Modified Circumpolar Deep Water that reaches the glacier grounding lines.

One sector of the East Antarctic margin has been especially responsive to warming over the past ~50 years (Li et al., 2016; Miles et al., 2016). On the Sabrina Coast, the Totten Glacier and Moscow University Ice Shelf system drain one eighth of the interior of the East Antarctic Ice Sheet (Figure 1.1; Aitken et al., 2016; Greenbaum et al., 2015). The catchment, called the Aurora Subglacial Basin (ASB), contains ice that is equivalent to 5.3 m of sea level rise, which exceeds all of West Antarctica (Morlighem et al., 2020). Ice loss and high melt rates (100 G tons/yr and 1 m/yr) are thought to be caused by the presence of warm modified Circumpolar Deep Water (mCDW) that reaches glacier grounding lines (Silvano et al., 2017; 2018). MCDW presence on the Sabrina Coast is significant because the ASB is grounded 1-2 km below sea level and a deep bathymetric trough crosses the continental shelf, and the continental shelf physical oceanographic dynamics allow mCDW access to glacier grounding (Aitken et al., 2016; Greenbaum et al., 2015; Rintoul et al., 2016; Silvano et al., 2018; 2019). On the Sabrina Coast

continental shelf, warm water is present today and associated with glacial thinning and ice discharge (Rintoul et al., 2016). However, regional observations of the oceanographic and climatic drivers of discharge are limited to the past several decades through remote sensing and geophysical data (Li et al., 2016; Miles et al., 2016; Rintoul et al., 2016). Thus, the question arises whether observed physical oceanographic conditions and glacial retreat are within or outside the bounds of natural variability. Whereas regional ice cores provide records of atmospheric warmth and circulation patterns (Van Ommen et al., 2004), there is a gap in information about ocean temperatures, which require well-resolved sedimentary records from close to the ice margin. This dissertation seeks to eliminate this data gap by establishing the deglacial to recent paleoceanographic history of the Sabrina Coast, East Antarctica, seaward of the climatically vulnerable Totten Glacier and Moscow University Ice Shelf system.

1.2 Research Aims and Objectives

The major aim of this dissertation is to provide Holocene paleoceanographic data from offshore an East Antarctic marine-terminating glacier system, which is the outlet of the largest EAIS catchment, the Aurora Subglacial Basin. In providing data for this aim, this dissertation explores the questions: 1) When did the region deglaciate?, 2) Are oceanic paleotemperature estimates attainable on the continental shelf?, and 3) Has warm water been present on the continental shelf during the Holocene? To answer these questions, my objectives were to: a) develop well-dated geochemical, micropaleontological and sedimentological records documenting paleoceanographic variations on the Sabrina Coast shelf since the last deglaciation, b) produce geochemical data to aid in the regional calibration of paleotemperature proxies, and c) produce a Holocene record of oceanic paleotemperatures from the Sabrina Coast and interpret

this record in the context of what is known about Antarctic environmental change over the past 12,000 years.

Chapter 2 explores the hypothesis that sediments recovered are deglacial to Holocene in age, which is tested using radiocarbon dating methods established in Antarctic sediments. To further characterize the sediments, the hypothesis that continuous, distinct lithologic units reflect changes in glacial retreat and changes in oceanographic conditions (grounding line retreat, sea ice cover, water column stratification, productivity) is tested using a multi-proxy (sedimentologic, micropaleontologic, and geochemical) approach. Chapter 3 tests the hypothesis that surface sediment planktic foraminifer Mg/Ca and TEX₈₆ values exhibit definable relationships with measured temperatures on the Sabrina Coast, East Antarctica. Then, Sabrina Coast upper ocean temperatures are reconstructed for the last ~1000 years to test the hypothesis that paleotemperatures exhibit similar trends as those observed in late Holocene ice core records. Chapter 4 tests hypothesis that deglaciation was driven by warmer regional ocean temperatures rather than sea level change by generating Mg/Ca and TEX₈₆ paleotemperature estimates that span the last ~16,500 years.

1.3 Cenozoic Antarctic Cryosphere Evolution

Much of the information known about the development of Antarctica's cryosphere is derived from ice-distal deep sea sediment cores and from Antarctic ice cores. Cenozoic climate has evolved over 65 million years from warm, Eocene greenhouse conditions to the glacial icehouse conditions of the late Cenozoic, associated with growth and loss of major ice sheets. Information about past climate is archived in proxies such as deep-sea benthic foraminifer stable oxygen isotopes that demonstrate deep ocean temperatures have cooled by ~15-12°C (Figure 1.2;

Kennett & Shackleton, 1975; Lear et al., 2000). During this long-term cooling trend, continental-scale ice sheets developed on Antarctica at the Oligocene-Eocene boundary (Oi-1; ~40 million years ago; Miller et al., 1987; 1991). Ice growth at Oi-1 is thought to be associated with the opening of the Drake and Tasman gateways to surface ocean circulation, which isolated Antarctica from lower latitude heat (Kennett, 1977) and decreasing atmospheric CO₂ concentrations (DeConto & Pollard, 2003). The second major climate step in the deep-sea record occurs during the middle Miocene Climate Transition (MMCT; 14.2-13.8 million years ago), when Antarctica's ice sheets expanded in association with meridional heat and moisture transport and ice albedo feedbacks (Kennett & Shackleton, 1975; Levy et al., 2016; Shevenell et al., 2008).

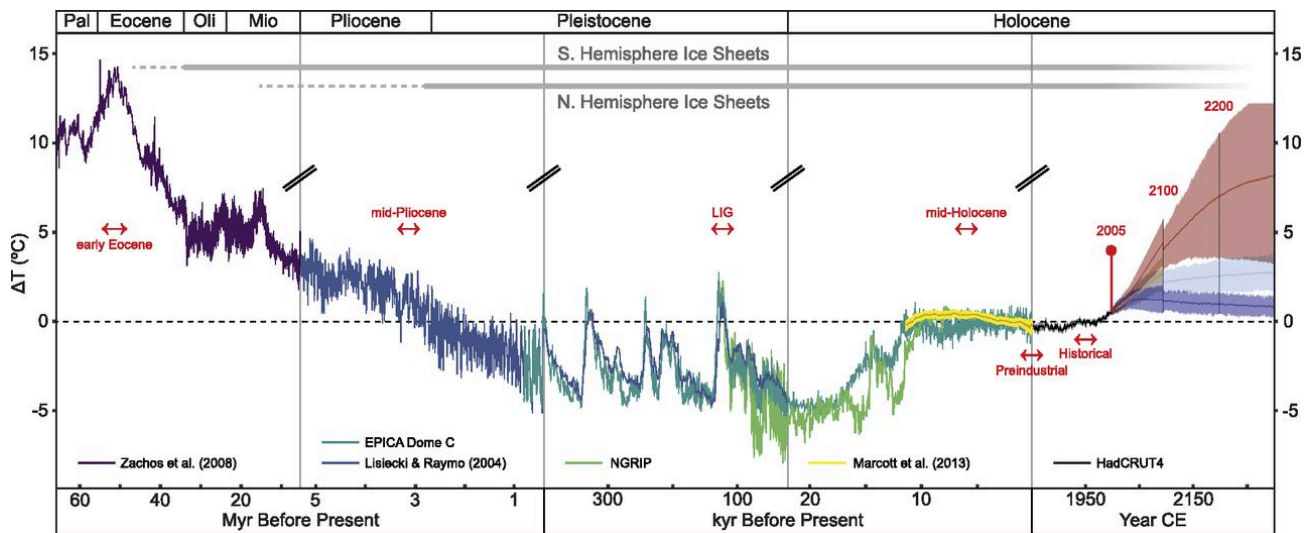


Figure 1.2 Global temperature and ice volume changes over the Cenozoic and future projections. Figure from Burke et al., 2018.

Following warming during the middle Pliocene, Earth's climate generally cooled over the last 4 million years, modulated by variations in Earth's orbit (Figure 1.2; Lear et al., 2000; Lisiecki & Raymo, 2005). Permanent ice sheets are thought to have grown in the northern

hemisphere ~2.7 million years ago, driven by the closure of the Central American Seaway and decreasing atmospheric CO₂ levels (Driscoll and Haug, 1998; Willeit et al., 2015). The sawtooth pattern of glacial-interglacial cycles, based on foraminifer $\delta^{18}\text{O}$ records (Emiliani, 1970; Paillard 2001; Shakun et al., 2015a), indicate a switch from a 41,000 to 100,000 year periodicity, thought to be driven by a change in Antarctic Ice Sheet volume (Elderfield et al., 2012; Raymo et al., 2006). Antarctic ice core records of the past 800,000 years provide more information on climatic conditions during glacial-interglacial transitions (Jouzel et al., 2007; Wolff et al., 2010), and δD -derived temperatures are in general agreement with deep-sea benthic foraminifer $\delta^{18}\text{O}$ records (Lisiecki & Raymo, 2005). Millennial scale variability in δD is thought to be controlled by local insolation changes induced by the obliquity cycle, whereas the long-term changes are induced by deep water formation changes, highlighting the importance of the Antarctic cryosphere and oceanography in global climate variability (EPICA Community Members, 2004; Jouzel et al., 2007; Lüthi et al., 2008). In Antarctica, the transition from the last glacial period to the Holocene interglacial is marked by rising atmospheric CO₂ (Anderson et al., 2009; Monnin et al., 2001; 2004), sea level rise (Bentley et al., 1999; Hodgson et al., 2016; Shakun et al. 2015b), and large-scale retreat of continental ice shelves from the shelf edge (Bentley et al., 2009; Hall et al., 2009; Mackintosh et al., 2014).

1.4 Development and importance of the East Antarctic Ice Sheet

Antarctica consists of two ice sheets containing 27 million km³ of ice (Fretwell et al., 2013). Two-thirds of the East Antarctic Ice Sheet (EAIS) is land based, while the West Antarctic Ice Sheet (WAIS) is mainly marine-based (grounded on bedrock or sediments below sea level). The EAIS and WAIS hold enough ice to raise sea level by ~53.3 m and 4.3 m, respectively, if

they were to melt (Fretwell et al., 2013). Ice sheet models show that early Antarctic glaciation began on isolated highlands in East Antarctica (Figure 1.3; Bo et al, 2009; Rose et al., 2013). Evidence exists for marine-terminating glaciers at the Sabrina Coast by the early to middle Eocene, indicating that marine-terminating glaciers may have existed in certain catchments before continental-scale ice growth (Gulick, Shevenell et al., 2017). Glacial and meltwater erosion were considered the dominant force on regional landscape evolution, until the middle to late Eocene (Shevenell et al., 2004, Lewis et al., 2006).

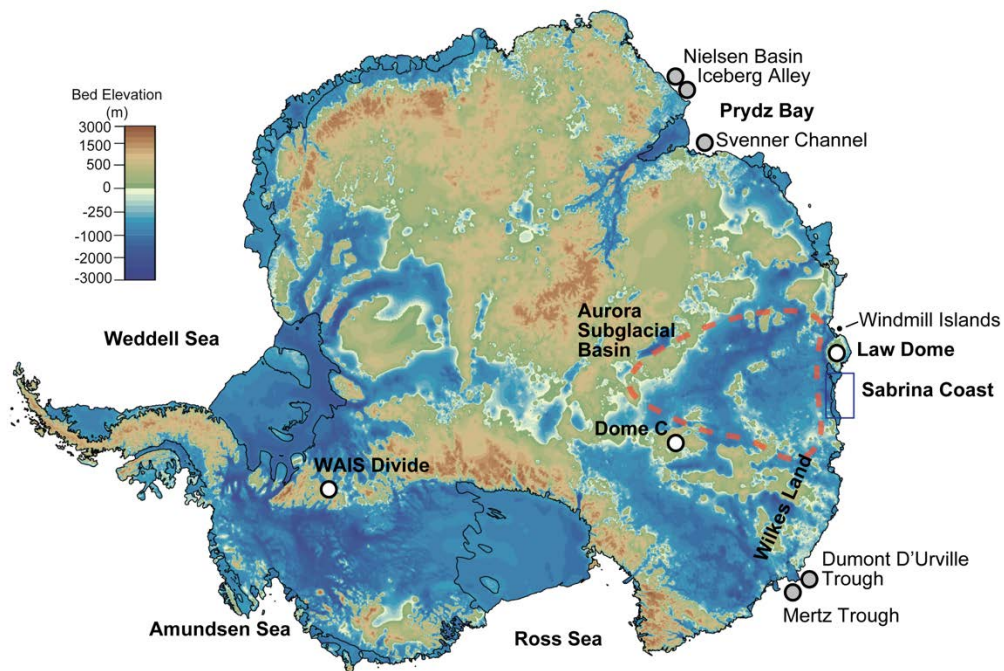


Figure 1.3 Antarctica with Bedmap2 elevations (Fretwell et al., 2013), annotated with key East Antarctic locations mentioned herein, Sabrina Coast (dark blue box), and Aurora Subglacial Basin (orange dashed line). Relevant ice cores (white circles) include the WAIS Divide ice core (WDC; WAIS Divide Project Members, 2013), EPICA Dome C ice core (EDC; EPICA Community Members, 2006), and the Dome Summit South ice core at Law Dome (Van Ommen et al., 2004). East Antarctic sediment records (gray circles) include Svenner Channel (Leventer et al., 2006), Iceberg Alley and Nielsen Basin (Harris & O'Brien, 1996; Leventer et al., 2006; Mackintosh et al., 2014), Dumont D'Urville Trough (Denis et al., 2009a; Maddison et al., 2012), and Mertz Trough (Domack et al., 1991; McMullen et al., 2006).

1.4.1 The Aurora Subglacial Basin

The advance and retreat of the East Antarctic ice sheet over glacial to interglacial timescales has impacted the topography of Wilkes Land, East Antarctica (Figure 1.3). One such sector of Antarctica that has been glacially active on millions of year timescales is the Aurora Subglacial Basin (ASB), a sparsely observed marine-based catchment in East Antarctica that extends from the Gamburtsev Mountains and Dome C in the south to the Sabrina Coast and Law Dome in the north (Figure 1.4). The ASB is bounded by the Terre Adélie Highlands to the east and the highlands of the Indo-Australo-Antarctic Suture to the west (Figure 1.4; Young et al., 2011). The ASB (287,000 km²) drains one eighth of the interior of EAIS, equivalent to 5.3 m of sea level (Aitken et al., 2016; Morlighem et al., 2020; Wright et al., 2012; Young et al., 2011). Geophysical data reveals that the catchment consists of overdeepened sub-basins, with elevations lower than the continental shelf (Aitken et al. 2014; 2016; Young et al., 2011). The ASB basement, scoured of sedimentary material, indicates repeated cycles of erosion during advance and retreat of the ice sheet (Figure 1.4; Aitken et al., 2016).

1.4.2 Climate-driven ice sheet instabilities

If current rates of greenhouse gas emissions continue, the Antarctic Ice Sheet could contribute up to 1 m of sea-level rise by 2100 (DeConto and Pollard, 2016). Data and models indicate that ice sheets grounded below sea level and located on landward-deepened beds are susceptible to marine ice sheet instability when warm ocean waters interact with grounded ice (Schoof, 2007, Jones et al., 2015, DeConto & Pollard, 2016; Young et al, 2011). Warm ocean water reduces ice mass by melting ice at the grounding line and the base of ice shelves, leading to acceleration and thinning of glacial systems (Figure 1.5; Shepard et al., 2004; Pollard et al.,

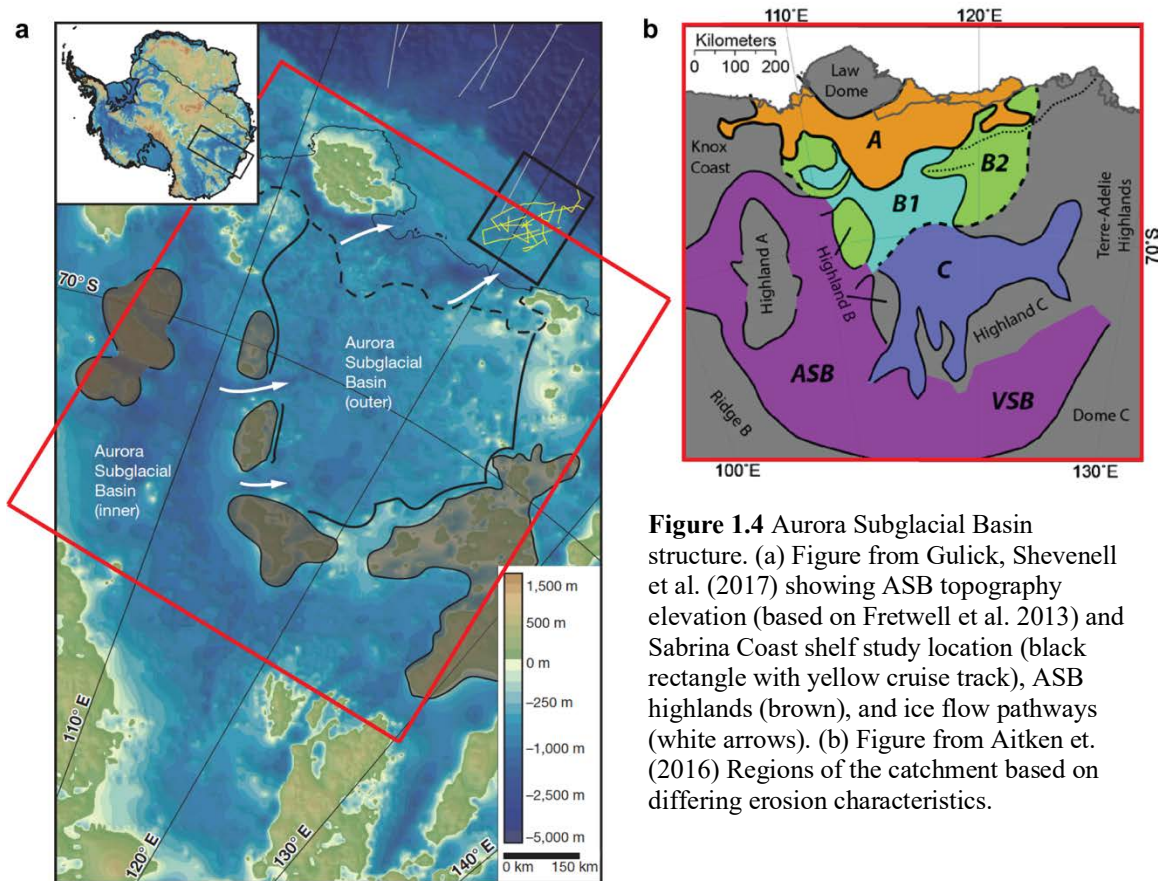


Figure 1.4 Aurora Subglacial Basin structure. (a) Figure from Gulick, Shevenell et al. (2017) showing ASB topography elevation (based on Fretwell et al. 2013) and Sabrina Coast shelf study location (black rectangle with yellow cruise track), ASB highlands (brown), and ice flow pathways (white arrows). (b) Figure from Aitken et. (2016) Regions of the catchment based on differing erosion characteristics.

2015). Other climate forcings contributing to ice sheet destabilization include sea level rise (eustatic forcing), which increases outlet glacier buoyancy, leading to flow acceleration, iceberg calving, and lift off of the grounded terminus (Jenkins et al., 2011). Another factor is atmospheric thermal forcing of the ice sheet through orbitally-paced local insolation (WAIS Divide Project Members, 2013), which increases surface melting, potentially leading to ice shelf disintegration, reducing back-stress and allowing accelerated flow of the glacier system buttressed by the ice shelf (Dupont & Alley, 2005). Surface melting results in increased basal lubrication and ice flow (Livingstone et al., 2012; Stearns et al., 2008).

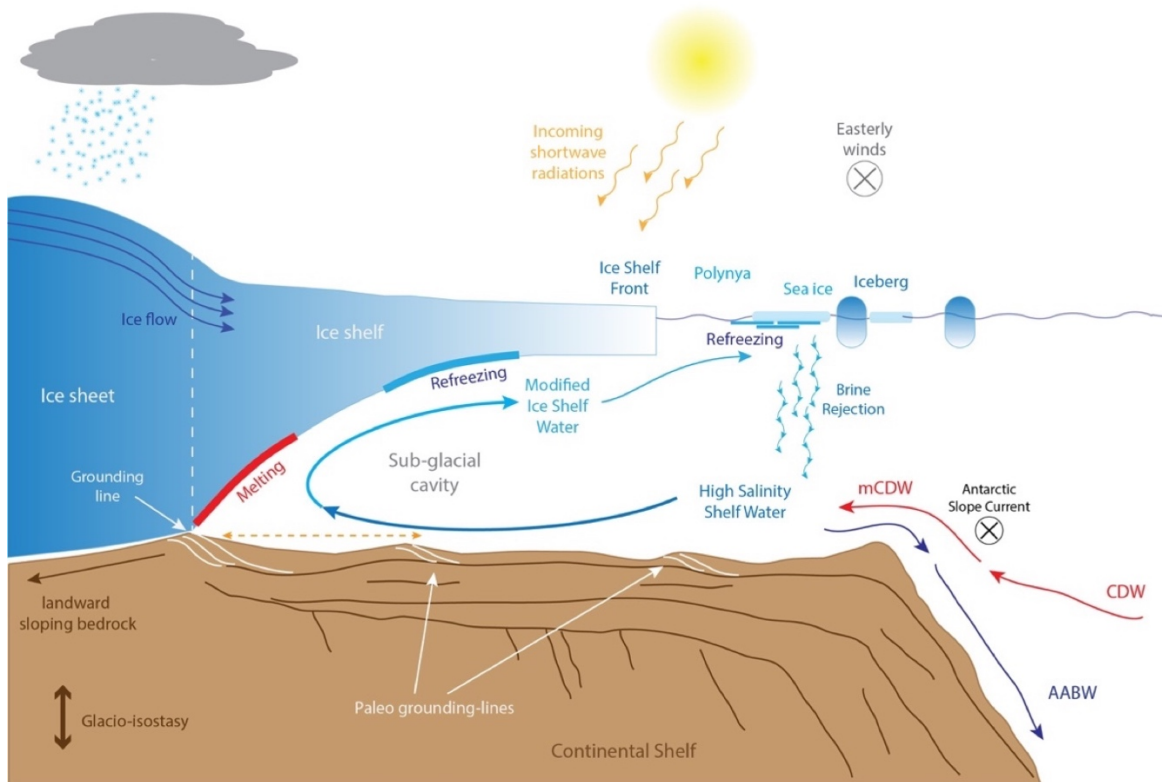


Figure 1.5 Illustration of processes impacting growth and loss of an ice shelf. These factors include warm ocean water, and wind (easterlies and westerlies). Figure from Colleoni & DeSantis (2015).

1.4.3 Aurora Subglacial Basin vulnerability to ice sheet instability

On the Sabrina Coast, models indicate that the ASB catchment can become progressively unstable under warm oceanic and atmospheric temperature conditions (Aitken et al., 2016). Under the modern-day configuration of the ice sheet, an increase in air temperature by +4°C and an increase in ocean temperature by +1°C results in glacial retreat from the coastal region and 0.9 m of global sea level rise (Aitken et al., 2016). However, the basin is divided by bedrock ridges between the coastal ocean sloping region and inland landward sloping region of the Aurora Subglacial Basin (Figure 1.4b; Aitken et al., 2016; Tooze et al., 2020; Young et al., 2011). The inland region bed is reverse-sloped, so retreat into the subglacial basin is subject to ocean-driven instabilities if ice retreats past the bedrock ridge between the coastal and inland

regions (Figure 1.4b; Aitken et al., 2016). At present-day air and ocean temperatures, ice sheet reconstructions must include ice-cliff failure in the model in order to cause ice retreat inland from the boundary ridge, suggesting that retreat into the Aurora Subglacial Basin interior is caused only under highly unstable conditions (Aitken et al., 2016). In ice sheet models, full retreat of the ASB is only projected if temperatures rise +15°C and ocean temperatures rise by +5°C (Aitken et al., 2016). The region also contains subglacial lake-like features and complex drainage networks connecting the ASB to the coast (Fricker et al., 2014; Siegert et al., 2005; Wright et al., 2012). ASB instability may be impacted by the presence of active subglacial hydrology, which can cause acceleration by meltwater lubrication at the bedrock surface (Dow et al., 2020; Stearns et al., 2008).

1.5 Physical Setting

1.5.1 Totten Glacier and the Sabrina Coast

Totten Glacier is a marine-terminating outlet glacier system that drains a majority of the ASB catchment. Totten Glacier and its associated tributaries terminate on the Sabrina Coast shelf (Figure 1.6), forming ice shelves (e.g., the Totten Ice Shelf and Moscow University Ice Shelf) landward of deep (1000-2000 m) regional grounding lines (Greenbaum et al., 2015). Regional grounding lines are connected to the intermediate and deep waters of the Southern Ocean via a deep cross-shelf trough and bedrock channels, which allow pathways for relatively warm (~0.5°C) water to move across the shelf and contribute to observed glacier thinning and ice mass loss (Aitken et al., 2016; Greenbaum et al., 2015; Rintoul et al., 2016). Satellite and airborne geophysical studies indicate substantial lowering of Totten Glacier's ice surface (1 m/yr) and the

regional transfer of grounded ice to the Southern Ocean (100 G tons/yr; Pritchard et al., 2009; Rignot et al., 2013; Shepherd & Wingham, 2007).

The Sabrina Coast was initially explored through hydrographic measurements at two stations on the outer continental shelf that identified warm ($>0^{\circ}\text{C}$) deep water presence (Bindoff et al., 2000; Williams et al., 2011), and through airborne geophysical surveys to map the ice sheet bed geometry draining into the Totten Glacier (Young et al., 2011). The observations led to the hypothesis that Totten Glacier was sensitive to marine ice sheet instabilities, similar to those observed in West Antarctica (Rignot & Jacobs, 2002; Shepherd et al., 2004), due to its deep (1000-2000 m) grounding line on a landward sloping bed, lubricated by an extensive subglacial drainage system (Rignot et al., 2006; Rignot et al., 2013; Greenbaum et al., 2015; Li et al., 2015; Aitken et al., 2016).

During the austral summer of 2014, the scientific part of research cruise NBP14-02 (Leventer et al., 2015) collected the first geophysical, sedimentological, and oceanographic data from the Sabrina Coast continental shelf (Figure 1.6) in the Dalton Polynya, east of Totten Glacier and west of Dalton Ice Tongue (115°E to 125°E). Prior to NBP14-02, the Sabrina Coast physical oceanography had not been characterized and the continental shelf had not been surveyed or sampled.

Multibeam sonar mapping revealed complex, glacially carved features with grounding line wedges, and bedrock channels indicating a complex glacial and deglacial history (Gulick, Shevenell et al., 2017; Fernandez et al., 2018; Leventer et al., 2015). The inner shelf is scoured free of sediments (Fernandez et al., 2018). The middle shelf consists of a thick sequence of glacially eroded Cenozoic age sediments, including a wide trough trending to the northwest in front of Totten Glacier (Figure 1.6b; Fernandez et al., 2018; Gulick, Shevenell, et al., 2017). The

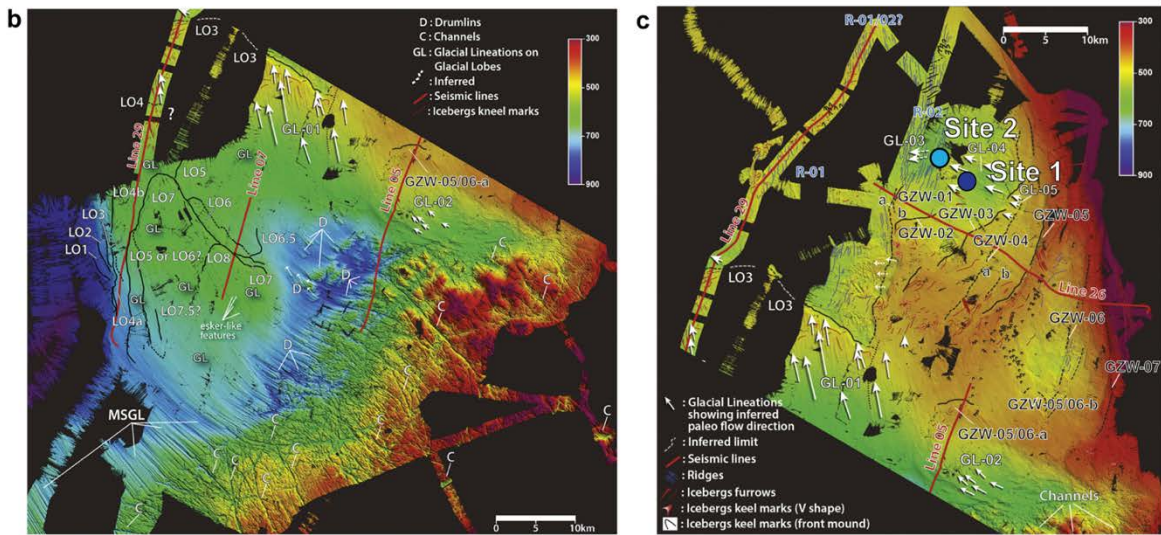
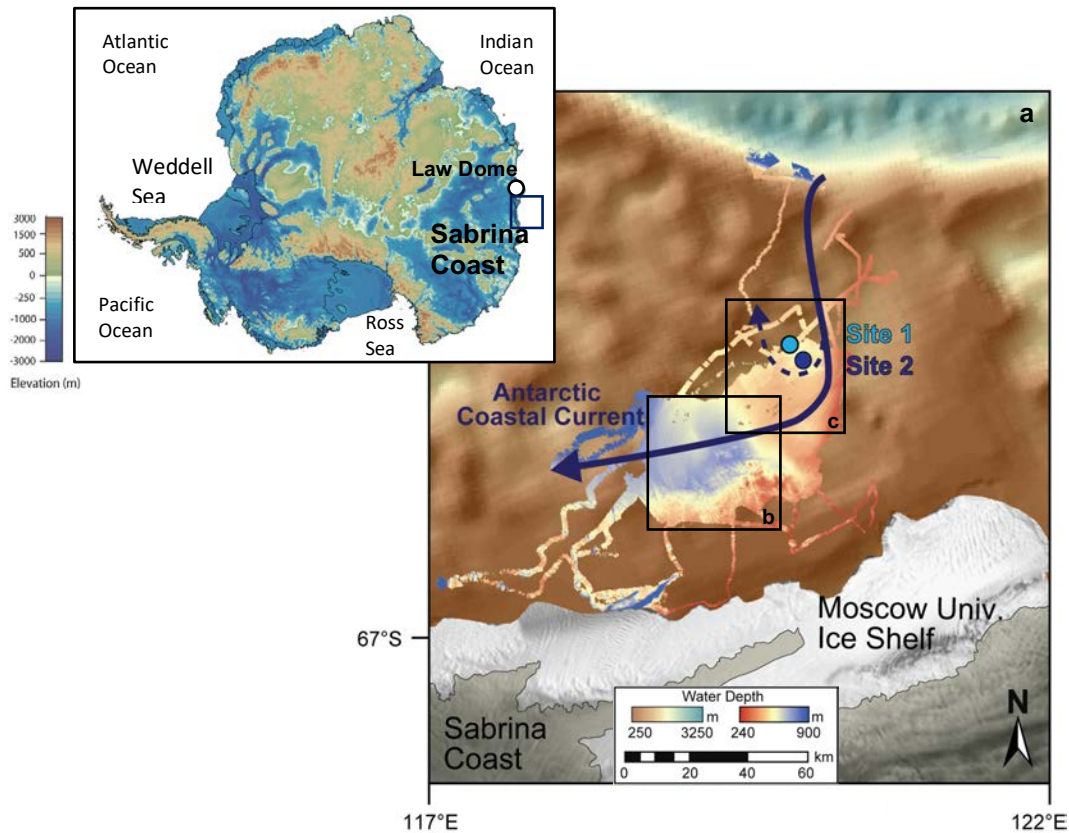


Figure 1.6 (a) Bathymetric map of the Sabrina Coast continental shelf. The shelf deepens to the west (cool colors) and is shallow in the east (warm colors). Core Sites 1 and 2 are ideally located in the path of the Antarctic Coastal Current (Figure 1.6a adapted from Gulick, Shevenell et al., 2017). (b) Bathymetry of the rugged inner shelf and deeper middle shelf areas. (c) Bathymetry of the shallow middle shelf area with core Sites 1 and 2 indicated (white arrows=ice flow direction based on glacial lineations; blue lines=ridges; black lines=grounding zone wedge interpretations). Figures b and c adapted from Fernandez et al. (2018).

seafloor on the western side of the survey region is deeply incised, with subparallel channels and ridges representing subglacial groundwater flow and past streaming ice in this region (Figure 1.6b; Fernandez et al., 2018).

Since 2014, several scientific expeditions have contributed to the understanding of Sabrina Coast shelf and slope oceanography and sedimentary dynamics. Expedition NBP15-03 surveyed the region and confirmed the role of regional bathymetry in steering deep-water access (Nitsche et al., 2017), while IN2017-V01 mapped and sampled sediments on the Sabrina Coast continental slope (Armand et al., 2018; Donda et al., 2020; Holder et al., 2020; O'Brien et al., 2020; Tooze et al., 2020). Continental shelf hydrography was characterized during several cruises between 2014 and 2016 (AU1402; Arroyo et al., 2019; Rintoul et al. 2016; Silvano et al. 2017; 2018; 2019), summarized in section 1.5.2, Sabrina Coast physical oceanographic setting.

1.5.2 Sabrina Coast physical oceanographic setting

The eastward-flowing Antarctic Circumpolar Current (ACC) is the major current system that defines the Antarctic polar region (Figure 1.7; Orsi et al., 1995). On the Sabrina Coast, two regional, westward flowing currents, the Antarctic Coastal Current, a surface current, and the Antarctic Slope Current, a deep current at the continental shelf-slope break, are driven by the strength and position of polar easterly winds (Gwyther et al., 2014; Massom et al., 1998). Wind stress at the continental shelf break east of the Dalton Ice Tongue leads to CDW upwelling on the continental shelf, then it flows south and west with the Antarctic Coastal Current (Greene et al., 2017). Observations from NBP14-02, as well as from Rintoul et al. (2016) and Silvano et al. (2017), indicate that relatively warm, nutrient rich, oxygen poor water is present below 400 m on the Sabrina Coast continental shelf, which mixes with local shelf waters to form mCDW (Figure

1.8). The distribution of mCDW is largely controlled by regional bathymetry, with the warmest (least modified) mCDW found on the outer shelf just west of Dalton Ice Tongue (Leventer et al., 2015; Rintoul et al., 2016). Warm mCDW can reach Totten Glacier and Moscow University Ice Shelf cavities via deep bathymetric channels (Figure 1.8; Greenbaum et al., 2015; Rintoul et al., 2016; Silvano et al., 2017). At the ice shelf fronts, these waters are 1 to 2°C above the local freezing point, which is warm enough to cause basal melting (Silvano et al., 2017).

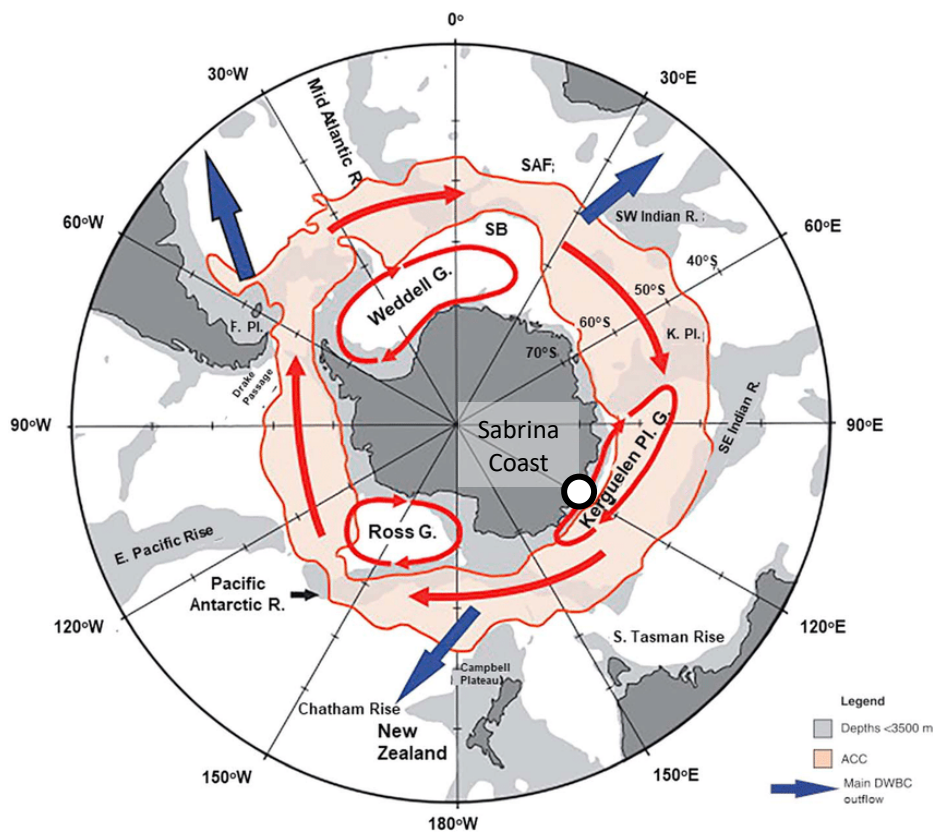


Figure 1.7 Primary Southern Ocean physical oceanographic features. Sabrina Coast study area indicated by white dot. Features include: (1) the Antarctic Circumpolar Current (ACC), the Subantarctic Front (SAF), and southern boundary of Upper Circumpolar Deep Water (SB); (2) the Ross, Weddell, and Kerguelen Plateau gyres (Park et al., 2009); and (3) the deep western boundary current (DWBC) outflow to the Southern Ocean (blue arrows). Figure modified from Carter et al., 2008.

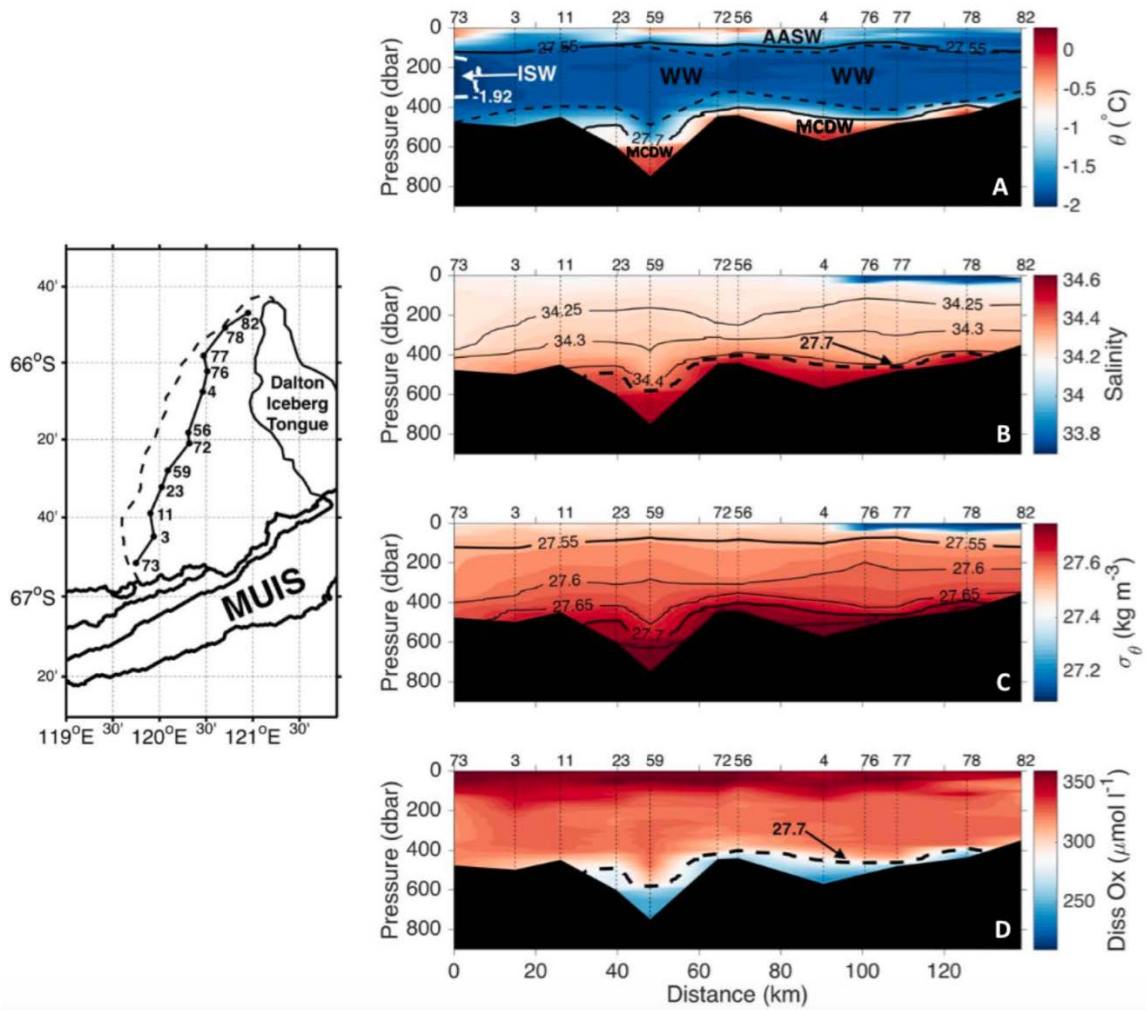


Figure 1.8 Physical oceanography of a meridional section through the Dalton Polynya. Figures show potential temperature, salinity, potential density, and dissolved oxygen. Ice Shelf Water indicated by dashed white line; Winter Water (WW) layer indicated by black dashed lines; modified Circumpolar Deep Water (mCDW) is below the $\sigma = 27.7 \text{ kg/m}^3$ contour; Antarctic Surface Water (AASW) is above the $\sigma = 27.55 \text{ kg/m}^3$ contour. Figure from Silvano et al., 2017.

The physical oceanography of the Sabrina Coast is also influenced by the Dalton Polynya (Figure 1.9), which forms when katabatic winds blow offshore from the EAIS, pushing sea ice away from the coast west of Dalton Ice Tongue (Jacobs et al., 2004; Khazendar et al., 2013; Rintoul et al., 2001). Profiles from the Sabrina Coast continental shelf show a strong density contrast between fresh, surface water (named Winter Water for its seasonal source) and saline

mCDW (Figure 1.8; Silvano et al., 2017), which stabilizes the water column. In strong polynyas, the offshore flow of katabatic wind creates Dense Shelf Water (also called High Salinity Shelf Water) as sea ice forms and brine is rejected (Tamura et al., 2016). However, Dense Shelf Water formation is not presently observed in the Dalton Polynya (Figure 1.10; Silvano et al., 2017; Tamura et al., 2016), which means mCDW can access grounding lines year-round (Silvano et al., 2017; 2018; 2019). The persistent presence of warm water on the continental shelf near the Totten Glacier and in the Dalton Polynya results in intensified ice shelf melt rates similar in magnitude to those observed in the Amundsen Sea Embayment (Figure 1.10; Leventer et al., 2015; Silvano et al., 2017; 2018).

The presence of the Dalton Ice Tongue inhibits the westward flow of sea ice and helps maintain the Dalton Polynya (Khazendar et al., 2013; Massom et al., 1998; Silvano et al., 2018; Tamura et al., 2008). Sea ice production is low in the Dalton Polynya ($51 \pm 10 \text{ km}^3/\text{yr}$) relative to other Antarctic polynyas (Massom et al., 1998; Tamura et al., 2016). On the Sabrina Coast shelf, the seasonal cycle of sea ice growth and decay is characterized by a minimum in yearly ice concentration in March. Ice concentration increases throughout austral autumn as air temperatures cool, then sea ice consolidates and attaches to the Totten Ice Shelf in May (Greene et al., 2018). The sea ice remains attached to the ice shelf throughout the austral winter, then the connection breaks in early austral summer and the region is filled with unconsolidated ice until it melts late in the summer season (Greene et al., 2018).

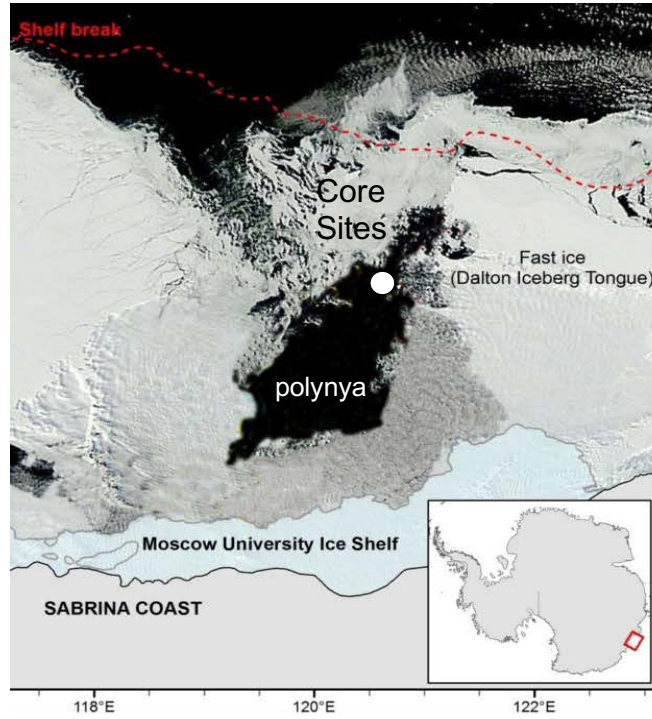


Figure 1.9 Satellite image of the Dalton Polynya from February 2014. Location of Dalton Polynya offshore the Sabrina Coast, to the west of the Dalton Iceberg Tongue. Image modified from A. Post, MODIS Aqua.

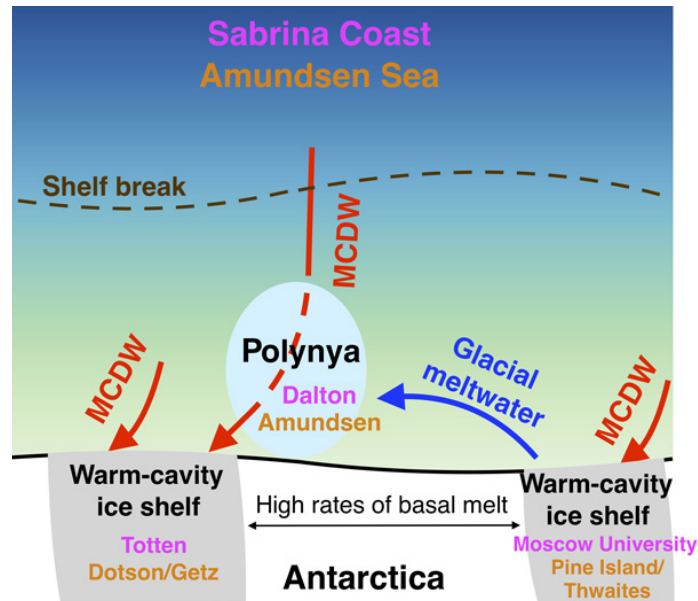


Figure 1.10 Schematic of Sabrina Coast continental shelf physical oceanography. On the Sabrina Coast Amundsen Sea continental shelves, modified Circumpolar Deep Water (mCDW) persists because the production of glacial meltwater prevents Dense Shelf Water (DSW) formation in polynyas. Otherwise, DSW formation would help block the incursion of mCDW. Figure from Silvano et al., 2019.

1.5.3 Sabrina Coast atmospheric processes

The physical oceanography of Antarctic continental shelves is strongly influenced by atmospheric circulation patterns. As a result of the strong pressure gradient between the Antarctic plateau and coastal regions, katabatic wind flow rapidly to the Antarctic coast (Yu et al., 2020 and references therein). Katabatic winds are significant to Antarctic shelf oceanography because they contribute to the formation and maintenance of polynyas (Massom et al., 1998) and can extend tens of km to ~100 km offshore (Massom et al., 1998). Along the Antarctic coast, the other major wind patterns are the westward flow of the polar easterlies and the strong westerly airflow driving the Antarctic Circumpolar Current (Figure 1.11; Van Den Broeke & Van Lipzig, 2004).

The record of atmospheric processes on the Sabrina Coast is well-chronicled in ice cores from Law Dome, a small (200 km wide), coastal (1400 m in elevation) ice dome just east of Totten Glacier (see Figure 1.3 for location; Goodwin et al., 1996). The Dome Summit South (DSS) ice core, at the center of Law Dome, experiences high annual snow accumulation (>1000 kg/m²/yr accumulation) due to its proximity to warm, northern air masses (Roberts et al., 2015). Despite its coastal location, Law Dome experiences low wind speeds (8.3 m/s) and minimal katabatic wind activity (Morgan et al., 1997). The Dome Summit South (DSS) ice core site, in close proximity to Casey Station on the western coast of Law Dome, provides a robust record of atmospheric processes since the last deglaciation to present (Curran et al., 1998; Massom et al. 2004; Masson-Delmotte, 2003; Souney et al., 2002; Van Ommen et al., 2004).

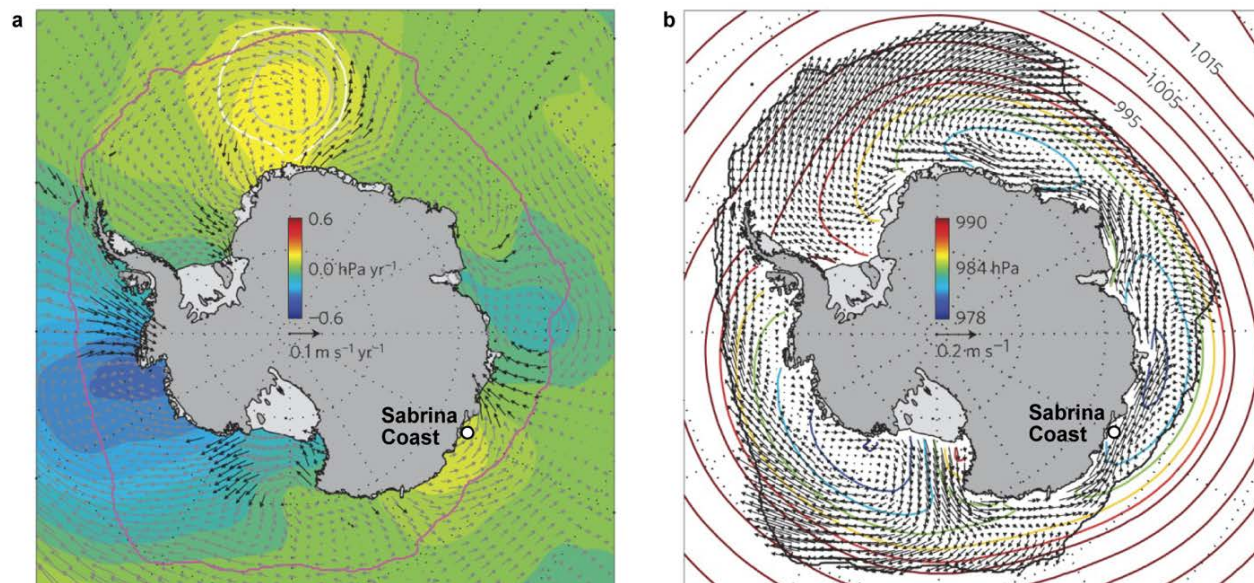


Figure 1.11 (a) Antarctic wind trend vectors (black) overlaid on trend in sea-level pressure (colored base map). (b) Sea ice motion vectors overlaid on modeled sea-level pressure (colored contours). Sabrina Coast study site indicated by white dots in each figure. Figures modified from Holland & Kwok, 2012.

1.5.4 Atmospheric and oceanic teleconnections

The Antarctic Ice Sheet is impacted by atmospheric temperature, precipitation, and wind patterns that propagate to ocean system (Kwok & Comiso, 2002; Marshall et al., 2004; Van Den Broeke & Van Lipzig, 2004). Climatological systems that influence atmospheric and oceanic processes around Antarctica are the Southern Annular Mode (SAM) and El Niño–Southern Oscillation (ENSO), two teleconnections that link the polar region with lower latitudes (Thompson & Solomon, 2002; Marshall et al., 2004). SAM modulates the sea level pressure gradient between middle (45°S) and southern latitudes (65°S), resulting in changes in snowfall accumulation, upwelling, and sea ice dynamics (Crosta et al., 2021; Raphael & Hobbs, 2014; Van Ommen et al., 2010; Vance et al., 2013). ENSO is a zonal pattern of atmospheric pressure and sea surface temperature in the equatorial and subtropical Pacific, which impacts the Pacific and Australian sectors of Antarctica (Fogt et al., 2011; Turner, 2004; Vance et al., 2013;). When

SAM is in a positive phase (Figure 1.12); sea level pressure is higher away from Antarctica, westerly winds are strengthened or further south, and upwelling of warm water can occur along continental shelves, including the Sabrina Coast shelf edge (Greene et al., 2017; Kwok and Comiso, 2002; Thompson et al., 2000). In addition to upwelling, SAM and ENSO can influence sea ice extent, polynya formation, and ice shelf melting (Paolo et al., 2018; Stammerjohn et al., 2008; Yuan, 2004), which is significant because fresher surface waters can reduce deep water formation and water column overturning, allowing mCDW to access regional grounding lines (Silvano et al., 2019).

The Sabrina Coast may be particularly sensitive to global climate variability. In the East Antarctic, south of Australia and New Zealand, ENSO and SAM patterns can interact with atmospheric blocking features, resulting in warm, moist air advected toward Antarctica (Massom et al., 2004; Renwick et al., 1998; Vance et al., 2013). Modeled incursions of mCDW onto the Sabrina Coast shelf result from wind-driven upwelling at the shelf edge north of the Dalton Iceberg Tongue (Greene et al., 2017). Upwelling of mCDW may change over time according to shifts in the phase of the SAM (Greene et al., 2017; Spence et al., 2014; Thoma et al., 2008). At present, warmer regional air temperatures, increased wind stress at the shelf edge, mCDW on the Sabrina Coast shelf, and regional ice mass loss are associated with the positive phase of SAM (Greene et al., 2017; Rintoul et al., 2016).

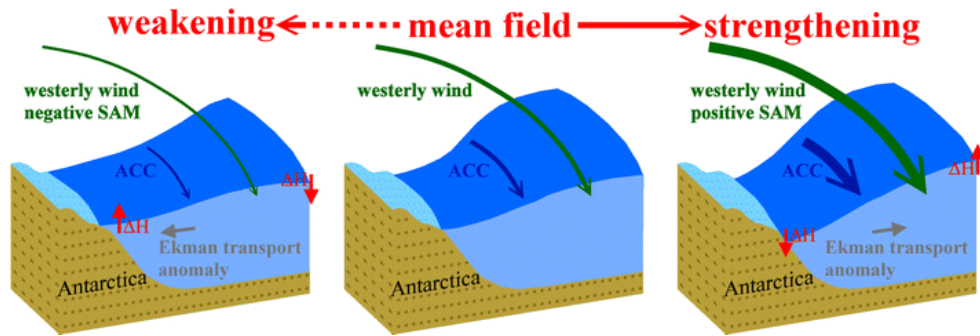


Figure 1.12 Depiction of SAM influence on the Antarctic Circumpolar Current and Southern Ocean. The effects of a positive SAM Index (right panel) and negative SAM Index (left panel) compared to mean conditions (center). Figure from Liao & Chao, 2017.

1.6 East Antarctic Deglacial to Recent Climate

Antarctic ice cores and marine sediment records provide context for past changes in the Antarctic cryosphere, atmospheric and oceanic circulation and temperature, and responses to global climate forcings. East Antarctic ice cores from Dome C and Law Dome record regional atmospheric conditions during deglaciation (Figure 1.3), including atmospheric warming during and after the Last Glacial Maximum (EPICA Community Members, 2006; Masson et al., 2000), followed by a cool period called the Antarctic Cold Reversal (ACR) between 14.6 and 12.7 thousand years before present (ka; EPICA Community Members, 2006; Pedro et al., 2011; Stenni et al., 2011). East Antarctic ice core records indicate the early Holocene was 1-2°C warmer than present, followed by general cooling through the Holocene, with shorter-term variability within the cooling trend (Masson et al., 2000; Masson-Delmotte et al., 2011). Local support for warmer atmospheric conditions during the early Holocene comes from coastal Law Dome, ~280 km to the southwest of our Sabrina Coast site, which indicates peak atmospheric warmth at ~11 ka, reduced sea ice extent, and less cyclonic activity between 12 and 9 ka (Curran et al., 1999; Masson et al., 2000; Morgan et al., 2002; Van Ommen et al., 2004). Law Dome also

records increased snow accumulation rates during the late Holocene after 5 ka (Van Ommen et al., 2004). Coastal East Antarctic ice cores document mid-Holocene warmth followed by late Holocene cooling (~5 to 0 ka), indicating that coastal sites are influenced by Southern Ocean and sub-Antarctic atmospheric circulation (Masson-Delmotte et al., 2011).

Circum-Antarctic marine sediment records document deglaciation as the onset of marine sedimentation at ~15 ka (Domack et al., 1998; Hemer & Harris, 2003; Mackintosh et al., 2014) and from the Amundsen Sea embayment by 16.4 ka (Kirshner et al., 2012; Smith et al., 2011). Regionally, deglaciation from EAIS proximal marine records ranges from ~10 to 15 ka (Leventer et al., 2006; Mackintosh et al., 2014). Sedimentary evidence from the Windmill Islands, on the inner continental shelf west of Law Dome, indicate deglaciation of the outermost islands by ~11-10 ka, likely associated with warm regional atmospheric temperatures (Goodwin & Zweck, 2000; Roberts, 2004).

By the early Holocene, many East Antarctic outlet glacier systems had begun to retreat from their maximum extents (Mackintosh et al., 2014). Marine sedimentary records from the Mertz Trough and Prydz Bay indicate persistent seasonally open marine conditions during the early to middle Holocene (Crosta et al., 2007; Denis et al., 2009a; Domack et al., 1998; Harris, 2000, Mackintosh et al., 2011). Middle Holocene open marine conditions coincide with records of rapid ice retreat in Larsemann and Vestfold Hills near Prydz Bay between 7.6 ka and 7 ka (Verleyen et al., 2005; Zwartz et al., 1998). On the East Antarctic margin, colder surface ocean temperatures and icier conditions dominate between ~4 to 1 ka (Denis et al., 2009b).

Furthermore, between 4 and 2.5 ka, glacial re-advance and thickening of the ice sheet in East Antarctica occurred at the Windmill Islands and Larsemann Hills, coincident with global sea level lowering of ~0.7 meters (Goodwin, 1996; 1998; Verleyen et al., 2005). Thus, there is

variability in timing of advance and retreat of East Antarctic outlet glaciers during the Holocene that had not yet been explored in the Sabrina Coast region prior to the research conducted in this dissertation.

1.7 Marine Sediments and Paleoceanographic Proxies

A wide variety of physical, geochemical, and micropaleontological tools can be used to reconstruct past climate conditions preserved in marine sediments. The following sections describe the applications, strengths, and limitations of several marine geologic tools and proxies that are implemented throughout the dissertation.

1.7.1 Lithology and physical properties

Utilizing lithologic features in sediment cores is the primary tool for interpreting depositional processes and inferring past glacial, biological, and oceanographic processes. Basic lithologic description involves characterizing sedimentary structures, thickness of lithologic sections, nature of contacts between sections, color, and sediment texture. Identifying lithofacies and associating them with depositional processes in a core can be useful for correlating between multiple cores across a region and characterizing the geologic and paleoceanographic history of large areas. In the Antarctic environment, sedimentation is impacted by a variety of factors, such as glacial activity (proximity of the ice sheet and ice shelves), the seasonal presence/absence of sea ice, and the seasonal deposition of organic material. Antarctic sediment and depositional associations are illustrated well in a figure from Smith et al. (2019), which covers commonly observed interpretations of open ocean, sub-ice shelf, subglacial lithofacies (Figure 1.13).

Physical properties of sediments, such as magnetic susceptibility, can provide further insight into depositional processes recorded in a sediment core. In sediment cores, magnetic susceptibility is a parameter that reflects the amount of magnetic minerals in a particular sediment horizon, measured by applying an external magnetic field (Thompson & Oldfield, 1986). Magnetic susceptibility is useful and widely applied in Antarctic settings to infer paleoproductivity and quantify the contribution of iron-bearing, terrigenous sediment versus biogenic sediment (Brachfeld et al., 2002; Kilfeather et al., 2011; Kirby et al., 1998; Leventer et al., 1996; McMullen et al., 2006). Other sediment physical properties such as grain size can provide insight into sediment transport processes (McCave et al., 2006; 2017). In Antarctic margin sediments, large clasts and coarse-grained material can indicate proximity of the grounding zone or transport by iceberg rafting (Smith et al., 2019 and references therein). Proximity to glacial systems is a challenge for recovering continuous sequences of Antarctic sediments because cycles of glacial advance and retreat can erase entire sequences from the sedimentary record (Smith et al., 2019).

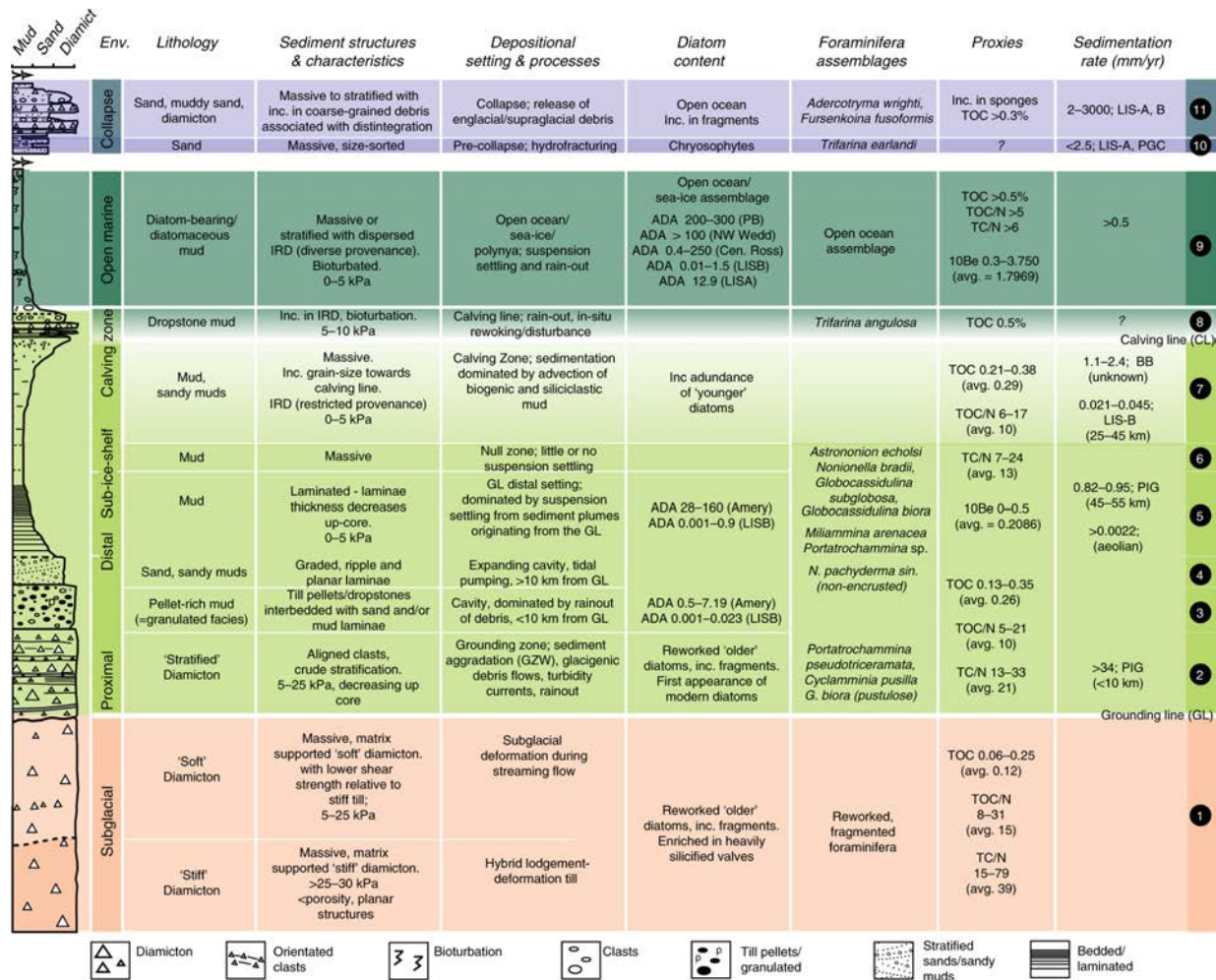


Figure 1.13 Idealized sedimentary sequence deposited under a retreating ice shelf. Figure from Smith et al. (2019).

1.7.2 Radiocarbon dating

Radiocarbon dating of Antarctic margin sediments relies on the incorporation of ^{14}C into calcium carbonate or organic matter. ^{14}C is an ideal chronometer for dating Holocene and Last Glacial Maximum sediments, within the ~50,000 year limit of ^{14}C decay (half life = 5730 ± 30 years) (Hajdas, 2008). Radiocarbon is produced in the upper atmosphere and enters circulation with the oceans as $^{14}\text{CO}_2$, and the decay “clock” begins once an organism dies and ceases to incorporate carbon (e.g. foraminifer calcification or algae photosynthesis) (Hajdas, 2008; Li et

al., 2021 and references therein). Several aspects of radiocarbon dating complicate its application in marine environments. Carbonate microfossils can be reworked through sediment transport or bioturbation, disturbing the steady deposition of sediment (Broecker et al., 2006). Another complication of dating marine deposits is the reservoir effect, the >550 year offset between the atmospheric ^{14}C age and the marine ^{14}C age, due to the relatively long timescale of circulation in the ocean (Berkman & Forman, 1996; Heaton et al., 2020; Stuiver et al., 2020). This offset is greater in Antarctic sediments, which are bathed in old, deep water; the average Antarctic marine reservoir age is 1300 ± 100 ^{14}C years (Berkman & Forman, 1996).

Often carbonate is not present in sufficient quantities or is not preserved in Antarctic sediments. Dating Antarctic sediment is further complicated by the presence of carbon from multiple sources that is incorporated into the bulk acid insoluble organic carbon (AIOM) radiocarbon dates, complicating development of Antarctic margin radiocarbon chronologies (Rosenheim et al., 2008, 2013). The Ramped PyrOx ^{14}C technique has been used successfully in Antarctic sediments to refine AIOM radiocarbon ages by utilizing differences in the thermal stability of allochthonous and autochthonous organic carbon in glacial marine sediments (Rosenheim et al., 2008; 2013; Subt et al., 2015; Venturelli et al., 2020). Ramped PyrOx uses a steady temperature ramp (5°C per minute up to 1000°C) to break down organic carbon and allow for separation of younger, reactive components from older, diagenetically stable material (Rosenheim et al., 2013). This approach is ideal because Ramped PyrOx-derived dates from the “youngest” (most reactive) organic carbon approaches, and in some cases, surpasses the accuracy of foraminifer-based ^{14}C dates (Subt et al., 2017).

1.7.3 ^{210}Pb dating

^{210}Pb is a useful tool to measure sediment accumulation rates for records up to ~120 years (half life = 22.3 years). ^{210}Pb dating is based on the principle that ^{210}Pb in recent sediments originates from the in situ decay of ^{226}Ra in minerals (“supported” ^{210}Pb) and the decay of atmospheric ^{222}Rn into ^{210}Pb (Appleby, 1992; Kirchner, 2011 and references therein). Upon deposition, the radionuclide adsorbs to suspended particles and is deposited in sediments. This unsupported or “excess” ^{210}Pb decays through time until it reaches the supported (background) level (Mackenzie et al., 1979).

Excess sedimentary ^{210}Pb activity is a function of changes in sedimentation rate and the amount of ^{210}Pb that is scavenged to the seafloor (Appleby, 1992; Kirchner, 2011 and references therein). Through the gradual deposition of overlying sediments through time, excess ^{210}Pb decreases with increasing depth in the sediment column. Thus, the depth profile can provide insight into sedimentary dynamics at the location of the core (Jaeger et al., 1999). The amount of excess ^{210}Pb reaching the sea floor is a function of particle concentration and adsorption surface availability, in addition to changes in sedimentation rates (Bettoli et al., 1998). Limitations to the applications of ^{210}Pb are the relatively short age range it can cover, and the dependence on a suitable depositional environment to preserve a consistent ^{210}Pb signal (i.e. little bioturbation or sediment remobilization; Kirchner, 2011). The concentration of water column particles and supply of ^{210}Pb can vary seasonally due sea ice cover, diatom spring blooms, and suspended lithogenic material during the summer melt season (Bettoli et al., 1998). The vertical profiles of ^{210}Pb in sediment cores can also be used to evaluate sediment dynamics, such as episodic deposition such as rapid deposit of a turbidite (Andresen et al., 2011; Jaeger et al., 1998). An added complication to ^{210}Pb dating is that an independent chronometer is recommended for

validation, such as a vertical profile of ^{137}Cs (Kirchner, 2011). Peak ^{137}Cs corresponds to the maximum concentration from 1963 global fallout, but much has decayed, making it more difficult to detect in samples (Baskaran et al., 2014). Additionally, less nuclear fallout was transported to the southern hemisphere, about one-third of northern hemisphere concentrations, so it is more difficult to detect ^{137}Cs in Antarctic sediments (Evrard et al., 2020)

1.7.4 Foraminifer assemblages

The presence of planktic and benthic foraminifera in Antarctic sediment allow us to identify changes in species assemblages and water mass characteristics. *Trifarina angulosa*, a shallow infaunal benthic foraminifer that prefers bottom current flow, also recognized as *Uvigerina angulosa* (Williamson, 1858), is present in sediments around the Antarctic margin (Hillenbrand et al., 2017; Mawbey et al., 2020). *Bulimina aculeata* is a shallow infaunal (~1 cm) foraminifer that prefers organic carbon-rich hemipelagic muds and is associated with water mass boundaries and mCDW ($>0^{\circ}\text{C}$) (Mackensen et al., 1985; 1990; McCorkle et al., 1990). *Neogloboquadrina pachyderma* (sinistral), a polar foraminifer that is the dominant planktic species in Antarctic assemblages, typically dwells at surface depths or at the ice-water interface (Hendry et al., 2009; Mikis et al., 2019).

Foraminifer assemblages in the Antarctic environment can be subject to limitations due to preservation (digenesis and/or dissolution; Mackensen et al., 1990; Murray & Pudsey, 2004). They are also subject to reworking by glacial advances and retreats or downslope transport, limiting their ability to serve as chronostratigraphic or paleoenvironmental indicators, so their presence in a sediment sequence must be scrutinized (Quilty, 2001; McKay et al., 2016). To use foraminifera as a paleoenvironmental proxy, it is essential to assess the relationships between the

living assemblages and the surface dead and downcore assemblages (Bergami et al., 2009; Murray & Pudsey, 2004).

1.7.5 Foraminifer stable isotopes

$\delta^{18}\text{O}$ in foraminifer calcium carbonate (CaCO_3) reflects the combined signal of the water temperature and $\delta^{18}\text{O}$ of the seawater in which the foraminifer calcified (Lea, 2014 and references therein). Due to its benthic, infaunal habitat, foraminifer *Uvigerina* spp. incorporates stable oxygen isotopes in equilibrium with seawater, providing reliable values of bottom water $\delta^{18}\text{O}$ (Shackleton, 1974). In planktic foraminifer *N. pachyderma* (s), $\delta^{18}\text{O}$ may be complicated by biological vital effects that cause foraminifera to incorporate $\delta^{18}\text{O}$ out of equilibrium with seawater and intratest variability in isotopic values (Kozdon et al., 2009; Mortyn & Charles, 2003; Nürnberg, 1995). *Neogloboquadrina pachyderma* (s) oxygen and carbon isotopes from western Antarctic Peninsula sediment traps demonstrate that *N. pachyderma* (s) calcifies at the ice-water interface during the winter, where biological activity and brine rejection result in undersaturation of CO_2 (Hendry et al., 2009). Although the setting elevates the ambient carbonate ion saturation $[\text{CO}_3^{2-}]$, isotopic incorporation is not as heavily influenced as trace metal uptake (less than 0.1‰; Hendry et al., 2009).

The $\delta^{13}\text{C}$ signature of foraminifers (stable carbon isotopes ^{12}C and ^{13}C) reflects both local biological and physical processes (Lea, 2014). Photosynthesizing organisms preferentially incorporate the lighter carbon isotope, resulting in high $\delta^{13}\text{C}$ surface water values, whereas deep water $\delta^{13}\text{C}$ is typically lighter due to respiration of organic matter (Lea, 2014). The resulting water column $\delta^{13}\text{C}$ gradient reflected in foraminifer values can be a useful tool to evaluate changes in water mass structure and source (Bostock et al., 2004; Mackensen, 2001). For

example the $\delta^{13}\text{C}$ signature of old, nutrient-rich Circumpolar Deep Water can impart a lighter $\delta^{13}\text{C}$ signature on foraminifera (Hillenbrand et al., 2017; Ninneman & Charles, 2002; Shevenell & Kennett, 2002).

1.7.6 Foraminifer trace elements

Relationships between ambient oceanographic conditions and foraminifer CaCO_3 geochemistry are commonly used to reconstruct paleoceanographic conditions globally. However, foraminifer CaCO_3 preservation in Antarctic sediments is patchy and often discontinuous due to high organic carbon fluxes, high sedimentation rates, and corrosive bottom waters (Jones et al., 2017; Moy et al., 2009). Rathburn and DeDeckker (1997) observed a relationship between shallow infaunal benthic foraminifer species, *Trifarina angulosa* (synonym: *Uvigerina angulosa*; Williamson, 1858), Mg/Ca and bottom water temperature in Prydz Bay, East Antarctica, suggesting its utility as a regional paleothermometer. The *Uvigerina* Mg/Ca paleotemperature proxy has since evolved and is a standard proxy for reconstructing past bottom water temperatures (Elderfield et al., 2006; 2010; Yu & Elderfield, 2008). *Trifarina angulosa* is observed in many Antarctic margin locations, including the Weddell, Ross, and Amundsen Seas (Mackensen et al., 1985; 1990; Mawbey et al., 2020). The *T. angulosa* Mg/Ca-temperature calibration developed by Mawbey et al. (2020) connects the robust *Uvigerina*-based temperature estimates with those from the ice-proximal Antarctic margin.

Foraminifer Mg/Ca paleothermometry is also impacted by factors related to environmental conditions or physiological effects, including local changes in the Mg/Ca of seawater due to meltwater influx and other ice-related complications (Vazquez Riveiros et al., 2016), salinity (Arbuszewski et al., 2010), carbonate ion concentration (Lear et al., 2010; Misra

et al., 2014; Yu & Elderfield, 2008), and preservation (diagenesis and/or dissolution; Brown & Elderfield, 1996; Regenberget al., 2014). A multi-element analytical approach enables the possibility to assess these uncertainties, including monitoring Li/Ca to evaluate seawater carbonate ion changes (Lear et al., 2010), Ba/Ca to assess meltwater influx (Hall & Chan, 2004), and Sr, Fe, Mn, and U as dissolution and cleaning indicators (Lea et al., 1999; Martin & Lea, 2002). A strength of *T. angulosa* as a shallow infaunal benthic species, is that the Mg/Ca ratios may be less likely be affected by carbonate ion concentration than epifaunal species (Elderfield et al., 2010). However, several aspects of the planktic *N. pachyderma* (s) habitat can complicate their use for paleothermometry. Due to dwelling in porous sea ice and subsurface ocean depths, *N. pachyderma* (s) trace element values may not reflect sea surface temperatures (Kohfeld et al., 1996; Nyland et al., 2006) and can be impacted by the carbonate saturation of sea water (Elderfield et al., 2006; Hendry et al., 2009).

1.7.7 Archaeal lipids

Due to inconsistent CaCO₃ preservation in Antarctic margin sediments, researchers have developed paleothermometers that do not rely on carbonate, including the TEX₈₆ (TetraEther IndeX of 86 carbons) paleothermometer (Etourneau et al. 2013; Ho et al., 2014; Kim et al. 2012; Schouten et al., 2002; Shevenell et al. 2011) to determine ice-proximal upper ocean temperatures. The TEX₈₆ paleothermometer is based on a ratio of membrane lipid structures (glycerol dialkyl glycerol tetraethers; GDGTs) synthesized by archaea abundant in epi- and mesopelagic low temperature marine environments (Kim et al., 2008; 2010; Schouten et al., 2002). The application of TEX₈₆ as a paleotemperature proxy is possible because GDGT

abundance and ocean temperature exhibit a positive relationship (Kim et al., 2008; 2010; Schouten et al., 2002; Tierney et al., 2019).

Marine archaeal production is strongly coupled with nutrient availability and surface water primary productivity, which vary seasonally in the Antarctic (Park et al., 2019). The export of archaeal GDGTs to sediments is highest in the late spring when diatom blooms dominated by *Chaetoceros* occur (Sjunneskog & Taylor, 2002), so GDGTs derived from Antarctic margin sediments likely reflect upper ocean spring temperatures (Church et al., 2003; Luria et al., 2014; Park et al., 2019). Marine archaea are the most abundant in late winter and early spring and generally concentrated at ~150 m, which likely corresponds to the depth of thermocline or pycnocline (Church et al., 2003; Luria et al., 2014). Along with depth of GDGT production and seasonality, additional factors that complicate the sedimentary distribution of GDGTs include temperature, pH, and oxygen concentration (Elling et al., 2015; Ingalls, 2016; Qin et al., 2015), differential source (terrestrial versus marine), differential rates of ammonia oxidation in the water column (Hurley et al., 2016), and differential degradation during transport and export to the sediment (Kim et al. 2008; Shah et al. 2008).

CHAPTER TWO:
DEGLACIAL TO HOLOCENE EVOLUTION OF ICE-OCEAN INTERACTIONS ON
THE SABRINA COAST SHELF, EAST ANTARCTICA

2.1 Chapter Contributions

K. J. Vadman created the figures and led chapter writing, counted laminations and clasts, created the composite depth section, prepared and analyzed all carbonate samples and seven of eight bulk sediment samples via Ramped PyrOx/dirt burner for radiocarbon analyses, generated the Bacon age model, and generated foraminifer assemblage and stable isotope data. A. Leventer generated all diatom data. T. M. King prepared one Ramped PyrOx sample.

2.2 Abstract

Glacier systems around Antarctica that are grounded below sea level are vulnerable to melting by contact with warm ocean water. Presently, the Totten Glacier system on the Sabrina Coast, East Antarctica is losing mass more rapidly than all other East Antarctic glaciers. The Aurora Subglacial Basin is primarily drained through the glaciers terminating along the Sabrina Coast. Incursions of deep, warm water ($>0^{\circ}\text{C}$) are known to move across the continental shelf and come into contact with the Totten Glacier system, leading to the highest rates of coastal thinning in East Antarctica. Today, this process is associated with regional, wind-driven currents that carry relatively warm bottom waters isolated by a $\sim 400\text{m}$ thick layer of near-freezing water, inshore, and the presence of a polynya, a region of open water where surface cooling by wind

creates new sea ice. The timing and mechanisms driving present-day thinning of the Totten Glacier system are not well understood because observational and instrumental records extend only a few decades. In order to put present day changes in ice volume into the context of natural variability, we utilized the record of past oceanographic conditions preserved in the middle continental shelf sediment offshore the Sabrina Coast.

The history of when glaciers retreated after the Last Glacial Maximum is preserved in shelf sediments around Antarctica. We collected sediment cores and determined when the Sabrina Coast shelf transitioned an ice-covered to open water environment by radiocarbon dating core material containing carbon formed at the time the sediment was deposited. We found that ice retreated from the continental shelf offshore Totten Glacier by ~16.5 thousand years ago. The timing of deglaciation occurred during increasing atmospheric warming, increasing concentrations of atmospheric CO₂, and enhanced Southern Ocean upwelling after the end of the Last Glacial Maximum. We also used sediment properties to identify the changes in environmental setting after deglaciation. Microscopic marine organisms exhibit environmental preferences for settings like sea ice presence, water mass stability, and nutrient availability in the present day, so we utilized the chemical composition and species presence of foraminifera and diatoms to infer the progression of past environmental conditions. These paleoceanographic characteristics include warm, productive surface water conditions during the early and middle Holocene, followed by variably cool conditions during the late Holocene, and presence of warm ocean water in the modern setting. Similarities to other regional East Antarctic sedimentary sequences indicate sensitivity to local and regional wind conditions, and potentially low-latitude climate forcings that drive patterns in Antarctic climate. These patterns are significant because

gradients between low latitudes and the poles are expected to change under future warm conditions, which will lead to impacts on ice volume and sea level rise.

2.3 Introduction

Large areas of the East Antarctic Ice Sheet (EAIS) are grounded below sea level and are susceptible to marine ice sheet instabilities similar to those presently influencing the West Antarctic Ice Sheet (WAIS) (DeConto & Pollard, 2016; Fretwell et al., 2013; Golledge et al., 2015; Morlighem et al., 2020). Marine-based EAIS catchments contain ~19 meters of sea level-equivalent ice (~5x that of the WAIS), therefore understanding the EAIS response to past and ongoing climate change is essential for predicting future sea levels (DeConto & Pollard, 2016; Fretwell et al., 2013; Golledge et al., 2015; Morlighem et al., 2020). However, current understanding is limited by East Antarctica's geographic inaccessibility and sparse ice-proximal oceanographic and marine geologic observations.

Numerical ice sheet and climate models indicate that ice mass in the Wilkes, Aurora, Recovery, and Lambert subglacial basin catchments is sensitive to climate perturbations, including warming ocean waters over Antarctica's continental shelves and sea level rise (DeConto & Pollard, 2016; Golledge et al., 2012; 2014; 2017). Remote sensing indicates that marine-terminating outlet glaciers draining the Aurora Subglacial Basin (ASB) catchment to the Sabrina Coast are presently experiencing the largest mass loss in East Antarctica (Fretwell et al., 2013; Li et al., 2015; Rignot et al., 2013; Rintoul et al., 2016; Schröder et al., 2019; Smith et al., 2020). The ASB catchment drains one eighth of the EAIS and contains 5.3 m of sea level equivalent ice (Greenbaum et al., 2015; Aitken et al., 2016). However, regional subglacial topography indicates that the catchment may be susceptible to progressive glacial instability,

making it difficult to assess the catchment's contribution to future sea level rise under existing warming scenarios (Aitken et al., 2016; Greenbaum et al., 2015; Gulick, Shevenell et al., 2017; Young et al., 2011, 2015). To better constrain models and understand how the marine-terminating outlet glaciers draining these catchments responded during past intervals of climatic warming and sea level rise, geologic data from Antarctica's continental shelves is required. The Sabrina Coast may be particularly sensitive to global climate variability. Currently, ice mass loss from the ASB catchment is driven, in part, by the presence and/or persistence of relatively warm, salty, nutrient-rich modified Circumpolar Deep Water (mCDW) on the Sabrina Coast continental shelf (Greene et al., 2017; Rintoul et al., 2016). Incursions of mCDW onto the Sabrina Coast shelf result from wind-driven upwelling at the shelf edge north of the Dalton Iceberg Tongue (Greene et al., 2017). These relatively warm offshore waters are then entrained in Antarctic Coastal Current, which flows southwestward along the western side of the Dalton Iceberg Tongue and across the Sabrina Coast shelf at depths >400m (Figure 2.1; Silvano et al., 2019). Regional bathymetric studies indicate the presence of both a cross shelf bathymetric trough and a series of deep channels carved into regional bedrock that may provide conduits for mCDW to access regional grounding lines (Fernandez et al., 2018; Greenbaum et al., 2015; Greene et al., 2017; Gulick, Shevenell et al., 2017; Nitsche et al., 2017; Rintoul et al., 2016). Over time, the vigor of shelf-edge upwelling of mCDW may change according to shifts in the phase of the Southern Annular Mode (SAM; Greene et al., 2017; Spence et al., 2014; Thoma et al., 2008), a pattern of atmospheric climate variability that impacts surface pressure and temperature gradients between mid and high southern hemisphere latitudes (Fogt et al., 2011; Marshall et al., 2011; Thompson & Solomon, 2002; Vance et al., 2013). At present, warmer regional air temperatures, increased wind stress at the shelf edge, mCDW on the Sabrina Coast

shelf, and regional ice mass loss are associated with the positive phase of SAM (Greene et al., 2017; Rintoul et al., 2016).

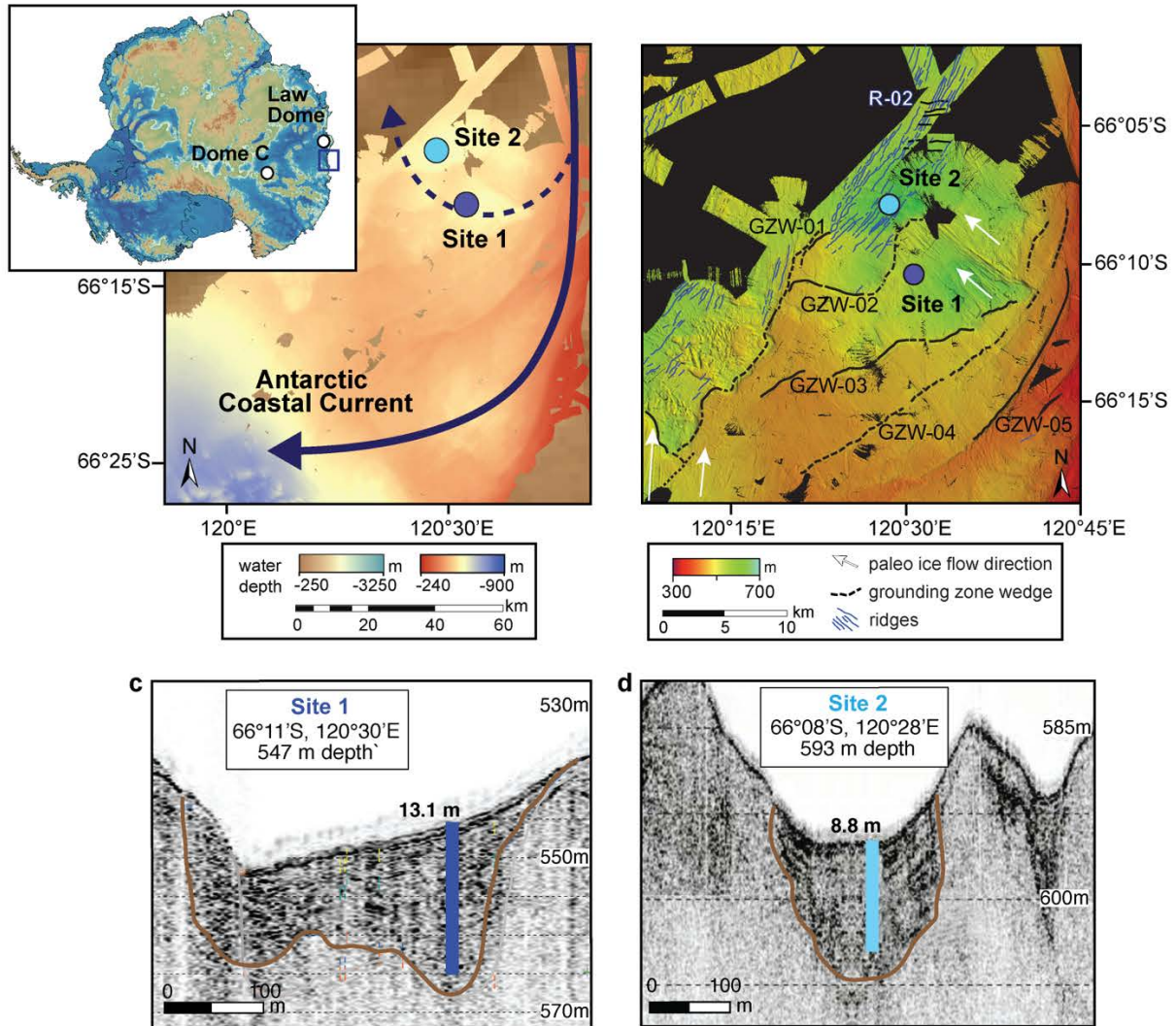


Figure 2.1 Sabrina Coast study location. (a) Sabrina Coast continental shelf bathymetry, East Antarctica (adapted from Gulick, Shevenell et al., 2017). Inset: Subglacial topography of Antarctica (Fretwell et al., 2013), with the Sabrina Coast (blue box), east of Law Dome (white dot). Multibeam bathymetry from the Dalton Polynya, offshore the Moscow University Ice Shelf was collected during U.S. Antarctic Program cruise NBP14-02 (Fernandez et al., 2018) with core sites indicated (Site 1, dark blue dot and Site 2, light blue dot). The Antarctic Coastal Current (approximated by the blue arrow) and local recirculation feature (approximated by the dashed arrow) are indicated. (b) Detailed multibeam bathymetry of study area, with geomorphological features indicating regional ice flow history (adapted from Fernandez et al., 2018). Site 1 is located in a small basin between grounding zone wedges (GZW) -02 and -03. Site 2 is located seaward of GZW-01 near a series of ridges (R-02). (c, d) Sub-bottom profiles across Sites 1 (c) and 2 (d) reveal sediment deposited in in ponded basins; basement indicated (brown lines). Marine sediment cores collected at Site 1 include: NBP14-02 JPC-27, JKC-53, KC-27B, and MC-45. Site 2 cores include NBP14-02 JPC-57 and MC-61.

To put present day ice-ocean interactions on the Sabrina Coast into context, we must look to regional records that document the past evolution of atmospheric conditions, continental shelf oceanography, and behavior of EAIS outlet glaciers. East Antarctic ice cores record warm early Holocene atmospheric temperatures during EAIS deglaciation (Masson-Delmotte et al., 2011; Mackintosh et al., 2014), followed by long-term Holocene cooling, possibly driven by decreasing local insolation (Renssen et al., 2005). EAIS ice cores from coastal and lower altitudes demonstrate higher variability through the Holocene (Masson-Delmotte et al., 2011). To evaluate Sabrina Coast oceanographic conditions and local ice sheet retreat since the last glaciation, we developed a suite of well-dated paleoenvironmental records from the Sabrina Coast continental shelf. We utilize lithology and physical properties to interpret changes in depositional setting, diatom and planktic foraminifer abundance to infer local surface productivity, and diatom assemblages to study regional changes in circulation, stratification, and sea ice. These data allow us to establish the timing of ice-stream retreat from the Sabrina Coast continental shelf following the Last Glacial Maximum, use sedimentology to understand style of deglaciation, and establish regional surface ocean paleoceanography through the Holocene. These records enable us to establish the natural variability of regional oceanography and outlet glacier behavior on the Sabrina Coast since the last deglaciation, which is critical for placing the current warming into a longer-term context.

2.4 Study Location: the Sabrina Coast, East Antarctica

2.4.1 Continental shelf morphology and glacial history

In 2014, the United States Antarctic Program cruise NBP14-02 collected the first geophysical, marine geologic, and physical oceanographic data from the Sabrina Coast (115°E to 125°E), East Antarctica, in a region bounded by Totten Glacier to the west and the Dalton

Iceberg Tongue to the east. The multibeam bathymetric survey conducted by NBP14-02 was the first ever performed on the Sabrina Coast continental shelf (Fernandez et al., 2018; Leventer et al., 2015), and revealed a glacially overdeepened 300 m to >1 km deep continental shelf with a glacially-carved, cross-shelf trough aligned with the present-day grounding line of Totten Glacier (Figure 2.1). Aerogeophysical surveys west of NBP14-02 multibeam data observed deep, wide troughs with little or no sediment cover leading into the Totten Glacier Ice Shelf cavity (Greenbaum et al., 2015). The troughs have been shown to host inflowing mCDW (Rintoul et al., 2016). The inner shelf is characterized by channelized bedrock, while the middle shelf is draped in sedimentary substrate, as indicated by crag and tail features and the onset of elongate megascale glacial lineations (Figure 2.1a). These features, aligned parallel to the trough axis, persist across the mid-shelf and were formed by a flowing ice stream (Fernandez et al., 2018). This study's core sites are located ~75 km to the east of the trough axis on the mid-shelf (Figure 2.1b). Chirp seismic data (2-6 kHz sweep frequency) revealed two middle shelf sites with ~9 to 13 m of acoustically transparent sediment (Figures 1c and 1d). The mid-shelf contains a series of grounding line wedges, banks, and ridges, changing to iceberg plow marks and gullies on the eastern outer shelf, near the Dalton Iceberg Tongue (Figure 2.1b). Taken together, these landforms reveal a complex deglacial history of the Sabrina Coast shelf (Fernandez et al., 2018).

2.4.2 Sabrina Coast physical oceanography

The Sabrina Coast physical oceanography is influenced by the Dalton Polynya, regional winds, and the Antarctic Coastal Current (Greene et al., 2017; Gwyther et al., 2014; Khazendar et al., 2013; Rintoul et al., 2016; Silvano et al., 2017; 2018). During NBP14-02 (January-March, 2014), physical oceanographic data from within the Dalton Polynya reveal a thin layer of

seasonal Antarctic Surface Water (AASW) overlying thick (~300m) near-freezing thermostad layer, often referred to as Winter Water. Below ~400 meters, over the middle and outer Dalton Polynya, relatively warm (~0.5°C), saline (~34.5), oxygen-poor (~5 mL/L) mCDW was observed in our study area where the Antarctic Coastal Current flows onshore. At present, the Winter Water overlying mCDW creates a strong density gradient that stabilizes the water column, inhibiting the formation of Dense Shelf Water (Whitworth et al., 1998) in the Dalton Polynya (Rintoul et al., 2016; Silvano et al., 2017; Tamura et al., 2016; Williams et al., 2011). The Dalton Polynya is a setting with weak Dense Shelf Water formation and convection, therefore incursions of mCDW are more likely (Miles et al., 2016). Thus, when the Dalton Polynya is weak, more mCDW crosses the shelf and is able to drive basal melt leading to thinning of the Totten Glacier (Khazendar et al., 2013; Nitsche et al., 2017; Rintoul et al., 2016, Silvano et al., 2018).

2.5 Methods

2.5.1 Sediment sampling, lithology, physical properties, and composite depths

At the two Sabrina Coast shelf core sites, multi-cores (MC), Kasten cores (KC), jumbo Kasten cores, (JKC), and jumbo piston cores (JPC) were deployed to collect a suite of sedimentary samples (Table 2.1). Cores MC-45, KC-27B, JKC-53, and JPC-27 were recovered at Site 1 and cores MC-61 and JPC-57 were recovered at Site 2 (Figures 2.1; Table 2.1). Kasten cores were visually described shipboard, while multi- and jumbo piston cores were split, visually described, and x-rayed at the Antarctic Core Repository at Florida State University. Magnetic susceptibility was measured at 1 cm resolution on multi- and jumbo piston cores using a GEOTEK multi-sensor core logger at Florida State University. Kasten core magnetic

susceptibility was measured shipboard on the archive u-channel at 0.5 cm intervals using a Bartington Magnetic Susceptibility Meter MS3 with a 45 mm loop sensor. Lithologic units and subunits were assigned using both visual core descriptions, x-rays, and magnetic susceptibility variations. Qualitative lamination and clast counts were conducted by counting the number of clasts >2 mm and laminations visible in the x-ray, per 10 cm depth interval.

Table 2.1 NBP14-02 sediment core locations, water depths, and core lengths.

Site	Core	Latitude	Longitude	Water Depth (m)	Core length (cm)
1	MC-45	66° 11.0069' S	120° 30.0591' E	537	35
	KC-27B	66° 11.0907' S	120° 30.2385' E	547	270
	JKC-53	66° 11.053' S	120° 30.208' E	545	520
	JPC-27	66° 11.0568' S	120° 30.1483' E	544	1310
2	MC-61	66° 07.691' S	120° 27.826' E	582	35
	JPC-57	66° 07.7325' S	120° 27.8407' E	583	875

General lithologic and magnetic susceptibility similarities between cores allowed us to construct a composite depth scale for cores from Sites 1 and 2 to address both piston core over-penetration and non-uniform compression. For example, JPC-27 and JPC-57 over penetrated by 56.5 and 72 cm, respectively. Core KC-27B was used as a reference core because it recovered an intact sediment water interface and was long enough to capture changes in magnetic susceptibility that could be associated with variations in the longer kasten and jumbo piston cores. To generate the composite section between 0 and 900 cmbsf (centimeters below sea floor), we used the lineage function in Analyseries 2.0 software (Paillard et al., 1996) to correlate the magnetic susceptibility records of JPC-27 and JKC-53 to the reference core. This function allows you to select tie points to link similar features in the records, such as magnetic susceptibility highs or lows, and “stretch and squeeze” one curve in reference to the other record. The KC-27B

reference core was 270 cm long, so the remaining lengths of the magnetic susceptibility records in JKC-53 and JPC-27 past the end of KC-27B were adjusted uniformly by 32 cm. The 32 cm accounts for the final offset in depth between corresponding points of the JPC-27 and JKC-53 records at 270 cmbsf. The resulting composite record, which includes all cores from Site 1, was then used as the reference record for Site 2, JPC-57 (Figure 2.2). The magnetic susceptibility records from all cores were normalized to JPC-27 values and plotted versus centimeters composite depth to 932 cmcd. Below 900 cmbsf in JPC-27 and 648 cmbsf in JPC-57, depths were not converted into the composite depth scale because of lithologic and micropaleontologic differences within Units IV and V at Sites 1 and 2 (Figure 2.3).

The magnetic susceptibility records in both MC-45 and MC-61 did not vary sufficiently to identify magnetic susceptibility highs or lows that could be linked to the composite depth record. Because both megacores recovered an intact sediment-water interface upon collection, are relatively short (30 cm), and not likely to be affected by non-uniform compression, they were converted directly into the composite depth scale without Analyseries (ex: 1 cmbsf = 1 cmcd).

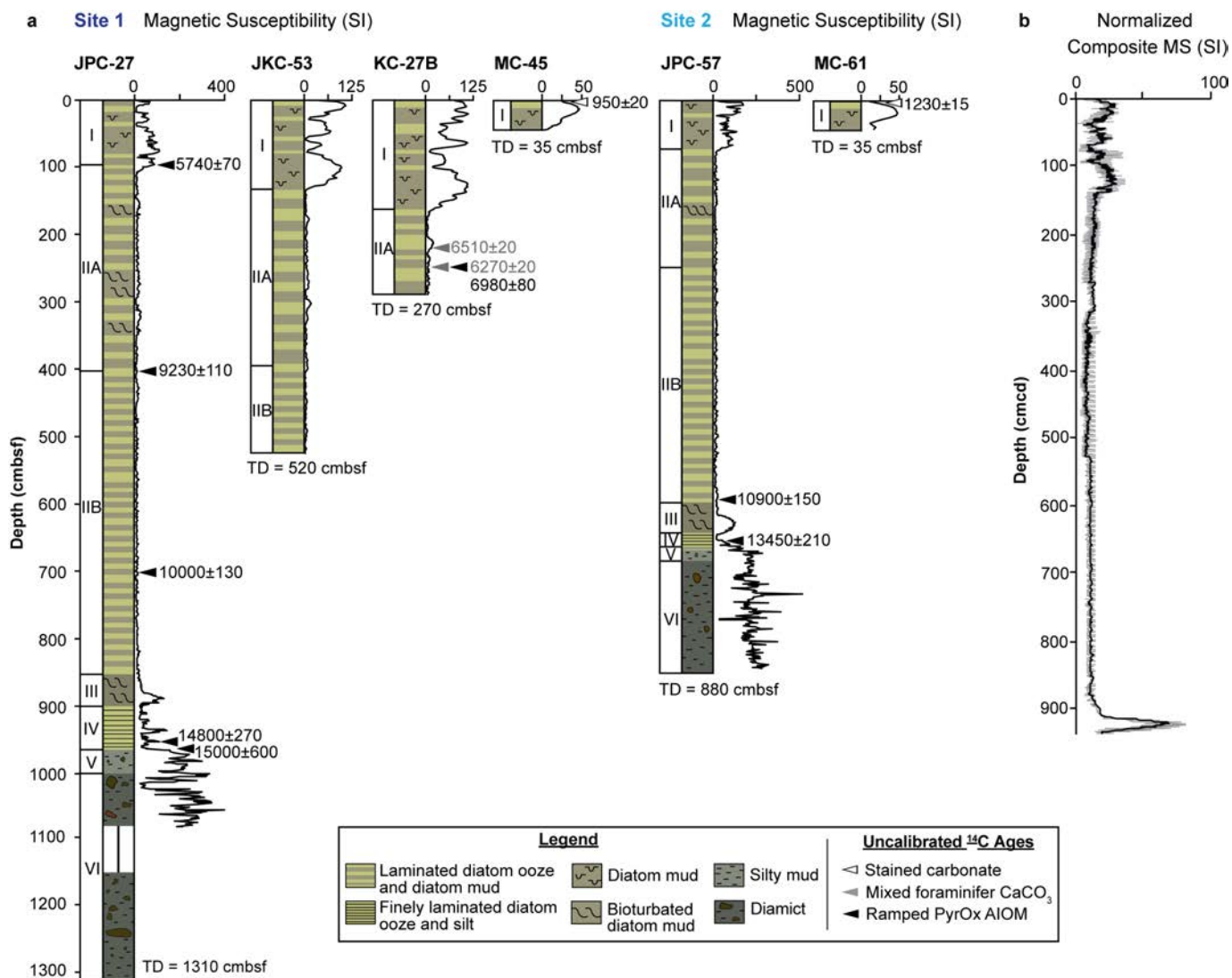


Figure 2.2 Sabrina Coast lithology, magnetic susceptibility (MS), composite depth, and radiocarbon ages. (a) Site 1 and 2 graphic lithologies with lithologic units (roman numerals) and MS versus depth (cmbsf) for NBP14-02 cores; locations of uncalibrated ¹⁴C ages indicated. Note that MS scales vary to emphasize relative changes. In JPC-27, MS was not recorded below 1100 cmbsf due to a gap in core recovery. (b) Normalized composite MS versus composite depth (cmcd) with 5-pt running mean. Units IV, V, and VI are excluded from the composite MS stack due to differences in lithologic features (see text).

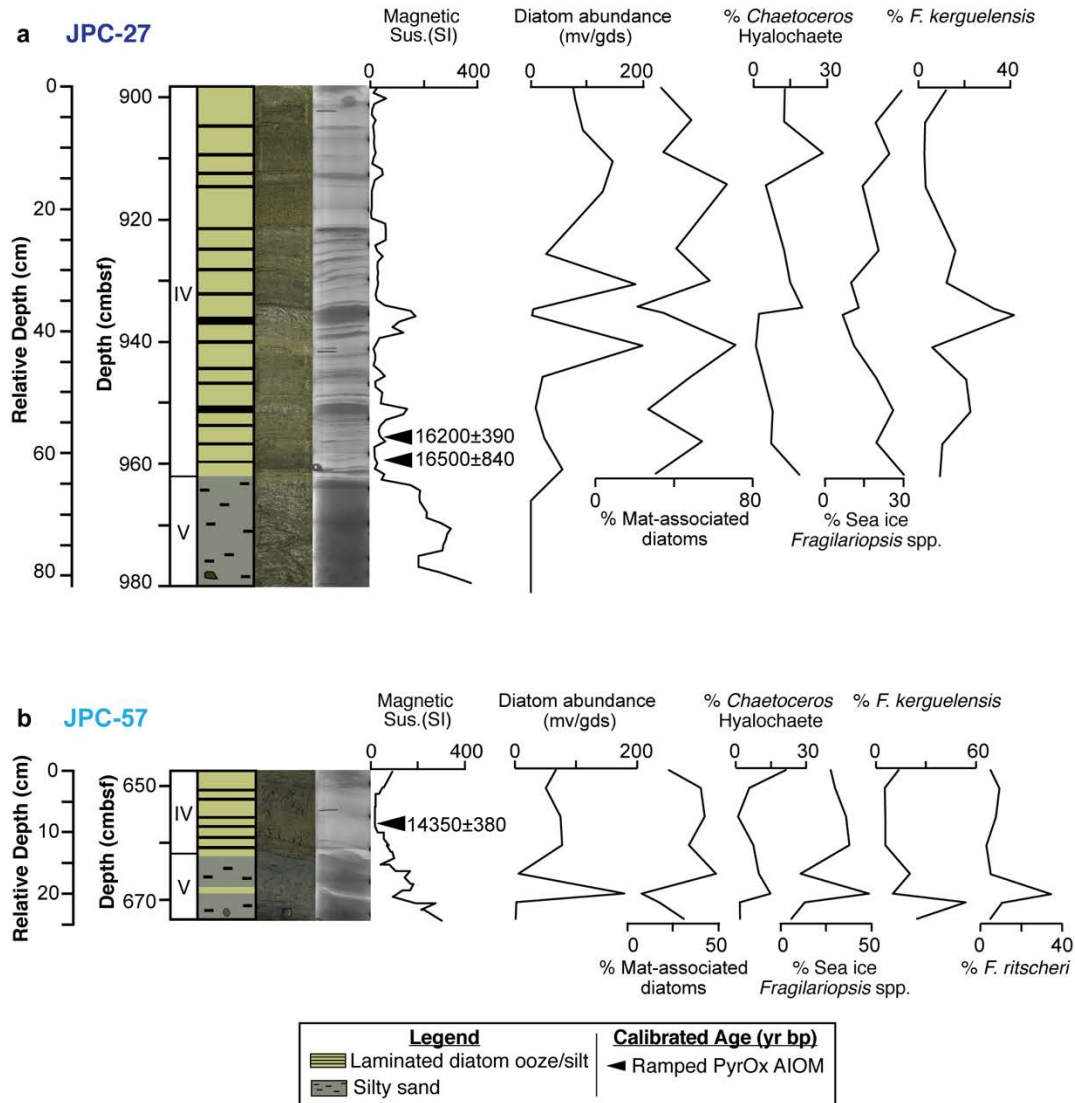


Figure 2.3 Sabrina Coast deglacial lithologies. (a) Site 1, JPC-27 graphic lithology with units (numbered column), core photo, x-ray, magnetic susceptibility (MS; SI units), total diatom abundance, and species-specific relative abundance data plotted versus depths in centimeters below sea floor (cmbsf). Black triangle indicates location of ^{14}C date and the calibrated age (cal yr BP) and error are listed. (b) Site 2, JPC-57 graphic lithology with units (numbered column), core photo, x-ray, magnetic susceptibility (SI units), total diatom abundance, and species-specific relative abundance data plotted versus depths in centimeters below sea floor (cmbsf). Black triangle indicates location of ^{14}C date and the calibrated age (cal yr BP) and error are listed. In panels a and b, the sea ice-associated *Fragilariopsis* group is dominated by *Fragilariopsis curta*, and includes *F. curta*, *F. cylindrus*, *F. lineata*, *F. obliquecostata*, *F. pseudonana*, *F. ritscheri*, *F. sublinearis*, *F. vanheurckii*, and *Fragilariopsis* spp. (unidentified).

2.5.2 Diatom assemblages

To evaluate changes in total diatom abundance and relative species abundance, we produced quantitative diatom slides at Colgate University according to the method described by Scherer (1994) and Warnock and Scherer (2014), which involves settling a known amount of sediment over a known surface area, yielding a random distribution of diatoms for quantitative evaluation. We counted at least 400 valves along slide transects at 1000x magnification on an Olympus BX60 microscope. Downcore at Site 1, we counted samples collected every 1 cm in core MC-45 and every 5 to 10 cm in JKC-53 (0-520 cmbsf) and JPC-27 (415-960 cmbsf) and integrated into one stratigraphically complete dataset on the composite depth scale (Leventer, 2017; doi: 10.15784/601258). At Site 2 (JPC-57), we counted 23 samples at 5 cm intervals from 585 to 675 cmbsf, and at 10 to 20 cm intervals from 675 to 720 cm where diatom abundance was low (0.03-0.05 mv/gds). Diatom data is distributed unevenly due to the sedimentation rate and sampling intervals, so we utilize a five-point running mean, overlaid on the raw data as a tool to visualize variations in absolute and relative abundances. Absolute diatom abundance values are reported as millions of valves per gram of dry sediment (mv/gds). This value is calculated by the expression $T = ((N * B) / (A * F)) / M$, where T = number of microfossils per unit mass, N = total number of microfossils counted, B = area of bottom of beaker (mm²), A = area of the microscope field of view (mm²), F = number of transects counted, and M = mass (g) of original sediment sample dispersed in beaker (Scherer, 1994). Relative abundance values for individual species are reported as percentages, calculated by dividing the number of valves of a species by the total valves counted. In our environmental interpretations, we utilize the diatom species and groups listed in Table 2.2.

Table 2.2 Summary of relationship between diatoms species and environmental conditions.

Species or group	Known ecology	Sabrina Coast Environmental conditions	References
<i>Chaetoceros</i> subg. <i>Hyalochaete</i>	Decreased nutrients, rapid stratification changes, spring bloom conditions	Wind-driven overturning of polynya	Leventer et al., 2006
<i>F. kerguelensis</i>	Antarctic Circumpolar Current-association, open water, ice-free conditions	Influence of offshore water masses, ice-free conditions	Crosta et al., 2005; Smetacek et al., 1997
Mat-associated diatoms (<i>Chaetoceros</i> subg. <i>Chaetoceros</i> , <i>Rhizosolenia</i> spp., <i>Proboscia</i> spp., <i>Corethron pennatum</i> , <i>Pseudonitzschia</i> , <i>Thalassiothrix antarctica</i> , <i>Trichotoxon reinboldii</i>)	Open ocean, stratified oligotrophic water	Stratified surface waters	Alley et al., 2018; Crawford, 1995; Crosta et al., 2005; McKay et al., 2000; Quéguiner, 2013; Singler & Villareal, 2005; Smetacek et al., 1985; Villareal et al., 1996
Sea ice associated species (<i>F. curta</i> , <i>F. cylindrus</i> , <i>F. lineata</i> , <i>F. obliquecostata</i> , <i>F. pseudonana</i> , <i>F. ritscheri</i> , <i>F. sublinearis</i> , <i>F. vanheurckii</i> , <i>Fragilariopsis</i> spp. (unidentified))	Sea ice presence: sea ice edge, or sea ice melting-induced stratified waters	Sea ice covered or ice edge environment, with possible melt-induced stratification or Dense Shelf Water formation	Armand et al., 2005; Crosta et al., 2004
<i>T. antarctica</i> T1	Cold water form of <i>T. antarctica</i> , associated with cool surface water and extended sea ice season	Cool open water, platelet sea ice	Buffen et al., 2007; Pike et al., 2009; Taylor et al., 2001
<i>T. gracilis</i> and <i>T. lentiginosa</i>	Cool open ocean	Influence of an offshore water masses, longer ice-free season	Crosta et al., 2005, 2005; Pondaven et al., 1998

2.5.3 Foraminifer assemblages and stable isotope analyses

We subsampled for foraminifer analyses at 0.5 to 5 cm intervals in multi-, Kasten, and piston cores. Multi-core subsamples between 0 and 10 cm were immediately subsampled and stained with Rose Bengal (3.8% formalin) solution to identify living (or recently living) foraminifers and mollusks (McCorkle et al., 1997; Murray & Pudsey, 2004). We washed samples through a 63 μm sieve on the ship to ensure foraminifer preservation. We generated foraminifer assemblages by counting all individuals in the $>150 \mu\text{m}$ size fraction in a 20 cc sediment sample. Planktic foraminifer *Neogloboquadrina pachyderma* (sinistral) tests were prepared for oxygen ($\delta^{18}\text{O}$) and carbon ($\delta^{13}\text{C}$) stable isotope analyses by picking 10-20 individuals from the $>150 \mu\text{m}$ fraction, weighing into $\sim 20\text{-}80 \mu\text{g}$ aliquots, crushing between glass slides, rinsed with methanol, and dried at 90°C . Samples were reacted with phosphoric acid to generate CO_2 , which was analyzed at the University of South Florida College of Marine Science (USF-CMS) using a Thermo Scientific MAT 253 light stable isotope ratio mass spectrometer equipped with a Gas

Bench II preparatory device. Stable isotope data were generated in random stratigraphic order from 56 sample depths. Duplicate analyses were conducted on ~20% of the samples (n=10) during the 12-month study interval. The standard deviation among replicates of CaCO₃ aliquots from the same sample depth is between 0.05 and 0.2‰ (mean: 0.1‰) for δ¹⁸O and δ¹³C. Data are expressed using standard delta (δ) notation in per mil (‰) relative to the Vienna Pee Dee Belemnite (VPDB) carbonate standard.

2.5.4 Radiocarbon sample and age model preparation

The chronology for Sites 1 and 2 is based on four calcium carbonate (CaCO₃) and seven acid insoluble organic matter (AIOM) samples (Table 2.3). For sample depths where CaCO₃ is abundant enough for reliable dating, 1-6 mg of foraminifer or mollusk CaCO₃ was picked, converted to CO₂, quantified, graphitized, and analyzed for ¹⁴C by accelerator mass spectrometry (AMS) at the National Ocean Science Accelerator Mass Spectrometer (NOSAMS) facility in Woods Hole, MA. When biogenic CaCO₃ was not available in datable quantities, bulk AIOM was prepared using the Ramped PyrOx (RPO) technique at USF-CMS (Rosenheim et al., 2008; 2013; Subt et al., 2015). Bulk sediment samples from seven depths were prepared using standard procedures to remove detrital/biogenic CaCO₃ and weighed to quantities required to produce ~5 datable aliquots of CO₂ upon thermochemical decomposition (~100 μmol C; ~10-40 μmol CO₂/aliquot; Rosenheim et al., 2008; 2013). Antarctic margin sediment data indicate that the youngest most reactive carbon is trapped in the lowest-temperature CO₂ aliquot (Rosenheim et al., 2008; 2013), so we analyzed the first aliquot of each of the seven samples for ¹⁴C by AMS at the Lawrence Livermore National Laboratory (LLNL) Center for Accelerator Mass Spectrometry (CAMS). A radiocarbon blank correction was applied to account for modern and dead

radiocarbon introduced during processing (Table 3; Venturelli et al., 2020; Fernandez et al., 2014; Subt et al., 2016, 2017). For more information on blank contamination, see Appendix A, Text A1 and Figure A1. To assess the validity of developing a chronology using both Ramped PyrOx AIOM and mixed foraminifer CaCO₃ ages, we analyzed AIOM and CaCO₃ from 256.5 cmbsf (Table 2.3).

Table 2.3 NBP14-02 radiocarbon results from CaCO₃ and the first aliquot of bulk sediment acid insoluble organic matter (AIOM) prepared via Ramped PyrOx. Sample information is indicated by sample ID, core ID, average depth in centimeters below sea floor (cmbsf), centimeters composite depth (cmcd), and sample type. CaCO₃ ¹⁴C dates were generated and internally corrected at NOSAMS (AMS Facility ID OS-), corrected for the local marine reservoir age, and calibrated in CALIB 8.2 using the Marine20 calibration curve (Stuiver, M., Reimer, P.J., and Reimer, R.W., 2020). The fraction modern for AIOM samples was generated by Lawrence Livermore (AMS facility ID LL-), a blank correction was applied (after Venturelli et al., 2020 and Fernandez et al., 2014), dates were corrected for the local marine reservoir, and samples were calibrated using CALIB 8.2 using the Marine20 calibration curve.

AMS Facility ID	Core ID	Avg. Depth (cmbsf)	Avg. Depth (cmcd)	Sample Type	CaCO ₃ (mg)	CO ₂ evolved (µgC)	Fraction modern (Fm) (± Error)	Blank Corr. Fm (± Error)	Blank Corr. ¹⁴ C Yr (±1σ Error)	Reservoir Correction (±1σ Error)	Calendar Age yr BP (±1σ Error)
OS-121676	MC-45	1.25	1.25	<i>N. pachyderma</i> (s)	1.4	-	0.8886 (0.0022)	-	950 (20)	950 (100)	modern
OS-121677	MC-61	1.25	1.25	Mollusk	6.4	-	0.8581 (0.0018)	-	1230 (15)	1230 (100)	modern
LL-175009	JPC-27	93	135	AIOM	-	218.7	0.4922 (0.0023)	0.4893 (0.0042)	5740 (70)	1230 (100)	5190 (170)
OS-121694	KC-27B	226.5	228.5	Mixed foraminifers	2.6	-	0.4448 (0.0011)	-	6510 (20)	950 (100)	6350 (130)
OS-121708	KC-27B	256.5	258.5	Mixed foraminifers	1.2	-	0.4579 (0.0012)	-	6270 (20)	950 (100)	6090 (130)
LL-175142	KC-27B	256.5	258.5	AIOM	-	217.1	0.4238 (0.0020)	0.4195 (0.0043)	6980 (80)	1230 (100)	6550 (160)
LL-176611	JPC-27	403	435	AIOM	-	227.2	0.3231 (0.0016)	0.3171 (0.0044)	9230 (110)	1230 (100)	8970 (220)
LL-176614	JPC-27	703	735	AIOM	-	223.7	0.2943 (0.0020)	0.2887 (0.0047)	10000 (130)	1230 (100)	9950 (230)
LL-175069	JPC-57	587	882	AIOM	-	233.4	0.2640 (0.0020)	0.2572 (0.0046)	10900 (150)	1230 (100)	11200 (280)
LL-175072	JPC-57	657	982	AIOM	-	240.0	0.1953 (0.0019)	0.1875 (0.0048)	13450 (210)	1230 (100)	14350 (380)
LL-176608	JPC-27	954	986	AIOM	-	212.5	0.1682 (0.0017)	0.1588 (0.0054)	14800 (270)	1230 (100)	16200 (390)
OS-156030	JPC-27	959	991	AIOM	-	94.76	0.1744 (0.0012)	0.1536 (0.0115)	15000 (600)	1230 (100)	16500 (840)

To establish the downcore chronology for NBP14-02 Sites 1 and 2, raw radiocarbon dates were calibrated to account for the local reservoir effect (Table 2.3). The local marine reservoir

ages were obtained from Rose Bengal-stained carbonates from 1.25 cm depth in cores MC-45 and MC-61. Calibrated ages were placed on the cmcd depth scale, then an age model was generated using Bacon 2.3 software (Blaauw & Christen, 2011).

2.6 Results

2.6.1 Lithology

The sedimentary sequence at Sites 1 and 2 consists of six lithologic units (Figure 2.2; Table 2.4). Cores NBP14-02 JPC-27 and JPC-57 contain all six units, which vary in thickness between cores (Table 2.3). Unit VI, at the base of the sediment sequence, consists of a homogenous dark gray clast-rich diamict, with faceted clasts (1-10 cm). Magnetic susceptibility is high and variable. At both sites, contact between Unit VI and Unit V is sharp and bioturbated (Figure 2.2, 2.3). Unit V consists of homogenous light to medium gray silty mud with angular clasts (<2 cm) that increase up-section. Magnetic susceptibility is generally high, but lower than in Unit VI. Diatom abundance is generally low, consisting of fragments of extinct species. In JPC-57, there is a single diatom rich-lamination in the middle of the unit (Figure 2.3). The boundary between Units V and IV is sharp and undulating. Unit IV consists of dusky yellow to light olive gray interlaminated diatom oozes and diatom-bearing muds. Laminations are wavy or discontinuous. JPC-27 Unit IV consists of 130 laminations, including 56 diatom ooze and 64 diatom-bearing mud laminations in the 60 cm unit. In JPC-57, there are 10 laminations, including 5 diatom ooze and 5 diatom-bearing mud laminations in the 15 cm unit (Figure 2.3). Magnetic susceptibility is relatively low and variable (Figure 2.3). At both sites, the boundary between Units IV and III is gradational and bioturbated (Figures 2.2, 2.3). Unit III consists of light olive gray bioturbated diatom-bearing mud with pyritized burrows and dispersed clasts (<1

cm). The boundary between Units III and II is gradational and bioturbated. Unit II consists of diatom oozes interbedded at the cm to dm scale with bioturbated diatom-bearing to -rich muds with dispersed clasts (<1 cm). Lower ooze boundaries are sharp and cross-bedding is sometimes visible. Although Unit II has the lowest magnetic susceptibility of the sedimentary sequence, clasts are present throughout the Unit. Unit II was subdivided into Subunit IIB and Subunit IIA based on diatom ooze thickness and total diatom abundance. Subunit IIB contains dm-scale interbeds of horizontal to wavy diatom oozes and diatom-rich muds. Subunit IIA contains cm-scale diatom oozes interbedded with bioturbated diatom-bearing to -rich muds, which increase up section. Generally, there are more laminations/beds in Subunit IIB, compared with IIA. Unit I consists of bioturbated diatom-bearing to -rich muds interbedded with dm- to cm-thick diatom ooze mats, which decrease in abundance up-section. Magnetic susceptibility is higher than Unit II, but few clasts are observed. All remaining results and discussion are now described on the centimeters composite depth (cmcd) scale for core sections I-III.

2.6.2 Diatom assemblages

Diatoms are present throughout the Sabrina Coast shelf sedimentary sequence, with variable absolute abundance ranging from 0.04 to 600 mv/gds (Figures 2.3, 2.4). At Sites 1 and 2, diatoms are extremely sparse (0.05-0.5 mv/gds) in lithologic Units VI and V, with common fragments and a relatively high proportion of extinct forms of Oligocene to late Miocene age (Leventer, 2017; doi: 10.15784/601258). At Site 2 (JPC-57), Unit V contains relatively low diatom abundance (1.8 mv/gds), with a high contribution of *Fragilariopsis kerguelensis* (54%). A single ~0.5 cm-thick diatom-rich layer (175 mv/gds) occurs in this unit in JPC-57 that is comprised of *Fragilariopsis ritscheri* (35%) and *Fragilariopsis rhombica* (12%). At both sites,

Table 2.4 Sabrina Coast shelf deglacial to Holocene lithologic and micropaleontologic summary.

Unit	JPC-27 Depth Range (cmbsf)	JPC-57 Depth Range (cmbsf)	Composite Depth Range (cmcd)	Age Range (cal yr BP)	Lithology	Magnetic Sus. (SI)	Total Diatom Abundance (mv/gds)	Planktic Foraminifer Abundance (#tests/cc)	<i>N. pachy.</i> $\delta^{13}\text{C}$ (‰VPDB)* Range	<i>N. pachy.</i> $\delta^{18}\text{O}$ (‰VPDB)* Range
I	0-95	0-75	0-135	0-5190	Interbedded (cm to dm) bioturbated diatom-bearing/-rich mud and diatom ooze. Dispersed clasts (<1 cm). Diatom oozes are less abundant up-section	-1 to 30	50-175	0-15	1.80-2.14	4.28-4.50
IIA	95-403	75-250	135-435	5190-8970	Interbedded (cm-scale) diatom ooze and bioturbated diatom rich mud with dispersed clasts (<1 cm). Diatom oozes have sharp lower contacts.	-1 to 2	70-250	0-18	1.58-2.12	4.10-4.49
IIB	403-856	250-603	435-882	8970-11200	Interbedded (dm-scale) diatom ooze and diatom-bearing mud with clasts (<1 cm). Lower unit boundary is sharp with visible bioturbation.	-1 to 2	65-590	0	no data	no data
III	856-898	603-647	888-931	11200-date unconstrained	Bioturbated diatom-bearing mud with pyritized burrows and clasts (<1 cm). Lower unit boundary is gradational and bioturbated.	2 to 95	60-170	0-1	no data	no data
IV	898-963	647-663	-	JPC-57: 14350 JPC-27: 16200	Thinly laminated dusky yellow to light olive gray diatom-bearing mud and diatom ooze. Laminations are wavy or discontinuous. 130 laminations in JPC-27 (65) and 10 in JPC-57. Lower unit boundary is sharp and undulating.	3 to 100	3-200	0-1	no data	no data
V	963-996	663-674	-	>16200	Homogenous light to medium gray silty mud with angular clasts (<2 cm) increasing up-section. Lower unit boundary is gradational and bioturbated.	75 to 200	0.1-0.5 except lamination 175	0-3	no data	no data
VI	996-1310	674-875	-	>16200	Homogenous dark gray clast-rich diamict. Faceted clasts (1-10 cm) of various lithologies.	100-400	<0.05	0	no data	no data

* $\delta^{13}\text{C}$ offset of +1.0‰ and $\delta^{18}\text{O}$ offset of +0.6‰ applied to *N. pachyderma* (s) (Hendry et al., 2009; Mortyn & Charles, 2003)

absolute abundance is variable (3-200 mv/gds) in the interlaminated diatom oozes and diatom-bearing muds of Unit IV, with abundance peaks associated with diatom oozes (Figures 2.2, 2.3). Diatom oozes consist of large mat-associated diatoms, which dominate single laminations within the unit (average: 44% of the total species assemblage) (Figure 2.3). In JPC-27, *Fragilariopsis*

kerguelensis contributes to the assemblage when mat-associated diatoms are not abundant (935-950 cmbsf; Figure 2.3). The diatom-bearing muds contain 4 mv/gds of mostly fragmented diatoms.

Unit III is characterized by low diatom abundances (60-170 mv/gds; Figures 2.2, 2.4). However, this unit contains the highest (20%) relative abundance of *Thalassiosira antarctica* T1 and *F. kerguelensis* (30-40%). Unit II is characterized by relatively high diatom abundance and is divided into Subunits IIB and IIA, based on total diatom abundance and mat-associated diatom abundance. Diatom oozes are between 1 and 10 cm thick. In Subunit IIB, diatom abundance is relatively high and variable, with the highest total abundance (590 mv/gds) at the base of the subunit and the lowest total abundance (100 mv/gds) at the top of the subunit; abundance variability reflects the alternation between diatom ooze and diatom-bearing mud lithologies (Figure 2.4). High total abundance at the base of Subunit IIB is related to the abrupt increase of *Chaetoceros* subg. *Hyalochaete*, which is at maximum abundance (~60%) in the lower half of Subunit IIB. Both the mat-associated species assemblage and sea ice-associated *Fragilariopsis* spp. increase up-section within Subunit IIB. In Subunit IIA, total diatom abundance is relatively low (70-250 mv/gds), driven by a decrease in the relative contribution of mat-associated diatoms and *Chaetoceros* subg. *Chaetoceros*. *Fragilariopsis kerguelensis* increases up-section, in association with *Thalassiosira gracilis* and *Thalassiosira lentiginosa* (Figure 2.4). In Unit I, total diatom abundance is relatively low (50-175 mv/gds), with a peak at 40 cmcd (320 mv/gds) associated with an increase in the relative abundance of *F. kerguelensis*. While the relative abundance of *F. kerguelensis*, *T. gracilis*, and *T. lentiginosa* increases up-section, large mat-associated diatoms form distinct laminated diatom oozes between 40 and 200 cmcd (Figure 2.4).

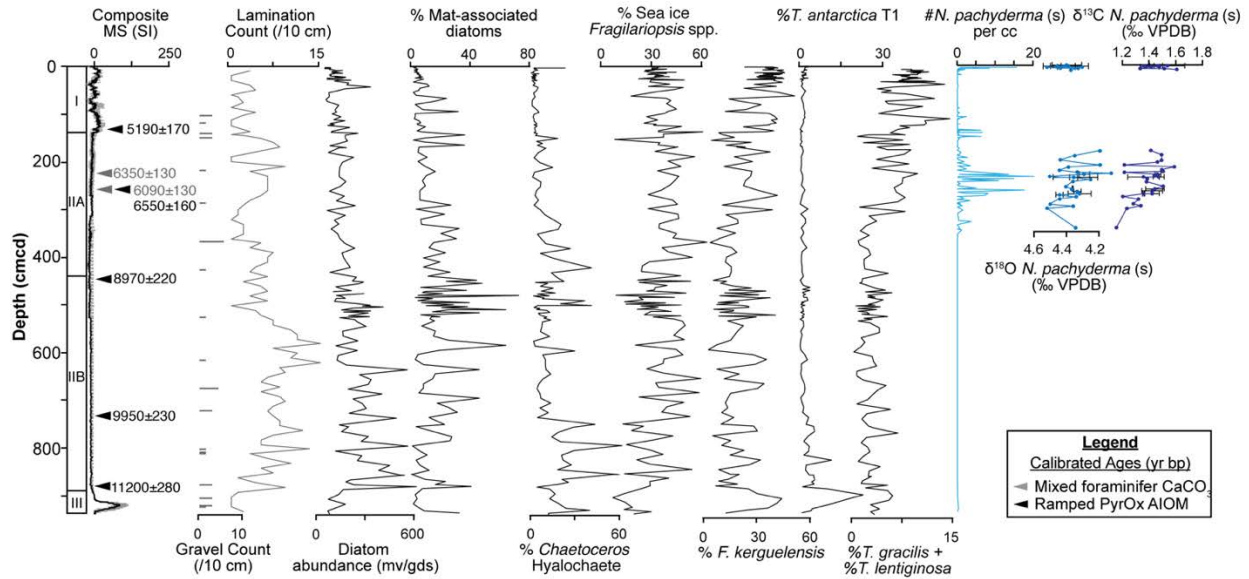


Figure 2.4 Sabrina Coast multiproxy record plotted against composite depth. Lithologic units; composite magnetic susceptibility; calibrated ages (cal yr BP); gravel counts (per 10 cm); lamination count (per 10 cm); diatom assemblages; *Neogloboquadrina pachyderma* (s) abundance; and *N. pachyderma* (s) $\delta^{18}\text{O}$ and $\delta^{13}\text{C}$ stable isotope records.

2.6.3 Foraminifer assemblages and stable isotopes

Well-preserved planktic foraminifer *Neogloboquadrina pachyderma* (s) tests are present in lithologic Units I-IV and are most abundant (~20 tests/cc) in Subunit IIA and surface sediments and rare (3 tests/cc) to absent in Units IIB-IV (Figure 2.4; Table 2.3).

Neogloboquadrina pachyderma (s) tests from Units I and II were analyzed for oxygen ($\delta^{18}\text{O}$) and carbon ($\delta^{13}\text{C}$) stable isotopes. The $\delta^{18}\text{O}$ and $\delta^{13}\text{C}$ values were adjusted by 0.6‰ and 1.0‰, respectively, to account for species vital effects (Hendry et al., 2009; Mortyn & Charles, 2003). In general, *N. pachyderma* (s) $\delta^{18}\text{O}$ and $\delta^{13}\text{C}$ are positively correlated (Figure 2.5). In Unit IIA, $\delta^{18}\text{O}$ values range between 4.2 and 4.5‰ (mean=4.3±0.1‰) and become more negative up-section. The $\delta^{13}\text{C}$ values range between 1.6‰ and 2.1‰ (mean=1.9±0.1‰) and become more positive up-section. In the surface sediments of Unit I, *N. pachyderma* (s) $\delta^{18}\text{O}$ values range between 4.3 and 4.5‰ (mean=4.4±0.06‰), which is not significantly different from Unit II

values. Unit I *N. pachyderma* (s) $\delta^{13}\text{C}$ values range between 1.8‰ and 2.1‰ (mean=2.0±0.1‰), not significantly different from Unit II values.

2.6.4 Downcore radiocarbon chronology

Our downcore radiocarbon chronology is based upon eight radiocarbon dates between 0 and 882 cmcd, two carbonate and six AIOM dates (Table 2.3; Figure 2.5). Ramped PyrOx AIOM and CaCO_3 -derived calendar ages were combined to generate the chronology, because paired dates are within 1σ error, similar to those in Antarctic Peninsula sediments (Table 2.3; Subt et al., 2016).

We established local marine reservoir ages from Rose Bengal-stained carbonates from 1.25 cm depth in cores MC-45 and MC-61. We obtained an uncalibrated AMS ^{14}C age of 950 ± 20 ^{14}C years from a monospecific planktic foraminifer, *N. pachyderma* (s), sample from core MC-45. In core MC-61, we obtained an uncalibrated AMS ^{14}C age of 1230 ± 15 ^{14}C years (Table 2.3) from a mollusk living on the seafloor at the time of collection. This age, which is indecipherable from the average Antarctic marine reservoir age of 1300 ± 100 ^{14}C years (Berkman & Forman, 1996), is the modern marine reservoir age for Sabrina Coast bottom water. Spatial and temporal variations in bottom water masses impact modern and downcore reservoir ages (King et al., 2018), so we use an uncertainty of 100 years for the reservoir age rather than the analytical uncertainty, which is consistent with the published literature (e.g., Berkman & Forman, 1996). As is standard in published Antarctic margin marine sediment records, we assume a constant reservoir correction downcore, which is not likely valid, given the known changes in the intermediate to deep Southern Ocean reservoir age since the last glaciation and more recently (King et al., 2018; Ninnemann & Charles, 2002; Skinner et al., 2010, 2019) and

the assumed changes in the relative influence of mCDW and meltwater on the Sabrina Coast shelf. However, no method currently exists to constrain past Antarctic margin reservoir age variations.

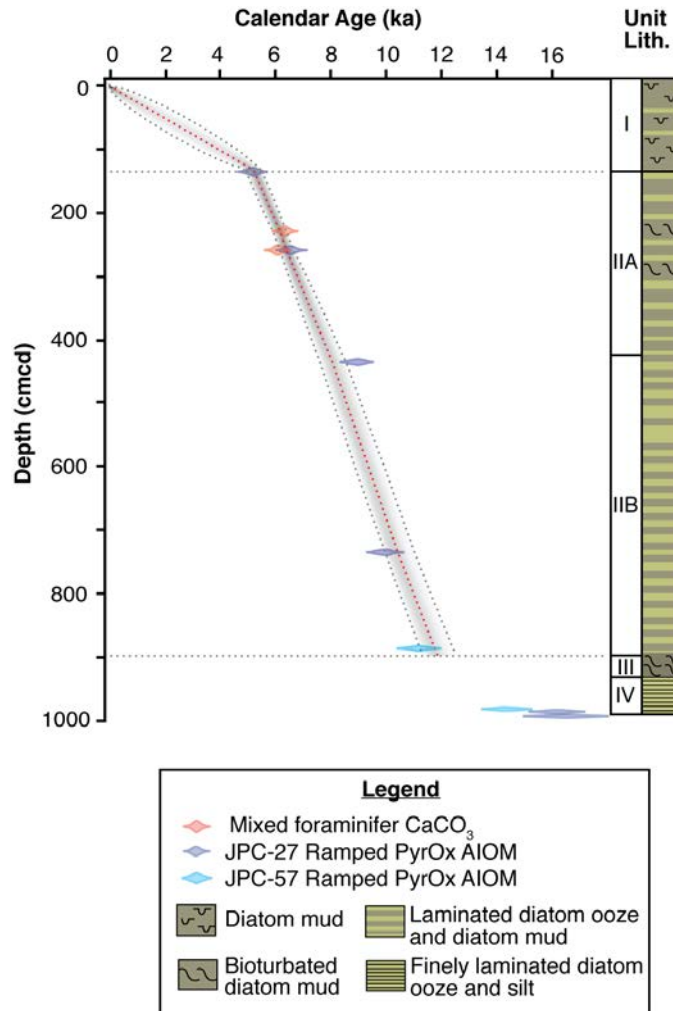


Figure 2.5 Calibrated ¹⁴C ages versus depth in centimeters composite depth. A composite graphic lithology and lithologic units are shown. Age model generated with Bacon 2.3 age modeling software showing calibrated ¹⁴C dates (colored symbols), the weighted mean (red curve) age, and 95% confidence intervals (shaded zone) for calculated ages (Blaauw & Christen, 2011). A downcore chronology is not developed below Unit IIB (see Section 2.6.4).

To establish the downcore chronology for NBP14-02 Sites 1 and 2, raw radiocarbon dates were calibrated to account for the local reservoir effect (Table 2.3). Calibrated ages were placed on the cmcd depth scale. We then generated an age model using Bacon 2.3 software (Figure 2.5;

Blaauw & Christen, 2011). This approach assumes that the accumulation rate changes at 135 cmcd (boundary between Unit I and IIA) and 888 cmcd (boundary between Unit IIB and Unit III), which is also informed by changes in lithology and magnetic susceptibility. The resulting age depth profile assumes that sedimentation was continuous, and gives, on average, a rate of 26 cm kyr⁻¹ in Unit I and 125 cm kyr⁻¹ in Unit II, providing a sampling resolution of ~40 yr cm⁻¹ and ~8 yr cm⁻¹, respectively. This age model results in uncertainty when converting data from the depth scale to time scale. In Unit I, the maximum uncertainty is ±850 years at 60 cmcd, near the midpoint of the unit where data is sparse. In Unit II, the maximum uncertainty is ±700 years at 888 cmcd, the base of Unit IIB. We terminate the downcore chronology at the base of Unit IIB, due to a lack of ¹⁴C dates in Unit III and differences in the thickness of Unit IV between Sites 1 and 2 (see Appendix A, Text A2, Figure A2).

2.7 Discussion

In targeting the first sediment record from the middle continental shelf of the Sabrina Coast, this study establishes the timing of deglaciation and documents the complete record of paleoceanographic variability from deglaciation to present. Radiocarbon chronology constrains the timing and nature of deglaciation across the shelf. Diatom and foraminifer fossil and geochemical data enable the reconstruction of the surface ocean paleoenvironmental variations, such as changes in primary productivity, stratification, polynya activity, sea-ice presence, and offshore influence. These data provide the basis for inferences about regional and global patterns of oceanographic and atmospheric variability to identify possible drivers for the paleoceanographic changes on the Sabrina Coast.

2.7.1 Sabrina Coast deglaciation (16.5 to ~14.4 ka)

The succession of sedimentary units provides an ice retreat history for the middle Sabrina Coast shelf. Unit VI is a diamict deposited sub-glacially or in a sub-ice shelf environment relatively close to the grounding line, indicated by the high magnetic susceptibility and site bathymetry suggesting streaming ice (Figure 2.1; Fernandez et al., 2018). Gravel layers in this unit suggest sub-ice shelf glaciomarine deposition during ice-sheet decoupling from the bed (Lowe & Anderson, 2002). Immediately overlying the diamict, Unit V, a silty mud with clasts, indicates deposition in a setting under ice shelf or fast ice cover, close to the grounding line. In core JPC-27, the initiation of seasonally open marine conditions on the middle Sabrina Coast shelf is shown by the abrupt transition between the gray mud (Unit V) and the lowermost diatom ooze of the laminated facies (Unit IV). In JPC-57 (Site 2), the presence of the *Fragilariopsis ritscheri* / *Fragilariopsis obliquecostata* lamination in Unit V suggests ice shelf retreat over this core site before the initiation of consistently open water, which we infer from a sequence of diatom mud and ooze laminations in Unit IV.

Ramped PyrOx-derived ^{14}C dates from both sites help us determine the timing and processes involved in the deglaciation of the Sabrina Coast continental shelf. The ^{14}C dates from Unit IV were collected as close as possible to the contact with the underlying silty muds of Unit V. This approach, used in other East Antarctic margin studies (Leventer et al., 2006; Mackintosh et al., 2011; Mackintosh et al., 2014), enables us to constrain the timing of the transition to open marine conditions. At Site 1, the more landward of the two sites, the minimum age of deglaciation was 16.5 ± 0.84 ka (15.0 ± 0.6 ^{14}C kyr, JPC-27). At Site 2, approximately three km from Site 1, the age obtained is 14.4 ± 0.38 ka (13.5 ± 0.21 ^{14}C kyr, JPC-57). The two-thousand-year difference in calibrated ages between laminated diatom ooze and silts of Unit IV at Site 1

(16.5 ± 0.84 ka) and Site 2 (14.4 ± 0.38 ka) could be related to either the incorporation of old carbon into the first split in JPC-27 or represent some temporal/spatial fluctuations of the ice margin prior to the deglaciation. We consider the incorporation of old carbon unlikely because the same was selected from diatom ooze with little to no contribution of allochthonous detrital material. Rather, we propose that the difference in age is better explained by the relative timing and onset of open marine conditions at the two sites.

The bathymetry of the Sabrina Coast shelf indicates a glacially carved cross shelf trough, which contained a fast-flowing ice stream (Fernandez et al., 2018; Gulick, Shevenell et al., 2017). We hypothesize that ice had retreated landward of the grounding zone wedge 2 (Figure 2.1b) by 16.5 ka and that three km away at Site 2, the area was clogged with sea ice and icebergs associated with deglaciation until the onset of open water conditions beginning at 14.4 ka. This interpretation is supported by iceberg furrows and keel marks observed in the region (Figure 2.1b; Fernandez et al., 2018). Further support for this hypothesis comes from both the abrupt nature of the contact between Units V and IV and the difference in the number of laminations in Unit IV between Sites 1 and 2. The earlier timing of deglaciation and the greater number of laminations at Site 1 suggests the open water conditions persisted longer at Site 1, whereas ice was likely clogged at Site 2. Furthermore, the single *Fragilariopsis ritscheri* lamination (669 cmbsf) within Unit V in JPC-57 at Site 2 suggests ice retreat prior to the deposition of the laminated facies, but heavy sea ice cover. *Fragilariopsis ritscheri* has been observed in areas of dense sea ice, including large floes separated by slushy brash ice in the Larsen A embayment (Table 2; Leventer, 2012 unpublished observation), and also associated with the summer sea ice edge environment, sea-ice-covered waters in summer, and surface melt pools (Armand et al., 2005; Crosta et al., 2004).

In Antarctic margin sequences, laminated diatom ooze and muds with variable magnetic susceptibility are often observed overlying silty muds and diamicts with high magnetic susceptibility in the glacial to deglacial sedimentary sequence (Leventer et al., 2006; Mackintosh et al., 2014; Taylor & Sjunneskog, 2002). It is hypothesized that laminated oozes and muds are deposited during seasonally open marine conditions in geographically restricted troughs on the shelf, and reflect the interplay between sediment-laden meltwater plumes and diatom blooms (Leventer et al., 2006). The diatoms preserved in the Sabrina Coast Unit IV deglacial laminations are different than in other shelf regions because of the diverse assemblage of large diatom species (e.g. *Chaetoceros* subg. *Chaetoceros*, *Rhizosolenia* spp., *Proboscia* spp., and *Corethron pennatum*). The species thrive in a productive, highly stratified water column and may accumulate in the water column over the course of the entire season before reaching the seafloor in tangled mats (Table 2; Alley et al., 2018; Crawford, 1995; McKay et al., 2000; Quéguiner, 2013; Singler & Villareal, 2005; Smetacek et al., 1985; Villareal et al., 1996). In general, the laminated ooze and silt was likely deposited in a seasonally open marine setting on a broad continental shelf with iceberg presence and glacial ice melt. The diatom muds within this unit may have formed during periodic subglacial meltwater input, interrupting diatom productivity and downward export.

Regionally, Sabrina Coast deglaciation precedes the timing of other East Antarctic margin marine records by one to five thousand years. Local terrestrial evidence from the Windmill Islands adjacent to Law Dome indicate that area started to deglaciate by ~10.5 ka (Cremer et al., 2003; Hodgson et al., 2003). Regionally, deglaciation from marine records recording East Antarctic Ice Sheet deglaciation range from ~10-15 ka (see Figure 2.6; Anderson et al., 2014 and references therein; Denis et al., 2009a; Leventer et al., 2006; Stickley et al.,

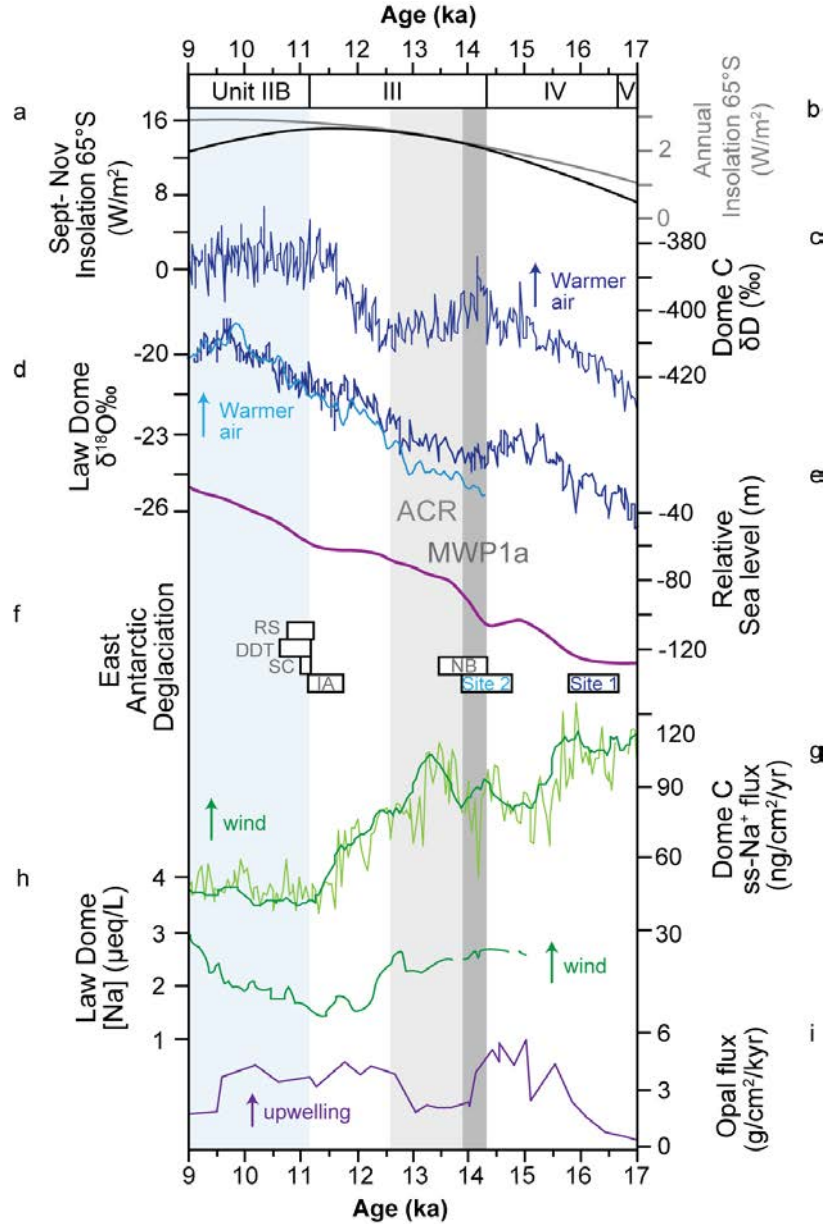


Figure 2.6 Regional proxy records of oceanic and atmospheric variability related to deglaciation and Holocene climate. Spring (a) and annual (b) insolation at 65°S (Laskar et al., 2014), (c) the EPICA Dome C δD record (EPICA Community Members, 2006), (d) the Law Dome $\delta^{18}O$ record (Plummer 2018; Morgan et al. 2002); and (e) global sea level curve (Lambeck et al., 2014). In (f), black boxes with Sabrina Coast Sites 1 and 2 deglacial age ranges (dark and light blue text), and black boxes with grey text indicate deglacial ages for Prydz Bay regions: Svenner Channel (SC; 11,000 cal yr bp; Leventer et al., 2006), Iceberg Alley (IA; 11,700 cal yr bp; Mackintosh et al., 2014), and Nielsen Basin (NB; 14,000 cal yr bp; Mackintosh et al., 2014), Adélie Land: Dumont D'Urville Trough (DDT; 10,600 cal yr bp; Domack et al., 1991; Denis et al., 2009a) and Ross Sea Drygalski Trough (RS; Anderson et al., 2014). (g) EPICA Dome C sodium flux (Röthlisberger et al., 2002); (h) Law Dome sodium concentration (Van Ommen et al., 2004); (i) opal flux (Anderson et al., 2009). Blue shade zone indicates early Holocene climate optimum in our record (Unit IIB), while the gray shaded zones indicate where existing Antarctic marine records observe Meltwater Pulse 1A (MWP1a; dark gray; Golledge et al., 2014; Weber et al., 2014) and the Antarctic Cold Reversal (ACR; light gray; EPICA Community Members, 2006; Pedro et al., 2011; Stenni et al., 2011).

2005). The difference in timing is potentially due to differences in chronological constraint, local physical oceanographic processes, and the geomorphology of the continental shelves at these sites, which direct the pattern of ice flow and retreat. However, the timing of deglaciation from more distal marine sediment core records is consistent with our Sabrina Coast record. Other records from the margin document early deglaciation, including beneath the Amery Ice Shelf in Prydz Bay, with the onset of marine sedimentation at ~15 ka (Domack et al., 1998; Hemer & Harris, 2003), near the Lambert/Amery drainage system at 18 ka (White et al., 2011), and from the Amundsen Sea embayment by 16.4 ka (Kirshner et al., 2012; Smith et al., 2011).

The similar oceanographic setting and timing of retreat between these outlet glacier systems and the Sabrina Coast might indicate a common forcing mechanism for deglaciation. Regional atmospheric conditions during deglaciation are recorded at Dome C and Law Dome (Figure 2.6), which document atmospheric warming after the Last Glacial Maximum (Figure 2.6; EPICA Community Members, 2006; Masson et al., 2000), consistent with our inferred Sabrina Coast deglaciation at 16.5 ± 0.84 ka. Both Prydz Bay and Amundsen Embayment which show similar timing of deglaciation are in locations similar to the Sabrina Coast: large catchments with offshore gyre systems where warm water is transported toward the continental shelf. There is a significant source of meltwater inferred from the southern hemisphere (Clark et al., 2009), so the timing of Sabrina Coast deglaciation is relevant to understanding the contribution of Antarctic glacial catchments to past sea level rise, including Meltwater Pulse 1a (MWP1a; 14.0-14.5 ka; Figure 6; Clark et al., 2009; Deschamps et al., 2012; Lambeck et al., 2014; Liu et al., 2016). Significantly, the timing of initial Sabrina Coast deglaciation precedes the timing of MWP1a, suggesting the regional glacier system could have contributed to sea level rise, prior to the retreat of most Antarctic sectors.

2.7.2 The Antarctic Cold Reversal (~14.4 to 11.2 ka)

Lower sedimentation rates and a shift in lithology towards a bioturbated diatom mud (Unit III) indicates a change in environmental conditions along the Sabrina Coast between ~14.4 and 11.2 ka. The relative decrease in diatom abundance, increased magnetic susceptibility, and the presence of pyrite lined burrows and several small (<1cm) clasts suggests that this unit was deposited relatively slowly in a sub-fast ice or sub-ice shelf environment (Domack et al., 1998; McKay et al., 2008; Prothro et al., 2017). However, the presence of the cool water form of *T. antarctica* (T1), open ocean-associated *F. kerguelensis*, and low abundances of sea ice-associated *Fragilariopsis* spp. suggest that these sites continued to be influenced by cool, open ocean waters present over the Sabrina Coast shelf (Crosta et al., 2004, 2005; Pondaven et al., 1998).

Taken together, the paleoenvironmental proxies and chronological constraints indicate that Unit III was deposited during the Antarctic Cold Reversal (ACR; Figure 2.6). The ACR is characterized by cool atmospheric conditions between 14.6 and 12.7 ka (EPICA Community Members, 2006; Pedro et al., 2011; Stenni et al., 2011), and variability in seasonal sea-ice extent and surface productivity (Fogwill et al., 2020). This period coincides with a range of time when increasing wind strength occurred in the sub-polar regions that may have led to enhanced upwelling and increased ocean heat transport (Figure 2.6; Anderson et al., 2009; McGlone et al., 2010; Röthlisberger et al., 2002; Van Ommen et al., 2004).

2.7.3 Early Holocene (11.2 to 9 ka)

During the early Holocene (11.2-9 ka, Unit IIB), high accumulation rates and the co-occurrence of mat- and sea ice-associated diatom species suggest that surface waters of the

Sabrina Coast were generally stratified and productive (Figure 2.7; Table 2.2; Taylor & Sjunneskog, 2002). Surface stratification could be caused by increased meltwater presence, weaker/less frequent storms, and/or the lack of a polynya system during the early Holocene. However, monospecific diatom oozes are also present in this interval, which indicate rapid flux to the sea floor, likely associated with breakdown of stratification by storms and/or changes in position/strength of the coastal current (Kemp & Villareal, 2013; Taylor & Sjunneskog, 2002).

Changes in the strength/position of the coastal current may have altered the amount of mCDW on the shelf, resulting in increased meltwater production and nutrient availability (Silvano et al., 2018; Figures 2.8, 2.9). Support for this interpretation comes from the lack of planktic foraminifers preserved in early Holocene Sabrina Coast sediments. However, it is difficult to determine if this lack of carbonate resulted from an increase in corrosive bottom waters (dissolution) and/or rapid sedimentation of discrete diatom bloom events (dilution; Mackensen et al., 1993). A similar lack of foraminifer carbonate is observed in interbedded early Holocene diatom oozes and muds from the Antarctic Peninsula and in the Weddell Sea, and linked to increased mCDW influence and surface stratification (Hillenbrand, et al., 2003; Shevenell & Kennett, 2002; Shevenell et al., 2011). We note that well-preserved foraminifers and abundant phytodetritus were found in surface sediments at Sites 1 and 2, which were bathed in relatively corrosive mCDW below 400 m. Discrete diatom oozes in recent sediments (e.g., the upper part of Unit I) occur less frequently than in the early Holocene, suggesting different upper ocean conditions compared to present.

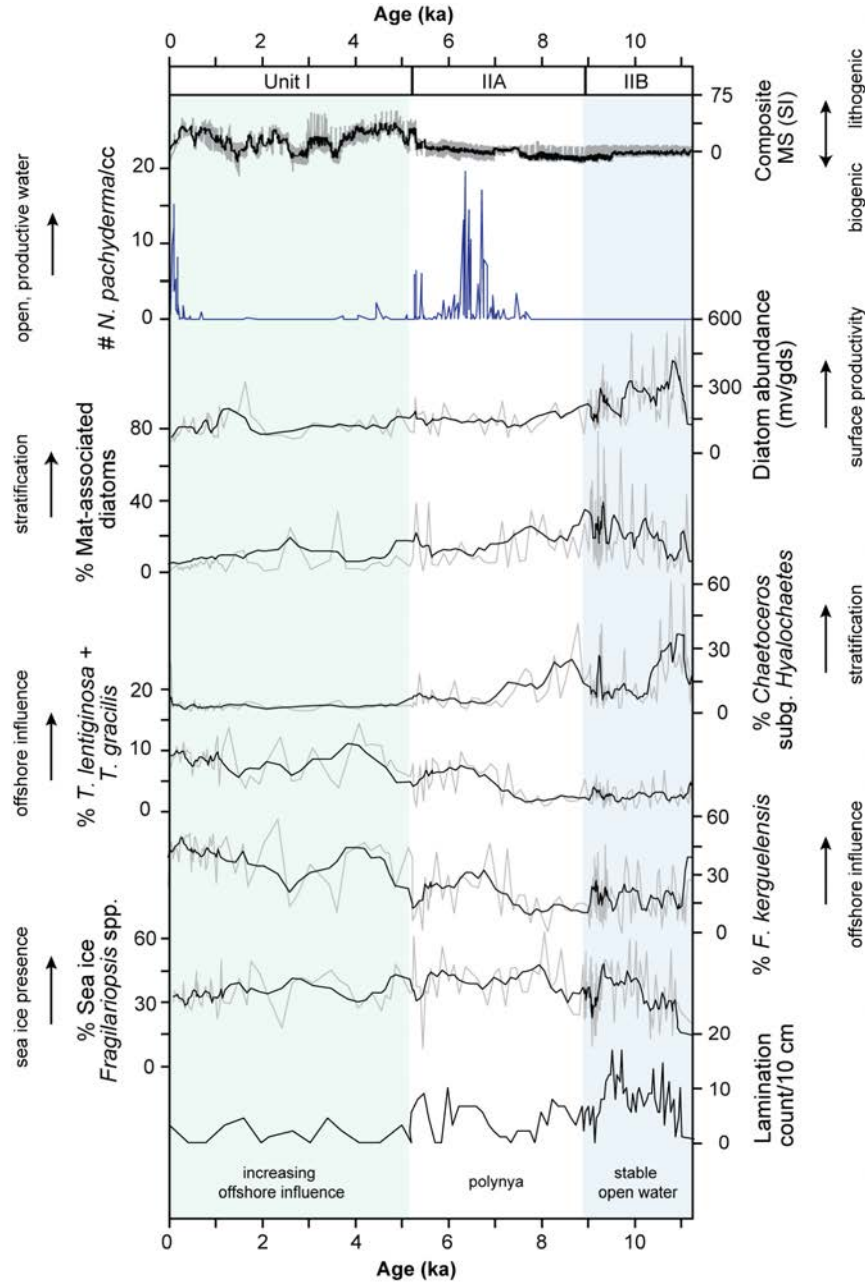


Figure 2.7 Sabrina Coast multiproxy environmental reconstruction plotted versus age. Includes lithologic units, composite magnetic susceptibility, *N. pachyderma* (s) abundance, diatom assemblages, and lamination counts per 10 cm. Thin gray lines include each data point; thicker black lines are 5-pt moving averages to highlight variations in data. Shaded and white zones indicate our interpretation of the early, middle, and late Holocene climate in our record.

Circum-Antarctic atmospheric and oceanic warmth, coincident with early Holocene austral spring insolation, is extensively documented in ice core and marine sediment records (e.g., Crosta et al., 2007; Denis et al., 2009a; EPICA Community Members, 2006; Masson et al., 2000; Mulvaney et al., 2012; Shevenell et al., 2011). High spring insolation at 65°S influences summer duration, by promoting earlier regional sea-ice retreat (Huybers & Denton, 2008; Shevenell et al., 2011; Stammerjohn et al., 2008; Vimeux et al., 2001). Sabrina Coast diatom abundance tracks local spring insolation through the Holocene, suggesting that on orbital timescales, the timing of spring sea ice breakout and the length of summer is critical for diatom productivity (Shevenell et al., 2011; Vimeux et al., 2001).

Local support for warmer atmospheric conditions comes from coastal Law Dome, ~280 km to the southwest of our Sabrina Coast site, which indicates peak atmospheric warmth at ~11 ka, reduced sea ice extent, and less cyclonic activity between 12 and 9 ka (Masson et al., 2000; Morgan et al., 2002; Van Ommen et al., 2004). Further sedimentary evidence from the Windmill Islands, immediately west of Law Dome, indicates deglaciation of the outermost islands by ~11-10 ka, likely associated with warm regional atmospheric temperatures (Goodwin & Zweck, 2000; Roberts, 2004). Farther afield, marine sedimentary records from Adélie Land, Prydz Bay, and the Mac.Robertson Shelf indicate open marine conditions along the East Antarctic margin during the early Holocene (Crosta et al., 2007; Denis et al., 2009a; Domack et al., 1998; Harris, 2000, Mackintosh et al., 2011).

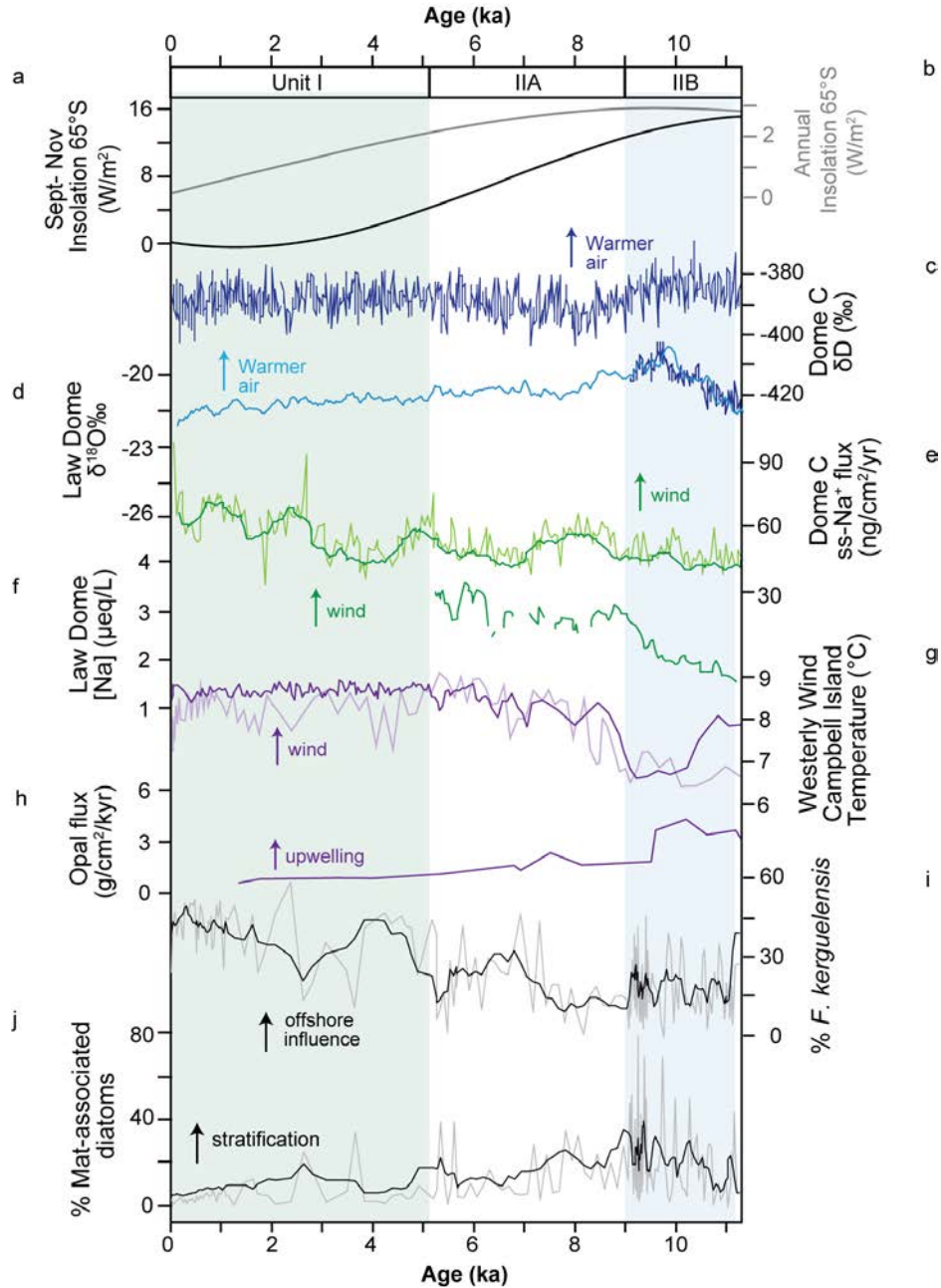


Figure 2.8 Sabrina Coast diatom assemblages plotted versus regional proxy records of oceanic and atmospheric variability related to Holocene climate. (a) Spring and (b) annual insolation at 65°S (Laskar et al., 2014); (c) the EPICA Dome C δD record (EPICA Community Members, 2006); (d) the Law Dome $\delta^{18}O$ record (dark blue, Plummer, 2018; light blue, Morgan et al. 2002); (e) EPICA Dome C sodium flux (Röthlisberger et al., 2002); (f) Law Dome sodium concentration (Van Ommen et al., 2004); (g) the westerly wind record from Campbell Island, NZ (purple curves, McGlone et al., 2010); (h) opal flux (Anderson et al., 2009). In diatom assemblage data, thin gray lines include each data point; thicker black lines are 5-pt moving averages. Shaded and white zones indicate our interpretation of the early, middle, and late Holocene climate in our record.

2.7.4 Early to middle Holocene (9 to 5.2 ka)

Along the Sabrina Coast, the early to middle Holocene (9-5.2 ka; Unit IIA) is a period of reduced stratification and/or nutrient input (Leventer et al., 2006), indicated by reduced contribution of mat-associated diatoms (Figure 2.7). Similarly, an increase in diatoms associated with offshore influence from 9 ka and 5.2 ka indicate that stratified surface water conditions gave way to a more well-mixed water column with increased open ocean influence (Figures 2.7, 2.9; Crosta et al., 2005). These conditions are similar to other East Antarctic margin records that indicate productive surface water conditions and less sea ice cover, suggesting a warmer setting between ~8 and 4 ka (Denis et al., 2009b; Kusahara et al., 2010). Well-preserved and abundant *N. pachyderma* (s) (Figure 2.7) indicate primary productivity on the continental shelf and conditions favorable for carbonate preservation such as presence of less corrosive, regional shelf water (Mackensen et al., 1993; Shevenell et al., 2002). The peak in *N. pachyderma* (s) presence may indicate increased nutrient availability and warmer, open-marine conditions (Figure 2.7; Asioli 1997; Bergami et al., 2009; Mikis et al., 2019). Furthermore, $\delta^{18}\text{O}$ values exhibit a ~0.3% shift to lighter isotopic values, indicating warmer and fresher surface waters, possibly indicating persistent meltwater in the system (Cape et al., 2019; Hillenbrand et al., 2017).

Throughout Unit IIA, diatom laminations become more wavy and irregular, suggesting disturbance during or after deposition (Harris, 2000). These characteristics are similar to a mid-shelf core from the Mac.Robertson shelf that records an episode of rapid accumulation from 3.6 ka to 6.5 ka characterized by cross-laminated sediments where brine rejection creates dense bottom water (Harris, 2000; Harris & O'Brien, 1996). The process of Dense Shelf Water formation possibly occurred on the Sabrina Coast during the middle Holocene, as shown by the matted and irregular diatom laminations throughout Unit IIA in Sites 1 and 2. This interpretation

is further supported by an age reversal in the foraminifer ^{14}C dates from 25 cm apart in this sequence, which indicates sediment disturbance, possibly as a result of deep current flow. If mCDW was present on the Sabrina Coast in the mid Holocene, mixing and cooling of upwelled mCDW, facilitated by the Antarctic Coastal Current, could also support the stability of a polynya and promote bottom water formation by the upward exchange of deep, warm water (Rintoul, 1998).

In Antarctic margin marine and terrestrial records, the mid Holocene is a period of productivity, retracted glacial margins, and diminished sea ice (Ingólfsson et al., 1998). The timing of the mid-Holocene optimum at Sabrina Coast Sites 1 and 2 also coincides records of rapid ice retreat in Larsemann and Vestfold Hills near Prydz Bay between 7 ka and 7.6 ka (Verleyen et al., 2005; Zwartz et al., 1998). Circum-Antarctic records of middle Holocene climate warmth including from Sites 1 and 2 are corroborated by changes in sea-salt concentrations at Law Dome (Figure 2.8) that suggest the regional climate shifted from a glacial setting similar to the present-day Antarctic interior, to the current maritime climate influenced by more northerly air masses starting around 7 kyr ago (Figure 2.8; Van Ommen et al., 2004).

2.7.5 Middle to late Holocene (5.2 to 0 ka)

The depositional environment of the latest-middle to late Holocene encompassing Unit I was markedly different from the early and middle Holocene (Unit IIB and Unit IIA). The lower boundary of Unit I, punctuated by a transition from laminated diatom ooze and diatom mud to a more slowly accumulating diatom mud with few laminations and bioturbation, suggests the region experienced a reduction in primary productivity on the shelf. Throughout this interval, the Sabrina Coast experienced a later onset of primary production and longer sea ice season,

demonstrated by the low contribution of *Chaetoceros* subg. *Hyalochaete*, a diatom typically associated with spring blooms (Leventer et al., 2006). Throughout this time period, the water column was progressively more influenced by offshore water masses, shown by the increased presence of diatom species *F. kerguelensis*, associated with open water, and *T. lentiginosa*, a pelagic open-ocean species (Crosta et al., 2004, 2005; Pondaven et al., 1998). Individual laminations become more abundant in the upper part of Unit I and likely reflect discrete depositional events when a highly stable upper water column was destratified (Kemp & Villareal, 2013). This sequence of diatom species suggests that the overall trend in offshore influence on upper ocean conditions was punctuated by episodes of stratification and rapid deposition (Figure 2.9). Similar sequences of late Holocene sediments from the West Antarctic Peninsula record offshore influence in the late Holocene punctuated by periods of changes in stratification (Shevenell & Kennett, 2002) associated with the varying influence of coastal and offshore water masses. The low preservation of foraminifera in Unit I (Figure 2.7) may be attributed to lower foraminifer productivity due to increased sea ice cover, an advanced glacial margin at this time (Goodwin, 1996), or low preservation potential of carbonate in slowly accumulating sediments (Hendry et al., 2008).

On the East Antarctic margin, a transition in oceanographic regime is observed around 5 ka in other records. The onset of the Late Holocene in marine cores occurs at ~5 ka for the Mertz-Ninnis Trough and at 4.3 ka for the Dumont D'Urville Trough (Domack et al., 1991). Regional records from Adélie Land and Prydz Bay indicate colder sea-surface waters, and icier conditions from ~4 to 1 ka (Denis et al., 2009b). Furthermore, between 2.5 ka and 4 ka, glacier re-advance and thickening of the ice sheet in East Antarctica occurred at the Windmill Islands and Larsemann Hills, and global sea level lowering of ~0.7 meters occurred (Goodwin, 1996;

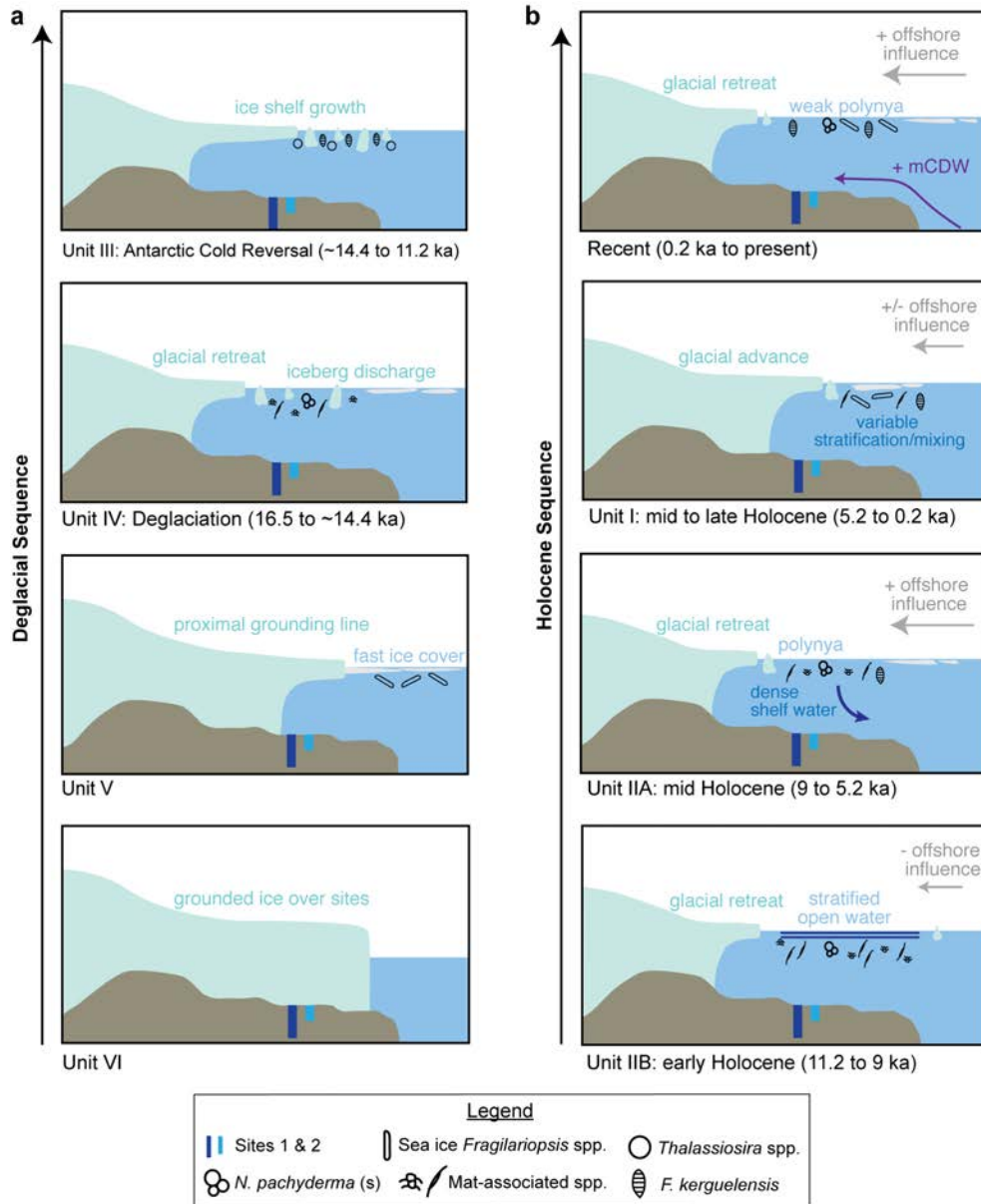


Figure 2.9 Conceptual model of deglacial to Holocene water column conditions. Including ice sheet, ice shelf, sea ice, microfossil deposition, and paleoenvironmental drivers (winds, currents) for (a) the deglacial sequence and (b) Holocene sequence, including recent conditions.

1998; Verleyen et al., 2005). East Antarctic coastal ice cores at Taylor Dome and Law Dome also record increased snow accumulation rates during this time (Steig et al., 2000; Van Ommen et al., 2004). The geological and ice core data are supported by model predictions that show a progressive increase of annual sea-ice cover since 5 ka (Renssen et al., 2005). These

observations and predictions are consistent with our inferred increase in terrigenous sediment supply (higher magnetic susceptibility values) at Sites 1 and 2, indicating greater sediment delivery to the mid continental shelf.

Middle to late Holocene records from the Antarctic margin and sub-Antarctic suggest a shift in atmospheric moisture content and circulation, indicating increasing influence of lower latitude climate signals (Figure 2.8; Van Ommen et al., 2004). Elevated East Antarctic ice core accumulation rates are attributed to enhanced meridional atmospheric temperature gradients, which enhance poleward transport of warm, moist, northern airmasses (Van Ommen et al., 2004; Vimeux et al., 2001). After ~5 ka, decreased local insolation caused a reduced latitudinal temperature gradient, reducing the amount of heat transferred to the high latitudes (Figure 8; Renssen et al., 2005). This reduction is consistent with the increase in sea-ice duration inferred from the Sabrina Coast sites and the re-advance of glaciers in the circum-Antarctic after 5 ka (Denis et al., 2009a; Ingólfsson et al., 1998), punctuated by periods of high productivity and surface ocean stratification.

2.7.6 Regional to global forcings of Sabrina Coast paleoceanography

The timing and characteristics of paleoceanographic change preserved in the deglacial through Holocene Sabrina Coast shelf sequence demonstrate that this region is sensitive to climate forcings on local to global scales. The record at NBP14-02 Sites 1 and 2 suggests the shelf is primarily influenced by local variability in polynya activity associated with coastal winds and currents. The Sabrina Coast and neighboring Law Dome lie further north than most of Antarctica's coastline, so this region is strongly influenced by maritime cyclonic activity today, which is closely linked to meridional circulation (Masson-Delmotte et al., 2004; Van Ommen et

al., 2004). We propose that local conditions from the deglacial through Holocene were impacted by regional to global-scale mechanisms with links to lower latitudes.

Long-term change through the deglacial to Holocene is governed by orbital forcing, which affects the latitudinal distribution of insolation and the thermal gradient between the high and low latitudes (Timmerman et al., 2009; Vimeux et al., 2001). Our deglacial record on the Sabrina Coast coincides with the timing of global ice mass loss at the end of the last glacial maximum (Weber et al., 2014) and is coincident with the increase in atmospheric temperatures and CO₂ recorded in high latitude ice core records (Figure 2.6; EPICA Community Members, 2006). Models and ice core evidence indicates that an orbital configuration with longer austral summers as well as atmospheric CO₂ increase around 17 ka BP played a key role in the deglacial temperature rise in Antarctica and the southern hemisphere by creating warm atmospheric conditions (Huybers & Denton, 2008; Timmerman et al., 2009; WAIS Divide Members 2013). The local orbital configuration (65°S) shows an increasing spring and annual insolation (Figure 2.6). This led to an increase in the temperature gradient from high to low latitudes during the spring and summer (Vimeux et al., 2001), enhancing southward atmospheric and oceanic transport (Vimeux et al., 2001). Sediment records of both atmospheric processes and warm water driving deglaciation are present around the Antarctic margin (Hillenbrand et al., 2010; 2017; Shevenell et al., 2011).

Mechanisms impacting millennial-scale Holocene climate trends might also be related to atmospheric and oceanographic perturbations generated at lower latitudes, linked to climatological patterns such as the Southern Annular Mode (SAM) and El Nino Southern Oscillation (ENSO; Clement et al., 1999; Fogt et al., 2011; Lamy et al., 2001; Marshall et al., 2011; Thompson & Solomon, 2002; Vance et al., 2013). ENSO is a zonal climate pattern of

varying atmospheric pressure and sea surface temperature in the tropical and subtropical Pacific, which impacts the Pacific sector of Antarctica via meso-scale eddies and cyclonic events (Vance et al., 2013; Fogt et al., 2011). The assemblage and lithological changes around 5 ka in our Sabrina Coast record occurred during a period of time when it is thought the modern-day frequencies of the El Niño Southern Oscillation (ENSO) were established (Clement et al., 1999; Hodell et al., 2001; Lamy et al., 2001). This alignment suggests the position of the westerly winds may influence the Sabrina Coast via low latitude teleconnections (Marshall et al., 2011; Thompson & Solomon, 2002). Similar low to high latitude teleconnections are recognized in the Antarctic Peninsula region (Abram et al., 2014; Shevenell et al., 2011; Shevenell & Kennett, 2002) as well as East Antarctic margin marine and ice core records (Cremer et al., 2003; Crosta et al., 2004; Vance et al., 2013), documenting the shift in late Holocene climate variability.

Models show that projected strengthening and a poleward shift of the westerlies under future scenarios of increased atmospheric CO₂ can produce significant subsurface warming of Antarctic coastal waters, leading to accelerated ice shelf melt in the future (Dinniman et al., 2012; Spence et al., 2014). This trend is significant because the Sabrina Coast record has revealed warmer conditions during the Holocene that are possibly related to influence from offshore water masses, as well as meltwater-enhanced stratification. These conditions possibly allowed incursions of warm deep water onto the continental shelf and closer to outlet glacier grounding lines.

2.8 Conclusion

We conclude that the Sabrina Coast, East Antarctica was sensitive to atmospheric forcing from the deglacial through the Holocene, and, as such, is likely more sensitive to anthropogenic

global warming than previously recognized. The onset of open marine conditions at 16.5 ka precedes the timing of deglaciation in all other East Antarctic records to date, indicating that this is a region naturally vulnerable to climate forcing. In modern sediments, diatom data, foraminifer assemblages, and geochemistry indicate a mixed water column with influence of offshore water masses, indicative of current mCDW and regional meltwater interaction at depth, but a more accurately dated approach to this high-resolution core top is necessary to better constrain the recent presence of relatively warm water on the shelf. In order to continue to fully assess the past oceanographic variability on the sensitive marine-based outlet systems on the Sabrina Coast and the Aurora Subglacial Basin, we must obtain more unambiguous records of mCDW influence on the shelf through quantification of past water column temperatures, and investigate more high resolution records from the recent past to constrain onset of the present day oceanographic regime. With support from modern physical oceanographic observations and models, the Sabrina Coast sediment record we present here suggests that regional winds have played a dominant role in driving polynya and ocean processes throughout the Holocene. Present-day, large-scale climate variability exerts an influence on regional to local processes on the Sabrina Coast. Therefore, we may anticipate an impact on Antarctic glacier systems and ice-sheet stability into the future if low latitude climate patterns increase in strength and frequency, with implications for global sea level rise.

CHAPTER THREE:

UPPER OCEAN WARMING ON THE SABRINA COAST SHELF SINCE 1000 CE

3.1 Chapter Contributions

Kara J. Vadman wrote this chapter and created all figures, prepared and analyzed all carbonate and sediment samples for radiocarbon analyses and ^{210}Pb dating, generated the Bacon age model, extracted and analyzed samples for GDGT analyses, and prepared and analyzed foraminifer stable isotopes and trace metals. ^{210}Pb data analysis in Excel and R was facilitated by J. M. Jaeger. A. Leventer generated all diatom data.

3.2 Abstract

Outlet glaciers on the Sabrina Coast drain one eighth of the East Antarctic Ice Sheet and are losing mass. Observations indicate that the Aurora Subglacial Basin catchment is susceptible to ocean thermal forcing. To understand the evolution of present-day ocean-ice interactions, we first validate the utility of two upper ocean paleothermometers, TEX_{86} and planktic foraminifer Mg/Ca ratios in Sabrina Coast surface sediments. We then use ^{210}Pb and ^{14}C dates, TEX_{86} paleothermometry, foraminifer and diatom assemblages, and foraminifer stable isotopes and trace metals to reconstruct ~1000 years of paleoenvironmental variations (temperature, sea ice, open water, stratification) on the middle continental shelf. Results reveal +2°C warming in the upper ocean, sea ice decline, increased open ocean influence since ~1300 CE, and 20th Century warming/freshening in the surface waters. We suggest regional temperature and ice variations

are driven by changes in wind-driven currents, which modulate delivery of offshore water masses to the shelf.

3.3 Introduction

Melting at deep regional grounding lines and basal melting of the Totten and Moscow University Ice Shelves on the Sabrina Coast, East Antarctica, is occurring at rates similar to West Antarctic outlet systems (Holland et al., 2019; Rignot et al., 2019). Observations demonstrate that thinning and retreat are associated with warmer regional air temperatures and the presence of warm water at or near regional grounding lines (Greene et al., 2017; Rintoul et al., 2016). Physical oceanographic observations indicate that modified Circumpolar Deep Water (mCDW) upwells at the continental shelf edge of the Sabrina Coast and flows southward across the shelf (Greene et al., 2017; Silvano et al., 2017; Silvano et al., 2018). Regional bathymetry (Fernandez et al., 2018; Greenbaum et al., 2015) steers deep water towards regional grounding lines (1000-2000 m) via glacially-carved cross-shelf bathymetric troughs (Greenbaum et al., 2015; Greene et al., 2017; Nitsche et al., 2017; Rintoul et al., 2016). As the Aurora Subglacial Basin, the marine-based catchment drained by Totten Glacier system, contains 5.3 meters of sea level equivalent ice, it is important understand its sensitivity ocean temperature (Morlighem et al., 2020).

To put recent warming and ice mass loss into context, we can look to high resolution ice core records of climate on decadal to centennial timescales. Law Dome, located on the western flank of the Sabrina Coast, is a coastal ice dome where the Dome Summit South record was recovered and subsequently interpreted (Masson et al., 2000; Morgan et al., 2002; Van Ommen et al., 2004). Over the past millennium, Law Dome ice cores record periods of enhanced atmospheric transport, changes in accumulation rate, and ion concentration, and air temperature

(Masson-Delmotte et al., 2003; Roberts et al., 2015; Souney et al., 2002; Vallelonga et al., 2017; Vance et al., 2013). Over the past several hundred years, high concentrations of sea salt ions transported to Law Dome suggest enhanced atmospheric circulation patterns around East Antarctica (Curran et al., 1998; Souney et al., 2002). Further, records measured from Casey Station, on the leeward, western flank of Law Dome, record a 2°C increase in atmospheric temperatures over the past 50 years (Masson-Delmotte et al., 2003; Miles et al., 2016; Souney et al., 2002). While atmospheric changes can account for a portion of ice mass changes observed on the Sabrina Coast (Miles et al., 2016), it remains unclear when the warm water observed today (~0.5°C) may have influenced the glacial outlet system in the past.

With limited long-term oceanographic observations from the Sabrina Coast, it remains difficult to fully assess the scale of natural variability of Sabrina Coast glaciers in response to ocean thermal forcing. Marine sediments collected on the Sabrina Coast shelf offer an opportunity to identify ocean temperature variations impacting current ocean-ice sheet interactions. To do so, we must first test the hypothesis that Sabrina Coast cores faithfully record current ocean temperatures, by applying two paleotemperature proxies, the TEX₈₆ (TetraEther INdeX of 86 carbons) paleothermometer and planktic foraminifer *N. pachyderma* (s) Mg/Ca-paleothermometry. If Sabrina Coast core top Mg/Ca and TEX₈₆ values fall on existing regional temperature calibration lines (Vazquez Riveiros et al., 2016; Shevenell et al., 2011 respectively), and if core top temperatures estimates are within error of measured water mass temperatures, then we can confidently apply generated paleotemperatures downcore.

TEX₈₆ and Mg/Ca of planktic foraminifera are two paleotemperatures proxies applied to cores on the Antarctic margin and they are ideal for providing independent temperature estimates. Where calcium carbonate is scarce in the sedimentary record, TEX₈₆ can provide

paleoenvironmental insight. On the Antarctic margin, warmer ocean temperatures and higher nutrients are observed to co-occur in association with mCDW incursions (Shevenell et al., 2011), so TEX₈₆ can potentially reflect the water mass. Although archaea communities have not been directly studied in the Sabrina Coast water column, TEX₈₆-derived temperatures likely reflect similar associations with warm subsurface water during the spring. This inference is supported by a recent study that identified an archaea abundance maximum in the subsurface waters (~200 m) of Prydz Bay, East Antarctica (Liu et al., 2020). To corroborate TEX₈₆ paleotemperatures, we utilize Mg/Ca of planktic *N. pachyderma* (s), which has a paleotemperature calibration for cold temperatures (Vazquez Riveiros et al., 2016). However, its use is complicated by the life cycle and depth habitat of *N. pachyderma* (Kohfeld et al., 1996; Nyland et al., 2006). Trace metal uptake in *N. pachyderma* (s) is also impacted by the concentration of carbonate ions ([CO₃²⁻]), complicating their use for paleothermometry (Hendry et al., 2009). To further evaluate core-top temperature proxies and establish that they can reconstruct realistic temperatures down-core, we will reconstruct the relative magnitude and timing of changes in upper ocean temperature through the latest Holocene in comparison to regional ice core records from Law Dome (Souney et al., 2002; Van Ommen et al., 2004; Curran et al., 1998). The Law Dome ice core record records atmospheric variability through the late Holocene, so we will test the hypothesis that Sabrina Coast upper ocean temperatures vary in response to similar atmospheric drivers as Law Dome.

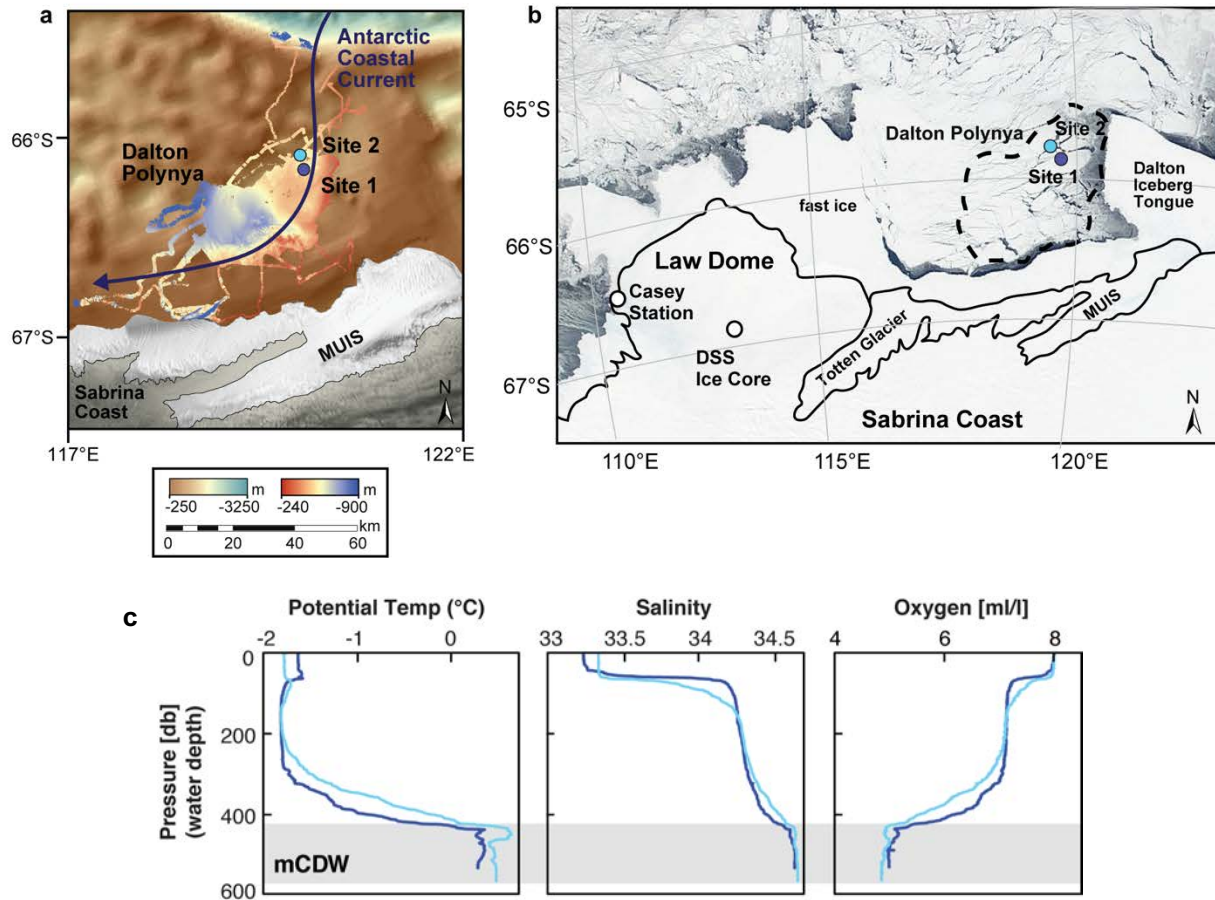


Figure 3.1 (a) Bathymetry of the Dalton Polynya on the Sabrina Coast continental shelf, East Antarctica, offshore Moscow University Ice Shelf (MUIS). Map adapted from Gulick, Shevenell et al., 2017. Water depth indicated by colored scale bars (left bar, from Bedmap2, Fretwell et al., 2013; right bar from NBP14-02 bathymetric survey). Site 1 and 2 marine sediment cores (blue dots) were collected during U.S. Antarctic Program cruise NBP14-02. The Antarctic Coastal Current (blue thick arrow) indicated. (b) Image adapted from Terra Modis image acquired October 21, 2001, showing location of core sites in relation to Casey Station and the Dome Summit South (DSS) ice core (white dots), Law Dome, and Dalton Iceberg Tongue. (c) Sabrina Coast CTD casts. NBP14-02 CTD-based potential temperature, salinity, and oxygen concentration data from Site 1 (dark blue; 547 m water depth; 66°11.06'S, 120°30.15'E) and Site 2 (light blue; 593 m water depth; 66°07.73'S, 120°27.84'E) at the location of sediment cores collected from the middle continental shelf. Modified Circumpolar Deep Water (mCDW) was observed at both sites >400 m (gray shading).

3.4 Materials and Methods

3.4.1 Lithology, magnetic susceptibility, and composite depth scale

In 2014, cruise NBP14-02 cored two sites on the middle continental shelf on the Sabrina Coast with ~9 to 13 m of sediment consisting of interbedded diatom mud and diatom ooze

(Figure 3.1). In this study, we present core MC-45 collected at Site 1 (66°11'S, 120°30'E; 547 m of water; 35 cm long) and core MC-61 from Site 2 (66°08'S, 120°28'E; 593 m of water; 35 cm long), both recovered with intact sediment water interfaces (Figure 3.2a; Table 3.1). Creating a composite depth scale allows us to tie regional paleoceanography into an integrated record.

In the previous chapter (Chapter 2), a composite depth scale established at Site 1 and Site 2 using the lineage function in Analyseries 2.0 software (Paillard et al., 1996) to correlate magnetic susceptibility records. Core KC-27B was used as a reference core because it recovered an intact sediment water interface and was long enough to capture changes in magnetic susceptibility apparent in the longer jumbo piston cores. Cores JPC-27 and JKC-53 were correlated to the reference core, accounting for overpenetration and compression. The resulting composite record from Site 1 was then used as the reference record for JPC-57 at Site 2 (Figure 3.2b).

Although Chapter 3 focuses on MC-45 and MC-61, using the Chapter 2 composite depth scale with kasten and jumbo piston cores is necessary because the MC-45 and MC-61 chronologies must be constrained by a ^{14}C date taken from below the megacores, at 135 cmcd (93 cmbsf) in JPC-27 (Figure 3.2a). When the composite record for Sites 1 and 2 was established in the previous chapter, the megacores MC-45 and MC-61 were assumed to convert directly into the composite depth scale without Analyseries (ex: 1 cmbsf = 1 cmcd). Both cores were 30 cm long, and magnetic susceptibility records in both MC-45 and MC-61 did not vary sufficiently to identify magnetic susceptibility highs or lows that could be linked to the composite depth record. Thus, when depths were converted to age in the previous chapter, MC-45 and MC-61 were equivalent in age. However, in Chapter 3, rather than integrate MC-45 and MC-61 directly into a composite record by assuming that all 30 cm of each core are equivalent in age and

depositional history, we utilize the results of ^{210}Pb dating to combine the proxy records of the two megacores. In other words, MC-45 proxy data was plotted using an age model that combines the MC-45 ^{210}Pb dates and the JPC-27 ^{14}C date, and the MC-61 proxy data was plotted using an age model with MC-61 ^{210}Pb ages and the same JPC-27 ^{14}C date. Then, the proxy data was merged together on a common age scale. The ^{210}Pb modeling for each core and Bacon age models are described in the following section of the methods.

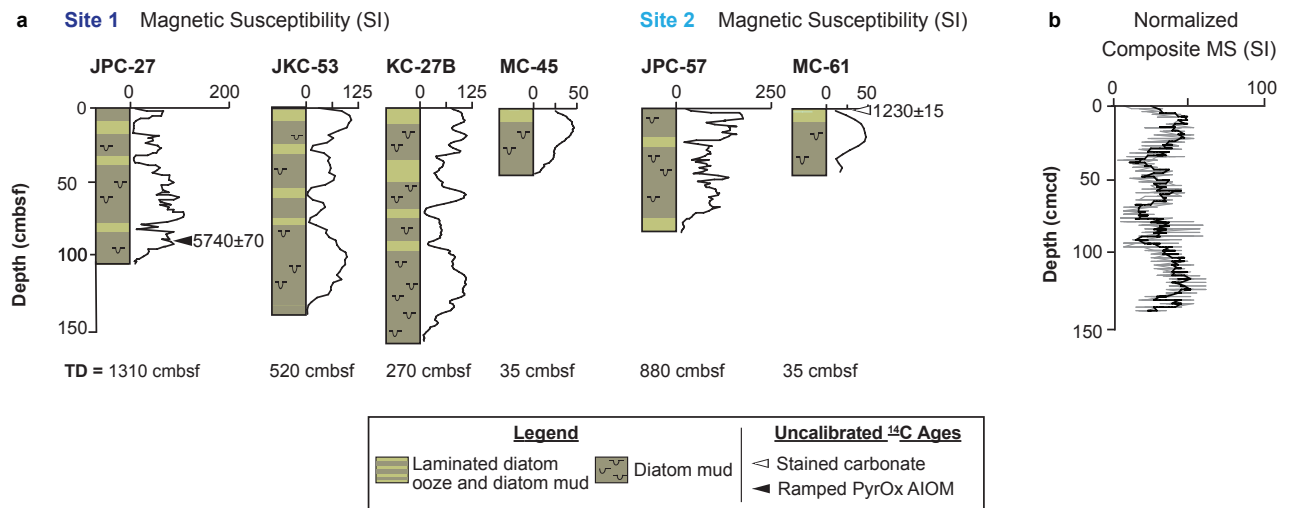


Figure 3.2 Sabrina Coast lithology and composite depth scale. (a) Site 1 and Site 2 graphic lithologies with and magnetic susceptibility versus depth (cmbsf) for the upper sections of NBP14-02 cores; locations of ^{14}C dates and uncalibrated ^{14}C ages indicated. Note that Magnetic Susceptibility (MS) scales vary to emphasize relative changes. (b) Normalized composite MS versus composite depth (cmcd). The lower sections of the Site 1 and Site 2 cores are excluded due to our focus on the megacore records and the upper ~135 cmcd. TD indicates total lengths of cores.

Table 3.1 NBP14-02 sediment core locations.

Site	Surface Ocean Temp. (°C)	mCDW Temp. (°C)	Core	Latitude	Longitude	Water Depth (m)	Core length (cm)
1	-1.7	0.3	MC-45	66° 11.0069' S	120° 30.0591' E	537	35
			KC-27B	66° 11.0907' S	120° 30.2385' E	547	270
			JKC-53	66° 11.053' S	120° 30.208' E	545	520
			JPC-27	66° 11.0568' S	120° 30.1483' E	544	1310
2	-1.6	0.5	MC-61	66° 07.691' S	120° 27.826' E	582	35
			JPC-57	66° 07.7325' S	120° 27.8407' E	583	875

3.4.2 Radiometric dating methods and age model

3.4.2.1 ^{210}Pb measurements

Homogenized dry sediments from 0.5 cm sample intervals between 0 and 20 cmbsf in MC-45 and MC-61 were analyzed over 48 hours by gamma spectrometry on Canberra High-Purity Germanium Coaxial Planar Photon detectors at the University of South Florida, College of Marine Science. Sediments were analyzed for total activities of ^{210}Pb (46.5 KeV), ^{214}Pb (295 and 351 KeV), ^{214}Bi (609 KeV), and ^{137}Cs (661 KeV). Supported ^{210}Pb (produced *in situ*) was estimated by the mean activities of ^{214}Pb and ^{214}Bi . To determine excess ^{210}Pb , supported ^{210}Pb was subtracted from measured ^{210}Pb .

3.4.2.2 ^{210}Pb ages

The ^{210}Pb age-depth models for each core were generated using the constant flux-constant sedimentation (CFCS) approach (after Wangner et al., 2020). Age-depth profiles were generated from mean sedimentation rates, calculated using a non-linear exponential model fit to excess ^{210}Pb activity (code developed by J.M. Jaeger, published in Wangner et al., 2020). Linear sedimentation rates (cm/yr) are porosity-corrected by using mass accumulation rates (MAR; g/cm²/yr) modeled from a non-linear fit of excess ^{210}Pb (dpm/g) versus cumulative mass depth (g/cm²) that are then normalized by a constant dry bulk density (g/cm³) at depth of excess activity profile. This sedimentation rate allows us to determine age versus depth (Table 3.2, 3.3).

Table 3.2 Modeled ²¹⁰Pb chronology for NBP1402 MC-45. C.I.=confidence interval.

Avg. Depth (cmbsf)	Median Age	Upper 95% C. I.	Lower 95% C. I.
0.5	2008	2008	2008
1.25	1999	2000	1998
1.75	1993	1994	1992
2.25	1987	1989	1985
2.75	1981	1983	1979
3.25	1975	1977	1972
3.75	1969	1972	1966
4.25	1963	1966	1960
4.75	1957	1960	1953
5.25	1951	1955	1947
5.75	1945	1949	1940
6.25	1939	1944	1934
6.75	1933	1938	1927
7.25	1927	1932	1921
7.75	1921	1927	1915
8.25	1915	1921	1908
8.75	1909	1915	1902
9.25	1903	1910	1895
9.75	1897	1904	1889
10.25	1891	1899	1883

Table 3.3 Modeled ²¹⁰Pb chronology for NBP1402 MC-61. C.I.=confidence interval.

Avg. Depth (cmbsf)	Median Age	Upper 95% C. I.	Lower 95% C. I.
0.25	2006	2007	2005
0.75	1991	1994	1987
1.25	1975	1980	1970
1.75	1960	1966	1952
2.25	1944	1953	1934
2.75	1929	1939	1916
3.25	1913	1926	1899
3.75	1898	1912	1881
4.25	1882	1898	1863

Table 3.4 Radiocarbon measurements. Core-top CaCO₃ sample (MC-61) used for Reservoir Correction and Ramped PyrOx AIOM ¹⁴C sample (JPC-27) used to constrain age model below ²¹⁰Pb. Sample information is indicated by sample ID, core ID, average depth in centimeters below sea floor (cmbsf), centimeters composite depth (cmcd), and sample type.

AMS Facility ID	Core ID	Avg. Depth (cmbsf)	Avg. Depth (cmcd)	Sample Type	CaCO ₃ (mg)	CO ₂ evolved (mgC)	Fraction modern (Fm) (± Error)	Blank Corr. Fm (± Error)	Blank Corr. ¹⁴ C Yr (±1σ Error)	Reservoir Correction (±1σ Error)	Calendar Age yr BP (±1σ Error)
OS-121677	MC-61	1.25	1.25	Mollusk	6.4	-	0.8581 (0.0018)	-	1230 (15)	1230 (100)	modern
LL-175009	JPC-27	93	135	AIOM	-	218.7	0.4922 (0.0023)	0.4893 (0.0042)	5740 (70)	1230 (100)	5190 (170)

3.4.2.3 Radiocarbon analyses

NBP14-02 radiocarbon results are derived from recently dead mollusk CaCO_3 , stained with Rose Bengal, and the first aliquot of bulk sediment acid insoluble organic matter (AIOM) prepared via accelerator mass spectrometry at the National Ocean Sciences Accelerator Mass Spectrometry facility (NOSAMS; OS-), and we apply that age as the local marine reservoir age (1230 ± 100 ^{14}C yr; Table 3.4). The fraction modern for the AIOM sample was generated by Lawrence Livermore AMS facility (LL-), a blank correction was applied (after Fernandez et al., 2014 and Venturelli et al., 2020), the date was corrected for the local marine reservoir age, and calibrated using CALIB 8.2 using the Marine20 calibration curve (Heaton et al., 2020; Stuiver et al., 2020).

3.4.2.4 Bayesian statistics modeling parameters

The age-depth model for MC-45 and MC-61 was developed using ^{210}Pb measurements and a radiocarbon (^{14}C) date from the first aliquot of bulk sediment acid insoluble organic matter (AIOM) prepared via Ramped PyrOx (Rosenheim et al., 2008; 2013) from core JPC-27. To create the final age model, ^{210}Pb and calibrated ^{14}C ages were combined using Bacon 2.3 software (Blaauw & Christen, 2011), which uses Bayesian statistics to obtain weighted mean sediment age-depth relationships with 95% confidence intervals. When generating the age-depth model in Bacon 2.3 (Blaauw & Christen, 2011), the following priors were used: acc.shape=1.5, acc.mean (y/cm)=50, mem.strength= 10, mem.mean= 0.7. The prior information are the assumptions that guide the age model, including an expected accumulation rate (acc. shape and acc.mean), how much the accumulation rate may have changed over time (mem. strength and mem.mean).

3.4.3 Archaeal lipid preparation, analysis, and calibration

3.4.3.1 Lipid extraction

We manually extracted and analyzed Glycerol Dialkyl Glycerol Tetraethers (GDGTs) in 23 samples from MC-45 and 19 samples from MC-61 using High Performance Liquid Chromatography-Mass Spectrometry (HPLC-MS) following published methods (Huguet et al., 2010; Schouten et al., 2007). We replicated 30% of the unknown analyses (n=14) throughout the study. Freeze dried sediment samples were homogenized, then archaeal lipids were manually extracted by ultrasonication using pure methanol (MeOH), dichloromethane: methanol (DCM:MeOH, 1:1 v/v), then pure DCM (3x). Eluent was dried down under continuous N₂ flow, rinsed with DCM, transferred to 4 mL vials, and dried down again under N₂. Each lipid extract was filtered using a PTFE 0.4 µm filter, dissolved in 50-150µL of 1% Isopropanol (IPA): Hexane (Hx) (v/v), then injected onto a High Pressure Liquid Chromatograph, attached to a Mass Spectrometer (HPLC-MS). Samples were stored at 4°C refrigeration before and after HPLC analysis.

3.4.3.2 High Performance Liquid Chromatography analyses

50 µL of sample was injected into an Agilent 1200 series high performance liquid chromatographer (HPLC), coupled to a Varian 320 triple-quad mass spectrometer (MS). GDGTs were separated on the HPLC-MS using two Prevail Cyano columns (2.1x150 mm, 3µm diameter, maintained at 30°C) and a gradient elution similar to that of Schouten et al. (2007) as follows: 1% IPA:hexane for 5 minutes, then a gradient to 1.8% IPA in 55 minutes (flow rate: 0.2 mL/min), followed by an automatic backflush of 10% IPA:hexane for 20 minutes, then column re-equilibration by flushing 1% IPA:hexane forward over 20 minutes. GDGTs were detected by

an atmospheric-pressure chemical ionization (APCI) source in single ion mode (scanning for m/z 1302, 1300, 1298, 1296, 1292, 1050, 1036, and 1022), coupled to the MS.

3.4.3.3 *TEX₈₆ quantification and monitoring*

TEX₈₆ values were calculated using manual integration of individual extracted ion chromatograms within the ChemStation software, based on the equation Schouten et al. (2002):

$$\text{TEX}_{86} = \frac{[\text{GDGT-2} + \text{GDGT-3} + \text{Cren isomer}]}{[\text{GDGT-1} + \text{GDGT-2} + \text{GDGT-3} + \text{Cren isomer}]}$$

We monitored external and internal reference materials with each set of unknown samples to assess consistency; NIOZ sediments from the Royal Institute for Sea Research, Den Burg, Netherlands (Schouten et al., 2013) and USF-CMS Antarctic Standard (AS-1; TEX₈₆ values=0.28±0.02). The internal standard AS-1 was made from a homogenized Holocene sediment sample (NBP01-07 JTC-17), collected from the east Antarctic Peninsula (64°40'S, 65°05'W). We also monitored several indices to assess NBP14-02 TEX₈₆ values for variables such as soil-derived GDGTs (BIT: Branched Isoprenoid Tetraether index; Hopmans et al., 2004), the relative input of methanotrophic archaeal components (Methane Index; Zhang et al., 2011) and non-thermal influences (Ring Index; Zhang et al., 2016).

3.4.4 Stable isotopes of foraminifer calcite

We analyzed tests of planktic foraminifer species *Neogloboquadrina pachyderma* (s) for stable oxygen (δ¹⁸O) and carbon (δ¹³C) isotopes. Due the small amount of foraminifer carbonate available, sample material larger than 150 μm was analyzed together, without separating by size fraction. For stable isotope analyses, ~20-80 μg of crushed, species-specific foraminifer tests were prepared from 0.5 cm sample intervals using standard procedures and analyzed on a

Thermo Scientific MAT 253 Stable Isotope Ratio Mass Spectrometer equipped with a Gas Bench II preparatory device. All isotopic values are expressed using standard δ notation in permil relative to Vienna Pee Dee Belemnite (‰VPDB).

Measurements of $\delta^{18}\text{O}$ and $\delta^{13}\text{C}$ were corrected using standard laboratory reference materials for sequence drift correction, amplitude, and quality control (Borba; $\delta^{13}\text{C}=2.87\pm 0.05\text{‰}$; $\delta^{18}\text{O}=-6.15\pm 0.09\text{‰}$), amplitude (TSF-1, equivalent to NBS-19; $\delta^{13}\text{C}=1.95\pm 0.05\text{‰}$; $\delta^{18}\text{O}=-2.2\pm 0.06\text{‰}$), and monitored for quality control (Atlantis-3 and ChiCal). These values are derived from repeat measurements of the reference materials at University of South Florida College of Marine Science. Long-term instrument precision is 0.08‰ for $\delta^{18}\text{O}$ and 0.05‰ for $\delta^{13}\text{C}$. For the MC-45 and MC-61 samples, the standard deviation among replicates from the same sample depth is 0.05-0.2‰ (Average: 0.1‰) for both $\delta^{18}\text{O}$ and $\delta^{13}\text{C}$.

3.4.5 Trace element/calcium analysis

We evaluated the surface ocean temperature signal using *Neogloboquadrina pachyderma* (s) tests (150-300 μm) from 14 sample depths across MC-61 and MC-45. Samples were prepared using standard foraminifer trace element cleaning procedures with both oxidative and reductive steps (Boyle and Keigwin, 1985/86; Martin and Lea, 2002), then analyzed using a ThermoFisher Element XR High Resolution-Inductively Coupled Plasma-Mass Spectrometer. Replicate analyses were conducted on ~50% of the samples over the length of the project as well as within each run (n=7).

All isotopes were measured in analog mode at low resolution (R=300), with the exception of ^{45}Sc , ^{55}Mn , and ^{56}Fe , which were measured in medium resolution (R=4000) to avoid spectral

interferences. Mg/Ca ratios are reported using the ^{24}Mg isotope due to its high natural abundance. All minor and trace elements are ratioed to ^{43}Ca . Elemental ratios in unknowns were determined using a suite of multi-element standards with varying concentrations of Mg, Ca, B, Ba, U, Cd, Mo, Li, Na, Mn, Sr, Fe, and Zn prepared to achieve a range of elemental ratios similar to those of foraminifers.

We converted raw counts to concentrations using linear calibration lines that included blank measurements and 3-4 multi-element standards and applied a noise correction factor following Schrag (1999). We removed matrix effects on sample Mg/Ca through corrections based on the ratio of known Mg/Ca to measured Mg/Ca in the Sample Matrix Standard (Rosenthal et al., 1999; Schrag, 1999) and in community standards ECRM, BAM, and CMSI (Greaves et al., 2008). We used community standards ECRM (Mg/Ca = 3.75 mmol/mol), BAM (Mg/Ca = 0.78 mmol/mol), and CMSI (Mg/Ca = 0.78 mmol/mol) to monitor accuracy (Greaves et al., 2008). Relative standard deviations for community standards were 1.8% (ECRM), 3.3% (BAM), and 3.5% (CMSI).

A suite of trace elements were measured to assess cleaning efficacy (Figure 3.3). Our monitoring results indicate adherent clays were removed completely, and no contamination was introduced in the cleaning process. Planktic *N. pachyderma* Mg/Ca is not correlated with Mn/Ca ($R^2=0.065$), Fe/Ca ($R^2=0.005$), and Al/Ca ($R^2=0.0025$). Maximum Mn/Ca and Fe/Ca, and Al/Ca in *N. pachyderma* are 0.06, 0.11, and 0.014 mmol/mol. Sr/Ca and Mg/Ca are not correlated in the *N. pachyderma* data ($R^2=0.0025$) (Figure 3).

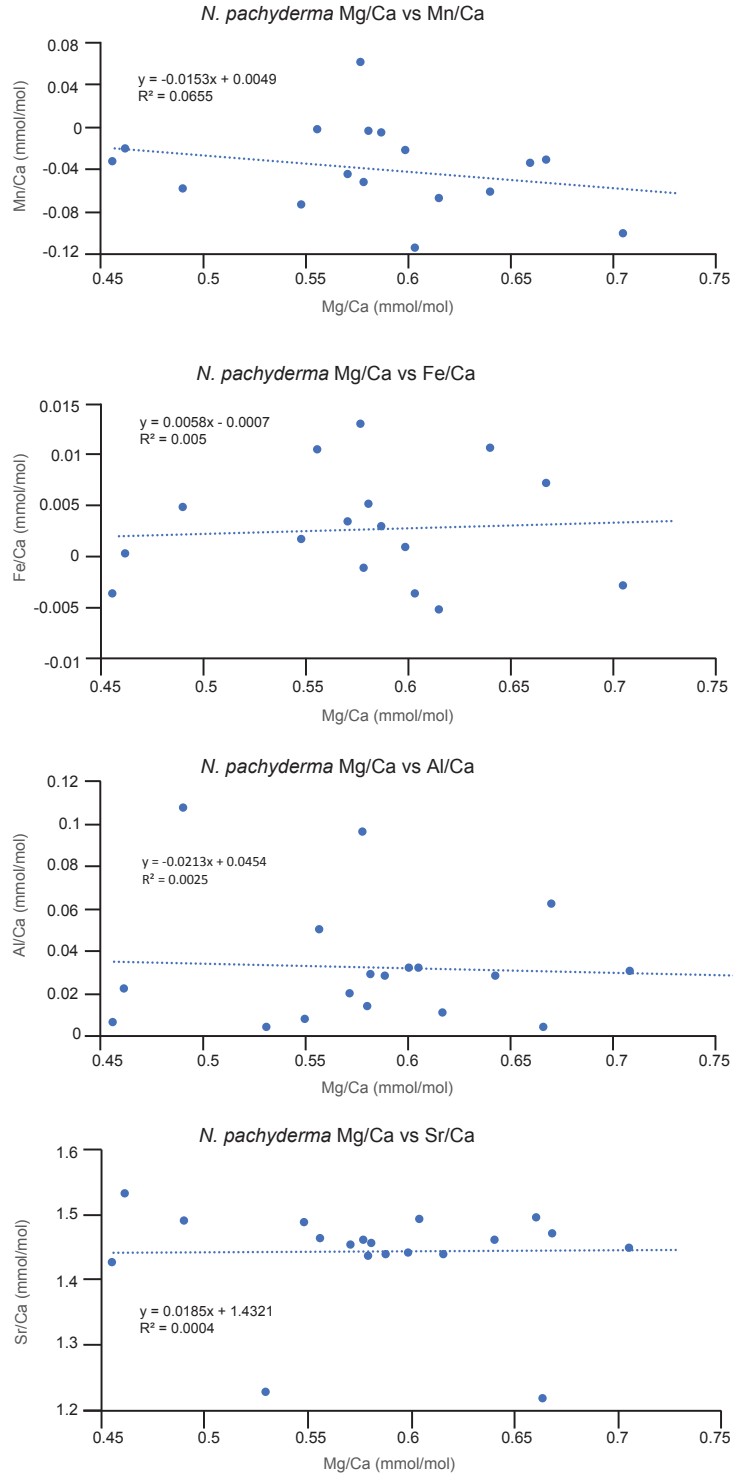


Figure 3.3 *N. pachyderma* (s) sample results for trace metals cleaning indicators. Plots show both MC-45 and MC-61 data (Mg/Ca vs. Mn/Ca, Fe/Ca, Al/Ca, and Sr/Ca in mmol/mol).

3.4.6 Diatom assemblages

Diatom assemblage data were generated for 30 samples at 1 cm resolution in MC-45 and MC-61 to evaluate changes in total diatom abundance and relative species abundance. Total diatom abundance is useful to understand overall surface ocean productivity, whereas relative species abundance indicates specific environmental parameters such as sea ice presence/absence, or water column stratification. Quantitative diatom slides were produced following the method described by Scherer (1994), which involves settling a known amount of sediment over a known surface area, yielding a random distribution of diatoms for quantitative evaluation.

We counted at least 400 diatom valves along slide transects at 1000x magnification on an Olympus BX60 microscope. Absolute diatom abundance values are reported as millions of valves per gram of dry sediment (mv/gds). This value is calculated by the expression $T = (N * B) / (A * F) / M$, where T=number of microfossils per unit mass, N=total number of microfossils counted, B=area of bottom of beaker (mm²), A=area of the microscope field of view (mm²), F=number of transects counted, and M=mass (g) of original sediment sample dispersed in beaker (Scherer, 1994). Relative abundance values for individual species are reported as percentages, calculated by dividing the number of valves of a species by the total valves counted. In our environmental interpretations, we utilize the diatom species and groups listed in Table 3.5.

Table 3.5 Summary of relationship between diatoms species and environmental conditions.

Species or group	Known ecology	Sabrina Coast Environmental conditions	References
<i>F. kerguelensis</i>	Antarctic Circumpolar Current-association, open water, ice-free conditions	Influence of offshore water masses, ice-free conditions	Crosta et al., 2005; Smetacek et al., 1997
Mat-associated diatoms (<i>Chaetoceros</i> subg. <i>Chaetoceros</i> , <i>Rhizosolenia</i> spp., <i>Proboscia</i> spp., <i>Corethron pennatum</i> , <i>Pseudonitzschia</i> , <i>Thalassiothrix antarctica</i> , <i>Trichotoxon reinboldii</i>)	Open ocean, stratified oligotrophic water	Stratified surface waters	Alley et al., 2018; Crawford, 1995; Crosta et al., 2005; McKay et al., 2000; Quéguiner, 2013; Singler & Villareal, 2005; Smetacek et al., 1985; Villareal et al., 1996
Sea ice associated species (<i>F. curta</i> , <i>F. cylindrus</i> , <i>F. lineata</i> , <i>F. obliquecostata</i> , <i>F. pseudonana</i> , <i>F. ritscheri</i> , <i>F. sublinearis</i> , <i>F. vanheurckii</i> , <i>Fragilariopsis</i> spp. (unidentified))	Sea ice presence: sea ice edge, or sea ice melting-induced stratified waters	Sea ice covered or ice edge environment, with possible melt-induced stratification or Dense Shelf Water formation	Armand et al., 2005; Crosta et al., 2004

3.5 Results

3.5.1 Chronology

We used a constant flux-constant sedimentation (CFCS) approach to model excess ^{210}Pb activity. The CFCS model assumes that the depositional system has a constant accumulation of sediments and a constant supply of excess ^{210}Pb (Appleby & Oldfield, 1992; Baskaran et al., 2014). This model is appropriate to apply to the megacores because both MC-45 and MC-61 show a constant decline in unsupported ^{210}Pb with depth (Figure 3.4a), similar to the “Type 1” profile described in Jaeger et al. (1999). Excess ^{210}Pb activity decays exponentially and reaches background level at ~10 cm in MC-45, and at ~6 cm in MC-61. The porosity-corrected modeled sedimentation rate is 0.08 cm/yr in MC-45 and 0.03 cm/yr in MC-61.

In order to constrain ages in the lower portion of the megacores, below the limit of ^{210}Pb , a ^{14}C date at 135 cmcd (93 cmbsf) from core JPC-27 was used as an additional chronological tie point in Bacon (Figure 3.5; Table 3.4). Chronological uncertainty expands in the Bacon age model beyond the ^{210}Pb datums, indicated by the gray error cloud (Figure 3.5). In the MC-45 age model (Figure 3.5a), the mean 95% confidence range of ages is 1236 years. The minimum range

in age error is 4 yr at the core top, and maximum is 1656 yr at 80 cmcd. In the MC-61 age model (Figure 3.5b), the mean 95% confidence range of ages is 1260 years. The minimum range age error is 9 yr at the core top, and the maximum is 1646 yr at 80 cmcd.

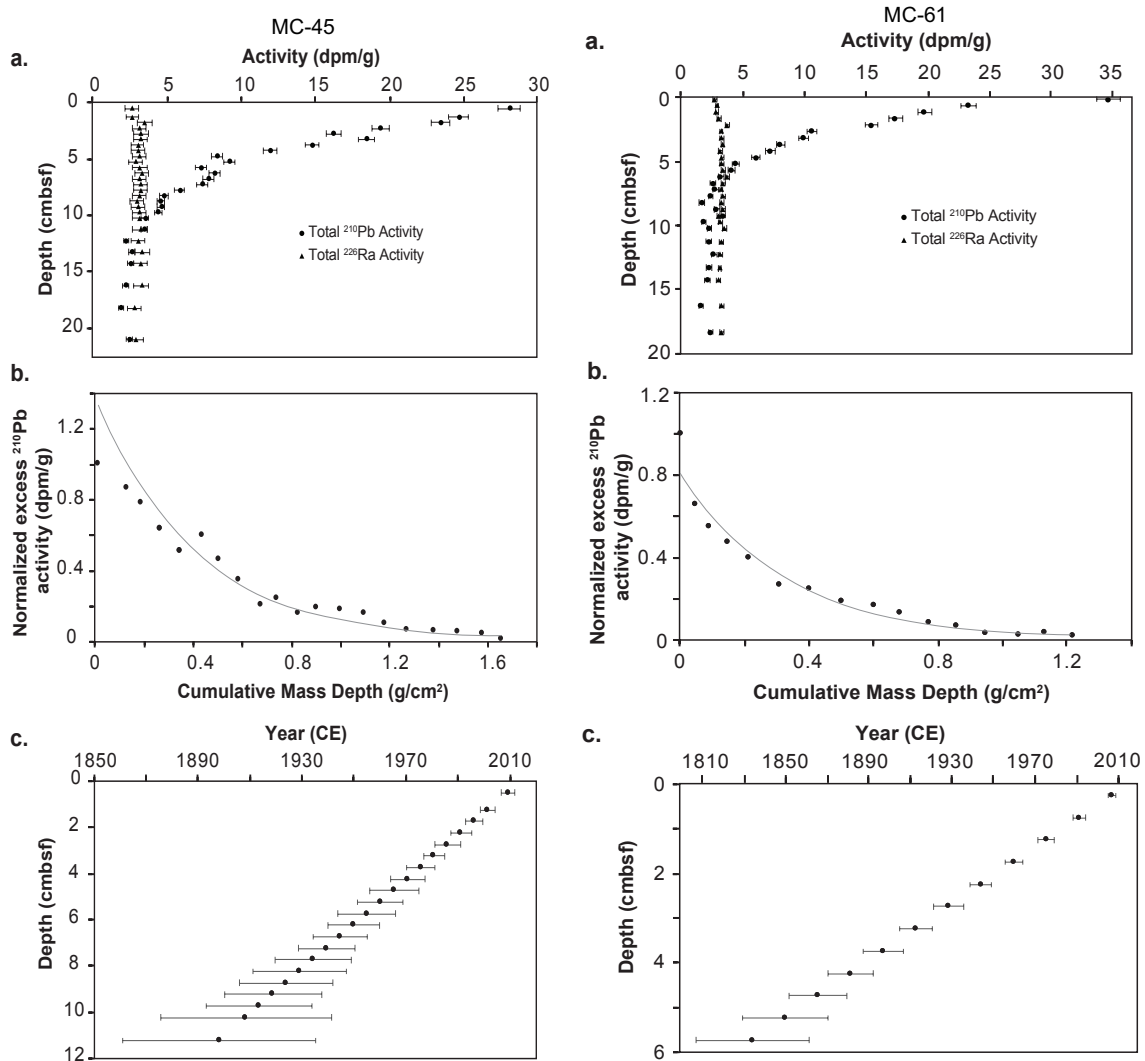


Figure 3.4 ^{210}Pb chronology and age-depth model for NBP14-02 MC-45 (left) and MC-61 (right). (a) Excess ^{210}Pb activity and total ^{226}Ra activity in disintegrations per minute per gram (dpm/g). (b) Normalized excess ^{210}Pb activity against cumulative mass depth (g/cm^2) with a non-linear exponential model used to establish mean sedimentation rates ($\text{g}/\text{cm}^2/\text{yr}$). (c) Age-depth model calculated from porosity-corrected sedimentation rates, with 95% confidence interval.

One way to explore how well the modeled ^{210}Pb ages in the upper depths of the megacores represent the ages deeper in the core is to extrapolate through the ^{210}Pb dates down to the depth of the first ^{14}C age. When projecting MC-45 ^{210}Pb ages through 135 cmcd, the estimated date based on the ^{210}Pb accumulation rate is 1620 yr bp, whereas the modeled age for the ^{14}C date is 5204 ± 300 yr bp. The MC-45 date at 135 cmcd is outside the 95% confidence interval (± 300). Furthermore, when comparing the array of ages in the extrapolated MC-45 ^{210}Pb projection between 0-135 cmcd using a paired two tailed t-test, the ages are significantly different than the array of ages in the Bacon age model ($t < 0.05$). When projecting MC-61 ^{210}Pb ages through 135 cmcd, the estimated date based on the ^{210}Pb accumulation rate is 4180 yr bp, whereas the modeled age for the ^{14}C date is 5204 ± 300 yr bp. Thus, the MC-61 date at 135 cmcd is also outside the 95% confidence interval (± 300). Like in MC-45, the array of ages in the modeled MC-61 ^{210}Pb projection between 0-135 cmcd is significantly different than the array of ages in the Bacon age model ($t < 0.05$; paired, two tailed t-test).

The proxy data plotted in this chapter fall between 0-30 cmcd, so it is also useful to compare only the upper 30 cmcd of the ^{210}Pb projected ages with the Bacon age model results. The MC-45 projected ages from 0-30 cmcd are significantly different than the Bacon age model ($t < 0.05$). However, the MC-61 ^{210}Pb projected dates between 0-30 cmcd are *not* significantly different than the Bacon age model ($t = 0.51$). This result indicates greater confidence in the MC-61 data when converted from the depth scale and represented on the age scale, which is illustrated by ghost plots (Figure 3.6). Heavily shaded areas indicate high certainty in the calendar ages for the particular proxy value (Figure 3.6). A possible consideration for difference in the age estimates between the ^{210}Pb projected ages and the dated ^{14}C sample at 135 cmcd (JPC-27) may be the occurrence of event sedimentation. The activity decay in the ^{210}Pb profiles

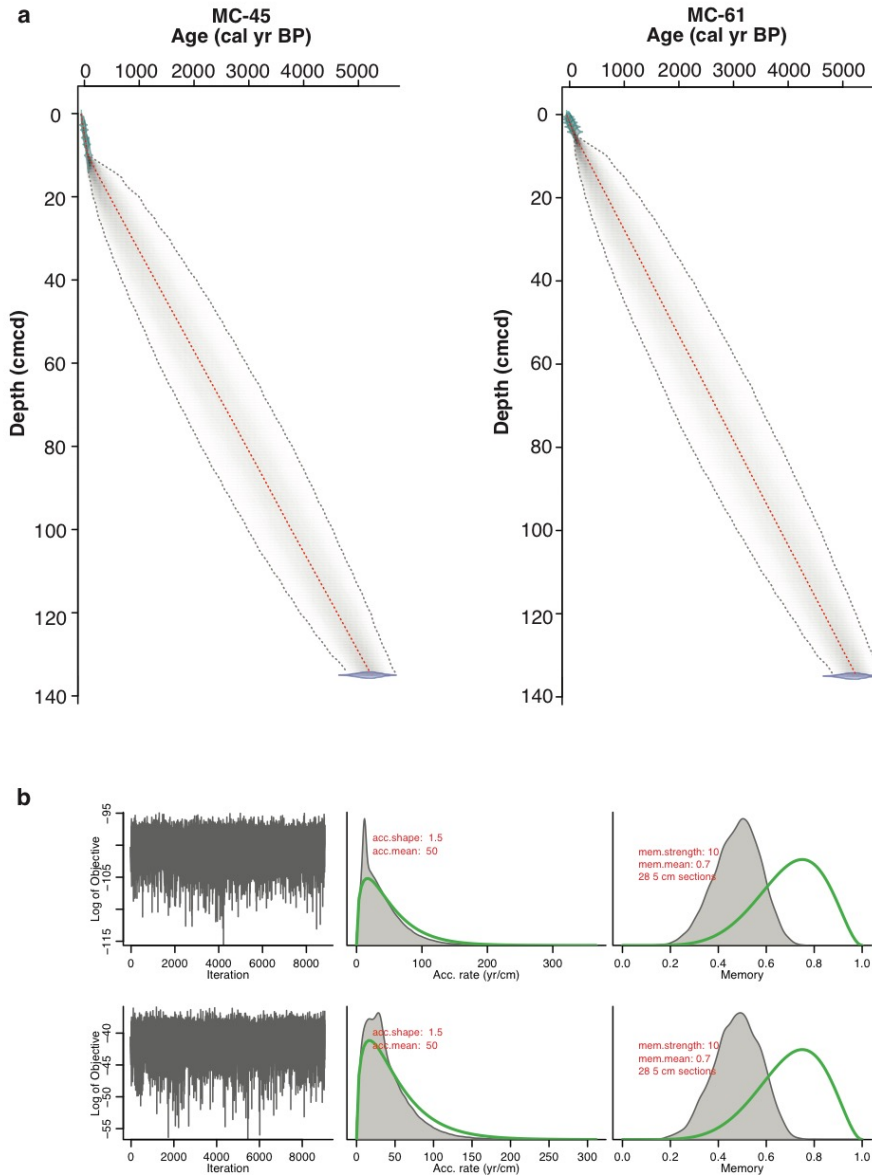


Figure 3.5 (a) Calendar age-depth model derived using Bacon 2.3 software (Blaauw & Christen, 2011). Including ^{210}Pb modeling and calibrated reservoir corrected Ramped PyrOx AIOM ^{14}C date at 135 cmcd. Red dotted line is the weighted mean average age and gray dotted lines indicate the 95% confidence interval. (b) Prior information for plotted age models (top: MC-45; bottom: MC-61). Left panels depicts the Markov chain Monte Carlo (MCMC) iterations. The middle panels depict the prior (green curves) and posterior (grey histograms) distributions for the accumulation rate, and the right panels depicts the prior and posterior distributions for memory.

of the megacores does not indicate a disruption in sedimentation, as both profiles decrease exponentially to a constant supported activity. Because the megacores were extruded and sampled vertically, there are not traditional photographs or x-radiographs of the length of the cores to better observe structures. These resources would aid in determining event sedimentation within the megacores in future analyses. When inspecting the lithology between 30 cm and 135 cmcd, the first laminated and massive diatom oozes occur only deeper in the cores sequence (35-40, 48-50, 67-75, 87-94, and 130-132 cmcd).

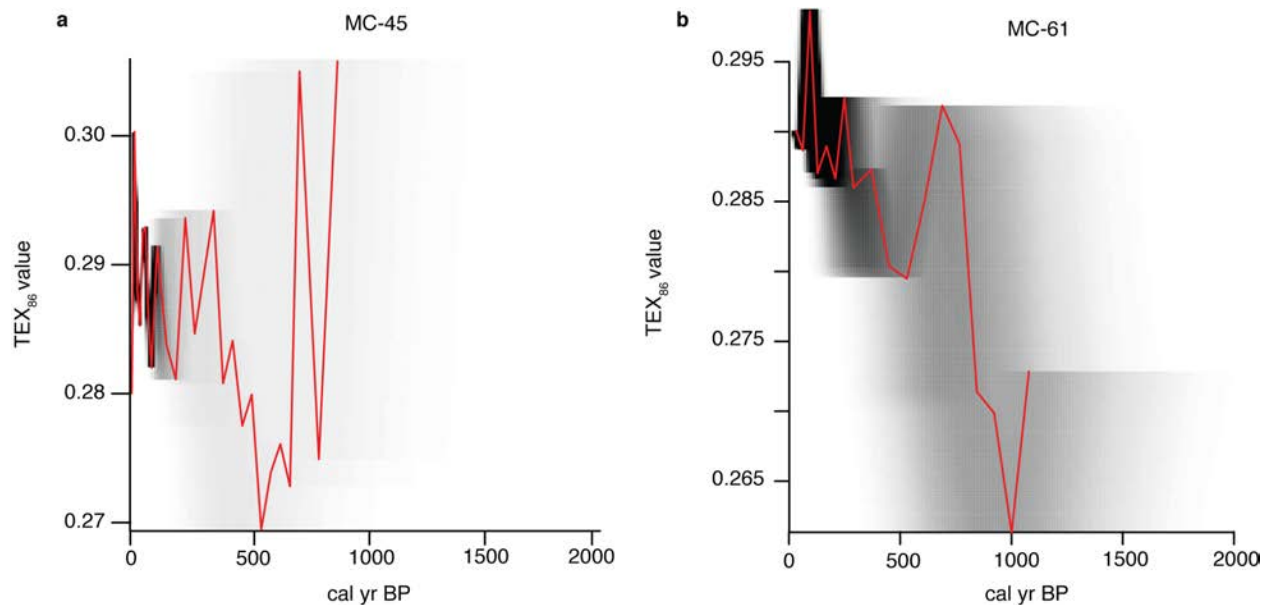


Figure 3.6 Proxy ghost plots with (a) MC-45 and (b) MC-61 TEX_{86} data. This exercise demonstrates that the age model is more robust in MC-61 because ^{210}Pb regression better aligns with the ^{14}C date at 135 cmcd. Shaded zones indicate uncertainty in time on the x-axis and red lines are median TEX_{86} value.

3.5.2 TEX_{86} -derived upper ocean temperatures

TEX_{86} values were converted to temperature using the Shevenell et al. (2011) calibration that is established in Antarctic sediments and produces realistic temperatures for the region ($TEX_{86}=0.0125*T+0.3038$). Shevenell et al. (2011) uses the global core top data set from Kim et

al., 2010 (n=223) with seven additional samples from the Anvers Island region. The calibration excludes core-tops from the Red Sea and the Arctic Ocean because these regional calibrations results in TEX₈₆-temperature relationships that diverge from the global linear regression (Pearson and Ingalls, 2013).

Calibrated core-top temperature values, reflective of the most recent upper ocean temperatures, are approximately -1.0 ± 0.49 °C for MC-45 and -1.6 ± 0.46 °C for MC-61. Errors of the core-top temperatures reflect the measurement uncertainty of replicate samples. The range of TEX₈₆-derived upper ocean temperatures in MC-45 is -2.8 to 0.5 °C and -3 to -0.5 °C in MC-61 (Figure 3.7) with a mean of -1.1 °C (n=41). Temperatures increase up-core in both MC-45 and MC-61 (Figure 3.7). When applied to the Sabrina Coast shelf sediments, the calibration produces some data points (n=10) below the regional freezing point of -1.8 °C (Silvano et al., 2016). However, we chose to include these points in our reconstruction as they are within calibration error (± 2.2 °C) of observed temperatures.

To evaluate how well the core top values from NBP14-02 align with existing calibrations, MC-45 and MC-61 core top values are plotted with published Antarctic TEX₈₆ values from Shevenell et al. (2011) and the global core top dataset (Tierney & Tingley, 2015). When added to the Antarctic samples, the data points from the Sabrina Coast fall within the global calibration dataset (Figure 3.8). This agreement of the Sabrina Coast surface data with the global dataset demonstrates the applicability of this calibration at our site. Note that the calibration from Shevenell et al. (2011) was utilized for converting TEX₈₆ values to temperature.

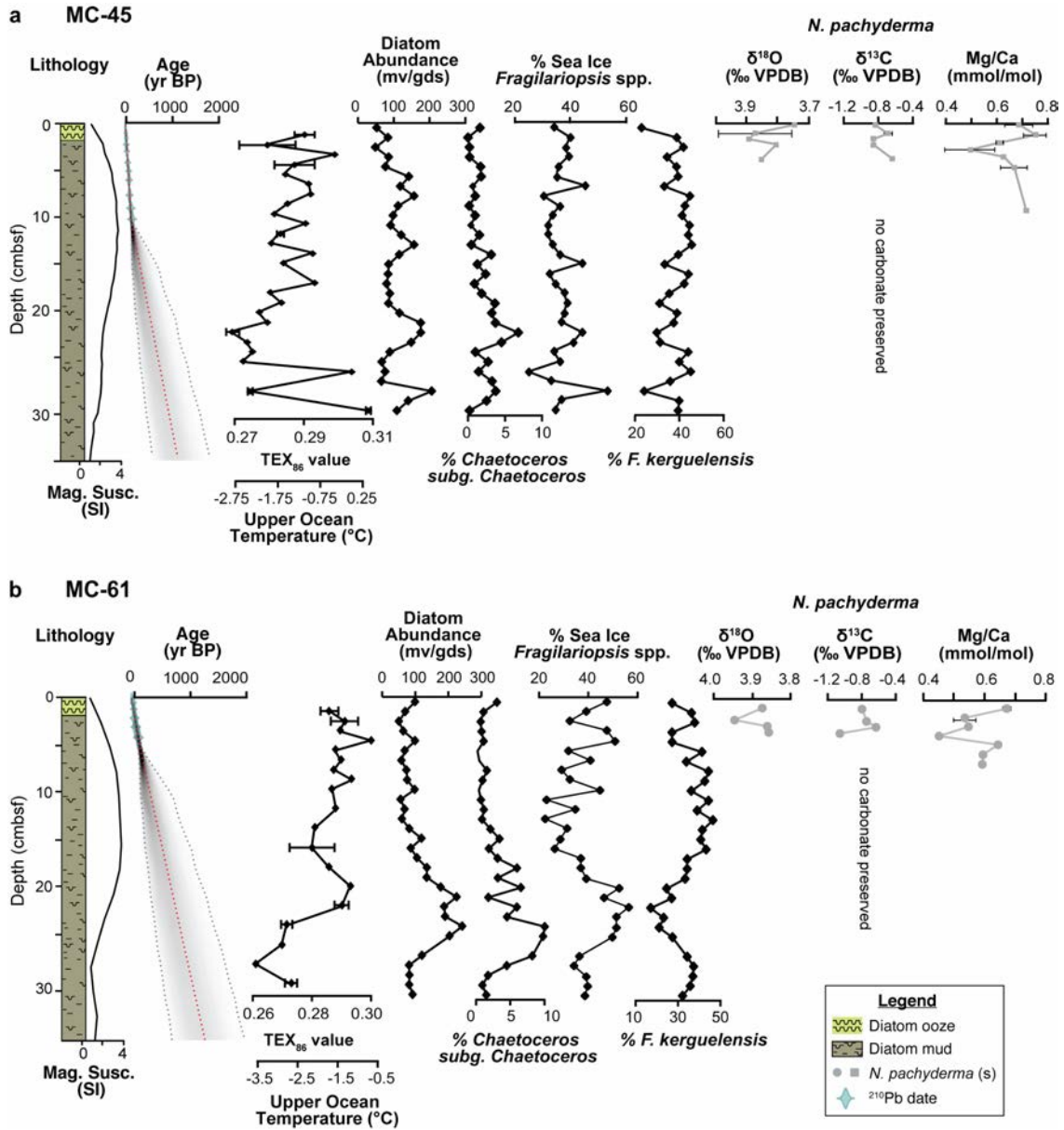


Figure 3.7 NBP14-02 cores (a) MC-45 and (b) MC-61 multiproxy record vs. depth. Graphic lithology, Magnetic Susceptibility, Calendar age-depth model, TEX_{86} values and calibrated upper ocean temperature ($^{\circ}C$), diatom abundance and species assemblage, and *N. pachyderma* (s) stable isotopes and Mg/Ca versus depth (centimeters below seafloor; cmbsf). Age-depth model is based on ^{210}Pb ages and calibrated reservoir corrected Ramped PyrOx AIOM ^{14}C date (see Figure 5). For TEX_{86} values, stable isotopes, and Mg/Ca values, error bars indicate the standard deviation of replicates.

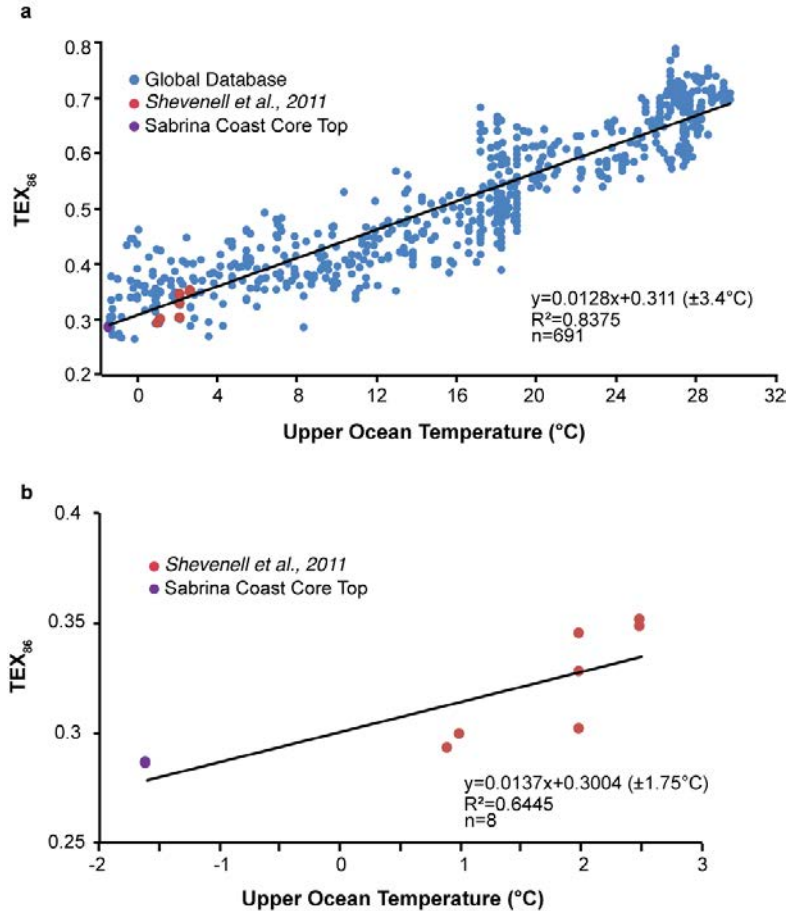


Figure 3.8 Comparison of global and Antarctic TEX₈₆ calibrations. (a) A TEX₈₆-temperature calibration that incorporates 691 core top samples from the TEX₈₆ database (Tierney & Tingley, 2015), seven samples from Shevenell et al., 2011, and two from the Sabrina Coast, East Antarctica (NBP 14-02). When added to the Antarctic samples (b), MC-45 and MC-61 data points from the Sabrina Coast falls on the global calibration. Note that the calibration from Shevenell et al., 2011 was utilized for converting TEX values to temperature for the figures in this chapter. This agreement demonstrates the applicability of the new data points on the global calibration.

3.5.3 *N. pachyderma* (s) stable isotopes

Planktic foraminifer species, *N. pachyderma* (s), is present (1-10 tests/cc of sediment) in MC-45 and MC-61 core tops from 0 to 10 cmbsf. Below 10 cmbsf in both megacores, foraminifers are absent or only present in trace amounts (<1 test/cc sediment; Figure 3.7). We applied species-specific offsets to *N. pachyderma* (s) to account for vital effects. The $\delta^{13}\text{C}$ values have been adjusted by +1.0‰ and the $\delta^{18}\text{O}$ values have been adjusted by +0.6‰ (Mortyn &

Charles, 2003; Hendry et al., 2009). In the upper 5 cm of MC-45 and MC-61, planktic foraminifer $\delta^{18}\text{O}$ exhibits more negative values up-section, while planktic $\delta^{13}\text{C}$ do not exhibit a clear trend (Figure 7). *Neogloboquadrina pachyderma* (s) $\delta^{18}\text{O}$ values range from 4.3‰ to 4.5‰ (mean=4.4±0.06‰) and $\delta^{13}\text{C}$ values range from 1.8‰ to 2.1‰ (mean=2.0±0.1‰).

3.5.4 *N. pachyderma* (s) trace metals

In the upper 10 cm of MC-45 and MC-61, *N. pachyderma* Mg/Ca values increase up-core from 0.4 to 0.7±0.04 mmol/mol (14 samples, replicates n=7). For paleotemperature estimates, *N. pachyderma* (s) Mg/Ca ratios were converted temperature using Vazquez Riveiros et al. (2016) equation $\text{Mg/Ca} = 0.58 \exp(0.08 \cdot T)$, $R^2=0.70$ (Figure 9a). This calibration incorporates data from high-latitude *N. pachyderma* studies (Elderfield & Ganssen, 2000; Nürnberg, 1995), and is valid from -1 to 9°C (1 σ calibration error=±0.9°C). The calibration excludes cores collected close to the sea ice edge, because when *N. pachyderma* (s) from sites close to the sea ice edge are included, the Mg/Ca correlation with temperature weakens ($R^2=0.35$), suggesting that salinity changes associated with either sea ice melt or *N. pachyderma* habitats within sea ice brine channels impacts foraminifer Mg/Ca (Hendry et al., 2009). Using the Vazquez Riveiros et al. (2016) calibration, *N. pachyderma* (s) values show an up-core increase in temperature from -2 to 2°C over the length of MC-45 and MC-61 (Figure 3.7). The average analytical error from replicate measurements is ±0.91°C, which is very close to the ±0.9°C calibration error.

When plotting NBP14-02 *N. pachyderma* (s) within the Vazquez Riveiros et al. (2016) calibration, MC-45 and MC-61 samples fall at the cold end of the calibration. Measured surface water temperature at the core sites are -1.6 to -1.7°C, (Figure 3.9). The addition of the Sabrina Coast data points to the calibration do not improve the correlation (Figure 3.9). This highlights

the difficulty of improving the cold end of the calibration, and may suggest that Sabrina Coast *N. pachyderma* (s) are subject to habitat and vital effect impacts similar to the excluded cores collected close to the sea ice edge in Vazquez Riveiros et al. (2016).

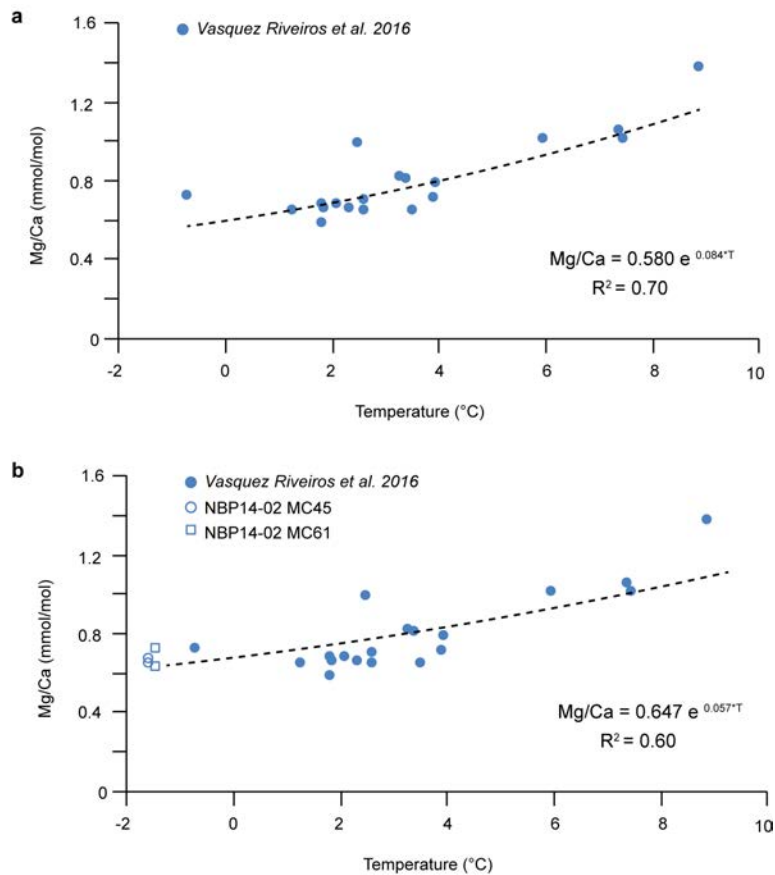


Figure 3.9 *N. pachyderma* (s) Mg/Ca calibration lines. (a) The original Mg/Ca-temperature calibration from Vazquez Riveiros et al. 2016 for *N. pachyderma* (s), between -1 and 9°C. (b) The Vazquez Riveiros et al. 2016 dataset from (a), plotted with NBP14-02 data points for MC-45 (open circles) and MC-61 (open squares).

3.5.5 Diatom assemblages

Total diatom abundance varies from 50 to 240 million valves per gram of dry sediment (mv/gds; Figure 3.7). In MC-45 and the upper 15 cm of MC-61, the system was dominated by *F. kerguelensis* (30-50%). In this same interval, sea ice indicator *Fragilariopsis* species are lower in

abundance (15-35%), and there are few mat-associated diatom species such as *Chaetoceros* subg. *Chaetoceros* (0-8%; Figure 3.7). In MC-61 from 15-30 cm, sea-associated (25-57%) and mat-associated diatoms (2-10 %) are relatively more abundant and there is a distinct drop in *F. kerguelensis* abundance (15-40%), concurrent with a general increase in total diatom abundance (Figure 3.7).

3.6 Discussion

3.6.1 Proxy validation over the 20th-21st centuries

Core top values of temperatures based on TEX₈₆ and Mg/Ca paleothermometry allow us to assess consistency between proxy reconstructions and measured ocean temperatures. In Sabrina Coast core top sediment (Figure 10), the TEX₈₆-derived temperature is $-1.01 \pm 0.49^\circ\text{C}$, which is consistent with the measured ocean temperatures in the upper 200 m taken during NBP14-02 CTD casts (-1.6 to -1.7°C). The core top temperatures successfully approximate the measured upper ocean temperature from CTD casts within the $\pm 2.2^\circ\text{C}$ calibration error (Shevenell et al., 2011). Furthermore, down-core trends in TEX₈₆ values vary similarly with instrumental air temperatures from Casey Station over the past 60 years (Masson-Delmotte et al., 2003), and air temperatures based on $\delta^{18}\text{O}$ from the Dome Summit South (DSS) ice core (Plummer et al., 2012), which demonstrate a net increase in temperature since 1960 (Figure 3.10). The similar trends in atmospheric and upper ocean temperatures lends confidence to TEX₈₆ as a reliable temperature proxy, within current calibration constraints.

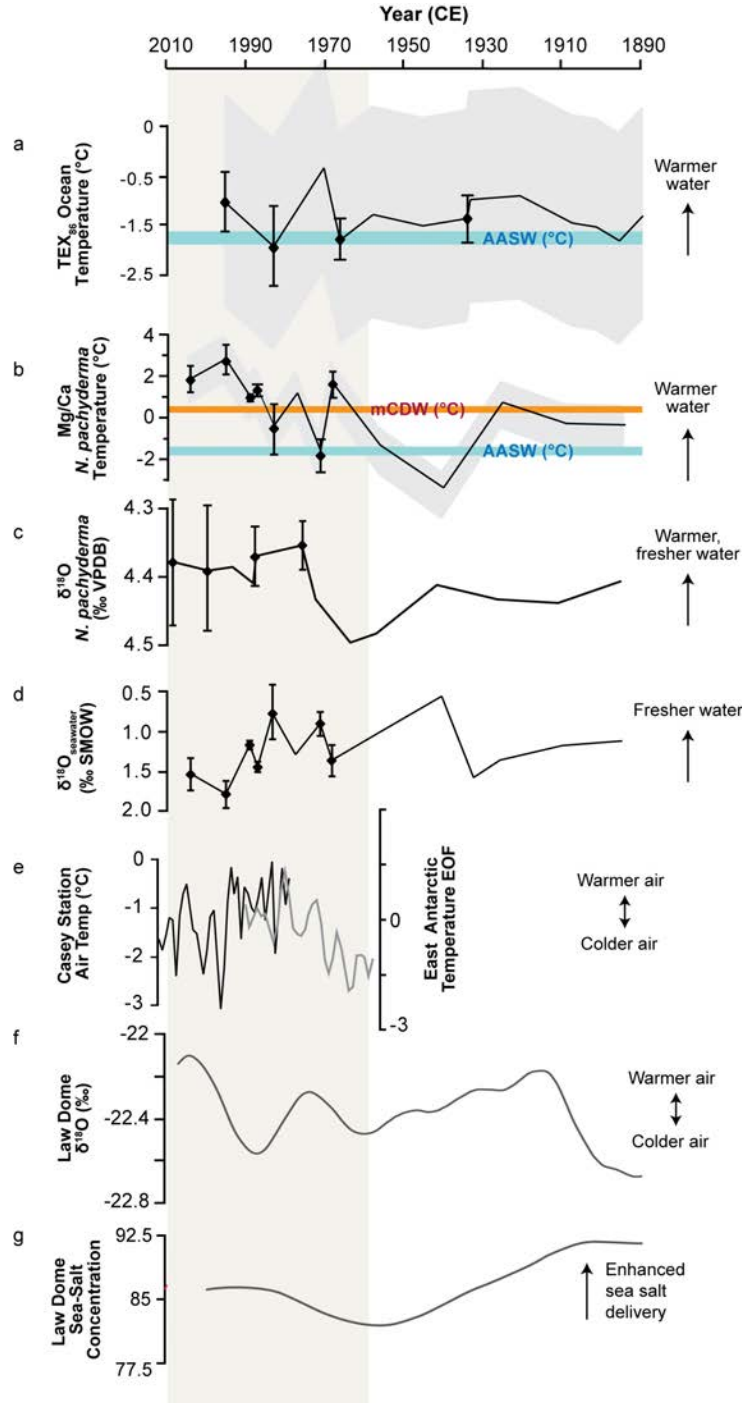


Figure 3.10 MC-45 and MC-61 data for the past 120 years. (a) TEX_{86} -based upper ocean temperatures; error bars represent standard deviation of replicates and grey shading indicates 2.2°C calibration error. (b) *N. pachyderma* (s) Mg/Ca-based temperatures; error bars represent standard deviation of replicates and grey shading indicates 0.9°C calibration error. (c) $\delta^{18}\text{O}$ of *N. pachyderma* (s). (d) Calculated $\delta^{18}\text{O}$ of seawater. (e) Casey Station temperature (black line; Miles et al., 2016) with East Antarctic stations air temperature EOF (grey line; Masson-Delmotte et al., 2003). (f) Law Dome DSS $\delta^{18}\text{O}$ (Plummer et al., 2012). (g) the record of sea salt delivery to Law Dome (Souney et al., 2002). An increase in warm and/or fresh water on the shelf occurs starting at approximately 1950. Modern-day mCDW temperature indicated by red bar (0.3 to 0.5°C) and modern Antarctic Surface Water (AASW; -1.6 to -1.7°C) indicated by blue bar.

The calibrated core-top Mg/Ca-temperature of $1.79 \pm 0.7^\circ\text{C}$ exceeds the present day measured surface water values of -1.6 to -1.7°C . The core top Mg/Ca-temperatures also falls outside of the $\pm 0.9^\circ\text{C}$ calibration error (Vazquez Riveiros et al. 2016). Though the core top Mg/Ca-temperature is elevated compared to current observed surface temperatures, the Sabrina Coast calibrated temperatures falls within the range of Antarctic Surface Water and mCDW deeper in the core (Figure 3.10b). This proxy may be impacted by effects not related to calcification temperature, including salinity and carbonate ion concentration. The role of sea ice in *N. pachyderma* (s) calcification is described by Hendry et al., 2009, where the species is observed high concentrations at the ice-water interface. Uptake of Mg in *N. pachyderma* (s) is likely impacted by the concentration of carbonate ions ($[\text{CO}_3^{2-}]$) at the ice-water interface and salinity differences between the sea ice and surface ocean (Hendry et al., 2009). However, evaluating the carbonate ion effect is outside the scope of this project and future assessment of indicators, such as foraminifer Li/Ca (Lear et al., 2010) is required for Mg/Ca evaluation.

The salinity of the surface ocean impacts Mg/Ca uptake, which can lead to underestimation or overestimation of ocean temperatures. Glacial and sea ice meltwater impact salinity by freshening the surface ocean, which can lower Mg/Ca values, whereas more saline waters have the opposite effect, resulting in overestimation of ocean temperatures (Arbuszewski et al., 2010; Hönisch et al., 2013; Lea et al., 1999). Salinity were made by calculating $\delta^{18}\text{O}_{\text{seawater}}$ values from Mg/Ca calcification temperature values and $\delta^{18}\text{O}_{\text{calcite}}$ values using the equation of Mashiotta et al. (1999) as follows: $\delta^{18}\text{O}_{\text{seawater}} = (\delta^{18}\text{O}_{\text{calcite}} + 0.27) - 4.38 - \sqrt{(4.38 - 4 * 0.1 * 16.9 - \text{Temp}) / (2 * 0.1)}$. The $\delta^{18}\text{O}$ values of *N. pachyderma* exhibit a warming and/or freshening trend from ~1950 to 2010, which varies similarly with warming surface ocean temperatures derived from *N. pachyderma* Mg/Ca over the same period (Figure 10). Through the $\delta^{18}\text{O}_{\text{seawater}}$

calculation, we can deconvolve that salinity did not vary significantly over the 120-year period (Figure 3.10d; $t > 0.05$). The lack of variation in $\delta^{18}\text{O}_{\text{seawater}}$ at the same time as the increase in Mg/Ca temperature suggests that ocean warming, rather than changes in salinity, are responsible for the trend in $\delta^{18}\text{O}_{\text{calcite}}$ over the 120-year period (Figure 3.10e). In context to regional records, Mg/Ca-temperatures vary similarly compared with instrumental air temperatures from Casey Station (Masson-Delmotte et al., 2003) and air temperatures based on $\delta^{18}\text{O}$ from the Dome Summit South (DSS) ice core (Plummer et al., 2012). Although further assessment of Mg/Ca-paleotemperatures are required, the ocean-ice core similarities suggest that the ocean temperature proxies are working and provide the first indications that oceanographic processes on the shelf are likely to impact the Sabrina Coast outlet glaciers.

3.6.2 Late Holocene paleoceanographic variability

We use our multiproxy record from the Sabrina Coast to reconstruct oceanographic changes over the past ~1000 years (Figure 3.11). We rely on a combination of TEX₈₆-based ocean temperatures and diatom assemblages to gain insight into the surface ocean to deep water structure at our study sites. Absolute diatom abundance and magnetic susceptibility are indicators of changes in diatom productivity (Armand et al., 2005; Leventer et al., 1998, 2002; Sjunneskog and Taylor, 2002). We use the relative abundance of diatom species to provide insight into the influence of offshore open ocean water masses (*F. kerguelensis*), changes in water column stratification (*Chaetoceros* subg. *Chaetoceros*), and sea ice presence (sea ice-associated *Fragilariopsis* spp.) (Armand et al., 2005, 2008; Kemp & Villareal, 2013; Leventer et al., 2002).

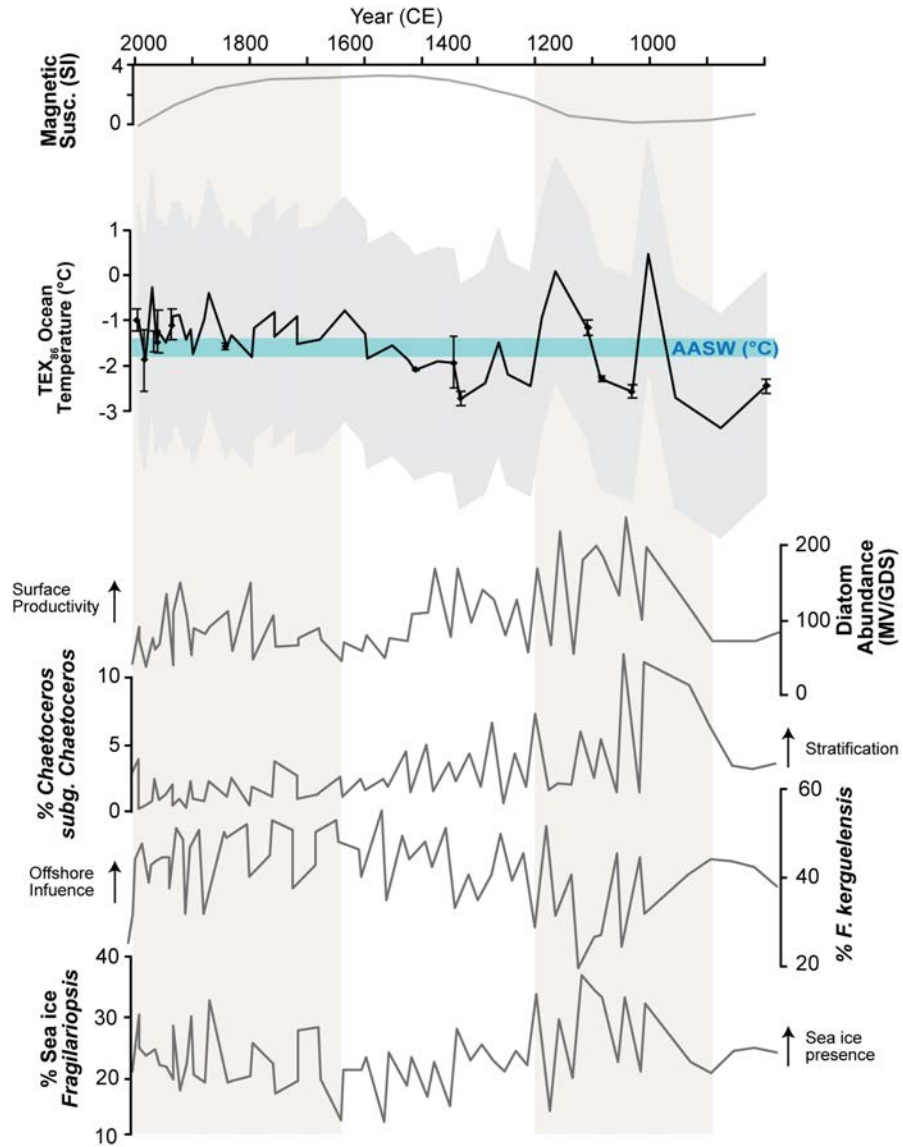


Figure 3.11 A composite of MC-45 and MC-61 multiproxy records vs. age. Primary axis shows 950-year record of magnetic susceptibility, TEX₈₆-derived upper ocean temperatures, total diatom abundance, and relative abundance of stratification indicator *Chaetoceros* subg. *Chaetoceros*, Antarctic Circumpolar Current (ACC)-associated *F. kerguelensis*, and sea ice-associated *Fragilariopsis* spp. TEX₈₆ error bars represent standard deviation of replicates and grey shading indicates calibration error. Modern-day Antarctic Surface Water (AASW; -1.6 to -1.7°C) indicated by blue bar. Alternating shaded zones denote time slices described in discussion (1000 to 1300 CE, 1300 to 1650 CE, 1650 CE to present).

Based on our proxy reconstruction, we identify three time periods with notable trends across the record: from ~1000 to 1300 CE, ~1300 to 1650 CE, and ~1650 CE to present. We qualify that due to the uncertainty in the age model below ^{210}Pb , the temporal aspects of the following inferences is tentative. Across the 1000-year-long record, TEX₈₆-based ocean temperatures and diatom data indicate a system dominated by sea ice melt and high stratification before 1300 CE, shifting to one more greatly influenced by the Antarctic Circumpolar Current after 1300 CE. From ~1000 to 1400 CE (Figure 3.11), TEX₈₆-derived ocean temperatures increase from -3 to 0.5°C while diatoms increase in absolute abundance, suggesting productive upper ocean conditions. There is a peak in water column stratification indicated by *Chaetoceros* group diatoms, while sea-ice associated *Fragilariopsis* spp. increase in abundance and offshore influence, and declining sea ice presence. From ~1400 to 1650 CE, the TEX₈₆ data record a ~0.75°C decrease in upper ocean temperature (Figure 3.11). Over this period, the diatom data indicate declining diatom abundance, a decline in stratification, an increase in offshore influence, and declining sea ice presence. From ~1650 CE to present, a 1°C increase in surface ocean temperatures is coincident with an increase in diatoms associated with offshore influence (Figure 11).

What climatic processes might be driving the ocean warming, sea ice decline, decreased stratification, and offshore influence since 1000 CE along the Sabrina Coast shelf? The record of ocean warming, sea ice decline, and decreased stratification on the Sabrina Coast may result from increased wind influence, as observed elsewhere on the Antarctic margin (Hillenbrand et al., 2017). A critical aspect of the Sabrina Coast oceanography is the influence of the Dalton Polynya, which links atmospheric processes to physical oceanography. For example, open water

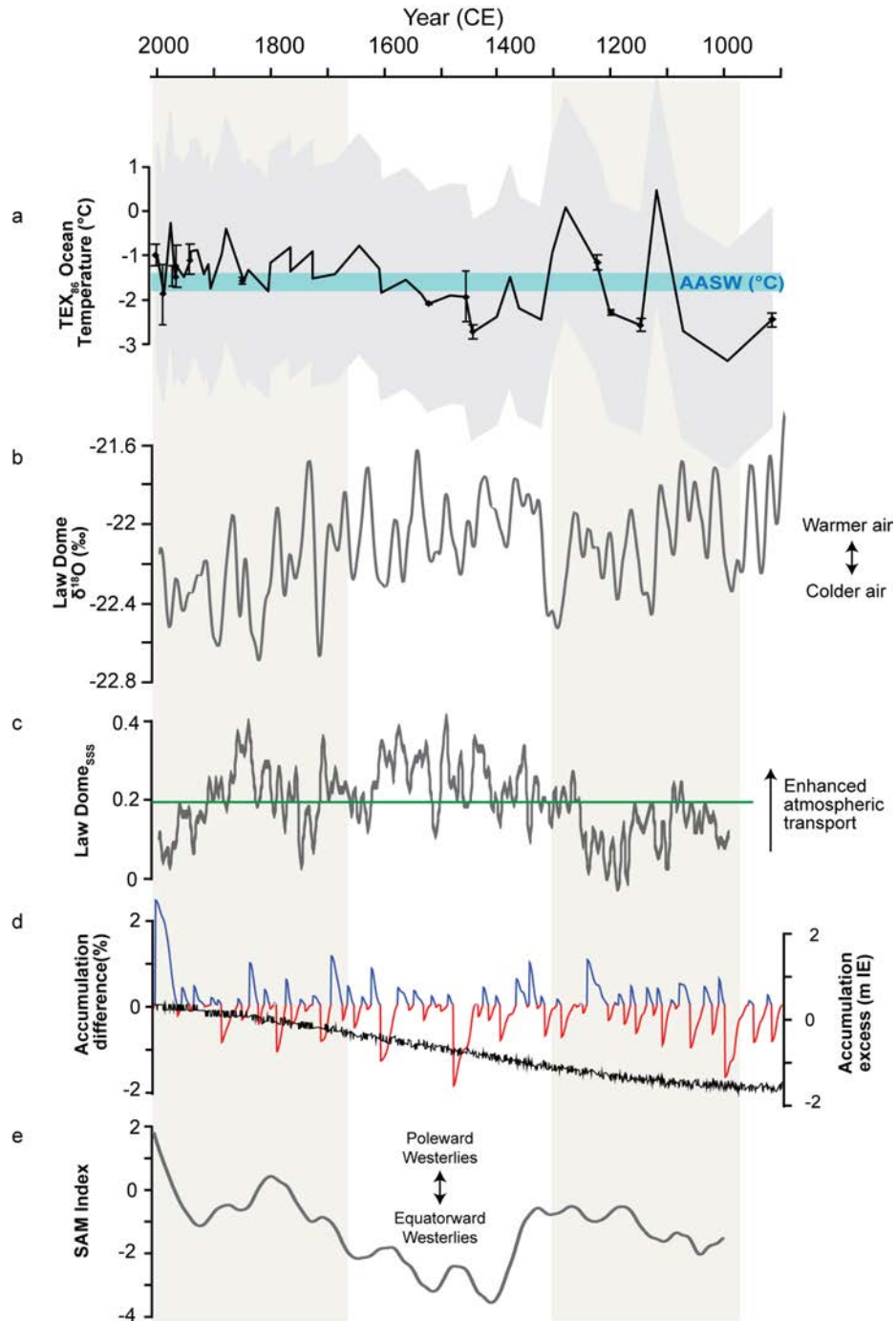


Figure 3.12 Sabrina Coast TEX₈₆ records vs. regional proxy records. (a) Sabrina Coast TEX₈₆-based paleotemperatures plotted with records of regional climate variability. TEX₈₆ error bars represent standard deviation of replicates and grey shading indicates calibration error. Modern-day Antarctic Surface Water (AASW; -1.6 to -1.7°C) indicated by blue bar. (b) Law Dome DSS δ¹⁸O (Plummer et al., 2012); (c) Record of Law Dome summer sea salt. The solid black line is a 10-year Gaussian smooth of the annual data with green line showing mean value (Vance et al., 2013); (d) Law Dome accumulation difference and accumulation excess (Roberts et al., 2015); and (e) a reconstruction of the Southern Annular Mode (SAM) from Abram et al., (2014) plotted as 70 yr loess filter.

conditions may be created by katabatic winds flowing offshore, opening the polynya, and pushing sea ice out (Massom et al., 1998; Moreau et al., 2019; Tamura et al., 2016).

The oceanographic conditions (such as sea ice cover, upwelling, and stratification) of the Australian sector of the Antarctic margin is influenced by regional atmospheric changes including the position of the southern hemisphere westerly winds (Masson-Delmotte et al., 2003; Vance et al., 2013), which transport warm, moist air from the north toward the Sabrina Coast when the westerlies are stronger (Roberts et al., 2015; Vance et al., 2013). Due to their coastal location, Law Dome ice cores provide an archive of Southern Ocean climate variability (Roberts et al., 2015), at time scales ranging from the last century (Morgan et al. 1985; Morgan et al. 1997) to 1000 CE. Comparison between our ocean temperature record and the Southern Annular Mode (SAM), over the interval from 1000 CE to present, reveals that the poleward position of the westerlies may have driven upper ocean warming on the Sabrina Coast (Figure 3.12; Abram et al., 2014). This is corroborated by an increase in sea salt concentration at Law Dome (Figure 3.12; Souney et al., 2002), which varies similarly with changes in the SAM index (Abram et al., 2014).

Over the past 1000 years, the overall trend in SAM has shifted toward a positive phase associated with intensified or southerly-shifted westerly winds (Figure 3.12; Abram et al., 2014). This is important because if the warming ocean temperature trend in the Sabrina Coast TEX₈₆ data persists, and if the westerlies remain in a positive mode, then we suggest that Sabrina Coast warming and ice mass loss will continue, driven by poleward shifting westerlies under high atmospheric CO₂ (Figure 3.12; MacFarling-Meure et al., 2006). This interpretation is supported by present day observations of surface melt and glacial retreat along the Sabrina Coast, which demonstrate that modern rates of ice sheet thinning are accelerating (Pritchard et al., 2012,

Rignot et al., 2013). This is also consistent with the increase in glacier discharge recorded in East Antarctic records (Crespin et al., 2014) and records of increased offshore influence in the Amundsen Sea, Adélie Land, and the Antarctic Peninsula during the 20th Century (Christ et al., 2015; King et al., 2018; Hillenbrand et al., 2017).

Identifying similarities between Law Dome records with Sabrina Coast upper ocean temperatures over the past century is important for understanding atmospheric and oceanographic processes impacting this sector of the Antarctic Margin. On the Sabrina Coast, Law Dome ice cores document increasing snow accumulation over the past century (Masson-Delmotte et al., 2003; Roberts et al., 2015) caused by meridional transport of warmer, northern air masses (Souney et al., 2002; Vance et al., 2013). Atmospheric circulation change is indicated by increased accumulation rates in Law Dome since 1900 CE, associated with changes in moisture delivery to the region (Roberts et al., 2015; Vance et al., 2013). This pattern of 20th Century change on the Sabrina Coast suggests a link to climatic variability from lower latitudes (Abram et al., 2014; Li, 2000; Saunders et al., 2018).

The TEX₈₆, diatom, and foraminifer proxy reconstructions allow us to assess utility of upper ocean temperature proxies and provide high resolution information on the upper ocean temperature and water column processes on the Sabrina Coast shelf for the past ~1000 years. Our record demonstrates that TEX₈₆ records variations in upper ocean temperatures are within realistic temperatures (not below the local freezing point of water: -1.8°C). Although the past century accounts for a small part (~0.5 °C) of the temperature increase in the TEX₈₆ record, Mg/Ca of planktic foraminifera exhibit a ~4°C warming. The weak but significant 1000-year warming trend ($R^2=0.2$, $t < 0.05$) observed in this study is similar to conditions observed in the early to mid-Holocene when regional temperatures were warmer than today, ice shelves

retreated, the westerlies shifted poleward, and atmospheric CO₂ rose towards pre-industrial levels (Abram et al., 2014; MacFarling-Meure et al., 2006; McGlone et al., 2010; Moreno et al., 2010; Shevenell et al., 2011). We can improve our understanding of the timing and drivers of paleoceanographic and environmental offshore the Sabrina Coast and the response of East Antarctic margin outlet systems if we continue to improve the age model in the cores presented, and if we expand the spatial resolution of marine sediment collected across the shelf and slope.

CHAPTER FOUR:
DEGLACIAL TO HOLOCENE OCEAN TEMPERATURE VARIABILITY ON THE
SABRINA COAST SHELF, EAST ANTARCTICA

4.1 Chapter Contributions

Kara J. Vadman wrote this chapter and created all figures, prepared and analyzed ^{210}Pb samples, prepared all carbonate ^{14}C samples, and seven of eight bulk sediment samples via Ramped PyrOx/dirt burner for radiocarbon analyses, generated the Bacon age model, extracted and analyzed samples for TEX_{86} measurements, and prepared and analyzed foraminifer stable isotopes and trace metals. Sortable silt data was prepared and analyzed by K. J. Vadman and R. Rivera. Data analysis resources for sortable silt measurements were provided by J. M. Jaeger. A. Leventer generated all diatom data. T. M. King prepared one Ramped PyrOx sample.

4.2 Abstract

Data to constrain the past influence of ocean temperature on the Sabrina Coast shelf is required to understand the role of warm water on marine-terminating outlet systems. In order to identify the magnitude and timing of ocean warming over the Sabrina Coast shelf, we present the first reconstruction of upper ocean and deep water temperatures from the deglacial (16,500 years before present) through the Holocene using two ocean temperature proxies, TEX_{86} and foraminifer Mg/Ca , in ice-proximal, Antarctic continental margin sediments. We show that surface ocean temperatures on the middle continental shelf cooled by $\sim 2^\circ\text{C}$ over the past 16,500

years towards present, with millennial-scale fluctuations of 1-2°C superimposed (calibration error: ± 2.2 °C). We also present deep-water temperatures derived from Mg/Ca of benthic foraminifer *Trifarina angulosa*, which show warmer temperatures in the middle Holocene than present day. We then compare ocean temperature reconstructions at our site with the record of sortable silt, to interpret whether bottom water currents were active. Together, the temperature and sortable silt reconstruction provide insight into potential source of warm water, which can be compared to records of southern hemisphere westerly wind patterns, to evaluate presence of teleconnections between the sub-Antarctic and Sabrina Coast region.

4.3 Introduction

The Aurora Subglacial Basin (ASB) is an extensive, sparsely observed, marine-based glacial catchment that drains one eighth of the interior of the East Antarctic Ice Sheet (EAIS; equivalent to ~ 5 m of sea level) via the Totten Glacier outlet system (Aitken et al., 2016; Greenbaum et al., 2015; Morlighem et al., 2020; Young et al., 2011). The Totten Glacier accelerates when easterly winds are strengthened or westerly winds are weakened (Greene et al., 2017). The glacier speed increased by $\sim 10\%$, corresponding to a 1 to 3 km grounding line retreat over a 26-year period (1988-2014; Li et al., 2015). Regional glacial grounding lines are susceptible to ocean warmth from intermediate waters (>500 m) of the Southern Ocean because a deep cross-shelf trough allows warm, nutrient-rich, modified Circumpolar Deep Water (mCDW) to move across the shelf (Aitken et al., 2016; Greenbaum et al., 2015; Rintoul et al., 2016). The warm water access to deep grounding lines results in observed regional glacier thinning and ice mass loss (Li et al., 2015; Mohajerani et al., 2018).

Dynamic ice sheet changes have global significance, but the drivers of Antarctica's ongoing and past ice retreat are poorly understood due to a scarcity of unambiguous paleoclimate records from ice-proximal Antarctic margin locations. Sabrina Coast sediments are ideal for quantitatively investigating the influence of ocean thermal forcing on the regional glacier system through the Holocene because they contain both foraminifer carbonate and organic biomarkers, and the sediments are recovered from a location in the path of current mCDW inflow (Figure 4.1a; Greene et al., 2017; Williams et al., 2011; Rintoul et al., 2016; Silvano et al. 2017). In addition, the study site is located 250 km to the northeast of Law Dome, where deglacial to Holocene atmospheric conditions are archived in ice cores (Morgan et al., 2002; Masson-Delmotte et al., 2003; Van Ommen et al., 2004). The proximity of our study site to Law Dome enables us to compare oceanographic variability documented in sediment cores with atmospheric signals archived in the ice core.

Reconstructing ocean temperatures from Antarctic coastal marine sediments has historically been difficult due to the scarcity of biogenic carbonate. An alternative approach is to employ the TetraEther IndeX of 86 carbon atoms (TEX₈₆ paleothermometry), which utilizes a ratio of membrane lipids from pelagic marine archaea (Huguet et al., 2010; Kim et al., 2008; Schouten et al., 2002), and has been applied to Antarctic sediments over a range of timescales to reconstruct upper ocean temperatures (Etourneau et al., 2013; Hartman et al., 2018; McKay et al., 2012; Shevenell et al., 2011). Here we investigate upper ocean paleotemperature trends on the Sabrina Coast shelf during the Holocene and associated paleoenvironmental conditions based on diatom assemblages that indicate shelf processes and offshore influence (Alley et al., 2018; Crawford, 1995; Smetacek et al., 1997; Villareal et al., 1996). We investigate shelf processes using mean sortable silt, a proxy for bottom current speed in order to test the association of

bottom currents with ocean paleotemperatures and link offshore influence to the ice-proximal continental shelf.

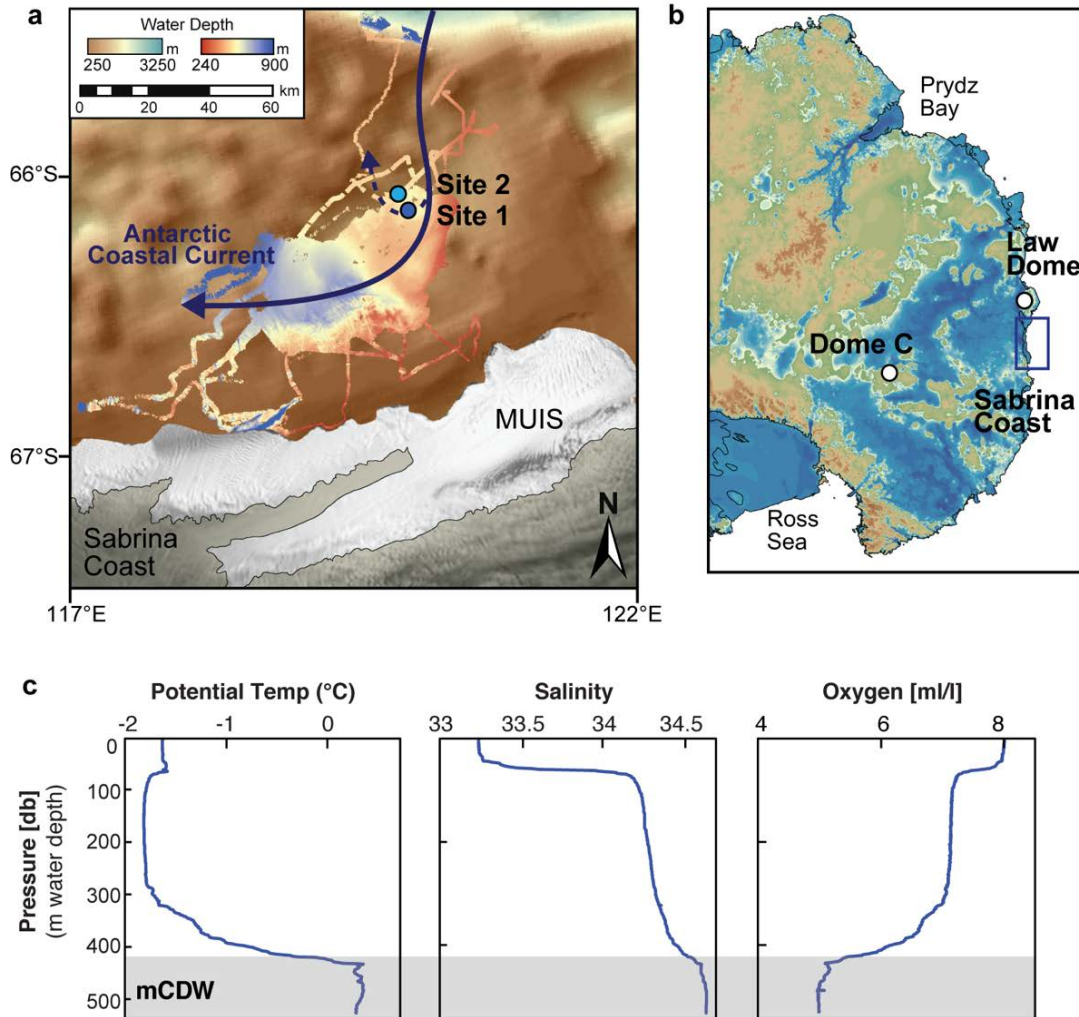


Figure 4.1 Sabrina Coast study location and oceanography. (a) Bathymetry of the Dalton Polynya on the Sabrina Coast continental shelf, East Antarctica (adapted from Gulick, Shevenell et al., 2017) collected during U.S. Antarctic Program cruise NBP14-02 with location of Site 1 marine sediment cores, MC-45, KC-27B, and JPC-27 (547 m water depth; 66°11.06'S, 120°30.15'E) Site 2 core JPC-57 (light blue; 593 m water depth; 66°07.73'S, 120°27.84'E). The Antarctic Coastal Current (blue thick arrow) and local recirculation feature (blue dashed arrow) indicated. MUIS=Moscow University Ice shelf. (b) Subglacial topography of East Antarctica (Fretwell et al., 2013), with the location of the Sabrina Coast indicated by the blue box, and the locations of Law Dome and Dome C (white dots). (c) NBP14-02 CTD-based potential temperature, salinity, and oxygen concentration data from Sites 1 (Leventer et al., 2015). Modified Circumpolar Deep Water (mCDW) is indicated by the gray shading below 400 m.

4.3.1 Sabrina Coast study area

Our study area is located within the Dalton Polynya, a weak polynya with low sea ice production and a lack of dense shelf water formation, which enables mCDW incursion onto the shelf (Silvano et al., 2018; Tamura et al., 2016). Observations and models suggest that shelf intrusions of relatively warm waters result from wind-driven upwelling at the continental shelf break north of the Dalton Iceberg Tongue (Greene et al., 2017). Upwelled mCDW is entrained into the wind-driven westward-flowing Antarctic Coastal Current (Greene et al., 2017; Gwyther et al., 2014; Massom et al., 1998), which transports the warm water onto the middle and inner continental shelf (Greene et al., 2017). Present day physical oceanographic observations from the Sabrina Coast continental shelf show mCDW below 400 m, with the warmest mCDW observed in the trough on the western side of the polynya and steered by regional bathymetry (Rintoul et al. 2016; Silvano et al. 2017; 2019). At both the Totten and Moscow University calving fronts, bottom waters are 1 to 2°C above the local freezing point, resulting in basal melt of these ice shelves at rates (4-10 m/yr) comparable to those observed in the Amundsen Sea, West Antarctica (4-15 m/yr; Depoorter et al., 2013; Rintoul et al., 2016; Silvano et al., 2017; 2018).

4.4 Methods

4.4.1 Sediment sampling, lithology, physical properties, and composite depths

On cruise NBP14-02, cores MC-45, KC-27B, and JPC-27 were recovered at Site 1 and JPC-57 was recovered from Site 2 (Table 4.1) on the middle continental shelf offshore the Sabrina Coast, East Antarctica. Lithologic units and subunits of cores were assigned using both visual core descriptions, x-rays, and magnetic susceptibility variations. General lithologic and magnetic susceptibility similarities between cores allowed us to construct a composite depth

scale for cores from Sites 1 and 2 to address both piston core over-penetration and non-uniform compression. To generate the composite section, we used the lineage function in Analyseries 2.0 software (Paillard et al., 1996) to correlate the magnetic susceptibility records of core JPC-27 to reference cores KC-27B, which recovered an intact sediment water interface. We assume MC-45 was recovered with an intact sediment-water interface, but the core is too short to serve as a reference core. Therefore, we assume the cmbsf values in MC-45 are equal to its depth on the cmcd scale. The Analyseries lineage function allows you to link similar variations between two curves, such as magnetic susceptibility highs or lows, and “stretch and squeeze” one curve in reference to the other record. The KC-27B reference core was 270 cm long, so the remaining lengths of the magnetic susceptibility records in JPC-27, past the end of KC-27B, was adjusted uniformly by 32 cm. The resulting composite record, which includes all cores from Site 1, was then used as the reference record for Site 2, JPC-57 (Figure 4.2b). The magnetic susceptibility records from all cores were normalized to JPC-27 values and plotted versus centimeters composite depth to 1115 cmcd (Figure 4.2b).

Table 4.1 NBP14-02 sediment core locations, water depths, and core lengths.

Site	Core	Latitude	Longitude	Water Depth (m)	Core length (cm)
1	MC-45	66° 11.0069' S	120° 30.0591' E	537	35
	KC-27B	66° 11.0907' S	120° 30.2385' E	547	270
	JPC-27	66° 11.0568' S	120° 30.1483' E	544	1310
2	JPC-57	66° 07.7325' S	120° 27.8407' E	583	875

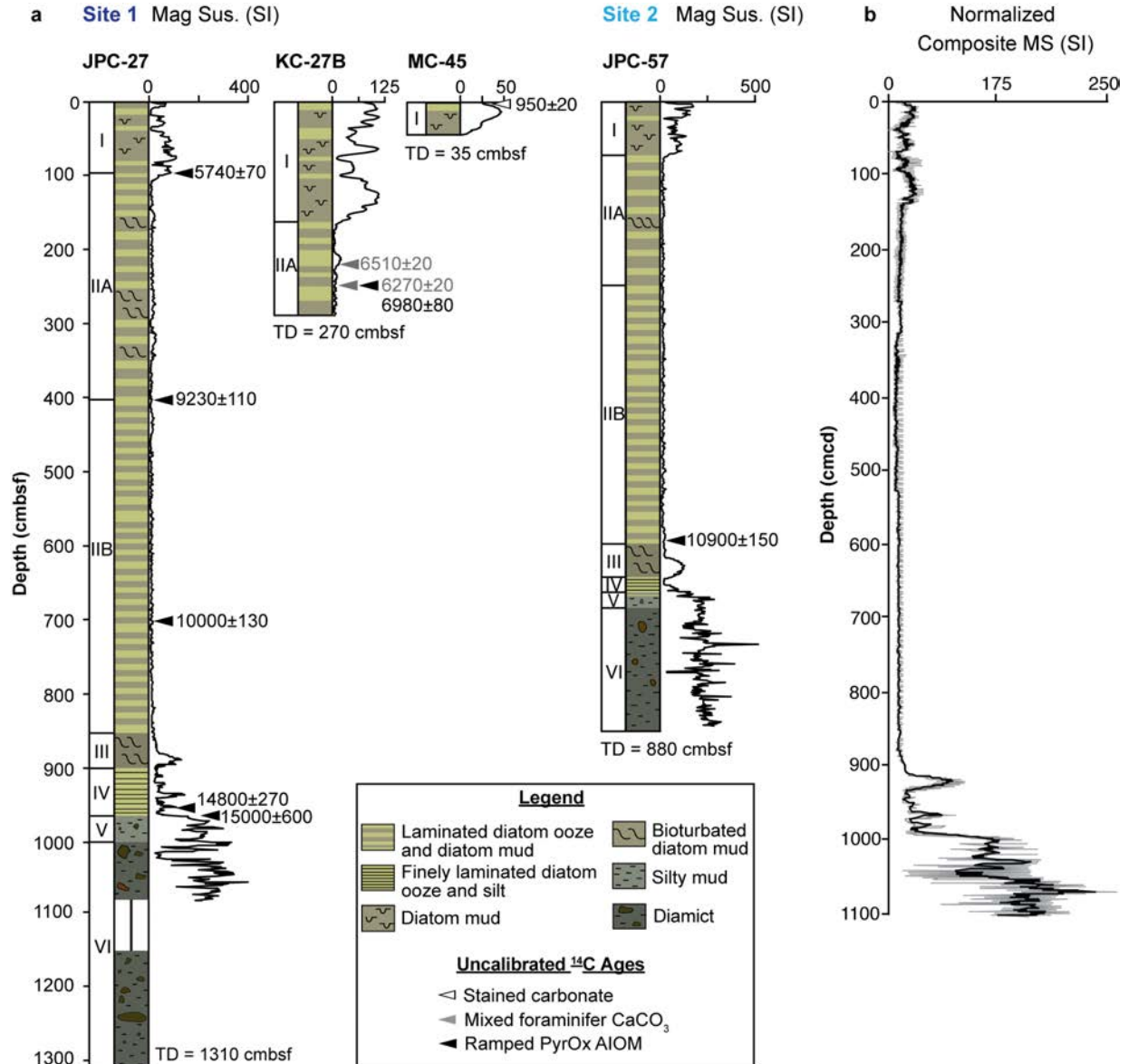


Figure 4.2 Lithology, radiocarbon ages, and composite depth scale. **(a)** Unit lithology, magnetic susceptibility (mag sus., SI), and blank corrected, uncalibrated ¹⁴C dates for Sites 1 and 2 plotted versus centimeters below sea floor (cmbsf). We utilize only one ¹⁴C date in from Site 2 to help constrain the lower boundary of Unit IIB. **(b)** Composite depth scale in centimeters composite depth (cmcd) for the entire sediment sequence.

4.4.2 ²¹⁰Pb and ¹⁴C sample preparation and age model

Age constraints between 0 and 991 cmcd for the composite stack (Figure 4.2) were achieved using a combination of ²¹⁰Pb dating (n=18), mixed foraminifer (n=2) radiocarbon (¹⁴C) dates, and the low temperature aliquot (RPO-1) of acid insoluble organic material (AIOM; n=8).

Measurements of ^{210}Pb were made on 0.5 cm intervals in core MC-45 using a Canberra High-Purity Germanium Coaxial Planar Photon detector and analyzed for total activities of ^{210}Pb (46.5 KeV), ^{214}Pb (295 and 351 KeV), ^{214}Bi (609 KeV), and ^{137}Cs (661 KeV). Supported ^{210}Pb (produced in situ) was estimated by the mean activities of ^{214}Pb and ^{214}Bi . To determine excess ^{210}Pb , supported ^{210}Pb was subtracted from measured ^{210}Pb . The ^{210}Pb age-depth models for each core were generated using the constant flux-constant sedimentation (CFCS) approach (after Wangner et al., 2020). Age-depth profiles were generated from mean sedimentation rates, calculated using a non-linear exponential model fit to excess ^{210}Pb activity (code developed by J.M. Jaeger, published in Wangner et al., 2020). Linear sedimentation rates (cm/yr) are porosity-corrected by using mass accumulation rates (MAR; $\text{g}/\text{cm}^2/\text{yr}$) modeled from a non-linear fit of excess ^{210}Pb (dpm/g) versus cumulative mass depth (g/cm^2) that are then normalized by a constant dry bulk density (g/cm^3) at depth of excess activity profile. This sedimentation rate allows us to determine ages corresponding to the depth in the cores.

For radiocarbon ages, foraminifer CaCO_3 samples were picked, converted to CO_2 , quantified, graphitized, and analyzed for ^{14}C by accelerator mass spectrometry (AMS) at the National Ocean Science Accelerator Mass Spectrometer (NOSAMS) facility in Woods Hole, MA. Bulk AIOM was prepared via the Ramped PyrOx (RPO) technique at USF College of Marine Science (Rosenheim et al., 2008; 2013; Subt et al., 2015). Published Antarctic margin sediment data indicate that the youngest most reactive carbon is trapped in the lowest-temperature CO_2 aliquot (Rosenheim et al., 2008; 2013), so we analyzed the first aliquot of each of each sample (RPO-1) for ^{14}C by AMS at the Lawrence Livermore National Laboratory (LLNL) Center for Accelerator Mass Spectrometry (CAMS). A radiocarbon blank correction was applied to account for modern and dead radiocarbon introduced during processing

(Venturelli et al., 2020; Fernandez et al., 2014; Subt et al., 2016, 2017).

The age model uses Bayesian statistics to model the MC-45 ²¹⁰Pb dates and ¹⁴C dates (Table 4.2). ²¹⁰Pb and calibrated ¹⁴C ages were entered into Bacon 2.3 software (Blaauw & Christen, 2011) to obtain weighted mean sediment age-depth relationships with 95% confidence intervals. The following prior information was used to generate the age-depth model: acc.shape= 1.5; mem.strength= 10; mem.mean= 0.7; boundary (cmcd)=135, 888; acc.mean (y/cm)=50, 10, 50, 20. The prior information inputs allow for modifications of the age model based on

Table 4.2 NBP14-02 R-code inputs for the Bacon-generated age model. Model uses ²¹⁰Pb, and radiocarbon from CaCO₃ and the first aliquot of bulk sediment acid insoluble organic matter (AIOM) prepared via Ramped PyrOx. Sample information is indicated by lab ID, Age (cal yr before 1950), Age error (1-sigma) in years, centimeters composite depth (cmcd), core code for applying the Marine20 calibration to radiocarbon samples, delta R (Reservoir age minus 550 years), and standard deviation of delta R. Negative numbers in Age column denote ²¹⁰Pb dates of samples deposited since 1950.

labID	Age (cal yr before 1950)	Age error	Depth (cmcd)	Core code	delta.R	delta.STD
MC-45 0.5 cm	-58	1	0.5	0	0	0
MC-45 1.25 cm	-49	2	1.25	0	0	0
MC-45 1.75 cm	-43	2	1.75	0	0	0
MC-45 2.25 cm	-37	4	2.25	0	0	0
MC-45 2.75 cm	-31	4	2.75	0	0	0
MC-45 3.25 cm	-25	5	3.25	0	0	0
MC-45 3.75 cm	-19	6	3.75	0	0	0
MC-45 4.25 cm	-13	6	4.25	0	0	0
MC-45 4.75 cm	-7	7	4.75	0	0	0
MC-45 5.25 cm	-1	8	5.25	0	0	0
MC-45 5.75 cm	5	9	5.75	0	0	0
MC-45 6.25 cm	11	10	6.25	0	0	0
MC-45 6.75 cm	17	11	6.75	0	0	0
MC-45 7.25 cm	23	11	7.25	0	0	0
MC-45 7.75 cm	29	12	7.75	0	0	0
MC-45 8.25 cm	35	13	8.25	0	0	0
MC-45 8.75 cm	41	13	8.75	0	0	0
MC-45 9.25 cm	47	15	9.25	0	0	0
JPC27 92-94 cm AIOM	5742	69	135	2	680	100
KC27B 225-228 cm CaCO ₃	6510	20	228.5	2	400	100
KC27B 255-258 cm AIOM	6978	82	258.5	2	680	100
KC27B 255-258 cm CaCO ₃	6270	20	258.5	2	400	100
JPC27 402-404 cm AIOM	9225	111	435	2	680	100
JPC27 702-704 cm AIOM	10008	132	735	2	680	100
JPC57 586-588 cm AIOM	10908	145	882	2	680	100
JPC57 656-658 cm AIOM	13446	206	982	2	680	100
JPC27 953-955 cm AIOM	14780	274	986	2	680	100
JPC27 958-960 cm AIOM	15047	603	991	2	680	100

knowledge of the sedimentology, such as sharp unit transitions and distinct changes in accumulation rate. Prior assumptions include an expected accumulation rate (acc. shape and acc.mean), and how much the accumulation rate may have changed over time (mem. strength and mem.mean). In this age model, we also apply boundaries at 135 and 888 cmcd to indicate transitions in lithologic units where accumulation rates are expected to change.

4.4.3 Lipid biomarker extraction and analysis

To generate TEX₈₆-derived paleotemperatures (Schouten et al., 2002), Glycerol Dialkyl Glycerol Tetraethers (GDGTs) were manually extracted from 124 samples from MC-45, KC-27B, and JPC-27 using High Performance Liquid Chromatography-Mass Spectrometry (HPLC-MS) following published methods (Schouten et al., 2007; Huguet et al., 2010). MC-45 was sampled every 1 cm, KC-27B was sampled every 5 cm, and JPC-27 was sampled every 5, 10, or 20 cm. Freeze-dried homogenized samples were ultrasonified three times each in methanol, methanol:dichloromethane (1:1 v/v), and dichloromethane. Lipid extracts were dried down under a nitrogen stream then brought up in a isopropanol:hexane (1:99 v/v) solution and filtered through a PTFE 0.4 µm filter. GDGT analyses were performed on an Agilent 1200 series High Performance Liquid Chromatographer coupled to a Varian 310 Atmospheric Pressure Chemical Ionization Mass Spectrometer. Samples (50 µL) were injected into a Prevail Cyano column to with a 0.2 mL/min to separate GDGTs. Relative GDGT abundance was quantified by monitoring ion signals 1302, 1300, 1298, 1296, and 1292' compounds and by integrating the area under the signal using the Agilent ChemStation software.

Replicates of 23% of the unknown samples (n=29) were analyzed throughout the study. The average standard deviation of replicate samples was ±0.008 TEX₈₆ units. External and

internal reference materials were monitored with each set of unknown samples to assess consistency; NIOZ sediments from the Royal Institute for Sea Research, Netherlands (Schouten et al., 2013) and an Antarctic Standard (AS-1; TEX_{86} value= 0.28 ± 0.02 for $n=20$ samples over the course of this study) from University of South Florida College of Marine Science (USF CMS). We also monitored several indices to assess NBP14-02 TEX_{86} values for variables such as soil-derived GDGTs (BIT: Branched Isoprenoid Tetraether index; Hopmans et al., 2004), the relative input of methanotrophic archaeal components (Methane Index; Zhang et al., 2011), and non-thermal influences (Ring Index; Zhang et al., 2016).

4.4.4 Foraminifer assemblages and stable isotopes

Benthic foraminifer *Trifarina angulosa* tests (150-300 μm) were picked from the >150 μm size fraction and ~ 20 -80 μg of crushed tests were prepared using standard procedures and analyzed on a Thermo Scientific MAT 253 IR-MS equipped with a Gas Bench II preparatory device at USF CMS. Samples ($n=36$) were taken at 0.5 cm intervals in MC-45 and 5 cm intervals in KC-27B, and JPC-27. Measurements of $\delta^{18}\text{O}$ and $\delta^{13}\text{C}$ were corrected using standard laboratory reference materials for sequence drift correction (Borba; $\delta^{13}\text{C}=2.87\pm 0.05\text{‰}$; $\delta^{18}\text{O}=-6.15\pm 0.09\text{‰}$), amplitude (TSF-1; $\delta^{13}\text{C}=1.95\pm 0.05\text{‰}$; $\delta^{18}\text{O}=-2.2\pm 0.06\text{‰}$), and monitored for quality control (Atlantis-3 and ChiCal). These values are derived from repeat measurements of the reference materials at University of South Florida College of Marine Science. All isotopic data are expressed using standard δ notation in per mil (‰) relative to the Vienna Pee Dee Belemnite (VPDB) carbonate standard. Long-term instrument precision is 0.08‰ for $\delta^{18}\text{O}$ and 0.05‰ for $\delta^{13}\text{C}$. In NBP14-02 samples, *T. angulosa* carbonate tests were scarce and duplicate analyses were conducted on $\sim 1\%$ of the samples ($n=2$). For measured samples, the standard deviation among

replicates of CaCO₃ aliquots from the same sample depth is 0.05-0.2‰ (Average: 0.1‰) for both δ¹⁸O and δ¹³C.

4.4.5 Foraminifer trace element/calcium ratios

Trifarina angulosa tests (100-300 μg) from MC-45, KC-27B, and JPC-27 were picked from the same sample intervals as stable isotopes (section 4.4.4), and prepared using standard foraminifer trace element cleaning procedures with both oxidative and reductive steps (Boyle & Keigwin, 1985/86; Martin & Lea, 2002). This protocol removes contamination from clays via rinses and ultrasonication with deionized water and methanol, organic matter with an oxidative solution of hydrogen peroxide in sodium hydroxide, and Mn- and Fe-oxides with a reductive solution of hydrazine and citric acid in ammonia.

Cleaned samples (n=10) were dissolved, then analyzed using a ThermoFisher Element XR HR-ICP-MS coupled with an ESI SC-4 DX autosampler. Duplicate analyses were not possible on *T. angulosa* tests due to limited sample mass, but repeat standard materials were monitored for reproducibility and drift throughout the analysis. Accuracy was monitored using community standards ECRM (Mg/Ca = 3.75 mmol/mol), BAM (Mg/Ca = 0.78 mmol/mol), and CMSI (Mg/Ca = 0.78 mmol/mol), values reported by Greaves et al. (2008). Relative standard deviations for community standards were 1.8% (ECRM), 3.3% (BAM), and 3.5% (CMSI).

All isotopes were measured in analog mode at low resolution (R=300), with the exception of ⁴⁵Sc, ⁵⁵Mn, and ⁵⁶Fe, which were measured in medium resolution (R=4000) to avoid spectral interferences. Mg/Ca ratios are reported using the ²⁴Mg isotope due to its high natural abundance. All minor and trace elements are ratioed to ⁴³Ca. Elemental ratios in unknowns were determined using a suite of multi-element standards with varying concentrations of Mg, Ca, B,

Ba, U, Cd, Mo, Li, Na, Mn, Sr, Fe, and Zn prepared to achieve a range of elemental ratios similar to those of foraminifers.

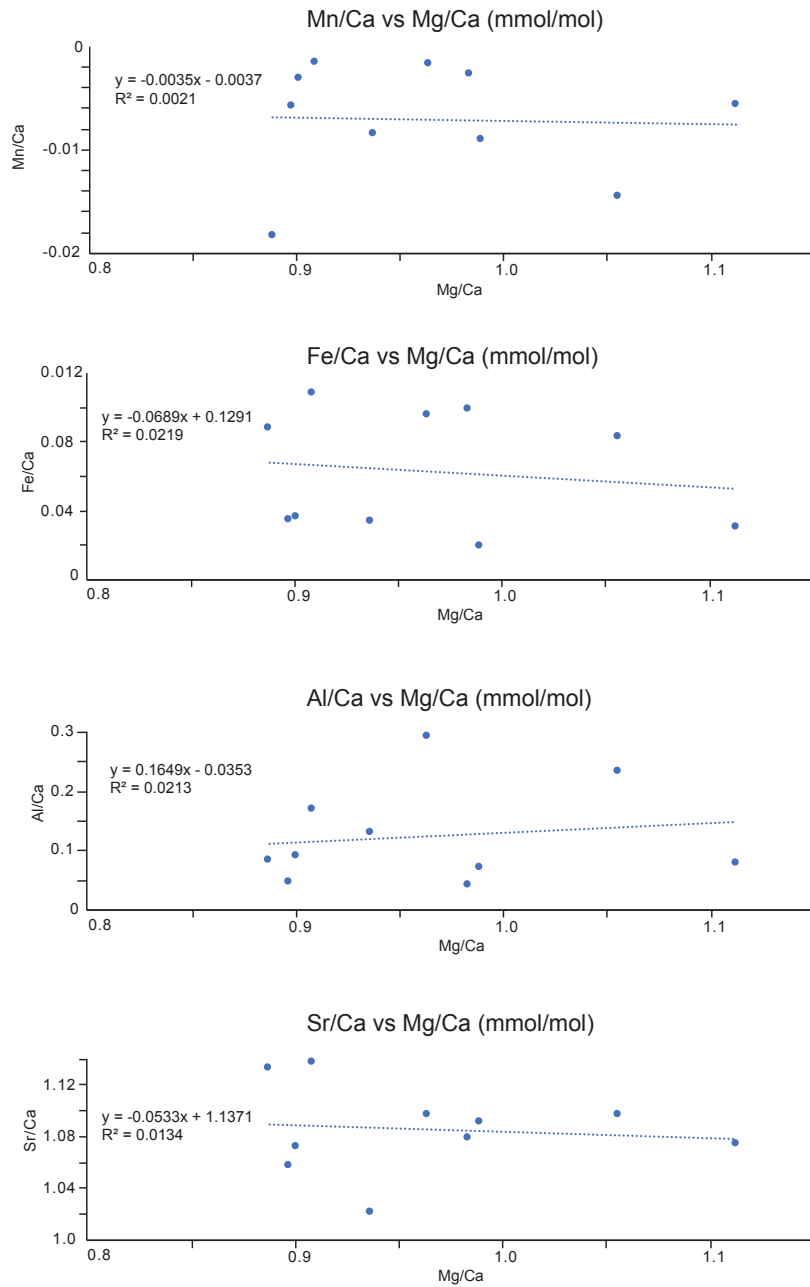


Figure 4.3 Trace metals cleaning indicators for *Trifarina angulosa*. Data show no trend that would suggest contamination during the cleaning process. Also note that Mn/Ca is at the detection limit.

Raw counts were converted to concentrations using linear calibration lines that included blank measurements and 3-4 multi-element standards and applied a noise correction factor following Schrag (1999). Matrix effects were removed from sample values through corrections based on the ratio of known Mg/Ca to measured Mg/Ca in the Sample Matrix Standard (Rosenthal et al., 1999; Schrag, 1999) and in community standards ECRM, BAM, and CMSI (Greaves et al., 2008).

A suite of trace elements were measured to assess cleaning efficacy (Figure 4.3). Our monitoring results indicate adherent clays were removed completely, and no contamination was introduced in the cleaning process. Mg/Ca is not correlated with Mn/Ca ($R^2=0.0021$), Fe/Ca ($R^2=0.0219$), Al/Ca ($R^2=0.0213$), or Sr/Ca ($R^2=0.0134$) in the *T. angulosa* data. Maximum Fe/Ca, and Al/Ca in *T. angulosa* are 0.011, and 0.3 mmol/mol. Mn/Ca is below the detection limit (maximum value -0.001).

4.4.6 Grain size

A record of sortable silt, which incorporates the 10-63 μm size fraction, was generated from NBP14-02 cores (McCave & Hall, 2006; McCave et al., 2017). 108 samples were analyzed with 30% replication ($n=32$) via laser diffraction using a Malvern MasterSizer 2000G at USF CMS. Like the TEX_{86} analyses, the sample resolution was adjusted depending on the length of the record: every 1 cm in MC-45 and every 5 cm in KC-27B. In JPC-27 samples were analyzed every 5, 10, or 25 cm. Freeze-dried sediment samples were homogenized (~ 500 mg), then organic matter, carbonate, and biogenic opal were removed following a modified method of Aiello & Ravello (2012) and Morlock & Froelich (1989). Samples were treated in a 10% H_2O_2 solution to remove organics followed by 1N HCl to remove carbonate. Then, samples were

treated with 2N NaOH and submerged in a hot water (85°C) bath for 24 hours to accelerate the removal of biogenic opal. Smear slides were created and examined to ensure that all biogenic opal had been removed. To disaggregate sediment prior to grain size analysis, samples were treated with a 0.5% NaO₃P (Calgon) solution for 30 minutes, then poured samples into the MasterSizer 2000G. Instrument performance was monitored by bracketing unknown sample runs with soda-lime glass bead standards in two size ranges, 20-38 µm (NIST SRM 1003c) and 106-355 µm (NIST SRM 1017b).

4.5 Results

4.5.1 Lithology and chronology

A lithologic, micropaleontologic, and paleotemperature record was generated from a 13.1-m-thick Holocene sediment sequence collected from Site 1 during cruise NBP14-02, using cores MC-45, KC-27B, and JPC-27. Six lithostratigraphic units in the cores are distinguished by lithologic and micropaleontologic properties established in Chapter 2, and vary from clast-rich muds to diatomaceous mud and ooze, which allow for paleoenvironmental interpretation. From the lower-most to upper-most unit: Unit VI is subglacial to ice proximal, Unit V is sub-ice shelf/fast ice, Unit VI is restricted/intermittent ice-proximal open marine, and Units III, IIB, IIA, and I are productive, seasonally open marine settings (Figure 4.2).

The downcore radiocarbon chronology between 0 and 991 cmcd is based upon 18 ²¹⁰Pb dates, two mixed foraminifer ¹⁴C dates, and eight low temperature aliquot (RPO-1) of eight acid insoluble organic matter ¹⁴C dates. An age model was generated using Bacon 2.3 software (Figure 4; Blaauw & Christen, 2011). This approach assumes that the accumulation rate changes at 135 cmcd (boundary between Unit I and IIA) 888 cmcd (boundary between Unit IIB and Unit

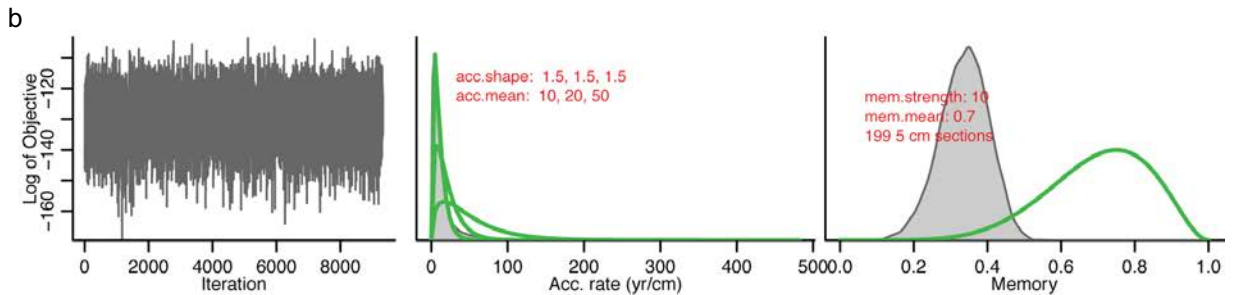
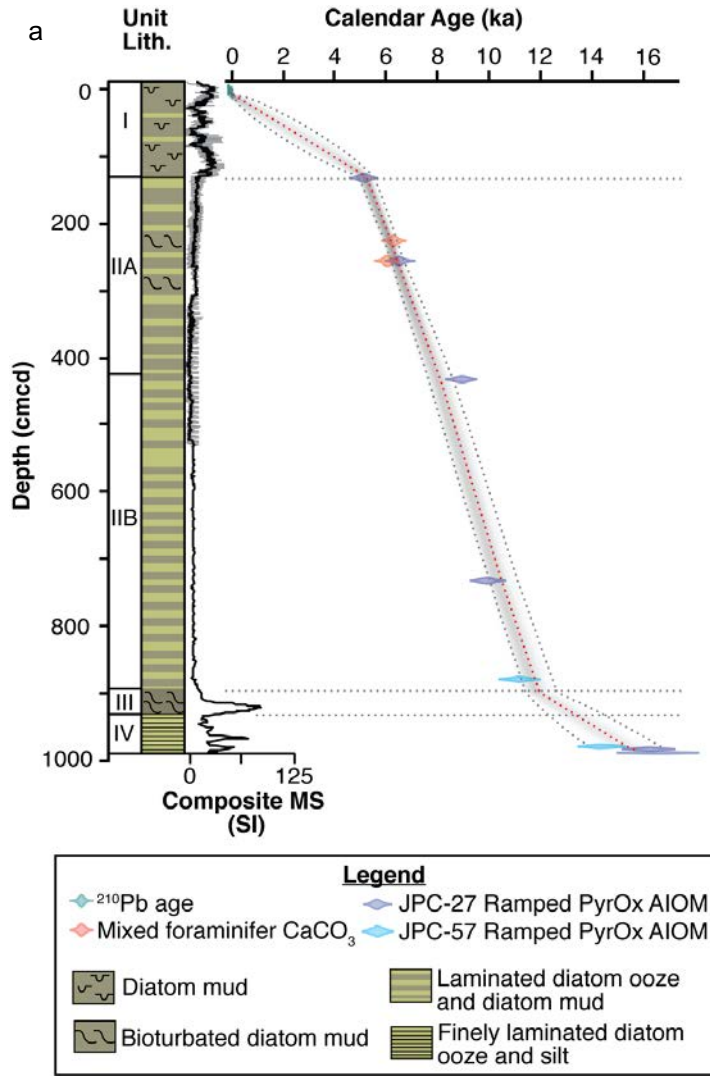


Figure 4.4 (a) Unit lithology, composite magnetic susceptibility (MS), and age model plotted versus centimeters composite depth. This age model combines the MC-45 ^{210}Pb dates and CaCO_3 and Ramped PyrOx AIOM ^{14}C dates (Table 2). To create the final age model, ^{210}Pb and blank corrected, calibrated ^{14}C dates were modeled using Bacon 2.3 software (Blaauw and Christen, 2011). (b) Prior information for Site 1 Bacon chronology. Left plot depicts the Markov chain Monte Carlo iterations (MCMC). The middle plot depicts the prior (green curves) and posterior (grey histograms) distributions for the accumulation rate, and the right plot depicts the prior and posterior distributions for memory.

III), and 931 cmcd (boundary between Unit III and Unit IIV), which is also informed by changes in lithology and magnetic susceptibility (Figure 4.4). In Unit I, the maximum age uncertainty is ± 850 years at 60 cmcd, near the midpoint of the unit where data is sparse. In Unit II, the maximum uncertainty is ± 700 years at 888 cmcd, the base of Unit IIB.

4.5.2 TEX₈₆ paleotemperatures

A centennial-scale resolution upper ocean paleotemperature record was generated (Figure 5) for Sabrina Coast cores. TEX₈₆ values were converted to upper ocean temperatures using the Shevenell et al. (2011) calibration that includes Antarctic core-top measurements. Shevenell et al. (2011) used the global core top data set from Kim et al. (2010) (n=223) with seven additional samples from the Anvers Island region, western Antarctic Peninsula. When applied to the Sabrina Coast shelf sediments, this calibration produces realistic temperatures, although some fall below the regional freezing point of -1.8°C (Silvano et al., 2016; n=10). However, we chose to include these points in our reconstruction as they are within calibration error ($\pm 2.2^{\circ}\text{C}$) of realistic temperatures. We also do not reject any TEX₈₆ data based on the BIT, Methane, or Ring indices that monitor external archaeal and non-thermal influences (Appendix D, Table D.19; Hopmans et al., 2004; Zhang et al., 2016).

Resulting Holocene paleotemperatures range from -3.3 to $2.9 \pm 2.2^{\circ}\text{C}$, with an average temperature of $-0.66 \pm 2.2^{\circ}\text{C}$ (Figure 4.3). The average standard deviation of replicate samples was ± 0.008 TEX₈₆ units, which is $\pm 0.48^{\circ}\text{C}$. TEX₈₆-derived paleotemperatures are relatively warm from 16.5-14.8 ka, varying between 0.1 and 2.9°C . Cooler temperatures persist between 14.8 ka and 13.5 ka. Temperatures exhibit a long-term cooling of 2°C from 11 to 1 thousand years before present (ka) and warming since 1.0 ka. Regional upper ocean temperatures

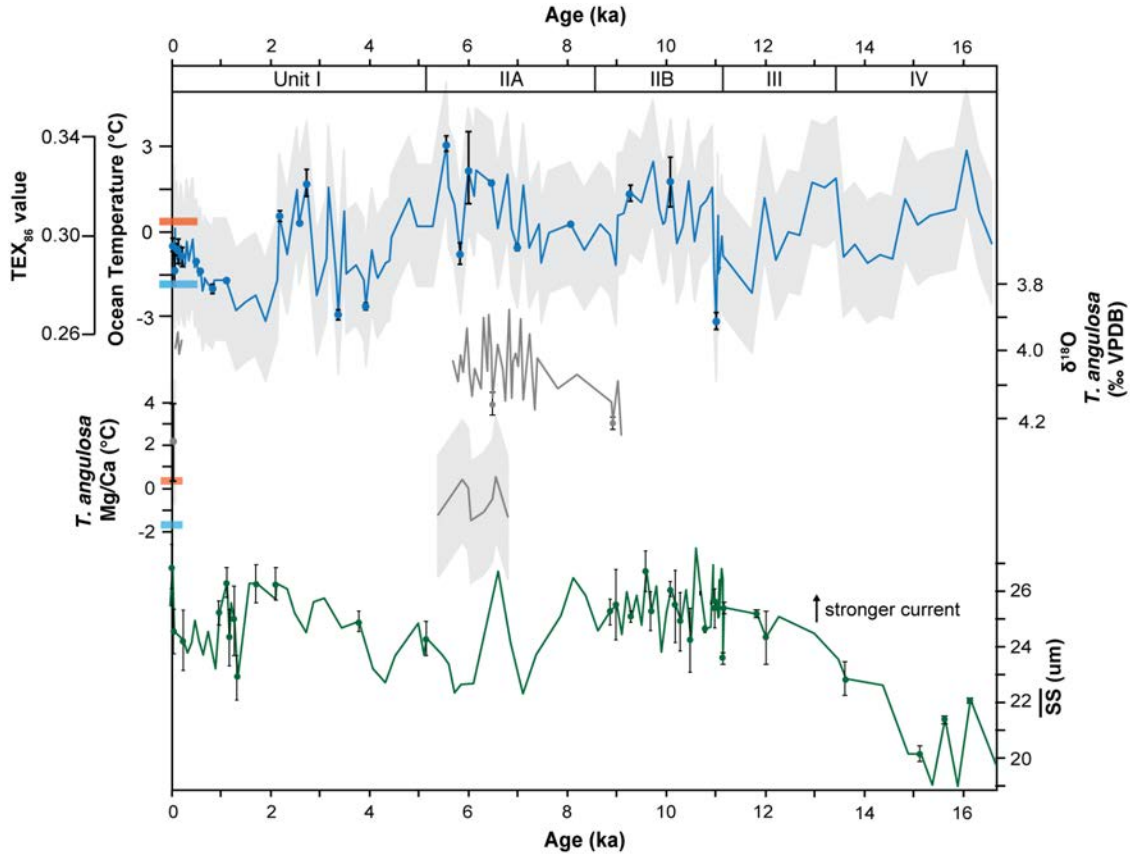


Figure 4.5 Sabrina Coast Holocene reconstruction of surface and bottom water conditions. Includes TEX_{86} values and upper ocean temperatures; $\delta^{18}O$ of *Trifarina angulosa*; Mg/Ca-derived paleotemperatures of *T. angulosa*; mean sortable silt (\overline{SS}). On the temperature axes, blue bars indicate modern Antarctic Surface Water temperature (-1.6 to -1.7 °C) and orange bars indicates modern mCDW temperature (0.3 to 0.5 °C) at the core site.

Table 4.3 TEX_{86} temperature t-table significance tests. Comparisons of relatively warm and cool periods during the Holocene demonstrated that temperatures of time slices are significantly different from neighboring time period. When $t < 0.05$, the variance or the standard deviation of the two sample sets are not equal (they are significantly different).

Time Range vs Time Range (ka)		T-test value
1.2 to 0	2.3 to 1.2	0.0018
2.3 to 1.2	3.4 to 2.3	0.0009
3.4 to 2.3	4.8 to 3.4	0.0401
4.8 to 3.4	7.1 to 4.8	0.0013
7.1 to 4.8	8.9 to 7.1	0.0004
8.9 to 7.1	10.8 to 8.9	0.0001

increased by 2°C over the past 1000 years, but have remained relatively stable over the past century (Figure 4.3). Superimposed on the Holocene cooling trend are a series of millennial-scale fluctuations in temperature ranging 2 to 4°C (Figure 4.5). Warm events occur from 10.8 to 8.9 ka, 7.1 to 4.8 ka, 3.4 to 2.3 ka, and 1.2 ka to the present. Periods of relatively cooler temperatures during the Holocene are at 8.9 to 7.1 ka, 4.8 to 3.4 ka, and 2.3 to 1.2 ka (Figure 4.5). Warmer and cooler periods significantly vary from one another ($t < 0.05$ for all comparison periods; Table 4.3).

4.5.3 *Trifarina angulosa* stable isotopes

Benthic foraminifer *T. angulosa* is present in lithologic Units I, IIA, and IIB (Figure 4.5). *Trifarina angulosa* stable isotope values have not been adjusted because the species, considered to be part of the genus *Uvigerina*, precipitates near isotopic equilibrium with the ambient water masses (McCorkle et al., 1997). In Unit I surface sediments (200 yr to present), *T. angulosa* $\delta^{18}\text{O}$ values vary from 3.8‰ to 4.0‰ (mean = 3.9 ± 0.06 ‰). The *T. angulosa* $\delta^{18}\text{O}$ values trend towards more negative values moving up-section from the middle Holocene to present. In Unit II, *T. angulosa* $\delta^{18}\text{O}$ exhibits centennial-scale fluctuations and values range from 3.8‰ to 4.5‰ (mean = 4.1 ± 0.2 ‰). There are sharp, repeated variations in *T. angulosa* $\delta^{18}\text{O}$ values of up to 0.5‰ from 8.5 to 7 ka.

4.5.4 *Trifarina angulosa* trace metals

For paleotemperature estimates, we analyzed *T. angulosa* Mg/Ca ratios from Sabrina Coast Site 1. *T. angulosa* Mg/Ca ratios were converted to temperature using Equation 4 from Mawbey et al., 2020, $\text{Mg/Ca} = 0.0651 * T + 1.102$ ($\pm 2.95^\circ\text{C}$), which integrates newly reported *T.*

angulosa core top measurements with global *Uvigerina* core top data (Figure 4.6). Mg/Ca temperature sensitivity is reduced at the cold end of the calibration. However, when combined with published *Uvigerina* spp. data, a robust linear correlation emerges (Figure 4.6). Sabrina Coast *T. angulosa* Mg/Ca ratios are lower than those from other locations on the Antarctic Margin, such as the Amundsen Sea and Weddell Sea (Mawbey et al., 2020). There is very little clay in the Sabrina Coast surface sediments, which may account for the lower Mg/Ca ratios. The presence of adherent clays leads to higher Mg/Ca values, which biases data toward warmer calibrated temperatures. The Sabrina Coast samples are also distinct from the others in Mawbey et al. (2020) in that they are not separated by size fraction (all >150 μm), and contain a spinose *T. angulosa* morphotype that may create a vital effect in Mg/Ca uptake (Mawbey et al., 2020).

At Sabrina Coast Site 1, the calibrated core-top (0-2 cmbsf) temperature for *T. angulosa* was $0.9 \pm 1.0^\circ\text{C}$ (analytical error of replicate samples, $n=2$), consistent with bottom water temperatures (>400 m) of $0.3\text{-}0.5^\circ\text{C}$, measured from NBP14-02 CTD casts. Down-core, *T. angulosa* present in Unit IIA exhibit temperature estimates between 0.23 and -1.3°C (Figure 4.5). Although the error envelope of the temperature calibration ($\pm 2.95^\circ\text{C}$) exceeds the range of temperature values in the calibrated *T. angulosa* samples (Figure 4.5), the Mawbey et al. (2020) calibration produces realistic temperatures for the Sabrina Coast samples.

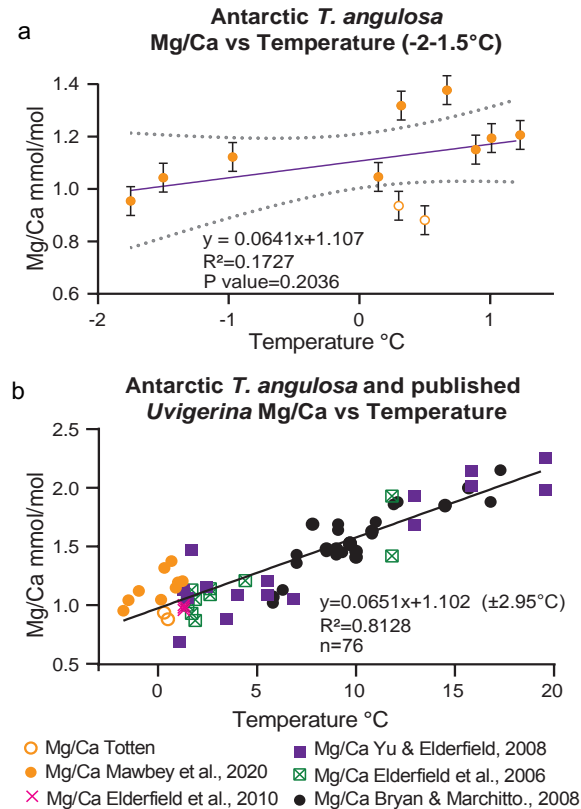


Figure 4.6 Mg/Ca-temperature calibrations from Mawbey et al., 2020. (a) *T. angulosa* data from West Antarctica (solid orange dots), Sabrina Coast (open orange dots), calibration Equation 2. (b) *T. angulosa* data from West Antarctica (solid orange dots), Sabrina Coast (open orange dots), and published collection of *Uvigerina* Mg/Ca data. We use Equation 4 in Mawbey et al., 2020 to calibrate the Sabrina Coast *T. angulosa* data in this chapter.

4.5.5 Sortable silt

Sortable silt measurements are presented as the mean size of the 10-63 μm sortable silt fraction ($\overline{\text{SS}}$), a proxy for paleocurrent speed (Figure 2; McCave et al., 2017; McCave & Hall, 2006). To assess changed in current speed, %SS and $\overline{\text{SS}}$ were calculated, which has a correlation coefficient of 0.52 (Figure 4.7). The mean sortable silt record shows $\sim 4 \mu\text{m}$ $\overline{\text{SS}}$ variations up-core throughout the Holocene (Figure 4.5). In our record, $\overline{\text{SS}}$ increases from 18 μm to 26 μm during the period from 16 to 11 ka. In the Holocene, $\overline{\text{SS}}$ remains stable from 11 to 8 ka (mean: 26 μm), decreases from 8 to 7 ka (26 to 23 μm), then increases from the middle Holocene to late

Holocene (23 to 27 μm , from 7 to 0 ka). Between 7 ka to 0 ka, $\overline{\text{SS}}$ values are data sparse, which precludes testing for significant trends, or comparing with TEX_{86} paleotemperature variations.

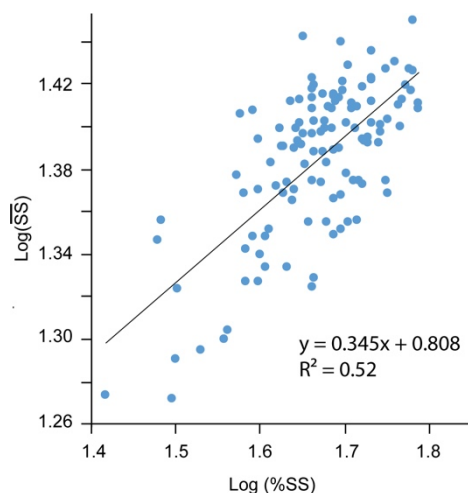


Figure 4.7 The log of calculated mean sortable silt ($\overline{\text{SS}}$) plotted against the log of present sortable silt (%SS). We use samples collected within open marine Units I-IV (blue circles) to determine an R^2 value ($r^2=0.52$). Sub-ice shelf and subglacial Units V and VI are excluded from the sortable silt dataset.

4.6 Discussion

4.6.1 Paleotemperature proxy validation

Throughout the deglacial to Holocene sequence, TEX_{86} -derived paleotemperatures (Figure 4.5) vary between temperatures typical of Antarctic Surface Water (-1.6 to -1.7°C) to values typical of or exceeding present-day mCDW (0.3 to 0.5 °C). Studies from the western Antarctic Peninsula demonstrate that TEX_{86} is a reliable indicator of warm upper ocean temperatures in the spring because marine archaea dwell in the deeper in surface water (50-150 m) at the interface with Circumpolar Deep Water (Kalanetra et al., 2009; Luria et al., 2014; Signori et al., 2018; Tolar et al., 2016). Although archaea communities have not been directly studied in the Sabrina Coast water column, TEX_{86} -derived temperatures likely reflect similar

associations with warm subsurface water during the spring. This inference is supported by a recent study that identified an abundance maximum of archaea in subsurface waters (~200 m) of Prydz Bay, East Antarctica (Liu et al., 2020).

Although benthic foraminifer carbonate is not preserved throughout the entire Holocene sequence, they are present in the middle Holocene, which can provide clarity on TEX₈₆ associations with temperature. In samples where *T. angulosa* was present, calibrated bottom water Mg/Ca-temperature fluctuations between -1.5 and 0.5 ±2.95 °C vary similarly with TEX₈₆-temperature fluctuations between -1.5 and 3 ±2.2 °C. The high variability in bottom water properties is also present in *T. angulosa* δ¹⁸O, which show warmer/fresher values when TEX₈₆ and Mg/Ca temperatures are higher, and cooler/saltier values when TEX₈₆ and Mg/Ca temperatures are lower (Figure 4.5). Further evaluation of δ¹⁸O_{seawater} is necessary to interpret the role, if any, that salinity and meltwater play on the benthic foraminifer values.

4.6.2 Deglacial paleoenvironmental conditions

The TEX₈₆ record presented in this study provides new information about the paleoceanographic conditions immediately following the deglaciation of the middle continental shelf on the Sabrina Coast. Regionally, Sabrina Coast deglaciation precedes the timing of other East Antarctic margin marine records by one to five thousand years. Deglaciation from marine records recording East Antarctic Ice Sheet deglaciation range from ~10-15 ka (Anderson et al. 2014 and references therein; Denis et al., 2009a; Leventer et al., 2006; Mackintosh et al., 2014). Regional atmospheric conditions during deglaciation at Dome C and Law Dome document atmospheric warming after the Last Glacial Maximum (Figure 4.8; EPICA Community Members, 2006; Masson et al., 2000), consistent with our inferred Sabrina Coast deglaciation at

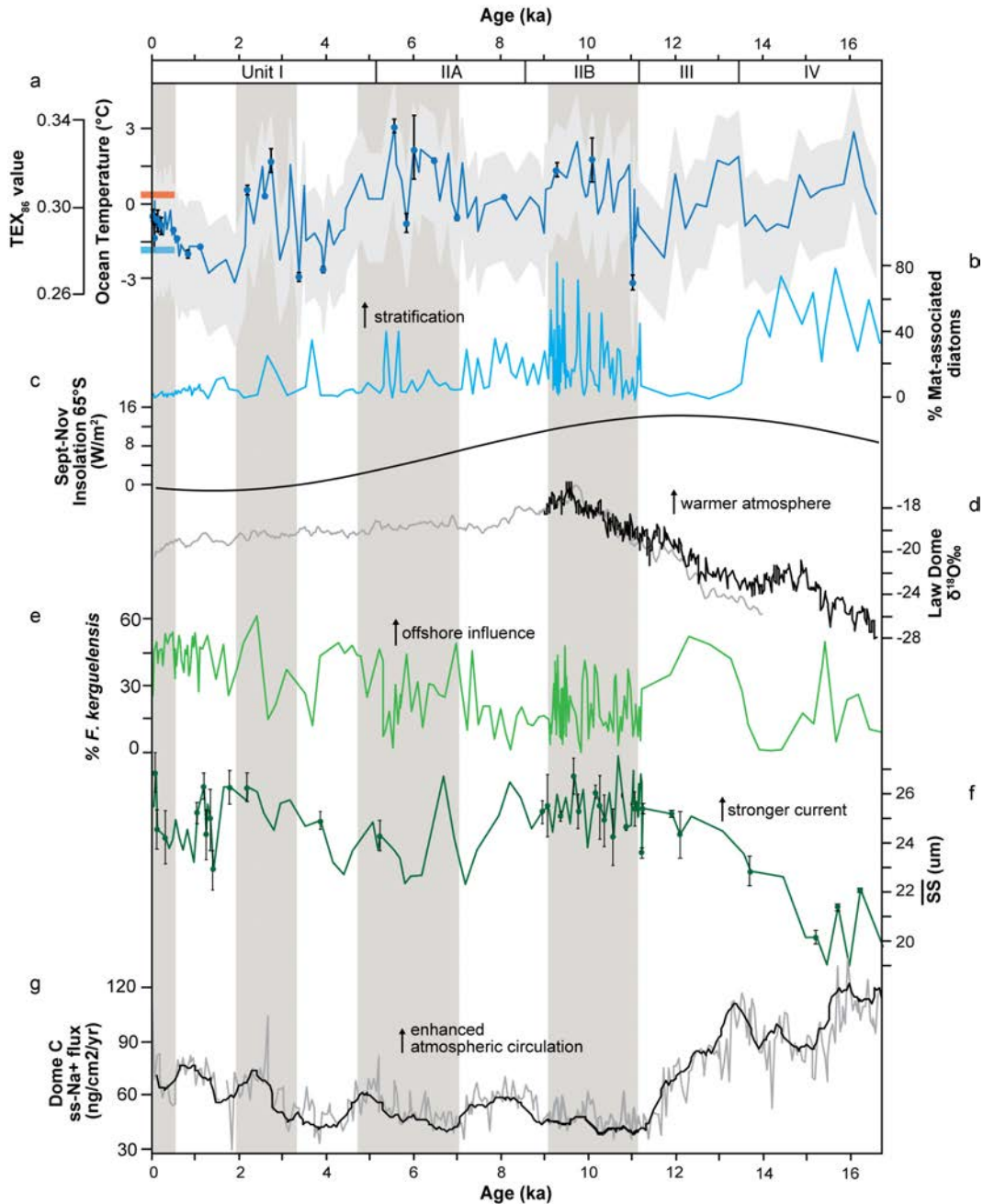


Figure 4.8 Sabrina Coast and regional Antarctic records of Holocene climate variability. Includes: (a) the Sabrina Coast upper ocean temperature record (this study). On the temperature axis, blue bar indicates modern Antarctic Surface Water temperature (-1.6 to -1.7 °C) and red bar indicates modern mCDW temperature (0.3 to 0.5 °C) at the core site; (b) Site 1 mat-associated diatom relative abundance (Chapter 2); (c) Austral spring insolation at 65°S (Laskar et al., 2004); (d) Law Dome $\delta^{18}\text{O}$ atmospheric temperature record (Morgan et al., 2002; Plummer, 2018); (e) Site 1 *Fragilariopsis kerguelensis* relative abundance (Chapter 2), (f) mean sortable silt record (SS); (g) EPICA Dome C sea salt sodium (ss- Na^+) flux record with 5-pt running mean (Röthlisberger et al., 2002).

16.5±0.84 ka. Because relatively warm waters are present at the initiation of an open water setting on the Sabrina Coast continental shelf, and deglaciation precedes the timing of Meltwater Pulse 1a (MWP1a; 14.0–14.5 ka; Clark et al., 2009; Deschamps et al., 2012; Lambeck et al., 2014; Liu et al., 2016), Sabrina Coast outlet glaciers are potential contributors to MWP1a sea level rise.

4.6.3 Holocene paleotemperature variations

Through the Holocene (11.2 to 1.0 ka), TEX₈₆ paleotemperatures exhibit a weak but significant ($R^2=0.14$, $t<0.05$) long-term cooling of 2°C with 2000 to 3000-year cycles of relatively cooler and warmer periods superimposed (Figure 4.8; Table 4.3). The TEX₈₆-based Holocene cooling trend agrees with temperature records of atmospheric warmth at Law Dome during the early and middle Holocene (Figure 4.8; Morgan et al., 2002; Plummer 2018), further supporting the regional utility of TEX₈₆ paleothermometry. The upper ocean cooling trend through the Holocene is also consistent with orbital-scale cooling resulting from a decline in austral summer insolation (Figure 4.8; Laskar et al., 2014).

A key to understanding what is driving temperature variations on the Sabrina Coast is to evaluate continental shelf oceanographic processes. An increase in \overline{SS} throughout the Holocene between 15 ka and 12 ka suggests bottom current intensification (Figure 4.8, McCave & Hall, 2006; McCave et al., 2017). Application of the sortable silt proxy requires specific conditions to be met, mainly that the sediments are fine grained muds and well sorted, and were transported and deposited by a single mechanism (Hass 2002; McCave et al., 2006). For these reasons, the method is mainly applied in deep ocean regions (Bianchi & McCave, 1999; McCave et al., 2014). To determine if current sorting or ice-rafting impact \overline{SS} , we evaluated the co-variance

between \overline{SS} and %SS (Figure 4.7; McCave & Hall, 2006; McCave & Andrews, 2019). The two parameters demonstrate a positive correlation ($R^2=0.52$), which just exceeds the proposed minimum correlation coefficient of 0.5 for a primarily current-influenced sortable silt record (McCave & Andrews, 2019). Although the correlation suggests we can utilize \overline{SS} trends as a paleoceanographic indicator of current flow, the use of sortable silt requires more scrutiny on a continental shelf than in deep sea applications because sediments may be introduced from multiple shelf sources. For example, deposition of the sediments may be derived from meltwater, or resuspension and across-shelf transport, as described by Sternal et al. (2014).

Although the use of \overline{SS} at the Sabrina Coast core sites is tentative, we offer an interpretation of the deglacial to Holocene \overline{SS} record. The increase in \overline{SS} from 21 μm to 26 μm from the deglaciation through early Holocene (~16 to 11 ka) indicates an increase in local bottom water activity. Smaller-scale variations in \overline{SS} values throughout the Holocene are not significantly different from the mean. The sedimentological and diatom records in the core provide further insight for interpreting Holocene current activity. Mat-forming diatoms species throughout the early to middle Holocene on the Sabrina Coast indicate intervals of strong stratification in surface waters followed by seasonal export of mats of diatoms (Figure 4.8). It may be possible that the energetic water mass sinking responsible for exporting diatom oozes is similar to turbulent events observed in the deep sea setting (McCave et al., 2017). Bottom current activity from dense shelf water export is further supported by cross bedded laminations in diatom oozes in the Sabrina Coast Holocene sediment, similar to those reported in Harris (2000) and Harris & O'Brien (1998).

Furthermore, \overline{SS} variations during the Holocene, increasing after 11 ka, vary similarly with an increase in abundance in the diatom *F. kerguelensis*, which is associated with open water

(Figure 8; Crosta et al., 2005). There is a notable increase in relative contribution of *F. kerguelensis* from ~13-11 ka, coincident with the inflection in \overline{SS} values across that period (Figure 4.8). There is also similar variability between wind intensity in the Australian sector of the sub-Antarctic (Saunders et al., 2018) and sea salt transport to Law Dome adjacent to the Sabrina Coast (tan shaded zones, Figure 4.8; Röthlisberger et al, 2002). Periodically warm ocean temperatures and elevated \overline{SS} during the Holocene suggest modulation by wind-driven processes, creating an open water polynya setting.

The Sabrina Coast may be particularly sensitive to global climate variability. Sabrina Coast oceanographic conditions today are approaching the magnitude of ocean warmth observed in the early to middle Holocene when there was open water over the continental shelf, regional productivity was high, the southern hemisphere westerly winds were shifted poleward (Saunders et al., 2018), and atmospheric CO₂ was rising (EPICA Community Members, 2006). We suggest that warming atmospheric temperatures and ocean currents driven by wind are the dominant oceanographic processes on the Sabrina Coast, which are influenced by perturbations from lower latitudes (Masson-Delmotte et al., 2003; Souney et al., 2002; Vance et al., 2013), similar to the western Antarctic Peninsula (Dinniman et al., 2012; Fogt et al., 2011; Shevenell et al., 2002; 2011).

4.6.4 Global importance

The Sabrina Coast marine-based catchment was sensitive to warmer upper ocean temperatures during the Holocene, and our data suggest that current conditions are on a trajectory to reach warm conditions similar to the early and middle Holocene. Our ocean temperature reconstruction indicates that present ocean temperatures and mCDW influence on

the Sabrina Coast outlet glaciers are within the range of natural Holocene variability (Figure 8). Although the late Holocene warm upper ocean temperature values have not yet exceeded early or middle Holocene upper ocean temperatures, Sabrina Coast ice mass loss will likely continue with accelerating atmospheric warming and higher $p\text{CO}_2$, leading to greater ice sheet instability and global sea level rise. Greater coverage of the deglacial to Holocene sediment record on the Sabrina Coast shelf, and further proxy validation through water column measurements are needed to improve our understanding of the spatial extent and timing of ocean warming.

CHAPTER FIVE:

CONCLUSION

This dissertation sets out to establish the first deglacial to Holocene sediment record for the continental shelf on the Sabrina Coast, East Antarctica. In Chapter 2, we dated the initiation of open water conditions after deglaciation on the middle Sabrina Coast continental shelf, which occurred at 16.5 ka. Sedimentological and micropaleontological data provided insight into the paleoceanography and paleoenvironment, such as stratification, sea ice presence/absence, and open water conditions during the Holocene. The reconstruction revealed that Holocene shelf conditions were impacted by polynya dynamics and ocean currents, driven by regional wind and atmospheric forcing patterns.

In Chapter 3, we presented a multiproxy record of oceanographic change from the Sabrina Coast shelf over the past ~1000 years. We found that ocean temperatures warmed by ~2°C over the 1000-year period, and upper ocean waters became warmer during the 20th Century. However, we recognize limitations in the current version of the age model, so identifying climate events within the 1000-year record is tentative. The TEX₈₆ and diatom assemblage record show ocean warming and increased influence of offshore water masses, which vary similarly with regional atmospheric circulation changes in Law Dome over the same ~1000-year period. A critical purpose of this chapter was also to test the applicability of existing paleotemperature calibrations with newly generated core top sediments. Both TEX₈₆ and planktic

N. pachyderma (s) values for the Sabrina Coast core tops fell within realistic ranges, and thus strengthen the cold end of the respective temperature calibrations.

In Chapter 4, Sabrina Coast sediments indicate warm ocean temperatures following the deglaciation at 16.5 ka, and significant millennial scale variations of upper ocean temperatures throughout the Holocene. Sortable silt data is relatively invariant during the Holocene and does not allow us to draw a conclusive association with warm water presence. Rather, the sortable silt data in conjunction with diatom assemblages and sedimentary structures provide insight into shelf water formation at the site. The Sabrina Coast Holocene TEX₈₆ record is the first marine record from East Antarctica to document ocean temperature changes consistent with local insolation forcing and atmospheric temperature and transport records from nearby ice core records. We determined that, although present-day temperatures are not above earlier Holocene values, the Sabrina Coast glacial systems may have responded to relatively warm water in the past.

Oceanographic variability on the Sabrina Coast may be associated with warmer maritime air advected from lower latitudes due to poleward shifts of the westerlies, which can increase upwelling of warm Circumpolar Deep Water onto the Sabrina Coast continental shelf. In the Sabrina Coast sediment record, both atmospheric and oceanic warming are implied as mechanisms driving local deglaciation. The Sabrina Coast region seems to be responding to low-latitude climate changes similar to parts of West Antarctica and the Antarctic Peninsula. The Sabrina Coast sediment record demonstrates sensitivity to warm ocean and atmospheric conditions, suggesting this sector of East Antarctica is more vulnerable to future warming and ice retreat than previously appreciated.

Modern day observations of oceanographic and ice behavior are critical to characterize the present processes on the Sabrina Coast continental shelf. Avenues to improve our understanding of the regional climatic changes and impacts on the Sabrina Coast involve continuing to collect water column measurements and surface sediment cores to improve regional paleotemperature calibrations. This study reflects the first deglacial to recent paleoenvironmental reconstructions from the Sabrina Coast shelf. Continued effort to core and drill in the region will contribute to understanding the timing and style of the last deglaciation in the Sabrina Coast sector and to characterizing earlier climate periods when major growth and collapse of the East Antarctic Ice Sheet occurred.

REFERENCES

- Adusumilli, S., Fricker, H. A., Medley, B., Padman, L., & Siegfried, M. R. (2020). Interannual variations in meltwater input to the Southern Ocean from Antarctic ice shelves. *Nature Geoscience*, 13(9), 616-620
- Aiello, I.W. & Ravelo, A.C., (2012). Evolution of marine sedimentation in the Bering Sea since the Pliocene. *Geosphere*, 8(6), 1231-1253.
- Aitken, A. R. A., Young, D. A., Ferraccioli, F., Betts, P. G., Greenbaum, J. S., Richter, T. G., Roberts, J. L., Blankenship, D.D., & Siegert, M. J. (2014). The subglacial geology of Wilkes Land, East Antarctica. *Geophysical Research Letters*, 41, 2390–2400
doi:10.1002/2014GL059405
- Aitken, A. R. A., Roberts, J. L., Van Ommen, T. D., Young, D. A., Golledge, N. R., Greenbaum, J. S., & Siegert, M. J. (2016). Repeated large-scale retreat and advance of Totten Glacier indicated by inland bed erosion. *Nature*, 533, 385-389. doi:10.1038/nature17447
- Alley, K., Patacca, K., Pike, J., Dunbar, R., & Leventer, A., 2018. Iceberg Alley, East Antarctic margin: Continuously laminated diatomaceous sediments from the late Holocene. *Marine Micropaleontology*, 140, 56-68.
- Anderson, J.B., Conway, H., Bart, P.J., Witus, A.E., Greenwood, S.L., McKay, R.M., et al. (2014). Ross Sea paleo-ice sheet drainage and deglacial history during and since the LGM. *Quaternary Science Reviews*, 100, 31-54.
- Anderson, R. F., Ali, S., Bradtmiller, L. I., Nielsen, S. H. H., Fleisher, M. Q., Anderson, B. E., & Burckle, L. H. (2009). Wind-driven upwelling in the Southern Ocean and the deglacial rise in atmospheric CO₂. *Science*, 323(5920), 1443-1448. doi: 10.1126/science.1167441
- Andresen, C. S., Straneo, F., Ribergaard, M. H., Bjørk, A. A., Andersen, T. J., Kuijpers, A., et al. (2012). Rapid response of Helheim Glacier in Greenland to climate variability over the past century. *Nature Geoscience*, 5(1), 37-41.
- Appleby, P. G. & Oldfield, F. (1992). Application of ²¹⁰Pb to sedimentation studies. In: M. Ivanovich & R.S. Harmon (eds.), *Uranium-series Disequilibrium: Applications to Earth, Marine & Environmental Sciences*, Oxford University Press, 731-778.
- Appleby, P.G. (1998). *Dating recent sediments by 210 Pb: Problems and solutions* (No. STUK-A-145).
- Arbuszewski, J., deMenocal, P., Kaplan, A., & Farmer, E.C. (2010). On the fidelity of shell-derived $\delta^{18}\text{O}_{\text{seawater}}$ estimates. *Earth and Planetary Science Letters*, 300(3-4), 185-196.
- Armand, L. K., Crosta, X., Romero, O., & Pichon, J. J. (2005). The biogeography of major diatom taxa in Southern Ocean sediments: 1. Sea ice related species. *Palaeogeography, Palaeoclimatology, Palaeoecology*, 223(1-2), 93-126. doi:10.1016/j.palaeo.2005.02.015
- Armand, L. K., Crosta, X., Quéguiner, B., Mosseri, J., & Garcia, N. (2008). Diatoms preserved in surface sediments of the northeastern Kerguelen Plateau. *Deep-Sea Research Pt. II*, 55(5), 677-692. doi:10.1016/j.dsr2.2007.12.032
- Armand, L., O'Brien, P., Armbrrecht, L., Barker, H., Caburlotto, A., Connell, T. et al. (2018).

- Interactions of the Totten Glacier with the Southern Ocean through multiple glacial cycles (IN2017-V01): Post-survey report. *Australian Antarctic Science Grant Program (AAS# 4333)*.
- Arroyo, M.C., Shadwick, E.H. and Tilbrook, B., 2019. Summer carbonate chemistry in the Dalton Polynya, East Antarctica. *Journal of Geophysical Research: Oceans*, 124(8), pp.5634-5653.
- Asioli, A. & Langone, L. (1997). Relationship between recent Planktic Foraminifera and water mass properties in the Western Ross Sea (Antarctica). *Geografia Fisica e Dinamica Quaternaria*, 20, 193-198.
- Barbara, L., Crosta, X., Massé, G., & Ther, O. (2010). Deglacial environments in eastern Prydz Bay, East Antarctica. *Quaternary Science Reviews*, 29, 2731-2740. doi:10.1016/j.quascirev.2010.06.027
- Baskaran, M., Nix, J., Kuyper, C., & Karunakara, N. (2014). Problems with the dating of sediment core using excess 210Pb in a freshwater system impacted by large scale watershed changes. *Journal of environmental radioactivity*, 138, 355-363.
- Bentley, M. J., Hodgson, D. A., Smith, J. A., Cofaigh, C. O., Domack, E. W., Larter, R. D., Roberts, S. J., Brachfeld, S., Leventer, A., Hjort, C., & Hillenbrand, C. D. (2009). Mechanisms of Holocene palaeoenvironmental change in the Antarctic Peninsula region. *The Holocene*, 19(1), 51-69. doi:10.1177/0959683608096603
- Bergami, C., Capotondi, L., Langone, L., Giglio, F. & Ravaioli, M. (2009). Distribution of living planktonic foraminifera in the Ross Sea and the Pacific sector of the Southern Ocean (Antarctica). *Marine Micropaleontology*, 73(1-2), 37-48.
- Berkman, P. A. & Forman, S. L. (1996). Pre-bomb radiocarbon and the reservoir correction for calcareous marine species in the Southern Ocean. *Geophysical Research Letters*, 23(4), 363-366. doi:10.1029/96GL00151
- Bettoli, M.G., Cantelli, L., Quarin, D., Ravanelli, M., Tositti, L. & Tubertini, O., (1998). Marine sediments and snow from Ross Sea region (Antarctica) dating by 210Pb method. *International Journal of Environmental Analytical Chemistry*, 71(3-4), 321-330.
- Bianchi, G.G. & McCave, I.N., (1999). Holocene periodicity in North Atlantic climate and deep-ocean flow south of Iceland. *Nature*, 397(6719), 515-517.
- Bianchi, C., & Gersonde, R. (2004). Climate evolution at the last deglaciation: the role of the Southern Ocean. *Earth and Planetary Science Letters*, 228(3-4), 407-424. doi:10.1016/j.epsl.2004.10.003
- Bindoff, N. L., Rosenberg, M. A. & Warner, M. J. (2000). On the circulation and water masses over the Antarctic continental slope and rise between 80 and 150 E. *Deep Sea Research Part II: Topical Studies in Oceanography*, 47(12-13), 2299-2326.
- Blaauw, M. & Christen, J. A. (2011). Flexible paleoclimate age-depth models using an autoregressive gamma process. *Bayesian Analysis*, 6(3), 457-474. <https://doi.org/10.1214/11-BA618>
- Bo, S., Siegert, M. J., Mudd, S. M., Sugden, D., Fujita, S., Xiangbin, C., Yunyun, J., Xueyuan, T. and Yuansheng, L. (2009). The Gamburtsev Mountains and the origin and early evolution of the Antarctic Ice Sheet. *Nature*, 459(7247), 690-693.
- Bostock, H. C., Opdyke, B. N., Gagan, M. K. & Fifield, L. K. (2004). Carbon isotope evidence for changes in Antarctic Intermediate Water circulation and ocean ventilation in the southwest Pacific during the last deglaciation. *Paleoceanography*, 19(4).

- Boyle E.A. & Keigwin, L.D. (1985). Comparison of Atlantic and Pacific paleochemical records for the last 215,000 years: changes in deep ocean circulation and chemical inventories. *Earth and Planetary Science Letters*, 76, 135-150, doi:10.1016/0012-821X(85)90154-2.
- Brachfeld, S.A., Banerjee, S.K., Guyodo, Y. and Acton, G.D. (2002). A 13,200 year history of century to millennial-scale paleoenvironmental change magnetically recorded in the Palmer Deep, western Antarctic Peninsula. *Earth and Planetary Science Letters*, 194(3-4), 311-326.
- Broecker, W., Barker, S., Clark, E., Hajdas, I. & Bonani, G. (2006). Anomalous radiocarbon ages for foraminifera shells. *Paleoceanography*, 21(2).
- Bryan, S.P. & Marchitto, T.M. (2008). Mg/Ca–temperature proxy in benthic foraminifera: New calibrations from the Florida Straits and a hypothesis regarding Mg/Li. *Paleoceanography*, 23(2).
- Buffen, A., Leventer, A., Rubin, A., & Hutchins, T. (2007). Diatom assemblages in surface sediments of the northwestern Weddell Sea, Antarctic Peninsula. *Marine Micropaleontology*, 62(1), pp.7-30.
- Burke, K.D., Williams, J.W., Chandler, M.A., Haywood, A.M., Lunt, D.J. & Otto-Bliesner, B.L. (2018). Pliocene and Eocene provide best analogs for near-future climates. *Proceedings of the National Academy of Sciences*, 115(52), 13288-13293.
- Cape, M.R., Vernet, M., Pettit, E.C., Wellner, J., Truffer, M., Akie, G., Domack, E., Leventer, A., Smith, C.R. & Huber, B.A. (2019). Circumpolar Deep Water impacts glacial meltwater export and coastal biogeochemical cycling along the west Antarctic Peninsula. *Frontiers in Marine Science*, 6, 144.
- Church, M. J., DeLong, E. F., Ducklow, H. W., Karner, M. B., Preston, C. M. & Karl, D. M. (2003). Abundance and distribution of planktonic Archaea and Bacteria in the waters west of the Antarctic Peninsula. *Limnology and Oceanography*, 48(5), 1893-1902.
- Clark, P. U., Dyke, A. S., Shakun, J. D., Carlson, A. E., Clark, J., Wohlfarth, B., et al. (2009). The last glacial maximum. *science*, 325(5941), 710-714. doi:10.1126/science.1172873
- Clement, A. C., Seager, R., & Cane, M. A. (1999). Orbital controls on the El Niño/Southern Oscillation and the tropical climate, *Paleoceanography*, 14, 441-456.
- Colleoni et al. (2018). Spatio-temporal variability of processes across Antarctic ice-bed–ocean interfaces, *Nature Communications*, 9, 2289.
- Crawford, R. M. (1995). The role of sex in the sedimentation of a marine diatom bloom. *Limnology and Oceanography*, 40(1), 200-204. doi:10.4319/lo.1995.40.1.0200
- Cremer, H., Gore, D., Melles, M. & Roberts, D. (2003). Palaeoclimatic significance of late Quaternary diatom assemblages from southern Windmill Islands, East Antarctica. *Palaeogeography, Palaeoclimatology, Palaeoecology*, 195(3-4), 261-280. doi:10.1016/S0031-0182(03)00361-4
- Crespin, J., Yam, R., Crosta, X., Massé, G., Schmidt, S., Campagne, P., & Shemesh, A. (2014). Holocene glacial discharge fluctuations and recent instability in East Antarctica. *Earth and Planetary Science Letters*, 394, 38-47. doi: 10.1016/j.epsl.2014.03.009
- Crosta, X., Sturm, A., Armand, L., & Pichon, J. J. (2004). Late Quaternary sea ice history in the Indian sector of the Southern Ocean as recorded by diatom assemblages. *Marine Micropaleontology*, 50(3-4), 209-223. doi:10.1016/S0377-8398(03)00072-0
- Crosta, X., Romero, O., Armand, L. K., & Pichon, J. J. (2005). The biogeography of major diatom taxa in Southern Ocean sediments: 2. Open ocean related species.

- Palaeogeography, Palaeoclimatology, Palaeoecology*, 223(1-2), 66-92.
doi:10.1016/j.palaeo.2005.03.028
- Crosta, X., Debret, M., Denis, D., Courty, M. A., & Ther, O. (2007). Holocene long-and short-term climate changes off Adélie Land, East Antarctica. *Geochemistry, Geophysics, Geosystems*, 8(11). doi:10.1029/2007GC001718
- Crosta, X., Etourneau, J., Orme, L. C., Dalaiden, Q., Campagne, P., Swingedouw, D., Goosse, H., Massé, G., Miettinen, A., McKay, R.M. & Dunbar, R. B. (2021). Multi-decadal trends in Antarctic sea-ice extent driven by ENSO–SAM over the last 2,000 years. *Nature Geoscience*, 14(3), 156-160.
- Curran, M.A., Van Ommen, T.D. & Morgan, V. (1998). Seasonal characteristics of the major ions in the high-accumulation Dome Summit South ice core, Law Dome, Antarctica. *Annals of Glaciology*, 27, 385-390.
- DeConto, R. M. & Pollard, D. (2016). Contribution of Antarctica to past and future sea-level rise. *Nature*, 531, 591-597. doi:10.1038/nature17145
- Denis, D., Crosta, X., Schmidt, S., Carson, D. S., Ganeshram, R.S., Renssen, H., et al. (2009a). Holocene glacier and deep water dynamics, Adélie Land region, East Antarctica. *Quaternary Science Reviews*, 28(13-14), 1291-1303. doi:10.1016/j.quascirev.2008.12.024
- Denis, D., Crosta, X., Schmidt, S., Carson, D. S., Ganeshram, R. S., Renssen, H., et al. (2009b). Holocene productivity changes off Adélie Land (East Antarctica). *Paleoceanography*, 24(3). doi:10.1029/2008PA001689
- Denis, D., Crosta, X., Barbara, L., Massé, G., Renssen, H., Ther, O., & Giraudeau, J. (2010). Sea ice and wind variability during the Holocene in East Antarctica: insight on middle–high latitude coupling. *Quaternary Science Reviews*, 29(27-28), pp.3709-3719. doi:10.1016/j.quascirev.2010.08.007
- Denton, G.H., Anderson, R.F., Toggweiler, J.R., Edwards, R.L., Schaefer, J.M., & Putnam, A.E. (2010). The last glacial termination. *Science*, 328(5986), 1652-1656. doi:10.1126/science.1184119
- Depoorter, M.A., Bamber, J.L., Griggs, J.A., Lenaerts, J.T., Ligtenberg, S.R., van den Broeke, M.R., & Moholdt, G. (2013). Calving fluxes and basal melt rates of Antarctic ice shelves. *Nature*, 502(7469), 89-92.
- Deschamps, P., Durand, N., Bard, E., Hamelin, B., Camoin, G., Thomas, A.L., et al., (2012). Ice-sheet collapse and sea-level rise at the Bølling warming 14,600 years ago. *Nature*, 483(7391), 559-564. doi: 10.1038/nature10902
- Dinniman, M.S., Klinck, J.M., & Hofmann, E.E. (2012). Sensitivity of circumpolar deep water transport and ice shelf basal melt along the West Antarctic Peninsula to changes in the winds. *Journal of Climate*, 25(14), 4799-4816. doi:10.1175/JCLI-D-11-00307.1
- Domack, E. W., Jull, A. T., & Nakao, S. (1991). Advance of East Antarctic outlet glaciers during the Hypsithermal: implications for the volume state of the Antarctic ice sheet under global warming. *Geology*, 19(11), 1059-1062.
- Domack, E. W., O'Brien, P. E., Harris, P. T., Taylor, F., Quilty, P. G., De Santis, L., & Raker, B. (1998). Late Quaternary sediment facies in Prydz Bay, East Antarctica and their relationship to glacial advance onto the continental shelf. *Antarctic Science*, 10(3), 236-246. doi:10.1017/S0954102098000339

- Donda, F., Leitchenkov, G., Brancolini, G., Romeo, R., De Santis, L., Escutia, C., O'Brien, P., Armand, L., Caburlotto, A., & Cotterle, D. (2020). The influence of Totten Glacier on the Late Cenozoic sedimentary record. *Antarctic Science*, 32(4), 288-300.
- Dow, C. F., McCormack, F. S., Young, D. A., Greenbaum, J. S., Roberts, J. L., & Blankenship, D. D. (2019). Totten Glacier subglacial hydrology determined from geophysics and modeling. *Earth and Planetary Science Letters*, 115961.
- Driscoll, N. W. & Haug, G. H. (1998). A short circuit in thermohaline circulation: A cause for northern hemisphere glaciation? *Science*, 282(5388), 436-438.
- Dupont, T. K. & Alley, R. B. (2005). Assessment of the importance of ice-shelf buttressing to ice-sheet flow. *Geophysical Research Letters*, 32(4).
- Elderfield, H. & Ganssen, G. (2000). Past temperature and $\delta^{18}\text{O}$ of surface ocean waters inferred from foraminiferal Mg/Ca ratios. *Nature*, 405, 442-445.
- Elderfield, H., Yu, J., Anand, P., Kiefer, T., & Nyland, B. (2006). Calibrations for benthic foraminiferal Mg/Ca paleothermometry and the carbonate ion hypothesis. *Earth and Planetary Science Letters*, 250(3-4), 633-649.
- Elderfield, H., Greaves, M., Barker, S., Hall, I.R., Tripathi, A., Ferretti, P., Crowhurst, S., Booth, L., & Daunt, C. (2010). A record of bottom water temperature and seawater $\delta^{18}\text{O}$ for the Southern Ocean over the past 440 kyr based on Mg/Ca of benthic foraminiferal *Uvigerina* spp. *Quaternary Science Reviews*, 29(1-2), 160-169.
- Elderfield, H., Ferretti, P., Greaves, M., Crowhurst, S., McCave, I.N., Hodell, D., & Piotrowski, A.M. (2012). Evolution of ocean temperature and ice volume through the mid-Pleistocene climate transition. *Science*, 337(6095), 704-709.
- Elling, F.J., Könneke, M., Mußmann, M., Greve, A., & Hinrichs, K.-U. (2015). Influence of temperature, pH, and salinity on membrane lipid composition and TEX₈₆ of marine planktonic thaumarchaeal isolates. *Geochimica et Cosmochimica Acta* 171, 238-255.
- Emile-Geay, J., Cobb, K. M., Mann, M. E., & Wittenberg, A. T. (2013). Estimating Central Equatorial Pacific SST variability over the Past Millennium. Part I: Methodology and Validation. *Journal of Climate*, 26(7), 2302-2328. doi:10.1175/JCLI-D-11-00510.1
- Emiliani, C. (1970). Pleistocene paleotemperatures. *Science*, 168(3933), 822-825.
- EPICA Community Members. (2006). One to one coupling of glacial climate variability in Greenland and Antarctica. *Nature*, 444, 195-198. doi:10.1038/nature05301
- Etourneau, J., Collins, L. G., Willmott, V., Kim, J. H., Barbara, L., Leventer, A., et al. (2013). Holocene climate variations in the western Antarctic Peninsula: evidence for sea ice extent predominantly controlled by changes in insolation and ENSO variability. *Climate of the Past*, 9, 1431-1446. doi:10.5194/cp-9-1431-2013
- Evrard, O., Chaboche, P. A., Ramon, R., Foucher, A. & Laceby, J. P. (2020). A global review of sediment source fingerprinting research incorporating fallout radiocesium (¹³⁷Cs). *Geomorphology*, 362, 107103.
- Fernandez, A., Santos, G. M., Williams, E. K., Pendergraft, M. A., Vetter, L., & Rosenheim, B. E. (2014). Blank corrections for ramped pyrolysis radiocarbon dating of sedimentary and soil organic carbon. *Analytical Chemistry*, 86(24), 12085-12092. doi:10.1021/ac502874j
- Fernandez, R., Gulick, S. P. S., Domack E., Montelli, A., Leventer, A., Shevenell, A. E., Frederick, B., & the NBP14-02 Science Party. (2018). Past ice stream and ice sheet changes on the continental shelf off Sabrina Coast, East Antarctica. *Geomorphology*, 317, 10-22. doi:10.1016/j.geomorph.2018.05.020

- Fogt, R. L., Bromwich, D. H., & Hines, K. M. (2011). Understanding the SAM influence on the South Pacific ENSO teleconnection. *Climate Dynamics*, 36, 1555–1576. doi:10.1007/s00382-010-0905-0
- Fogwill, C. J., Turney, C. S. M., Menviel, L., Baker, A., Weber, M. E., Ellis, B., et al. (2020). Southern Ocean carbon sink enhanced by sea-ice feedbacks at the Antarctic Cold Reversal. *Nature Geoscience*, 13(7), 489-497.
- Fretwell, P., Pritchard, H. D., Vaughan, D. G., Bamber, J. L., Barrand, N. E., Bell, R., et al. (2013). Bedmap2: improved ice bed, surface and thickness datasets for Antarctica. *Cryosphere*, 7, 375-393. doi:10.5194/tc-7-375-2013
- Golledge, N. R., Fogwill, C. J., Mackintosh, A. N., & Buckley, K. M. (2012). Dynamics of the last glacial maximum Antarctic ice-sheet and its response to ocean forcing. *Proceedings of the National Academy of Science*, 109(40), 16052-16056. doi:10.1073/pnas.1205385109
- Golledge, N. R., Menviel, L., Carter, L., Fogwill, C. J., England, M. H., Cortese, G., & Levy, R. H. (2014). Antarctic contribution to meltwater pulse 1A from reduced Southern Ocean overturning. *Nature Communications*, 5. doi: 10.1038/ncomms6107
- Golledge, N. R., Kowalewski, D. E., Naish, T. R., Levy, R. H., Fogwill, C. J., & Gasson, E. G. W. (2015). The multi-millennial Antarctic commitment to future sea-level rise. *Nature*, 526, 421-425. doi:10.1038/nature15706
- Golledge, N. R., Levy, R. H., McKay, R. M., & Naish, T. R. (2017). East Antarctic Ice Sheet most vulnerable to Weddell Sea warming. *Geophysical Research Letters* 44(5), 2343e2351.
- Goodwin, I. D. (1996). A mid to late Holocene readvance of the Law Dome ice margin, Budd Coast, East Antarctica. *Antarctic Science*, 8(4), 395-406. doi:10.1017/S0954102096000570
- Goodwin, I. D. (1998). Did changes in Antarctic ice volume influence late Holocene sea-level lowering?. *Quaternary Science Reviews*, 17(4-5), 319-332. doi:10.1016/S0277-3791(97)00051-6
- Goodwin, I. D. & Zweck, C. (2000). Glacio-isostasy and glacial ice load at Law Dome, Wilkes land, east Antarctica. *Quaternary Research*, 53(3), 285-293. doi:10.1006/qres.1999.2125
- Greaves, M., Caillon, N., Rebaubier, H., Bartoli, G., Bohaty, S., Cacho, I., Clarke, L., Cooper, M., Daunt, C., Delaney, M., & DeMenocal, P. (2008). Interlaboratory comparison study of calibration standards for foraminiferal Mg/Ca thermometry. *Geochemistry, Geophysics, Geosystems*, 9(8).
- Greenbaum, J. S., Blankenship, D. D., Young, D. A., Richter, T. G., Roberts, J. L., Aitken, A. R. A., et al. (2015). Ocean access to a cavity beneath Totten Glacier in East Antarctica. *Nature Geoscience*, 8(4), 294-298. doi:10.1038/ngeo2388
- Greene, C. A., Blankenship, D. D., Gwyther, D. E., Silvano, A., & van Wijk, E. (2017). Wind causes Totten Ice Shelf melt and acceleration. *Science Advances*, 3(11), e1701681. doi: 0.1126/sciadv.1701681
- Greene, C. A., Young, D. A., Gwyther, D. E., Galton-Fenzi, B. K. & Blankenship, D. D. (2018). Seasonal dynamics of Totten Ice Shelf controlled by sea ice buttressing. *Cryosphere*, 12(9), 2869-2882. doi:10.5194/tc-12-2869-2018
- Gulick, S. P. S., Shevenell, A. E., Montelli, A., Fernandez, R., Smith, C., Warny, S., et al. (2017). Initiation and long-term instability of the East Antarctic Ice Sheet. *Nature*, 552(7684), 225. doi:10.1038/nature25026

- Gwyther, D. E., Galton-Fenzi, B. K., Hunter, J. R., & Roberts, J. L. (2014). Simulated melt rates for the Totten and Dalton ice shelves. *Ocean Science*, *10*(3), 267. doi:10.5194/os-10-267-2014
- Hajdas, I. (2008). Radiocarbon dating and its applications in Quaternary studies. *E&G Quaternary Science Journal*, *57*(1/2), 2-24.
- Hall, B. L. (2009). Holocene glacial history of Antarctica and the sub-Antarctic islands. *Quaternary Science Reviews*, *28*(21-22), 2213-2230. doi:0.1016/j.quascirev.2009.06.011
- Hall, A. & Visbeck, M. (2002). Synchronous variability in the southern hemisphere atmosphere, sea ice, and ocean resulting from the annular mode. *Journal of Climate*, *15*(21), 3043-3057.
- Hall, J. M. & Chan, L. H. (2004). Ba/Ca in *Neogloboquadrina pachyderma* as an indicator of deglacial meltwater discharge into the western Arctic Ocean. *Paleoceanography*, *19*(1).
- Harris, P. T. (2000). Ripple cross-laminated sediments on the East Antarctic Shelf: evidence for episodic bottom water production during the Holocene?. *Marine Geology*, *170*(3-4), 317-330. doi:10.1016/S0025-3227(00)00096-7
- Harris, P. T. & O'Brien, P. E. (1996). Geomorphology and sedimentology of the continental shelf adjacent to Mac. Robertson Land, East Antarctica: a scalped shelf. *Geo-Marine Letters*, *16*(4), 287-296.
- Harris, P. T. & O'Brien, P. E. (1998). Bottom currents, sedimentation and ice-sheet retreat facies successions on the Mac Robertson shelf, East Antarctica. *Marine Geology*, *151*(1), 47-72.
- Hartman, J.D., Sangiorgi, F., Salabarnada, A., Peterse, F., Houben, A.J., Schouten, S., et al. (2018). Paleoenvironment and ice sheet variability offshore Wilkes Land, Antarctica—Part 3: Insights from Oligocene–Miocene TEX 86-based sea surface temperature reconstructions. *Climate of the Past*, *14*(9), 1275-1297.
- Hass, H. C. (2002). A method to reduce the influence of ice-rafted debris on a grain size record from northern Fram Strait, Arctic Ocean. *Polar Research*, *21*(2), 299-306.
- Heaton, T. J., Köhler, P., Butzin, M., Bard, E., Reimer, R. W., Austin, et al. (2020). Marine20—the marine radiocarbon age calibration curve (0–55,000 cal BP). *Radiocarbon*, 1-42.
- Hemer, M. A. & Harris, P. T. (2003). Sediment core from beneath the Amery Ice Shelf, East Antarctica, suggests mid-Holocene ice-shelf retreat. *Geology*, *31*(2), 127-130.
- Hendry, K. R. & Rickaby, R. E. (2008). Opal (Zn/Si) ratios as a nearshore geochemical proxy in coastal Antarctica. *Paleoceanography and Paleoclimatology*, *23*(2). doi:10.1029/2007PA001576
- Hendry, K. R., Rickaby, R. E., Meredith, M. P., & Elderfield, H. (2009). Controls on stable isotope and trace metal uptake in *Neogloboquadrina pachyderma* (sinistral) from an Antarctic sea-ice environment. *Earth and Planetary Science Letters*, *278*(1-2), 67-77. doi:10.1016/j.epsl.2008.11.026
- Hillenbrand, C. D., Grobe, H., Diekmann, B., Kuhn, G., & Fütterer, D. K. (2003). Distribution of clay minerals and proxies for productivity in surface sediments of the Bellingshausen and Amundsen seas (West Antarctica)—Relation to modern environmental conditions. *Marine Geology*, *193*(3-4), pp.253-271. doi:10.1016/S0025-3227(02)00659-X
- Hillenbrand, C. D., Smith, J. A., Kuhn, G., Esper, O., Gersonde, R., Larter, R. D., et al. (2010). Age assignment of a diatomaceous ooze deposited in the western Amundsen Sea Embayment after the Last Glacial Maximum. *Journal of Quaternary Science: Published for the Quaternary Research Association*, *25*(3), 280-295. doi:10.1002/jqs.1308

- Hillenbrand, C. D., Smith, J. A., Hodell, D. A., Greaves, M., Poole, C. R., Kender, S., et al. (2017). West Antarctic Ice Sheet retreat driven by Holocene warm water incursions. *Nature*, 547(7661), 43. doi:10.1038/nature22995
- Hodgson, D. A., McMinn, A., Kirkup, H., Cremer, H., Gore, D., Melles, M., et al. (2003). Colonization, succession, and extinction of marine floras during a glacial cycle: A case study from the Windmill Islands (east Antarctica) using biomarkers. *Paleoceanography*, 18(3). doi:10.1029/2002PA000775
- Hodgson, D. A., Whitehouse, P. L., De Cort, G., Berg, S., Verleyen, E., Tavernier, I., et al. (2016). Rapid early Holocene sea-level rise in Prydz Bay, East Antarctica. *Global and Planetary Change*, 139, 128-140.
- Hodell, D. A., Kanfoush, S. L., Shemesh, A., Crosta, X., Charles, C. D., & Guilderson, T. P. (2001). Abrupt cooling of Antarctic surface waters and sea ice expansion in the South Atlantic sector of the Southern Ocean at 5000 cal yr BP. *Quaternary Research*, 56(2), 191-198. doi: 10.1006/qres.2001.2252
- Holder, L., Duffy, M., Opdyke, B., Leventer, A., Post, A., O'Brien, P. & Armand, L.K. (2020). Controls since the Mid-Pleistocene Transition on Sedimentation and Primary Productivity Downslope of Totten Glacier, East Antarctica. *Paleoceanography and Paleoclimatology*, p.e2020PA003981.
- Holland, P.R. & Kwok, R. (2012). Wind-driven trends in Antarctic sea-ice drift. *Nature Geoscience*, 5(12), 872-875.
- Holland, P. R., Bracegirdle, T. J., Dutrieux, P., Jenkins, A., & Steig, E. J. (2019). West Antarctic ice loss influenced by internal climate variability and anthropogenic forcing. *Nature Geoscience*, 12(9), 18-724.
- Hönisch, B., Allen, K.A., Lea, D.W., Spero, H.J., Eggins, S.M., Arbuszewski, J., deMenocal, P., Rosenthal, Y., Russell, A.D., & Elderfield, H. (2013). The influence of salinity on Mg/Ca in planktic foraminifers—Evidence from cultures, core-top sediments and complementary $\delta^{18}\text{O}$. *Geochimica et Cosmochimica Acta*, 121, 196-213.
- Hopmans, E. C., Weijers, J. W. H., Schefuß, E., Herfort, L., Sinninghe Damsté, J. S., & Schouten, S. (2004). A novel proxy for terrestrial organic matter in sediments based on branched and isoprenoid tetraether lipids. *Earth and Planetary Science Letters*, 224(1-2), 107-116. doi:10.1016/j.epsl.2004.05.012
- Huguet, C., Martens-Habben, W., Urakawa, H., Stahl, D. A., & Ingalls, A. E. (2010). Comparison of extraction methods for quantitative analysis of core and intact polar glycerol dialkyl glycerol tetraethers (GDGTs) in environmental samples. *Limnology and Oceanography: Methods*, 8, 127-145. https://doi.org/10.4319/lom.2010.8.12
- Hurley, S. J., Elling, F. J., Könneke, M., Buchwald, C., Wankel, S. D., Santoro, A. E., et al. (2016). Influence of ammonia oxidation rate on thaumarchaeal lipid composition and the TEX86 temperature proxy. *Proceedings of the National Academy of Sciences*, 113(28), 7762–7767. https://doi.org/10.1073/pnas.1518534113
- Huybers, P. & Denton, G. (2008). Antarctic temperature at orbital timescales controlled by local summer duration. *Nature Geoscience*, 1(11), 787-792. doi:10.1038/ngeo311
- Ingalls, A.E. (2016). Signal from the subsurface. *Nature Geoscience* 9, 572-573.
- Ingólfsson, Ó., Hjort, C., Berkman, P. A., Björck, S., Colhoun, E., Goodwin, I. D., et al. (1998). Antarctic glacial history since the Last Glacial Maximum: an overview of the record on land. *Antarctic Science*, 10(3), 326-344. doi:10.1017/S095410209800039X
- Jacobs, S. S. (1991). On the nature and significance of the Antarctic Slope Front. *Marine Chemistry*, 35(1-4), 9-24. doi:10.1016/S0304-4203(09)90005-6

- Jacobs, S. S. (2004). Bottom water production and its links with the thermohaline circulation. *Antarctic Science*, 16(4), 427-437. doi:10.1017/S095410200400224X
- Jacobs, S. S., Jenkins, A., Giulivi, C. F. & Dutrieux, P. (2011). Stronger ocean circulation and increased melting under Pine Island Glacier ice shelf. *Nature Geoscience*, 4(8), 519-523. doi:10.1038/ngeo1188
- Jaeger, J. M., Nittrouer, C. A., Scott, N. D. & Milliman, J. D. (1998). Sediment accumulation along a glacially impacted mountainous coastline: North-east Gulf of Alaska. *Basin Research*, 10(1), 155-173.
- Jenkins, A., Dutrieux, P., Jacobs, S., Steig, E.J., Gudmundsson, G.H., Smith, J. & Heywood, K.J. (2016). Decadal ocean forcing and Antarctic ice sheet response: Lessons from the Amundsen Sea. *Oceanography*, 29(4), pp.106-117.
- Jones, R. S., Mackintosh, A. N., Norton, K. P., Golledge, N. R., Fogwill, C. J., Kubik, et al. (2015). Rapid Holocene thinning of an East Antarctic outlet glacier driven by marine ice sheet instability. *Nature Communications*, 6(1), 1-9.
- Jones, E. M., Fenton, M., Meredith, M. P., Clargo, N. M., Ossebaar, S., Ducklow, H. W., Venables, H. J. & de Baar, H. J. (2017). Ocean acidification and calcium carbonate saturation states in the coastal zone of the West Antarctic Peninsula. *Deep Sea Research Part II: Topical Studies in Oceanography*, 139, 181-194.
- Jouzel, J., Masson-Delmotte, V., Cattani, O., Dreyfus, G., Falourd, S., Hoffmann, G., Minster, B., Nouet, J., Barnola, J.M., Chappellaz, J. & Fischer, H. (2007). Orbital and millennial Antarctic climate variability over the past 800,000 years. *Science*, 317(5839), 793-796.
- Jun, S. Y., Kim, J. H., Choi, J., Kim, S. J., Kim, B. M. & An, S. I. (2020). The internal origin of the west-east asymmetry of Antarctic climate change. *Science Advances*, 6(24), p.eaaz149
- Kaiser, J., Schefuß, E., Lamy, F., Mohtadi, M., & Hebbeln, D. (2008). Glacial to Holocene changes in sea surface temperature and coastal vegetation in north central Chile: high versus low latitude forcing. *Quaternary Science Reviews*, 27(21-22), 2064-2075. doi:10.1016/j.quascirev.2008.08.025
- Kalanetra, K. M., Bano, N., & Hollibaugh, J. T. (2009). Ammonia-oxidizing archaea in the Arctic Ocean and Antarctic coastal waters. *Environmental Microbiology*, 11(9), 2434-2445. doi:10.1111/j.1462-2920.2009.01974
- Kemp, A. E. S., & Villareal, T. A. (2013). High diatom production and export in stratified waters—A potential negative feedback to global warming. *Progress in Oceanography*, 119, 4-23. doi:10.1016/j.pocean.2013.06.004
- Kennett, J.P. & Shackleton, N.J. (1975). Laurentide ice sheet meltwater recorded in Gulf of Mexico deep-sea cores. *Science*, 188(4184), 147-150.
- Kennett, J. P. (1977). Cenozoic evolution of Antarctic glaciation, the circum-Antarctic Ocean, and their impact on global paleoceanography. *Journal of geophysical research*, 82(27), 3843-3860.
- Khazendar, A., Schodlok, M. P., Fenty, I., Ligtenberg, S. R. M., Rignot, E., & Van den Broeke, M. R. (2013). Observed thinning of Totten Glacier is linked to coastal polynya variability. *Nature Communications*, 4. doi:10.1038/ncomms3857
- Kilfeather, A. A., Cofaigh, C.Ó., Lloyd, J.M., Dowdeswell, J. A., Xu, S. & Moreton, S. G. (2011). Ice-stream retreat and ice-shelf history in Marguerite Trough, Antarctic Peninsula: Sedimentological and foraminiferal signatures. *Bulletin*, 123(5-6), 997-1015.
- Kim, J.-H., Schouten, S. Hoppmans, E.C., Donner, B., & Sinninghe Damste, J. S. (2008). Global

- core top calibration of the TEX₈₆ paleothermometer in the ocean. *Geochimica et Cosmochimica Acta*, 72, 1154-1173.
- Kim, J.-H., Van der Meer, J., Schouten, S., Helmke, P., Willmott, V., Sangiorgi, F., Koç, N., Hopmans, E. C. and Damsté, J. S. S. (2010). New indices and calibrations derived from the distribution of crenarchaeal isoprenoid tetraether lipids: Implications for past sea surface temperature reconstructions. *Geochimica et Cosmochimica Acta*, 74(16), 4639-4654.
- Kim, J.-H., Crosta, X., Willmott, V., Renssen, H., Bonnin, J., Helmke, P., Schouten, S. & Sinninghe Damste, J. S. (2012). Holocene subsurface temperature variability in the eastern Antarctic continental margin. *Geophysical Research Letters*, 39, L06705, doi:10.1029/2012GL051157
- King, T. M., Rosenheim, B. E., Post, A. L., Gabris, T., Burt, T., & Domack, E. W. (2018). Large-Scale Intrusion of Circumpolar Deep Water on Antarctic Margin Recorded by Stylasterid Corals. *Paleoceanography and Paleoclimatology*, 33(11), 1306-1321.
- Kirby, M. E., Domack, E. W. & McClennen, C. E. (1998). Magnetic stratigraphy and sedimentology of Holocene glacial marine deposits in the Palmer Deep, Bellingshausen Sea, Antarctica: implications for climate change? *Marine Geology*, 152(4), 247-259.
- Kirchner, G. (2011). ²¹⁰Pb as a tool for establishing sediment chronologies: examples of potentials and limitations of conventional dating models. *Journal of Environmental Radioactivity*, 102(5), 490-494.
- Kirshner, A. E., Anderson, J. B., Jakobsson, M., O'Regan, M., Majewski, W., & Nitsche, F. O. (2012). Post-LGM deglaciation in Pine island Bay, west Antarctica. *Quaternary Science Reviews*, 38, 11-26. doi:10.1016/j.quascirev.2012.01.017
- Kohfeld, K. E., Fairbanks, R. G., Smith, S.L. & Walsh, I. D. (1996). Neogloboquadrina pachyderma (sinistral coiling) as paleoceanographic tracers in polar oceans: Evidence from Northeast Water Polynya plankton tows, sediment traps, and surface sediments. *Paleoceanography*, 11(6), 679-699.
- Kusahara, K., Hasumi, H., & Tamura, T. (2010). Modeling sea ice production and dense shelf water formation in coastal polynyas around East Antarctica. *Journal of Geophysical Research: Oceans*, 115, C10006. doi:10.1029/2010JC006133
- Lambeck, K., Rouby, H., Purcell, A., Sun, Y., & Sambridge, M. (2014). Sea level and global ice volumes from the Last Glacial Maximum to the Holocene. *Proceedings of the National Academy of Sciences*, 111(43), 15296-15303. doi:10.1073/pnas.1411762111
- Lamy, F., Hebbeln, D., Röhl, U., & Wefer, G. (2001). Holocene rainfall variability in southern Chile: a marine record of latitudinal shifts of the Southern Westerlies. *Earth and Planetary Science Letters*, 185(3-4), 369-382. doi:10.1016/S0012-821X(00)00381-2
- Laskar, F. I., Pallamraju, D., & Veenadhari, B. (2014). Vertical coupling of atmospheres: dependence on strength of sudden stratospheric warming and solar activity. *Earth, Planets and Space*, 66(94). doi: 10.1186/1880-5981-66-94
- Liau, J.R. & Chao, B.F. (2017). Variation of Antarctic circumpolar current and its intensification in relation to the southern annular mode detected in the time-variable gravity signals by GRACE satellite. *Earth, Planets and Space*, 69(1), 1-9.
- Lea, D.W., Mashiotta, T.A. & Spero, H.J. (1999). Controls on magnesium and strontium uptake in planktonic foraminifera determined by live culturing. *Geochimica et Cosmochimica Acta*, 63(16), 2369-2379.

- Lea, D. W. (2014). Elemental and Isotopic Proxies of Past Ocean Temperatures. *Treatise on Geochemistry: Second Edition*. Elsevier Ltd, 373-397.
- Lear, C. H., Elderfield, H. and Wilson, P. A. (2000). Cenozoic deep-sea temperatures and global ice volumes from Mg/Ca in benthic foraminiferal calcite. *Science*, 287(5451), 269-272.
- Lear, C.H., Mawbey, E.M. & Rosenthal, Y. (2010). Cenozoic benthic foraminiferal Mg/Ca and Li/Ca records: Toward unlocking temperatures and saturation states. *Paleoceanography*, 25(4).
- Leventer, A., Domack, E.W., Ishman, S.E., Brachfeld, S., McClennen, C.E. & Manley, P. (1996). Productivity cycles of 200–300 years in the Antarctic Peninsula region: understanding linkages among the sun, atmosphere, oceans, sea ice, and biota. *Geological Society of America Bulletin*, 108(12), 1626-1644.
- Leventer, A. (1998). The fate of Antarctic “sea ice diatoms” and their use as paleoenvironmental indicators. *Antarctic sea ice. Biological processes, interactions and variability*, 121-137. doi:10.1029/AR073p0121
- Leventer, A. (2017). NBP1402 diatom data. U.S. Antarctic Program (USAP) Data Center. doi: 10.15784/601258.
- Leventer, A., Domack, E., Barkoukis, A., McAndrews, B., & Murray, J. (2002). Laminations from the Palmer Deep: A diatom-based interpretation. *Paleoceanography*, 17(3). doi:10.1029/2001PA000624
- Leventer, A., Domack, E., Dunbar, R., Pike, J., Stickley, C., Maddison, E., et al. (2006). Marine sediment record from the East Antarctic margin reveals dynamics of ice sheet recession. *GSA Today*, 16, 4-10. doi:10.1130/GSAT01612A.1
- Leventer, A., Domack, E., Gulick, S. P. S., Huber, B., Orsi, A., & Shevenell, A. E. (2015). Sabrina Coast Marine Record of Cryosphere – Ocean Dynamics. *Marine Science Faculty Publications*. 573.
- Levy, R., Harwood, D., Florindo, F., Sangiorgi, F., Tripathi, R., Von Eynatten, H., et al. (2016). Antarctic ice sheet sensitivity to atmospheric CO₂ variations in the early to mid-Miocene. *Proceedings of the National Academy of Sciences*, 113(13), 3453-3458.
- Li, W., Li, X., Mei, X., Zhang, F., Xu, J., Liu, C., Wei, C. & Liu, Q. (2021). A review of current and emerging approaches for Quaternary marine sediment dating. *Science of The Total Environment*, 146522.
- Li, X., Rignot, E., Morlighem, M., Mouginot, J., & Scheuchl, B. (2015). Grounding line retreat of Totten Glacier, East Antarctica, 1996 to 2013. *Geophysical Research Letters*, 42(19), 8049-8056. doi:10.1002/2015GL065701
- Lisiecki, L.E. and Raymo, M.E. (2005). A Pliocene-Pleistocene stack of 57 globally distributed benthic $\delta^{18}\text{O}$ records. *Paleoceanography*, 20(1).
- Liu, J., Milne, G.A., Kopp, R.E., Clark, P.U., & Shennan, I. (2016). Sea-level constraints on the amplitude and source distribution of Meltwater Pulse 1A. *Nature Geoscience*, 9(2), 130-134. doi:10.1038/ngeo2616
- Liu, R., Han, Z., Zhao, J., Zhang, H., Li, D., Ren, J., Pan, J. & Zhang, H. (2020). Distribution and source of glycerol dialkyl glycerol tetraethers (GDGTs) and the applicability of GDGT-based temperature proxies in surface sediments of Prydz Bay, East Antarctica. *Polar Research*, 39.
- Livingstone, S. J., Cofaigh, C. Ó., Stokes, C. R., Hillenbrand, C. D., Vieli, A. & Jamieson, S. S., (2012). Antarctic palaeo-ice streams. *Earth-Science Reviews*, 111(1-2), 90-128.

- Lowe, A.L. & Anderson, J.B. (2002). Reconstruction of the West Antarctic ice sheet in Pine Island Bay during the Last Glacial Maximum and its subsequent retreat history. *Quaternary Science Reviews*, 21, 16-17, 1879-1897.
- Luria, C., Ducklow, H., & Amaral-Zettler, L. (2014). Marine bacterial, archaeal and eukaryotic diversity and community structure on the continental shelf of the western Antarctic Peninsula. *Aquatic Microbial Ecology*, 73(2), 107–121. doi:10.3354/ame01703
- Lüthi, D., M. Le Floch, B. Bereiter, T. Blunier, J.-M. Barnola, et al. (2008). High-resolution carbon dioxide concentration record 650,000-800,000 years before present. *Nature* 453, 379-382. doi:10.1038/nature06949.
- MacFarling Meure, C., Etheridge, D., Trudinger, C., Steele, P., & Langenfelds, R. (2006). Law Dome CO₂, CH₄ and N₂O ice core records extended to 2000 years bp. *Geophysical Research Letters*, 33, L14810. doi: 10.1029/2006GL026152
- Mackensen, A., Sejrup, H.P. & Jansen, E. (1985). The distribution of living benthic foraminifera on the continental slope and rise off southwest Norway. *Marine Micropaleontology*, 9(4), 275-306.
- Mackensen, A., Grobe, H., Kuhn, G. & Fu, D.K. (1990). Benthic foraminiferal assemblages from the eastern Weddell Sea between 68 and 73 S: Distribution, ecology and fossilization potential. *Marine micropaleontology*, 16(3-4), 241-283.
- Mackensen, A. (2001). Oxygen and carbon stable isotope tracers of Weddell Sea water masses: new data and some paleoceanographic implications. *Deep Sea Research Part I: Oceanographic Research Papers*, 48(6), pp.1401-1422. doi:0.1016/S0967-0637(00)00093-5
- Mackensen, A., Fu, D. K., Grobe, H. & Schmiedl, G. (1993). Benthic foraminiferal assemblages from the eastern South Atlantic Polar Front region between 35 and 57 S: distribution, ecology and fossilization potential. *Marine Micropaleontology*, 22(1-2), pp.33-69. doi: 10.1016/0377-8398(93)90003-G
- Mackenzie, A., Baxter, M., Mckinley, I., Swan, D. and Jack, W. (1979). The determination of ¹³⁴Cs, ¹³⁷Cs, ²¹⁰Pb, ²²⁶Ra and ²²⁸Ra concentrations in nearshore marine sediments and seawater. *Journal of Radioanalytical and Nuclear Chemistry*, 48(1-2), 29-47.
- Mackintosh, A. N., Verleyen, E., O'Brien, P. E., White, D. A., Jones, R. S., McKay, R., et al. (2013). Retreat History of the East Antarctic Ice Sheet since the Last Glacial Maximum. *Quaternary Science Reviews*, 100, 10-30. doi:10.1016/j.quascirev.2013.07.024
- Mackintosh, A., Golledge, N., Domack, E., Dunbar, R., Leventer, A., White, D., et al. (2011). Retreat of the East Antarctic ice sheet during the last glacial termination. *Nature Geoscience*, 4(3), 195. doi:10.1038/NNGEO1061
- Mackintosh, A. N., Verleyen, E., O'Brien, P. E., White, D. A., Jones, R. S., McKay, R., et al. (2014). Retreat history of the East Antarctic Ice Sheet since the last glacial maximum. *Quaternary Science Reviews*, 100, 10-30. doi:10.1016/j.quascirev.2013.07.024
- Maddison, E. J., Pike, J., Leventer, A., Dunbar, R., Brachfeld, S., Domack, E. W., Manley, P. & McClennen, C. (2006). Post-glacial seasonal diatom record of the Mertz Glacier Polynya, East Antarctica. *Marine Micropaleontology*, 60(1), 66-88.
- Marchitto, T. M. (2006). Precise multi-elemental ratios in small foraminiferal samples determined by sector field ICP-MS. *Geochemistry, Geophysics, Geosystems*, 7, Q05P13. doi:10.1029/2005GC001018.

- Marshall, G. J., Stott, P.A., Turner, J., Connolley, W. M., King, J. C. and Lachlan-Cope, T. A. (2004). Causes of exceptional atmospheric circulation changes in the Southern Hemisphere. *Geophysical Research Letters*, 31(14).
- Marshall, G. J., Di Battista, S., Naik, S. S., & Thamban, M. (2011). Analysis of a regional change in the sign of the SAM–temperature relationship in Antarctica. *Climate Dynamics*, 36(1-2), 277-287. doi:10.1007/s00382-009-0682-9
- Martin, P. A. & Lea, D. W. (2002). A simple evaluation of cleaning procedures on fossil benthic foraminiferal Mg/Ca. *Geochemistry, Geophysics, Geosystems*, 3, 1-8.
- Mashiotta, T. A., Lea, D. W., & Spero, H. J. (1999). Glacial–interglacial changes in Subantarctic sea surface temperature and $\delta^{18}\text{O}$ -water using foraminiferal Mg. *Earth and Planetary Science Letters*, 170(4), 417-432.
- Massom, R. A., Harris, P. T., Michael, K. J., & Potter, M. J. (1998). The distribution and formative processes of latent-heat polynyas in East Antarctica. *Annals of Glaciology*, 27(1), 420-426. doi:10.3189/1998AoG27-1-420-426
- Massom, R. A., Pook, M. J., Comiso, J. C., Adams, N., Turner, J., Lachlan-Cope, T. & Gibson, T. T. (2004). Precipitation over the interior East Antarctic ice sheet related to midlatitude blocking-high activity. *Journal of Climate*, 17(10), 1914-1928.
- Masson, V., Vimeux, F., Jouzel, J., Morgan, V., Delmotte, M., Ciais, P., et al. (2000). Holocene climate variability in Antarctica based on 11 ice-core isotopic records. *Quaternary Research*, 54(3), 348-358. doi:10.1006/qres.2000.2172
- Masson-Delmotte, V., Stenni, B., & Jouzel, J. (2004). Common millennial-scale variability of Antarctic and Southern Ocean temperatures during the past 5000 years reconstructed from the EPICA Dome C ice core. *The Holocene*, 14(2), 145-151. doi:10.1191/0959683604hl697ft
- Mawbey, E., Hendry, K., Greaves, M., Hillenbrand, C. D., Mackensen, A., Kuhn, G., et al. (2020). Mg/Ca-Temperature Calibration for Polar Benthic foraminiferal species for reconstruction of bottom water temperatures in the Antarctic shelf regions. *Geochimica et Cosmochimica Acta*, 283, 54-66.
- McCave, I.N., & Hall, I.R., (2006). Size sorting in marine muds: Processes, pitfalls, and prospects for paleoflow-speed proxies. *Geochemistry, Geophysics, Geosystems*, 7(10).
- McCave, I.N., Crowhurst, S.J., Kuhn, G., Hillenbrand, C.D., & Meredith, M.P. (2014). Minimal change in Antarctic Circumpolar Current flow speed between the last glacial and Holocene. *Nature Geoscience*, 7(2), 113-116.
- McCave, I. N., Thornalley, D. J. R., & Hall, I. R., (2017). Relation of sortable silt grain-size to deep-sea current speeds: Calibration of the ‘Mud Current Meter’. *Deep Sea Research Part I: Oceanographic Research Papers*, 127, 1-12.
- McCave, I. N., & Andrews, J. T. (2019). Distinguishing current effects in sediments delivered to the ocean by ice. Principles, methods and examples. *Quaternary Science Reviews*, 212, 92–107.
- McCorkle, D., Corliss, B. H., & Farnham, C. A. (1997). Vertical distributions and stable isotopic compositions of live (stained) benthic foraminifera from the North Carolina and California continental margins. *Deep-Sea Research*, 44, 983-1024. doi:10.1016/S0967-0637(97)00004-6

- McGlone, M. S., Turney, C. S., Wilmshurst, J. M., Renwick, J., & Pahnke, K. (2010). Divergent trends in land and ocean temperature in the Southern Ocean over the past 18,000 years. *Nature Geoscience*, 3(9), 622. doi:10.1038/NCEO931
- McCorkle, D.C., Corliss, B.H., & Farnham, C.A. (1997). Vertical distributions and stable isotopic compositions of live (stained) benthic foraminifera from the North Carolina and California continental margins. *Deep Sea Research Part I: Oceanographic Research Papers*, 44(6), 983-1024.
- McKay, R. M. L., Villareal, T. A., & La Roche, J. (2000). Vertical migration by *Rhizosolenia* spp. (Bacillariophyceae): Implications for Fe acquisition. *Journal of Phycology*, 36(4), 669-674. doi:10.1046/j.1529-8817.2000.99125.x
- McKay, R.M., Dunbar, G.B., Naish, T.R., Barrett, P.J., Carter, L. & Harper, M. (2008). Retreat history of the Ross Ice Sheet (Shelf) since the Last Glacial Maximum from deep-basin sediment cores around Ross Island. *Palaeogeography, Palaeoclimatology, Palaeoecology*, 260(1-2), 245-261.
- McKay, R., Golledge, N.R., Maas, S., Naish, T., Levy, R., Dunbar, G. & Kuhn, G. (2016). Antarctic marine ice-sheet retreat in the Ross Sea during the early Holocene. *Geology*, 44(1), 7-10.
- McMullen, K., Domack, E., Leventer, A., Olson, C., Dunbar, R., & Brachfeld, S. (2006). Glacial morphology and sediment formation in the Mertz Trough, East Antarctica. *Palaeogeography, Palaeoclimatology, Palaeoecology*, 231(1-2), 169-180.
- Mikis, A., Hendry, K. R., Pike, J., Schmidt, D. N., Edgar, K. M., Peck, V., et al. (2019). Temporal variability in foraminiferal morphology and geochemistry at the West Antarctic Peninsula: a sediment trap study. *Biogeosciences*, 16, 3267-3282.
- Miles, B. W., Stokes, C. R., & Jamieson, S. S. (2016). Pan-ice-sheet glacier terminus change in East Antarctica reveals sensitivity of Wilkes Land to sea-ice changes. *Science Advances*, 2(5), p.e1501350. doi:10.1126/sciadv.1501350
- Miles, B. W., Stokes, C. R., & Jamieson, S. S. (2018). Velocity increases at Cook Glacier, East Antarctica linked to ice shelf loss and a subglacial flood event. *The Cryosphere*, 12(10), 3123-3136. doi:10.5194/tc-12-3123-2018
- Miller, K. G., Fairbanks, R. G. & Mountain, G. S. (1987). Tertiary oxygen isotope synthesis, sea level history, and continental margin erosion. *Paleoceanography*, 2(1), 1-19.
- Miller, K. G., Wright, J. D. and Fairbanks, R. G. (1991). Unlocking the ice house: Oligocene-Miocene oxygen isotopes, eustasy, and margin erosion. *Journal of Geophysical Research: Solid Earth*, 96(B4), 6829-6848.
- Misra, S., Greaves, M., Owen, R., Kerr, J., Elmore, A.C., & H. Elderfield. (2014). Determination of B/Ca of natural carbonates by HR-ICP-MS. *Geochemistry, Geophysics, Geosystems*, 15, 1617-1628. doi:10.1002/2013GC005049.
- Mohajerani, Y., Velicogna, I. & Rignot, E. (2018). Mass loss of Totten and Moscow University glaciers, East Antarctica, using regionally optimized GRACE mascons. *Geophysical Research Letters*, 45(14), 7010-7018.
- Monnin, E., Indermühle, A., Dällenbach, A., Flückiger, J., Stauffer, B., Stocker, T.F., Raynaud, D. & Barnola, J.M. (2001). Atmospheric CO₂ concentrations over the last glacial termination. *Science*, 291(5501), 112-114.
- Monnin, E., Steig, E. J., Siegenthaler, U., Kawamura, K., Schwander, J., Stauffer, B., et al. (2004). Evidence for substantial accumulation rate variability in Antarctica during the Holocene, through synchronization of CO₂ in the Taylor Dome, Dome C and DML ice

- cores. *Earth and Planetary Science Letters*, 224(1-2), 45-54.
<https://doi.org/10.1016/j.epsl.2004.05.007>
- Montelli, A., Gulick, S. P. S., Fernandez, R., Frederick, B. C., Shevenell, A. E., Leventer, A., & Blankenship, D. D. (2020). Seismic stratigraphy of the Sabrina Coast shelf, East Antarctica: Early history of dynamic meltwater-rich glaciations. *GSA Bulletin*, 132(3-4), 545-561.
- Moreau, S., Lannuzel, D., Janssens, J., Arroyo, M.C., Corkill, M., Cougnon, E., et al. (2019). Sea ice meltwater and circumpolar deep water drive contrasting productivity in three Antarctic polynyas. *Journal of Geophysical Research: Oceans*, 124(5), 2943-2968.
- Morgan, V.I. (1985). An oxygen isotope—climate record from the Law Dome, Antarctica. *Climatic Change*, 7(4), 415-426.
- Morgan, V. & Van Ommen, T.D. (1997). Seasonality in late-Holocene climate from ice-core records. *The Holocene*, 7(3), 351-354.
- Morgan, V. I., Wookey, C. W., Li, J., Van Ommen, T. D., Skinner, W. and Fitzpatrick, M. F. (1997). Site information and initial results from deep ice drilling on Law Dome, Antarctica. *Journal of Glaciology*, 43(143), 3-10.
- Morgan, V., Delmotte, M., Van Ommen, T., Jouzel, J., Chappellaz, J., Woon, S., Masson-Delmotte, V., & Raynaud, D., (2002). Relative timing of deglacial climate events in Antarctica and Greenland. *Science*, 297(5588), 1862-1864.
- Morlighem, M., Rignot, E., Binder, T., Blankenship, D., Drews, R., Eagles, G., et al. (2020). Deep glacial troughs and stabilizing ridges unveiled beneath the margins of the Antarctic ice sheet. *Nature Geoscience*, 13(2), pp.132-137. doi: 10.1038/s41561-019-0510-8
- Mortlock, R.A. & Froelich, P.N. (1989). A simple method for the rapid determination of biogenic opal in pelagic marine sediments. *Deep Sea Research Part A. Oceanographic Research Papers*, 36(9), 1415-1426.
- Mortyn, P. G. & Charles, C. D. (2003). Planktonic foraminiferal depth habitat and $\delta^{18}\text{O}$ calibrations: Plankton tow results from the Atlantic sector of the Southern Ocean. *Paleoceanography*, 18(2). doi:10.1029/2001PA000637
- Moy, A. D., Howard, W. R., Bray, S. G. and Trull, T. W. (2009). Reduced calcification in modern Southern Ocean planktonic foraminifera. *Nature Geoscience*, 2(4), 276-280.
- Mulvaney, R., Abram, N.J., Hindmarsh, R.C., Arrowsmith, C., Fleet, L., Triest, J., et al. (2012). Recent Antarctic Peninsula warming relative to Holocene climate and ice-shelf history. *Nature*, 489(7414), 141-144. doi: 10.1038/nature11391
- Murray, J.W. & Pudsey, C.J. (2004). Living (stained) and dead foraminifera from the newly ice-free Larsen Ice Shelf, Weddell Sea, Antarctica: ecology and taphonomy. *Marine Micropaleontology*, 53(1-2), 67-81.
- Ninnemann, U. S. & Charles, C. D. (2002). Changes in the mode of Southern Ocean circulation over the last glacial cycle revealed by foraminiferal stable isotopic variability. *Earth and Planetary Science Letters*, 201(2), 383-396. doi:10.1016/S0012-821X(02)00708-2
- Nitsche, F. O., Porter, D., Williams, G., Cougnon, E. A., Fraser, A. D., Correia, R., & Guerrero, R. (2017). Bathymetric control of warm ocean water access along the East Antarctic Margin. *Geophysical Research Letters*, 44(17), 8936-8944. doi:10.1002/2017GL074433
- Noble, T.L., Rohling, E.J., Aitken, A.R.A., Bostock, H.C., Chase, Z., Gomez, N., et al. (2020). The Sensitivity of the Antarctic Ice Sheet to a Changing Climate: Past, Present, and Future. *Reviews of Geophysics*, 58(4), p.e2019RG000663.

- Nürnberg, D. (1995). Magnesium in tests of *Neogloboquadrina pachyderma* sinistral from high northern and southern latitudes. *The Journal of Foraminiferal Research*, 25(4), 350–368.
- Nyland, B.F., Jansen, E., Elderfield, H., & Andersson, C. (2006). *Neogloboquadrina pachyderma* (dex. and sin.) Mg/Ca and $\delta^{18}\text{O}$ records from the Norwegian Sea. *Geochemistry, Geophysics, Geosystems*, 7(10).
- O'Brien, P.E., Post, A.L., Edwards, S., Martin, T., Caburlotto, A., Donda, F., et al. (2020). Continental slope and rise geomorphology seaward of the Totten Glacier, East Antarctica (112 E-122 E). *Marine Geology*, 427, 106221.
- Orsi, A. H., Whitworth, T., & Nowlin, W. D. (1995). On the meridional extent and fronts of the Antarctic Circumpolar Current. *Deep-Sea Research Part I*, 42(5), 641-673.
- Orsi, A. H. & Wiederwohl, C. L. 2009. A recount of Ross Sea Waters. *Deep Sea Research II*, 56, 778-795.
- Paillard, D., Labeyrie, L., & Yiou, P. (1996). Macintosh program performs time-series analysis. *Eos. Transactions AGU*, 77(39), 379-379. doi:10.1029/96EO00259
- Paillard, D. (2001). Glacial cycles: toward a new paradigm. *Reviews of Geophysics*, 39(3), 325-346.
- Palmer, A. S., van Ommen, T. D., Curran, M. A., Morgan, V., Souney, J. M. & Mayewski, P. A. (2001). High-precision dating of volcanic events (AD 1301–1995) using ice cores from Law Dome, Antarctica. *Journal of Geophysical Research: Atmospheres*, 106(D22), 28089-28095.
- Paolo, F. S., Fricker, H. A., & Padman, L. (2015). Volume loss from Antarctic ice shelves is accelerating. *Science*, 348(6232), 327-331. doi:10.1126/science.aaa0940
- Park, Y.H., Vivier, F., Roquet, F. & Kestenare, E. (2009). Direct observations of the ACC transport across the Kerguelen Plateau. *Geophysical Research Letters*, 36(18).
- Park, E., Hefter, J., Fischer, G., Iversen, M. H., Ramondenc, S., Nöthig, E. M. and Mollenhauer, G. (2019). Seasonality of archaeal lipid flux and GDGT-based thermometry in sinking particles of high-latitude oceans: Fram Strait (79 N) and Antarctic Polar Front (50 S). *Biogeosciences*, 16(11), 2247-2268.
- Pearson, A. & Ingalls, A.E. (2013). Assessing the use of archaeal lipids as marine environmental proxies. *Annual Review of Earth and Planetary Sciences*, 41(1).
- Pedro, J. B., Van Ommen, T. D., Rasmussen, S.O., Morgan, V. I., Chappellaz, J., Moy, A. D., et al. (2011). The last deglaciation: timing the bipolar seesaw. *Climate of the Past*, 7(2), 671-683. doi:10.5194/cp-7-671-2011
- Perlwitz, J., Pawson, S., Fogt, R. L., Nielsen, J. E. & Neff, W. D. (2008). Impact of stratospheric ozone hole recovery on Antarctic climate. *Geophysical Research Letters*, 35(8).
- Pike, J., Swann, G. E., Leng, M. J., & Snelling, A. M. (2013). Glacial discharge along the west Antarctic Peninsula during the Holocene. *Nature Geoscience*, 6(3), 199. doi:10.1038/NCEO1703
- Plummer, C. T., Curran, M., Van Ommen, T. D., Rasmussen, S. O., Moy, A. D., Vance, T. R., Clausen, H. B., Vinther B. M., & Mayewski, P. A. (2012). An independently dated 2000-yr volcanic record from Law Dome, East Antarctica, including a new perspective on the dating of the 1450s CE eruption of Kuwae, Vanuatu. *Climate of the Past*, 8(6), 1929.
- Plummer, C. T. (2018). *A Holocene Trace Chemistry Record from Law Dome Ice Cores* (Doctoral Dissertation). Retrieved from University of Tasmania Open Access Repository (<https://eprints.utas.edu.au/28348/>). Hobart, Tasmania: University of Tasmania.

- Pollard, D. & DeConto, R. M. (2005). Hysteresis in Cenozoic Antarctic ice-sheet variations. *Global and Planetary Change*, 45(1-3), 9-21. doi:0.1016/j.gloplacha.2004.09.011
- Pollard, D., DeConto, R. M., & Alley, R. B. (2015). Potential Antarctic Ice Sheet retreat driven by hydrofracturing and ice cliff failure. *Earth and Planetary Science Letters*, 412, 112-121.
- Pondaven, P., Fravallo, C., Ruiz-Pino, D., Tréguer, P., Quéguiner, B., & Jeandel, C. (1998). Modelling the silica pump in the Permanently Open Ocean Zone of the Southern Ocean. *Journal of Marine Systems.*, 17(1), 587-619. doi:10.1016/S0924-7963(98)00066-9
- Post, A. L., Lavoie, C., Domack, E. W., Leventer, A., Shevenell, A. E., & Fraser, A. D. (2017). Environmental drivers of benthic communities and habitat heterogeneity on an East Antarctic shelf. *Antarctic Science*, 29(1), 17-32. doi:10.1017/S0954102016000468
- Presti, M., De Santis, L., Busetti, M., & Harris, P. T. (2003). Late Pleistocene and Holocene sedimentation on the George V continental shelf, East Antarctica. *Deep Sea Research Part II: Topical Studies in Oceanography*, 50(8-9), pp.1441-1461. doi:10.1016/S0967-0645(03)00068-7
- Pritchard, H. D., Arthern, R. J., Vaughan, D. G., & Edwards, L. A. (2009). Extensive dynamic thinning on the margins of the Greenland and Antarctic ice sheets. *Nature*, 461(7266), 971-975. doi:10.1038/nature08471
- Pritchard, H. D., Ligtenberg, S. R. M., Fricker, H. A., Vaughan, D. G., van den Broeke, M. R., & Padman, L. (2012). Antarctic ice-sheet loss driven by basal melting of ice shelves. *Nature*, 484, 502-505. doi:10.1038/nature10968
- Prothro, L. O., Simkins, L. M., Majewski, W., & Anderson, J. B., 2018. Glacial retreat patterns and processes determined from integrated sedimentology and geomorphology records. *Marine Geology*, 395, 104-119.
- Purkey, S.G. & Johnson, G.C. (2010). Warming of global abyssal and deep Southern Ocean waters between the 1990s and 2000s: Contributions to global heat and sea level rise budgets. *Journal of Climate*, 23(23), 6336-6351.
- Qin, W., Carlson, L. T., Armbrust, E. V., Devol, A. H., Moffett, J. W., Stahl, D. A., & Ingalls, A. E. (2015). Confounding effects of oxygen and temperature on the TEX₈₆ signature of marine Thaumarchaeota. *Proceedings of the National Academy of Sciences USA* 112, 10979–10984.
- Quéguiner, B. (2013). Iron fertilization and the structure of planktonic communities in high nutrient regions of the Southern Ocean. *Deep-Sea Research Pt. II*, 90, 43-54. doi:10.1016/j.dsr2.2012.07.024
- Quilty, P.G. (2001). Reworked Paleocene and Eocene foraminifera, Mac. Robertson Shelf, East Antarctica: paleoenvironmental implications. *Journal of Foraminiferal Research*, 31(4), 369-384.
- Raphael, M. N. & Hobbs, W. (2014). The influence of the large-scale atmospheric circulation on Antarctic sea ice during ice advance and retreat seasons. *Geophysical Research Letters*, 41(14), 5037-5045.
- Rathburn, A.E. & Corliss, B.H. (1994). The ecology of living (stained) deep-sea benthic foraminifera from the Sulu Sea. *Paleoceanography*, 9(1), 87-150.
- Rathburn, A.E. & P. DeDeckker. 1997. Magnesium and strontium compositions of Recent benthic foraminifera from the Coral Sea, Australia and Prydz Bay, Antarctica. *Marine Micropaleontology* 32, 231-248, doi:10.1016/S0377-8398(97)00028-5
- Raymo, M. E., Lisiecki, L. E. & Nisancioglu, K. H. (2006). Plio-Pleistocene ice volume, Antarctic climate, and the global $\delta^{18}\text{O}$ record. *Science*, 313(5786), 492-495.
- Regenberg, M., Regenberg, A., Garbe-Schönberg, D. & Lea, D.W. (2014). Global dissolution

- effects on planktonic foraminiferal Mg/Ca ratios controlled by the calcite-saturation state of bottom waters. *Paleoceanography*, 29(3), 127-142.
- Renssen, H., Goosse, H., Fichefet, T., Masson-Delmotte, V., & Koç, N. (2005). Holocene climate evolution in the high-latitude southern hemisphere simulated by a coupled atmosphere-sea ice-ocean-vegetation model. *The Holocene*, 15(7), 951-964. doi:10.1191/0959683605hl869ra
- Renwick, J. A. (1998). ENSO-related variability in the frequency of South Pacific blocking. *Monthly Weather Review*, 126(12), 3117-3123.
- Reynolds, L. A. & Thunell, R. C. (1986). Seasonal production and morphologic variation of *Neogloboquadrina pachyderma* (Ehrenberg) in the northeast Pacific. *Micropaleontology*, 1-18. doi:10.2307/1485696
- Rignot, E. & Jacobs, S. (2002). Rapid bottom melting widespread near Antarctic Ice Sheet grounding lines. *Science*, 296, 2020-2023. doi:10.1126/science.1070942
- Rignot, E., Bamber, J. L., van den Broeke, M. R., Davis, C., Li, Y., van de Berg, W. J., & van Meijgaard, E. (2008). Recent Antarctic ice mass loss from radar interferometry and regional climate modeling. *Nature Geoscience*, 1, 106-110. doi:10.1038/ngeo102
- Rignot, E., Jacobs, S., Mouginot, J., & Scheuchl, B. (2013). Ice Shelf Melting Around Antarctica. *Science*, 341, 266-270. doi:10.1126/science.1235798
- Rintoul, S. R. (1998). On the origin and influence of Adélie Land Bottom Water. Pp. 151–171 in *Ocean, Ice, Atmosphere: Interactions at the Antarctic Continental Margin*. Antarctic Research Series, vol. 75, S.S. Jacobs and R.F. Weiss, eds, American Geophysical Union, Washington, D.C.
- Rintoul, S. R., Silvano, A., Pena-Molino, B., van Wijk, E., Rosenberg, M., Greenbaum, J. S., & Blankenship, D. D. (2016). Ocean heat drives rapid basal melt of the Totten Ice Shelf. *Science Advances*, 2(12), p.e1601610.
- Roberts, J., Plummer, C., Vance, T., Van Ommen, T., Moy, A., Poynter, S., Treverrow, A., Curran, M. and George, S. (2015). A 2000-year annual record of snow accumulation rates for Law Dome, East Antarctica. *Climate of the Past*, 11(5), 697-707.
- Rose, K. C., Ferraccioli, F., Jamieson, S. S., Bell, R.E., Corr, H., Creyts, T. T., Braaten, D., Jordan, T. A., Fretwell, P. T. and Damaske, D. (2013). Early East Antarctic Ice Sheet growth recorded in the landscape of the Gamburtsev Subglacial Mountains. *Earth and Planetary Science Letters*, 375, 1-12.
- Rosenheim, B. E., Day, M. B., Schrum, H., Domack E. W., Benthien, A., & Hayes, J. M. (2008). Antarctic sediment chronology by programmed temperature pyrolysis: Methodology and data treatment. *Geochemistry, Geophysics, Geosystems*, 9, Q04005. doi:10.1029/2007GC001816
- Rosenheim, B. E., Santoro, J. A., Gunter, M., & Domack, E. W. (2013). Improving Antarctic sediment ¹⁴C dating using ramped pyrolysis: An example from the Hugo Island trough. *Radiocarbon*, 55, 115-126. doi:10.2458/azu_js_rc.v55i1.16234
- Rosenthal, Y., Field, M. P., & Sherrell, R. M. (1999). Precise determination of element/calcium ratios in calcareous samples using sector field inductively coupled plasma mass spectrometry. *Analytical chemistry*, 71(15), 3248-3253.
- Röthlisberger, R., Mulvaney, R., Wolff, E. W., Hutterli, M. A., Bigler, M., Sommer, S., & Jouzel, J. (2002). Dust and sea salt variability in central East Antarctica (Dome C) over the last 45 kyrs and its implications for southern high-latitude climate. *Geophysical Research Letters*, 29(20), 24-1. doi:10.1029/2002GL015186

- Saunders, K. M., Roberts, S. J., Perren, B., Butz, C., Sime, L., Davies, S., et al. (2018). Holocene dynamics of the southern hemisphere westerly winds and possible links to CO₂ outgassing. *Nature Geoscience*, *11*, 650-655. doi:0.1038/s41561-018-0186-5
- Scherer, R. P. (1994). A new method for the determination of absolute abundance of diatoms and other silt-sized sedimentary particles. *Journal of Paleolimnology*, *12*(2), 171-179.
- Schoof, C. (2007). Ice sheet grounding line dynamics: Steady states, stability, and hysteresis. *Journal of Geophysical Research: Earth Surface*, *112*(F3).
- Schouten, S., Hopmans, E.C., Schefuß, E., & J. S. S. Damsté. 2002. Distributional variations in marine crenarchaeotal membrane lipids: A new tool for reconstructing ancient sea water temperatures? *Earth and Planetary Science Letters*, *204*, 265-274. doi:10.1016/S0012-821X(02)00979-2.
- Schouten, S., Hopmans, E.C., & J. S. S. Damsté. 2004. The effect of maturity and depositional redox conditions on archaeal tetraether lipid paleothermometry. *Organic Geochemistry*, *35*, 567-571, doi:10.1016/j.orggeochem.2004.01.012.
- Schrag, D. P., (1999). Rapid analysis of high-precision Sr/Ca ratios in corals and other marine carbonates. *Paleoceanography*, *14*(2), 97-102.
- Schröder, L., Horwath, M., Dietrich, R., Helm, V., Van Den Broeke, M. R., & Ligtenberg, S. R. (2019). Four decades of Antarctic surface elevation changes from multi-mission satellite altimetry. *The Cryosphere*, *13*(2), 427-449.
- Sedwick, P. N., Harris, P. T., Robertson, L. G., McMurtry, G. M., Cremer, M. D., & Robinson, P. (1998). A geochemical study of marine sediments from the Mac.Robertson shelf, East Antarctica: initial results and paleoenvironmental implications. *Annals of Glaciology*, *27*(1), 268-274. doi:10.3189/1998AoS27-1-268-274
- Shackleton, N. J. (1974). Attainment of isotopic equilibrium between ocean water and the benthonic foraminifera genus *Uvigerina*: isotopic changes in the ocean during the last glacial. *Colloques Internationaux du Centre National de la Recherche Scientifique*, *219*, 203-209.
- Shackleton, N. J. (1997). The deep-sea sediment record and the Pliocene-Pleistocene boundary. *Quaternary International*, *40*, 33-35.
- Shah, S. R., Mollenhauer, G., Ohkouchi, N., Eglinton, T. I. & Pearson, A. (2008). Origins of archaeal tetraether lipids in sediments: Insights from radiocarbon analysis. *Geochimica et Cosmochimica Acta*, *72*, 4577-4594.
- Shakun, J. D., Lea, D. W., Lisiecki, L. E. and Raymo, M. E. (2015a). An 800-kyr record of global surface ocean $\delta^{18}\text{O}$ and implications for ice volume-temperature coupling. *Earth and Planetary Science Letters*, *426*, 58-68.
- Shakun, J. D., Clark, P. U., He, F., Lifton, N. A., Liu, Z. & Otto-Bliesner, B. L. (2015b). Regional and global forcing of glacier retreat during the last deglaciation. *Nature Communications*, *6*(1), 1-7.
- Shepherd, A., Wingham, D., & Rignot, E. (2004). Warm ocean is eroding West Antarctic Ice Sheet. *Geophysical Research Letters*, *31*, L23402. doi:10.1029/2004GL021106
- Shepherd, A. & Wingham, D. (2007). Recent sea-level contributions of the Antarctic and Greenland Ice Sheets. *Science*, *315*, 1529-1532.
- Shevenell, A. E. & Kennett J. P. (2002). Shevenell, A.E. and Kennett, J.P., 2002. Antarctic Holocene climate change: A benthic foraminiferal stable isotope record from Palmer Deep. *Paleoceanography*, *17*(2), PAL-9. doi:10.1029/2000PA000596

- Shevenell, A. E., Kennett, J. P. & Lea, D. W. (2004). Middle Miocene southern ocean cooling and Antarctic cryosphere expansion. *Science*, 305(5691), 1766-1770.
- Shevenell, A. E., Ingalls, A. E., Domack, E. W., & Kelly, C. (2011). Holocene Southern Ocean surface temperature variability west of the Antarctic Peninsula. *Nature*, 470(7333), 250. doi:10.1038/nature09751
- Shevenell, A. E. & Bohaty, S. M. (2012). Southern exposure: New paleoclimate insights from Southern Ocean and Antarctic margin sediments. *Oceanography*, 25, 106-117. doi:10.5670/oceanog.2012.82
- Sigman, D. M. & Boyle, E. A. (2000). Glacial/interglacial variations in atmospheric carbon dioxide. *Nature*, 407(6806), 859.
- Signori, C. N., Pellizari, V. H., Enrich-Prast, A., & Sievert, S. M. (2018). Spatiotemporal dynamics of marine bacterial and archaeal communities in surface waters off the northern Antarctic Peninsula. *Deep-Sea Research Part II: Topical Studies in Oceanography*, 149, 150-160. doi:10.1016/j.dsr2.2017.12.017
- Silvano, A., Rintoul, S.R. & Herraiz-Borreguero, L., 2016. Ocean-ice shelf interaction in East Antarctica. *Oceanography*, 29(4), 130-143.
- Silvano, A., Rintoul, S. R., Peña-Molino, B., & Williams, G. D. (2017). Distribution of water masses and meltwater on the continental shelf near the Totten and Moscow University ice shelves. *Journal of Geophysical Research Oceans*, 122, 2050–2068. doi:10.1002/2016JC012115
- Silvano, A., Rintoul, S. R., Peña-Molino, B., Hobbs, W. R., van Wijk, E., Aoki, S., Tamura, T. & Williams, G. D. (2018). Freshening by glacial meltwater enhances melting of ice shelves and reduces formation of Antarctic Bottom Water. *Science Advances*, 4(4), eaap9467. doi:10.1126/sciadv.aap9467
- Silvano, A., Rintoul, S.R., Kusahara, K., Peña-Molino, B., van Wijk, E., Gwyther, D.E. & Williams, G.D. (2019). Seasonality of warm water intrusions onto the continental shelf near the Totten Glacier. *Journal of Geophysical Research: Oceans*, 124(6), pp.4272-4289. doi:10.1029/2018JC014634
- Simmonds, I. & Jacka, T. H. (1995). Relationship between the interannual variability of Antarctic sea-ice and the Southern Oscillation index. *Journal of Climate* 8, 637-647.
- Singler, H. R. & Villareal, T. A. (2005). Nitrogen inputs into the euphotic zone by vertically migrating *Rhizosolenia* mats. *Journal of Plankton Research*, 27(6), 545-556.
- Skinner, L.C., Fallon, S., Waelbroeck, C., Michel, E., & Barker, S. (2010). Ventilation of the deep Southern Ocean and deglacial CO₂ rise. *Science*, 328(5982), 1147-1151. doi: 10.1126/science.1183627
- Skinner, L. C., Muschitiello, F., & Scrivner, A. E. (2019). Marine Reservoir Age Variability Over the Last Deglaciation: Implications for Marine Carbon Cycling and Prospects for Regional Radiocarbon Calibrations. *Paleoceanography and Paleoclimatology*, 34(11), 1807-1815. doi: 10.1029/2019PA003667
- Smetacek, V. S. (1985). Role of sinking in diatom life-history cycles: ecological, evolutionary and geological significance. *Marine Biology*, 84(3), pp.239-251.
- Smetacek, V., De Baar, H.J.W., Bathmann, U. V., Lochte, K., & Van Der Loeff, M. R. (1997). Ecology and biogeochemistry of the Antarctic Circumpolar Current during austral spring: a summary of Southern Ocean JGOFS cruise ANT X/6 of RV Polarstern. *Deep Sea Research Part II: Topical Studies in Oceanography*, 44(1-2), 1-21. doi: 10.1016/S0967-0645(96)00100-2

- Smith, J. A., Hillenbrand, C. D., Kuhn, G., Larter, R. D., Graham, A. G., Ehrmann, W., et al. (2011). Deglacial history of the West Antarctic Ice Sheet in the western Amundsen Sea embayment. *Quaternary Science Reviews*, 30(5-6), 488-505. doi:10.1016/j.quascirev.2010.11.020
- Smith, J. A., Andersen, T. J., Shortt, M., Gaffney, A. M., Truffer, M., Stanton, T. P., et al. (2016). Sub-ice-shelf sediments record history of twentieth-century retreat of Pine Island Glacier. *Nature*, 541(7635), 77–80. <https://doi.org/10.1038/nature20136>
- Smith, J. A., Graham, A. G., Post, A. L., Hillenbrand, C.D., Bart, P. J. & Powell, R. D. (2019). The marine geological imprint of Antarctic ice shelves. *Nature communications*, 10(1), 1-16.
- Spence, P., Griffies, S. M., England, M. H., Hogg, A. M., Saenko, O. A., & Jourdain, N. C. (2014). Rapid subsurface warming and circulation changes of Antarctic coastal waters by poleward shifting winds. *Geophysical Research Letters*, 41(13), 4601-4610. doi:10.1002/2014GL060613
- Stammerjohn, S. E., Martinson, D. G., Smith, R.C., Yuan, X. and Rind, D. (2008). Trends in Antarctic annual sea ice retreat and advance and their relation to El Niño–Southern Oscillation and Southern Annular Mode variability. *Journal of Geophysical Research: Oceans*, 113(C3).
- Steig, E. J., Hart, C. P., White, J. W., Cunningham, W. L., Davis, M. D., & Saltzman, E. S. (1998). Changes in climate, ocean and ice-sheet conditions in the Ross embayment, Antarctica, at 6 ka. *Annals of Glaciology*, 27, 305-310. doi:10.3189/1998AoG27-1-305-310
- Steig, E. J., Morse, D. L., Waddington, E. D., Stuiver, M., Grootes, P. M., Mayewski, P. A., et al. (2000). Wisconsinan and Holocene climate history from an ice core at Taylor Dome, western Ross Embayment, Antarctica. *Geografiska Annaler: Series A, Physical Geography*, 82(2-3), 213-235. doi:10.1111/j.0435-3676.2000.00122.x
- Steig, E. J., Ding, Q., Battisti, D. S., & Jenkins, A. (2012). Tropical forcing of Circumpolar Deep Water inflow and outlet glacier thinning in the Amundsen Sea Embayment, West Antarctica. *Annals of Glaciology*, 53(60), 19-28. doi: 0.3189/2012AoG60A110
- Stenni, B., Masson-Delmotte, V., Johnsen, S., Jouzel, J., Longinelli, A., Monnin, E., et al. (2001). An oceanic cold reversal during the last deglaciation. *Science*, 293(5537), 2074-2077. doi:10.1126/science.1059702
- Sternal, B., Szczuciski, W., Forwick, M., Zajączkowski, M., Lorenc, S. and Przytarska, J. (2014). Postglacial variability in near-bottom current speed on the continental shelf off south-west Spitsbergen. *Journal of Quaternary Science*, 29(8), 767-777.
- Stickley, C. E., Pike, J., Leventer, A., Dunbar, R., Domack, E. W., Brachfeld, S., et al. (2005). Deglacial ocean and climate seasonality in laminated diatom sediments, Mac. Robertson Shelf, Antarctica. *Palaeogeography, Palaeoclimatology, Palaeoecology*, 227(4), 290-310. doi:10.1016/j.palaeo.2005.05.021
- Stuiver, M., Reimer, P. J., and Reimer, R. W. (2020). CALIB. 2020. Available online: <http://calib.org>
- Subt, C., Fangman, K. A., Wellner, J. S., & Rosenheim, B. E. (2015). Sediment chronology in Antarctic deglacial sediments: Reconciling organic carbon ¹⁴C ages to carbonate ¹⁴C ages using Ramped PyrOx. *Holocene*, 26, 265-273. doi:10.1177/0959683615608688
- Subt, C., Fangman, K. A., Wellner, J. S., & Rosenheim, B. E. (2016). Sediment chronology in Antarctic deglacial sediments: Reconciling organic carbon 14C ages to carbonate 14C

- ages using Ramped PyrOx. *The Holocene*, 26(2), 265-273.
doi:10.1177/0959683615608688
- Subt, C., Yoon, H. I., Yoo, K. C., Lee, J. I., Leventer, A., Domack, E. W., & Rosenheim, B. E. (2017). Sub-ice shelf sediment geochronology utilizing novel radiocarbon methodology for highly detrital sediments. *Geochemistry, Geophysics, Geosystems*, 18(4), 1404-1418. doi:10.1002/2016GC006578
- Tamura, T., Ohshima, K. I., Fraser, A. D., & Williams, G. D. (2016). Sea ice production variability in Antarctic coastal polynyas. *Journal of Geophysical Research Oceans*, 121(5), 2967-2979.
- Taylor, F., Whitehead, J. & Domack, E. (2001). Holocene paleoclimate change in the Antarctic Peninsula: evidence from the diatom, sedimentary and geochemical record. *Marine Micropaleontology*, 41(1-2), 25-43.
- Taylor, F., & Sjunneskog, C. (2002). Postglacial marine diatom record of the Palmer deep, Antarctic Peninsula (ODP Leg 178, site 1098) 2. Diatom assemblages. *Paleoceanography*, 17(3). doi:10.1029/2000PA000564
- Thoma, M., Jenkins, A., Holland, D., & Jacobs, S. (2008). Modelling circumpolar deep water intrusions on the Amundsen Sea continental shelf, Antarctica. *Geophysical Research Letters*, 35(18). doi:10.1029/2008GL034939
- Thompson, R. & Oldfield, F. (1986). Magnetic properties of natural materials. In Springer, *Environmental Magnetism*, 21-38.
- Thompson, A. F., Stewart, A. L., Spence, P., & Heywood, K. J. (2018). The Antarctic Slope Current in a changing climate. *Reviews of Geophysics*, 56(4), pp.741-770. doi:10.1029/2018RG000624
- Thompson, D. W., Wallace, J. M. & Hegerl, G. C. (2000). Annular modes in the extratropical circulation. Part II: Trends. *Journal of Climate*, 13(5), 1018-1036.
- Thompson, D. W. & Solomon, S. (2002). Interpretation of recent southern hemisphere climate change. *Science*, 296(5569), 895-899. doi:10.1126/science.1069270
- Tierney, J. E., Malevich, S. B., Gray, W., Vetter, L. and Thirumalai, K. (2019). Bayesian calibration of the Mg/Ca paleothermometer in planktic foraminifera. *Paleoceanography and Paleoclimatology*, 34(12), 2005-2030.
- Timmermann, A., Timm, O., Stott, L., & Menviel, L. (2009). The roles of CO₂ and orbital forcing in driving southern hemispheric temperature variations during the last 21 000 yr. *Journal of Climate*, 22(7), 1626-1640. doi:10.1175/2008JCLI2161.1
- Toggweiler, J. R. & Samuels, B. (1998). On the ocean's large-scale circulation near the limit of no vertical mixing. *Journal of Physical Oceanography*, 28, 1832-1852.
- Tolar, B. B., Ross, M. J., Wallsgrave, N. J., Liu, Q., Aluwihare, L. I., Popp, B. N., & Hollibaugh, J. T. (2016). Contribution of ammonia oxidation to chemoautotrophy in Antarctic coastal waters. *ISME Journal*, 10(11), 2605–2619. doi:10.1038/ismej.2016.61
- Tooze, S., Halpin, J.A., Noble, T.L., Chase, Z., O'Brien, P.E. & Armand, L. (2020). Scratching the surface: a marine sediment provenance record from the continental slope of central Wilkes Land, East Antarctica. *Geochemistry, Geophysics, Geosystems*, 21(11), p.e2020GC009156.
- Turner, J., 2004. The El Nino-Southern Oscillation and Antarctica. *International Journal of Climatology: A Journal of the Royal Meteorological Society*, 24(1), 1-31.

- Uda, I., Sugai, A., Itoh, Y. H. & Itoh, T. (2001). Variation in molecular species of polar lipids from *Thermoplasma acidophilum* depends on growth temperature. *Lipids*, 36(1), 103-105.
- Van Den Broeke, M.R. & Van Lipzig, N.P. (2004). Changes in Antarctic temperature, wind and precipitation in response to the Antarctic Oscillation. *Annals of Glaciology*, 39, 119-126.
- Van Ommen, T. D., Morgan, V., & Curran, M. A. (2004). Deglacial and Holocene changes in accumulation at Law Dome, East Antarctica. *Annals of Glaciology*, 39, 359-365. doi:10.3189/172756404781814221
- Van Ommen, T.D. & Morgan, V. (2010). Snowfall increase in coastal East Antarctica linked with southwest Western Australian drought. *Nature Geoscience*, 3(4), 267-272.
- Vance, T. R., Van Ommen, T. D., Curran, M. A., Plummer, C. T. and Moy, A. D. (2013). A millennial proxy record of ENSO and eastern Australian rainfall from the Law Dome ice core, East Antarctica. *Journal of Climate*, 26(3), 710-725. doi:10.1175/JCLI-D-12-00003.1
- Varma, V., Prange, M., Lamy, F., Merkel, U. & Schulz, M. (2011). Solar-forced shifts of the Southern Hemisphere Westerlies during the Holocene. *Climate of the Past* 7, 339–347.
- Vázquez Riveiros, N., Govin, A., Waelbroeck, C., Mackensen, A., Michel, E., Moreira, S., Bouinot, T., Caillon, N., Orgun, A., & Brandon, M. (2006). Mg/Ca thermometry in planktic foraminifera: Improving paleotemperature estimations for *G. bulloides* and *N. pachyderma* left. *Geochemistry, Geophysics, Geosystems*, 17(4), 1249-1264.
- Venturelli, R. A., Siegfried, M. R., Roush, K. A., Li, W., Burnett, J., Zook, R., et al. (2020). Mid-Holocene grounding line retreat and readvance at Whillans Ice Stream, West Antarctica. *Geophysical Research Letters*, 47(15), e2020GL088476. doi: 10.1029/2020GL088476
- Verleyen, E., Hodgson, D. A., Milne, G. A., Sabbe, K., & Vyverman, W. (2005). Relative sea-level history from the Lambert Glacier region, East Antarctica, and its relation to deglaciation and Holocene glacier readvance. *Quaternary Research*, 63(1), 45-52. doi:10.1016/j.yqres.2004.09.005
- Villareal, T. A., Woods, S., Moore, J. K., & Culver Rymysz, K. (1996). Vertical migration of *Rhizosolenia* mats and their significance to NO_3^- fluxes in the central North Pacific gyre. *Journal of Plankton Research*, 18(7), 1103-1121. doi:10.1093/plankt/18.7.1103
- Vimeux, F., Masson, V., Jouzel, J., Petit, J. R., Steig, E. J., Stievenard, M., et al. (2001). Holocene hydrological cycle changes in the southern hemisphere documented in East Antarctic deuterium excess records. *Climate Dynamics*, 17(7), 503-513.
- Wåhlin, A. K., Yuan, X., Björk, G., & Nohr, C. (2010). Inflow of Warm Circumpolar Deep Water in the Central Amundsen Shelf. *Journal of Physical Oceanography* 40, 1427-1434.
- WAIS Divide Project Members. (2013). Onset of deglacial warming in West Antarctica driven by local orbital forcing. *Nature*, 500(7463), 440.
- Wangner, D. J., Sicre, M.A., Kjeldsen, K. K., Jaeger, J. M., Björk, A. A., Vermassen, F., Sha, L., Kjær, K. H., Klein, V. and Andresen, C. S. (2020). Sea Surface Temperature Variability on the SE-Greenland Shelf (1796–2013 CE) and Its Influence on Thrym Glacier in Nørre Skjoldungesund. *Paleoceanography and Paleoclimatology*, 35(3), p.e2019PA003692. doi: 10.1029/2019PA003692
- Warnock, J. P. & Scherer, R. P. (2015). A revised method for determining the absolute abundance of diatoms. *Journal of Paleolimnology*, 53 (1), pp.157-163. doi:10.1007/s10933-014-9808-0

- Whitworth, T., Orsi, A. H., Kim, S-J., Nowlin, W. D., & R. A. Locarnini. (1998). Water Masses and Mixing Near the Antarctic Slope Front. *Antarctic Research Series*, 75, 1-27.
- Weber, M. E., Clark, P. U., Kuhn, G., Timmermann, A., Sprenk, D., Gladstone, R., et al. (2014). Millennial-scale variability in Antarctic ice-sheet discharge during the last deglaciation. *Nature*, 510(7503), 134. doi:10.1038/nature13397
- Willeit, M., Ganopolski, A., Calov, R., Robinson, A. & Maslin, M. (2015). The role of CO₂ decline for the onset of Northern Hemisphere glaciation. *Quaternary Science Reviews*, 119, 22-34.
- Williams, E. K., Rosenheim, B. E., McNichol, A. P. & Masiello, C. A. (2014). Charring and non-additive chemical reactions during ramped pyrolysis: applications to the characterization of sedimentary and soil organic material. *Organic Geochemistry*, 77, 106-114, doi:10.1016/j.orggeochem.2014.10.006.
- Williams, G. D., Nicol, S., Aoki, S., Meijers, A. J. S., Bindoff, N. L., Iijima, Y., et al. (2011), Surface oceanography of BROKE-West along the Antarctic margin of the south-west Indian Ocean (30-80°E). *Deep-Sea Research Pt. II*, 57, 738-757. doi:10.1016/j.dsr2.2009.04.020
- Wingham, D. J., Siegert, M. J., Shepherd, A. & Muir, A. S. (2006). Rapid discharge connects Antarctic subglacial lakes. *Nature*, 440, 1033-1036, doi:10.1038/nature04660.
- Wolff, E. W., Barbante, C., Becagli, S., Bigler, M., Boutron, C.F., Castellano, E., et al. (2010). Changes in environment over the last 800,000 years from chemical analysis of the EPICA Dome C ice core. *Quaternary Science Reviews*, 29(1-2), 285-295.
- Wright, A. P., Young, D. A., Roberts, J. L., Schroeder, D. M., Bamber, J. L., Dowdeswell, J. A., et al. (2012). Evidence of a hydrological connection between the ice divide and ice sheet margin in the Aurora Subglacial Basin, East Antarctica. *Journal of Geophysical Research: Earth Surface*, 117(F1). doi:10.1029/2011JF002066
- Young, D. A., Wright, A. P., Roberts, J. L., Warner, R. C., Young, N. W., Greenbaum, J. S., et al. (2011). A dynamic early East Antarctic Ice Sheet suggested by ice-covered fjord landscapes. *Nature*, 474, 72–75. doi:10.1038/nature10114
- Yu, J. & Elderfield, H. (2008). Mg/Ca in the benthic foraminifera *Cibicides wuellerstorfi* and *Cibicides mundulus*: Temperature versus carbonate ion saturation. *Earth and Planetary Science Letters*, 276(1-2), 129-139.
- Yu, L., Zhong, S. & Sun, B. (2020). The climatology and trend of surface wind speed over Antarctica and the Southern Ocean and the implication to wind energy application. *Atmosphere*, 11(1), p.108.
- Yuan, X. (2004). ENSO-related impacts on Antarctic sea ice: a synthesis of phenomenon and mechanisms. *Antarctic Science*, 16(4), 415.
- Zachos, J., Pagani, M., Sloan, L., Thomas, E., & Billups, K. (2001). Trends, rhythms, and aberrations in global climate 65 Ma to present. *Science*, 292(5517), 686-693.
- Zhang, Y. G., Zhang, C. L., Liu, X. L., Li, L., Hinrichs, K. U. & Noakes, J. E. (2011). Methane Index: A tetraether archaeal lipid biomarker indicator for detecting the instability of marine gas hydrates. *Earth and Planetary Science Letters*, 307(3-4), 525-534.
- Zhang, Y. G., Pagani, M., & Wang, Z. (2016). Ring Index: A new strategy to evaluate the integrity of TEX86 paleothermometry. *Paleoceanography*, 31(2), 220–232. <https://doi.org/10.1002/2015PA002848>
- Zwartz, D., Bird, M., Stone, J., & Lambeck, K. (1998). Holocene sea-level change and ice-sheet history in the Vestfold Hills, East Antarctica. *EPSL*, 155(1-2), 131-145

APPENDIX A:

CHAPTER 2 SUPPLEMENTARY MATERIAL

Text A1.

We apply a blank correction of $1.15 \pm 0.91 \mu\text{g}$ and a modern blank of $2.52 \pm 1.65 \mu\text{g}$ (Figure A1) as determined by the 2015-2019 compilation of Venturelli et al. (2020). We determine the mass of (a) modern and (b) dead contributions of carbon from the Ramped PyrOx ^{14}C system by repeatedly analyzing graphite ($n=37$) and oxalic acid ($n=32$), respectively, using the methods outlined in Fernandez et al (2014). Past work has noted that a reduction in blank contamination in the RPO system was made when Teflon tubing was replaced with stainless steel and copper tubing (Subt et al., 2017), and we build upon previously reported blank values with the addition of more analyses of our internal standards. Neither modern nor dead blank contamination appear to have any relationship with time, allowing compilation of blank determinations over a longer period of time.

Text A2.

Figure A2 demonstrates two different Bayesian models for ages in the laminated sequences in JPC-57 and JPC-27. Unit IV is interpreted as initiation of open water at the sites. The difference between the ages at the two core sites is 1850 calendar years, not accounting for error. Because of the differing number of laminations in Unit IV in each core, which could be a result of missing time or a differential lack in deposition in the cores, as well as the lack of age constraint on Unit III, we elect to not assign a chronology through either of the lowest data points from JPC-27 and JPC-57.

Table A1. JPC-27 and JPC-57 deglacial radiocarbon dates

Core	Avg. depth (cmbsf)	Avg. Depth (cmcd)	Age (cal yr BP)
JPC-57	657 cmbsf	982 cmcd	14250±380
JPC-27	954 cmbsf	986 cmcd	16200±390

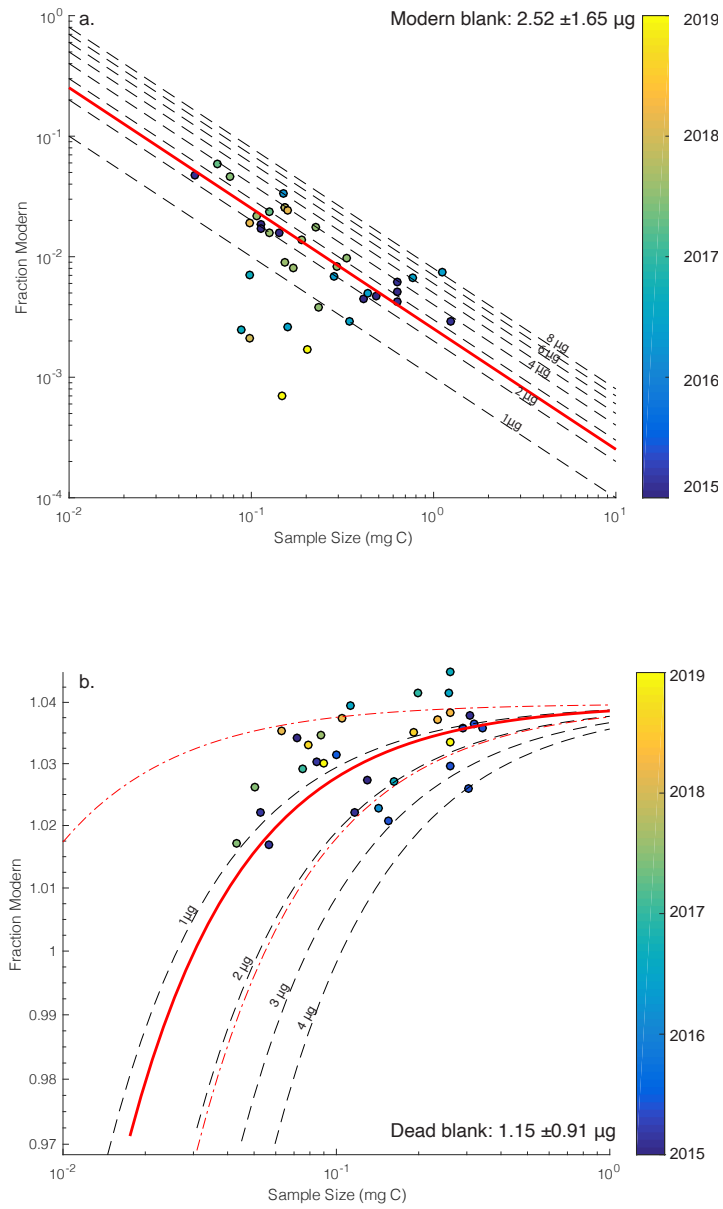


Figure A1. Determinations of (a) modern and (b) dead contributions of carbon.

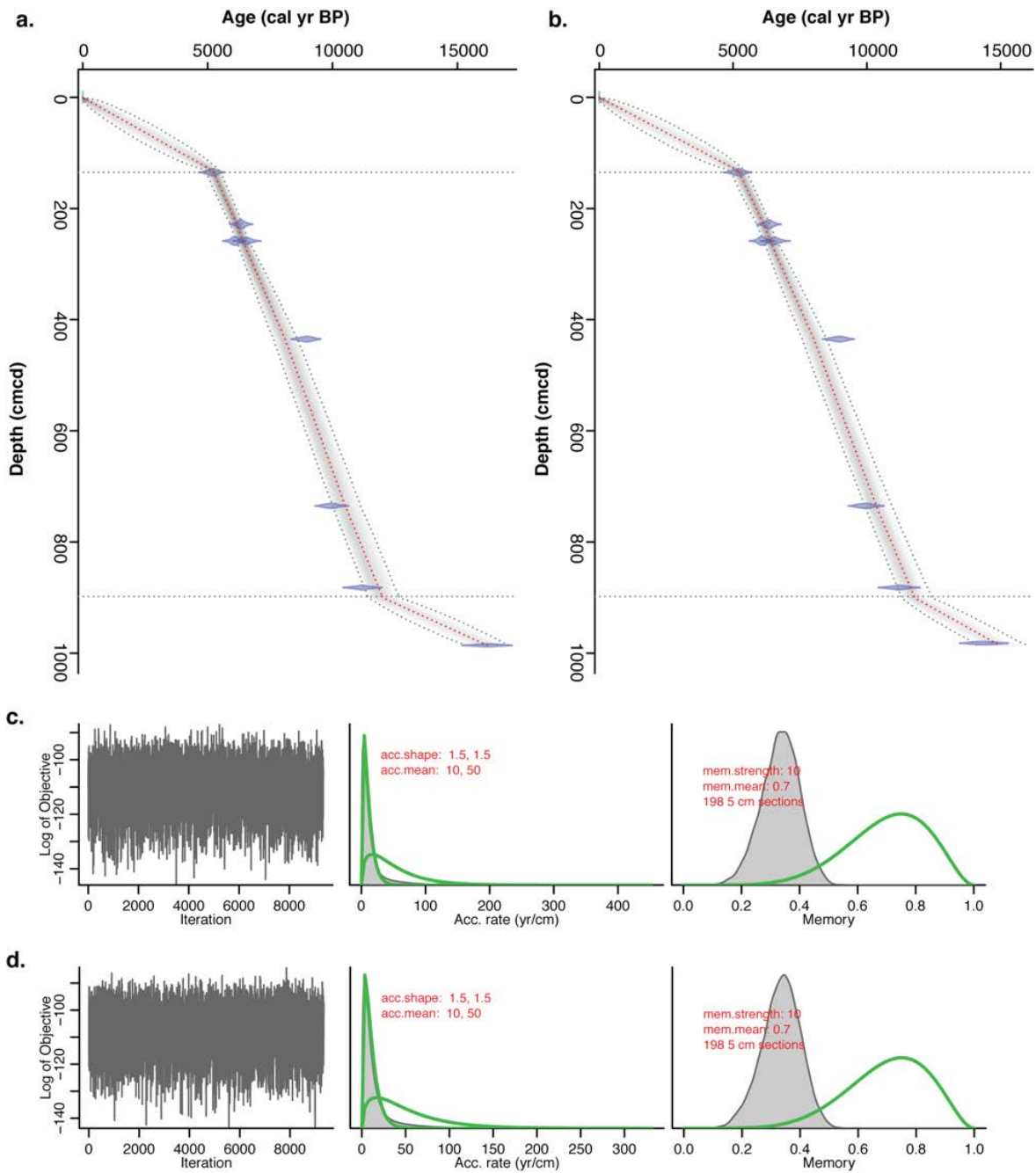


Figure A2. Alternative chronology for JPC-27 and JPC-57. (a) Chronology excluding deepest JPC-57 data point and (b) chronology excluding deepest JPC-27 data point for Sabrina Coast. (c) Priors for panel a, and (d) priors for panel b. Left panels depicts the Markov chain Monte Carlo (MCMC) iterations. The middle panels depicts the prior (green curves) and posterior (grey histograms) distributions for the accumulation rate, and the right panels depicts the prior and posterior distributions for memory.

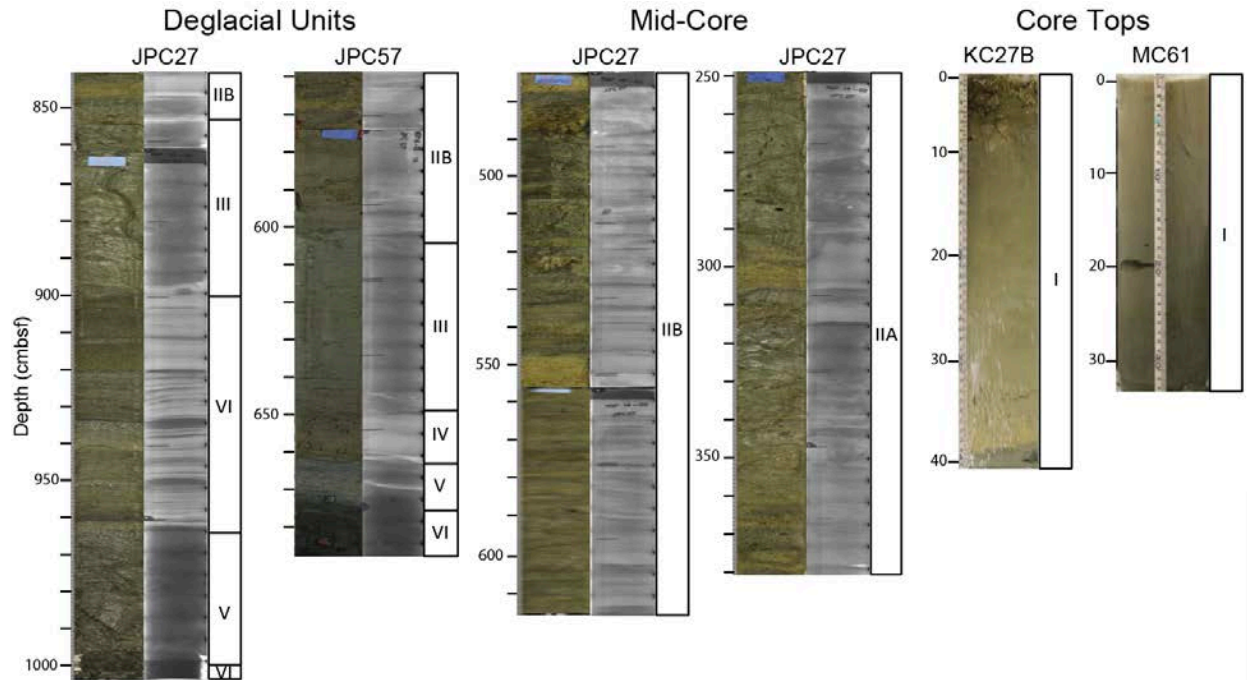


Figure A3. Core photos and x-radiographs of representative lithologic units.

APPENDIX B:

CHAPTER 3 SUPPLEMENTARY MATERIAL

Table B1. NBP14-02 R-code inputs for the MC-45 Bacon-generated age model. Model uses Lead-210 (^{210}Pb), and radiocarbon from the first aliquot of bulk sediment acid insoluble organic matter (AIOM) prepared via Ramped PyrOx. Sample information is indicated by lab ID, Age (cal yr before 1950), Age error (1-sigma) in years, centimeters composite depth (cmcd), core code for applying the Marine20 calibration to radiocarbon samples, delta R (Reservoir age minus 550 years), and standard deviation of delta R.

labID	Age (cal yr before 1950)	Age error	Depth (cmcd)	Core code	delta.R	delta.STD
MC-45 Pb-1	-58	1	0.5	0	0	0
MC-45 Pb-2	-49	2	1.25	0	0	0
MC-45 Pb-3	-43	2	1.75	0	0	0
MC-45 Pb-4	-37	4	2.25	0	0	0
MC-45 Pb-5	-31	4	2.75	0	0	0
MC-45 Pb-6	-25	5	3.25	0	0	0
MC-45 Pb-7	-19	6	3.75	0	0	0
MC-45 Pb-8	-13	6	4.25	0	0	0
MC-45 Pb-9	-7	7	4.75	0	0	0
MC-45 Pb-10	-1	8	5.25	0	0	0
MC-45 Pb-11	5	9	5.75	0	0	0
MC-45 Pb-12	11	10	6.25	0	0	0
MC-45 Pb-13	17	11	6.75	0	0	0
MC-45 Pb-14	23	11	7.25	0	0	0
MC-45 Pb-15	29	12	7.75	0	0	0
MC-45 Pb-16	35	13	8.25	0	0	0
MC-45 Pb-17	41	13	8.75	0	0	0
MC-45 Pb-18	47	15	9.25	0	0	0
JPC27 92-94	5742	69	135	2	680	100

Table B2. NBP14-02 R-code inputs for the MC-61 Bacon-generated age model. Model uses Lead-210 (^{210}Pb), and radiocarbon from the first aliquot of bulk sediment acid insoluble organic matter (AIOM) prepared via Ramped PyrOx. Sample information is indicated by lab ID, Age (cal yr before 1950), Age error (1-sigma) in years, centimeters composite depth (cmd), core code for applying the Marine20 calibration to radiocarbon samples, delta R (Reservoir age minus 550 years), and standard deviation of delta R

labID	Age (cal yr before 1950)	Age error	Depth (cmd)	Core code	delta.R	delta.STD
MC-61 Pb-1	-56	2	0.25	0	0	0
MC-61 Pb-2	-41	7	0.75	0	0	0
MC-61 Pb-3	-25	10	1.25	0	0	0
MC-61 Pb-4	-10	13	1.75	0	0	0
MC-61 Pb-5	6	19	2.25	0	0	0
MC-61 Pb-6	21	23	2.75	0	0	0
MC-61 Pb-7	37	27	3.25	0	0	0
MC-61 Pb-8	52	31	3.75	0	0	0
MC-61 Pb-9	68	35	4.25	0	0	0
JPC27 92-94	5742	69	135	2	680	100

APPENDIX C:

CHAPTER 4 SUPPLEMENTARY MATERIAL

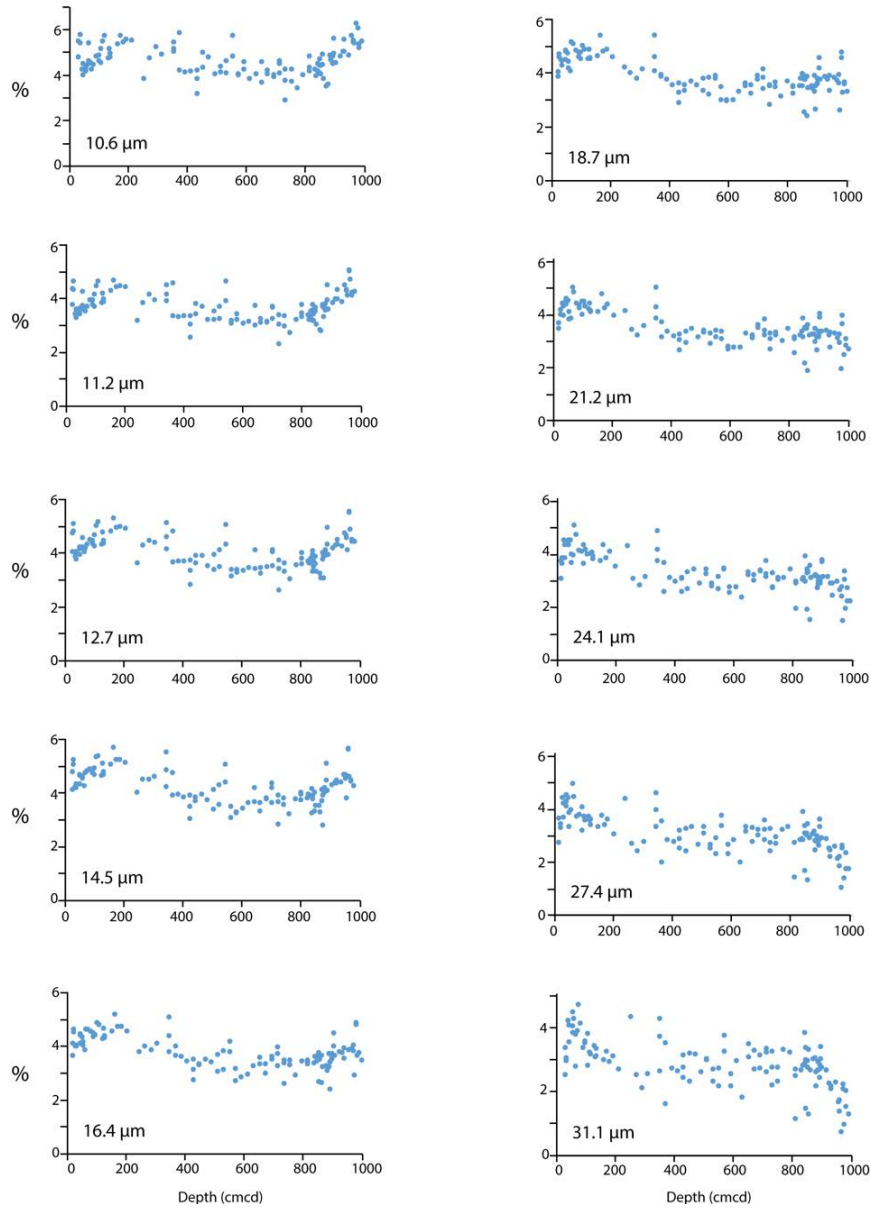


Figure C1. Relative abundance (%) of individual bins in the sortable silt size range (10-31 μm) plotted against centimeters composite depth (cmcd).

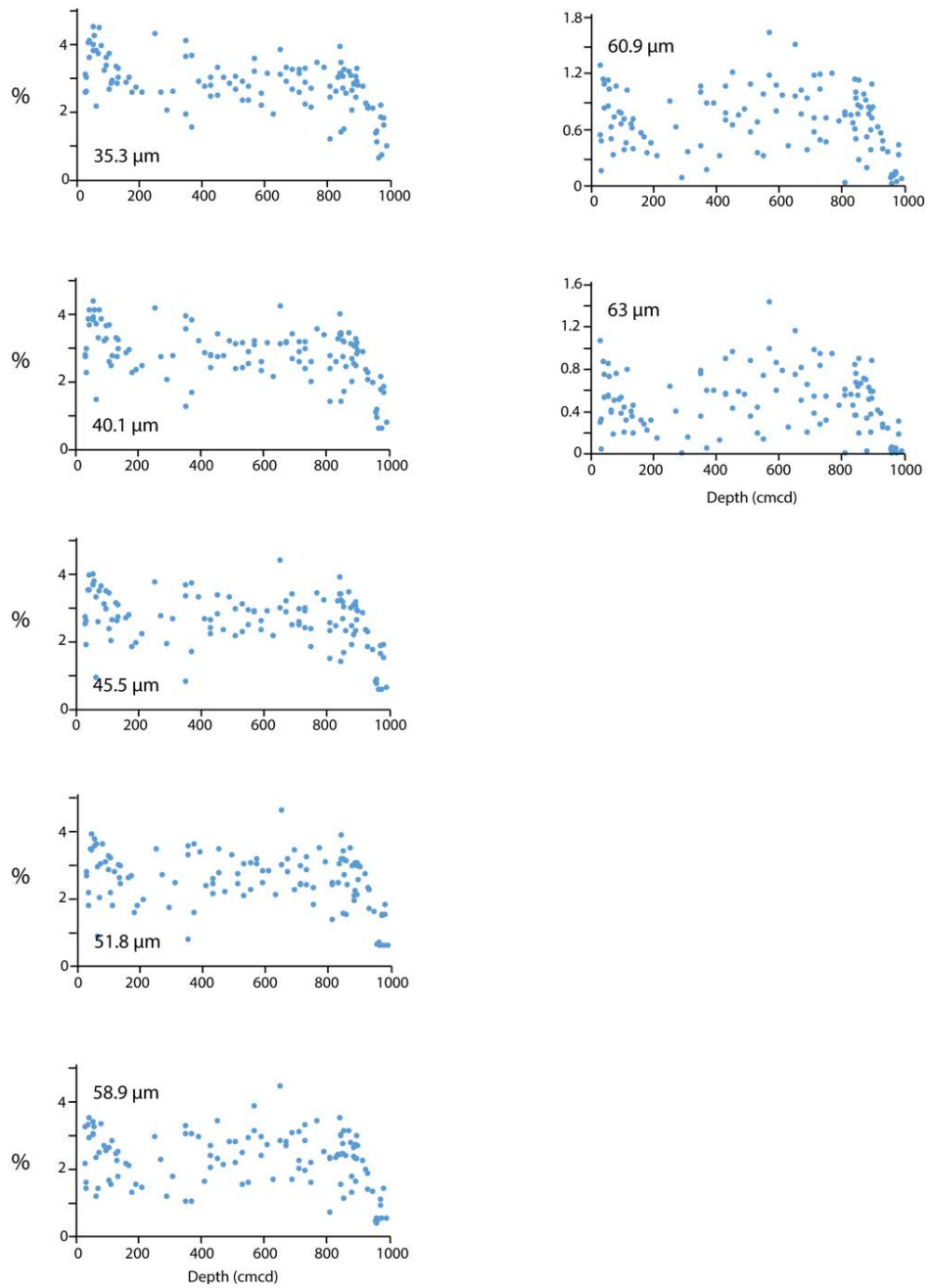


Figure C1. (continued) Relative abundance (%) of individual bins in the sortable silt size range (35-63 μm) plotted against centimeters composite depth (cmcd).

APPENDIX D:

ADDITIONAL DATA TABLES AND FIGURES

Text D1.

Diatom Data repository can be found at

Leventer, A. (2017). NBP1402 diatom data. U.S. Antarctic Program (USAP) Data Center.
doi: 10.15784/601258.

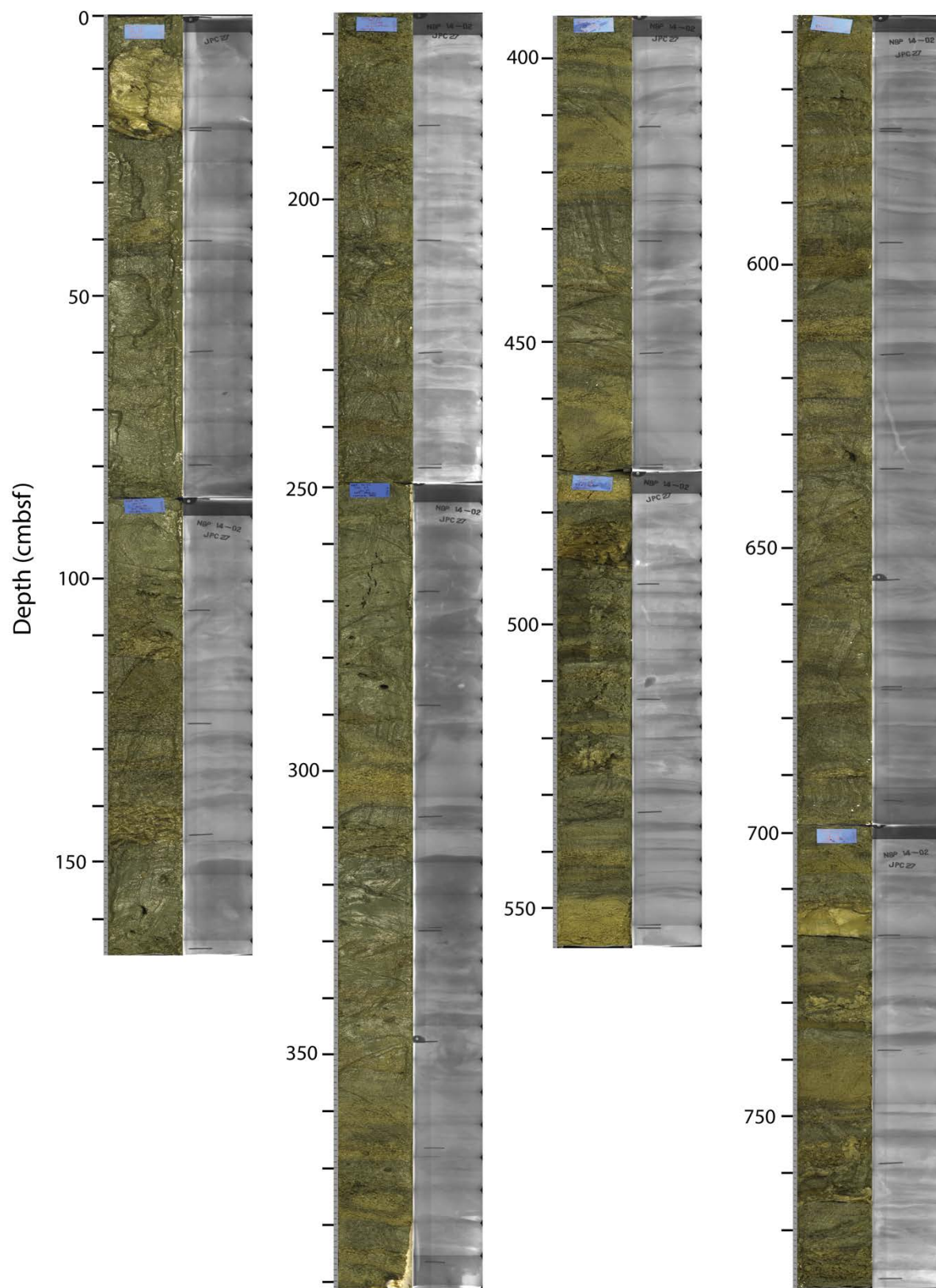


Figure D1. NBP14-02 JPC-27 core photos and x-rays.

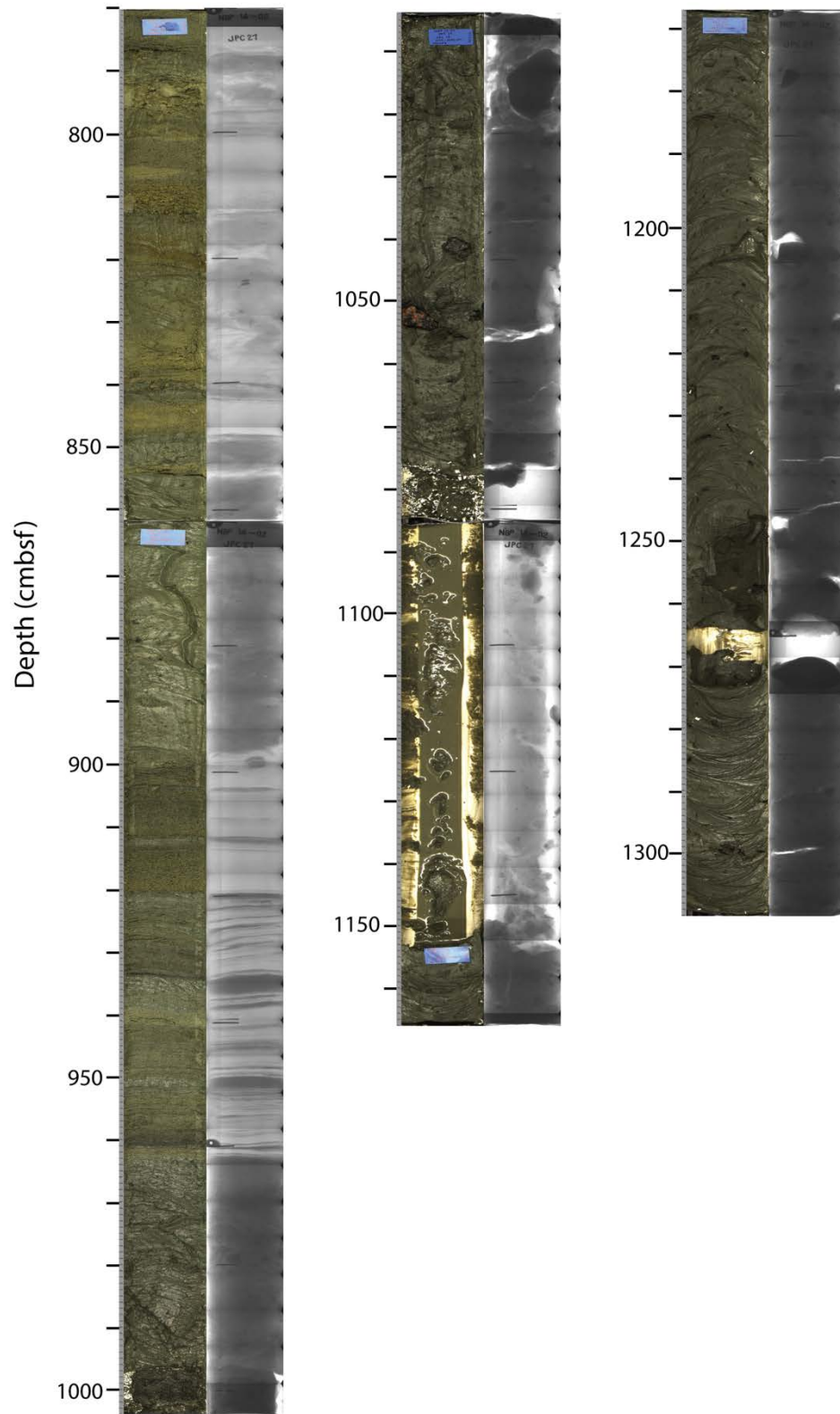


Figure D1. (continued) NBP14-02 JPC-27 core photos and x-ray

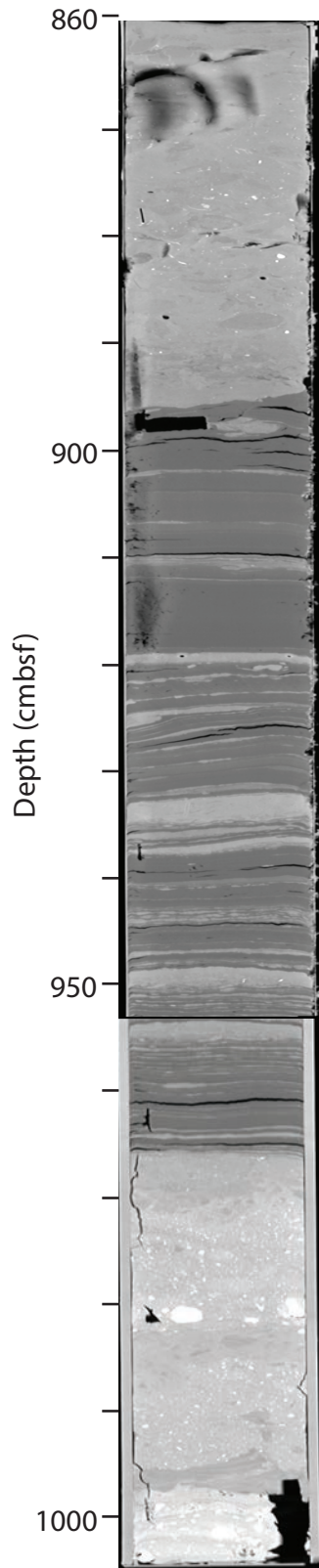


Figure D2. NBP14-02 JPC27 CT scan (861-1004 cmbsf).

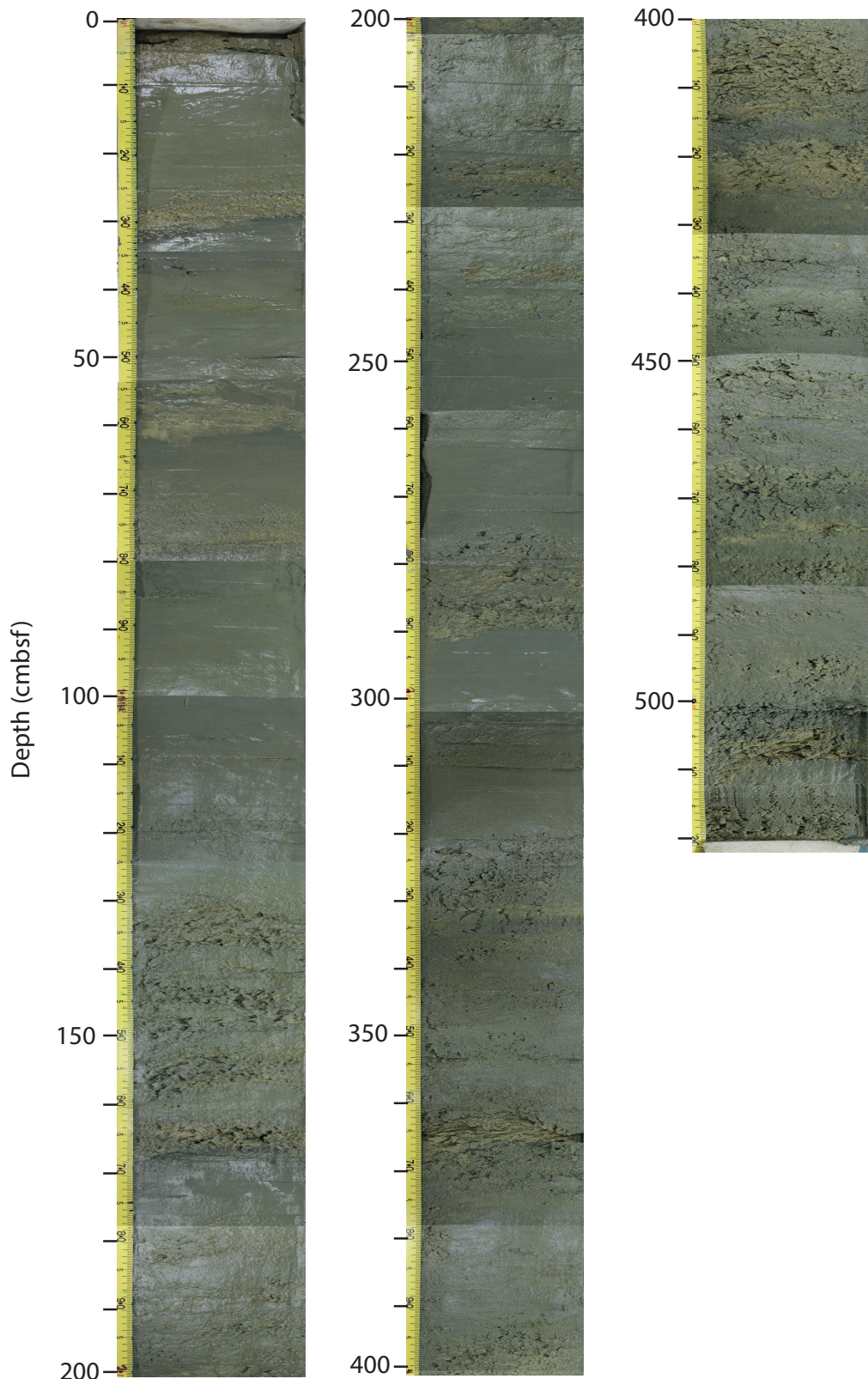


Figure D3. NBP14-02 JKC-53 core photos.

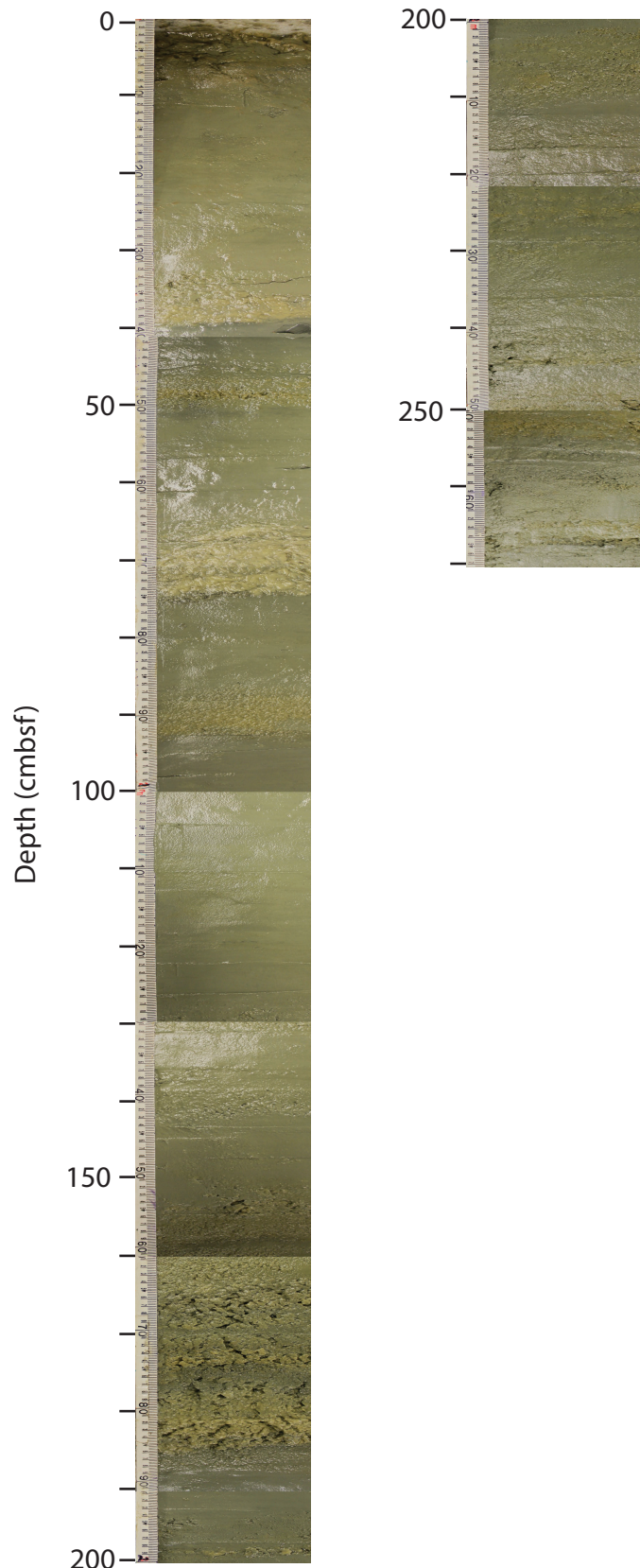


Figure D4. NBP14-02 KC-27B core photos.

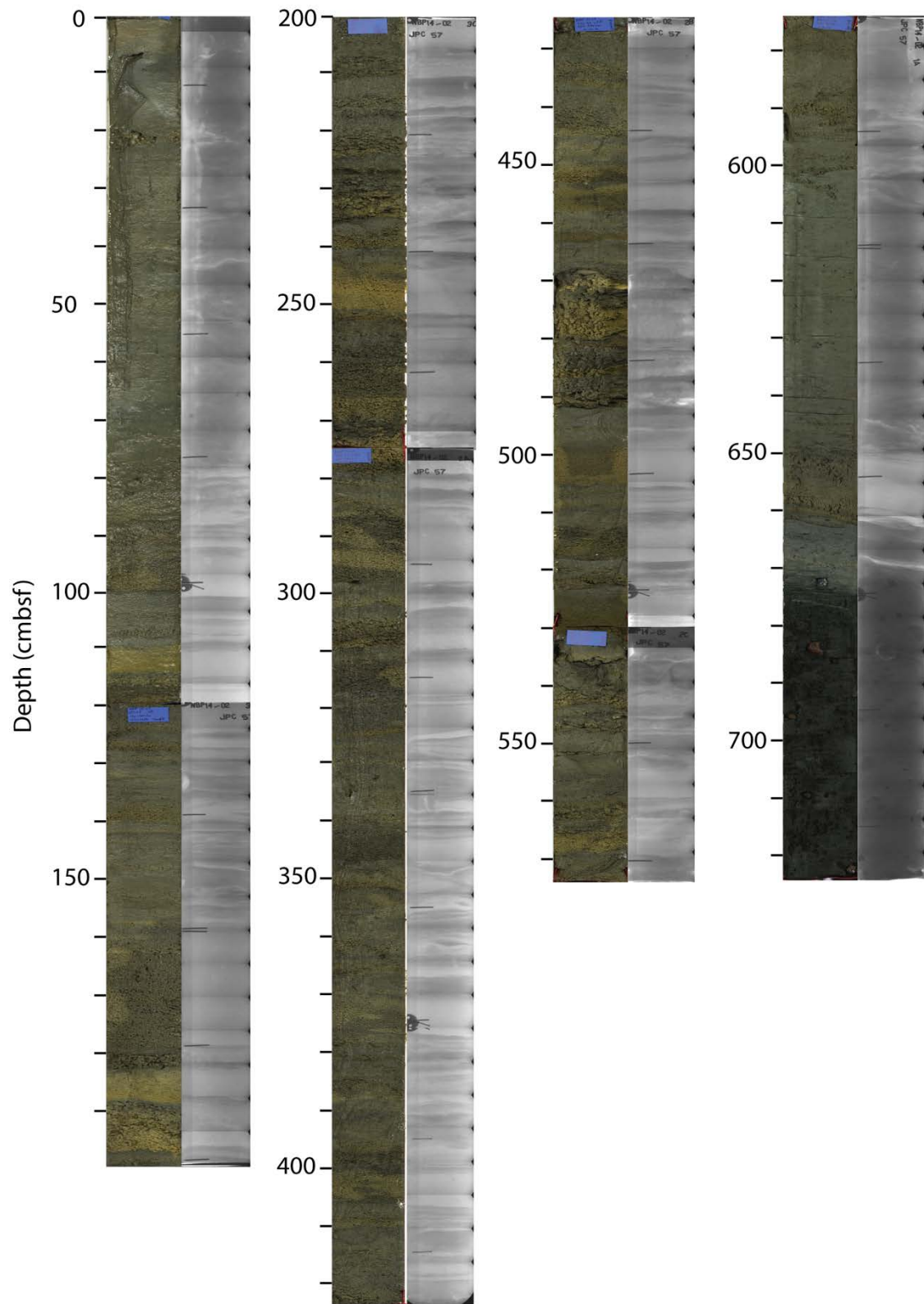


Figure D5. NBP14-02 JPC-57 core photos and x-rays.

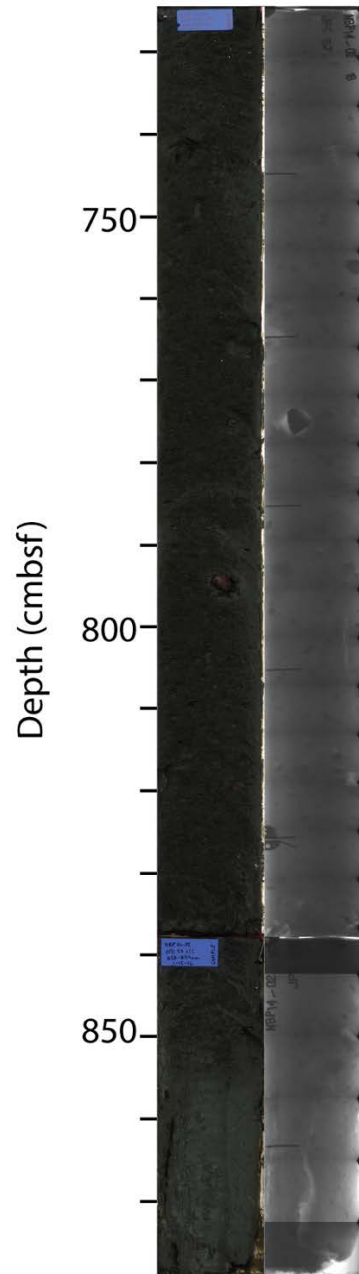


Figure D5. (continued) NBP14-02 JPC-57 core photos and x-rays.

Table D1. NBP14-02 magnetic susceptibility tie points. Depths in centimeters below sea floor (cmbsf) and centimeters composite depth (cmcd).

JPC27 Tie depth (cmbsf)	KC27B Reference Depth (cmbsf)	JKC53 Tie depth (cmbsf)	KC27B Reference Depth (cmbsf)	KC57 Tie depth (cmbsf)	KC27B Reference Depth (cmbsf)	JPC57 Tie depth (cmbsf)	JPC27 Reference Depth (cmcd)
60.661	0.360	0.5	13.5	0.5	13.5	0	72
61.606	2.299	11	17	12	17	75	135
63.502	3.999	28	38.5	37	38.5	250	435
66.088	7.968	36	42	42	42	587	882
73.636	16.853	47.5	56	51.5	56	602	888
85.504	29.097	58.5	66	65	66	648	932
88.793	33.230	66	80	72	80	657	982
93.468	39.661	72.5	90.5	77	90.5	663	995
109.371	62.397	83.5	101.5	95.5	101.5	676	1032
111.584	66.990	102.5	121	117	121		
115.805	72.996	110.5	131	130	131		
122.499	77.325	137.5	144		144		
130.845	86.009	161.5	181		181		
186.271	150.132	176	185.5		185.5		
268.899	243.792	179.45	206				

Table D.2 Cores with centimeters below sea floor (cmbsf) centimeters composite depth (cmcd) and Magnetic Susceptibility (Mag Susc) in cgs. $SI=cgs*4\pi$.

JPC27 depth (cmbsf)	JPC27 depth (cmcd)	JPC27 Mag Susc (cgs)	KC27B depth (cmbsf)	KC27B depth (cmcd)	KC27B Mag Susc (cgs)	JKC53 depth (cmbsf)	JKC53 depth (cmcd)	JKC53 Mag Susc (cgs)	MC45 depth (cmcd)	MC45 Mag Susc (cgs)	JPC57 depth (cmbsf)	JPC57 CMCD	JPC57 Mag Susc (cgs)	KC57 depth (cmbsf)	KC57 depth (cmcd)	KC57 Mag Susc (cgs)
0	56.48	-0.57	0	2	1.44	0	13.15	0	0	-1.15	0	72	0.39	0	5.8	-0.08
1	56.88	0.45	0.5	2.5	1.35	0.5	13.44	0	1	-0.66	2.5	74.1	0.65	0.5	5.98	0.57
2	57.28	1.8	1	3	1.26	1	13.73	0	2	-0.09	5	76.2	1.46	1	6.17	0.64
3	58.29	1.69	1.5	3.5	0.88	1.5	14.03	0	3	0.13	7.5	78.3	2.66	1.5	6.36	0.21
4	59.36	1.62	2	4	0.6	2	14.32	0	4	0.47	10	80.4	3.31	2	6.54	0.21
5	59.83	0.86	2.5	4.5	0.42	2.5	14.61	1.31	5	0.76	12.5	82.5	3.25	2.5	6.73	0.57
6	60.22	0.59	3	5	1.54	3	14.9	1.46	6	0.85	15	84.6	3.11	3	6.92	0.35
7	60.6	-0.11	3.5	5.5	2	3.5	15.19	1.39	7	1.05	17.5	86.7	3.11	3.5	7.1	0.21
8	60.99	-0.5	4	6	2.38	4	15.49	1.39	8	1.18	20	88.8	3.07	4	7.29	0.14
9	61.95	-0.54	4.5	6.5	2.75	4.5	15.78	1.01	9	1.19	22.5	90.9	3.21	4.5	7.47	0.35
10	68.96	-0.65	5	7	2.56	5	16.09	1.31	10	1.25	25	93	2.77	5	7.66	0.35
11	69.96	-0.66	5.5	7.5	2.56	5.5	16.4	1.61	11	1.35	27.5	95.1	2.01	5.5	7.85	0.42
12	70.97	-0.68	6	8	2.47	6	16.71	1.68	12	1.22	30	97.2	1.88	6	8.03	0.21
13	71.97	-0.65	6.5	8.5	2.38	6.5	17.02	1.83	13	1.26	32.5	99.3	2	6.5	8.22	0.35
14	72.98	-0.66	7	9	2.47	7	17.33	1.91	14	1.13	35	101.4	2.07	7	8.41	0.64
15	73.99	-0.72	7.5	9.5	1.82	7.5	17.74	1.83	15	1.07	37.5	103.5	2.11	7.5	8.59	0.5
16	74.99	-0.73	8	10	1.44	8	18.34	1.91	16	0.95	40	105.6	1.97	8	8.78	0.28
17	75.97	-0.6	8.5	10.5	1.82	8.5	18.94	2.06	17	0.73	42.5	107.7	2.19	8.5	8.97	0.57
18	76.82	1.03	9	11	2.28	9	19.54	2.36	18	0.64	45	109.8	2.26	9	9.15	0.5
19	77.66	1.44	9.5	11.5	2.19	9.5	20.03	2.28	19	0.41	47.5	111.9	2.16	9.5	9.34	0.71
20	78.73	0.52	10	12	2.38	10	20.52	2.06	20	0.21	50	114	2.42	10	9.52	0.85
21	79.81	0.86	10.5	12.5	2.75	10.5	21.01	2.28	21	0.02	52.5	116.1	2.54	10.5	9.71	1
22	80.88	0.94	11	13	2.47	11	21.51	2.58	22	-0.11	55	118.2	2.32	11	9.9	1.21
23	81.95	0.96	11.5	13.5	1.72	11.5	22.01	1.91	23	-0.15	57.5	120.3	2.2	11.5	10.08	1.5
24	82.89	0.31	12	14	1.63	12	22.52	1.83	24	-0.23	60	122.4	2.44	12	10.27	1.64
25	83.83	1.27	12.5	14.5	2.1	12.5	23.03	1.31	25	-0.14	62.5	124.5	2.65	12.5	10.46	1.14
26	84.77	1.34	13	15	1.82	13	23.54	1.24	26	-0.22	65	126.6	2.58	13	10.64	1.21
27	85.71	1.54	13.5	15.5	1.72	13.5	24.05	0.94	27	-0.21	67.5	128.7	2.51	13.5	10.83	1.14
28	86.65	1.6	14	16	1.72	14	24.56	0.79	28	-0.29	70	130.8	2.55	14	11.02	1.07
29	87.59	1.34	14.5	16.5	1.91	14.5	25.26	0.94	29	-0.44	72.5	132.9	2.36	14.5	11.2	1.07
30	88.35	1.22	15	17	2.28	15	26.07	1.39	30	-0.54	75	135	2.02	15	11.39	0.78
31	89.11	0.96	15.5	17.5	2.47	15.5	26.5	0.94	31	-0.95	77.5	139.3	1.58	15.5	11.57	0.78
32	89.87	0.49	16	18	2.19	16	26.93	0.79	32	-0.94	80	143.6	1.07	16	11.76	0.85
33	90.64	-0.51	16.5	18.5	2.47	16.5	27.36	0.94	33	-1.1	82.5	147.9	0.66	16.5	11.95	0.92

Table D.2 (continued)

34	91.33	-0.68	17	19	2.66	17	27.79	1.09	34	-1.19	85	152.1	0.52	17	12.13	0.92
35	92	-0.68	17.5	19.5	2.66	17.5	29.23	0.94	35	-1.3	87.5	156.4	0.43	17.5	12.32	0.57
36	92.67	-0.68	18	20	2.66	18	30.66	0.71	36	-1.66	90	160.7	0.36	18	12.51	0.28
37	93.34	-0.54	18.5	20.5	2.28	18.5	31.24	1.24	37	-2.02	92.5	165	0.32	18.5	12.69	0
38	94.01	-0.28	19	21	2.38	19	31.6	1.31	38	-2.48	95	169.3	0.36	19	13.32	0.14
39	94.68	0.53	19.5	21.5	2.56	19.5	31.96	1.31			97.5	173.6	0.26	19.5	13.94	0.21
40	95.36	1.15	20	22	2.47	20	32.32	1.31			100	177.9	0.34	20	14.57	0.21
41	96.64	1.52	20.5	22.5	2.28	20.5	32.68	1.39			102.5	182.1	0.36	20.5	15.19	0.21
42	97.93	1.55	21	23	2	21	33.07	1.09			105	186.4	0.35	21	15.81	-0.29
43	99.22	1.3	21.5	23.5	2	21.5	33.49	0.86			107.5	190.7	0.31	21.5	16.44	-0.29
44	100.46	0.94	22	24	1.82	22	33.91	0.56			110	195	0.3	22	17.06	-0.36
45	101.19	0.88	22.5	24.5	1.91	22.5	34.33	0.49			112.5	199.3	0.25	22.5	17.69	-0.08
46	101.93	1.69	23	25	1.82	23	34.75	0.34			115	203.6	0.29	23	18.31	0.28
47	102.66	2.29	23.5	25.5	1.91	23.5	35.17	0.56			117.5	207.9	0.22	23.5	18.94	0.42
48	103.4	2.32	24	26	2	24	35.59	0.56			120	212.1	0.33	24	19.72	0
49	104.13	2.26	24.5	26.5	1.82	24.5	36.35	0.49			122.5	216.4	0.23	24.5	20.5	0.07
50	104.87	2.33	25	27	1.72	25	37.19	0.49			125	220.7	0.29	25	21.28	0.07
51	105.6	2.68	25.5	27.5	2	25.5	38.02	0.49			127.5	225	0.26	25.5	22.06	0.35
52	106.34	2.64	26	28	2.1	26	38.86	0.56			130	229.3	0.35	26	22.84	0.28
53	107.07	2.21	26.5	28.5	1.91	26.5	39.7	0.56			132.5	233.6	0.39	26.5	23.62	0.14
54	107.81	1.63	27	29	1.35	27	40.19	0.41			135	237.9	0.36	27	24.4	0.28
55	108.54	1.58	27.5	29.5	0.51	27.5	40.44	0.19			137.5	242.1	0.32	27.5	25.18	0.07
56	109.28	1.73	28	30	0.42	28	40.69	0.11			140	246.4	0.3	28	25.96	0
57	110.01	1.67	28.5	30.5	0.23	28.5	40.94	0.19			142.5	250.7	0.33	28.5	26.74	-0.22
58	110.75	2.28	29	31	0.32	29	41.19	0.26			145	255	0.38	29	27.52	0
59	111.48	1.66	29.5	31.5	0.7	29.5	41.44	0.34			147.5	259.3	0.34	29.5	28.3	0.21
60	112.22	1.21	30	32	1.07	30	41.7	0.34			150	263.6	0.38	30	29.08	-0.08
61	112.96	2.39	30.5	32.5	2.19	30.5	41.97	0.34			152.5	267.9	0.38	30.5	29.86	0
62	113.58	3.12	31	33	1.63	31	42.24	0.26			155	272.1	0.32	31	30.64	0
63	113.89	2.66	31.5	33.5	1.16	31.5	42.51	0.34			157.5	276.4	0.37	31.5	31.42	-0.08
64	114.21	1.44	32	34	0.32	32	42.78	0.71			160	280.7	0.32	32	32.13	0
65	114.52	1.56	32.5	34.5	-0.24	32.5	43.06	1.01			162.5	285	0.25	32.5	32.63	0
66	114.83	1.66	33	35	-0.24	33	43.34	1.31			165	289.3	0.23	33	33.12	-0.15
67	115.14	2.4	33.5	35.5	-0.14	33.5	43.62	1.46			167.5	293.6	0.21	33.5	33.62	-0.43
68	115.45	1.52	34	36	-0.33	34	43.89	1.53			170	297.9	0.21	34	34.12	-0.72
69	115.76	2.25	34.5	36.5	-0.42	34.5	44.17	1.53			172.5	302.1	0.18	34.5	34.62	-0.58
70	116.07	2.11	35	37	-0.42	35	44.45	1.39			175	306.4	0.18	35	35.11	-0.65
71	116.38	2.68	35.5	37.5	-0.7	35.5	44.72	1.46			177.5	310.7	0.2	35.5	35.61	-0.93
72	116.69	2.58	36	38	-0.7	36	45	1.61			180	315	0.26	36	36.11	-1.22
73	117	3.43	36.5	38.5	-0.7	36.5	46.07	1.31			182.5	319.3	0.3	36.5	36.79	-1.29

Table D.2 (continued)

74	119.49	3.42	37	39	-0.7	37	47.21	0.56			185	323.6	0.21	37	37.53	-1.36
75	122.18	3.52	37.5	39.5	-0.61	37.5	48.35	0.64			187.5	327.9	0.26	37.5	38.28	-1.29
76	124.65	3.45	38	40	-0.61	38	49.09	0.79			190	332.1	0.2	38	39.02	-1.29
77	125.72	3.46	38.5	40.5	-0.79	38.5	49.23	1.46			192.5	336.4	0.22	38.5	39.76	-1.15
78	126.79	2.95	39	41	-0.79	39	49.38	1.31			195	340.7	0.15	39	40.5	-0.86
79	127.85	2.15	39.5	41.5	-0.61	39.5	49.52	1.39			197.5	345	0.23	39.5	41.24	-0.86
80	128.92	2.06	40	42	-0.61	40	49.67	1.39			200	349.3	0.2	40	41.99	-0.29
81	129.57	0.19	40.5	42.5	-0.61	40.5	49.81	1.46			202.5	353.6	0.25	40.5	42.73	-0.08
82	130.16	-0.03	41	43	0.04	41	49.95	1.46			205	357.9	0.35	41	43.47	0.21
83	130.74	1.33	41.5	43.5	0.6	41.5	50.1	1.53			207.5	362.1	0.27	41.5	44.14	0.28
84	131.33	-0.42	42	44	0.7	42	50.24	1.53			210	366.4	0.34	42	44.74	0.35
85	131.92	-0.21	42.5	44.5	0.23	42.5	50.38	1.53			212.5	370.7	0.3	42.5	45.34	0.35
86	132.5	2.44	43	45	0.42	43	50.53	1.24			215	375	0.32	43	45.94	0.35
87	132.98	2.68	43.5	45.5	-0.05	43.5	50.67	1.09			217.5	379.3	0.37	43.5	46.53	0.14
88	133.33	2.03	44	46	-0.33	44	50.81	1.39			220	383.6	0.4	44	47.13	0.28
89	133.67	2.07	44.5	46.5	-0.24	44.5	50.96	1.61			222.5	387.9	0.72	44.5	47.73	-0.29
90	134.01	2.13	45	47	-0.24	45	51.12	1.98			225	392.1	0.68	45	48.33	0.71
91	134.35	2.33	45.5	47.5	-0.52	45.5	53.5	0.64			227.5	396.4	0.33	45.5	48.93	0.42
92	134.69	1.7	46	48	-0.79	46	54.6	1.98			230	400.7	0.29	46	49.53	0.42
93	135.04	2.4	46.5	48.5	-0.89	46.5	55.72	1.83			232.5	405	0.24	46.5	50.12	0.5
94	135.38	2.37	47	49	-0.79	47	56.84	2.13			235	409.3	0.23	47	50.72	0.64
95	135.72	2.65	47.5	49.5	-0.33	47.5	57.95	2.21			237.5	413.6	0.35	47.5	51.32	0.64
96	136.06	1.99	48	50	-0.52	48	58.59	1.98			240	417.9	0.32	48	51.92	0.57
97	136.4	1.85	48.5	50.5	0.14	48.5	59.2	1.91			242.5	422.1	0.21	48.5	52.52	0.57
98	136.75	1.3	49	51	0.42	49	59.81	1.68			245	426.4	0.23	49	53.11	0.57
99	137.09	0.53	49.5	51.5	0.42	49.5	60.42	1.91			247.5	430.7	0.19	49.5	53.71	0.71
100	137.43	0.5	50	52	0.23	50	61.03	1.53			250	435	0.17	50	54.31	0.64
101	137.77	0.6	50.5	52.5	0.23	50.5	61.64	1.39			252.5	438.3	0.23	50.5	54.91	0.78
102	138.12	0.46	51	53	0.23	51	62.25	1.24			255	441.6	0.27	51	55.51	0.71
103	138.46	0.15	51.5	53.5	-0.24	51.5	62.86	1.31			257.5	444.9	0.27	51.5	56.11	0.78
104	138.8	0.12	52	54	0.14	52	63.47	1.31			260	448.3	0.28	52	56.7	0.78
105	139.14	-0.21	52.5	54.5	0.32	52.5	64.08	1.31			262.5	451.6	0.17	52.5	57.3	0.78
106	139.48	-0.39	53	55	0.23	53	64.69	1.46			265	454.9	0.2	53	57.9	0.78
107	139.83	-0.61	53.5	55.5	0.23	53.5	65.34	1.46			267.5	458.2	0.19	53.5	58.4	0.71
108	140	-0.4	54	56	0.14	54	66.12	0.64			270	461.5	0.19	54	58.89	0.64
109	141	-0.54	54.5	56.5	0.42	54.5	66.9	0.34			272.5	464.8	0.2	54.5	59.39	0.64
110	142	-0.65	55	57	1.07	55	67.42	0.34			275	468.2	0.18	55	59.89	0.42
111	143	-0.69	55.5	57.5	1.26	55.5	67.89	0.26			277.5	471.5	0.19	55.5	60.38	-0.29
112	144	-0.71	56	58	1.54	56	68.36	0.11			280	474.8	0.2	56	60.88	-0.15
113	145	-0.72	56.5	58.5	1.44	56.5	68.82	0.11			282.5	478.1	0.22	56.5	61.38	-0.15

Table D.2 (continued)

114	146	-0.47	57	59	0.88	57	69.29	0.04			285	481.4	0.3	57	61.87	-0.36
115	147	-0.57	57.5	59.5	0.6	57.5	69.76	0.04			287.5	484.7	0.22	57.5	62.37	-0.22
116	148	-0.64	58	60	0.79	58	70.23	0.04			290	488.1	0.2	58	62.86	-0.43
117	149	-0.5	58.5	60.5	0.79	58.5	70.7	-0.04			292.5	491.4	0.2	58.5	63.36	-0.43
118	150	-0.54	59	61	0.7	59	71.17	0.04			295	494.7	0.24	59	63.86	-0.22
119	151	-0.55	59.5	61.5	0.7	59.5	71.64	0.11			297.5	498	0.23	59.5	64.35	0
120	152	-0.53	60	62	0.51	60	72.1	0.11			300	501.3	0.28	60	64.85	0.07
121	153	-0.64	60.5	62.5	0.51	60.5	72.57	0.11			302.5	504.6	0.28	60.5	65.35	0
122	154	-0.68	61	63	0.42	61	73.04	0.19			305	508	0.25	61	65.84	-0.15
123	155	-0.58	61.5	63.5	0.6	61.5	73.51	0.04			307.5	511.3	0.19	61.5	66.34	-0.22
124	156	-0.69	62	64	0.42	62	73.98	0.04			310	514.6	0.2	62	66.84	-0.29
125	157	-0.66	62.5	64.5	0.32	62.5	74.45	0.11			312.5	517.9	0.25	62.5	67.33	-0.43
126	158	-0.64	63	65	0.14	63	74.92	0.19			315	521.2	0.21	63	67.83	-0.5
127	159	-0.55	63.5	65.5	0.14	63.5	75.39	0.19			317.5	524.5	0.3	63.5	68.33	-0.58
128	160	-0.4	64	66	-0.14	64	76.14	0.34			320	527.8	0.29	64	68.82	-0.58
129	161	-0.61	64.5	66.5	-0.89	64.5	77.21	0.41			322.5	531.2	0.31	64.5	69.25	-0.65
130	162	-0.54	65	67	-1.26	65	78.28	0.79			325	534.5	0.29	65	69.48	-0.86
131	163	-0.49	65.5	67.5	-2.01	65.5	79.36	1.31			327.5	537.8	0.29	65.5	69.71	-0.79
132	164	-0.61	66	68	-1.26	66	80.48	1.46			330	541.1	0.34	66	69.94	-0.72
133	165	-0.64	66.5	68.5	-1.26	66.5	81.83	1.46			332.5	544.4	0.36	66.5	70.17	-0.72
134	166	-0.43	67	69	-1.26	67	83.17	1.24			335	547.7	0.35	67	70.4	-0.58
135	167	-0.46	67.5	69.5	-1.26	67.5	84.52	1.16			337.5	551.1	0.25	67.5	70.63	-0.72
136	168	-0.42	68	70	-1.26	68	85.86	1.09			340	554.4	0.3	68	70.86	-0.65
137	169	-0.51	68.5	70.5	-1.35	68.5	87.21	1.24			342.5	557.7	0.19	68.5	71.09	-0.72
138	170	-0.43	69	71	-1.26	69	88.01	1.09			345	561	0.25	69	71.32	-0.79
139	171	-0.33	69.5	71.5	-1.35	69.5	88.65	0.41			347.5	564.3	0.27	69.5	71.55	-0.65
140	172	-0.61	70	72	-1.35	70	89.29	0.19			350	567.6	0.22	70	71.78	-0.65
141	173	-0.68	70.5	72.5	-1.35	70.5	89.94	0.19			352.5	571	0.24	70.5	72.01	-0.65
142	174	-0.73	71	73	-1.45	71	90.58	0.04			355	574.3	0.34	71	72.24	-0.36
143	175	-0.75	71.5	73.5	-1.35	71.5	91.22	0.04			357.5	577.6	0.29	71.5	72.47	0
144	176	-0.73	72	74	-1.45	72	91.86	0.04			360	580.9	0.32	72	72.69	0.21
145	177	-0.73	72.5	74.5	-1.45	72.5	92.5	-0.11			362.5	584.2	0.3	72.5	72.92	0.21
146	178	-0.61	73	75	-1.35	73	92.85	0.11			365	587.5	0.23	73	73.15	0.14
147	179	-0.38	73.5	75.5	-1.45	73.5	93.11	0.56			367.5	590.9	0.3	73.5	73.38	0.14
148	180	-0.5	74	76	-1.26	74	93.38	0.64			370	594.2	0.2	74	73.61	0.07
149	181	-0.53	74.5	76.5	-1.17	74.5	93.65	0.56			372.5	597.5	0.15	74.5	73.84	-0.15
150	182	-0.13	75	77	-0.52	75	93.91	0.64			375	600.8	0.28	75	74.07	-0.15
151	183	-0.13	75.5	77.5	-0.24	75.5	94.18	0.71			377.5	604.1	0.27	75.5	74.3	-0.22
152	184	-0.07	76	78	-0.33	76	94.45	0.86			380	607.4	0.32	76	74.53	-0.29
153	185	-0.03	76.5	78.5	-0.33	76.5	94.71	0.79			382.5	610.7	0.29	76.5	74.76	-0.29

Table D.2 (continued)

154	186	-0.05	77	79	-0.42	77	94.98	0.71			385	614.1	0.26	77	74.99	-0.5
155	187	-0.05	77.5	79.5	-0.24	77.5	95.25	0.79			387.5	617.4	0.28	77.5	75.22	-0.43
156	188	-0.07	78	80	0.04	78	95.51	1.39			390	620.7	0.24	78	75.45	-0.36
157	189	-0.24	78.5	80.5	-0.05	78.5	96.07	1.46			392.5	624	0.27	78.5	75.74	-0.29
158	190	-0.24	79	81	-0.05	79	96.8	1.53			395	627.3	0.33	79	76.06	-0.29
159	191	0	79.5	81.5	0.04	79.5	97.54	1.53			397.5	630.6	0.22	79.5	76.37	-0.36
160	192	-0.13	80	82	0.14	80	98.28	1.61			400	634	0.18	80	76.69	-0.36
161	193	-0.21	80.5	82.5	-0.05	80.5	99.01	1.76			402.5	637.3	0.21	80.5	77	-0.29
162	194	-0.44	81	83	-0.14	81	99.75	1.83			405	640.6	0.2	81	77.32	-0.15
163	195	-0.4	81.5	83.5	-0.33	81.5	100.49	1.91			407.5	643.9	0.28	81.5	77.64	-0.22
164	196	-0.46	82	84	-0.14	82	101.22	2.13			410	647.2	0.34	82	77.95	-0.08
165	197	-0.47	82.5	84.5	-0.24	82.5	101.96	2.06			412.5	650.5	0.3	82.5	78.27	0.07
166	198	-0.54	83	85	-0.33	83	102.7	2.13			415	653.9	0.28	83	78.58	0.21
167	199	-0.54	83.5	85.5	-0.42	83.5	103.43	2.28			417.5	657.2	0.24	83.5	78.9	0.28
168	200	-0.55	84	86	-0.33	84	103.88	2.06			420	660.5	0.24	84	79.22	0.28
169	201	-0.62	84.5	86.5	-0.24	84.5	104.3	2.21			422.5	663.8	0.23	84.5	79.53	0.21
170	202	0	85	87	-0.24	85	104.72	2.06			425	667.1	0.3	85	79.85	0.07
171	203	-0.71	85.5	87.5	-0.05	85.5	105.15	1.98			427.5	670.4	0.3	85.5	80.16	0
172	204	-0.58	86	88	-0.24	86	105.57	1.91			430	673.8	0.3	86	80.48	0.14
173	205	-0.64	86.5	88.5	-0.42	86.5	105.99	1.98			432.5	677.1	0.29	86.5	80.8	0.28
174	206	-0.49	87	89	-0.79	87	106.41	1.83			435	680.4	0.24	87	81.11	0.21
175	207	-0.28	87.5	89.5	-0.7	87.5	106.83	1.76			437.5	683.7	0.26	87.5	81.43	0.28
176	208	-0.42	88	90	-0.98	88	107.25	1.76			440	687	0.22	88	81.74	0.28
177	209	-0.47	88.5	90.5	-1.26	88.5	107.67	1.76			442.5	690.3	0.18	88.5	82.06	0.28
178	210	-0.5	89	91	-1.26	89	108.09	1.91			445	693.6	0.22	89	82.37	0.21
179	211	-0.58	89.5	91.5	-1.26	89.5	108.51	1.76			447.5	697	0.2	89.5	82.69	0.21
180	212	-0.55	90	92	-1.26	90	108.93	1.76			450	700.3	0.23	90	83.01	0.35
181	213	-0.51	90.5	92.5	-1.35	90.5	109.35	1.83			452.5	703.6	0.17	90.5	83.32	0.14
182	214	-0.62	91	93	-1.35	91	109.77	1.76			455	706.9	0.24	91	83.64	-0.08
183	215	-0.66	91.5	93.5	-0.42	91.5	110.19	1.61			457.5	710.2	0.31	91.5	83.95	-0.08
184	216	-0.44	92	94	-0.98	92	110.61	1.68			460	713.5	0.26	92	84.27	0.14
185	217	-0.47	92.5	94.5	-0.33	92.5	111.03	1.68			462.5	716.9	0.29	92.5	84.59	0.28
186	218	-0.47	93	95	-0.14	93	111.45	1.76			465	720.2	0.25	93	84.9	0.07
187	219	-0.49	93.5	95.5	0.14	93.5	111.8	1.61			467.5	723.5	0.32	93.5	85.22	0.21
188	220	-0.44	94	96	0.23	94	112.14	1.46			470	726.8	0.21	94	85.53	0.28
189	221	-0.53	94.5	96.5	0.14	94.5	112.48	1.68			472.5	730.1	0.24	94.5	85.85	0.21
190	222	-0.54	95	97	0.32	95	112.82	1.53			475	733.4	0.22	95	86.16	0.28
191	223	-0.51	95.5	97.5	0.23	95.5	113.16	1.53			477.5	736.8	0.22	95.5	86.48	0.71
192	224	-0.62	96	98	0.42	96	113.5	1.83			480	740.1	0.22	96	86.8	0.35
193	225	-0.66	96.5	98.5	0.42	96.5	114.07	1.61			482.5	743.4	0.21	96.5	87.11	0.42

Table D.2 (continued)

194	226	-0.65	97	99	0.42	97	114.64	1.53			485	746.7	0.26	97	87.43	-0.29
195	227	-0.51	97.5	99.5	0.42	97.5	115.21	1.68			487.5	750	0.29	97.5	87.74	0.42
196	228	-0.44	98	100	0.51	98	115.79	1.76			490	753.3	0.31	98	88.06	0.21
197	229	-0.49	98.5	100.5	0.32	98.5	116.36	1.91			492.5	756.7	0.28	98.5	88.38	0.14
198	230	-0.44	99	101	0.32	99	116.76	1.76			495	760	0.29	99	88.69	0.21
199	231	-0.66	99.5	101.5	0.42	99.5	117.16	1.91			497.5	763.3	0.31	99.5	89.01	0.28
200	232	-0.66	100	102	0.32	100	117.56	1.91			500	766.6	0.18	100	89.32	0.21
201	233	-0.33	100.5	102.5	0.51	100.5	117.96	1.98			502.5	769.9	0.18	100.5	89.64	0.07
202	234	-0.29	101	103	0.79	101	118.36	1.91			505	773.2	0.17	101	89.95	0.21
203	235	-0.49	101.5	103.5	1.44	101.5	118.76	2.13			507.5	776.6	0.2	101.5	90.27	0.21
204	236	-0.65	102	104	0.7	102	119.16	2.21			510	779.9	0.29	102	90.59	0
205	237	-0.68	102.5	104.5	0.7	102.5	119.55	2.36			512.5	783.2	0.22	102.5	90.9	-0.22
206	238	-0.65	103	105	0.7	103	119.67	1.98			515	786.5	0.14	103	91.22	-0.08
207	239	-0.54	103.5	105.5	0.88	103.5	119.78	1.83			517.5	789.8	0.22	103.5	91.77	0.07
208	240	-0.54	104	106	0.6	104	119.9	1.83			520	793.1	0.29	104	92.32	0.14
209	241	-0.32	104.5	106.5	0.51	104.5	120.01	1.76			522.5	796.4	0.31	104.5	92.87	0
210	242	-0.4	105	107	0.6	105	120.13	1.98			525	799.8	0.26	105	93.42	0
211	243	-0.55	105.5	107.5	0.79	105.5	120.24	1.68			527.5	803.1	0.17	105.5	93.97	0.07
212	244	-0.62	106	108	0.88	106	120.36	1.53			530	806.4	0.19	106	94.52	0.07
213	245	-0.66	106.5	108.5	0.51	106.5	120.47	1.83			532.5	809.7	0.19	106.5	95.07	0.07
214	246	-0.54	107	109	0.7	107	120.59	1.61			535	813	0.23	107	95.62	0.14
215	247	-0.51	107.5	109.5	0.98	107.5	120.7	1.53			537.5	816.3	0.3	107.5	96.17	0.21
216	248	-0.62	108	110	1.07	108	120.81	1.31			540	819.7	0.26	108	96.72	0.28
217	249	-0.6	108.5	110.5	1.16	108.5	120.93	1.31			542.5	823	0.18	108.5	97.27	0.28
218	250	-0.47	109	111	1.26	109	121.13	1.31			545	826.3	0.21	109	97.82	0.5
219	251	-0.38	109.5	111.5	1.26	109.5	121.74	1.31			547.5	829.6	0.26	109.5	98.37	0.64
220	252	-0.5	110	112	0.98	110	122.36	1.53			550	832.9	0.28	110	99.66	1
221	253	-0.65	110.5	112.5	0.98	110.5	122.98	2.13			552.5	836.2	0.31	110.5	101.18	0.92
222	254	-0.43	111	113	1.16	111	123.18	1.98			555	839.6	0.22	111	102.7	0.92
223	255	-0.51	111.5	113.5	1.26	111.5	123.38	1.53			557.5	842.9	0.16	111.5	104.22	1
224	256	-0.6	112	114	1.07	112	123.57	1.76			560	846.2	0.22	112	105.74	1.14
225	257	-0.64	112.5	114.5	0.79	112.5	123.76	2.06			562.5	849.5	0.22	112.5	107.26	1
226	258	-0.36	113	115	0.7	113	123.96	2.06			565	852.8	0.15	113	108.78	1
227	259	-0.42	113.5	115.5	0.7	113.5	124.15	1.98			567.5	856.1	0.15	113.5	110.3	1.07
228	260	-0.39	114	116	0.98	114	124.34	1.98			570	859.5	0.27	114	111.82	1.21
229	261	-0.31	114.5	116.5	1.35	114.5	124.53	2.21			572.5	862.8	0.15	114.5	113.35	1.28
230	262	-0.42	115	117	1.44	115	125.44	1.91			575	866.1	0.14	115	114.87	1.21
231	263	-0.57	115.5	117.5	1.54	115.5	126.41	1.61			577.5	869.4	0.2	115.5	116.39	1.28
232	264	-0.64	116	118	1.54	116	127.2	1.76			580	872.7	0.15	116	117.91	1.21
233	265	-0.31	116.5	118.5	1.54	116.5	128.11	1.68			582.5	876	0.2	116.5	119.43	1.43

Table D.2 (continued)

234	266	-0.44	117	119	1.54	117	129.03	1.31			585	879.3	0.22	117	119.88	1.71
235	267	-0.24	117.5	119.5	1.63	117.5	129.95	1.24			587.5	882.2	0.18	117.5	120.26	1.14
236	268	-0.33	118	120	1.44	118	130.87	1.01			590	883.2	0.17	118	120.64	1.28
237	269	-0.36	118.5	120.5	1.26	118.5	131.82	1.39			592.5	884.2	0.12	118.5	121.02	1.43
238	270	-0.66	119	121	1.07	119	132.71	1.39			595	885.2	0.2	119	121.41	1.21
239	271	-0.71	119.5	121.5	1.63	119.5	133.09	1.46			597.5	886.2	0.33	119.5	121.79	1
240	272	-0.62	120	122	1.54	120	133.47	1.39			600	887.2	0.29	120	122.17	0.78
241	273	-0.54	120.5	122.5	1.72	120.5	133.85	1.39			602.5	888.5	0.38	120.5	122.55	0.78
242	274	-0.36	121	123	1.91	121	134.23	1.31			605	890.9	0.51	121	122.93	0.64
243	275	-0.38	121.5	123.5	1.26	121.5	134.61	1.31			607.5	893.3	0.59	121.5	123.31	0.42
244	276	-0.24	122	124	1.82	122	134.99	1.24			610	895.7	0.69	122	123.69	0.28
245	277	-0.4	122.5	124.5	1.91	122.5	135.37	1.31			612.5	898	0.75	122.5	124.07	0.5
246	278	-0.55	123	125	1.72	123	135.75	1.46			615	900.4	0.95	123	124.46	0.42
247	279	-0.55	123.5	125.5	1.26	123.5	136.13	1.46			617.5	902.8	1.33	123.5	124.84	0.42
248	280	-0.53	124	126	1.16	124	136.51	1.31			620	905.2	2.54	124	125.22	0.64
249	281	-0.56	124.5	126.5	1.07	124.5	136.89	1.39			622.5	907.6	4.89	124.5	125.6	0.85
250	282	-0.46	125	127	1.26	125	137.08	1.24			625	910	7.17	125	125.98	0.78
251	283	-0.39	125.5	127.5	1.16	125.5	137.17	1.09			627.5	912.4	8.21	125.5	126.36	0.57
252	284	-0.43	126	128	1.07	126	137.26	0.86			630	914.8	9.33	126	126.74	0.42
253	285	-0.38	126.5	128.5	0.88	126.5	137.36	0.94			632.5	917.2	9.93	126.5	127.12	0.35
254	286	-0.65	127	129	0.88	127	137.45	0.94			635	919.6	9.91	127	127.5	0.35
255	287	-0.61	127.5	129.5	0.7	127.5	137.54	0.86			637.5	922	9.71	127.5	127.89	0.35
256	288	-0.16	128	130	0.32	128	137.63	0.79			640	924.3	9.17	128	128.27	0.28
257	289	-0.24	128.5	130.5	0.23	128.5	137.72	0.79			642.5	926.7	8.32	128.5	128.65	0.07
258	290	-0.24	129	131	-0.05	129	137.82	0.64			645	929.1	7.45	129	129.03	0.07
259	291	-0.27	129.5	131.5	0.32	129.5	137.91	0.71			647.5	931.5	6.27	129.5	129.52	0.35
260	292	-0.24	130	132	0.42	130	138	0.64			650	943.1	4.03	130	130.11	0.57
261	293	-0.25	130.5	132.5	1.16	130.5	138.09	0.49			652.5	957	2.14	130.5	130.71	1.21
262	294	-0.28	131	133	1.26	131	138.38	0.56			655	970.9	1.31	131	131.3	0.78
263	295	-0.16	131.5	133.5	1.26	131.5	138.72	0.64			657.5	983.1	0.75	131.5	131.9	0.78
264	296	-0.36	132	134	1.16	132	139.05	0.49			660	988.5	1.16	132	132.49	0.92
265	297	-0.17	132.5	134.5	1.26	132.5	139.39	0.71			662.5	993.9	2.42	132.5	132.75	0.92
266	298	-0.1	133	135	1.07	133	139.73	0.79			665	1000.7	4.59	133	133.01	0.92
267	299	-0.27	133.5	135.5	0.79	133.5	140.25	0.64			667.5	1007.8	5.97	133.5	133.26	1
268	300	-0.33	134	136	0.7	134	140.77	0.71			670	1014.9	7.14	134	133.51	1
269	301	-0.32	134.5	136.5	0.7	134.5	141.3	0.64			672.5	1022	10.42	134.5	133.77	0.92
270	302	-0.44	135	137	0.7	135	141.82	0.71			675	1029.2	15.29	135	134.02	0.85
271	303	-0.28	135.5	137.5	-0.14	135.5	142.34	0.94			677.5	1037.5	17.69	135.5	134.28	0.85
272	304	-0.07	136	138	-0.61	136	143.24	0.71			680	1040	18.88	136	134.53	0.85
273	305	0	136.5	138.5	-0.42	136.5	144.15	0.56			682.5	1042.5	19.82	136.5	134.78	0.85

Table D.2 (continued)

274	306	0.06	137	139	-0.05	137	144.5	0.86			685	1045	21.26	137	135.04	0.92
275	307	0.02	137.5	139.5	0.04	137.5	145	1.16			687.5	1047.5	21.39	137.5	135.29	1.5
276	308	-0.29	138	140	-0.05	138	145.5	0.64			690	1050	21.95	138	135.55	1
277	309	-0.27	138.5	140.5	-0.05	138.5	146	0.71			692.5	1052.5	21.27	138.5	135.8	0.71
278	310	-0.33	139	141	-0.05	139	146.5	0.64			695	1055	20.44	139	136.06	0.78
279	311	-0.39	139.5	141.5	-0.05	139.5	148	0.71			697.5	1057.5	20.21	139.5	136.31	0.78
280	312	-0.4	140	142	0.04	140	148.5	0.64			700	1060	19.91	140	136.56	0.78
281	313	-0.49	140.5	142.5	0.04	140.5	149	0.64			702.5	1062.5	19.79	140.5	136.82	0.78
282	314	-0.53	141	143	-0.14	141	149.5	0.64			705	1065	19.86	141	137.07	0.71
283	315	-0.35	141.5	143.5	-0.24	141.5	150	0.56			707.5	1067.5	19.85	141.5	137.33	0.78
284	316	-0.16	142	144	-0.14	142	150.5	0.71			710	1070	19.87	142	137.58	0.78
285	317	-0.14	142.5	144.5	-0.05	142.5	151	0.71			712.5	1072.5	20.23	142.5	137.83	0.71
286	318	-0.18	143	145	0.14	143	151.5	0.86			715	1075	20.31	143	138.09	0.71
287	319	-0.21	143.5	145.5	0.23	143.5	152	0.86			717.5	1077.5	20.16	143.5	138.34	0.78
288	320	-0.18	144	146	0.32	144	152.5	0.71			720	1080	20.16	144	138.6	0.71
289	321	-0.29	144.5	146.5	0.32	144.5	153	0.64			722.5	1082.5	20.15	144.5	138.85	0.78
290	322	-0.47	145	147	0.23	145	153.5	0.49			725	1085	20.4	145	139.1	0.64
291	323	-0.33	145.5	147.5	0.23	145.5	154	0.56			727.5	1087.5	20.78	145.5	139.36	0.64
292	324	-0.32	146	148	0.04	146	154.5	0.49			730	1090	21.56	146	139.61	0.64
293	325	-0.35	146.5	148.5	0.14	146.5	155	0.49			732.5	1092.5	22.18	146.5	139.87	0.42
294	326	-0.5	147	149	-0.05	147	155.5	0.49			735	1095	22.24	147	140.12	0.35
295	327	-0.68	147.5	149.5	-0.05	147.5	156	0.56			737.5	1097.5	22.28	147.5	140.37	0.57
296	328	-0.66	148	150	-0.14	148	156.5	0.56			740	1100	23.68	148	140.63	0.57
297	329	-0.73	148.5	150.5	-0.24	148.5	157	0.41			742.5	1102.5	24.99	148.5	140.88	0.57
298	330	-0.69	149	151	-0.24	149	157.5	0.41			745	1105	24.66	149	141.14	0.57
299	331	-0.69	149.5	151.5	-0.14	149.5	158	0.34			747.5	1107.5	24.01	149.5	141.39	0.5
300	332	-0.71	150	152	-0.14	150	158.5	0.34			750	1110	24.53	150	141.64	0.5
301	333	-0.71	150.5	152.5	-0.05	150.5	159	0.49			752.5	1112.5	26	150.5	141.9	0.42
302	334	-0.75	151	153	-0.14	151	159.5	0.49			755	1115	28.55	151	142.15	0.21
303	335	-0.73	151.5	153.5	-0.05	151.5	160	0.56			757.5	1117.5	28.95	151.5	142.41	0.35
304	336	-0.71	152	154	-0.14	152	160.5	0.56			760	1120	25.54	152	142.66	0.42
305	337	-0.66	152.5	154.5	0.04	152.5	161	0.56			762.5	1122.5	24.71	152.5	142.91	0.42
306	338	-0.25	153	155	0.14	153	161.5	0.34			765	1125	24.51	153	143.17	0.35
307	339	-0.44	153.5	155.5	0.14	153.5	162	0.49			767.5	1127.5	25.07	153.5	143.42	-0.29
308	340	-0.42	154	156	0.04	154	162.5	0.41			770	1130	27.46	154	143.68	0.42
309	341	-0.43	154.5	156.5	0.04	154.5	163	0.49			772.5	1132.5	33.79	154.5	143.93	0.35
310	342	-0.66	155	157	-0.05	155	163.5	0.71			775	1135	41.23	155	144.19	0.28
311	343	-0.69	155.5	157.5	0.04	155.5	164	0.49			777.5	1137.5	36.07	155.5	144.44	0.21
312	344	-0.16	156	158	-0.14	156	164.5	0.64			780	1140	28.93	156	145.09	0.14
313	345	-0.73	156.5	158.5	-0.24	156.5	165	0.49			782.5	1142.5	25.59	156.5	145.87	0

Table D.2 (continued)

314	346	-0.68	157	159	-0.24	157	165.5	0.41			785	1145	24.58	157	146.65	0
315	347	0.06	157.5	159.5	-0.24	157.5	166	0.41			787.5	1147.5	23.87	157.5	147.42	0.14
316	348	0.22	158	160	-0.33	158	166.5	0.26			790	1150	24	158	148.2	0.14
317	349	0.19	158.5	160.5	-0.24	158.5	167	0.26			792.5	1152.5	24.18	158.5	148.98	0.14
318	350	0.04	159	161	-0.33	159	167.5	0.41			795	1155	23.78	159	149.75	0.07
319	351	0.08	159.5	161.5	-0.24	159.5	168	0.49			797.5	1157.5	23.78	159.5	150.53	0.07
320	352	-0.1	160	162	-0.24	160	168.5	0.34			800	1160	23.97	160	151.31	0
321	353	0.04	160.5	162.5	0.04	160.5	169	0.34			802.5	1162.5	23.64	160.5	152.08	0.07
322	354	0.16	161	163	0.04	161	169.5	0.34			805	1165	23.33	161	152.86	0.07
323	355	0.08	161.5	163.5	-0.05	161.5	170	0.26			807.5	1167.5	23.43	161.5	153.64	0
324	356	0.09	162	164	-0.05	162	170.5	0.34			810	1170	23.81	162	154.41	0
325	357	0.15	162.5	164.5	-0.05	162.5	171	0.26			812.5	1172.5	23.87	162.5	155.19	0
326	358	-0.05	163	165	-0.05	163	171.5	0.41			815	1175	23.68	163	155.97	0
327	359	-0.02	163.5	165.5	-0.05	163.5	172	0.49			817.5	1177.5	24.02	163.5	156.74	-0.08
328	360	-0.17	164	166	-0.05	164	172.5	0.49			820	1180	24.96	164	157.52	0
329	361	-0.16	164.5	166.5	-0.05	164.5	173	0.41			822.5	1182.5	25.11	164.5	158.3	0
330	362	-0.29	165	167	-0.14	165	173.5	0.41			825	1185	24.65	165	159.07	0
331	363	-0.24	165.5	167.5	-0.05	165.5	174	0.41			827.5	1187.5	24.1	165.5	159.85	0
332	364	-0.36	166	168	-0.05	166	174.5	0.49			830	1190	24.25	166	160.63	-0.08
333	365	-0.27	166.5	168.5	-0.14	166.5	175	0.34			832.5	1192.5	24.63	166.5	161.4	-0.15
334	366	-0.27	167	169	-0.14	167	175.5	0.49			835	1195	26.21	167	162.18	0.57
335	367	-0.35	167.5	169.5	-0.14	167.5	176	0.49			837.5	1197.5	26.48	167.5	162.96	-0.15
336	368	-0.24	168	170	-0.14	168	176.5	0.56			840	1200	25	168	163.73	-0.22
337	369	-0.29	168.5	170.5	-0.24	168.5	177	0.64			842.5	1202.5	24.25	168.5	164.51	-0.22
338	370	-0.58	169	171	-0.24	169	177.5	0.56			845	1205	23.88	169	165.29	-0.15
339	371	-0.53	169.5	171.5	-0.14	169.5	178	0.64			847.5	1207.5	24.05	169.5	166.06	-0.22
340	372	-0.57	170	172	-0.24	170	178.5	0.64			850	1210	23.53	170	166.84	-0.15
341	373	-0.31	170.5	172.5	-0.24	170.5	179	0.64			852.5	1212.5	22.65	170.5	167.62	-0.29
342	374	-0.57	171	173	-0.33	171	179.5	0.71			855	1215	22.09	171	168.4	-0.36
343	375	-0.11	171.5	173.5	-0.33	171.5	180	0.79			857.5	1217.5	21.43	171.5	169.17	-0.29
344	376	0.06	172	174	-0.33	172	180.5	0.86			860	1220	21.07	172	169.95	-0.29
345	377	-0.5	172.5	174.5	-0.33	172.5	181	0.79			862.5	1222.5	19.95	172.5	170.73	-0.22
346	378	-0.4	173	175	-0.33	173	181.5	0.71			865	1225	16.44	173	171.5	-0.29
347	379	-0.27	173.5	175.5	-0.52	173.5	182	0.79			867.5	1227.5	12.72	173.5	172.28	-0.29
348	380	-0.4	174	176	-0.52	174	182.5	0.79			870	1230	6.61	174	173.06	-0.29
349	381	-0.33	174.5	176.5	-0.52	174.5	183	0.71			872.5	1232.5	1.89	174.5	173.83	-0.29
350	382	-0.39	175	177	-0.52	175	183.5	0.79			875	1235	0.7	175	174.61	-0.36
351	383	-0.65	175.5	177.5	-0.52	175.5	184	0.71						175.5	175.39	-0.36
352	384	-0.58	176	178	-0.52	176	184.5	0.86						176	176.16	-0.29
353	385	-0.53	176.5	178.5	-0.52	176.5	185	0.86						176.5	176.94	-0.29

Table D.2 (continued)

354	386	-0.58	177	179	-0.61	177	185.5	0.79						177	177.72	-0.29
355	387	-0.62	177.5	179.5	-0.61	177.5	186	0.86						177.5	178.49	-0.22
356	388	-0.68	178	180	-0.61	178	186.5	0.79						178	179.27	-0.29
357	389	-0.64	178.5	180.5	-0.61	178.5	187	0.79						178.5	180.05	-0.29
358	390	-0.66	179	181	-0.61	179	187.5	0.79						179	180.82	-0.29
359	391	-0.66	179.5	181.5	-0.7	179.5	188	0.71						179.5	181.6	-0.22
360	392	-0.66	180	182	-0.7	180	188.5	0.64						180	182.38	-0.22
361	393	-0.69	180.5	182.5	-0.7	180.5	189	0.49						180.5	183.15	-0.29
362	394	-0.69	181	183	-0.79	181	189.5	0.49						181	183.93	-0.29
363	395	-0.68	181.5	183.5	-0.61	181.5	190	0.56						181.5	184.71	-0.29
364	396	-0.66	182	184	-0.7	182	190.5	0.64						182	185.48	-0.36
365	397	-0.66	182.5	184.5	-0.7	182.5	191	0.71						182.5	186.26	-0.29
366	398	-0.69	183	185	-0.33	183	191.5	0.64						183	187.04	-0.36
367	399	-0.69	183.5	185.5	-0.7	183.5	192	0.56						183.5	187.81	-0.36
368	400	-0.64	184	186	-0.7	184	192.5	0.56						184	188.59	-0.36
369	401	-0.51	184.5	186.5	-0.61	184.5	193	0.56						184.5	189.37	-0.43
370	402	-0.47	185	187	-0.61	185	193.5	0.56						185	190.14	-0.36
371	403	-0.51	185.5	187.5	-0.52	185.5	194	0.56						185.5	190.92	-0.36
372	404	-0.61	186	188	-0.42	186	194.5	0.64						186	191.7	-0.43
373	405	-0.62	186.5	188.5	-0.42	186.5	195	0.64						186.5	192.47	-0.36
374	406	-0.64	187	189	-0.42	187	195.5	0.64						187	193.25	-0.36
375	407	-0.66	187.5	189.5	-0.42	187.5	196	0.79						187.5	194.03	-0.36
376	408	-0.68	188	190	-0.42	188	196.5	0.56						188	194.81	-0.36
377	409	-0.68	188.5	190.5	-0.42	188.5	197	0.49						188.5	195.58	-0.08
378	410	-0.72	189	191	-0.42	189	197.5	0.49						189	196.36	-0.36
379	411	-0.49	189.5	191.5	-0.42	189.5	198	0.49						189.5	197.14	-0.43
380	412	-0.46	190	192	-0.42	190	198.5	0.56						190	197.91	-0.43
381	413	-0.42	190.5	192.5	-0.42	190.5	199	0.56						190.5	198.69	-0.58
382	414	-0.49	191	193	-0.52	191	199.5	0.71						191	199.47	-0.65
383	415	-0.6	191.5	193.5	-0.52	191.5	200	0.56						191.5	200.24	-0.58
384	416	-0.66	192	194	-0.52	192	200.5	0.49						192	201.02	-0.58
385	417	-0.51	192.5	194.5	-0.52	192.5	201	0.56						192.5	201.8	-0.58
386	418	-0.66	193	195	-0.52	193	201.5	0.49						193	202.57	-0.5
387	419	-0.62	193.5	195.5	-0.61	193.5	202	0.56						193.5	203.35	-0.58
388	420	-0.62	194	196	-0.61	194	202.5	0.56						194	204.13	-0.5
389	421	-0.61	194.5	196.5	-0.7	194.5	203	0.49						194.5	204.9	-0.5
390	422	-0.57	195	197	-0.52	195	203.5	0.49						195	205.68	-0.58
391	423	-0.6	195.5	197.5	-0.61	195.5	204	0.41						195.5	206.46	-0.5
392	424	-0.83	196	198	-0.61	196	204.5	0.49						196	207.23	-0.58
393	425	-0.62	196.5	198.5	-0.52	196.5	205	0.56						196.5	208.01	-0.58

Table D.2 (continued)

394	426	-0.69	197	199	-0.61	197	205.5	0.56						197	208.79	-0.58
395	427	-0.76	197.5	199.5	-0.61	197.5	206	0.56						197.5	209.56	-0.65
396	428	-0.77	198	200	-0.7	198	206.5	0.49						198	210.34	-0.58
397	429	-0.76	198.5	200.5	-0.7	198.5	207	0.49						198.5	211.12	-0.58
398	430	-0.75	199	201	-0.89	199	207.5	0.49						199	211.89	-0.5
399	431	-0.73	199.5	201.5	-0.79	199.5	208	0.56						199.5	212.67	-0.58
400	432	-0.61	200	202	-0.89	200	208.5	0.56						200	213.45	-0.58
401	433	-0.71	200.5	202.5	-0.89	200.5	209	0.56						200.5	214.22	-0.65
402	434	-0.73	201	203	-0.89	201	209.5	0.49						201	215	-0.65
403	435	-0.73	201.5	203.5	-0.89	201.5	210	0.49						201.5	215.78	-0.65
404	436	-0.49	202	204	-0.79	202	210.5	0.56						202	216.55	-0.65
405	437	-0.53	202.5	204.5	-0.89	202.5	211	0.49						202.5	217.33	-0.58
406	438	-0.6	203	205	-0.79	203	211.5	0.49						203	218.11	-0.58
407	439	-0.58	203.5	205.5	-0.89	203.5	212	0.56						203.5	218.88	-0.65
408	440	-0.68	204	206	-0.98	204	212.5	0.56						204	219.66	-0.58
409	441	-0.71	204.5	206.5	-0.89	204.5	213	0.56						204.5	220.44	-0.65
410	442	-0.73	205	207	-0.98	205	213.5	0.56						205	221.22	-0.58
411	443	-0.71	205.5	207.5	-0.98	205.5	214	0.56						205.5	221.99	-0.58
412	444	-0.71	206	208	-0.98	206	214.5	0.49						206	222.77	-0.58
413	445	-0.71	206.5	208.5	-1.07	206.5	215	0.49						206.5	223.55	-0.65
414	446	-0.72	207	209	-1.07	207	215.5	0.49						207	224.32	-0.72
415	447	-0.69	207.5	209.5	-1.07	207.5	216	0.49						207.5	225.1	-0.72
416	448	-0.71	208	210	-0.98	208	216.5	0.56						208	225.88	-0.72
417	449	-0.53	208.5	210.5	-0.98	208.5	217	0.56						208.5	226.65	-0.72
418	450	-0.62	209	211	-0.98	209	217.5	0.41						209	227.43	-0.72
419	451	-0.65	209.5	211.5	-0.89	209.5	218	0.49						209.5	228.21	-0.79
420	452	-0.68	210	212	-0.98	210	218.5	0.49						210	228.98	-0.65
421	453	-0.68	210.5	212.5	-0.61	210.5	219	0.49						210.5	229.76	-0.65
422	454	-0.51	211	213	-0.79	211	219.5	0.49						211	230.54	-0.72
423	455	-0.47	211.5	213.5	-0.79	211.5	220	0.49						211.5	231.31	-0.72
424	456	-0.42	212	214	-0.7	212	220.5	0.49						212	232.09	-0.72
425	457	-0.4	212.5	214.5	-0.61	212.5	221	0.26						212.5	232.87	-0.58
426	458	-0.44	213	215	-0.61	213	221.5	0.34						213	233.64	-0.58
427	459	-0.39	213.5	215.5	-0.7	213.5	222	0.41						213.5	234.42	-0.65
428	460	-0.42	214	216	-0.61	214	222.5	0.49						214	235.2	-0.65
429	461	-0.17	214.5	216.5	-0.61	214.5	223	0.34						214.5	235.97	-0.79
430	462	-0.21	215	217	-0.61	215	223.5	0.34						215	236.75	-0.79
431	463	-0.36	215.5	217.5	-0.61	215.5	224	0.41						215.5	237.53	-0.79
432	464	-0.35	216	218	-0.7	216	224.5	0.34						216	238.3	-0.86
433	465	-0.29	216.5	218.5	-0.61	216.5	225	0.34						216.5	239.08	-0.86

Table D.2 (continued)

434	466	-0.54	217	219	-0.61	217	225.5	0.34						217	239.86	-0.79
435	467	-0.51	217.5	219.5	-0.61	217.5	226	0.41						217.5	240.63	-0.79
436	468	-0.61	218	220	-0.7	218	226.5	0.34						218	241.41	-0.86
437	469	-0.54	218.5	220.5	-0.61	218.5	227	0.26						218.5	242.19	-0.72
438	470	-0.2	219	221	-0.61	219	227.5	0.34						219	242.96	-0.79
439	471	-0.5	219.5	221.5	-0.7	219.5	228	0.34						219.5	243.74	-0.79
440	472	-0.36	220	222	-0.61	220	228.5	0.26						220	244.52	-0.79
441	473	-0.4	220.5	222.5	-0.79	220.5	229	0.41						220.5	245.29	-0.79
442	474	-0.43	221	223	-0.61	221	229.5	0.49						221	246.07	-0.72
443	475	-0.35	221.5	223.5	-0.52	221.5	230	0.34						221.5	246.85	-0.79
444	476	-0.38	222	224	-0.61	222	230.5	0.19						222	247.63	-0.79
445	477	-0.32	222.5	224.5	-0.61	222.5	231	0.26						222.5	248.4	-0.79
446	478	-0.33	223	225	-0.61	223	231.5	0.34						223	249.18	-0.79
447	479	-0.36	223.5	225.5	-0.7	223.5	232	0.26						223.5	249.96	-0.79
448	480	-0.38	224	226	-0.61	224	232.5	0.26						224	250.73	-0.79
449	481	-0.4	224.5	226.5	-0.61	224.5	233	0.26						224.5	251.51	-0.86
450	482	-0.47	225	227	-0.52	225	233.5	0.26						225	252.29	-0.86
451	483	-0.42	225.5	227.5	-0.61	225.5	234	0.19						225.5	253.06	-0.86
452	484	-0.66	226	228	-0.61	226	234.5	0.26						226	253.84	-0.86
453	485	-0.6	226.5	228.5	-0.61	226.5	235	0.19						226.5	254.62	-0.86
454	486	-0.66	227	229	-0.7	227	235.5	0.19						227	255.39	-0.79
455	487	-0.65	227.5	229.5	-0.7	227.5	236	0.19						227.5	256.17	-0.86
456	488	-0.68	228	230	-0.79	228	236.5	0.19						228	256.95	-0.79
457	489	-0.71	228.5	230.5	-0.61	228.5	237	0.26						228.5	257.72	-0.79
458	490	-0.73	229	231	-0.7	229	237.5	0.19						229	258.5	-0.86
459	491	-0.72	229.5	231.5	-0.7	229.5	238	0.19						229.5	259.28	-0.86
460	492	-0.73	230	232	-0.61	230	238.5	0.19						230	260.05	-0.79
461	493	-0.72	230.5	232.5	-0.7	230.5	239	0.26						230.5	260.83	-0.79
462	494	-0.75	231	233	-0.61	231	239.5	0.26						231	261.61	-0.79
463	495	-0.71	231.5	233.5	-0.7	231.5	240	0.26						231.5	262.38	-0.79
464	496	-0.72	232	234	-0.7	232	240.5	0.26						232	263.16	-0.86
465	497	-0.75	232.5	234.5	-0.79	232.5	241	0.19						232.5	263.94	-0.79
466	498	-0.73	233	235	-0.79	233	241.5	0.26						233	264.71	-0.86
467	499	-0.71	233.5	235.5	-0.79	233.5	242	0.19						233.5	265.49	-0.86
468	500	-0.73	234	236	-0.89	234	242.5	0.19						234	266.27	-0.86
469	501	-0.65	234.5	236.5	-0.89	234.5	243	0.11						234.5	267.04	-0.86
470	502	-0.69	235	237	-0.89	235	243.5	0.11						235	267.82	-0.86
471	503	-0.61	235.5	237.5	-0.89	235.5	244	0.19						235.5	268.6	-0.86
472	504	-0.55	236	238	-0.98	236	244.5	0.11						236	269.37	-0.79
473	505	-0.73	236.5	238.5	-0.89	236.5	245	0.11						236.5	270.15	-0.86

Table D.2 (continued)

474	506	-0.69	237	239	-0.98	237	245.5	0.11						237	270.93	-0.79
475	507	-0.69	237.5	239.5	-0.89	237.5	246	0.04						237.5	271.7	-0.86
476	508	-0.31	238	240	-0.89	238	246.5	0.04						238	272.48	-0.79
477	509	-0.82	238.5	240.5	-0.98	238.5	247	0.11						238.5	273.26	-0.79
478	510	-0.62	239	241	-0.98	239	247.5	0.11						239	274.03	-0.79
479	511	-0.39	239.5	241.5	-0.89	239.5	248	0.19						239.5	274.81	-0.79
480	512	-0.32	240	242	-0.98	240	248.5	0.04						240	275.59	-0.79
481	513	-0.42	240.5	242.5	-0.89	240.5	249	0.04						240.5	276.37	-0.79
482	514	-0.71	241	243	-0.89	241	249.5	0.04						241	277.14	-0.72
483	515	-0.72	241.5	243.5	-0.89	241.5	250	0.04						241.5	277.92	-0.79
484	516	-0.75	242	244	-0.98	242	250.5	0.04						242	278.7	-0.86
485	517	-0.73	242.5	244.5	-1.07	242.5	251	0.04						242.5	279.47	-0.93
486	518	-0.76	243	245	-0.98	243	251.5	0.04						243	280.25	-0.93
487	519	-0.75	243.5	245.5	-0.79	243.5	252	-0.04						243.5	281.03	-0.93
488	520	-0.73	244	246	-0.89	244	252.5	0.04						244	281.8	-0.86
489	521	-0.54	244.5	246.5	-0.89	244.5	253	0.11						244.5	282.58	-0.93
490	522	-0.58	245	247	-0.79	245	253.5	0.04						245	283.36	-0.86
491	523	-0.61	245.5	247.5	-0.79	245.5	254	0.26						245.5	284.13	-0.93
492	524	-0.65	246	248	-0.89	246	254.5	0.19						246	284.91	-0.93
493	525	-0.6	246.5	248.5	-0.89	246.5	255	0.19						246.5	285.69	-0.93
494	526	-0.54	247	249	-0.89	247	255.5	0.11						247	286.46	-0.93
495	527	-0.65	247.5	249.5	-0.89	247.5	256	0.19						247.5	287.24	-0.93
496	528	-0.64	248	250	-0.98	248	256.5	0.04						248	288.02	-1.01
497	529	-0.5	248.5	250.5	-0.98	248.5	257	0.04						248.5	288.79	-0.93
498	530	-0.57	249	251	-0.98	249	257.5	0.11						249	289.57	-0.86
499	531	-0.65	249.5	251.5	-1.07	249.5	258	0.04						249.5	290.35	-0.86
500	532	-0.6	250	252	-1.07	250	258.5	0.04						250	291.12	-0.86
501	533	-0.62	250.5	252.5	-0.98	250.5	259	-0.04						250.5	291.9	-0.86
502	534	-0.68	251	253	-0.89	251	259.5	0.04						251	292.68	-0.86
503	535	-0.69	251.5	253.5	-0.98	251.5	260	0.11						251.5	293.45	-0.86
504	536	-0.62	252	254	-0.98	252	260.5	0.11						278		
505	537	-0.62	252.5	254.5	-1.07	252.5	261	0.19								
506	538	-0.33	253	255	-1.07	253	261.5	0.19								
507	539	-0.43	253.5	255.5	-0.98	253.5	262	0.19								
508	540	-0.72	254	256	-0.98	254	262.5	0.11								
509	541	-0.65	254.5	256.5	-0.98	254.5	263	0.04								
510	542	-0.61	255	257	-0.98	255	263.5	0.04								
511	543	-0.49	255.5	257.5	-0.98	255.5	264	0.11								
512	544	-0.39	256	258	-1.07	256	264.5	0.11								
513	545	-0.64	256.5	258.5	-0.89	256.5	265	0.11								

Table D.2 (continued)

514	546	-0.62	257	259	-0.89	257	265.5	0.11										
515	547	-0.44	257.5	259.5	-0.89	257.5	266	0.04										
516	548	-0.46	258	260	-0.89	258	266.5	-0.04										
517	549	-0.72	258.5	260.5	-0.89	258.5	267	0.04										
518	550	-0.72	259	261	-0.98	259	267.5	0.11										
519	551	-0.32	259.5	261.5	-0.98	259.5	268	0.11										
520	552	-0.66	260	262	-0.98	260	268.5	0.04										
521	553	-0.64	260.5	262.5	-0.98	260.5	269	-0.04										
522	554	-0.65	261	263	-0.89	261	269.5	0.04										
523	555	-0.72	261.5	263.5	-0.98	261.5	270	0.04										
524	556	-0.72	262	264	-1.07	262	270.5	0.04										
525	557	-0.71	262.5	264.5	-1.07	262.5	271	0.19										
526	558	-0.54	263	265	-0.98	263	271.5	0.19										
527	559	-0.6	263.5	265.5	-0.89	263.5	272	0.19										
528	560	-0.36	264	266	-0.98	264	272.5	0.19										
529	561	-0.58	264.5	266.5	-0.89	264.5	273	0.19										
530	562	-0.65	265	267	-0.98	265	273.5	0.11										
531	563	-0.69	265.5	267.5	-0.89	265.5	274	0.04										
532	564	-0.66	266	268	-0.98	266	274.5	0.19										
533	565	-0.66	266.5	268.5	-0.89	266.5	275	0.19										
534	566	-0.44	267	269	-0.89	267	275.5	0.19										
535	567	-0.55	267.5	269.5	-1.07	267.5	276	0.11										
536	568	-0.69	268	270	-1.07	268	276.5	0.11										
537	569	-0.58	268.5	270.5	-0.89	268.5	277	0.11										
538	570	-0.5	269	271	-0.89	269	277.5	-0.04										
539	571	-0.71				269.5	278	0.04										
540	572	-0.71				270	278.5	0.04										
541	573	-0.73				270.5	279	0.04										
542	574	-0.68				271	279.5	0.04										
543	575	-0.69				271.5	280	0.11										
544	576	-0.69				272	280.5	0.04										
545	577	-0.66				272.5	281	-0.04										
546	578	-0.66				273	281.5	-0.04										
547	579	-0.75				273.5	282	0.04										
548	580	-0.72				274	282.5	-0.04										
549	581	-0.73				274.5	283	0.04										
550	582	-0.73				275	283.5	0.04										
551	583	-0.73				275.5	284	-0.04										
552	584	-0.76				276	284.5	-0.11										
553	585	-0.69				276.5	285	-0.04										

Table D.2 (continued)

554	586	-0.61				277	285.5	-0.04									
555	587	-0.66				277.5	286	-0.04									
556	588	-0.49				278	286.5	-0.04									
557	589	-0.51				278.5	287	-0.11									
558	590	-0.35				279	287.5	-0.04									
559	591	-0.68				279.5	288	-0.04									
560	592	-0.71				280	288.5	-0.11									
561	593	-0.69				280.5	289	-0.11									
562	594	-0.54				281	289.5	-0.11									
563	595	-0.68				281.5	290	-0.19									
564	596	-0.68				282	290.5	-0.11									
565	597	-0.4				282.5	291	-0.04									
566	598	-0.22				283	291.5	-0.11									
567	599	-0.44				283.5	292	-0.11									
568	600	-0.5				284	292.5	-0.04									
569	601	-0.44				284.5	293	-0.04									
570	602	-0.5				285	293.5	-0.19									
571	603	-0.6				285.5	294	-0.11									
572	604	-0.68				286	294.5	-0.11									
573	605	-0.44				286.5	295	-0.11									
574	606	-0.66				287	295.5	-0.11									
575	607	-0.42				287.5	296	-0.11									
576	608	-0.55				288	296.5	-0.11									
577	609	-0.62				288.5	297	-0.11									
578	610	-0.44				289	297.5	-0.19									
579	611	-0.39				289.5	298	-0.11									
580	612	-0.6				290	298.5	-0.11									
581	613	-0.72				290.5	299	-0.11									
582	614	-0.58				291	299.5	0.04									
583	615	-0.53				291.5	300	-0.04									
584	616	-0.53				292	300.5	0.04									
585	617	-0.65				292.5	301	0.04									
586	618	-0.71				293	301.5	0.11									
587	619	-0.65				293.5	302	0.11									
588	620	-0.49				294	302.5	0.19									
589	621	-0.65				294.5	303	0.19									
590	622	-0.4				295	303.5	0.11									
591	623	-0.5				295.5	304	0.19									
592	624	-0.53				296	304.5	0.19									
593	625	-0.53				296.5	305	0.19									

Table D.2 (continued)

594	626	-0.68				297	305.5	0.19									
595	627	-0.65				297.5	306	0.19									
596	628	-0.65				298	306.5	0.19									
597	629	-0.71				298.5	307	0.19									
598	630	-0.72				299	307.5	0.11									
599	631	-0.73				299.5	308	0.11									
600	632	-0.76				300	308.5	0.11									
601	633	-0.73				300.5	309	0.19									
602	634	-0.39				301	309.5	0.19									
603	635	-0.44				301.5	310	0.19									
604	636	-0.6				302	310.5	0.19									
605	637	-0.6				302.5	311	0.26									
606	638	-0.6				303	311.5	0.26									
607	639	-0.51				303.5	312	0.19									
608	640	-0.65				304	312.5	0.11									
609	641	-0.68				304.5	313	0.11									
610	642	-0.75				305	313.5	0.11									
611	643	-0.75				305.5	314	-0.64									
612	644	-0.71				306	314.5	-0.71									
613	645	-0.27				306.5	315	-0.64									
614	646	-0.4				307	315.5	-0.79									
615	647	-0.44				307.5	316	-0.71									
616	648	-0.6				308	316.5	-0.71									
617	649	-0.5				308.5	317	-0.79									
618	650	-0.71				309	317.5	-0.86									
619	651	-0.51				309.5	318	-0.86									
620	652	-0.69				310	318.5	-0.86									
621	653	-0.68				310.5	319	-0.79									
622	654	-0.66				311	319.5	-0.71									
623	655	-0.43				311.5	320	-0.79									
624	656	-0.58				312	320.5	-0.86									
625	657	-0.65				312.5	321	-0.71									
626	658	-0.64				313	321.5	-0.71									
627	659	-0.46				313.5	322	-0.71									
628	660	-0.44				314	322.5	-0.79									
629	661	-0.64				314.5	323	-0.94									
630	662	-0.55				315	323.5	-0.94									
631	663	-0.66				315.5	324	-0.86									
632	664	-0.62				316	324.5	-0.94									
633	665	-0.61				316.5	325	-0.86									

Table D.2 (continued)

634	666	-0.69				317	325.5	-0.86									
635	667	-0.61				317.5	326	-0.86									
636	668	-0.51				318	326.5	-0.86									
637	669	-0.58				318.5	327	-0.94									
638	670	-0.64				319	327.5	-0.94									
639	671	-0.61				319.5	328	-0.94									
640	672	-0.58				320	328.5	-0.94									
641	673	-0.51				320.5	329	-0.94									
642	674	-0.46				321	329.5	-1.01									
643	675	-0.51				321.5	330	-1.09									
644	676	-0.61				322	330.5	-1.09									
645	677	-0.53				322.5	331	-1.09									
646	678	-0.57				323	331.5	-1.09									
647	679	-0.65				323.5	332	-1.09									
648	680	-0.62				324	332.5	-1.09									
649	681	-0.64				324.5	333	-1.09									
650	682	-0.61				325	333.5	-1.09									
651	683	-0.53				325.5	334	-1.09									
652	684	-0.62				326	334.5	-1.09									
653	685	-0.6				326.5	335	-1.09									
654	686	-0.61				327	335.5	-1.09									
655	687	-0.6				327.5	336	-0.94									
656	688	-0.43				328	336.5	-0.86									
657	689	-0.49				328.5	337	-1.01									
658	690	-0.57				329	337.5	-1.01									
659	691	-0.6				329.5	338	-1.01									
660	692	-0.62				330	338.5	-0.94									
661	693	-0.61				330.5	339	-1.09									
662	694	-0.49				331	339.5	-1.01									
663	695	-0.25				331.5	340	-1.01									
664	696	-0.24				332	340.5	-1.09									
665	697	-0.49				332.5	341	-1.09									
666	698	-0.51				333	341.5	-1.09									
667	699	-0.53				333.5	342	-1.01									
668	700	-0.55				334	342.5	-1.09									
669	701	-0.64				334.5	343	-1.09									
670	702	-0.62				335	343.5	-1.09									
671	703	-0.66				335.5	344	-1.01									
672	704	-0.61				336	344.5	-1.09									
673	705	-0.55				336.5	345	-1.16									

Table D.2 (continued)

674	706	-0.54				337	345.5	-1.01									
675	707	-0.5				337.5	346	-1.01									
676	708	-0.44				338	346.5	-1									
677	709	-0.62				338.5	347	-1									
678	710	-0.68				339	347.5	-1									
679	711	-0.64				339.5	348	-1									
680	712	-0.65				340	348.5	-1									
681	713	-0.64				340.5	349	-0.94									
682	714	-0.43				341	349.5	-1.09									
683	715	-0.31				341.5	350	-1.01									
684	716	-0.36				342	350.5	-1.09									
685	717	-0.39				342.5	351	-1.09									
686	718	-0.55				343	351.5	-1.09									
687	719	-0.6				343.5	352	-1.01									
688	720	-0.42				344	352.5	-1.01									
689	721	-0.66				344.5	353	-1.01									
690	722	-0.77				345	353.5	-1.09									
691	723	-0.4				345.5	354	-1.01									
692	724	-0.55				346	354.5	-1.01									
693	725	-0.6				346.5	355	-1.01									
694	726	-0.35				347	355.5	-1.01									
695	727	-0.38				347.5	356	-1.01									
696	728	-0.57				348	356.5	-1.01									
697	729	-0.64				348.5	357	-1.01									
698	730	-0.61				349	357.5	-1.01									
699	731	-0.44				349.5	358	-1.09									
700	732	-0.6				350	358.5	-1.09									
701	733	-0.55				350.5	359	-1.09									
702	734	-0.58				351	359.5	-1.09									
703	735	-0.69				351.5	360	-1.09									
704	736	-0.71				352	360.5	-1.09									
705	737	-0.72				352.5	361	-1.09									
706	738	-0.33				353	361.5	-1.09									
707	739	-0.39				353.5	362	-1.16									
708	740	-0.42				354	362.5	-1.09									
709	741	-0.35				354.5	363	-1.16									
710	742	-0.65				355	363.5	-1.09									
711	743	-0.69				355.5	364	-1.01									
712	744	-0.71				356	364.5	-1.01									
713	745	-0.75				356.5	365	-1.09									

Table D.2 (continued)

714	746	-0.71				357	365.5	-1.01									
715	747	-0.69				357.5	366	-1.09									
716	748	-0.71				358	366.5	-1.09									
717	749	-0.49				358.5	367	-1.01									
718	750	-0.64				359	367.5	-1.09									
719	751	-0.4				359.5	368	-1.16									
720	752	-0.43				360	368.5	-1.09									
721	753	-0.47				360.5	369	-1.09									
722	754	-0.4				361	369.5	-1.16									
723	755	-0.49				361.5	370	-1.09									
724	756	-0.6				362	370.5	-1.16									
725	757	-0.64				362.5	371	-1.16									
726	758	-0.64				363	371.5	-1.16									
727	759	-0.62				363.5	372	-1									
728	760	-0.46				364	372.5	-1.16									
729	761	-0.64				364.5	373	-1.09									
730	762	-0.64				365	373.5	-1.16									
731	763	-0.65				365.5	374	-1.09									
732	764	-0.66				366	374.5	-1.09									
733	765	-0.64				366.5	375	-1.16									
734	766	-0.36				367	375.5	-1.09									
735	767	-0.25				367.5	376	-1.09									
736	768	-0.55				368	376.5	-1.16									
737	769	-0.62				368.5	377	-1.16									
738	770	-0.68				369	377.5	-1.09									
739	771	-0.71				369.5	378	-0.86									
740	772	-0.72				370	378.5	-0.79									
741	773	-0.68				370.5	379	-0.86									
742	774	-0.69				371	379.5	-0.94									
743	775	-0.71				371.5	380	-1.01									
744	776	-0.72				372	380.5	-0.86									
745	777	-0.68				372.5	381	-0.86									
746	778	-0.69				373	381.5	-1.01									
747	779	-0.64				373.5	382	-1.09									
748	780	-0.36				374	382.5	-1.09									
749	781	-0.6				374.5	383	-1.09									
750	782	-0.64				375	383.5	-1.01									
751	783	-0.42				375.5	384	-1.01									
752	784	-0.36				376	384.5	-1.09									
753	785	-0.4				376.5	385	-1.01									

Table D.2 (continued)

754	786	-0.64				377	385.5	-1.01									
755	787	-0.64				377.5	386	-0.94									
756	788	-0.68				378	386.5	-0.94									
757	789	-0.64				378.5	387	-0.94									
758	790	-0.54				379	387.5	-0.94									
759	791	-0.6				379.5	388	-0.94									
760	792	-0.42				380	388.5	-1.01									
761	793	-0.57				380.5	389	-1.01									
762	794	-0.6				381	389.5	-0.94									
763	795	-0.6				381.5	390	-1.09									
764	796	-0.51				382	390.5	-1.01									
765	797	-0.6				382.5	391	-1.09									
766	798	-0.51				383	391.5	-1.09									
767	799	-0.39				383.5	392	-1.01									
768	800	-0.44				384	392.5	-1.01									
769	801	-0.33				384.5	393	-1.01									
770	802	-0.54				385	393.5	-0.94									
771	803	-0.61				385.5	394	-1.01									
772	804	-0.6				386	394.5	-1.09									
773	805	-0.69				386.5	395	-1.09									
774	806	-0.68				387	395.5	-1.09									
775	807	-0.66				387.5	396	-1.09									
776	808	-0.69				388	396.5	-1.09									
777	809	-0.6				388.5	397	-1.01									
778	810	-0.55				389	397.5	-1.01									
779	811	-0.55				389.5	398	-1.01									
780	812	-0.68				390	398.5	-1.09									
781	813	-0.58				390.5	399	-1.01									
782	814	-0.55				391	399.5	-1.01									
783	815	-0.49				391.5	400	-1.09									
784	816	-0.57				392	400.5	-1.09									
785	817	-0.58				392.5	401	-1.09									
786	818	-0.6				393	401.5	-1.09									
787	819	-0.62				393.5	402	-1.16									
788	820	-0.62				394	402.5	-1.16									
789	821	-0.54				394.5	403	-1.09									
790	822	-0.38				395	403.5	-1.09									
791	823	-0.43				395.5	404	-1.16									
792	824	-0.53				396	404.5	-1.09									
793	825	-0.6				396.5	405	-1.16									

Table D.2 (continued)

794	826	-0.68				397	405.5	-1.16									
795	827	-0.65				397.5	406	-1.16									
796	828	-0.65				398	406.5	-1.16									
797	829	-0.65				398.5	407	-1.16									
798	830	-0.57				399	407.5	-1.09									
799	831	-0.57				399.5	408	-1.16									
800	832	-0.51				400	408.5	-1.16									
801	833	-0.55				400.5	409	-1.24									
802	834	-0.55				401	409.5	-1.16									
803	835	-0.61				401.5	410	-1.16									
804	836	-0.61				402	410.5	-1.16									
805	837	-0.6				402.5	411	-1.16									
806	838	-0.58				403	411.5	-1.16									
807	839	-0.62				403.5	412	-1.16									
808	840	-0.62				404	412.5	-1.24									
809	841	-0.64				404.5	413	-1.24									
810	842	-0.69				405	413.5	-1.24									
811	843	-0.66				405.5	414	-1.24									
812	844	-0.71				406	414.5	-1.24									
813	845	-0.66				406.5	415	-1.31									
814	846	-0.6				407	415.5	-1.24									
815	847	-0.51				407.5	416	-1.24									
816	848	-0.43				408	416.5	-1.24									
817	849	-0.43				408.5	417	-1.24									
818	850	-0.46				409	417.5	-1.24									
819	851	-0.5				409.5	418	-1.31									
820	852	-0.64				410	418.5	-1.31									
821	853	-0.57				410.5	419	-1.24									
822	854	-0.5				411	419.5	-1.31									
823	855	-0.1				411.5	420	-1.24									
824	856	0.16				412	420.5	-1.24									
825	857	-0.2				412.5	421	-1.31									
826	858	-0.2				413	421.5	-1.24									
827	859	-0.29				413.5	422	-1.31									
828	860	-0.32				414	422.5	-1.24									
829	861	-0.29				414.5	423	-1.24									
830	862	-0.35				415	423.5	-1.24									
831	863	-0.36				415.5	424	-1.24									
832	864	-0.46				416	424.5	-1.24									
833	865	-0.58				416.5	425	-1.24									

Table D.2 (continued)

834	866	-0.65				417	425.5	-1.16									
835	867	-0.66				417.5	426	-1.09									
836	868	-0.71				418	426.5	-1.09									
837	869	-0.66				418.5	427	-1.16									
838	870	-0.73				419	427.5	-1									
839	871	-0.68				419.5	428	-1									
840	872	-0.62				420	428.5	-1									
841	873	-0.68				420.5	429	-1.09									
842	874	-0.6				421	429.5	-1.01									
843	875	-0.25				421.5	430	-1.01									
844	876	-0.55				422	430.5	-1.01									
845	877	-0.72				422.5	431	-1.09									
846	878	-0.72				423	431.5	-1.09									
847	879	-0.72				423.5	432	-1.01									
848	880	-0.71				424	432.5	-1.01									
849	881	-0.72				424.5	433	-1.01									
850	882	-0.31				425	433.5	-1.01									
851	883	-0.06				425.5	434	-0.94									
852	884	-0.09				426	434.5	-0.94									
853	885	-0.28				426.5	435	-0.94									
854	886	-0.32				427	435.5	-1.01									
855	887	-0.62				427.5	436	-0.94									
856	888	-0.14				428	436.5	-0.94									
857	889	0.04				428.5	437	-0.86									
858	890	-0.02				429	437.5	-0.86									
859	891	0.02				429.5	438	-0.94									
860	892	0.04				430	438.5	-1.01									
861	893	-0.17				430.5	439	-1.01									
862	894	-0.33				431	439.5	-1.09									
863	895	0.33				431.5	440	-1.09									
864	896	0				432	440.5	-1.01									
865	897	-0.1				432.5	441	-1.09									
866	898	0.23				433	441.5	-1.09									
867	899	0.49				433.5	442	-1.09									
868	900	0.44				434	442.5	-1.09									
869	901	0.53				434.5	443	-1.16									
870	902	0.5				435	443.5	-1.09									
871	903	0.64				435.5	444	-1.16									
872	904	0.53				436	444.5	-1.09									
873	905	0.52				436.5	445	-1.16									

Table D.2 (continued)

874	906	0.61				437	445.5	-1.09									
875	907	0.56				437.5	446	-1.09									
876	908	0.74				438	446.5	-1.09									
877	909	0.66				438.5	447	-1.09									
878	910	0.82				439	447.5	-1.09									
879	911	0.72				439.5	448	-1.09									
880	912	0.66				440	448.5	-1.09									
881	913	1.08				440.5	449	-1.09									
882	914	1.11				441	449.5	-1.16									
883	915	1.34				441.5	450	-1.16									
884	916	2.27				442	450.5	-1.16									
885	917	4				442.5	451	-1.16									
886	918	3.77				443	451.5	-1.16									
887	919	4.28				443.5	452	-1.16									
888	920	4.94				444	452.5	-1.09									
889	921	5.52				444.5	453	-1.16									
890	922	6.76				445	453.5	-1.16									
891	923	7.56				445.5	454	-1.09									
892	924	6.06				446	454.5	-1.16									
893	925	5.2				446.5	455	-1.16									
894	926	4.34				447	455.5	-1.16									
895	927	4.19				447.5	456	-1.09									
896	928	5.02				448	456.5	-1.09									
897	929	6.05				448.5	457	-1.16									
898	930	1.28				449	457.5	-1.16									
899	931	0.59				449.5	458	-1.16									
900	932	2.98				450	458.5	-1.24									
901	933	0.72				450.5	459	-1.16									
902	934	0.3				451	459.5	-1.24									
903	935	0.21				451.5	460	-1.16									
904	936	0.95				452	460.5	-1.16									
905	937	0.45				452.5	461	-1.16									
906	938	0.72				453	461.5	-1.16									
907	939	0.62				453.5	462	-1.24									
908	940	0.69				454	462.5	-1.16									
909	941	0.99				454.5	463	-1.16									
910	942	0.53				455	463.5	-1.24									
911	943	0.34				455.5	464	-1.24									
912	944	2.18				456	464.5	-1.24									
913	945	2.31				456.5	465	-1.24									

Table D.2 (continued)

914	946	0.81				457	465.5	-1.16									
915	947	0.25				457.5	466	-1.24									
916	948	0.27				458	466.5	-0.94									
917	949	0.27				458.5	467	-0.86									
918	950	0.24				459	467.5	-0.94									
919	951	0.1				459.5	468	-0.94									
920	952	0.19				460	468.5	-0.94									
921	953	2.82				460.5	469	-0.94									
922	954	2.86				461	469.5	-0.94									
923	955	2.89				461.5	470	-0.94									
924	956	0.91				462	470.5	-0.86									
925	957	1.31				462.5	471	-0.86									
926	958	2.34				463	471.5	-0.86									
927	959	1.36				463.5	472	-0.86									
928	960	1.27				464	472.5	-0.86									
929	961	1.48				464.5	473	-0.86									
930	962	1.33				465	473.5	-0.86									
931	963	1.44				465.5	474	-0.86									
932	964	0.99				466	474.5	-0.94									
933	965	1.18				466.5	475	-0.94									
934	966	2.76				467	475.5	-0.79									
935	967	7.65				467.5	476	-0.79									
936	968	8.56				468	476.5	-0.86									
937	969	5.45				468.5	477	-0.86									
938	970	4.18				469	477.5	-0.86									
939	971	6.29				469.5	478	-0.94									
940	972	1.73				470	478.5	-0.94									
941	973	0.59				470.5	479	-0.86									
942	974	0.85				471	479.5	-0.94									
943	975	0.91				471.5	480	-1.01									
944	976	0.6				472	480.5	-1.09									
945	977	1.8				472.5	481	-1.09									
946	978	2.7				473	481.5	-0.94									
947	979	0.91				473.5	482	-1.01									
948	980	0.99				474	482.5	-0.94									
949	981	2.28				474.5	483	-1.01									
950	982	1.92				475	483.5	-0.94									
951	983	6.98				475.5	484	-0.86									
952	984	6.25				476	484.5	-0.71									
953	985	3.01				476.5	485	-0.79									

Table D.2 (continued)

954	986	1.93				477	485.5	-0.86									
955	987	1.55				477.5	486	-0.86									
956	988	1.73				478	486.5	-0.86									
957	989	2.79				478.5	487	-0.86									
958	990	0.76				479	487.5	-0.94									
959	991	0.78				479.5	488	-0.94									
960	992	1.32				480	488.5	-1.01									
961	993	0.79				480.5	489	-0.94									
962	994	2.67				481	489.5	-0.94									
963	995	2.09				481.5	490	-0.94									
964	996	7.62				482	490.5	-0.86									
965	997	9.49				482.5	491	-0.94									
966	998	9.36				483	491.5	-0.94									
967	999	9.39				483.5	492	-0.86									
968	1000	10.73				484	492.5	-0.94									
969	1001	10.72				484.5	493	-0.94									
970	1002	13.47				485	493.5	-0.94									
971	1003	15.32				485.5	494	-0.94									
972	1004	14.59				486	494.5	-0.86									
973	1005	14.37				486.5	495	-0.94									
974	1006	13.89				487	495.5	-1.01									
975	1007	13.74				487.5	496	-1.01									
976	1008	9.18				488	496.5	-1.01									
977	1009	9.19				488.5	497	-1.01									
978	1010	13.19				489	497.5	-1.01									
979	1011	16.31				489.5	498	-1.09									
980	1012	19.19				490	498.5	-1.01									
981	1013	11.16				490.5	499	-1.01									
982	1014	7.84				491	499.5	-1.01									
983	1015	9.52				491.5	500	-1.01									
984	1016	11.56				492	500.5	-1.09									
985	1017	14.71				492.5	501	-1.09									
986	1018	14.47				493	501.5	-0.94									
987	1019	14.57				493.5	502	-1.09									
988	1020	13.03				494	502.5	-1.01									
989	1021	13.34				494.5	503	-1.09									
990	1022	13.93				495	503.5	-1.09									
991	1023	12.87				495.5	504	-1.01									
992	1024	13.42				496	504.5	-1.01									
993	1025	13.5				496.5	505	-1.09									

Table D.2 (continued)

994	1026	9.96				497	505.5	-1.09									
995	1027	5.94				497.5	506	-1.09									
996	1028	7.3				498	506.5	-1.01									
997	1029	11.71				498.5	507	-1.01									
998	1030	15.91				499	507.5	-1.09									
999	1031	21.53				499.5	508	-1.01									
1000	1032	17.5				500	508.5	-1.01									
1001	1033	20.88				500.5	509	-0.94									
1002	1034	20.32				501	509.5	-1.09									
1003	1035	12.4				501.5	510	-1.09									
1004	1036	9.16				502	510.5	-1.09									
1005	1037	2.05				502.5	511	-1.01									
1006	1038	5.92				503	511.5	-1.01									
1007	1039	9.63				503.5	512	-1.09									
1008	1040	17.55				504	512.5	-1.09									
1009	1041	12.1				504.5	513	-1.09									
1010	1042	10.73				505	513.5	-1.09									
1011	1043	3.15				505.5	514	-1.16									
1012	1044	0.25				506	514.5	-1.16									
1013	1045	0.31				506.5	515	-1.16									
1014	1046	1.09				507	515.5	-1.09									
1015	1047	1.75				507.5	516	-1.09									
1016	1048	1.58				508	516.5	-1.09									
1017	1049	1.31				508.5	517	-1.09									
1018	1050	0.63				509	517.5	-1.09									
1019	1051	0.67				509.5	518	-1.16									
1020	1052	3.5				510	518.5	-1.09									
1021	1053	15.53				510.5	519	-1.16									
1022	1054	5.95				511	519.5	-1.09									
1023	1055	4.95				511.5	520	-1.09									
1024	1056	18.15				512	520.5	-1.16									
1025	1057	19.27				512.5	521	-1.09									
1026	1058	18.06				513	521.5	-1.09									
1027	1059	16.77				513.5	522	-1.09									
1028	1060	4.71				514	522.5	-1.16									
1029	1061	11.42				514.5	523	-1.09									
1030	1062	18.5				515	523.5	-1.16									
1031	1063	15.8				515.5	524	-1.09									
1032	1064	19.8				516	524.5	-1.09									
1033	1065	19.59				516.5	525	-1.16									

Table D.2 (continued)

1034	1066	12.39				517	525.5	-1.09											
1035	1067	12.47				517.5	526	-1.01											
1036	1068	18.53				518	526.5	-1.01											
1037	1069	20.17				518.5	527	-1.16											
1038	1070	21.92				519	527.5	-1.09											
1039	1071	16.65				519.5	528	-1.09											
1040	1072	18.86																	
1041	1073	22.14																	
1042	1074	17.82																	
1043	1075	18.24																	
1044	1076	9.7																	
1045	1077	10.08																	
1046	1078	13.58																	
1047	1079	15.35																	
1048	1080	13.01																	
1049	1081	10.93																	
1050	1082	13.69																	
1051	1083	26.14																	
1052	1084	14.3																	
1053	1085	20.52																	
1054	1086	17.74																	
1055	1087	18.89																	
1056	1088	9																	
1057	1089	6.19																	
1058	1090	15.11																	
1059	1091	17.61																	
1060	1092	18.02																	
1061	1093	18.14																	
1062	1094	15.81																	
1063	1095	18.22																	
1064	1096	15.72																	
1065	1097	16.09																	
1066	1098	12.26																	
1067	1099	10.66																	
1068	1100	17.75																	
1069	1101	17.02																	
1070	1102	14.73																	
1071	1103	14.22																	
1072	1104	16.16																	
1073	1105	15.63																	

Table D.2 (continued)

1074	1106	11.51														
1075	1107	13.31														
1076	1108	17.78														
1077	1109	3.97														
1078	1110	0.2														
1079	1111	0.05														
1080	1112	0.02														
1081	1113	-0.01														
1082	1114	-0.02														
1083	1115	-0.01														

Table D.3 Calcium carbonate (CaCO₃) radiocarbon data.

Sample ID	Avg Depth (cmbf)	Avg Depth (cmcd)	Type	Mass (mg)	Fraction modern	Fm Err ±	Uncorrected Age (¹⁴ C yr)	Age Err ±	d13C	Calibrated Median age (cal yr BP)	1 sigma ±	2 sigma ±	Rounded Calibrated age (cal yr BP)	1 sigma ±	2 sigma ±
KC27B 225-228	226.5	228.5	Mixed foram	2.6	0.4448	0.0011	6510	20	0.48	6345	127	276	6350	130	280
KC27B 255-258	256.5	258.5	Mixed foram	1.2	0.4579	0.0012	6270	20	0.43	6087	129	256.5	6090	130	260
MC45(6) 1-1.5	1.25	1.25	<i>N. pachyderma</i> (s)	1.4	0.8886	0.0022	950	20	0.75	>Modern					
MC45(6) 1-1.5	1.25	1.25	Mollusk	6.4	0.8581	0.0018	1230	15	-5.22	>Modern					

Table D.4 Ramped PyrOx radiocarbon data.

Lab ID number	Sample	Avg Depth (cmcd)	M (μmol manometric)	mgC	error μgC	μgC	Fm	error	Blank corrected Fm	error	Blank corrected age (^{14}C yr)	error	Calib. age (cal yr BP)	1 σ err	2 σ err	Round Calib. age (cal yr BP)	1 σ err	2 σ err
175009	DB 1274-1 (JPC27 92-94 cm)	135	18.208	218692.1	11.02	218.69	0.4922	0.0023	0.4893	0.0042	5742	69	5191	173	323	5190	170	320
175010	DB 1274-2		22.386	268873.1	13.55	268.87	0.4917	0.0020	0.4894	0.0035	5741	58	-	-	-	-	-	-
175068	DB-1274-5		28.043	336818.0	16.98	336.82	0.4680	0.0018	0.4658	0.0030	6137	51	-	-	-	-	-	-
175069	DB 1277-1 (JPC57 586-588)	882	19.436	233441.3	11.77	233.44	0.2640	0.0020	0.2572	0.0046	10908	145	11191	281	545	11200	280	540
175070	DB 1277-2		25.886	310910.8	15.67	310.91	0.2574	0.0016	0.2522	0.0036	11065	114	-	-	-	-	-	-
175071	DB 1277-5		12.501	150146.6	7.57	150.15	0.2348	0.0029	0.2234	0.0073	12040	264	-	-	-	-	-	-
175072	DB 1276-1 (JPC57 656-658)	982	19.984	240023.2	12.10	240.02	0.1953	0.0019	0.1875	0.0048	13446	206	14354	375	693	14350	380	690
175073	DB 1276-2		40.048	481007.3	24.24	481.01	0.1876	0.0017	0.1836	0.0028	13616	122	-	-	-	-	-	-
175074	DB 1276-5		10.289	123578.8	6.23	123.58	0.1622	0.0054	0.1458	0.0104	15466	573	-	-	-	-	-	-
175142	DB-1330-1 (KC27B 255-258)	258.5	18.075	217094.7	10.94	217.09	0.4238	0.0020	0.4195	0.0043	6978	82	6546	159	314	6550	160	310
175140	DB-1330-2		19.852	238437.8	12.02	238.44	0.4267	0.0020	0.4229	0.0040	6914	76	-	-	-	-	-	-
175141	DB-1330-6		16.354	196424.1	9.90	196.42	0.4029	0.0024	0.3977	0.0049	7406	100	-	-	-	-	-	-
176608	DB 1442 1 (JPC27 953-955)	986	17.69	212470.5	10.71	212.47	0.1682	0.0017	0.1588	0.0054	14780	274	16210	395	772	16200	390	770
176609	DB 1442 2		20.37	244659.4	12.33	244.66	0.1330	0.0018	0.1243	0.0050	16749	321	-	-	-	-	-	-
176610	DB 1442 5		19.26	231327.4	11.66	231.33	0.1281	0.0018	0.1188	0.0053	17114	357	-	-	-	-	-	-
176611	DB 1451-1 (JPC27 402-404)	435	18.913	227159.7	11.45	227.16	0.3231	0.0016	0.3171	0.0044	9225	111	8966	222	412	8970	220	410
176612	DB 1451-2		18.333	220193.4	11.10	220.19	0.3120	0.0017	0.3057	0.0046	9521	120	-	-	-	-	-	-
176613	DB 1451-5		10.995	132058.4	6.66	132.06	0.3020	0.0035	0.2912	0.0080	9911	219	-	-	-	-	-	-
176614	DB 1453-1 (JPC27 702-704)	735	18.621	223652.5	11.27	223.65	0.2943	0.0020	0.2877	0.0047	10008	132	9943	233	447	9950	230	450
176615	DB 1453-2		19.031	228576.9	11.52	228.58	0.2822	0.0016	0.2755	0.0045	10355	132	-	-	-	-	-	-
176616	DB 1453-5		32.777	393676.9	19.84	393.68	0.2782	0.0013	0.2743	0.0028	10391	82	-	-	-	-	-	-
156030	DB-1866-1 (JPC27 958-960)	991	7.89	94764.9	4.78	94.76	0.1744	0.0012	0.1536	0.0115	15047	603	16522	835.5	1569	16500	840	1570
156130	DB-1866-5		20.68	248382.7	12.52	248.38	0.1564	0.0011	0.1482	0.0046	15338	249	-	-	-	-	-	-

Table D.5 NBP1402 MC-45 ²¹⁰Pb data.

Depth Range	Avg depth (cmbsf)	Interval thick (cm)	Dry Bulk Density	Cum Mass	Pb210_Tot	Pb210_Tot_unc	Ra226_Tot	Ra226_Tot_unc	XsPb210	Excess Activity Uncertainty (dpm/g)	ln(Excess Activity) (dpm/g)	ln(Excess Activity) (dpm/g)
0-1	0.5	1	0.06	0.00	28.10	0.73	2.63	0.45	25.47	0.86	3.24	-0.16
1-1.5	1.25	1	0.20	0.20	24.70	0.65	2.66	0.43	22.04	0.78	3.09	-0.25
1.5-2	1.75	0.5	0.20	0.30	23.48	0.64	3.50	0.50	19.99	0.82	3.00	-0.20
2-2.5	2.25	0.5	0.26	0.43	19.42	0.57	3.15	0.46	16.28	0.74	2.79	-0.31
2.5-3	2.75	0.5	0.27	0.56	16.26	0.53	3.24	0.48	13.01	0.72	2.57	-0.33
3-3.5	3.25	0.5	0.30	0.71	18.46	0.56	3.21	0.48	15.26	0.74	2.72	-0.30
3.5-4	3.75	0.5	0.23	0.83	14.81	0.48	3.03	0.44	11.78	0.66	2.47	-0.42
4-4.5	4.25	0.5	0.28	0.97	11.98	0.45	3.08	0.46	8.90	0.65	2.19	-0.44
4.5-5	4.75	0.5	0.30	1.12	8.41	0.38	3.11	0.47	5.30	0.60	1.67	-0.50
5-5.5	5.25	0.5	0.21	1.22	9.22	0.40	2.89	0.45	6.33	0.60	1.85	-0.51
5.5-6	5.75	0.5	0.29	1.37	7.32	0.35	3.17	0.47	4.15	0.59	1.42	-0.53
6-6.5	6.25	0.5	0.25	1.49	8.24	0.37	3.29	0.48	4.95	0.61	1.60	-0.50
6.5-7	6.75	0.5	0.33	1.66	7.79	0.37	3.13	0.48	4.66	0.60	1.54	-0.51
7-7.5	7.25	0.5	0.33	1.82	7.39	0.36	3.23	0.48	4.16	0.60	1.43	-0.51
7.5-8	7.75	0.5	0.28	1.97	5.85	0.31	3.24	0.48	2.62	0.57	0.96	-0.56
8-8.5	8.25	0.5	0.30	2.11	4.82	0.29	3.14	0.47	1.69	0.55	0.52	-0.59
8.5-9	8.75	0.5	0.38	2.30	4.59	0.28	2.94	0.46	1.65	0.54	0.50	-0.61
9-9.5	9.25	0.5	0.32	2.46	4.60	0.28	3.08	0.47	1.52	0.54	0.42	-0.61
9.5-10	9.75	0.5	0.33	2.63	4.41	0.28	3.14	0.48	1.27	0.55	0.24	-0.60
10-10.5	10.25	0.5	0.26	2.76	3.53	0.24	3.14	0.47	0.39	0.53	-0.95	-0.64
11-11.5	11.25	1	0.27	3.03	3.47	0.25	3.20	0.48	0.27	0.54	-1.32	-0.61
12-12.5	12.25	1	0.35	3.38	2.26	0.20	3.03	0.46	-0.77	0.50	-	-0.70
13-13.5	13.25	1	0.25	3.63	2.66	0.21	3.34	0.47	-0.68	0.52	-	-0.66
14-14.5	14.25	1	0.34	3.98	2.54	0.20	3.20	0.46	-0.65	0.51	-	-0.68
16-16.5	16.25	2	0.42	4.81	2.20	0.19	3.27	0.48	-1.07	0.52	-	-0.66
18-18.5	18.25	2	0.35	5.51	1.87	0.18	2.78	0.44	-0.91	0.48	-	-0.74
20-22	21	2	0.39	6.30	2.50	0.21	2.92	0.46	-0.42	0.50	-	-0.69

Table D.6 NBP1402 MC-61 ²¹⁰Pb data.

Depth Range	Avg depth (cmbsf)	Interval thick (cm)	Dry Bulk Density	Cum Mass	Pb210_Tot	Pb210_Tot_unc	Ra226_Tot	Ra226_Tot_unc	XsPb210	Excess Activity Uncertainty (dpm/g)	ln(Excess Activity) (dpm/g)	ln(Excess Activity) (dpm/g)
0-0.5	0.25	0.5	0.13	0.00	34.71	0.94	2.779	0.155	31.93	0.96	3.46	-0.05
0.5-1	0.75	0.5	0.15	0.07	23.40	0.64	2.932	0.147	20.47	0.65	3.02	-0.43
1-1.5	1.25	0.5	0.15	0.15	19.79	0.58	2.910	0.147	16.88	0.60	2.83	-0.51
1.5-2	1.75	0.5	0.19	0.24	17.42	0.55	3.078	0.150	14.34	0.57	2.66	-0.57
2-2.5	2.25	0.5	0.22	0.35	15.43	0.50	3.717	0.164	11.71	0.53	2.46	-0.63
2.5-3	2.75	0.5	0.32	0.51	10.66	0.42	3.268	0.153	7.39	0.45	2.00	-0.80
3-3.5	3.25	0.5	0.31	0.66	9.96	0.40	3.282	0.152	6.68	0.43	1.90	-0.85
3.5-4	3.75	0.5	0.33	0.83	8.08	0.36	3.384	0.156	4.69	0.40	1.55	-0.92
4-4.5	4.25	0.5	0.33	1.00	7.26	0.35	3.202	0.151	4.06	0.38	1.40	-0.97
4.5-5	4.75	0.5	0.28	1.13	6.11	0.32	3.368	0.156	2.74	0.36	1.01	-1.03
5-5.5	5.25	0.5	0.30	1.28	4.45	0.27	3.320	0.154	1.13	0.31	0.13	-1.16
5.5-6	5.75	0.5	0.29	1.43	4.07	0.27	3.471	0.160	0.60	0.31	-0.51	-1.17
6-6.5	6.25	0.5	0.30	1.57	3.24	0.23	3.729	0.164	-0.49	0.28	-	-1.26
6.5-7	6.75	0.5	0.34	1.75	2.61	0.21	3.470	0.160	-0.86	0.27	-	-1.32
7-7.5	7.25	0.5	0.27	1.88	2.79	0.21	3.271	0.150	-0.48	0.26	-	-1.36
7.5-8	7.75	0.5	0.30	2.03	2.39	0.20	3.407	0.158	-1.01	0.26	-	-1.36
8-8.5	8.25	0.5	0.28	2.17	1.68	0.17	3.294	0.156	-1.61	0.23	-	-1.46
8.5-9	8.75	0.5	0.33	2.34	2.88	0.22	3.420	0.159	-0.54	0.27	-	-1.29
9-9.5	9.25	0.5	0.27	2.47	3.39	0.24	3.099	0.152	0.29	0.29	-	-1.25
9.5-10	9.75	0.5	0.37	2.66	1.85	0.18	3.241	0.153	-1.39	0.23	-	-1.45
10-10.5	10.25	0.5	0.30	2.81	2.29	0.20	3.553	0.160	-1.27	0.25	-	-1.37
11-11.5	11.25	1	0.35	3.15	2.26	0.20	3.354	0.158	-1.09	0.25	-	-1.38
12-12.5	12.25	1	0.25	3.40	2.66	0.21	3.241	0.154	-0.58	0.26	-	-1.33
13-13.5	13.25	1	0.35	3.75	2.34	0.20	3.247	0.153	-0.91	0.25	-	-1.38
14-14.5	14.25	1	0.40	4.15	2.15	0.19	3.107	0.151	-0.96	0.24	-	-1.41
16-16.5	16.25	2	0.29	4.72	1.66	0.17	3.360	0.158	-1.70	0.23	-	-1.47
18-18.5	18.25	2	0.32	5.37	2.42	0.20	3.292	0.155	-0.87	0.25	-	-1.37

Table D.7 NBP1402 MC-45 ^{210}Pb age model results.

Depth in core (cmbfsf)	Years before 2014	agemid	agehigh	agelow	pos error	neg error
0.5	6	2008	2008	2008	0	0
1.25	15	1999	2000	1998	1	1
1.75	21	1993	1994	1992	1	1
2.25	27	1987	1989	1985	2	2
2.75	33	1981	1983	1979	2	2
3.25	39	1975	1977	1972	2	3
3.75	45	1969	1972	1966	3	3
4.25	51	1963	1966	1960	3	3
4.75	57	1957	1960	1953	3	4
5.25	63	1951	1955	1947	4	4
5.75	69	1945	1949	1940	4	5
6.25	75	1939	1944	1934	5	5
6.75	81	1933	1938	1927	5	6
7.25	87	1927	1932	1921	5	6
7.75	93	1921	1927	1915	6	6
8.25	99	1915	1921	1908	6	7
8.75	105	1909	1915	1902	6	7
9.25	111	1903	1910	1895	7	8
9.75	117	1897	1904	1889	7	8
10.25	123	1891	1899	1883	8	8
11.25	135	1879	1887	1870	8	9
12.25	147	1867	1876	1857	9	10
13.25	159	1855	1865	1844	10	11
14.25	171	1843	1853	1831	10	12
16.25	195	1819	1831	1806	12	13
18.25	219	1795	1808	1780	13	15
21	252	1762	1777	1745	15	17

Table D.8 NBP1402 MC-61 ²¹⁰Pb age model results

Depth in core (cmbsf)	Years before 2014	agemid	agehigh	agelow	pos error	neg error
0.25	8	2006	2007	2005	1	1
0.75	23	1991	1994	1987	3	4
1.25	39	1975	1980	1970	5	5
1.75	54	1960	1966	1952	6	8
2.25	70	1944	1953	1934	9	10
2.75	85	1929	1939	1916	10	13
3.25	101	1913	1926	1899	13	14
3.75	116	1898	1912	1881	14	17
4.25	132	1882	1898	1863	16	19
4.75	147	1867	1885	1845	18	22
5.25	163	1851	1871	1828	20	23
5.75	178	1836	1858	1810	22	26
6.25	194	1820	1844	1792	24	28
6.75	209	1805	1830	1774	25	31
7.25	225	1789	1817	1757	28	32
7.75	240	1774	1803	1739	29	35
8.25	255	1759	1790	1721	31	38
8.75	271	1743	1776	1703	33	40
9.25	286	1728	1762	1686	34	42
9.75	302	1712	1749	1668	37	44
10.25	317	1697	1735	1650	38	47
11.25	348	1666	1708	1615	42	51
12.25	379	1635	1681	1579	46	56
13.25	410	1604	1654	1544	50	60
14.25	441	1573	1626	1508	53	65
16.25	503	1511	1572	1437	61	74
18.25	565	1449	1518	1366	69	83

Table D.9 Foraminifer assemblages (raw test counts)

Counts (raw)										
Cruise	Core	Avg depth (cmbsf)	Composite Depth (cmcd)	<i>N. pachyderma</i> (s)	<i>Trifarina angulosa</i>	<i>Bulimina aculeata</i>	<i>Globocassidulina</i>	<i>Cibicoides</i> spp.	other	Total Count
NBP 14-02	MC45(6)	0	0	13	6	12	0	0	0	31
NBP 14-02	MC45(6)	0.5	0.5	95	2	5	11	0	0	113
NBP 14-02	MC45(6)	1.25	1.25	64	33	8	6	0	0	111
NBP 14-02	MC45(6)	1.75	1.75	14	8	9	0	0	0	31
NBP 14-02	MC45(6)	2.25	2.25	17	7	7	0	0	0	31
NBP 14-02	MC45(6)	2.75	2.75	18	7	8	0	0	0	33
NBP 14-02	MC45(6)	3.25	3.25	17	5	7	0	0	0	29
NBP 14-02	MC45(6)	3.75	3.75	13	2	5	1	0	0	21
NBP 14-02	MC45(6)	4.25	4.25	10	3	3	0	0	0	16
NBP 14-02	MC45(6)	5.25	5.25	3	2	2	0	0	0	7
NBP 14-02	MC45(6)	5.75	5.75	3	1	2	0	0	13	19
NBP 14-02	MC45(6)	6.75	6.75	2	0	0	0	0	1	3
NBP 14-02	MC45(6)	7.25	7.25	2	0	0	0	0	0	2
NBP 14-02	MC45(6)	7.75	7.75	3	0	0	1	0	0	4
NBP 14-02	MC45(6)	8.25	8.25	4	0	0	0	0	0	4
NBP 14-02	MC45(6)	8.75	8.75	0	0	0	0	0	0	0
NBP 14-02	MC45(6)	9.75	9.75	3	0	1	0	0	0	4
NBP 14-02	MC45(6)	10.5	10.5	1	0	0	0	0	0	1
NBP 14-02	MC45(6)	11.5	11.5	0	0	0	0	0	0	0
NBP 14-02	MC45(6)	12.5	12.5	0	0	0	0	0	0	0
NBP 14-02	MC45(6)	14.5	14.5	0	0	0	0	0	0	0
NBP 14-02	MC45(6)	16.5	16.5	0	0	0	0	0	0	0
NBP 14-02	MC45(6)	18.5	18.5	0	0	0	0	0	0	0
NBP 14-02	MC45(6)	20.5	20.5	0	0	0	0	0	0	0
NBP 14-02	MC45(6)	22.5	22.5	0	0	0	0	0	0	0
NBP 14-02	MC45(6)	24.5	24.5	0	0	0	0	0	0	0
NBP 14-02	MC45(6)	26.5	26.5	0	0	0	0	0	0	0
NBP 14-02	MC45(6)	28.5	28.5	0	0	0	0	0	0	0
NBP 14-02	MC45(6)	30.5	30.5	0	0	0	0	0	0	0
NBP 14-02	MC61(4)	0.75	0.75	65	2	7	5	0	0	79
NBP 14-02	MC61(4)	1.25	1.25	57	2	9	2	0	0	70
NBP 14-02	MC61(4)	1.75	1.75	75	2	4	5	0	0	86

Table D.9 (continued)

NBP 14-02	MC61(4)	2.25	2.25	47	1	6	1	0	0	55
NBP 14-02	MC61(4)	2.75	2.75	28	1	4	1	0	0	34
NBP 14-02	MC61(4)	3.25	3.25	44	2	9	0	0	0	55
NBP 14-02	MC61(4)	3.75	3.75	44	0	3	0	0	0	47
NBP 14-02	MC61(4)	4.25	4.25	7	0	1	0	0	0	8
NBP 14-02	MC61(4)	4.75	4.75	1	0	0	0	0	0	1
NBP 14-02	MC61(4)	5.25	5.25	4	0	0	0	0	0	4
NBP 14-02	MC61(4)	5.75	5.75	0	0	0	0	0	0	0
NBP 14-02	MC61(4)	6.25	6.25	1	0	0	0	0	0	1
NBP 14-02	MC61(4)	6.75	6.75	0	0	0	0	0	0	0
NBP 14-02	MC61(4)	7.25	7.25	0	0	0	0	0	2	2
NBP 14-02	MC61(4)	7.75	7.75	0	0	0	0	0	0	0
NBP 14-02	MC61(4)	8.25	8.25	0	0	0	0	0	0	0
NBP 14-02	MC61(4)	8.75	8.75	0	0	0	0	0	0	0
NBP 14-02	MC61(4)	9.25	9.25	0	0	0	0	0	0	0
NBP 14-02	MC61(4)	9.75	9.75	0	0	0	0	0	0	0
NBP 14-02	MC61(4)	10.5	10.5	0	0	0	0	0	0	0
NBP 14-02	MC61(4)	12.5	12.5	0	0	0	0	0	0	0
NBP 14-02	MC61(4)	16.5	16.5	0	0	0	0	0	0	0
NBP 14-02	MC61(4)	20.5	20.5	0	0	0	0	0	0	0
NBP 14-02	MC61(4)	24.5	24.5	0	0	0	0	0	0	0
NBP 14-02	MC61(4)	28.5	28.5	0	0	0	0	0	0	0
NBP 14-02	MC61(4)	31.5	31.5	0	0	0	0	0	0	0
NBP 14-02	KC27B	1.5	3.5	166	9	14	8	0	7	204
NBP 14-02	KC27B	4.5	6.5	38	3	4	6	0	3	54
NBP 14-02	KC27B	7.5	9.5	10	2	0	0	0	0	12
NBP 14-02	KC27B	31.5	33.5	1	0	0	0	0	0	1
NBP 14-02	KC27B	36.5	38.5	4	5	0	2	0	0	11
NBP 14-02	KC27B	51.5	53.5	0	1	0	0	0	0	1
NBP 14-02	KC27B	61.5	63.5	0	1	0	0	0	0	1
NBP 14-02	KC27B	76.5	78.5	1	1	0	0	0	0	2
NBP 14-02	KC27B	91.5	93.5	0	4	0	0	0	0	4
NBP 14-02	KC27B	101.5	103.5	0	2	0	0	0	0	2
NBP 14-02	KC27B	106.5	108.5	9	3	0	0	0	0	12
NBP 14-02	KC27B	111.5	113.5	0	3	0	0	0	0	3
NBP 14-02	KC27B	116.5	118.5	0	6	0	0	0	0	6
NBP 14-02	KC27B	126.5	128.5	0	6	0	0	0	0	6

Table D.9 (continued)

NBP 14-02	KC27B	141.5	143.5	0	5	1	0	0	0	6
NBP 14-02	KC27B	146.5	148.5	1	6	0	0	0	0	7
NBP 14-02	KC27B	151.5	153.5	0	4	0	0	0	0	4
NBP 14-02	KC27B	161.5	163.5	0	21	0	0	0	2	23
NBP 14-02	KC27B	166.5	168.5	0	4	0	0	0	0	4
NBP 14-02	KC27B	171.5	173.5	0	8	0	0	0	2	10
NBP 14-02	KC27B	176.5	178.5	18	11	0	0	0	0	29
NBP 14-02	KC27B	181.5	183.5	1	7	0	0	0	1	9
NBP 14-02	KC27B	186.5	188.5	52	30	0	0	0	0	82
NBP 14-02	KC27B	191.5	193.5	6	33	0	0	0	3	42
NBP 14-02	KC27B	196.5	198.5	36	44	0	0	0	0	80
NBP 14-02	KC27B	201.5	203.5	33	34	0	0	1	1	69
NBP 14-02	KC27B	206.5	208.5	19	14	0	0	0	1	34
NBP 14-02	KC27B	211.5	213.5	46	15	0	0	0	4	65
NBP 14-02	KC27B	216.5	218.5	39	12	5	0	1	2	59
NBP 14-02	KC27B	221.5	223.5	265	22	0	0	1	0	288
NBP 14-02	KC27B	226.5	228.5	396	7	1	42	1	1	448
NBP 14-02	KC27B	231.5	233.5	293	17	0	7	0	24	341
NBP 14-02	KC27B	236.5	238.5	213	21	0	0	2	6	242
NBP 14-02	KC27B	241.5	243.5	15	33	0	0	0	10	58
NBP 14-02	KC27B	246.5	248.5	7	3	0	1	0	10	21
NBP 14-02	KC27B	251.5	253.5	96	17	0	24	0	3	140
NBP 14-02	KC27B	256.5	258.5	346	18	0	99	0	16	479
NBP 14-02	KC27B	261.5	263.5	159	19	0	8	0	5	191
NBP 14-02	KC27B	266.5	268.5	143	8	0	11	2	35	199
NBP 14-02	KC27B	269.5	271.5	9	6	0	0	0	0	15
NBP 14-02	JKC 53	4.5	15.8	20	2	1	0	0	0	23
NBP 14-02	JKC 53	141.5	150	11	40	1	0	0	28	80
NBP 14-02	JKC53	221.5	230	6	1	0	2	0	0	9
NBP 14-02	JKC53	226.5	235	25	7	0	0	0	0	32
NBP 14-02	JKC53	261.5	270	25	9	0	0	0	0	34
NBP 14-02	JKC53	266.5	275	34	10	0	1	0	2	47
NBP 14-02	JKC53	271.5	280	65	10	0	1	0	4	80
NBP 14-02	JKC53	276.5	285	16	7	0	3	0	0	26
NBP 14-02	JKC53	281.5	290	25	8	0	0	0	0	33
NBP 14-02	JKC53	286.5	295	9	2	0	0	0	0	11
NBP 14-02	JKC53	291.5	300	28	4	0	0	0	0	32

Table D.9 (continued)

NBP 14-02	JKC53	296.5	305	3	0	0	0	0	0	3
NBP 14-02	JKC53	301.5	310	1	9	0	0	0	0	10
NBP 14-02	JKC53	306.5	315	5	9	0	0	0	0	14
NBP 14-02	JKC53	311.5	320	5	2	0	0	0	0	7
NBP 14-02	JKC 53	321.5	330	0	0	0	0	0	0	0
NBP 14-02	JKC53	331.5	340	22	4	0	0	0	0	26
NBP 14-02	JKC53	341.5	350	0	9	0	0	0	0	9
NBP 14-02	JKC53	346.5	355	1	2	0	0	0	0	3
NBP 14-02	JKC 53	351.5	360	0	0	0	0	0	0	0
NBP 14-02	JKC53	356.5	365	0	4	0	0	0	0	4
NBP 14-02	JKC53	366.5	375	0	3	0	0	0	0	3
NBP 14-02	JKC53	376.5	385	0	12	0	0	0	0	12
NBP 14-02	JKC53	381.5	390	0	2	0	0	0	0	2
NBP 14-02	JKC 53	391.5	400	0	3	0	0	0	0	3
NBP 14-02	JKC 53	396.5	405	0	0	0	0	0	0	0
NBP 14-02	JKC53	401.5	410	0	4	0	0	0	0	4
NBP 14-02	JKC 53	416.5	425	0	0	0	0	0	0	0
NBP 14-02	JKC 53	436.5	445	0	24	0	0	0	5	29
NBP 14-02	JKC53	446.5	455	0	2	0	0	0	0	2
NBP 14-02	JKC53	451.5	460	0	2	0	0	0	0	2
NBP 14-02	JKC53	456.5	465	0	7	0	0	0	0	7
NBP 14-02	JKC53	461.5	470	0	28	0	0	0	0	28
NBP 14-02	JKC53	466.5	475	0	29	0	0	0	0	29
NBP 14-02	JKC 53	471.5	480	0	0	0	0	0	0	0
NBP 14-02	JKC53	481.5	490	0	5	0	0	0	0	5
NBP 14-02	JKC 53	486.5	495	0	2	0	0	0	0	2
NBP 14-02	JKC53	491.5	500	0	5	0	0	0	0	5
NBP 14-02	JKC53	496.5	505	0	10	0	0	0	0	10
NBP 14-02	JKC53	511.5	520	0	4	0	0	0	0	4
NBP 14-02	KC 57	1.5	6.35	19	2	3	0	0	0	24
NBP 14-02	KC 57	4.5	7.47	0	0	0	0	0	1	1
NBP 14-02	KC 57	7.5	8.59	0	0	0	0	0	0	0
NBP 14-02	KC 57	10.5	9.71	0	0	0	0	0	1	1
NBP 14-02	KC 57	13.5	10.83	0	0	0	0	0	0	0
NBP 14-02	KC 57	16.5	11.95	0	0	0	0	0	0	0
NBP 14-02	KC 57	21.5	16.44	0	0	0	0	0	0	0
NBP 14-02	KC 57	26.5	23.62	0	0	0	0	0	0	0

Table D.9 (continued)

NBP 14-02	KC 57	31.5	31.42	0	0	0	0	0	0	0
NBP 14-02	KC 57	36.5	36.8	0	0	0	0	0	0	0
NBP 14-02	KC 57	41.5	44.15	0	0	0	0	0	0	0
NBP 14-02	KC 57	46.5	50.12	0	0	0	0	0	0	0
NBP 14-02	KC 57	51.5	56.1	0	0	0	0	0	0	0
NBP 14-02	KC 57	56.5	61.37	0	0	0	0	0	0	0
NBP 14-02	KC 57	61.5	66.34	0	0	0	0	0	0	0
NBP 14-02	KC 57	66.5	70.17	0	0	0	0	0	0	0
NBP 14-02	KC 57	71.5	72.5	0	13	0	0	0	0	13
NBP 14-02	KC 57	76.5	74.8	0	12	0	0	0	3	15
NBP 14-02	KC 57	81.5	77.6	0	13	0	0	0	1	14
NBP 14-02	KC 57	86.5	80.8	0	5	0	0	0	2	7
NBP 14-02	KC 57	91.5	83.95	2	13	0	0	0	2	17
NBP 14-02	KC 57	96.5	87.11	10	36	0	0	0	6	52
NBP 14-02	KC 57	101.5	90.27	0	2	0	0	0	5	7
NBP 14-02	KC 57	106.5	95.1	11	7	0	0	0	10	28
NBP 14-02	KC 57	111.5	104.2	46	16	1	0	0	87	150
NBP 14-02	KC 57	116.5	119.4	14	4	0	0	0	4	22
NBP 14-02	KC 57	121.5	123.3	0	14	0	0	0	1	15
NBP 14-02	KC 57	126.5	127.1	1	30	0	0	0	5	36
NBP 14-02	KC 57	131.5	131.8	120	15	0	0	0	45	180
NBP 14-02	KC 57	136.5	134.7	11	4	0	0	0	3	18
NBP 14-02	KC 57	141.5	137.3	130	16	0	2	0	11	159
NBP 14-02	KC 57	146.5	139.8	4	0	0	0	0	1	5
NBP 14-02	KC 57	151.5	142.4	8	4	3	0	0	2	17
NBP 14-02	KC 57	156.5	145.8	122	9	0	0	0	16	147
NBP 14-02	KC 57	156.5	145.8	51	26	1	4	0	0	82
NBP 14-02	KC 57	161.5	153.6	1	0	0	0	0	3	4
NBP 14-02	KC 57	171.5	169.2	9	39	0	1	43	0	92
NBP 14-02	KC 57	176.5	176	1	11	0	0	0	12	24
NBP 14-02	KC 57	181.5	184.7	0	1	0	0	0	1	2
NBP 14-02	KC 57	186.5	192.5	0	0	0	0	0	0	0
NBP 14-02	KC 57	191.5	200.2	0	13	0	0	0	15	28
NBP 14-02	KC 57	196.5	208.01	2	1	0	0	0	7	10
NBP 14-02	KC 57	201.5	215.8	0	0	0	0	0	1	1
NBP 14-02	KC 57	206.5	223.5	11	25	0	0	0	4	40
NBP 14-02	KC 57	211.5	231.3	3	7	0	0	0	4	14

Table D.9 (continued)

NBP 14-02	KC 57	216.5	239.1	0	8	0	0	0	9	17
NBP 14-02	KC 57	221.5	246.84	0	0	0	0	0	0	0
NBP 14-02	KC 57	226.5	254.6	0	0	0	0	0	0	0
NBP 14-02	KC 57	231.5	262.4	3	1	0	0	0	5	9
NBP 14-02	KC 57	236.5	270.2	0	0	0	0	0	0	0
NBP 14-02	KC 57	241.5	277.9	0	5	0	0	0	29	34
NBP 14-02	KC 57	246.5	285.7	0	0	0	0	0	0	0
NBP 14-02	KC 57	251.5	292.7	0	0	0	0	0	0	0
NBP 14-02	KC 57	326.5	339.5	0	0	0	0	0	0	0
NBP 14-02	KC 57	386.5	399.5	0	19	0	0	0	1	20
NBP 14-02	JPC 27	1	56.8	0	0	0	0	0	0	0
NBP 14-02	JPC 27	4	59.4	0	0	0	0	0	0	0
NBP 14-02	JPC 27	8	60.9	0	0	0	0	0	0	0
NBP 14-02	JPC 27	13	71.9	0	0	0	0	0	0	0
NBP 14-02	JPC 27	18	76.8	0	0	0	0	0	0	0
NBP 14-02	JPC 27	23	81.9	0	0	0	0	0	0	0
NBP 14-02	JPC 27	29	87.5	0	0	0	0	0	0	0
NBP 14-02	JPC 27	34	91.3	0	0	0	0	0	0	0
NBP 14-02	JPC 27	39	94.7	0	0	0	0	0	0	0
NBP 14-02	JPC 27	44	100.5	0	0	0	0	0	0	0
NBP 14-02	JPC 27	49	104.1	5	1	0	0	0	1	7
NBP 14-02	JPC 27	51.5	106	20	6	0	0	0	1	27
NBP 14-02	JPC 27	54	107.8	0	0	0	0	0	0	0
NBP 14-02	JPC 27	59	111.5	0	0	0	0	0	0	0
NBP 14-02	JPC 27	64	114.2	0	0	0	0	0	0	0
NBP 14-02	JPC 27	69	115.8	0	0	0	0	0	0	0
NBP 14-02	JPC 27	74	119.5	0	1	0	0	0	0	1
NBP 14-02	JPC 27	79	127.9	0	0	0	0	0	0	0
NBP 14-02	JPC 27	84	131.3	0	0	0	0	0	0	0
NBP 14-02	JPC 27	86	132.5	0	0	0	0	0	0	0
NBP 14-02	JPC 27	91	134.4	0	0	0	0	0	0	0
NBP 14-02	JPC 27	96	136.1	0	0	0	0	0	0	0
NBP 14-02	JPC 27	101	137.8	0	0	0	0	0	0	0
NBP 14-02	JPC 27	106	139.5	0	0	0	0	0	0	0
NBP 14-02	JPC 27	131	163	3	0	0	0	0	0	3
NBP 14-02	JPC 27	151	183	9	14	0	0	0	9	32
NBP 14-02	JPC 27	176	208	67	8	0	0	0	16	91

Table D.9 (continued)

NBP 14-02	JPC 27	201	233	87	0	0	0	0	11	98
NBP 14-02	JPC 27	211	243	5	6	0	0	0	3	14
NBP 14-02	JPC 27	231	263	42	10	0	0	0	3	55
NBP 14-02	JPC 27	251	283	0	0	0	0	0	0	0
NBP 14-02	JPC 27	291	323	71	8	0	1	0	0	80
NBP 14-02	JPC 27	306	338	13	1	0	0	0	2	16
NBP 14-02	JPC 27	406	438	0	15	0	0	0	0	15
NBP 14-02	JPC 27	431	463	0	0	2	0	0	1	3
NBP 14-02	JPC 27	826	858	0	1	0	0	0	0	1
NBP 14-02	JPC 27	831	863	0	1	0	0	0	0	1
NBP 14-02	JPC 27	866	898	1	0	0	0	0	0	1
NBP 14-02	JPC 27	891	923	6	12	0	0	0	3	21
NBP 14-02	JPC 27	896	928	1	7	0	0	0	1	9
NBP 14-02	JPC 27	926	958	18	0	0	0	0	0	18
NBP 14-02	JPC 27	951	983	11	2	0	0	0	11	24
NBP 14-02	JPC 27	961	993	45	0	0	0	0	0	45

Table D.10 Foraminifer assemblages (percent abundance; # tests/cubic cm of sediment).

Total Abundance (#/cc)							
Core	Depth (cmbfsf)	Composite Depth (cmcd)	<i>N. pachyderma</i> (s)	<i>Trifarina angulosa</i>	<i>Bulimina aculeata</i>	<i>Globocassidulina</i>	Other
MC45(6)	0	0	0.65	0.3	0.6	0	0
MC45(6)	0.5	0.5	4.75	0.1	0.25	0.55	0
MC45(6)	1.25	1.25	3.2	1.65	0.4	0.3	0
MC45(6)	1.75	1.75	0.7	0.4	0.45	0	0
MC45(6)	2.25	2.25	0.85	0.35	0.35	0	0
MC45(6)	2.75	2.75	0.9	0.35	0.4	0	0
MC45(6)	3.25	3.25	0.85	0.25	0.35	0	0
MC45(6)	3.75	3.75	0.65	0.1	0.25	0.05	0
MC45(6)	4.25	4.25	0.5	0.15	0.15	0	0
MC45(6)	5.25	5.25	0.15	0.1	0.1	0	0
MC45(6)	5.75	5.75	0.15	0.05	0.1	0	0.65
MC45(6)	6.75	6.75	0.1	0	0	0	0.05
MC45(6)	7.25	7.25	0.1	0	0	0	0
MC45(6)	7.75	7.75	0.15	0	0	0.05	0
MC45(6)	8.25	8.25	0.2	0	0	0	0
MC45(6)	8.75	8.75	0	0	0	0	0
MC45(6)	9.75	9.75	0.15	0	0.05	0	0
MC45(6)	10.5	10.5	0.05	0	0	0	0
MC45(6)	11.5	11.5	0	0	0	0	0
MC45(6)	12.5	12.5	0	0	0	0	0
MC45(6)	14.5	14.5	0	0	0	0	0
MC45(6)	16.5	16.5	0	0	0	0	0
MC45(6)	18.5	18.5	0	0	0	0	0
MC45(6)	20.5	20.5	0	0	0	0	0
MC45(6)	22.5	22.5	0	0	0	0	0
MC45(6)	24.5	24.5	0	0	0	0	0
MC45(6)	26.5	26.5	0	0	0	0	0
MC45(6)	28.5	28.5	0	0	0	0	0
MC45(6)	30.5	30.5	0	0	0	0	0
MC61(4)	0.75	0.75	3.25	0.1	0.35	0.25	0
MC61(4)	1.25	1.25	2.85	0.1	0.45	0.1	0
MC61(4)	1.75	1.75	3.75	0.1	0.2	0.25	0
MC61(4)	2.25	2.25	2.35	0.05	0.3	0.05	0

Table D.10 (continued)

MC61(4)	2.75	2.75	1.4	0.05	0.2	0.05	0
MC61(4)	3.25	3.25	2.2	0.1	0.45	0	0
MC61(4)	3.75	3.75	2.2	0	0.15	0	0
MC61(4)	4.25	4.25	0.35	0	0.05	0	0
MC61(4)	4.75	4.75	0.05	0	0	0	0
MC61(4)	5.25	5.25	0.2	0	0	0	0
MC61(4)	5.75	5.75	0	0	0	0	0
MC61(4)	6.25	6.25	0.05	0	0	0	0
MC61(4)	6.75	6.75	0	0	0	0	0
MC61(4)	7.25	7.25	0	0	0	0	0.1
MC61(4)	7.75	7.75	0	0	0	0	0
MC61(4)	8.25	8.25	0	0	0	0	0
MC61(4)	8.75	8.75	0	0	0	0	0
MC61(4)	9.25	9.25	0	0	0	0	0
MC61(4)	9.75	9.75	0	0	0	0	0
MC61(4)	10.5	10.5	0	0	0	0	0
MC61(4)	12.5	12.5	0	0	0	0	0
MC61(4)	16.5	16.5	0	0	0	0	0
MC61(4)	20.5	20.5	0	0	0	0	0
MC61(4)	24.5	24.5	0	0	0	0	0
MC61(4)	28.5	28.5	0	0	0	0	0
MC61(4)	31.5	31.5	0	0	0	0	0
KC27B	1.5	3.5	8.3	0.45	0.7	0.4	0.35
KC27B	4.5	6.5	1.9	0.15	0.2	0.3	0.15
KC27B	7.5	9.5	0.5	0.1	0	0	0
KC27B	31.5	33.5	0.05	0	0	0	0
KC27B	36.5	38.5	0.2	0.25	0	0.1	0
KC27B	51.5	53.5	0	0.05	0	0	0
KC27B	61.6	63.6	0	0.05	0	0	0
KC27B	76.5	78.5	0.05	0.05	0	0	0
KC27B	91.5	93.5	0	0.2	0	0	0
KC27B	101.5	103.5	0	0.1	0	0	0
KC27B	106.5	108.5	0.45	0.15	0	0	0
KC27B	111.5	113.5	0	0.15	0	0	0
KC27B	116.5	118.5	0	0.3	0	0	0
KC27B	126.5	128.5	0	0.3	0	0	0
KC27B	141.5	143.5	0	0.25	0.05	0	0

Table D.10 (continued)

KC27B	146.5	148.5	0.05	0.3	0	0	0
KC27B	151.5	153.5	0	0.2	0	0	0
KC27B	161.5	163.5	0	1.05	0	0	0.1
KC27B	166.5	168.5	0	0.2	0	0	0
KC27B	171.5	173.5	0	0.4	0	0	0.1
KC27B	176.5	178.5	0.9	0.55	0	0	0
KC27B	181.5	183.5	0.05	0.35	0	0	0.05
KC27B	186.5	188.5	2.6	1.5	0	0	0
KC27B	191.5	193.5	0.3	1.65	0	0	0.15
KC27B	196.5	198.5	1.8	2.2	0	0	0
KC27B	201.5	203.5	1.65	1.7	0	0	0.05
KC27B	206.5	208.5	0.95	0.7	0	0	0.05
KC27B	211.5	213.5	2.3	0.75	0	0	0.2
KC27B	216.5	218.5	1.95	0.6	0.25	0	0.1
KC27B	221.5	223.5	13.25	1.1	0	0	0
KC27B	226.5	228.5	19.8	0.35	0.05	2.1	0.05
KC27B	231.5	233.5	14.65	0.85	0	0.35	1.2
KC27B	236.5	238.5	10.65	1.05	0	0	0.3
KC27B	241.5	243.5	0.75	1.65	0	0	0.5
KC27B	246.5	248.5	0.35	0.15	0	0.05	0.5
KC27B	251.5	253.5	4.8	0.85	0	1.2	0.15
KC27B	256.5	258.5	17.3	0.9	0	4.95	0.8
KC27B	261.5	263.5	7.95	0.95	0	0.4	0.25
KC27B	266.5	268.5	7.15	0.4	0	0.55	1.75
KC27B	269.5	271.5	0.45	0.3	0	0	0
JKC 53	4.5	15.8	1	0.1	0.05	0	0
JKC 53	141.5	150	0.55	2	0.05	0	1.4
JKC53	221.5	230	0.3	0.05	0	0.1	0
JKC53	226.5	235	1.25	0.35	0	0	0
JKC53	261.5	270	1.25	0.45	0	0	0
JKC53	266.5	275	1.7	0.5	0	0.05	0.1
JKC53	271.5	280	3.25	0.5	0	0.05	0.2
JKC53	276.5	285	0.8	0.35	0	0.15	0
JKC53	281.5	290	1.25	0.4	0	0	0
JKC53	286.5	295	0.45	0.1	0	0	0
JKC53	291.5	300	1.4	0.2	0	0	0
JKC53	296.5	305	0.15	0	0	0	0

Table D.10 (continued)

JKC53	301.5	310	0.05	0.45	0	0	0
JKC53	306.5	315	0.25	0.45	0	0	0
JKC53	311.5	320	0.25	0.1	0	0	0
JKC 53	321.5	330	0	0	0	0	0
JKC53	331.5	340	1.1	0.2	0	0	0
JKC53	341.5	350	0	0.45	0	0	0
JKC53	346.5	355	0.05	0.1	0	0	0
JKC 53	351.5	360	0	0	0	0	0
JKC53	356.5	365	0	0.2	0	0	0
JKC53	366.5	375	0	0.15	0	0	0
JKC53	376.5	385	0	0.6	0	0	0
JKC53	381.5	390	0	0.1	0	0	0
JKC 53	391.5	400	0	0.15	0	0	0
JKC 53	396.5	405	0	0	0	0	0
JKC53	401.5	410	0	0.2	0	0	0
JKC 53	416.5	425	0	0	0	0	0
JKC 53	436.5	445	0	1.2	0	0	0.25
JKC53	446.5	455	0	0.1	0	0	0
JKC53	451.5	460	0	0.1	0	0	0
JKC53	456.5	465	0	0.35	0	0	0
JKC53	461.5	470	0	1.4	0	0	0
JKC53	466.5	475	0	1.45	0	0	0
JKC 53	471.5	480	0	0	0	0	0
JKC53	481.5	490	0	0.25	0	0	0
JKC 53	486.5	495	0	0.1	0	0	0
JKC53	491.5	500	0	0.25	0	0	0
JKC53	496.5	505	0	0.5	0	0	0
JKC53	511.5	520	0	0.2	0	0	0
KC 57	1.5	6.35	0.95	0.1	0.15	0	0
KC 57	4.5	7.47	0	0	0	0	0.05
KC 57	7.5	8.59	0	0	0	0	0
KC 57	10.5	9.71	0	0	0	0	0.05
KC 57	13.5	10.83	0	0	0	0	0
KC 57	16.5	11.95	0	0	0	0	0
KC 57	21.5	16.44	0	0	0	0	0
KC 57	26.5	23.62	0	0	0	0	0
KC 57	31.5	31.42	0	0	0	0	0

Table D.10 (continued)

KC 57	36.5	36.8	0	0	0	0	0
KC 57	41.5	44.15	0	0	0	0	0
KC 57	46.5	50.12	0	0	0	0	0
KC 57	51.5	56.1	0	0	0	0	0
KC 57	56.5	61.37	0	0	0	0	0
KC 57	61.5	66.34	0	0	0	0	0
KC 57	66.5	70.17	0	0	0	0	0
KC 57	71.5	72.5	0	0.65	0	0	0
KC 57	76.5	74.8	0	0.6	0	0	0.15
KC 57	81.5	77.6	0	0.65	0	0	0.05
KC 57	86.5	80.8	0	0.25	0	0	0.1
KC 57	91.5	83.95	0.1	0.65	0	0	0.1
KC 57	96.5	87.11	0.5	1.8	0	0	0.3
KC 57	101.5	90.27	0	0.1	0	0	0.25
KC 57	106.5	95.1	0.55	0.35	0	0	0.5
KC 57	111.5	104.2	2.3	0.8	0.05	0	4.35
KC 57	116.5	119.4	0.7	0.2	0	0	0.2
KC 57	121.5	123.3	0	0.7	0	0	0.05
KC 57	126.5	127.1	0.05	1.5	0	0	0.25
KC 57	131.5	131.8	6	0.75	0	0	2.25
KC 57	136.5	134.7	0.55	0.2	0	0	0.15
KC 57	141.5	137.3	6.5	0.8	0	0.1	0.55
KC 57	146.5	139.8	0.2	0	0	0	0.05
KC 57	151.5	142.4	0.4	0.2	0.15	0	0.1
KC 57	156.5	145.8	6.1	0.45	0	0	0.8
KC 57	156.5	145.8	2.55	1.3	0.05	0.2	0
KC 57	161.5	153.6	0.05	0	0	0	0.15
KC 57	171.5	169.2	0.45	1.95	0	0.05	0
KC 57	176.5	189.5	0.05	0.55	0	0	0.6
KC 57	181.5	184.7	0	0.05	0	0	0.05
KC 57	186.5	192.5	0	0	0	0	0
KC 57	191.5	200.2	0	0.65	0	0	0.75
KC 57	196.5	208.01	0.1	0.05	0	0	0.35
KC 57	201.5	215.8	0	0	0	0	0.05
KC 57	206.5	223.5	0.55	1.25	0	0	0.2
KC 57	211.5	231.3	0.15	0.35	0	0	0.2
KC 57	216.5	239.1	0	0.4	0	0	0.45

Table D.10 (continued)

KC 57	221.5	246.84	0	0	0	0	0
KC 57	226.5	254.6	0	0	0	0	0
KC 57	231.5	262.4	0.15	0.05	0	0	0.25
KC 57	236.5	270.2	0	0	0	0	0
KC 57	241.5	277.9	0	0.25	0	0	1.45
KC 57	246.5	285.7	0	0	0	0	0
KC 57	251.5	292.7	0	0	0	0	0
KC 57	326.5	339.5	0	0	0	0	0
KC 57	386.5	399.5	0	0.95	0	0	0.05
JPC 27	1	56.8	0	0	0	0	0
JPC 27	4	59.4	0	0	0	0	0
JPC 27	8	60.9	0	0	0	0	0
JPC 27	13	71.9	0	0	0	0	0
JPC 27	18	76.8	0	0	0	0	0
JPC 27	23	81.9	0	0	0	0	0
JPC 27	29	87.5	0	0	0	0	0
JPC 27	34	91.3	0	0	0	0	0
JPC 27	39	94.7	0	0	0	0	0
JPC 27	44	100.5	0	0	0	0	0
JPC 27	49	104.1	0.25	0.05	0	0	0.05
JPC 27	51.5	106	1	0.3	0	0	0.05
JPC 27	54	107.8	0	0	0	0	0
JPC 27	59	111.5	0	0	0	0	0
JPC 27	64	114.2	0	0	0	0	0
JPC 27	69	115.8	0	0	0	0	0
JPC 27	74	119.5	0	0.05	0	0	0
JPC 27	79	127.9	0	0	0	0	0
JPC 27	84	131.3	0	0	0	0	0
JPC 27	86	132.5	0	0	0	0	0
JPC 27	91	134.4	0	0	0	0	0
JPC 27	96	136.1	0	0	0	0	0
JPC 27	101	137.8	0	0	0	0	0
JPC 27	106	139.5	0	0	0	0	0
JPC 27	131	163	0.15	0	0	0	0
JPC 27	151	183	0.45	0.7	0	0	0.45
JPC 27	176	208	3.35	0.4	0	0	0.8
JPC 27	201	233	4.35	0	0	0	0.55

Table D.10 (continued)

JPC 27	211	243	0.25	0.3	0	0	0.15
JPC 27	231	263	2.1	0.5	0	0	0.15
JPC 27	251	283	0	0	0	0	0
JPC 27	291	323	3.55	0.4	0	0.05	0
JPC 27	306	338	0.65	0.05	0	0	0.1
JPC 27	406	438	0	0.75	0	0	0
JPC 27	431	463	0	0	0.1	0	0.05
JPC 27	826	858	0	0.05	0	0	0
JPC 27	831	863	0	0.05	0	0	0
JPC 27	866	898	0.05	0	0	0	0
JPC 27	891	923	0.3	0.6	0	0	0.15
JPC 27	896	928	0.05	0.35	0	0	0.05
JPC 27	926	958	0.9	0	0	0	0
JPC 27	946	978	0.35	0	0	0	0
JPC 27	951	983	0.55	0.1	0	0	0.55
JPC 27	956	988	0	0	0	0	0
JPC 27	961	993	2.25	0	0	0	0

Table D.11 MC-45 foraminifer stable isotopes. *Neogloboquadrina pachyderma* (s) $\delta^{18}\text{O}$ adjusted +0.6‰ and $\delta^{13}\text{C}$ adjusted +1.0‰ (Hendry et al., 2009; Mortyn & Charles, 2003). *Trifarina angulosa* $\delta^{13}\text{C}$ adjusted +0.85‰ (Hillenbrand et al., 2017). *Bulimina aculeata* $\delta^{13}\text{C}$ adjusted -0.7‰ (Mackensen et al., 2003).

Cruise	Core ID	Depth (cmbsf)	Depth (cmcd)	Age (calendar year before 2014)	<i>N. Pachyderma</i> (s)				<i>T. angulosa</i>			<i>B. aculeata</i>			<i>G. subglobosa</i>	
					$\delta^{18}\text{O}$ (‰ VPDB)	Adjusted $\delta^{18}\text{O}$ (‰ VPDB)	$\delta^{13}\text{C}$ (‰ VPDB)	Adjusted $\delta^{13}\text{C}$ (‰ VPDB)	$\delta^{18}\text{O}$ (‰ VPDB)	$\delta^{13}\text{C}$ (‰ VPDB)	Adjusted $\delta^{13}\text{C}$ (‰ VPDB)	$\delta^{18}\text{O}$ (‰ PDB)	$\delta^{13}\text{C}$ (‰ PDB)	Adjusted $\delta^{13}\text{C}$ (‰ VPDB)	$\delta^{18}\text{O}$ (‰ PDB)	$\delta^{13}\text{C}$ (‰ PDB)
NBP14-02	MC45 (6)	0.5	0.5	6	3.801	4.401	0.84	1.84	3.981	-0.354	0.496	3.745	-0.121	-0.821	4.019	0.719
NBP14-02	MC45 (6)	0.5	0.5	6	3.677	4.277	1.193	2.193								
NBP14-02	MC45 (6)	0.5	0.5	6	3.858	4.458	1.119	2.119								
NBP14-02	MC45 (6)	0.75	0.75	11											3.960	0.817
NBP14-02	MC45 (6)	1.25	1.25	15	3.864	4.464	1.011	2.011				3.787	-0.004	-0.704	3.924	0.702
NBP14-02	MC45 (6)	1.25	1.25	15	3.718	4.318	0.932	1.932				3.953	0.060	-0.640		
NBP14-02	MC45 (6)	1.75	1.75	21	3.686	4.286	1.143	2.143	3.888	-0.177	0.673	3.891	-0.135	-0.835		
NBP14-02	MC45 (6)	2.25	2.25	27	3.748	4.348	1.067	2.067	4.016	-0.345	0.505	3.802	-0.138	-0.838		
NBP14-02	MC45 (6)	2.25	2.25	27	3.803	4.403	0.97	1.97								
NBP14-02	MC45 (6)	2.25	2.25	27	3.719	4.319	1.123	2.123								
NBP14-02	MC45 (6)	3.25	3.25	39	3.78	4.38	0.991	1.991								
NBP14-02	MC45 (6)	3.25	3.25	39	3.729	4.329	0.861	1.861								
NBP14-02	MC45 (6)	4.25	4.25	51	3.896	4.496	0.908	1.908								

Table D.12 MC-61 foraminifer stable isotopes. *Neogloboquadrina pachyderma* (s) $\delta^{18}\text{O}$ adjusted +0.6‰ and $\delta^{13}\text{C}$ adjusted +1.0‰ (Hendry et al., 2009; Mortyn & Charles, 2003). *Bulimina aculeata* $\delta^{13}\text{C}$ adjusted -0.7‰ (Mackensen et al., 2003).

Cruise	Core ID	Depth (cmbsf)	Depth (cmcd)	Age (calendar year before 2014)	<i>N. Pachyderma</i>				<i>B. aculeata</i>			<i>G. subglobosa</i>	
					$\delta^{18}\text{O}$ (‰ VPDB)	Adjusted $\delta^{18}\text{O}$ (‰ VPDB)	$\delta^{13}\text{C}$ (‰ VPDB)	Adjusted $\delta^{13}\text{C}$ (‰ VPDB)	$\delta^{18}\text{O}$ (‰ PDB)	$\delta^{13}\text{C}$ (‰ PDB)	Adjusted $\delta^{13}\text{C}$ (‰ VPDB)	$\delta^{18}\text{O}$ (‰ VPDB)	$\delta^{13}\text{C}$ (‰ VPDB)
NBP14-02	MC61	0.75	0.75	23	3.811	4.411	1.039	2.039	4.201	0.436	-0.264	3.999	0.062
NBP14-02	MC61	1.25	1.25	39	3.834	4.434	0.967	1.967	3.991	-0.160	-0.860		
NBP14-02	MC61	1.75	1.75	54	3.885	4.485	0.91	1.91					
NBP14-02	MC61	2.25	2.25	70	3.812	4.412	0.87	1.87	3.945	-0.028	-0.728		
NBP14-02	MC61	2.75	2.75	85	3.835	4.435	0.852	1.852	3.862	0.082	-0.618		
NBP14-02	MC61	3.25	3.25	101	3.839	4.439	0.821	1.821	3.859	-0.341	-1.041		
NBP14-02	MC61	3.75	3.75	116	3.808	4.408	0.853	1.853					

Table D.13 KC-27B foraminifer stable isotopes. *Neogloboquadrina pachyderma* (s) $\delta^{18}\text{O}$ adjusted +0.6‰ and $\delta^{13}\text{C}$ adjusted +1.0‰ (Hendry et al., 2009; Mortyn & Charles, 2003). *Trifarina angulosa* $\delta^{13}\text{C}$ adjusted +0.85‰ (Hillenbrand et al., 2017). *Bulimina aculeata* $\delta^{13}\text{C}$ adjusted -0.7‰ (Mackensen et al., 2003).

Cruise	Core ID	Depth (cmbfsf)	Depth (cmcd)	Age (Cal yr before 1950)	<i>N. Pachyderma</i> (s)				<i>T. angulosa</i>			<i>B. aculeata</i>			<i>G. subglobosa</i>	
					$\delta^{18}\text{O}$ (‰ VPDB)	Adjusted $\delta^{18}\text{O}$ (‰ VPDB)	$\delta^{13}\text{C}$ (‰ VPDB)	Adjusted $\delta^{13}\text{C}$ (‰ VPDB)	$\delta^{18}\text{O}$ (‰ VPDB)	$\delta^{13}\text{C}$ (‰ VPDB)	Adjusted $\delta^{13}\text{C}$ (‰ VPDB)	$\delta^{18}\text{O}$ (‰ PDB)	$\delta^{13}\text{C}$ (‰ PDB)	Adjusted $\delta^{13}\text{C}$ (‰ VPDB)	$\delta^{18}\text{O}$ (‰ PDB)	$\delta^{13}\text{C}$ (‰ PDB)
NBP14-02	KC27B	1.5	3.5	-23	3.676	4.276	0.978	1.978	3.937	-0.279	0.571	3.858	0.091	-0.609	3.760	0.543
NBP14-02	KC27B	4.5	6.5	8	3.705	4.305	1.025	2.025				3.849	0.057	-0.643	3.773	0.714
NBP14-02	KC27B	4.5	6.5	8											3.627	0.680
NBP14-02	KC27B	7.5	9.5	35	3.748	4.348	1.144	2.144								
NBP14-02	KC27B	161.5	163.5	5486					4.054	-0.527	0.323					
NBP14-02	KC27B	171.5	173.5	5585					4.173	-0.202	0.648					
NBP14-02	KC27B	176.5	178.5	5635	3.566	4.166	0.893	1.893	4.023	-0.461	0.389					
NBP14-02	KC27B	181.5	183.5	5685					4.119	-0.199	0.651					
NBP14-02	KC27B	186.5	188.5	5735	3.726	4.326	1.002	2.002	3.865	-0.917	-0.067					
NBP14-02	KC27B	191.5	193.5	5784					4.131	-0.349	0.501					
NBP14-02	KC27B	196.5	198.5	5834	3.81	4.41	1.004	2.004	4.261	-0.533	0.317					
NBP14-02	KC27B	201.5	203.5	5884	3.677	4.277	0.968	1.968	4.099	-0.519	0.331					
NBP14-02	KC27B	206.5	208.5	5933	3.562	4.162	0.65	1.65								
NBP14-02	KC27B	211.5	213.5	5982	3.763	4.363	1.119	2.119	4.218	-0.509	0.341					
NBP14-02	KC27B	216.5	218.5	6032	3.812	4.412	1.004	2.004	3.802	-0.991	-0.141					
NBP14-02	KC27B	221.5	223.5	6081	3.718	4.318	1.015	2.015	4.025	-0.746	0.104					
NBP14-02	KC27B	226.5	228.5	6130	3.696	4.296	0.985	1.985	3.787	-1.012	-0.162					

Table D.13 (continued)

NBP14 -02	KC27B	226.5	228.5	6130	3.649	4.249	0.947	1.947								
NBP14 -02	KC27B	231.5	233.5	6174	3.803	4.403	0.945	1.945	3.980	-0.398	0.452					
NBP14 -02	KC27B	231.5	233.5	6174	3.871	4.471	1.036	2.036								
NBP14 -02	KC27B	231.5	233.5	6174	3.768	4.368	0.945	1.945								
NBP14 -02	KC27B	236.5	238.5	6214	3.63	4.23	0.867	1.867	4.111	-0.472	0.378					
NBP14 -02	KC27B	241.5	243.5	6255	3.735	4.335	0.862	1.862	3.959	-0.485	0.365					
NBP14 -02	KC27B	251.5	253.5	6337	3.776	4.376	1.019	2.019	4.103	-0.482	0.368					
NBP14 -02	KC27B	256.5	258.5	6379	3.741	4.341	0.878	1.878	4.289	-0.724	0.126					
NBP14 -02	KC27B	256.5	258.5	6379	3.745	4.345	1	2								
NBP14 -02	KC27B	261.5	263.5	6424	3.731	4.331	0.981	1.981	3.756	-0.702	0.148					
NBP14 -02	KC27B	261.5	263.5	6424	3.698	4.298	0.844	1.844								
NBP14 -02	KC27B	266.5	268.5	6471	3.65	4.25	0.864	1.864								
NBP14 -02	KC27B	266.5	268.5	6471	3.752	4.352	0.962	1.962								

Table D.14 JKC-53 foraminifer stable isotopes. *Neogloboquadrina pachyderma* (s) $\delta^{18}\text{O}$ adjusted +0.6‰ and $\delta^{13}\text{C}$ adjusted +1.0‰ (Hendry et al., 2009; Mortyn & Charles, 2003). *Trifarina angulosa* $\delta^{13}\text{C}$ adjusted +0.85‰ (Hillenbrand et al., 2017).

Cruise	Core ID	Depth (cmbsf)	Depth (cmcd)	Age (Cal yr before 1950)	<i>N. Pachyderma</i>				<i>T. angulosa</i>		
					$\delta^{18}\text{O}$ (‰ VPDB)	Adjusted $\delta^{18}\text{O}$ (‰ VPDB)	$\delta^{13}\text{C}$ (‰ VPDB)	Adjusted $\delta^{13}\text{C}$ (‰ VPDB)	$\delta^{18}\text{O}$ (‰ VPDB)	$\delta^{13}\text{C}$ (‰ VPDB)	Adjusted $\delta^{13}\text{C}$ (‰ VPDB)
NBP14-02	JKC53	216.5	225	6096	3.501	4.101	0.655	1.655	4.113	-0.649	0.201
NBP14-02	JKC53	226.5	235	6190	3.756	4.356	0.938	1.938	4.205	-0.458	0.392
NBP14-02	JKC53	226.5	235	6190	3.721	4.321	0.729	1.729	4.329	-0.579	0.271
NBP14-02	JKC53	261.5	270	6485	3.802	4.402	0.824	1.824	4.269	-0.614	0.236
NBP14-02	JKC53	261.5	270	6485	3.834	4.434	0.836	1.836			
NBP14-02	JKC53	266.5	275	6531	3.722	4.322	0.639	1.639	4.011	-0.782	0.068
NBP14-02	JKC53	271.5	280	6577	3.82	4.42	0.786	1.786	4.085	-0.870	-0.020
NBP14-02	JKC53	276.5	285	6623					3.810	-0.887	-0.037
NBP14-02	JKC53	281.5	290	6669	3.879	4.479	0.735	1.735	4.281	-0.340	0.510
NBP14-02	JKC53	286.5	295	6716	3.729	4.329	0.809	1.809			
NBP14-02	JKC53	291.5	300	6763	3.892	4.492	0.673	1.673	3.897	-0.367	0.483
NBP14-02	JKC53	301.5	310	6857					4.340	-0.481	0.369
NBP14-02	JKC53	306.5	315	6903					4.038	-0.963	-0.113
NBP14-02	JKC53	331.5	340	7135	3.714	4.314	0.579	1.579			
NBP14-02	JKC53	341.5	350	7229					4.215	-0.426	0.424
NBP14-02	JKC53	376.5	385	7552					4.133	-0.477	0.373
NBP14-02	JKC53	456.5	465	8253					4.295	-0.634	0.216
NBP14-02	JKC53	461.5	470	8293					4.376	-0.288	0.562
NBP14-02	JKC53	461.5	470	8293					4.442	-0.344	0.506
NBP14-02	JKC53	481.5	490	8448					4.172	-0.642	0.208
NBP14-02	JKC53	496.5	505	8566					4.487	-0.584	0.266

Table D.15 Processed and calibrated trace metals data for *Trifarina angulosa* (species: T).

Sample name	depth (cmbsf)	depth (cmcd)	age (yr bp)	Species	Initial weight (µg)	# shells	Avg shell mass	Mawbey 2020 Eq#4 Calibrated Temp (°C)	Ca conc (ppm) based on Ca43	Recovery (%)	CMSTD Adjusted Mg24 Ca43 (mmol/mol)	CMSTD Adjusted Mg24 Ca44 (mmol/mol)	CMSTD Adjusted Mg25 Ca43 (mmol/mol)	CMSTD Adjusted Mg25 Ca44 (mmol/mol)
Mawbey MC61 (0.5 C) 0.5-3.5	1.5	1.5	46.5	T	-	-	-	-1.46	-	-	0.881	-	-	-
Mawbey MC45 (0.3 C) 1-1.5 cm	1.25	1.25	15.0	T	-	-	-	-0.56	-	-	0.936	-	-	-
AI MC45 1.5-2	1.75	1.75	21.0	T	126	16	7.88	2.33	57.2	32%	1.11	1.09	1.08	1.05
AI JKC53 140-143	141.5	150	5407.1	T	229	24	9.54	-1.13	68.1	55%	0.90	0.96	0.84	0.89
AI KC27B 185-188	186.5	188.5	5889.6	T	160	25	6.40	0.23	42.4	60%	0.98	0.78	0.90	0.72
AI KC27B 195-198	196.5	198.5	6014.9	T	207	38	5.45	-0.10	46.8	66%	0.96	1.03	0.87	0.93
AI KC27B 200-203	201.5	203.5	6077.6	T	137	39	3.51	-1.34	31.7	65%	0.89	0.71	0.81	0.65
AI KC27B 220-233	221.5	223.5	6328.2	T	134	18	3.78	-1.00	45.4	49%	0.91	0.73	0.85	0.69
AI KC27B 235-238	236.5	238.5	6516.2	T	104	20	5.20	-0.54	22.8	67%	0.94	1.05	0.91	1.02
AI KC27B 240-243	241.5	243.5	6578.8	T	192	42	4.57	0.32	30.0	77%	0.99	1.00	0.96	0.96
AI KC27B 260-263	261.5	263.5	6829.4	T	130	32	4.06	-1.19	46.3	47%	0.90	0.85	0.84	0.79
AI JKC53 435-438	436.5	445	9103.9	T	100	26	3.85	1.40	36.2	46%	1.06	0.86	1.03	0.85

Table D.15 (continued)

Sample name	Li Ca43 ($\mu\text{mol}/\text{mol}$)	Li Ca44 ($\mu\text{mol}/\text{mol}$)	Na Ca43 (mmol/mol)	Na Ca44 (mol/mol)	Al Ca43 (mmol/mol)	Al Ca44 (mmol/mol)	Sr Ca43 (mmol/mol)	Sr Ca44 (mmol/mol)	Ba135 Ca43 ($\mu\text{mol}/\text{mol}$)	Ba135 Ca44 ($\mu\text{mol}/\text{mol}$)	Ba137 Ca43 ($\mu\text{mol}/\text{mol}$)	Ba137 Ca44 ($\mu\text{mol}/\text{mol}$)	U Ca43 (nmol/mol)	U Ca44 (nmol/mol)	Al Ca43 (mmol/mol)	Al Ca44 (mmol/mol)	Mn Ca43 (mmol/mol)	Mn Ca44 (mmol/mol)	Fe Ca43 (mmol/mol)	Fe Ca44 (mmol/mol)
Mawbey MC61 (0.5 C) 0.5-3.5	-	-	-	-	-	-	-	-	-	-	-	-	-	-	-	-	-	-	-	-
Mawbey MC45 (0.3 C) 1-1.5 cm	-	-	-	-	-	-	-	-	-	-	-	-	-	-	-	-	-	-	-	-
Al MC45 1.5-2	16.10	16.63	4.33	4.47	0.08	0.09	1.07	1.11	1.86	1.92	3.35	3.46	71.44	73.86	0.08	0.08	-0.01	-0.01	0.03	0.03
Al JKC53 140-143	16.70	17.30	4.42	4.59	0.07	0.07	1.07	1.11	1.23	1.27	2.29	2.38	265.58	286.97	0.09	0.09	0.00	0.00	0.04	0.04
Al KC27B 185- 188	16.49	14.46	4.45	3.89	0.04	0.04	1.08	0.94	1.33	1.16	2.32	2.03	1906.11	1695.95	0.04	0.04	0.00	0.00	0.11	0.10
Al KC27B 195- 198	16.29	16.86	4.15	4.30	0.22	0.23	1.10	1.14	1.84	1.91	3.38	3.50	366.33	395.30	0.29	0.30	0.00	0.00	0.09	0.10
Al KC27B 200- 203	17.14	15.21	4.29	3.80	0.09	0.08	1.13	1.00	1.62	1.43	3.02	2.67	3282.80	2955.36	0.08	0.07	-0.02	-0.02	0.10	0.09
Al KC27B 220- 233	19.17	17.03	4.28	3.80	0.18	0.16	1.14	1.01	1.94	1.72	3.50	3.11	2388.11	2153.46	0.17	0.15	0.00	0.00	0.12	0.11
Al KC27B 235- 238	14.26	16.66	3.98	4.65	0.14	0.17	1.02	1.19	1.85	2.16	3.12	3.64	1508.32	1764.57	0.13	0.15	-0.01	-0.01	0.03	0.03
Al KC27B 240- 243	15.38	16.37	4.16	4.43	0.08	0.09	1.09	1.16	1.10	1.17	2.04	2.17	2392.73	2550.85	0.07	0.08	-0.01	-0.01	0.02	0.02
Al KC27B 260- 263	14.98	15.26	4.16	4.24	0.05	0.05	1.06	1.08	1.50	1.53	2.64	2.69	1493.42	1523.33	0.05	0.05	-0.01	-0.01	0.03	0.03
Al JKC53 435-438	17.39	15.59	4.25	3.81	0.24	0.22	1.10	0.98	1.54	1.38	2.71	2.43	5319.94	4840.41	0.24	0.21	-0.01	-0.01	0.09	0.08

Table D.16 Raw trace metals data for *Trifarina angulosa* in counts per second.

Sequence Name	Avg Depth (cmbsf)	Avg Depth (cmd)	Li7(LR) Intensity AVG	Na23(LR) Intensity AVG [cps]	Mg24(LR) Intensity AVG [cps]	Mg25(LR) Intensity AVG [cps]	Al27(LR) Intensity AVG [cps]	Ca43(LR) Intensity AVG [cps]	Ca44(LR) Intensity AVG [cps]	Sr87++(LR) Intensity AVG [cps]	Sr88(LR) Intensity AVG [cps]	Y89(LR) Intensity AVG [cps]	Ba135(LR) Intensity AVG [cps]	Ba137(LR) Intensity AVG [cps]	U238(LR) Intensity AVG [cps]	Al27(MR) Intensity AVG [cps]	Se45(MR) Intensity AVG [cps]	Mn55(MR) Intensity AVG [cps]	Fe56(MR) Intensity AVG [cps]
026-AI NBP1402 JKC53 140-143	141.5	150	6.36E+04	1.34E+08	2.11E+07	2.28E+06	7.69E+05	1.50E+08	4.12E+07	5.23E+05	3.59E+08	3.23E+07	1.78E+05	2.23E+05	2.04E+05	1.01E+05	1.51E+06	1.00E+06	7.76E+05
027-AI NBP1402 KC27B 185-188	186.5	188.5	1.87E+04	3.19E+07	3.93E+06	3.12E+05	1.74E+05	3.49E+07	2.09E+07	1.05E+05	9.13E+07	9.15E+06	5.35E+04	6.22E+04	3.09E+04	1.78E+04	3.37E+05	2.26E+05	1.90E+05
026-AI NBP1402 KC27B 190-193	190.5	192.5	1.80E+04	2.99E+07	3.48E+06	2.76E+05	1.35E+05	3.18E+07	1.88E+07	9.85E+04	8.49E+07	9.56E+06	5.15E+04	5.85E+04	2.99E+04	1.40E+04	3.37E+05	2.27E+05	2.86E+05
025-AI NBP1402 KC27B 195-198	196.5	198.5	5.53E+04	1.13E+08	1.87E+07	2.01E+06	1.29E+06	1.29E+08	3.57E+07	4.60E+05	3.15E+08	3.20E+07	1.78E+05	2.22E+05	1.92E+05	1.72E+05	1.51E+06	1.00E+06	9.36E+05
025-AI NBP1402 KC27B 200-203	201.5	203.5	1.89E+04	3.14E+07	3.82E+06	3.05E+05	2.32E+05	3.46E+07	2.06E+07	1.06E+05	9.23E+07	9.83E+06	5.65E+04	6.64E+04	4.25E+04	2.31E+04	3.42E+05	2.32E+05	1.74E+05
029-AI NBP1402 KC27B 220-233	221.5	223.5	2.01E+04	3.25E+07	3.96E+06	3.17E+05	4.36E+05	3.60E+07	2.15E+07	1.10E+05	9.55E+07	9.24E+06	5.95E+04	7.34E+04	4.16E+04	4.43E+04	3.36E+05	2.29E+05	2.04E+05
032-AI NBP1402 KC27B 235-238	236.5	238.5	1.64E+04	2.68E+07	3.27E+06	2.60E+05	2.38E+05	2.96E+07	1.77E+07	9.31E+04	7.90E+07	9.08E+06	5.14E+04	5.82E+04	2.01E+04	2.42E+04	3.31E+05	2.21E+05	1.19E+05
031-AI NBP1402 KC27B 240-243	241.5	243.5	1.72E+04	2.83E+07	3.46E+06	2.75E+05	1.99E+05	3.11E+07	1.88E+07	9.57E+04	8.33E+07	8.99E+06	4.93E+04	5.59E+04	4.05E+04	2.02E+04	3.27E+05	2.17E+05	1.16E+05
033-AI NBP1402 KC27B 260-263	261.5	263.5	1.84E+04	3.08E+07	3.69E+06	2.90E+05	1.88E+05	3.41E+07	2.08E+07	1.03E+05	8.95E+07	8.73E+06	5.39E+04	6.46E+04	3.80E+04	1.94E+04	3.14E+05	2.11E+05	1.29E+05
028-AI NBP1402 JKC53 435-438	436.5	445	1.88E+04	3.11E+07	3.94E+06	3.19E+05	4.82E+05	3.44E+07	2.04E+07	1.05E+05	9.08E+07	9.44E+06	5.51E+04	6.42E+04	7.50E+04	4.93E+04	3.35E+05	2.24E+05	1.71E+05

Table D.17 Processed and calibrated trace metals data for *N. pachyderma* (s) (species: NPS).

Sample name	depth (cmbsf)	depth (cmcd)	age (yr bp)	Species	Initial weight (µg)	# shells	Avg shell mass (ug)	Vazquez Riveiros 2014 Calibrated Temp (°C)	Repl Avg	Repl stdev	Ca conc (ppm) based on Ca43	Recovery (%)	CMSTD Adjusted Mg24 Ca43 (mmol/mol)	CMSTD Adjusted Mg24 Ca44 (mmol/mol)	CMSTD Adjusted Mg25 Ca43 (mmol/mol)	CMSTD Adjusted Mg25 Ca44 (mmol/mol)
AH MC61 0.5-1	0.75	0.75	23.0	NPS	251	18	13.94	0.99			85.08	49%	0.641	0.628	0.611	0.599
AH MC61 0.5-1 repl	0.75	0.75	23.0	NPS	251	18	13.94	1.47			103.89	38%	0.661	0.652	0.636	0.628
AH MC61 1-1.5	1.25	1.25	39.0	NPS	295	21	14.05	-2.31			42.26	79%	0.490	0.482	0.466	0.459
AH MC61 1-1.5 repl	1.25	1.25	39.0	NPS	295	21	14.05	-0.86			84.53	57%	0.549	0.541	0.537	0.530
AH MC61 1.5-2	1.75	1.75	54.0	NPS	420	53	7.92	-1.36			180.23	36%	0.530	0.520	0.511	0.503
AH MC61 2-2.5	2.25	2.25	70.0	NPS	256	30	8.53	-3.30			82.42	52%	0.456	0.445	0.426	0.417
AG15 MC61 2.5-3	2.75	2.75	85.0	NPS	118	12	9.83	0.62			40.6	48%	0.577	0.610	0.575	0.603
AH MC61 3-3.5	3.25	3.25	101.0	NPS	230	23	10.00	-0.35			107.45	30%	0.579	0.564	0.568	0.554
AH MC61 3.5-4	3.75	3.75	116.0	NPS	202	22	9.18	-0.42			87.07	35%	0.571	0.561	0.541	0.533
AH MC45 0-1	0.5	0.5	6.0	NPS	320.5	24	13.35	2.81	1.8	1.4	110.50	48%	0.711	0.726	0.650	0.664
AH MC45 0-1 repl	0.5	0.5	6.0	NPS	320.5	24	13.35	0.77			117.30	45%	0.616	0.617	0.583	0.584
AH MC45 1-1.5	1.25	1.25	15.0	NPS	353.5	21	16.83	3.82	3.0	1.1	127.48	46%	0.768	0.787	0.707	0.724
AH MC45 1-1.5 repl	1.25	1.25	15.0	NPS	353.5	21	16.83	2.19			140.13	41%	0.706	0.691	0.661	0.648
AF3MC45 1.5-2	1.75	1.75	21.0	NPS	298	25	11.92	0.31	0.5	0.2	151.9	24%	0.581	0.595	0.520	0.528
AG18 MC45 1.5-2	1.75	1.75	21.0	NPS	493	33	14.94	0.59			175.4	47%	0.588	0.608	0.553	0.569
AF4 MC45 2-2.5	2.25	2.25	27.0	NPS	245	33	7.42	-0.01	-1.9	2.6	109.0	33%	0.556	0.580	0.481	0.497
AG21 MC45 2-2.5	2.25	2.25	27.0	NPS	271	31	8.74	-3.72			97.6	46%	0.462	0.431	0.320	0.291
AF5MC45 2.5-3	2.75	2.75	33.0	NPS	277	51	5.43	0.70			110.1	40%	0.599	0.613	0.536	0.545
AH KC27B 0-3	1.5	3.5	42.0	NPS	325	28	11.61	1.68	1.1	0.8	116.38	46%	0.664	0.663	0.603	0.603
AH KC27B 0-3 repl	1.5	3.5	42.0	NPS	325	28	11.61	0.49			112.59	48%	0.604	0.603	0.551	0.551
AF6.7 MC45 3-4	3.5	3.5	42.0	NPS	202	25	8.08	2.39			55.1	59%	0.668	0.702	0.633	0.661
AH KC27B 3-6	4.5	6.5	78.0	NPS	316	38	8.32	2.34			101.76	52%	0.706	0.699	0.656	0.650
AF21 KC27B 185-188	186.5	188.5	5889.6	NPS	153	37	4.14	-2.57			62.1	39%	0.443	0.472	0.360	0.378
AF9.10 KC27B 195-203	199	201	6046.2	NPS	233	67	3.48	-3.67			68.5	56%	0.439	0.432	0.393	0.384
AH JPC 27 175-177	176	208	6134.0	NPS	261	11	23.73	-4.85			89.97	48%	0.407	0.394	0.369	0.358

Table D.17 (continued)

AF14 KC27B 210-213	211.5	213.5	6202.9	NPS	144	54	2.67	-1.28			56.7	41%	0.515	0.524	0.462	0.466
AH KC27B 220-223	221.5	223.5	6328.2	NPS	310.5	50	6.21	-3.96	-4.1	0.2	133.23	36%	0.423	0.423	0.381	0.381
AH KC27B 220-223 repl	221.5	223.5	6328.2	NPS	310.5	50	6.21	-4.29			98.23	53%	0.415	0.412	0.384	0.381
AF15 KC27B 220-223	221.5	223.5	6328.2	NPS	113	26	4.35	-2.97			39.8	47%	0.429	0.457	0.406	0.428
AH JPC 27 200-202	201	233	6447.2	NPS	230	20	11.50	-4.22			46.04	70%	0.417	0.414	0.349	0.347
AH KC27B 230-233	231.5	233.5	6453.5	NPS	393.5	50	7.87	-5.08	-4.4	1.0	132.20	50%	0.402	0.386	0.373	0.360
AH KC27B 230-233 repl	231.5	233.5	6453.5	NPS	393.5	50	7.87	-3.64			135.00	49%	0.430	0.433	0.391	0.394
AH KC27B 235-238	236.5	238.5	6516.2	NPS	326	50	6.52	-0.09	-2.3	3.1	126.63	42%	0.577	0.576	0.518	0.517
AH KC27B 235-238 repl	236.5	238.5	6516.2	NPS	326	50	6.52	-4.43			132.27	39%	0.411	0.407	0.380	0.377
AH KC27B 250-253	251.5	253.5	6704.1	NPS	300	50	6.00	-4.35			130.28	35%	0.410	0.409	0.354	0.354
AG2 KC27B 255-258	256.5	258.5	6766.8	NPS	265	87	3.05	-2.80			140.7	20%	0.436	0.464	0.391	0.411
AF18 JPC27 230-232	231	263	6823.2	NPS	124	30	4.13	-3.99			46.6	44%	0.396	0.422	0.357	0.375
AH KC27B 260-263	261.5	263.5	6829.4	NPS	318	50	6.36	-2.89	-2.6	0.4	114.90	46%	0.467	0.460	0.432	0.426
AH KC27B 260-263 repl	261.5	263.5	6829.4	NPS	318	50	6.36	-2.26			172.32	19%	0.500	0.484	0.474	0.460
AF22 JKC53 270-273	271.5	280	7036.2	NPS	343	53	6.47	-3.25			109.2	52%	0.431	0.447	0.372	0.382
AG8 JKC53 280-283	281.5	290	7161.5	NPS	354	47	7.53	-1.32			130.4	45%	0.497	0.522	0.464	0.483
AG20 JKC53 280-283	281.5	290	7161.5	NPS	396	55	7.20	-2.27			149.1	44%	0.474	0.484	0.434	0.439
AG7 JKC53 290-293	291.5	300	7286.8	NPS	292	41	7.12	-2.19			152.2	22%	0.457	0.487	0.413	0.435
AG19 JKC53 290-293	291.5	300	7286.8	NPS	470	80	5.88	-5.20			153.3	51%	0.373	0.383	0.336	0.340
AF20 JPC27 925-927	926	958	14943.9	NPS	91	18	5.06	-5.25			36.7	39%	0.385	0.381	0.325	0.318

Table D.17 (continued)

Sample name	Li Ca43 (μmol/mol)	Li Ca44 (μmol/mol)	Na Ca43 (mmol/mol)	Na Ca44 (mmol/mol)	Al Ca43 (mmol/mol)	Al Ca44 (mmol/mol)	Sr Ca43 (mmol/mol)	Sr Ca44 (mmol/mol)	Ba135 Ca43 (μmol/mol)	Ba135 Ca44 (μmol/mol)	Ba137 Ca43 (μmol/mol)	Ba137 Ca44 (μmol/mol)	U Ca43 (nmol/mol)	U Ca44 (nmol/mol)	Al Ca43 (mmol/mol)	Al Ca44 (mmol/mol)	Mn Ca43 (mmol/mol)	Mn Ca44 (mmol/mol)	Fe Ca43 (mmol/mol)	Fe Ca44 (mmol/mol)
AH MC61 0.5-1	20.918	20.288	6.510	6.314	0.029	0.027	1.459	1.401	0.721	0.693	1.231	1.182	204.123	196.200	0.344	82.784	-0.006	-0.006	0.011	0.011
AH MC61 0.5-1 repl	19.805	19.347	6.372	6.224	0.287	0.283	1.495	1.473	0.868	0.855	1.518	1.496	1145.838	1130.298	3.726	919.758	-0.003	-0.003	0.155	0.153
AH MC61 1-1.5	23.687	23.040	6.388	6.214	0.107	0.105	1.489	1.466	0.764	0.753	1.337	1.317	576.083	568.017	2.177	537.248	-0.006	-0.006	0.005	0.005
AH MC61 1-1.5 repl	20.370	19.877	6.370	6.215	0.009	0.009	1.487	1.464	0.736	0.725	1.334	1.313	1122.689	1106.411	0.094	23.277	-0.007	-0.007	0.002	0.002
AH MC61 1.5-2	15.118	14.690	5.638	5.478	0.005	0.005	1.227	1.222	2.685	2.673	2.692	2.681	8.961	8.931	0.005	0.005	0.102	0.102	0.061	0.061
AH MC61 2-2.5	15.713	15.207	5.624	5.442	0.007	0.007	1.427	1.411	0.825	0.815	1.410	1.394	26.634	26.307	0.065	18.844	-0.003	-0.003	-0.004	-0.004
AG15 MC61 2.5-3	13.875	14.307	5.577	5.750	0.096	0.099	1.460	1.506	1.077	1.111	1.618	1.668	26.135	26.950	0.130	0.134	0.006	0.006	0.013	0.013
AH MC61 3-3.5	16.905	16.317	5.972	5.765	0.015	0.014	1.434	1.391	0.848	0.823	1.502	1.457	35.490	34.380	0.146	41.425	-0.005	-0.005	-0.001	-0.001
AH MC61 3.5-4	17.277	16.804	5.975	5.813	0.020	0.020	1.452	1.431	1.231	1.213	2.101	2.070	28.034	27.597	0.241	69.530	-0.005	-0.005	0.003	0.003
AH MC45 0-1	20.328	20.459	6.501	6.543	0.210	0.208	1.468	1.452	1.472	1.456	2.659	2.630	1416.863	1400.765	1.876	910.875	0.187	0.185	0.061	0.061
AH MC45 0-1 repl	19.130	18.913	6.899	6.821	0.012	0.012	1.438	1.451	0.966	0.975	1.666	1.681	76.353	76.979	0.115	34.503	-0.007	-0.007	-0.005	-0.005
AH MC45 1-1.5	22.599	22.806	7.249	7.315	0.111	0.111	1.503	1.500	1.063	1.061	1.935	1.931	734.339	732.567	0.820	401.812	0.021	0.021	0.028	0.028
AH MC45 1-1.5 repl	20.699	20.071	6.908	6.698	0.031	0.031	1.449	1.428	1.320	1.302	2.291	2.258	67.013	66.010	0.275	80.555	-0.010	-0.010	-0.003	-0.003
AF3MC45 1.5-2	18.135	18.260	6.577	6.623	0.030	0.030	1.456	1.466	1.052	1.059	1.860	1.873	118.597	119.406	0.038	0.038	-0.001	-0.001	0.005	0.005
AG18 MC45 1.5-2	17.239	17.504	6.581	6.682	0.029	0.029	1.437	1.459	1.043	1.059	1.738	1.764	72.590	73.705	0.039	0.040	-0.001	-0.001	0.003	0.003
AF4 MC45 2-2.5	15.070	15.394	6.023	6.153	0.051	0.052	1.463	1.494	1.010	1.031	1.789	1.827	90.754	92.697	0.063	0.065	0.000	0.000	0.010	0.010
AG21 MC45 2-2.5	16.560	15.728	6.167	5.852	0.023	0.022	1.530	1.453	0.949	0.902	1.647	1.566	64.675	62.205	0.024	0.023	-0.002	-0.002	0.000	0.000
AF5MC45 2.5-3	14.467	14.571	6.390	6.436	0.033	0.033	1.441	1.451	2.909	2.930	5.116	5.153	52.445	52.823	0.034	0.034	-0.002	-0.002	0.001	0.001
AH KC27B 0-3	20.809	20.517	6.644	6.551	0.005	0.005	1.217	1.218	2.618	2.619	2.638	2.639	6.374	6.375	0.005	0.005	0.106	0.106	0.064	0.064
AH KC27B 0-3 repl	18.796	18.521	6.389	6.296	0.032	0.032	1.492	1.461	0.850	0.832	1.476	1.445	65.416	63.971	0.290	84.091	-0.011	-0.011	-0.004	-0.004
AF6.7 MC45 3-4	15.951	16.369	6.792	6.970	0.062	0.064	1.470	1.509	0.971	0.996	1.750	1.796	99.097	101.690	0.065	0.067	-0.003	-0.003	0.007	0.007
AH KC27B 3-6	19.967	19.545	6.748	6.606	0.161	0.159	1.456	1.437	1.481	1.463	2.638	2.605	1103.984	1090.274	1.264	545.288	0.189	0.187	0.071	0.070
AF21 KC27B 185-188	9.431	9.798	4.899	5.089	0.064	0.066	1.465	1.522	0.689	0.716	1.192	1.238	299.340	311.202	0.080	0.083	-0.001	-0.001	0.036	0.038
AF9.10 KC27B 195-203	9.672	9.519	4.974	4.895	0.050	0.049	1.471	1.448	0.732	0.721	1.312	1.291	539.262	530.871	0.052	0.051	-0.003	-0.003	0.062	0.061

Table D.17 (continued)

AH JPC 27 175-177	13.012	12.494	5.336	5.123	0.862	0.851	1.449	1.430	1.583	1.563	2.857	2.820	2386.268	2355.817	6.487	2798.423	0.208	0.206	0.072	0.071
AF14 KC27B 210-213	9.774	9.812	5.233	5.253	0.021	0.021	1.511	1.517	0.723	0.726	1.264	1.269	648.001	650.668	0.022	0.022	-0.003	-0.003	0.014	0.014
AH KC27B 220-223	13.908	13.700	5.402	5.320	0.330	0.332	1.421	1.429	2.039	2.051	3.617	3.637	1114.052	1120.327	2.368	1040.591	0.136	0.137	0.116	0.117
AH KC27B 220-223 repl	14.160	13.850	5.357	5.239	0.036	0.035	1.540	1.508	0.860	0.842	1.448	1.418	186.414	182.408	0.348	101.074	-0.023	-0.023	-0.009	-0.009
AF15 KC27B 220-223	10.994	11.434	5.371	5.585	0.045	0.046	1.461	1.520	0.683	0.710	1.176	1.223	732.648	761.947	0.050	0.052	-0.001	-0.001	0.005	0.005
AH JPC 27 200-202	16.318	15.983	5.483	5.370	0.515	0.511	1.425	1.415	2.735	2.716	4.864	4.831	2125.045	2110.603	4.572	1984.285	0.234	0.233	0.108	0.108
AH KC27B 230-233	15.018	14.353	5.908	5.646	0.861	0.500	0.573	0.333	3.911	2.273	-1.272	-0.739	86.388	50.197	7.695	1953.712	0.083	0.048	-0.045	-0.026
AH KC27B 230-233 repl	14.279	14.164	6.211	6.161	0.004	0.004	1.213	1.219	2.584	2.596	2.576	2.588	5.250	5.280	0.005	0.005	0.111	0.112	0.066	0.067
AH KC27B 235-238	13.534	13.337	5.246	5.169	0.005	0.005	1.232	1.237	2.696	2.707	2.705	2.716	8.823	8.851	0.005	0.004	0.106	0.106	0.062	0.063
AH KC27B 235-238 repl	12.912	12.616	5.490	5.364	0.548	0.553	0.153	0.155	26.485	26.705	46.592	46.979	2274.612	2295.985	0.778	0.000	0.159	0.160	0.200	0.202
AH KC27B 250-253	13.152	12.949	5.622	5.534	0.019	0.020	1.430	1.439	0.846	0.852	1.503	1.513	57.018	57.329	0.187	55.785	-0.007	-0.007	-0.006	-0.006
AG2 KC27B 255-258	10.905	11.321	5.322	5.525	0.043	0.045	1.489	1.546	0.783	0.813	1.383	1.436	884.008	918.085	0.052	0.054	-0.002	-0.002	0.018	0.019
AF18 JPC27 230-232	11.723	12.190	5.487	5.705	0.039	0.041	1.493	1.553	0.623	0.648	1.273	1.323	192.660	200.336	0.044	0.046	-0.003	-0.003	0.007	0.008
AH KC27B 260-263	15.488	15.106	5.127	5.000	0.158	0.155	0.168	0.166	20.093	19.813	35.576	35.079	4.886	4.823	0.211	0.000	0.004	0.004	0.002	0.002
AH KC27B 260-263 repl	15.335	14.742	5.309	5.103	0.009	0.008	1.517	1.450	0.742	0.709	1.294	1.237	672.816	643.704	0.122	29.246	-0.008	-0.007	0.002	0.001
AF22 JKC53 270-273	12.178	12.434	5.776	5.898	0.011	0.012	1.495	1.526	0.769	0.785	1.342	1.370	553.627	565.257	0.015	0.016	-0.002	-0.002	0.000	0.000
AG8 JKC53 280-283	15.041	15.462	6.525	6.708	0.009	0.010	1.493	1.535	0.887	0.912	1.603	1.648	2784.696	2863.055	0.011	0.012	-0.003	-0.003	0.020	0.020
AG20 JKC53 280-283	13.693	13.798	5.978	6.024	0.023	0.023	1.494	1.506	0.871	0.877	1.504	1.515	1731.126	1745.805	0.031	0.031	-0.001	-0.001	0.001	0.001
AG7 JKC53 290-293	14.536	15.089	6.139	6.373	0.040	0.041	1.464	1.520	1.299	1.349	2.311	2.399	648.566	673.336	0.046	0.048	0.001	0.001	0.084	0.087
AG19 JKC53 290-293	13.070	13.272	5.843	5.933	0.024	0.025	1.486	1.509	0.829	0.842	1.395	1.417	99.258	100.869	0.035	0.035	0.001	0.001	0.035	0.036
AF20 JPC27 925-927	13.316	13.209	5.828	5.781	0.059	0.059	1.553	1.541	0.471	0.467	0.969	0.961	58.730	58.299	0.074	0.073	-0.001	-0.001	0.001	0.001

Table D.18 Raw trace metals data for *N. pachyderma* (s) in counts per second.

Sequence Name	Avg Depth (cmbst)	Avg Depth (cmcd)	Li7(LR) Intensity AVG	Na23(LR) Intensity AVG [cps]	Mg24(LR) Intensity AVG [cps]	Mg25(LR) Intensity AVG [cps]	Al27(LR) Intensity AVG [cps]	Ca43(LR) Intensity AVG [cps]	Ca44(LR) Intensity AVG [cps]	Sr87+(LR) Intensity AVG [cps]	Sr88(LR) Intensity AVG [cps]	Y89(LR) Intensity AVG [cps]	Ba135(LR) Intensity AVG [cps]	Ba137(LR) Intensity AVG [cps]	U238(LR) Intensity AVG [cps]	Al27(MR) Intensity AVG [cps]	Sc45(MR) Intensity AVG [cps]	Mn55(MR) Intensity AVG [cps]	Fe56(MR) Intensity AVG [cps]
025-AF3 MC45 1.5-2	1.75	1.75	8.96E+04	2.48E+08	2.45E+07	2.51E+06	7.81E+05	2.17E+08	9.08E+07	9.21E+05	5.89E+08	2.96E+07	1.94E+05	2.53E+05	8.47E+03	9.01E+04	1.33E+06	8.71E+05	5.43E+05
050-AG18 MC45 1.5-2	1.75	1.75	8.57E+04	2.38E+08	2.15E+07	2.07E+06	6.08E+05	2.05E+08	8.71E+07	8.35E+05	5.74E+08	2.59E+07	1.87E+05	2.49E+05	8.84E+03	6.99E+04	1.12E+06	7.39E+05	4.31E+05
026-AF4 MC45 2-2.5	2.25	2.25	6.88E+04	1.90E+08	2.09E+07	2.13E+06	8.94E+05	1.81E+08	7.52E+07	7.72E+05	4.86E+08	2.98E+07	1.72E+05	2.14E+05	5.17E+03	1.02E+05	1.36E+06	8.81E+05	5.72E+05
055-AG21 MC45 2-2.5	2.25	2.25	5.72E+04	1.47E+08	1.52E+07	1.43E+06	4.79E+05	1.40E+08	6.07E+07	5.79E+05	3.89E+08	2.43E+07	1.38E+05	1.68E+05	3.94E+03	5.29E+04	1.07E+06	7.05E+05	3.96E+05
028-AF5 MC45 2.5-3	2.75	2.75	6.85E+04	1.97E+08	2.09E+07	2.10E+06	6.85E+05	1.81E+08	7.56E+07	7.68E+05	4.87E+08	2.96E+07	2.73E+05	3.94E+05	3.48E+03	7.56E+04	1.32E+06	8.66E+05	4.97E+05
029-AF6.7 MC45 3-4	3.5	3.5	5.41E+04	1.38E+08	1.66E+07	1.71E+06	6.58E+05	1.31E+08	5.48E+07	5.54E+05	3.48E+08	2.93E+07	1.45E+05	1.69E+05	3.31E+03	7.32E+04	1.31E+06	8.62E+05	5.12E+05
038-AF21 KC27B 185-188	186.5	188.5	4.68E+04	1.20E+08	1.48E+07	1.45E+06	6.73E+05	1.30E+08	5.45E+07	5.49E+05	3.49E+08	2.77E+07	1.36E+05	1.54E+05	9.02E+03	7.78E+04	1.25E+06	8.18E+05	5.97E+05
031-AF9.10 KC27B 195-203	199	201	5.02E+04	1.33E+08	1.61E+07	1.62E+06	6.58E+05	1.43E+08	6.07E+07	6.04E+05	3.83E+08	2.92E+07	1.45E+05	1.67E+05	1.74E+04	7.69E+04	1.32E+06	8.61E+05	8.01E+05
032-AF14 KC27B 210-213	211.5	213.5	4.73E+04	1.23E+08	1.55E+07	1.57E+06	4.18E+05	1.30E+08	5.51E+07	5.67E+05	3.52E+08	2.87E+07	1.38E+05	1.56E+05	1.70E+04	4.91E+04	1.32E+06	8.53E+05	5.34E+05
034-AF15 KC27B 220-223	221.5	223.5	4.51E+04	1.09E+08	1.40E+07	1.42E+06	4.74E+05	1.16E+08	4.88E+07	4.91E+05	3.06E+08	2.88E+07	1.34E+05	1.46E+05	1.34E+04	5.50E+04	1.31E+06	8.52E+05	4.83E+05
041-AF26 KC27B 225-228	226.5	228.5	3.94E+04	8.94E+07	1.24E+07	1.23E+06	5.12E+05	9.58E+07	4.10E+07	4.01E+05	2.51E+08	2.74E+07	1.23E+05	1.32E+05	3.15E+03	5.93E+04	1.25E+06	8.15E+05	4.74E+05
043-AG2 KC27B 255-258	256.5	258.5	6.41E+04	1.91E+08	1.89E+07	1.82E+06	8.77E+05	1.93E+08	8.05E+07	8.11E+05	5.46E+08	2.75E+07	1.68E+05	2.12E+05	6.55E+04	9.89E+04	1.21E+06	7.94E+05	6.04E+05
040-AF22 JKC53 270-273	271.5	280	6.05E+04	1.72E+08	1.72E+07	1.67E+06	4.12E+05	1.67E+08	7.05E+07	7.13E+05	4.67E+08	2.75E+07	1.54E+05	1.86E+05	2.98E+04	4.65E+04	1.22E+06	7.94E+05	4.34E+05
047-AG8 JKC53 280-283	281.5	290	7.37E+04	2.10E+08	1.93E+07	1.86E+06	4.10E+05	1.88E+08	7.92E+07	7.80E+05	5.31E+08	2.79E+07	1.75E+05	2.26E+05	2.42E+05	4.67E+04	1.18E+06	8.01E+05	6.24E+05
053-AG20 JKC53 280-283	281.5	290	7.02E+04	2.02E+08	1.86E+07	1.76E+06	5.12E+05	1.89E+08	8.10E+07	7.89E+05	5.42E+08	2.65E+07	1.69E+05	2.18E+05	1.74E+05	5.67E+04	1.11E+06	7.44E+05	4.10E+05
046-AG7 JKC53 290-293	291.5	300	7.58E+04	2.16E+08	1.95E+07	1.85E+06	8.53E+05	1.99E+08	8.32E+07	8.19E+05	5.59E+08	2.70E+07	2.06E+05	2.84E+05	6.43E+04	9.50E+04	1.16E+06	8.15E+05	1.28E+06
052-AG19 JKC53 290-293	291.5	300	6.76E+04	1.97E+08	1.70E+07	1.60E+06	5.15E+05	1.87E+08	7.97E+07	7.84E+05	5.35E+08	2.57E+07	1.63E+05	2.08E+05	1.10E+04	5.95E+04	1.14E+06	7.41E+05	7.31E+05
035-AF18 JPC27 230-232	231	263	4.70E+04	1.16E+08	1.42E+07	1.43E+06	4.79E+05	1.21E+08	5.10E+07	5.20E+05	3.25E+08	2.87E+07	1.34E+05	1.52E+05	4.86E+03	5.57E+04	1.31E+06	8.44E+05	4.93E+05
037-AF20 JPC27 925-927	926	958	4.59E+04	1.08E+08	1.33E+07	1.33E+06	5.09E+05	1.11E+08	4.77E+07	4.75E+05	2.99E+08	2.83E+07	1.27E+05	1.39E+05	2.00E+03	5.83E+04	1.26E+06	8.33E+05	4.56E+05
044-AG6 JPC27 960-962	961	993	5.07E+04	1.30E+08	1.41E+07	1.36E+06	5.27E+05	1.33E+08	5.71E+07	5.65E+05	3.68E+08	2.66E+07	1.38E+05	1.60E+05	4.75E+03	6.02E+04	1.19E+06	8.04E+05	4.53E+05
049-AG15 MC61 2.5-3	2.75	2.75	4.24E+04	9.71E+07	1.24E+07	1.21E+06	5.27E+05	1.01E+08	4.35E+07	4.21E+05	2.73E+08	2.58E+07	1.26E+05	1.41E+05	1.73E+03	6.00E+04	1.16E+06	7.61E+05	4.31E+05

Table D.19 NBP1402 TEX₈₆ values and calibrated temperatures using Shevenell et al., 2011; BIT index; Ring Index; Methane Index

Cruise	Core	Av Depth (cmbsf)	Av Depth (cmcd)	1302 GDGT-0	1300 GDGT-1	1298 GDGT-2	1296 GDGT-3	1292 crenarchaeol	1292 Cren. Isomer	1050 GDGT-I	1036 GDGT-II	1022 GDGT-III	TEX86	TEX86-derived temp (°C)	BIT	Delta RI (RI _{TEX} -RI _{sample})	Methane Index
NBP1402	MC45	1.5	1.5	1.35E+09	1.15E+08	2.33E+07	1.52E+07	1.28E+09	7.76E+06	9.84E+07	1.54E+08	6.68E+07	0.287	-1.355	0.200	0.756	0.107
NBP1402	MC45	1.5	1.5	2.56E+09	1.74E+08	3.88E+07	1.97E+07	2.22E+09	1.43E+07	4.00E+07	6.24E+07	3.32E+07	0.296	-0.663	0.057	0.674	0.094
NBP1402	MC45	2.5	2.5	1.38E+09	1.36E+08	2.93E+07	1.75E+07	1.30E+09	9.44E+06	1.65E+08	2.77E+08	1.24E+08	0.292	-0.940	0.303	0.735	0.123
NBP1402	MC45	2.5	2.5	5.25E+09	3.46E+08	7.16E+07	3.68E+07	3.43E+09	1.82E+07	9.46E+07	1.37E+08	7.44E+07	0.268	-2.863	0.082	0.434	0.116
NBP1402	MC45	3.5	3.5	6.19E+09	4.37E+08	9.96E+07	4.74E+07	5.09E+09	4.08E+07	1.67E+08	2.43E+08	1.33E+08	0.300	-0.279	0.096	0.613	0.102
NBP1402	MC45	4.5	4.5	3.87E+09	2.65E+08	5.84E+07	2.79E+07	3.04E+09	2.54E+07	1.19E+08	1.69E+08	8.38E+07	0.297	-0.582	0.109	0.575	0.103
NBP1402	MC45	4.5	4.5	2.45E+09	1.60E+08	3.33E+07	1.73E+07	1.88E+09	1.16E+07	6.19E+07	8.94E+07	4.46E+07	0.280	-1.931	0.095	0.574	0.100
NBP1402	MC45	5.5	5.5	3.11E+09	2.11E+08	4.48E+07	2.26E+07	2.45E+09	1.68E+07	8.82E+07	1.18E+08	6.18E+07	0.285	-1.482	0.098	0.594	0.101
NBP1402	MC45	6.5	6.5	3.96E+09	2.62E+08	5.89E+07	2.82E+07	3.16E+09	2.12E+07	1.34E+08	1.66E+08	8.33E+07	0.293	-0.903	0.108	0.596	0.099
NBP1402	MC45	7.5	7.5	2.18E+09	2.19E+08	4.76E+07	2.60E+07	2.08E+09	1.70E+07	4.79E+08	5.98E+08	2.58E+08	0.293	-0.871	0.391	0.744	0.122
NBP1402	MC45	8.5	8.5	5.13E+09	3.48E+08	7.61E+07	4.03E+07	3.73E+09	2.29E+07	2.03E+08	2.18E+08	1.09E+08	0.286	-1.420	0.124	0.514	0.110
NBP1402	MC45	9.5	9.5	4.67E+09	3.26E+08	6.90E+07	3.52E+07	4.06E+09	2.39E+07	2.05E+08	2.12E+08	1.08E+08	0.282	-1.744	0.114	0.688	0.095
NBP1402	MC45	10.5	10.5	2.93E+09	1.97E+08	4.29E+07	2.32E+07	2.32E+09	1.50E+07	1.27E+08	1.22E+08	6.08E+07	0.291	-0.991	0.118	0.590	0.102
NBP1402	MC45	11.5	11.5	9.38E+09	6.65E+08	1.40E+08	7.43E+07	7.45E+09	5.11E+07	5.18E+08	4.25E+08	2.27E+08	0.285	-1.495	0.136	0.598	0.105
NBP1402	MC45	11.5	11.5	4.05E+09	2.73E+08	5.86E+07	3.08E+07	3.13E+09	1.81E+07	2.09E+08	1.79E+08	9.48E+07	0.282	-1.708	0.134	0.576	0.103
NBP1402	MC45	12.5	12.5	4.77E+09	3.05E+08	6.40E+07	3.35E+07	3.49E+09	2.16E+07	2.51E+08	1.75E+08	9.33E+07	0.281	-1.815	0.130	0.528	0.103
NBP1402	MC45	13.5	13.5	2.50E+09	2.44E+08	5.34E+07	2.95E+07	2.24E+09	1.84E+07	7.92E+08	5.55E+08	2.45E+08	0.294	-0.814	0.416	0.686	0.126
NBP1402	MC45	14.5	14.5	1.29E+10	8.87E+08	1.96E+08	9.75E+07	8.65E+09	5.94E+07	6.64E+08	4.07E+08	2.08E+08	0.285	-1.531	0.129	0.437	0.119
NBP1402	MC45	16.5	16.5	1.36E+10	1.02E+09	2.36E+08	1.17E+08	1.11E+10	7.27E+07	8.83E+08	4.80E+08	2.53E+08	0.294	-0.769	0.127	0.614	0.109
NBP1402	MC45	17.5	17.5	1.49E+10	1.05E+09	2.39E+08	1.19E+08	1.03E+10	5.01E+07	8.65E+08	4.56E+08	2.47E+08	0.281	-1.840	0.133	0.464	0.120
NBP1402	MC45	18.5	18.5	9.35E+09	6.14E+08	1.34E+08	6.85E+07	5.79E+09	4.13E+07	5.06E+08	2.88E+08	1.55E+08	0.284	-1.575	0.141	0.369	0.123
NBP1402	MC45	19.5	19.5	8.47E+09	6.39E+08	1.35E+08	7.14E+07	7.19E+09	3.89E+07	5.13E+08	3.05E+08	1.55E+08	0.277	-2.132	0.119	0.665	0.105
NBP1402	MC45	19.5	19.5	1.18E+10	8.15E+08	1.77E+08	8.80E+07	7.87E+09	4.88E+07	6.91E+08	4.05E+08	2.19E+08	0.278	-2.074	0.143	0.442	0.120
NBP1402	MC45	20.5	20.5	4.21E+09	2.98E+08	6.20E+07	3.37E+07	3.68E+09	2.01E+07	2.12E+08	1.31E+08	6.88E+07	0.280	-1.910	0.101	0.696	0.096
NBP1402	MC45	21.5	21.5	6.73E+09	4.61E+08	9.25E+07	5.03E+07	4.67E+09	2.47E+07	2.86E+08	1.77E+08	7.77E+07	0.267	-2.977	0.104	0.490	0.114
NBP1402	MC45	21.5	21.5	4.97E+09	3.33E+08	6.65E+07	3.61E+07	3.52E+09	2.19E+07	2.28E+08	1.38E+08	7.33E+07	0.272	-2.516	0.111	0.505	0.109
NBP1402	MC45	22.5	22.5	9.81E+09	7.05E+08	1.45E+08	7.92E+07	6.75E+09	4.19E+07	4.55E+08	2.67E+08	1.39E+08	0.274	-2.392	0.113	0.473	0.120
NBP1402	MC45	22.5	22.5	6.37E+09	4.36E+08	9.34E+07	4.94E+07	5.30E+09	2.36E+07	3.10E+08	1.74E+08	9.41E+07	0.276	-2.217	0.098	0.653	0.098
NBP1402	MC45	23.5	22.5	6.53E+09	4.26E+08	8.80E+07	4.47E+07	4.69E+09	2.71E+07	2.77E+08	1.88E+08	1.02E+08	0.273	-2.479	0.108	0.518	0.106
NBP1402	MC45	24.5	24.5	1.12E+09	6.85E+07	1.53E+07	8.83E+06	1.02E+09	5.90E+06	4.57E+07	3.61E+07	1.90E+07	0.305	0.096	0.090	0.716	0.083
NBP1402	MC45	26.5	26.5	6.13E+09	4.04E+08	8.18E+07	4.27E+07	4.21E+09	2.56E+07	2.67E+08	1.83E+08	9.55E+07	0.271	-2.613	0.115	0.478	0.111
NBP1402	MC45	27.5	27.5	2.34E+09	1.60E+08	3.10E+07	1.77E+07	1.95E+09	1.22E+07	1.19E+08	7.88E+07	4.57E+07	0.276	-2.234	0.111	0.655	0.096
NBP1402	MC45	27.5	27.5	1.70E+09	1.15E+08	2.27E+07	1.31E+07	1.43E+09	7.48E+06	8.93E+07	6.55E+07	3.55E+07	0.274	-2.387	0.117	0.669	0.095

Table D.19 (continued)

NBP1402	MC45	29.5	29.5	1.54E+09	1.08E+08	2.53E+07	1.50E+07	1.38E+09	8.22E+06	4.11E+08	2.08E+08	6.66E+07	0.310	0.495	0.332	0.686	0.097
NBP1402	MC45	29.5	29.5	1.19E+09	7.02E+07	1.55E+07	9.88E+06	1.02E+09	6.11E+06	7.76E+07	4.47E+07	2.25E+07	0.310	0.485	0.125	0.647	0.085
NBP1402	MC61	1.5	1.5	6.49E+09	4.59E+08	1.01E+08	5.00E+07	5.06E+09	3.57E+07	1.22E+08	1.76E+08	9.04E+07	0.2893	-1.160	0.071	0.575	0.107
NBP1402	MC61	1.5	1.5	5.85E+09	4.16E+08	8.95E+07	4.30E+07	5.10E+09	3.03E+07	9.43E+07	1.50E+08	8.36E+07	0.28112	-1.814	0.060	0.691	0.097
NBP1402	MC61	2.5	2.5	6.09E+09	4.41E+08	1.01E+08	4.90E+07	4.65E+09	3.62E+07	1.42E+08	2.04E+08	1.08E+08	0.2962	-0.608	0.089	0.546	0.112
NBP1402	MC61	2.5	2.5	6.18E+09	4.56E+08	9.81E+07	5.08E+07	5.41E+09	3.21E+07	1.22E+08	1.86E+08	8.96E+07	0.28408	-1.578	0.068	0.690	0.100
NBP1402	MC61	3.5	3.5	5.53E+09	4.09E+08	8.87E+07	4.50E+07	4.72E+09	3.25E+07	1.40E+08	1.95E+08	1.03E+08	0.28871	-1.208	0.085	0.661	0.103
NBP1402	MC61	4.5	4.5	6.89E+09	4.75E+08	1.09E+08	5.34E+07	5.20E+09	4.00E+07	1.88E+08	2.36E+08	1.27E+08	0.29869	-0.408	0.096	0.534	0.108
NBP1402	MC61	5.5	5.5	7.23E+09	5.20E+08	1.15E+08	5.83E+07	5.16E+09	3.57E+07	2.57E+08	3.02E+08	1.45E+08	0.28709	-1.337	0.120	0.493	0.118
NBP1402	MC61	6.5	6.5	8.23E+09	6.08E+08	1.34E+08	6.75E+07	6.33E+09	4.57E+07	3.09E+08	3.25E+08	1.57E+08	0.28902	-1.183	0.111	0.561	0.113
NBP1402	MC61	7.5	7.5	6.88E+09	5.07E+08	1.11E+08	5.59E+07	4.85E+09	3.69E+07	2.35E+08	2.60E+08	1.47E+08	0.2867	-1.368	0.117	0.480	0.121
NBP1402	MC61	8.5	8.5	5.73E+09	4.15E+08	9.49E+07	4.41E+07	4.44E+09	3.25E+07	2.22E+08	2.38E+08	1.36E+08	0.29251	-0.903	0.118	0.565	0.110
NBP1402	MC61	9.5	9.5	6.88E+09	5.11E+08	1.12E+08	5.33E+07	5.52E+09	3.91E+07	3.07E+08	2.69E+08	1.51E+08	0.28603	-1.421	0.116	0.604	0.109
NBP1402	MC61	11.5	11.5	7.83E+09	5.98E+08	1.32E+08	6.25E+07	6.49E+09	4.70E+07	4.41E+08	3.23E+08	1.62E+08	0.28737	-1.315	0.125	0.632	0.108
NBP1402	MC61	13.5	13.5	7.83E+09	5.67E+08	1.21E+08	6.04E+07	5.55E+09	3.96E+07	5.03E+08	3.28E+08	1.68E+08	0.28043	-1.869	0.152	0.493	0.118
NBP1402	MC61	15.5	15.5	7.76E+09	6.00E+08	1.31E+08	6.80E+07	6.61E+09	4.59E+07	4.68E+08	3.10E+08	1.75E+08	0.28986	-1.115	0.126	0.654	0.107
NBP1402	MC61	15.5	15.5	6.35E+09	4.53E+08	9.57E+07	4.75E+07	4.62E+09	2.39E+07	3.06E+08	2.02E+08	1.06E+08	0.26922	-2.766	0.117	0.529	0.114
NBP1402	MC61	17.5	17.5	9.87E+09	6.85E+08	1.48E+08	7.45E+07	7.32E+09	5.11E+07	4.43E+08	2.90E+08	1.47E+08	0.2851	-1.496	0.107	0.534	0.110
NBP1402	MC61	19.5	19.5	7.47E+09	5.80E+08	1.28E+08	6.60E+07	6.81E+09	4.49E+07	5.08E+08	2.86E+08	1.42E+08	0.29192	-0.950	0.121	0.718	0.101
NBP1402	MC61	21.5	21.5	9.43E+09	6.72E+08	1.55E+08	7.82E+07	7.12E+09	4.49E+07	5.06E+08	2.87E+08	1.66E+08	0.29226	-0.923	0.119	0.541	0.112
NBP1402	MC61	21.5	21.5	5.56E+09	3.38E+08	7.53E+07	3.79E+07	4.34E+09	2.22E+07	2.46E+08	1.25E+08	8.16E+07	0.28614	-1.413	0.095	0.586	0.094
NBP1402	MC61	23.5	23.5	6.26E+09	4.09E+08	8.53E+07	4.40E+07	4.74E+09	2.10E+07	3.10E+08	1.49E+08	1.01E+08	0.26882	-2.799	0.106	0.570	0.102
NBP1402	MC61	23.5	23.5	4.84E+09	3.16E+08	6.52E+07	3.37E+07	4.25E+09	2.04E+07	2.49E+08	1.25E+08	7.81E+07	0.27409	-2.377	0.096	0.710	0.088
NBP1402	MC61	25.5	25.5	4.67E+09	3.51E+08	7.29E+07	3.62E+07	3.69E+09	2.06E+07	1.64E+08	1.26E+08	8.24E+07	0.26991	-2.712	0.092	0.604	0.110
NBP1402	MC61	27.5	27.5	4.39E+09	3.36E+08	6.36E+07	3.40E+07	3.69E+09	2.14E+07	2.21E+08	1.51E+08	8.85E+07	0.26137	-3.394	0.111	0.670	0.105
NBP1402	MC61	29.5	29.5	2.98E+09	2.25E+08	4.59E+07	2.52E+07	2.78E+09	1.56E+07	1.36E+08	1.14E+08	6.68E+07	0.2784	-2.032	0.102	0.757	0.096
NBP1402	MC61	29.5	29.5	2.17E+09	1.44E+08	2.74E+07	1.64E+07	1.87E+09	8.81E+06	8.67E+07	7.13E+07	3.67E+07	0.26743	-2.910	0.094	0.699	0.091
NBP1402	KC27B	31.5	33.5	1.08E+10	7.83E+08	1.61E+08	8.51E+07	8.45E+09	5.09E+07	5.01E+08	2.93E+08	1.63E+08	0.275	-2.337	0.102	0.589	0.108
NBP1402	KC27B	36.5	38.5	1.62E+09	1.16E+08	2.28E+07	1.16E+07	1.49E+09	6.38E+06	1.57E+08	7.01E+07	5.82E+07	0.260	-3.486	0.161	0.762	0.091
NBP1402	KC27B	41.5	43.5	4.31E+09	3.26E+08	5.85E+07	3.52E+07	3.98E+09	2.34E+07	2.30E+08	1.59E+08	8.55E+07	0.264	-3.152	0.107	0.762	0.095
NBP1402	KC27B	46.5	48.5	6.53E+09	4.69E+08	9.29E+07	4.76E+07	5.32E+09	3.13E+07	3.50E+08	1.64E+08	8.64E+07	0.268	-2.846	0.101	0.639	0.102
NBP1402	KC27B	51.5	53.5	6.77E+09	5.55E+08	1.03E+08	5.49E+07	4.96E+09	3.29E+07	3.56E+08	0.00E+00	1.56E+08	0.256	-3.837	0.094	0.541	0.125
NBP1402	KC27B	56.5	58.5	5.35E+09	3.86E+08	8.04E+07	4.31E+07	4.32E+09	2.32E+07	3.34E+08	0.00E+00	1.11E+08	0.275	-2.273	0.093	0.622	0.105
NBP1402	KC27B	61.5	63.5	2.77E+09	1.80E+08	3.94E+07	1.99E+07	2.36E+09	1.30E+07	1.27E+08	8.11E+07	4.04E+07	0.287	-1.345	0.095	0.669	0.091
NBP1402	KC27B	66.5	68.5	2.57E+09	1.49E+08	3.61E+07	2.20E+07	2.08E+09	1.14E+07	2.41E+08	0.00E+00	0.00E+00	0.318	1.142	0.104	0.586	0.090
NBP1402	KC27B	71.5	73.5	1.19E+09	6.68E+07	1.71E+07	1.05E+07	1.03E+09	5.45E+06	1.15E+08	0.00E+00	0.00E+00	0.331	2.154	0.101	0.637	0.083
NBP1402	KC27B	71.5	73.5	2.17E+08	1.11E+07	2.33E+06	2.07E+06	1.90E+08	6.50E+05	1.91E+07	6.61E+06	5.94E+06	0.313	0.708	0.143	0.676	0.075

Table D.19 (continued)

NBP1402	KC27B	76.5	78.5	8.29E+09	6.01E+08	1.18E+08	6.16E+07	6.05E+09	3.97E+07	3.36E+08	0.00E+00	0.00E+00	0.267	-2.917	0.053	0.533	0.114
NBP1402	KC27B	76.5	78.5	3.32E+09	2.31E+08	4.51E+07	2.39E+07	2.69E+09	1.53E+07	1.30E+08	9.71E+07	4.79E+07	0.268	-2.901	0.093	0.633	0.100
NBP1402	KC27B	81.5	83.5	7.21E+09	5.20E+08	1.14E+08	5.81E+07	5.96E+09	3.58E+07	4.09E+08	0.00E+00	1.51E+08	0.286	-1.455	0.086	0.634	0.103
NBP1402	KC27B	86.5	88.5	5.69E+09	4.17E+08	8.71E+07	4.65E+07	4.22E+09	2.53E+07	3.15E+08	0.00E+00	1.06E+08	0.276	-2.231	0.091	0.539	0.115
NBP1402	KC27B	91.5	93.5	2.06E+09	1.50E+08	3.11E+07	1.72E+07	1.88E+09	9.52E+06	1.02E+08	0.00E+00	7.00E+07	0.278	-2.046	0.084	0.737	0.095
NBP1402	KC27B	96.5	98.5	6.13E+09	4.29E+08	8.92E+07	4.91E+07	4.61E+09	3.01E+07	3.39E+08	0.00E+00	1.28E+08	0.282	-1.753	0.092	0.549	0.109
NBP1402	KC27B	101.5	103.5	2.77E+09	1.90E+08	3.66E+07	1.95E+07	2.03E+09	1.08E+07	1.25E+08	7.61E+07	4.61E+07	0.260	-3.473	0.108	0.548	0.107
NBP1402	KC27B	101.5	103.5	5.90E+09	4.28E+08	8.84E+07	4.53E+07	4.42E+09	3.22E+07	3.17E+08	2.47E+08	1.27E+08	0.280	-1.940	0.135	0.545	0.112
NBP1402	KC27B	106.5	108.5	5.90E+09	4.28E+08	8.84E+07	4.53E+07	4.42E+09	3.22E+07	3.17E+08	2.47E+08	1.27E+08	0.280	-1.940	0.135	0.545	0.112
NBP1402	JPC27	6	60.2	1.09E+09	7.69E+07	1.83E+07	1.35E+07	1.05E+09	2.66E+06	3.71E+08	2.05E+08	9.18E+07	0.309	0.432	0.389	0.757	0.094
NBP1402	JPC27	6	60.2	6.03E+09	3.63E+08	8.59E+07	4.55E+07	4.07E+09	2.55E+07	2.53E+08	1.19E+08	5.97E+07	0.302	-0.152	0.096	0.432	0.108
NBP1402	JPC27	11	70	9.73E+08	6.07E+07	1.50E+07	7.53E+06	8.82E+08	3.80E+06	9.17E+07	4.44E+07	2.77E+07	0.303	-0.101	0.157	0.711	0.086
NBP1402	JPC27	11	70	1.03E+09	6.22E+07	1.39E+07	8.44E+06	9.19E+08	4.60E+06	6.51E+07	2.89E+07	2.05E+07	0.302	-0.125	0.111	0.702	0.084
NBP1402	JPC27	26	84.8	2.10E+09	1.39E+08	3.83E+07	1.61E+07	2.01E+09	1.07E+07	1.35E+08	1.04E+08	5.51E+07	0.319	1.213	0.128	0.741	0.087
NBP1402	JPC27	31	89.1	2.05E+09	1.52E+08	2.85E+07	1.44E+07	1.91E+09	9.23E+06	1.67E+08	1.05E+08	5.62E+07	0.256	-3.852	0.129	0.777	0.092
NBP1402	JPC27	31	89.1	3.16E+09	2.31E+08	4.29E+07	2.48E+07	2.53E+09	1.46E+07	1.64E+08	9.77E+07	5.20E+07	0.262	-3.307	0.110	0.624	0.105
NBP1402	JPC27	36	92.7	1.65E+09	1.08E+08	2.89E+07	1.14E+07	1.52E+09	7.68E+06	1.37E+08	8.09E+07	4.17E+07	0.308	0.304	0.146	0.718	0.088
NBP1402	JPC27	46	101.9	1.24E+09	8.53E+07	1.64E+07	8.76E+06	1.08E+09	7.18E+06	1.18E+08	7.37E+07	4.09E+07	0.275	-2.306	0.177	0.705	0.092
NBP1402	JPC27	51	105.6	1.98E+09	1.37E+08	3.10E+07	1.65E+07	1.48E+09	8.44E+06	3.47E+08	2.21E+08	6.14E+07	0.290	-1.109	0.298	0.535	0.110
NBP1402	JPC27	56	109.2	2.37E+09	1.68E+08	3.31E+07	1.82E+07	2.15E+09	1.28E+07	2.19E+08	1.15E+08	7.34E+07	0.276	-2.213	0.159	0.735	0.092
NBP1402	JPC27	61	113.0	2.31E+09	1.44E+08	3.01E+07	1.70E+07	2.06E+09	9.79E+06	1.45E+08	9.31E+07	5.20E+07	0.283	-1.630	0.124	0.716	0.085
NBP1402	JPC27	66	114.8	2.43E+09	1.63E+08	3.41E+07	1.85E+07	2.29E+09	1.21E+07	1.55E+08	1.19E+08	6.41E+07	0.284	-1.562	0.128	0.769	0.085
NBP1402	JPC27	71	116.4	3.58E+09	2.29E+08	5.12E+07	2.75E+07	3.01E+09	1.77E+07	2.61E+08	1.63E+08	9.63E+07	0.296	-0.634	0.148	0.645	0.092
NBP1402	JPC27	76	124.5	1.79E+09	1.18E+08	3.08E+07	1.37E+07	1.74E+09	9.56E+06	1.55E+08	9.99E+07	6.93E+07	0.314	0.831	0.157	0.763	0.085
NBP1402	JPC27	81	128.9	1.06E+09	9.03E+07	1.95E+07	1.25E+07	9.86E+08	6.91E+06	3.68E+08	2.67E+08	1.22E+08	0.301	-0.211	0.434	0.724	0.110
NBP1402	JPC27	101	137.8	6.46E+09	4.40E+08	1.03E+08	5.43E+07	5.44E+09	3.23E+07	3.64E+08	1.89E+08	1.22E+08	0.301	-0.250	0.110	0.637	0.098
NBP1402	JPC27	126	158	9.11E+08	5.54E+07	1.47E+07	9.89E+06	1.01E+09	4.56E+06	1.25E+08	8.32E+07	7.40E+07	0.345	3.283	0.219	0.849	0.073
NBP1402	JPC27	126	158	1.76E+09	9.46E+07	2.37E+07	1.54E+07	1.74E+09	8.48E+06	4.99E+07	3.38E+07	3.26E+07	0.335	2.465	0.063	0.763	0.071
NBP1402	JPC27	131	163	5.80E+09	3.27E+08	7.98E+07	4.83E+07	5.46E+09	2.55E+07	1.58E+08	8.84E+07	8.22E+07	0.319	1.255	0.057	0.731	0.077
NBP1402	JPC27	141	173	2.80E+09	1.71E+08	4.27E+07	2.31E+07	2.52E+09	1.17E+07	1.46E+08	5.21E+07	5.20E+07	0.312	0.630	0.090	0.695	0.086
NBP1402	JPC27	151	183	1.67E+09	1.15E+08	2.43E+07	1.46E+07	1.35E+09	5.76E+06	2.81E+08	2.08E+08	6.18E+07	0.280	-1.926	0.290	0.620	0.102
NBP1402	JPC27	151	183	1.54E+09	9.45E+07	2.07E+07	1.24E+07	1.32E+09	6.32E+06	7.30E+07	6.57E+07	3.74E+07	0.294	-0.767	0.118	0.670	0.088
NBP1402	JPC27	161	193	1.35E+09	1.09E+08	2.92E+07	1.89E+07	1.45E+09	1.12E+07	6.54E+08	3.65E+08	1.83E+08	0.352	3.849	0.453	0.800	0.097
NBP1402	JPC27	161	193	6.73E+09	4.47E+08	1.03E+08	5.71E+07	5.64E+09	3.55E+07	4.36E+08	2.44E+08	1.49E+08	0.304	0.001	0.128	0.631	0.097
NBP1402	JPC27	171	203	8.48E+09	5.03E+08	1.25E+08	6.79E+07	6.51E+09	3.89E+07	3.58E+08	1.71E+08	1.36E+08	0.315	0.914	0.093	0.538	0.096
NBP1402	JPC27	176	208	1.40E+09	1.00E+08	2.39E+07	1.64E+07	1.37E+09	8.39E+06	2.67E+08	1.87E+08	9.75E+07	0.327	1.873	0.287	0.745	0.093
NBP1402	JPC27	201	233	1.23E+09	7.22E+07	1.81E+07	1.04E+07	1.14E+09	5.49E+06	2.22E+08	1.27E+08	7.94E+07	0.320	1.311	0.273	0.716	0.081

Table D.19 (continued)

NBP1402	JPC27	201	233	2.03E+09	1.07E+08	2.75E+07	1.48E+07	1.70E+09	8.54E+06	6.96E+07	3.90E+07	2.98E+07	0.323	1.536	0.075	0.620	0.080
NBP1402	JPC27	211	243	9.08E+09	5.35E+08	1.24E+08	6.49E+07	6.73E+09	4.25E+07	4.18E+08	2.17E+08	1.64E+08	0.302	-0.163	0.106	0.521	0.097
NBP1402	JPC27	211	243	5.24E+09	3.14E+08	7.12E+07	3.79E+07	4.19E+09	2.42E+07	2.49E+08	1.35E+08	9.45E+07	0.298	-0.486	0.102	0.599	0.091
NBP1402	JPC27	226	258	1.69E+09	1.20E+08	2.98E+07	1.92E+07	1.73E+09	8.98E+06	2.29E+08	1.69E+08	9.97E+07	0.326	1.760	0.223	0.795	0.088
NBP1402	JPC27	231	263	8.82E+09	6.15E+08	1.43E+08	7.78E+07	6.74E+09	4.28E+07	2.49E+08	2.00E+08	1.17E+08	0.300	-0.301	0.077	0.545	0.110
NBP1402	JPC27	241	273	3.01E+09	2.01E+08	3.98E+07	2.79E+07	2.60E+09	1.39E+07	2.16E+08	1.17E+08	7.58E+07	0.288	-1.231	0.136	0.678	0.093
NBP1402	JPC27	241	273	5.41E+09	3.71E+08	8.47E+07	4.49E+07	4.08E+09	2.39E+07	2.50E+08	1.30E+08	8.27E+07	0.293	-0.900	0.102	0.542	0.109
NBP1402	JPC27	251	283	2.48E+09	2.34E+08	5.29E+07	3.44E+07	2.48E+09	2.29E+07	5.16E+08	4.36E+08	2.04E+08	0.320	1.309	0.318	0.763	0.114
NBP1402	JPC27	261	293	2.57E+09	1.75E+08	3.46E+07	2.23E+07	2.38E+09	1.48E+07	2.12E+08	1.56E+08	8.25E+07	0.290	-1.081	0.159	0.742	0.088
NBP1402	JPC27	276	308	1.82E+09	1.47E+08	3.16E+07	2.24E+07	1.70E+09	9.75E+06	5.21E+08	2.87E+08	1.68E+08	0.302	-0.165	0.365	0.724	0.106
NBP1402	JPC27	281	313	3.43E+09	2.20E+08	3.95E+07	3.04E+07	2.85E+09	1.71E+07	1.80E+08	1.21E+08	8.32E+07	0.284	-1.622	0.119	0.649	0.092
NBP1402	JPC27	291	323	5.41E+09	3.30E+08	6.32E+07	5.12E+07	4.60E+09	2.53E+07	2.95E+08	2.09E+08	1.78E+08	0.298	-0.504	0.129	0.658	0.088
NBP1402	JPC27	326	358	2.44E+09	1.62E+08	3.41E+07	2.13E+07	2.32E+09	1.48E+07	2.11E+08	1.62E+08	9.50E+07	0.302	-0.169	0.168	0.754	0.085
NBP1402	JPC27	326	358	2.11E+09	1.30E+08	2.86E+07	1.72E+07	1.76E+09	1.05E+07	1.04E+08	8.01E+07	4.73E+07	0.302	-0.131	0.116	0.633	0.091
NBP1402	JPC27	351	383	1.30E+09	8.24E+07	1.54E+07	1.20E+07	1.25E+09	6.21E+06	1.01E+08	5.07E+07	5.31E+07	0.289	-1.144	0.141	0.786	0.080
NBP1402	JPC27	376	408	1.28E+09	7.58E+07	1.40E+07	1.20E+07	1.47E+09	6.73E+06	7.88E+07	4.56E+07	5.75E+07	0.302	-0.174	0.110	0.948	0.065
NBP1402	JPC27	391	423	5.65E+09	3.42E+08	7.52E+07	4.60E+07	5.08E+09	2.35E+07	1.37E+08	8.99E+07	8.94E+07	0.297	-0.534	0.059	0.711	0.083
NBP1402	JPC27	401	433	1.83E+09	1.04E+08	2.10E+07	1.44E+07	1.43E+09	5.42E+06	1.14E+08	5.26E+07	3.35E+07	0.282	-1.755	0.123	0.595	0.089
NBP1402	JPC27	406	438	4.58E+09	2.65E+08	6.00E+07	3.70E+07	3.60E+09	1.99E+07	1.34E+08	7.16E+07	6.61E+07	0.306	0.166	0.070	0.574	0.091
NBP1402	JPC27	426	458	2.71E+09	1.59E+08	3.69E+07	2.23E+07	2.23E+09	1.10E+07	6.94E+07	5.98E+07	4.35E+07	0.307	0.264	0.072	0.613	0.089
NBP1402	JPC27	451	483	4.46E+09	2.57E+08	5.72E+07	3.97E+07	4.03E+09	1.92E+07	2.08E+08	1.05E+08	7.08E+07	0.312	0.618	0.087	0.701	0.080
NBP1402	JPC27	451	483	3.22E+09	1.99E+08	5.12E+07	3.26E+07	2.74E+09	1.10E+07	6.06E+08	2.77E+08	1.45E+08	0.323	1.509	0.273	0.625	0.093
NBP1402	JPC27	501	533	9.12E+08	6.17E+07	1.36E+07	1.01E+07	9.78E+08	4.29E+06	1.54E+08	9.41E+07	6.77E+07	0.312	0.662	0.244	0.861	0.080
NBP1402	JPC27	526	558	3.06E+09	1.86E+08	4.70E+07	2.65E+07	3.01E+09	1.49E+07	9.02E+07	5.78E+07	5.58E+07	0.322	1.469	0.063	0.768	0.079
NBP1402	JPC27	551	583	3.03E+09	1.59E+08	3.92E+07	2.87E+07	2.50E+09	1.10E+07	6.57E+07	3.78E+07	3.55E+07	0.332	2.271	0.053	0.588	0.083
NBP1402	JPC27	576	608	5.61E+09	3.42E+08	8.11E+07	4.82E+07	4.30E+09	2.38E+07	1.88E+08	1.31E+08	1.30E+08	0.309	0.434	0.095	0.543	0.098
NBP1402	JPC27	596	628	1.78E+09	1.10E+08	2.69E+07	1.46E+07	1.61E+09	6.17E+06	6.99E+07	4.09E+07	4.42E+07	0.302	-0.172	0.088	0.712	0.086
NBP1402	JPC27	606	638	3.72E+09	2.47E+08	5.66E+07	3.03E+07	3.46E+09	2.04E+07	1.13E+08	8.47E+07	6.11E+07	0.303	-0.085	0.069	0.735	0.088
NBP1402	JPC27	626	658	2.34E+09	1.24E+08	3.19E+07	2.03E+07	2.34E+09	1.15E+07	8.69E+07	5.32E+07	5.12E+07	0.339	2.846	0.076	0.767	0.070
NBP1402	JPC27	626	658	3.86E+09	2.24E+08	5.09E+07	3.23E+07	3.45E+09	1.54E+07	1.03E+08	6.09E+07	5.80E+07	0.306	0.146	0.061	0.698	0.081
NBP1402	JPC27	641	673	2.20E+09	1.46E+08	4.02E+07	1.76E+07	2.18E+09	8.92E+06	9.09E+07	5.46E+07	4.22E+07	0.314	0.788	0.079	0.781	0.085
NBP1402	JPC27	651	683	4.75E+09	2.80E+08	6.20E+07	3.47E+07	3.54E+09	1.95E+07	1.07E+08	7.08E+07	6.10E+07	0.293	-0.854	0.063	0.536	0.096
NBP1402	JPC27	676	708	5.78E+09	3.53E+08	8.01E+07	4.78E+07	4.97E+09	2.38E+07	1.94E+08	1.34E+08	1.23E+08	0.301	-0.258	0.083	0.664	0.088
NBP1402	JPC27	701	733	9.77E+08	6.26E+07	1.47E+07	9.35E+06	1.01E+09	5.72E+06	1.76E+08	1.00E+08	9.23E+07	0.322	1.479	0.267	0.815	0.079
NBP1402	JPC27	726	758	2.32E+09	1.39E+08	2.99E+07	1.98E+07	2.10E+09	8.04E+06	9.24E+07	5.97E+07	8.59E+07	0.293	-0.825	0.102	0.723	0.082
NBP1402	JPC27	751	783	5.63E+09	3.04E+08	6.96E+07	4.71E+07	4.29E+09	2.01E+07	9.13E+07	7.26E+07	6.10E+07	0.310	0.494	0.050	0.540	0.089
NBP1402	JPC27	776	808	2.14E+09	9.92E+07	2.36E+07	1.48E+07	2.06E+09	6.79E+06	7.08E+07	4.88E+07	5.91E+07	0.313	0.734	0.080	0.770	0.062

NBP1402	JPC27	801	833	1.18E+09	6.84E+07	1.59E+07	1.09E+07	1.10E+09	5.38E+06	1.22E+08	7.82E+07	8.00E+07	0.320	1.292	0.203	0.721	0.079
NBP1402	JPC27	811	843	2.63E+09	1.69E+08	2.88E+07	2.55E+07	2.60E+09	1.11E+07	1.30E+08	9.29E+07	1.07E+08	0.279	-1.950	0.112	0.824	0.079
NBP1402	JPC27	821	853	3.07E+09	2.07E+08	3.28E+07	2.47E+07	2.40E+09	1.13E+07	1.41E+08	1.06E+08	8.70E+07	0.249	-4.353	0.122	0.618	0.099
NBP1402	JPC27	821	853	5.36E+09	3.29E+08	6.06E+07	3.90E+07	4.07E+09	1.66E+07	1.35E+08	1.02E+08	8.79E+07	0.261	-3.444	0.074	0.585	0.095
NBP1402	JPC27	826	858	6.85E+09	3.94E+08	8.66E+07	6.14E+07	5.22E+09	2.62E+07	2.22E+08	1.46E+08	1.05E+08	0.306	0.204	0.083	0.543	0.094
NBP1402	JPC27	831	863	2.75E+09	1.69E+08	3.04E+07	2.45E+07	2.52E+09	1.03E+07	2.01E+08	9.60E+07	7.56E+07	0.278	-2.058	0.129	0.754	0.081
NBP1402	JPC27	841	873	8.51E+09	5.82E+08	1.03E+08	8.58E+07	7.39E+09	3.86E+07	2.20E+08	1.88E+08	1.71E+08	0.281	-1.816	0.073	0.690	0.094
NBP1402	JPC27	851	883	2.00E+09	1.57E+08	3.07E+07	2.36E+07	1.76E+09	1.32E+07	3.67E+08	2.90E+08	1.49E+08	0.301	-0.251	0.314	0.675	0.106
NBP1402	JPC27	851	883	5.61E+09	3.06E+08	6.21E+07	4.09E+07	4.40E+09	2.07E+07	1.43E+08	1.07E+08	6.27E+07	0.288	-1.267	0.066	0.594	0.085
NBP1402	JPC27	856	888	7.55E+09	4.58E+08	8.98E+07	6.01E+07	5.31E+09	3.31E+07	3.42E+08	0.00E+00	1.62E+08	0.285	-1.465	0.087	0.489	0.102
NBP1402	JPC27	861	893	3.30E+09	1.90E+08	3.36E+07	2.28E+07	2.71E+09	1.32E+07	2.87E+08	2.46E+08	1.48E+08	0.268	-2.843	0.201	0.657	0.083
NBP1402	JPC27	866	898	8.25E+09	4.59E+08	1.03E+08	7.23E+07	6.44E+09	3.27E+07	6.69E+08	0.00E+00	2.83E+08	0.312	0.644	0.129	0.561	0.089
NBP1402	JPC27	871	903	5.21E+09	3.42E+08	6.77E+07	4.73E+07	4.64E+09	2.05E+07	6.31E+08	4.39E+08	2.70E+08	0.283	-1.626	0.224	0.714	0.089
NBP1402	JPC27	876	908	4.18E+09	2.58E+08	5.16E+07	3.97E+07	3.58E+09	1.72E+07	4.31E+08	3.32E+08	1.84E+08	0.296	-0.598	0.209	0.665	0.088
NBP1402	JPC27	881	913	2.68E+09	1.63E+08	3.01E+07	2.60E+07	2.57E+09	1.11E+07	2.90E+08	2.37E+08	1.34E+08	0.292	-0.952	0.204	0.782	0.078
NBP1402	JPC27	881	913	9.93E+09	5.61E+08	1.14E+08	8.45E+07	7.91E+09	3.92E+07	5.75E+08	4.53E+08	2.61E+08	0.298	-0.496	0.140	0.598	0.087
NBP1402	JPC27	886	918	9.38E+09	5.28E+08	1.28E+08	8.99E+07	7.45E+09	4.53E+07	6.56E+08	0.00E+00	3.12E+08	0.333	2.309	0.115	0.550	0.091
NBP1402	JPC27	886	918	3.45E+09	1.56E+08	3.43E+07	2.61E+07	2.88E+09	1.16E+07	1.40E+08	1.04E+08	6.25E+07	0.316	1.015	0.096	0.630	0.069
NBP1402	JPC27	886	918	7.91E+09	4.38E+08	9.60E+07	6.77E+07	6.81E+09	3.08E+07	4.58E+08	3.41E+08	2.27E+08	0.307	0.285	0.131	0.661	0.081
NBP1402	JPC27	891	923	3.02E+09	1.75E+08	3.72E+07	2.96E+07	3.13E+09	1.43E+07	3.33E+08	1.92E+08	1.37E+08	0.316	1.009	0.174	0.831	0.071
NBP1402	JPC27	896	928	6.48E+09	3.49E+08	7.95E+07	5.94E+07	5.64E+09	2.58E+07	4.92E+08	0.00E+00	2.41E+08	0.321	1.345	0.115	0.656	0.079
NBP1402	JPC27	901	933	7.44E+08	3.98E+07	7.57E+06	5.73E+06	7.85E+08	2.53E+06	5.83E+07	3.58E+07	4.66E+07	0.285	-1.527	0.152	0.889	0.063
NBP1402	JPC27	906	938	1.80E+09	1.23E+08	2.54E+07	1.71E+07	1.80E+09	7.80E+06	7.55E+07	5.91E+07	8.02E+07	0.291	-1.049	0.107	0.817	0.084
NBP1402	JPC27	911	943	3.76E+09	2.57E+08	4.87E+07	3.38E+07	3.62E+09	1.85E+07	8.76E+07	7.41E+07	1.07E+08	0.282	-1.720	0.069	0.792	0.085
NBP1402	JPC27	916	948	1.37E+09	8.87E+07	1.80E+07	1.15E+07	1.43E+09	5.98E+06	7.53E+07	5.91E+07	7.72E+07	0.286	-1.451	0.129	0.873	0.076
NBP1402	JPC27	921	953	1.46E+09	9.34E+07	1.67E+07	1.12E+07	1.59E+09	6.66E+06	9.16E+07	5.77E+07	5.94E+07	0.270	-2.694	0.116	0.929	0.071
NBP1402	JPC27	921	953	3.63E+09	2.11E+08	4.28E+07	2.90E+07	2.97E+09	1.75E+07	1.29E+08	8.46E+07	9.50E+07	0.297	-0.508	0.094	0.624	0.086
NBP1402	JPC27	926	958	1.41E+09	9.47E+07	2.15E+07	1.40E+07	1.43E+09	7.38E+06	2.64E+08	1.30E+08	1.15E+08	0.312	0.619	0.263	0.809	0.083
NBP1402	JPC27	931	963	2.17E+09	1.24E+08	2.49E+07	1.94E+07	2.11E+09	8.60E+06	7.04E+07	0.00E+00	4.89E+07	0.300	-0.323	0.053	0.789	0.073
NBP1402	JPC27	936	968	1.56E+09	9.46E+07	1.96E+07	1.23E+07	1.44E+09	9.36E+06	6.32E+07	4.44E+07	4.50E+07	0.304	0.011	0.096	0.734	0.080
NBP1402	JPC27	946	978	2.79E+09	1.62E+08	3.68E+07	2.18E+07	2.61E+09	1.34E+07	1.38E+08	5.90E+07	5.94E+07	0.308	0.344	0.089	0.739	0.077
NBP1402	JPC27	946	978	5.92E+08	2.83E+07	6.31E+06	3.74E+06	6.46E+08	2.39E+06	2.47E+07	1.05E+07	1.08E+07	0.306	0.136	0.066	0.902	0.056
NBP1402	JPC27	951	983	2.29E+09	1.84E+08	4.88E+07	2.78E+07	2.36E+09	1.57E+07	5.11E+08	3.24E+08	2.95E+08	0.334	2.382	0.323	0.785	0.099
NBP1402	JPC27	956	988	3.21E+09	1.75E+08	4.03E+07	2.39E+07	3.00E+09	1.64E+07	1.15E+08	0.00E+00	7.54E+07	0.315	0.930	0.060	0.732	0.073
NBP1402	JPC27	956	988	4.33E+09	2.59E+08	5.71E+07	3.21E+07	3.90E+09	1.97E+07	1.41E+08	7.09E+07	9.30E+07	0.296	-0.621	0.072	0.717	0.082
NBP1402	JPC27	961	993	2.15E+09	1.44E+08	2.62E+07	1.83E+07	2.79E+09	1.46E+07	1.38E+08	8.87E+07	9.70E+07	0.291	-1.027	0.104	1.074	0.063

Table D.20 NBP1402 Grain Size data.

Core	Avg depth (cmcd)	<0.46 bin	0.523	0.594	0.675	0.767	0.872	0.991	1.13	1.28	1.45	1.65	1.88	2.13	2.42	2.75	3.12	3.55	4.03	4.58	5.21	5.92	6.72	7.64	8.68	9.86
MC-45	1.25	0.00	0.00	0.00	0.00	0.00	0.00	0.00	0.15	0.56	0.88	1.21	1.46	1.66	2.07	2.46	2.76	3.09	3.21	3.28	3.36	3.44	3.51	3.66	3.74	3.80
MC-45	2.25	0.00	0.00	0.00	0.00	0.00	0.00	0.00	0.09	0.36	0.93	1.15	1.29	1.43	1.85	2.33	2.65	2.91	2.92	2.82	2.78	2.85	2.99	3.24	3.45	3.61
MC-45	2.25	0.00	0.00	0.00	0.00	0.00	0.00	0.00	0.13	0.53	0.86	1.11	1.23	1.34	1.71	2.09	2.36	2.59	2.62	2.57	2.61	2.72	2.88	3.11	3.28	3.40
MC-45	3.25	0.00	0.00	0.00	0.00	0.00	0.00	0.00	0.10	0.58	1.07	1.32	1.38	1.46	1.91	2.42	2.74	2.99	2.97	2.85	2.86	3.04	3.30	3.66	3.91	4.05
MC-45	3.25	0.00	0.00	0.00	0.00	0.00	0.00	0.00	0.17	0.65	1.02	1.36	1.58	1.76	2.20	2.64	2.93	3.19	3.22	3.23	3.36	3.61	3.93	4.30	4.48	4.48
MC-45	8.25	0.00	0.00	0.00	0.00	0.00	0.00	0.00	0.12	0.62	1.09	1.33	1.39	1.48	1.93	2.44	2.77	3.01	2.98	2.86	2.88	3.07	3.35	3.72	3.96	4.08
MC-45	8.25	0.00	0.00	0.00	0.00	0.00	0.00	0.00	0.15	0.68	1.16	1.46	1.59	1.71	2.20	2.74	3.11	3.43	3.46	3.37	3.39	3.54	3.77	4.10	4.36	4.53
MC-45	10.25	0.00	0.00	0.00	0.00	0.00	0.00	0.00	0.15	0.69	1.18	1.47	1.57	1.68	2.17	2.73	3.12	3.46	3.49	3.38	3.38	3.51	3.72	4.04	4.30	4.46
MC-45	12.25	0.00	0.00	0.00	0.00	0.00	0.00	0.00	0.14	0.64	1.10	1.38	1.49	1.61	2.07	2.59	2.96	3.28	3.31	3.22	3.23	3.35	3.55	3.87	4.12	4.30
MC-45	14.25	0.00	0.00	0.00	0.00	0.00	0.00	0.00	0.13	0.61	1.06	1.33	1.43	1.53	1.98	2.49	2.85	3.16	3.18	3.09	3.10	3.22	3.43	3.75	4.00	4.18
MC-45	16.25	0.00	0.00	0.00	0.00	0.00	0.00	0.00	0.14	0.64	1.08	1.38	1.50	1.63	2.09	2.61	2.98	3.31	3.35	3.28	3.30	3.42	3.61	3.92	4.15	4.32
MC-45	18.25	0.00	0.00	0.00	0.00	0.00	0.00	0.00	0.16	0.66	1.07	1.39	1.56	1.71	2.17	2.66	3.01	3.35	3.42	3.40	3.44	3.56	3.74	4.02	4.23	4.39
MC-45	21	0.00	0.00	0.00	0.00	0.00	0.00	0.00	0.00	0.13	0.64	0.91	1.19	1.44	1.89	2.34	2.68	3.03	3.16	3.25	3.36	3.49	3.66	3.92	4.12	4.29
MC-45	25	0.00	0.00	0.00	0.00	0.00	0.00	0.00	0.20	0.68	1.03	1.39	1.66	1.87	2.31	2.75	3.08	3.44	3.57	3.62	3.71	3.80	3.92	4.12	4.26	4.37
MC-45	27	0.00	0.00	0.00	0.00	0.00	0.00	0.00	0.00	0.08	0.43	0.65	0.83	1.02	1.40	1.82	2.17	2.54	2.74	2.88	3.06	3.28	3.52	3.87	4.15	4.40
MC-45	27	0.00	0.00	0.00	0.00	0.00	0.00	0.00	0.00	0.07	0.39	0.61	0.80	0.97	1.31	1.69	1.99	2.30	2.46	2.62	2.86	3.13	3.44	3.80	4.02	4.16
MC-45	31	0.00	0.00	0.00	0.00	0.00	0.00	0.00	0.17	0.56	0.84	1.12	1.32	1.47	1.82	2.16	2.41	2.68	2.76	2.78	2.85	2.95	3.09	3.32	3.51	3.71
MC-45	31	0.00	0.00	0.00	0.00	0.00	0.00	0.00	0.14	0.51	0.79	1.07	1.26	1.41	1.76	2.10	2.34	2.60	2.67	2.69	2.76	2.88	3.04	3.29	3.49	3.67
MC-45	33	0.00	0.00	0.00	0.00	0.00	0.00	0.00	0.09	0.46	0.83	1.09	1.25	1.40	1.79	2.22	2.53	2.82	2.89	2.89	2.94	3.05	3.22	3.50	3.74	3.95
MC-45	35	0.00	0.00	0.00	0.00	0.00	0.00	0.00	0.15	0.67	1.11	1.40	1.52	1.65	2.11	2.63	2.99	3.30	3.33	3.25	3.26	3.36	3.55	3.87	4.13	4.34
MC-45	35	0.00	0.00	0.00	0.00	0.00	0.00	0.00	0.12	0.58	0.99	1.24	1.33	1.43	1.83	2.29	2.61	2.88	2.88	2.78	2.77	2.88	3.07	3.38	3.64	3.86
KC-27B	32.5	0.00	0.00	0.00	0.00	0.00	0.00	0.00	0.02	0.22	0.75	1.06	1.38	1.67	2.17	2.69	3.10	3.55	3.78	3.97	4.18	4.36	4.55	4.80	4.92	4.96
KC-27B	32.5	0.00	0.00	0.00	0.00	0.00	0.00	0.00	0.04	0.21	0.65	0.93	1.19	1.43	1.85	2.27	2.59	2.94	3.11	3.28	3.51	3.75	4.00	4.28	4.39	4.37
KC-27B	36.5	0.00	0.00	0.00	0.00	0.00	0.00	0.00	0.08	0.40	0.76	1.08	1.37	1.63	2.09	2.54	2.90	3.33	3.56	3.78	4.01	4.21	4.39	4.63	4.75	4.82
KC-27B	36.5	0.00	0.00	0.00	0.00	0.00	0.00	0.00	0.00	0.11	0.57	0.83	1.07	1.32	1.80	2.32	2.75	3.24	3.54	3.81	4.10	4.37	4.62	4.93	5.10	5.20
KC-27B	42.5	0.00	0.00	0.00	0.00	0.00	0.00	0.00	0.08	0.44	0.79	1.00	1.09	1.18	1.53	1.92	2.19	2.46	2.56	2.61	2.74	2.95	3.19	3.49	3.67	3.78
KC-27B	46.5	0.00	0.00	0.00	0.00	0.00	0.00	0.00	0.07	0.39	0.75	1.04	1.26	1.46	1.87	2.30	2.62	2.99	3.17	3.31	3.47	3.61	3.74	3.92	3.99	4.03
KC-27B	46.5	0.00	0.00	0.00	0.00	0.00	0.00	0.00	0.12	0.46	0.74	0.96	1.09	1.20	1.52	1.86	2.14	2.45	2.61	2.71	2.85	2.99	3.13	3.32	3.44	3.54
KC-27B	56.5	0.00	0.00	0.00	0.00	0.00	0.00	0.00	0.14	0.52	0.80	1.05	1.22	1.37	1.72	2.08	2.35	2.65	2.79	2.89	3.03	3.19	3.35	3.57	3.73	3.89
KC-27B	56.9	0.00	0.00	0.00	0.00	0.00	0.00	0.00	0.13	0.45	0.70	1.00	1.24	1.43	1.77	2.11	2.38	2.68	2.82	2.91	3.03	3.13	3.25	3.44	3.58	3.75
KC-27B	56.9	0.00	0.00	0.00	0.00	0.00	0.00	0.00	0.09	0.45	0.79	1.02	1.15	1.27	1.64	2.03	2.31	2.57	2.62	2.61	2.66	2.79	2.99	3.27	3.49	3.67
KC-27B	62.5	0.00	0.00	0.00	0.00	0.00	0.00	0.00	0.07	0.40	0.75	0.97	1.07	1.18	1.52	1.91	2.21	2.52	2.66	2.74	2.86	3.04	3.24	3.53	3.75	3.93
KC-27B	66.5	0.00	0.00	0.00	0.00	0.00	0.00	0.00	0.15	0.60	0.97	1.27	1.44	1.60	2.02	2.46	2.78	3.08	3.15	3.15	3.22	3.36	3.54	3.81	3.98	4.10
KC-27B	66.5	0.00	0.00	0.00	0.00	0.00	0.00	0.00	0.20	0.76	1.22	1.60	1.85	2.08	2.63	3.18	3.56	3.92	3.99	3.99	4.07	4.22	4.42	4.72	4.88	4.91

Table D.20 (continued)

KC-27B	72.5	0.00	0.00	0.00	0.00	0.00	0.00	0.00	0.09	0.47	0.90	1.32	1.70	2.03	2.58	3.10	3.46	3.81	3.87	3.86	3.86	3.86	3.89	4.01	4.07	4.09
KC-27B	76.5	0.00	0.00	0.00	0.00	0.00	0.00	0.00	0.12	0.50	0.83	1.05	1.15	1.25	1.59	1.96	2.23	2.51	2.61	2.64	2.72	2.84	3.01	3.26	3.48	3.70
JPC-27	82.0	0.00	0.00	0.00	0.00	0.00	0.00	0.00	0.16	0.57	0.84	1.03	1.08	1.15	1.48	1.86	2.15	2.41	2.49	2.49	2.59	2.77	3.02	3.36	3.65	3.90
JPC-27	91.3	0.00	0.00	0.00	0.00	0.00	0.00	0.00	0.10	0.47	0.82	1.11	1.30	1.47	1.87	2.29	2.60	2.92	3.03	3.09	3.20	3.36	3.57	3.87	4.09	4.27
JPC-27	100.5	0.00	0.00	0.00	0.00	0.00	0.00	0.00	0.12	0.57	0.97	1.26	1.41	1.56	2.01	2.48	2.82	3.13	3.20	3.17	3.23	3.38	3.60	3.92	4.17	4.34
JPC-27	100.5	0.00	0.00	0.00	0.00	0.00	0.00	0.00	0.15	0.52	0.82	1.12	1.36	1.55	1.93	2.30	2.60	2.92	3.05	3.14	3.26	3.39	3.55	3.77	3.93	4.08
JPC-27	107.8	0.00	0.00	0.00	0.00	0.00	0.00	0.00	0.12	0.49	0.83	1.12	1.31	1.48	1.87	2.28	2.59	2.90	3.00	3.04	3.13	3.26	3.43	3.68	3.87	4.02
JPC-27	107.8	0.00	0.00	0.00	0.00	0.00	0.00	0.00	0.15	0.66	1.12	1.44	1.60	1.75	2.24	2.78	3.18	3.54	3.62	3.58	3.61	3.73	3.92	4.21	4.44	4.59
JPC-27	114.2	0.00	0.00	0.00	0.00	0.00	0.00	0.00	0.00	0.14	0.69	0.93	1.12	1.31	1.81	2.38	2.84	3.30	3.49	3.58	3.73	3.93	4.15	4.47	4.70	4.88
JPC-27	119.5	0.00	0.00	0.00	0.00	0.00	0.00	0.00	0.00	0.04	0.17	0.50	0.66	0.86	1.24	1.69	2.10	2.54	2.84	3.12	3.45	3.80	4.15	4.58	4.87	5.08
JPC-27	131.3	0.00	0.00	0.00	0.00	0.00	0.00	0.00	0.11	0.56	0.99	1.27	1.41	1.54	1.99	2.49	2.85	3.19	3.25	3.22	3.27	3.39	3.58	3.87	4.09	4.23
JPC-27	134.4	0.00	0.00	0.00	0.00	0.00	0.00	0.00	0.07	0.32	0.90	1.16	1.37	1.57	2.05	2.58	2.96	3.33	3.44	3.45	3.52	3.65	3.84	4.15	4.38	4.57
JPC-27	137.8	0.00	0.00	0.00	0.00	0.00	0.00	0.00	0.10	0.32	0.78	1.09	1.39	1.64	2.07	2.49	2.81	3.16	3.28	3.36	3.48	3.60	3.75	3.98	4.14	4.25
JPC-27	137.8	0.00	0.00	0.00	0.00	0.00	0.00	0.00	0.08	0.43	0.84	1.20	1.50	1.75	2.22	2.68	3.02	3.38	3.51	3.59	3.70	3.82	3.97	4.20	4.34	4.42
JPC-27	163	0.00	0.00	0.00	0.00	0.00	0.00	0.00	0.00	0.00	0.04	0.51	0.89	1.28	1.79	2.31	2.78	3.31	3.62	3.92	4.18	4.35	4.48	4.67	4.74	4.80
JPC-27	173	0.00	0.00	0.00	0.00	0.00	0.00	0.00	0.00	0.00	0.03	0.32	0.54	0.78	1.16	1.61	2.09	2.65	3.06	3.44	3.83	4.15	4.44	4.76	4.95	5.11
JPC-27	183	0.00	0.00	0.00	0.00	0.00	0.00	0.00	0.00	0.09	0.51	0.90	1.25	1.58	2.15	2.74	3.20	3.66	3.85	3.95	4.07	4.18	4.32	4.56	4.72	4.85
JPC-27	193	0.00	0.00	0.00	0.00	0.00	0.00	0.00	0.00	0.04	0.31	0.63	0.88	1.17	1.76	2.44	3.01	3.54	3.77	3.85	3.99	4.17	4.38	4.67	4.86	4.97
JPC-27	213	0.00	0.00	0.00	0.00	0.00	0.00	0.00	0.00	0.04	0.18	0.64	1.06	1.48	2.07	2.67	3.19	3.75	4.03	4.26	4.45	4.56	4.66	4.84	4.92	4.97
JPC-27	253	0.00	0.37	0.59	0.52	0.41	0.31	0.25	0.28	0.40	0.64	0.99	1.37	1.62	1.92	2.17	2.40	2.72	2.87	3.02	3.11	3.13	3.13	3.22	3.29	3.40
JPC-27	273	0.00	0.00	0.00	0.00	0.00	0.00	0.00	0.13	0.47	0.77	1.15	1.51	1.79	2.22	2.63	2.97	3.39	3.60	3.79	3.95	4.03	4.08	4.19	4.23	4.27
JPC-27	293	0.00	0.00	0.00	0.00	0.00	0.00	0.00	0.19	0.68	1.08	1.54	1.95	2.30	2.89	3.44	3.84	4.28	4.44	4.55	4.64	4.67	4.70	4.81	4.81	4.77
JPC-27	313	0.00	0.28	0.37	0.21	0.09	0.02	0.07	0.35	0.72	1.10	1.47	1.76	1.98	2.43	2.87	3.21	3.60	3.75	3.85	3.95	4.05	4.14	4.31	4.38	4.41
JPC-27	353	0.00	0.00	0.00	0.00	0.00	0.00	0.00	0.24	0.83	1.27	1.73	2.06	2.31	2.86	3.44	3.89	4.31	4.33	4.27	4.28	4.34	4.48	4.71	4.75	4.65
JPC-27	353	0.00	0.00	0.00	0.00	0.00	0.00	0.00	0.00	0.00	0.00	0.03	0.20	0.38	0.63	0.94	1.27	1.66	1.99	2.35	2.76	3.16	3.58	4.06	4.45	4.77
JPC-27	353	0.00	0.00	0.00	0.00	0.00	0.00	0.00	0.00	0.00	0.02	0.15	0.47	0.79	1.15	1.52	1.88	2.35	2.72	3.15	3.56	3.86	4.12	4.40	4.54	4.63
JPC-27	373	0.00	0.00	0.00	0.00	0.00	0.00	0.06	0.31	0.79	1.18	1.58	1.90	2.17	2.68	3.13	3.42	3.77	3.95	4.14	4.43	4.76	5.07	5.40	5.47	5.38
JPC-27	373	0.00	0.15	0.20	0.12	0.06	0.02	0.06	0.22	0.44	0.71	1.02	1.32	1.56	1.91	2.20	2.39	2.65	2.82	3.03	3.28	3.51	3.71	3.89	3.90	3.83
JPC-27	393	0.00	0.00	0.00	0.00	0.00	0.00	0.00	0.10	0.42	0.78	1.19	1.55	1.83	2.29	2.75	3.13	3.53	3.65	3.73	3.78	3.75	3.72	3.76	3.73	3.71
JPC-27	413	0.00	0.00	0.00	0.00	0.00	0.00	0.00	0.23	0.86	1.41	1.99	2.36	2.49	2.85	3.36	3.94	4.52	4.60	4.51	4.32	4.03	3.79	3.75	3.73	3.75
JPC-27	433	0.00	1.04	1.38	0.80	0.40	0.22	0.33	0.74	1.23	1.75	2.21	2.46	2.46	2.63	2.86	3.25	3.93	4.36	4.47	4.38	4.07	3.65	3.32	3.08	2.92
JPC-27	433	0.00	0.00	0.00	0.00	0.00	0.00	0.00	0.08	0.55	1.12	1.56	1.82	1.93	2.25	2.64	3.12	3.84	4.33	4.54	4.59	4.48	4.25	4.09	3.95	3.83
JPC-27	433	0.00	0.00	0.00	0.00	0.00	0.00	0.00	0.06	0.45	0.95	1.38	1.69	1.80	2.06	2.37	2.82	3.52	4.01	4.27	4.36	4.26	4.04	3.86	3.67	3.52
JPC-27	453	0.00	0.00	0.00	0.00	0.00	0.00	0.00	0.08	0.22	0.50	0.79	1.10	1.34	1.65	1.92	2.15	2.45	2.64	2.89	3.19	3.46	3.71	3.97	4.03	3.98
JPC-27	453	0.00	0.00	0.00	0.00	0.00	0.00	0.00	0.13	0.47	0.77	1.15	1.50	1.76	2.14	2.47	2.75	3.12	3.39	3.74	4.14	4.50	4.79	5.02	4.93	4.67
JPC-27	473	0.00	0.00	0.00	0.00	0.00	0.00	0.01	0.25	0.76	1.15	1.49	1.66	1.73	2.01	2.32	2.62	3.11	3.52	3.87	4.22	4.50	4.66	4.75	4.65	4.43
JPC-27	493	0.00	0.06	0.09	0.07	0.05	0.05	0.12	0.28	0.51	0.85	1.29	1.75	2.03	2.33	2.53	2.71	3.08	3.37	3.71	3.97	4.09	4.08	4.04	3.87	3.71

Table D.20 (continued)

JPC-27	513	0.00	0.00	0.00	0.00	0.00	0.00	0.00	0.00	0.27	0.92	1.40	1.89	2.18	2.26	2.57	2.95	3.33	3.74	3.79	3.78	3.77	3.74	3.76	3.88	3.89	3.81
JPC-27	513	0.00	0.00	0.00	0.00	0.00	0.00	0.00	0.00	0.15	0.64	1.09	1.48	1.77	2.00	2.52	3.11	3.58	4.00	4.03	3.96	3.86	3.74	3.67	3.75	3.82	3.90
JPC-27	533	0.00	0.00	0.00	0.00	0.00	0.00	0.00	0.04	0.33	0.84	1.22	1.63	1.96	2.21	2.75	3.32	3.77	4.14	4.10	4.01	3.89	3.72	3.63	3.67	3.68	3.68
JPC-27	533	0.00	0.00	0.00	0.00	0.00	0.00	0.00	0.00	0.21	0.83	1.32	1.72	1.96	2.18	2.78	3.49	4.04	4.45	4.41	4.27	4.13	4.00	3.95	4.04	4.08	4.13
JPC-27	553	0.00	0.00	0.00	0.00	0.00	0.00	0.00	0.00	0.07	0.41	0.79	1.05	1.22	1.41	1.87	2.37	2.72	3.00	2.98	2.88	2.86	2.95	3.18	3.59	3.97	4.26
JPC-27	553	0.00	0.00	0.00	0.00	0.00	0.00	0.00	0.00	0.15	0.53	0.88	1.29	1.67	1.99	2.52	3.04	3.42	3.79	3.83	3.83	3.86	3.91	4.07	4.44	4.78	5.06
JPC-27	573	0.00	0.16	0.24	0.19	0.14	0.10	0.10	0.10	0.16	0.28	0.49	0.79	1.12	1.36	1.64	1.86	2.01	2.22	2.34	2.57	2.86	3.14	3.43	3.72	3.78	3.68
JPC-27	573	0.00	0.00	0.04	0.25	0.31	0.32	0.25	0.19	0.20	0.35	0.69	1.13	1.43	1.68	1.84	2.02	2.33	2.56	2.91	3.22	3.44	3.61	3.79	3.80	3.72	
JPC-27	593	0.00	0.00	0.00	0.00	0.00	0.00	0.04	0.20	0.53	0.87	1.29	1.65	1.89	2.22	2.52	2.80	3.22	3.54	3.92	4.31	4.57	4.69	4.70	4.42	4.04	
JPC-27	593	0.00	0.00	0.00	0.00	0.00	0.00	0.05	0.24	0.63	0.99	1.43	1.81	2.07	2.46	2.81	3.11	3.55	3.87	4.26	4.67	4.97	5.13	5.17	4.87	4.40	
JPC-27	613	0.00	0.00	0.00	0.00	0.00	0.00	0.00	0.21	0.70	1.10	1.59	2.00	2.25	2.66	3.08	3.41	3.72	3.68	3.61	3.51	3.38	3.31	3.38	3.42	3.45	
JPC-27	633	0.00	0.61	0.81	0.45	0.19	0.06	0.16	0.56	1.06	1.58	2.06	2.35	2.41	2.62	2.78	2.97	3.49	4.03	4.52	4.88	5.01	4.85	4.57	4.15	3.77	
JPC-27	653	0.00	0.00	0.00	0.00	0.00	0.00	0.00	0.10	0.25	0.54	0.79	1.06	1.27	1.58	1.89	2.14	2.37	2.40	2.41	2.42	2.44	2.55	2.78	3.00	3.22	
JPC-27	653	0.00	0.17	0.32	0.37	0.35	0.30	0.23	0.22	0.31	0.56	0.98	1.47	1.80	2.16	2.48	2.79	3.16	3.25	3.33	3.35	3.30	3.32	3.54	3.79	4.03	
JPC-27	673	0.00	0.00	0.00	0.00	0.00	0.00	0.00	0.26	0.85	1.22	1.62	1.86	1.96	2.25	2.51	2.72	3.09	3.39	3.74	4.12	4.42	4.54	4.54	4.27	3.94	
JPC-27	673	0.00	0.00	0.00	0.00	0.00	0.00	0.00	0.23	0.77	1.17	1.58	1.85	1.97	2.27	2.53	2.74	3.10	3.38	3.71	4.06	4.33	4.43	4.41	4.15	3.82	
JPC-27	693	0.00	0.00	0.00	0.00	0.00	0.00	0.00	0.12	0.51	0.92	1.33	1.66	1.84	2.14	2.42	2.71	3.18	3.50	3.75	3.91	3.95	3.88	3.83	3.69	3.57	
JPC-27	693	0.00	0.00	0.00	0.00	0.00	0.00	0.03	0.34	0.95	1.42	1.88	2.14	2.22	2.46	2.65	2.86	3.34	3.82	4.26	4.58	4.72	4.61	4.39	4.04	3.71	
JPC-27	713	0.00	0.00	0.01	0.05	0.27	0.32	0.29	0.27	0.31	0.54	1.02	1.62	2.06	2.43	2.65	2.84	3.20	3.44	3.76	3.97	3.99	3.94	3.97	3.95	4.00	
JPC-27	713	0.00	0.00	0.00	0.00	0.00	0.00	0.00	0.16	0.58	0.96	1.42	1.86	2.20	2.70	3.10	3.39	3.75	3.89	4.00	4.07	4.08	4.07	4.15	4.17	4.17	
JPC-27	713	0.00	0.00	0.00	0.00	0.00	0.00	0.00	0.14	0.47	0.77	1.17	1.57	1.88	2.29	2.61	2.83	3.11	3.23	3.34	3.44	3.49	3.54	3.66	3.69	3.68	
JPC-27	733	0.00	0.28	0.43	0.41	0.44	0.50	0.60	0.77	0.95	1.23	1.63	1.98	2.10	2.21	2.25	2.43	2.93	3.36	3.70	3.83	3.67	3.36	3.07	2.80	2.64	
JPC-27	733	0.00	0.00	0.00	0.00	0.00	0.00	0.00	0.26	0.92	1.41	1.89	2.16	2.24	2.51	2.81	3.23	3.95	4.50	4.81	4.90	4.78	4.50	4.27	4.05	3.89	
JPC-27	733	0.00	0.00	0.00	0.00	0.00	0.00	0.00	0.17	0.75	1.27	1.62	1.73	1.72	1.97	2.31	2.70	3.30	3.70	3.87	3.91	3.84	3.68	3.56	3.46	3.39	
JPC-27	753	0.00	1.34	1.94	1.45	1.04	0.76	0.66	0.79	0.98	1.26	1.57	1.81	1.93	2.18	2.44	2.74	3.23	3.57	3.81	3.95	3.94	3.81	3.69	3.52	3.38	
JPC-27	753	0.00	0.00	0.00	0.00	0.00	0.00	0.05	0.36	0.96	1.46	1.94	2.24	2.36	2.69	3.03	3.43	4.06	4.51	4.78	4.92	4.88	4.68	4.47	4.20	3.94	
JPC-27	773	0.00	0.26	0.36	0.23	0.12	0.06	0.10	0.25	0.49	0.80	1.19	1.59	1.89	2.32	2.71	2.99	3.30	3.38	3.44	3.43	3.35	3.25	3.21	3.13	3.08	
JPC-27	793	0.00	0.00	0.00	0.00	0.00	0.00	0.00	0.30	0.81	1.16	1.53	1.82	2.07	2.57	3.03	3.32	3.59	3.59	3.54	3.49	3.45	3.44	3.53	3.57	3.60	
JPC-27	813	0.00	0.21	0.28	0.16	0.08	0.04	0.14	0.49	0.94	1.45	2.01	2.50	2.83	3.41	4.00	4.53	5.12	5.29	5.34	5.31	5.14	4.94	4.83	4.64	4.44	
JPC-27	813	0.00	0.33	0.44	0.25	0.11	0.04	0.11	0.34	0.68	1.07	1.53	1.93	2.21	2.66	3.12	3.55	4.03	4.20	4.29	4.30	4.20	4.07	4.02	3.90	3.80	
JPC-27	813	0.00	0.00	0.00	0.00	0.00	0.00	0.00	0.16	0.78	1.36	1.73	1.88	2.01	2.54	3.19	3.71	4.18	4.21	4.06	3.93	3.85	3.82	3.89	3.92	3.90	
JPC-27	833	0.00	0.10	0.11	0.06	0.02	0.06	0.26	0.60	0.91	1.23	1.56	1.88	2.18	2.73	3.24	3.55	3.82	3.81	3.79	3.78	3.74	3.74	3.74	3.85	3.87	3.86
JPC-27	838	0.00	0.00	0.00	0.00	0.00	0.00	0.00	0.11	0.49	0.90	1.35	1.73	1.92	2.18	2.40	2.67	3.16	3.55	3.87	4.08	4.12	4.01	3.90	3.72	3.60	
JPC-27	843	0.00	0.00	0.00	0.00	0.00	0.00	0.00	0.06	0.17	0.41	0.73	1.10	1.36	1.65	1.89	2.10	2.42	2.63	2.90	3.17	3.38	3.55	3.73	3.77	3.76	
JPC-27	843	0.00	0.30	0.44	0.35	0.27	0.22	0.22	0.31	0.47	0.74	1.12	1.53	1.84	2.20	2.49	2.70	3.00	3.19	3.45	3.72	3.92	4.07	4.22	4.19	4.10	
JPC-27	848	0.00	0.00	0.00	0.00	0.00	0.00	0.01	0.19	0.55	0.86	1.21	1.50	1.75	2.18	2.61	2.93	3.23	3.29	3.33	3.40	3.48	3.60	3.79	3.90	3.96	
JPC-27	848	0.00	0.79	1.31	1.31	1.24	1.15	1.06	1.08	1.14	1.42	1.90	2.44	2.79	3.25	3.61	3.91	4.29	4.40	4.55	4.59	4.47	4.30	4.19	3.99	3.79	

Table D.20 (continued)

JPC-27	848	0.00	0.00	0.00	0.00	0.00	0.00	0.00	0.15	0.61	0.98	1.31	1.52	1.73	2.21	2.70	3.03	3.29	3.27	3.21	3.25	3.38	3.60	3.93	4.13	4.24
JPC-27	853	0.00	0.00	0.00	0.00	0.00	0.00	0.01	0.23	0.67	1.03	1.41	1.67	1.79	2.04	2.26	2.47	2.85	3.16	3.48	3.77	3.98	4.05	4.06	3.90	3.71
JPC-27	853	0.00	0.00	0.00	0.00	0.00	0.00	0.00	0.24	0.79	1.18	1.60	1.86	1.98	2.27	2.53	2.77	3.18	3.50	3.82	4.14	4.38	4.48	4.50	4.33	4.08
JPC-27	858	0.00	0.00	0.00	0.00	0.00	0.00	0.00	0.08	0.51	0.98	1.27	1.41	1.54	1.98	2.43	2.72	2.99	3.06	3.07	3.19	3.40	3.64	3.90	4.02	4.03
JPC-27	858	0.00	1.29	1.78	1.15	0.67	0.40	0.42	0.71	1.08	1.46	1.83	2.11	2.32	2.78	3.19	3.49	3.90	4.18	4.48	4.84	5.15	5.34	5.42	5.16	4.70
JPC-27	863	0.00	0.00	0.00	0.00	0.00	0.00	0.08	0.36	0.89	1.35	1.83	2.15	2.27	2.53	2.77	3.02	3.48	3.76	3.92	4.00	3.98	3.87	3.80	3.66	3.52
JPC-27	873	0.00	0.00	0.00	0.00	0.00	0.00	0.13	0.49	0.84	1.18	1.48	1.69	1.82	2.18	2.59	2.93	3.25	3.28	3.26	3.21	3.12	3.06	3.10	3.10	3.14
JPC-27	878	0.00	0.15	0.28	0.32	0.32	0.31	0.30	0.38	0.55	0.89	1.40	1.92	2.19	2.42	2.52	2.64	3.00	3.32	3.74	4.09	4.23	4.19	4.04	3.69	3.37
JPC-27	883	0.00	0.00	0.00	0.00	0.00	0.00	0.01	0.25	0.75	1.19	1.68	2.08	2.34	2.76	3.13	3.44	3.91	4.25	4.59	4.94	5.18	5.28	5.29	5.01	4.61
JPC-27	883	0.00	0.00	0.00	0.00	0.00	0.00	0.04	0.36	0.96	1.39	1.77	1.96	2.07	2.45	2.83	3.14	3.56	3.83	4.06	4.36	4.65	4.83	4.94	4.79	4.52
JPC-27	888	0.00	0.00	0.00	0.00	0.00	0.00	0.00	0.20	0.74	1.15	1.48	1.67	1.83	2.26	2.70	3.01	3.38	3.56	3.68	3.87	4.09	4.29	4.49	4.50	4.36
JPC-27	888	0.00	0.00	0.00	0.00	0.00	0.00	0.00	0.22	0.82	1.31	1.77	2.06	2.20	2.54	2.79	2.94	3.25	3.56	4.02	4.63	5.22	5.61	5.74	5.33	4.62
JPC-27	894	0.00	0.00	0.00	0.00	0.00	0.00	0.00	0.20	0.72	1.11	1.42	1.60	1.78	2.29	2.85	3.27	3.64	3.69	3.63	3.61	3.64	3.72	3.91	4.01	4.04
JPC-27	894	0.00	0.00	0.00	0.00	0.00	0.00	0.00	0.26	0.99	1.51	1.88	2.04	2.21	2.82	3.50	3.98	4.38	4.38	4.24	4.15	4.14	4.19	4.35	4.42	4.40
JPC-27	894	0.00	0.00	0.00	0.00	0.00	0.00	0.00	0.18	0.68	1.07	1.38	1.57	1.75	2.24	2.79	3.21	3.60	3.67	3.63	3.62	3.64	3.71	3.88	3.99	4.05
JPC-27	898	0.00	0.00	0.00	0.00	0.00	0.00	0.00	0.00	0.00	0.03	0.37	0.60	0.89	1.36	1.92	2.47	3.07	3.45	3.77	4.07	4.32	4.53	4.80	4.96	5.04
JPC-27	898	0.00	0.00	0.00	0.00	0.00	0.00	0.00	0.00	0.04	0.16	0.44	0.54	0.73	1.20	1.80	2.34	2.87	3.15	3.32	3.52	3.75	3.98	4.26	4.41	4.46
JPC-27	903	0.00	0.00	0.00	0.00	0.00	0.00	0.00	0.14	0.54	0.89	1.27	1.58	1.85	2.32	2.81	3.19	3.60	3.73	3.81	3.87	3.91	3.96	4.08	4.11	4.09
JPC-27	918	0.00	0.00	0.00	0.00	0.00	0.00	0.00	0.12	0.56	1.00	1.34	1.57	1.78	2.27	2.81	3.21	3.61	3.73	3.74	3.80	3.88	3.99	4.20	4.30	4.34
JPC-27	928	0.00	0.00	0.00	0.00	0.00	0.00	0.00	0.15	0.59	1.00	1.39	1.70	1.97	2.50	3.05	3.48	3.91	4.05	4.11	4.18	4.24	4.32	4.50	4.57	4.56
JPC-27	933	0.00	0.00	0.00	0.00	0.00	0.00	0.00	0.22	0.79	1.23	1.65	1.95	2.22	2.78	3.36	3.77	4.19	4.32	4.39	4.52	4.68	4.87	5.12	5.19	5.11
JPC-27	933	0.00	0.20	0.27	0.16	0.08	0.02	0.05	0.24	0.54	0.90	1.30	1.68	1.97	2.43	2.86	3.22	3.66	3.89	4.09	4.28	4.40	4.50	4.63	4.63	4.57
JPC-27	948	0.00	0.56	0.80	0.56	0.35	0.21	0.20	0.34	0.59	0.94	1.39	1.85	2.18	2.64	3.06	3.43	3.89	4.13	4.34	4.48	4.51	4.48	4.51	4.46	4.41
JPC-27	958	0.00	0.00	0.00	0.00	0.00	0.00	0.00	0.23	0.85	1.35	1.80	2.12	2.39	2.98	3.59	4.04	4.50	4.64	4.69	4.76	4.85	4.97	5.18	5.26	5.22
JPC-27	963	0.00	0.52	0.69	0.41	0.20	0.09	0.15	0.41	0.75	1.16	1.61	2.03	2.35	2.88	3.37	3.76	4.25	4.48	4.67	4.83	4.90	4.95	5.05	5.04	4.97
JPC-27	963	0.00	0.28	0.37	0.21	0.09	0.03	0.07	0.40	0.85	1.33	1.81	2.23	2.56	3.14	3.68	4.10	4.58	4.76	4.87	4.98	5.04	5.08	5.19	5.16	5.05
JPC-27	968	0.00	0.00	0.00	0.00	0.00	0.00	0.00	0.29	1.03	1.61	2.19	2.62	2.95	3.67	4.42	5.02	5.63	5.77	5.75	5.70	5.60	5.49	5.48	5.32	5.04
JPC-27	973	0.00	0.00	0.00	0.00	0.00	0.00	0.00	0.00	0.04	0.30	0.71	1.19	1.57	2.00	2.38	2.78	3.34	3.76	4.22	4.63	4.91	5.12	5.39	5.52	5.62
JPC-27	973	0.00	0.00	0.00	0.00	0.00	0.00	0.00	0.00	0.11	0.59	0.90	1.19	1.46	1.97	2.52	3.00	3.54	3.87	4.15	4.45	4.73	5.00	5.34	5.53	5.64
JPC-27	978	0.00	0.00	0.00	0.00	0.00	0.00	0.00	0.05	0.54	1.18	1.66	2.03	2.36	3.07	3.83	4.42	5.04	5.28	5.37	5.47	5.55	5.61	5.75	5.74	5.60
JPC-27	983	0.00	0.00	0.00	0.00	0.00	0.00	0.00	0.06	0.52	1.10	1.50	1.76	2.00	2.60	3.29	3.87	4.43	4.59	4.73	4.69	4.68	4.70	4.82	4.88	4.86
JPC-27	983	0.00	0.00	0.00	0.00	0.00	0.00	0.00	0.08	0.59	1.20	1.60	1.84	2.07	2.70	3.43	4.03	4.59	4.73	4.69	4.68	4.68	4.70	4.82	4.83	4.76
JPC-27	993	0.00	0.00	0.00	0.00	0.00	0.00	0.00	0.20	0.85	1.43	1.93	2.30	2.63	3.33	4.02	4.52	5.05	5.22	5.27	5.30	5.29	5.26	5.32	5.24	5.07
JPC-27	998	0.00	0.00	0.00	0.00	0.00	0.00	0.00	0.07	0.53	1.08	1.48	1.76	2.04	2.65	3.31	3.83	4.37	4.58	4.79	4.88	4.97	5.13	5.17	5.11	

Table D.20 (continued)

Core	Avg depth (cmcd)	10 bin	11.2	12.7	14.5	16.4	18.7	21.2	24.1	27.4	31.1	35.3	40.1	45.6	51.8	58.9	63
MC-45	1.25	0.42	3.45	3.92	4.26	4.04	4.33	4.07	4.01	3.83	3.59	3.44	3.30	3.11	2.71	2.19	0.91
MC-45	2.25	0.41	3.36	3.89	4.33	4.25	4.76	4.70	4.84	4.76	4.54	4.34	4.11	3.77	3.15	2.36	0.89
MC-45	2.25	0.38	3.14	3.66	4.09	4.04	4.52	4.47	4.64	4.67	4.61	4.61	4.58	4.39	3.84	3.06	1.23
MC-45	3.25	0.45	3.67	4.13	4.44	4.19	4.56	4.43	4.57	4.53	4.28	3.92	3.44	2.88	2.32	1.88	0.84
MC-45	3.25	0.49	3.86	4.15	4.28	3.97	4.34	4.27	4.41	4.25	3.79	3.19	2.55	2.03	1.70	1.55	0.74
MC-45	8.25	0.45	3.65	4.07	4.33	4.07	4.44	4.36	4.54	4.52	4.25	3.81	3.24	2.67	2.19	1.89	0.90
MC-45	8.25	0.51	4.12	4.65	4.95	4.59	4.77	4.31	4.02	3.57	3.12	2.85	2.70	2.50	2.04	1.37	0.42
MC-45	10.25	0.50	4.07	4.60	4.91	4.57	4.78	4.34	4.08	3.66	3.25	3.01	2.87	2.67	2.17	1.38	0.39
MC-45	12.25		3.94	4.47	4.81	4.50	4.75	4.38	4.19	3.81	3.40	3.13	2.96	2.74	2.29	1.64	0.56
MC-45	14.25	0.47	3.83	4.34	4.66	4.37	4.63	4.31	4.19	3.90	3.59	3.42	3.34	3.18	2.72	2.01	0.72
MC-45	16.25	0.48	3.94	4.47	4.79	4.47	4.70	4.29	4.06	3.68	3.31	3.12	3.04	2.87	2.38	1.61	0.51
MC-45	18.25	0.49	4.02	4.58	4.93	4.60	4.80	4.34	4.04	3.62	3.25	3.08	2.97	2.72	2.08	1.19	0.28
MC-45	21	0.48	3.96	4.54	4.94	4.67	4.95	4.53	4.28	3.85	3.43	3.19	3.11	3.03	2.69	2.09	0.78
MC-45	25	0.49	3.99	4.55	4.91	4.59	4.79	4.33	4.03	3.57	3.09	2.75	2.50	2.23	1.78	1.18	0.36
MC-45	27	0.50	4.11	4.71	5.08	4.75	5.01	4.65	4.56	4.35	4.10	3.91	3.70	3.34	2.77	2.12	0.85
MC-45	27	0.46	3.75	4.21	4.53	4.33	4.80	4.79	5.05	5.04	4.72	4.25	3.67	3.09	2.61	2.33	1.13
MC-45	31	0.42	3.50	4.12	4.59	4.42	4.72	4.37	4.22	3.98	3.82	3.87	3.99	3.90	3.29	2.26	0.73
MC-45	31	0.42	3.44	3.98	4.37	4.14	4.41	4.14	4.16	4.12	4.09	4.14	4.16	4.01	3.56	2.94	1.23
MC-45	33	0.45	3.68	4.25	4.66	4.46	4.81	4.54	4.45	4.18	3.88	3.73	3.67	3.55	3.11	2.39	0.90
MC-45	35	0.49	4.01	4.58	4.95	4.65	4.92	4.53	4.32	3.94	3.55	3.32	3.16	2.88	2.26	1.37	0.33
MC-45	35	0.44	3.59	4.12	4.47	4.22	4.51	4.26	4.26	4.17	4.04	3.98	3.87	3.57	2.97	2.26	0.89
KC-27B	32.5	0.55	4.37	4.73	4.77	4.16	4.06	3.45	3.08	2.71	2.49	2.53	2.70	2.76	2.42	1.70	0.54
KC-27B	32.5	0.48	3.78	4.06	4.12	3.71	3.88	3.68	3.72	3.62	3.36	3.05	2.75	2.57	2.52	2.55	1.28
KC-27B	36.5	0.54	4.33	4.82	5.05	4.56	4.59	4.00	3.65	3.27	3.03	2.97	2.92	2.65	1.97	1.10	0.16
KC-27B	36.5	0.58	4.63	5.09	5.24	4.67	4.70	4.15	3.84	3.41	2.95	2.57	2.25	1.95	1.62	1.24	0.48
KC-27B	42.5	0.42	3.41	3.87	4.21	4.06	4.49	4.40	4.51	4.41	4.19	4.00	3.81	3.56	3.13	2.62	1.13
KC-27B	46.5	0.45	3.60	4.04	4.32	4.04	4.28	3.96	3.85	3.67	3.52	3.54	3.63	3.57	3.09	2.30	0.83
KC-27B	46.5	0.40	3.26	3.78	4.20	4.08	4.47	4.30	4.32	4.20	4.06	4.04	4.07	3.98	3.53	2.76	1.07
KC-27B	56.5	0.44	3.62	4.22	4.68	4.50	4.83	4.49	4.35	4.07	3.82	3.75	3.78	3.71	3.22	2.39	0.85
KC-27B	56.9	0.43	3.53	4.14	4.63	4.48	4.85	4.57	4.49	4.27	4.03	3.93	3.88	3.72	3.20	2.37	0.85
KC-27B	56.9	0.42	3.41	3.93	4.31	4.13	4.50	4.35	4.47	4.50	4.47	4.46	4.34	4.01	3.39	2.68	1.12
KC-27B	62.5	0.44	3.64	4.20	4.60	4.39	4.74	4.51	4.52	4.41	4.27	4.19	4.08	3.82	3.26	2.56	1.02
KC-27B	66.5	0.46	3.73	4.22	4.54	4.24	4.44	4.09	3.98	3.85	3.75	3.75	3.66	3.34	2.67	1.83	0.62
KC-27B	66.5	0.54	4.27	4.58	4.62	4.08	4.17	3.82	3.68	3.33	2.76	2.11	1.45	0.96	0.81	0.92	0.49
KC-27B	72.5	0.45	3.63	4.03	4.24	3.89	4.09	3.86	3.94	3.96	3.86	3.66	3.25	2.62	1.84	1.10	0.33

Table D.20 (continued)

KC-27B	76.5	0.42	3.53	4.19	4.75	4.68	5.17	5.00	5.06	4.93	4.68	4.43	4.07	3.52	2.75	1.96	0.73
JPC-27	82.0	0.44	3.69	4.32	4.82	4.67	5.09	4.82	4.73	4.44	4.11	3.92	3.82	3.68	3.28	2.64	1.06
JPC-27	91.3	0.48	3.94	4.51	4.89	4.60	4.84	4.40	4.12	3.71	3.34	3.19	3.18	3.15	2.79	2.13	0.78
JPC-27	100.5	0.49	3.96	4.46	4.74	4.39	4.60	4.23	4.07	3.78	3.49	3.33	3.22	3.01	2.57	1.99	0.77
JPC-27	100.5	0.46	3.77	4.36	4.78	4.52	4.76	4.33	4.09	3.78	3.56	3.55	3.63	3.52	2.94	2.02	0.65
JPC-27	107.8	0.45	3.71	4.26	4.66	4.46	4.79	4.48	4.34	4.06	3.79	3.67	3.63	3.46	2.91	2.07	0.71
JPC-27	107.8	0.51	4.17	4.67	4.92	4.47	4.54	4.00	3.64	3.19	2.80	2.62	2.56	2.42	1.98	1.29	0.38
JPC-27	114.2	0.55	4.46	5.04	5.35	4.91	5.03	4.48	4.15	3.69	3.19	2.79	2.43	2.06	1.64	1.21	0.46
JPC-27	119.5	0.57	4.63	5.16	5.38	4.84	4.88	4.30	3.98	3.54	3.13	2.87	2.74	2.68	2.52	2.24	1.01
JPC-27	131.3	0.47	3.85	4.33	4.63	4.31	4.54	4.19	4.01	3.70	3.40	3.28	3.26	3.17	2.71	1.94	0.66
JPC-27	134.4	0.51	4.20	4.77	5.10	4.73	4.90	4.40	4.07	3.56	3.07	2.79	2.70	2.66	2.37	1.75	0.61
JPC-27	137.8	0.48	3.87	4.37	4.68	4.36	4.55	4.13	3.91	3.58	3.31	3.22	3.22	3.11	2.68	1.98	0.71
JPC-27	137.8	0.49	3.99	4.48	4.78	4.42	4.58	4.10	3.79	3.40	3.08	2.96	2.93	2.75	2.20	1.38	0.39
JPC-27	163	0.53	4.30	4.80	5.06	4.60	4.65	4.09	3.75	3.33	2.98	2.83	2.81	2.75	2.38	1.70	0.56
JPC-27	173	0.57	4.67	5.30	5.68	5.25	5.39	4.77	4.33	3.74	3.22	2.96	2.90	2.82	2.41	1.66	0.52
JPC-27	183	0.54	4.41	4.97	5.25	4.77	4.83	4.23	3.85	3.37	2.90	2.54	2.22	1.87	1.45	1.01	0.35
JPC-27	193	0.55	4.46	4.97	5.23	4.77	4.90	4.39	4.08	3.60	3.08	2.67	2.32	2.01	1.64	1.21	0.46
JPC-27	213	0.55	4.44	4.92	5.13	4.60	4.59	3.95	3.52	3.04	2.67	2.51	2.44	2.27	1.79	1.12	0.32
JPC-27	253	0.38	3.16	3.64	3.99	3.84	4.22	4.14	4.31	4.36	4.31	4.26	4.13	3.79	3.13	2.33	0.90
JPC-27	273	0.47	3.84	4.29	4.49	4.04	4.01	3.44	3.07	2.70	2.49	2.53	2.71	2.78	2.45	1.79	0.63
JPC-27	293	0.52	4.14	4.46	4.49	3.90	3.80	3.21	2.82	2.39	2.08	2.00	2.04	1.98	1.57	0.92	0.09
JPC-27	313	0.49	3.94	4.39	4.61	4.16	4.15	3.55	3.15	2.75	2.52	2.56	2.73	2.72	2.23	1.38	0.36
JPC-27	353	0.50	3.92	4.16	4.22	3.85	4.09	3.86	3.74	3.31	2.61	1.87	1.23	0.85	0.75	0.82	0.43
JPC-27	353	0.54	4.48	5.14	5.52	5.15	5.41	5.00	4.87	4.58	4.25	4.05	3.90	3.69	3.22	2.58	1.06
JPC-27	353	0.52	4.16	4.62	4.84	4.44	4.62	4.26	4.16	3.94	3.71	3.59	3.52	3.38	2.99	2.41	1.00
JPC-27	373	0.58	4.58	4.82	4.76	4.06	3.86	3.13	2.56	1.98	1.59	1.52	1.65	1.73	1.45	0.81	0.17
JPC-27	373	0.42	3.33	3.68	3.92	3.69	3.95	3.70	3.65	3.54	3.49	3.62	3.80	3.77	3.25	2.39	0.88
JPC-27	393	0.41	3.30	3.69	3.94	3.65	3.76	3.35	3.09	2.82	2.70	2.85	3.16	3.34	3.04	2.33	0.87
JPC-27	413	0.42	3.35	3.70	3.85	3.49	3.55	3.17	2.97	2.75	2.63	2.70	2.81	2.71	2.16	1.28	0.32
JPC-27	433	0.32	2.54	2.84	3.03	2.80	2.90	2.66	2.59	2.50	2.42	2.41	2.38	2.25	1.96	1.60	0.70
JPC-27	433	0.42	3.36	3.73	3.91	3.55	3.61	3.23	3.07	2.87	2.74	2.74	2.77	2.69	2.35	1.88	0.77
JPC-27	433	0.38	3.04	3.34	3.48	3.16	3.26	3.05	3.11	3.16	3.11	2.98	2.72	2.43	2.20	2.12	1.06
JPC-27	453	0.43	3.40	3.63	3.70	3.37	3.54	3.33	3.32	3.24	3.18	3.25	3.37	3.39	3.13	2.70	1.21
JPC-27	453	0.50	3.81	3.92	3.85	3.36	3.35	2.92	2.67	2.41	2.31	2.45	2.71	2.84	2.51	1.82	0.64
JPC-27	473	0.47	3.69	3.90	3.94	3.54	3.69	3.45	3.43	3.32	3.14	2.97	2.72	2.38	1.99	1.68	0.75
JPC-27	493	0.40	3.19	3.51	3.72	3.44	3.55	3.15	2.90	2.64	2.58	2.80	3.16	3.33	2.98	2.21	0.81
JPC-27	513	0.41	3.22	3.38	3.40	3.09	3.35	3.31	3.43	3.31	2.98	2.62	2.34	2.22	2.20	2.20	1.08

Table D.20 (continued)

JPC-27	513	0.44	3.53	3.94	4.13	3.73	3.79	3.40	3.25	3.07	2.96	3.00	3.08	2.98	2.48	1.71	0.57
JPC-27	533	0.41	3.23	3.50	3.56	3.17	3.20	2.88	2.77	2.66	2.66	2.85	3.10	3.15	2.73	1.94	0.68
JPC-27	533	0.46	3.69	4.11	4.30	3.86	3.84	3.28	2.90	2.52	2.29	2.29	2.38	2.32	1.89	1.20	0.35
JPC-27	553	0.48	3.92	4.32	4.38	3.83	3.81	3.37	3.15	2.88	2.69	2.71	2.86	2.95	2.75	2.31	0.98
JPC-27	553	0.57	4.63	5.07	5.04	4.23	3.91	3.14	2.67	2.30	2.16	2.29	2.51	2.53	2.06	1.24	0.31
JPC-27	573	0.40	3.06	3.15	3.08	2.75	2.99	3.08	3.47	3.73	3.74	3.53	3.18	2.91	2.86	3.05	1.63
JPC-27	573	0.40	3.17	3.39	3.48	3.22	3.47	3.36	3.42	3.36	3.22	3.13	3.06	2.95	2.72	2.46	1.18
JPC-27	593	0.42	3.21	3.27	3.23	2.89	3.00	2.79	2.75	2.64	2.53	2.51	2.57	2.64	2.56	2.32	1.07
JPC-27	593	0.46	3.42	3.40	3.28	2.90	2.98	2.69	2.54	2.31	2.15	2.16	2.29	2.39	2.25	1.88	0.79
JPC-27	613	0.38	3.06	3.34	3.40	3.00	3.01	2.74	2.75	2.82	2.94	3.09	3.12	2.94	2.55	2.13	0.96
JPC-27	633	0.40	3.15	3.45	3.64	3.32	3.31	2.77	2.36	1.98	1.80	1.89	2.11	2.21	1.93	1.33	0.43
JPC-27	653	0.37	3.01	3.43	3.65	3.37	3.53	3.29	3.30	3.32	3.45	3.79	4.21	4.44	4.17	3.52	1.51
JPC-27	653	0.46	3.73	4.11	4.17	3.64	3.63	3.28	3.22	3.13	3.05	3.06	3.08	3.02	2.70	2.22	0.96
JPC-27	673	0.42	3.23	3.45	3.62	3.38	3.54	3.20	3.00	2.77	2.69	2.86	3.13	3.23	2.86	2.11	0.76
JPC-27	673	0.40	3.10	3.25	3.31	3.03	3.23	3.11	3.21	3.27	3.27	3.26	3.14	2.90	2.53	2.20	1.01
JPC-27	693	0.39	3.12	3.49	3.76	3.55	3.77	3.49	3.39	3.23	3.12	3.20	3.38	3.44	3.10	2.42	0.94
JPC-27	693	0.40	3.13	3.48	3.80	3.66	3.92	3.59	3.36	3.01	2.72	2.63	2.64	2.53	2.06	1.31	0.38
JPC-27	713	0.45	3.64	4.11	4.36	4.00	4.14	3.80	3.72	3.55	3.31	3.09	2.86	2.60	2.22	1.76	0.73
JPC-27	713	0.46	3.68	4.04	4.18	3.76	3.82	3.39	3.15	2.83	2.59	2.53	2.57	2.52	2.17	1.58	0.57
JPC-27	713	0.41	3.24	3.53	3.64	3.30	3.43	3.21	3.23	3.22	3.20	3.21	3.16	2.99	2.69	2.45	1.17
JPC-27	733	0.29	2.32	2.61	2.81	2.65	2.82	2.68	2.73	2.73	2.72	2.81	2.94	3.04	2.92	2.61	1.18
JPC-27	733	0.42	3.38	3.73	3.89	3.51	3.53	3.07	2.76	2.40	2.17	2.19	2.36	2.45	2.18	1.54	0.49
JPC-27	733	0.37	3.02	3.41	3.66	3.40	3.55	3.29	3.27	3.25	3.24	3.24	3.15	2.93	2.57	2.23	1.02
JPC-27	753	0.37	2.95	3.31	3.56	3.33	3.50	3.22	3.11	2.93	2.75	2.63	2.55	2.41	2.11	1.72	0.72
JPC-27	753	0.42	3.34	3.63	3.82	3.53	3.67	3.30	3.05	2.67	2.31	2.09	1.99	1.90	1.65	1.25	0.46
JPC-27	773	0.34	2.73	3.04	3.21	2.98	3.15	3.01	3.11	3.20	3.28	3.42	3.52	3.48	3.16	2.69	1.19
JPC-27	793	0.40	3.21	3.57	3.76	3.48	3.68	3.46	3.42	3.31	3.21	3.25	3.34	3.27	2.78	1.98	0.69
JPC-27	813	0.48	3.76	4.00	4.01	3.45	3.25	2.54	1.95	1.41	1.11	1.15	1.39	1.53	1.25	0.56	0.04
JPC-27	813	0.42	3.30	3.61	3.75	3.40	3.48	3.13	2.96	2.71	2.48	2.37	2.36	2.37	2.19	1.82	0.75
JPC-27	813	0.43	3.44	3.79	3.94	3.53	3.53	3.09	2.89	2.73	2.67	2.72	2.73	2.59	2.24	1.84	0.79
JPC-27	833	0.43	3.39	3.69	3.80	3.43	3.53	3.20	3.05	2.83	2.64	2.56	2.55	2.50	2.25	1.83	0.75
JPC-27	838	0.40	3.19	3.62	3.93	3.68	3.79	3.35	3.10	2.86	2.79	2.98	3.22	3.23	2.74	1.91	0.67
JPC-27	843	0.41	3.30	3.64	3.87	3.67	3.99	3.85	3.93	3.89	3.83	3.88	3.97	3.92	3.49	2.78	1.13
JPC-27	843	0.45	3.53	3.80	3.89	3.48	3.52	3.14	2.97	2.83	2.84	3.08	3.38	3.43	2.88	1.91	0.60
JPC-27	848	0.44	3.54	3.94	4.14	3.79	3.90	3.49	3.29	3.06	2.95	3.09	3.34	3.43	3.07	2.38	0.93
JPC-27	848	0.41	3.18	3.32	3.23	2.71	2.56	2.14	1.90	1.65	1.44	1.35	1.38	1.46	1.42	1.21	0.50
JPC-27	848	0.47	3.75	4.09	4.16	3.70	3.76	3.44	3.41	3.36	3.34	3.40	3.41	3.27	2.87	2.35	1.00

Table D.20 (continued)

JPC-27	853	0.40	3.17	3.50	3.76	3.56	3.77	3.46	3.30	3.07	2.93	3.01	3.18	3.22	2.84	2.17	0.86
JPC-27	853	0.44	3.42	3.70	3.89	3.63	3.83	3.50	3.30	2.99	2.73	2.66	2.71	2.72	2.44	1.92	0.76
JPC-27	858	0.44	3.52	3.86	4.02	3.69	3.87	3.60	3.55	3.43	3.29	3.21	3.15	3.05	2.81	2.48	1.12
JPC-27	858	0.49	3.66	3.60	3.32	2.68	2.42	1.87	1.53	1.30	1.27	1.45	1.67	1.71	1.40	0.88	0.28
JPC-27	863	0.38	3.03	3.32	3.51	3.27	3.46	3.22	3.12	2.90	2.65	2.49	2.42	2.36	2.18	1.88	0.84
JPC-27	873	0.35	2.84	3.23	3.52	3.33	3.52	3.26	3.16	3.03	2.99	3.15	3.40	3.49	3.16	2.47	0.98
JPC-27	878	0.36	2.80	3.05	3.28	3.14	3.41	3.23	3.22	3.12	3.03	3.04	3.08	3.01	2.69	2.18	0.92
JPC-27	883	0.49	3.69	3.77	3.71	3.27	3.31	2.95	2.73	2.44	2.15	2.00	1.96	1.94	1.76	1.39	0.52
JPC-27	883	0.48	3.75	4.00	4.13	3.78	3.89	3.45	3.15	2.80	2.58	2.57	2.63	2.48	1.89	1.01	0.20
JPC-27	888	0.47	3.67	3.88	3.90	3.47	3.52	3.14	2.96	2.74	2.64	2.78	3.02	3.12	2.77	2.07	0.76
JPC-27	888	0.46	3.33	3.07	2.79	2.43	2.63	2.66	2.87	2.98	2.92	2.75	2.49	2.23	2.02	1.85	0.84
JPC-27	894	0.45	3.56	3.89	3.99	3.57	3.61	3.20	3.00	2.78	2.67	2.78	3.01	3.10	2.77	2.13	0.82
JPC-27	894	0.48	3.82	4.11	4.16	3.65	3.63	3.16	2.89	2.61	2.41	2.39	2.43	2.34	1.92	1.26	0.38
JPC-27	894	0.45	3.62	4.01	4.18	3.77	3.80	3.34	3.09	2.86	2.81	3.00	3.23	3.21	2.68	1.81	0.59
JPC-27	898	0.56	4.50	4.95	5.10	4.55	4.57	4.01	3.69	3.31	2.98	2.84	2.79	2.68	2.32	1.81	0.72
JPC-27	898	0.49	3.94	4.33	4.48	4.06	4.20	3.87	3.78	3.59	3.38	3.23	3.12	2.98	2.70	2.36	1.08
JPC-27	903	0.45	3.59	3.93	4.07	3.68	3.76	3.36	3.15	2.90	2.73	2.75	2.87	2.92	2.67	2.12	0.83
JPC-27	918	0.48	3.83	4.18	4.29	3.83	3.85	3.40	3.14	2.84	2.66	2.70	2.85	2.87	2.48	1.77	0.62
JPC-27	928	0.50	3.98	4.30	4.35	3.81	3.76	3.23	2.88	2.49	2.23	2.20	2.32	2.38	2.11	1.56	0.56
JPC-27	933	0.55	4.33	4.51	4.35	3.60	3.36	2.77	2.45	2.20	2.06	2.05	2.04	1.90	1.54	1.09	0.39
JPC-27	933	0.50	3.98	4.34	4.46	3.96	3.91	3.31	2.89	2.44	2.14	2.11	2.25	2.33	2.06	1.45	0.47
JPC-27	948	0.49	3.89	4.27	4.39	3.89	3.84	3.29	2.96	2.58	2.26	2.07	1.94	1.79	1.48	1.04	0.36
JPC-27	958	0.57	4.49	4.75	4.66	3.94	3.74	3.10	2.65	2.14	1.66	1.32	1.07	0.86	0.61	0.34	0.08
JPC-27	963	0.54	4.31	4.64	4.68	4.07	3.93	3.26	2.76	2.21	1.71	1.38	1.14	0.93	0.63	0.29	0.02
JPC-27	963	0.55	4.32	4.58	4.54	3.86	3.63	2.92	2.40	1.84	1.37	1.07	0.90	0.80	0.64	0.42	0.12
JPC-27	968	0.54	4.11	4.12	3.79	2.98	2.61	1.96	1.49	1.04	0.72	0.58	0.58	0.62	0.57	0.39	0.10
JPC-27	973	0.63	5.05	5.56	5.66	4.87	4.56	3.64	3.02	2.50	2.20	2.14	2.12	1.91	1.40	0.72	0.15
JPC-27	973	0.63	5.02	5.50	5.62	4.92	4.77	3.96	3.33	2.63	2.06	1.79	1.73	1.68	1.38	0.85	0.13
JPC-27	978	0.61	4.72	4.87	4.61	3.69	3.26	2.48	1.93	1.39	0.95	0.68	0.59	0.62	0.59	0.40	0.04
JPC-27	983	0.53	4.22	4.50	4.46	3.80	3.65	3.08	2.73	2.34	1.99	1.77	1.65	1.56	1.38	1.10	0.43
JPC-27	983	0.52	4.11	4.42	4.44	3.81	3.58	2.82	2.24	1.73	1.49	1.57	1.82	1.94	1.67	1.10	0.33
JPC-27	993	0.55	4.26	4.42	4.25	3.53	3.31	2.69	2.24	1.73	1.27	0.95	0.78	0.69	0.58	0.41	0.08
JPC-27	998	0.56	4.39	4.65	4.55	3.82	3.60	2.97	2.59	2.18	1.82	1.58	1.46	1.37	1.19	0.90	0.33

Table D.20 (continued)

Core	Avg depth (cmcd)	66.9 bin	76	86.4	98.1	111	127	144	163	186	211	240	272	310	352	400	454	516	586	666	756	859	976	1110	1260<
MC-45	1.25	0.69	1.17	0.92	0.71	0.44	0.16	0.02	0.00	0.00	0.00	0.00	0.00	0.00	0.00	0.00	0.00	0.00	0.00	0.00	0.00	0.00	0.00	0.00	0.00
MC-45	2.25	0.59	0.79	0.39	0.14	0.00	0.00	0.00	0.00	0.00	0.00	0.00	0.00	0.00	0.00	0.00	0.00	0.00	0.00	0.00	0.00	0.00	0.00	0.00	0.00
MC-45	2.25	0.87	1.25	0.61	0.18	0.03	0.00	0.00	0.00	0.00	0.00	0.00	0.00	0.00	0.00	0.00	0.00	0.00	0.00	0.00	0.00	0.00	0.00	0.00	0.00
MC-45	3.25	0.67	1.15	0.77	0.28	0.00	0.00	0.00	0.00	0.00	0.00	0.00	0.00	0.00	0.00	0.00	0.00	0.00	0.00	0.00	0.00	0.00	0.00	0.00	0.00
MC-45	3.25	0.60	1.00	0.57	0.16	0.00	0.00	0.00	0.00	0.00	0.00	0.00	0.00	0.00	0.00	0.00	0.00	0.00	0.00	0.00	0.00	0.00	0.00	0.00	0.00
MC-45	8.25	0.75	1.37	1.00	0.41	0.00	0.00	0.00	0.00	0.00	0.00	0.00	0.00	0.00	0.00	0.00	0.00	0.00	0.00	0.00	0.00	0.00	0.00	0.00	0.00
MC-45	8.25	0.22	0.17	0.04	0.13	0.16	0.06	0.00	0.00	0.00	0.00	0.00	0.00	0.00	0.00	0.00	0.00	0.00	0.00	0.00	0.00	0.00	0.00	0.00	0.00
MC-45	10.25	0.18	0.06	0.00	0.00	0.00	0.00	0.00	0.00	0.00	0.00	0.00	0.00	0.00	0.00	0.00	0.00	0.00	0.00	0.00	0.00	0.00	0.00	0.00	0.00
MC-45	12.25	0.34	0.40	0.22	0.26	0.28	0.19	0.03	0.00	0.00	0.00	0.00	0.00	0.00	0.00	0.00	0.00	0.00	0.00	0.00	0.00	0.00	0.00	0.00	0.00
MC-45	14.25	0.45	0.58	0.31	0.25	0.18	0.01	0.00	0.00	0.00	0.00	0.00	0.00	0.00	0.00	0.00	0.00	0.00	0.00	0.00	0.00	0.00	0.00	0.00	0.00
MC-45	16.25	0.28	0.30	0.20	0.31	0.31	0.14	0.02	0.00	0.00	0.00	0.00	0.00	0.00	0.00	0.00	0.00	0.00	0.00	0.00	0.00	0.00	0.00	0.00	0.00
MC-45	18.25	0.10	0.06	0.14	0.30	0.28	0.15	0.02	0.00	0.00	0.00	0.00	0.00	0.00	0.00	0.00	0.00	0.00	0.00	0.00	0.00	0.00	0.00	0.00	0.00
MC-45	21	0.51	0.64	0.28	0.16	0.16	0.18	0.03	0.00	0.00	0.00	0.00	0.00	0.00	0.00	0.00	0.00	0.00	0.00	0.00	0.00	0.00	0.00	0.00	0.00
MC-45	25	0.19	0.20	0.16	0.27	0.23	0.01	0.00	0.00	0.00	0.00	0.00	0.00	0.00	0.00	0.00	0.00	0.00	0.00	0.00	0.00	0.00	0.00	0.00	0.00
MC-45	27	0.62	0.97	0.62	0.31	0.11	0.01	0.00	0.00	0.00	0.00	0.00	0.00	0.00	0.00	0.00	0.00	0.00	0.00	0.00	0.00	0.00	0.00	0.00	0.00
MC-45	27	0.95	1.74	1.28	0.58	0.05	0.00	0.00	0.00	0.00	0.00	0.00	0.00	0.00	0.00	0.00	0.00	0.00	0.00	0.00	0.00	0.00	0.00	0.00	0.00
MC-45	31	0.42	0.56	0.62	0.94	0.96	0.62	0.13	0.02	0.00	0.00	0.00	0.00	0.00	0.00	0.00	0.00	0.00	0.00	0.00	0.00	0.00	0.00	0.00	0.00
MC-45	31	0.91	1.42	0.85	0.45	0.22	0.12	0.07	0.05	0.05	0.06	0.04	0.00	0.00	0.00	0.00	0.00	0.00	0.00	0.00	0.00	0.00	0.00	0.00	0.00
MC-45	33	0.60	0.82	0.45	0.32	0.24	0.15	0.05	0.00	0.00	0.00	0.00	0.00	0.00	0.00	0.00	0.00	0.00	0.00	0.00	0.00	0.00	0.00	0.00	0.00
MC-45	35	0.11	0.02	0.00	0.00	0.00	0.00	0.00	0.00	0.00	0.00	0.00	0.00	0.00	0.00	0.00	0.00	0.00	0.00	0.00	0.00	0.00	0.00	0.00	0.00
MC-45	35	0.63	0.95	0.57	0.37	0.25	0.15	0.04	0.02	0.06	0.09	0.10	0.09	0.09	0.07	0.05	0.02	0.02	0.07	0.11	0.03	0.00	0.00	0.00	0.00
KC-27B	32.5	0.30	0.26	0.06	0.06	0.07	0.07	0.03	0.00	0.00	0.00	0.00	0.00	0.00	0.00	0.00	0.00	0.00	0.00	0.00	0.00	0.00	0.00	0.00	0.00
KC-27B	32.5	1.06	1.85	1.21	0.64	0.27	0.13	0.05	0.05	0.11	0.17	0.19	0.16	0.12	0.06	0.01	0.00	0.00	0.00	0.00	0.00	0.00	0.00	0.00	0.00
KC-27B	36.5	0.04	0.02	0.00	0.00	0.00	0.00	0.00	0.00	0.00	0.00	0.00	0.00	0.00	0.00	0.00	0.00	0.00	0.00	0.00	0.00	0.00	0.00	0.00	0.00
KC-27B	36.5	0.33	0.42	0.15	0.05	0.00	0.00	0.00	0.00	0.00	0.00	0.00	0.00	0.00	0.00	0.00	0.00	0.00	0.00	0.00	0.00	0.00	0.00	0.00	0.00
KC-27B	42.5	0.87	1.49	1.12	0.81	0.53	0.31	0.19	0.17	0.19	0.20	0.14	0.05	0.03	0.01	0.00	0.00	0.00	0.00	0.00	0.00	0.00	0.00	0.00	0.00
KC-27B	46.5	0.53	0.69	0.42	0.43	0.45	0.39	0.18	0.09	0.07	0.05	0.03	0.00	0.00	0.00	0.00	0.00	0.00	0.00	0.00	0.00	0.00	0.00	0.00	0.00
KC-27B	46.5	0.74	1.07	0.68	0.56	0.51	0.48	0.29	0.16	0.11	0.11	0.13	0.17	0.22	0.23	0.20	0.12	0.06	0.05	0.08	0.14	0.15	0.08	0.00	0.00
KC-27B	56.5	0.53	0.67	0.39	0.39	0.39	0.35	0.13	0.07	0.02	0.00	0.00	0.00	0.00	0.00	0.00	0.00	0.00	0.00	0.00	0.00	0.00	0.00	0.00	0.00
KC-27B	56.9	0.54	0.73	0.49	0.50	0.41	0.14	0.02	0.00	0.00	0.00	0.00	0.00	0.00	0.00	0.00	0.00	0.00	0.00	0.00	0.00	0.00	0.00	0.00	0.00
KC-27B	56.9	0.84	1.39	0.95	0.59	0.27	0.01	0.00	0.00	0.00	0.00	0.00	0.00	0.00	0.00	0.00	0.00	0.00	0.00	0.00	0.00	0.00	0.00	0.00	0.00
KC-27B	62.5	0.73	1.05	0.54	0.24	0.12	0.11	0.10	0.07	0.03	0.00	0.00	0.00	0.00	0.00	0.00	0.00	0.00	0.00	0.00	0.00	0.00	0.00	0.00	0.00
KC-27B	66.5	0.38	0.49	0.33	0.38	0.38	0.18	0.02	0.00	0.00	0.00	0.00	0.00	0.00	0.00	0.00	0.00	0.00	0.00	0.00	0.00	0.00	0.00	0.00	0.00
KC-27B	66.5	0.41	0.64	0.17	0.00	0.00	0.00	0.00	0.00	0.00	0.00	0.00	0.00	0.00	0.00	0.00	0.00	0.00	0.00	0.00	0.00	0.00	0.00	0.00	0.00

Table D.20 (continued)

KC-27B	72.5	0.18	0.08	0.00	0.00	0.00	0.00	0.00	0.00	0.00	0.00	0.00	0.00	0.00	0.00	0.00	0.00	0.00	0.00	0.00	0.00	0.00	0.00	0.00	0.00	0.00
KC-27B	76.5	0.50	0.73	0.46	0.34	0.27	0.25	0.11	0.03	0.00	0.00	0.00	0.00	0.00	0.00	0.00	0.00	0.00	0.00	0.00	0.00	0.00	0.00	0.00	0.00	0.00
JPC-27	82.0	0.75	1.12	0.66	0.39	0.23	0.15	0.06	0.04	0.03	0.03	0.00	0.00	0.00	0.00	0.00	0.00	0.00	0.00	0.00	0.00	0.00	0.00	0.00	0.00	0.00
JPC-27	91.3	0.50	0.67	0.41	0.38	0.33	0.19	0.03	0.00	0.00	0.00	0.00	0.00	0.00	0.00	0.00	0.00	0.00	0.00	0.00	0.00	0.00	0.00	0.00	0.00	0.00
JPC-27	100.5	0.53	0.71	0.24	0.06	0.02	0.00	0.00	0.00	0.00	0.00	0.00	0.00	0.00	0.00	0.00	0.00	0.00	0.00	0.00	0.00	0.00	0.00	0.00	0.00	0.00
JPC-27	100.5	0.38	0.45	0.32	0.37	0.29	0.05	0.00	0.00	0.00	0.00	0.00	0.00	0.00	0.00	0.00	0.00	0.00	0.00	0.00	0.00	0.00	0.00	0.00	0.00	0.00
JPC-27	107.8	0.44	0.56	0.37	0.37	0.29	0.09	0.01	0.00	0.00	0.00	0.00	0.00	0.00	0.00	0.00	0.00	0.00	0.00	0.00	0.00	0.00	0.00	0.00	0.00	0.00
JPC-27	107.8	0.20	0.25	0.30	0.45	0.38	0.09	0.01	0.00	0.00	0.00	0.00	0.00	0.00	0.00	0.00	0.00	0.00	0.00	0.00	0.00	0.00	0.00	0.00	0.00	0.00
JPC-27	114.2	0.31	0.43	0.20	0.10	0.02	0.00	0.00	0.00	0.00	0.00	0.00	0.00	0.00	0.00	0.00	0.00	0.00	0.00	0.00	0.00	0.00	0.00	0.00	0.00	0.00
JPC-27	119.5	0.79	1.34	0.91	0.54	0.23	0.04	0.00	0.00	0.00	0.00	0.00	0.00	0.00	0.00	0.00	0.00	0.00	0.00	0.00	0.00	0.00	0.00	0.00	0.00	0.00
JPC-27	131.3	0.39	0.47	0.32	0.40	0.39	0.25	0.02	0.00	0.00	0.00	0.00	0.00	0.00	0.00	0.00	0.00	0.00	0.00	0.00	0.00	0.00	0.00	0.00	0.00	0.00
JPC-27	134.4	0.35	0.16	0.00	0.00	0.00	0.00	0.00	0.00	0.00	0.00	0.00	0.00	0.00	0.00	0.00	0.00	0.00	0.00	0.00	0.00	0.00	0.00	0.00	0.00	0.00
JPC-27	137.8	0.46	0.59	0.34	0.31	0.27	0.16	0.02	0.00	0.00	0.00	0.00	0.00	0.00	0.00	0.00	0.00	0.00	0.00	0.00	0.00	0.00	0.00	0.00	0.00	0.00
JPC-27	137.8	0.19	0.21	0.28	0.47	0.41	0.05	0.00	0.00	0.00	0.00	0.00	0.00	0.00	0.00	0.00	0.00	0.00	0.00	0.00	0.00	0.00	0.00	0.00	0.00	0.00
JPC-27	163	0.32	0.30	0.09	0.17	0.25	0.07	0.01	0.00	0.00	0.00	0.00	0.00	0.00	0.00	0.00	0.00	0.00	0.00	0.00	0.00	0.00	0.00	0.00	0.00	0.00
JPC-27	173	0.27	0.24	0.06	0.08	0.12	0.11	0.02	0.00	0.00	0.00	0.00	0.00	0.00	0.00	0.00	0.00	0.00	0.00	0.00	0.00	0.00	0.00	0.00	0.00	0.00
JPC-27	183	0.22	0.28	0.14	0.10	0.07	0.03	0.00	0.00	0.00	0.00	0.00	0.00	0.00	0.00	0.00	0.00	0.00	0.00	0.00	0.00	0.00	0.00	0.00	0.00	0.00
JPC-27	193	0.31	0.44	0.26	0.14	0.06	0.00	0.00	0.00	0.00	0.00	0.00	0.00	0.00	0.00	0.00	0.00	0.00	0.00	0.00	0.00	0.00	0.00	0.00	0.00	0.00
JPC-27	213	0.15	0.08	0.01	0.02	0.04	0.04	0.02	0.00	0.00	0.00	0.00	0.00	0.00	0.00	0.00	0.00	0.00	0.00	0.00	0.00	0.00	0.00	0.00	0.00	0.00
JPC-27	253	0.63	0.94	0.59	0.41	0.28	0.07	0.01	0.00	0.00	0.00	0.00	0.00	0.00	0.00	0.00	0.00	0.00	0.00	0.00	0.00	0.00	0.00	0.00	0.00	0.00
JPC-27	273	0.40	0.56	0.48	0.56	0.54	0.48	0.37	0.33	0.34	0.30	0.27	0.21	0.15	0.08	0.03	0.00	0.00	0.00	0.00	0.00	0.00	0.00	0.00	0.00	0.00
JPC-27	293	0.00	0.00	0.00	0.00	0.00	0.00	0.00	0.00	0.00	0.00	0.00	0.00	0.00	0.00	0.00	0.00	0.00	0.00	0.00	0.00	0.00	0.00	0.00	0.00	0.00
JPC-27	313	0.15	0.12	0.14	0.26	0.22	0.04	0.00	0.00	0.00	0.00	0.00	0.00	0.00	0.00	0.00	0.00	0.00	0.00	0.00	0.00	0.00	0.00	0.00	0.00	0.00
JPC-27	353	0.35	0.54	0.14	0.00	0.00	0.00	0.00	0.00	0.00	0.00	0.00	0.00	0.00	0.00	0.00	0.00	0.00	0.00	0.00	0.00	0.00	0.00	0.00	0.00	0.00
JPC-27	353	0.78	1.28	0.95	0.72	0.44	0.13	0.02	0.00	0.00	0.00	0.00	0.00	0.00	0.00	0.00	0.00	0.00	0.00	0.00	0.00	0.00	0.00	0.00	0.00	0.00
JPC-27	353	0.75	1.29	1.04	0.85	0.52	0.11	0.01	0.00	0.00	0.00	0.00	0.00	0.00	0.00	0.00	0.00	0.00	0.00	0.00	0.00	0.00	0.00	0.00	0.00	0.00
JPC-27	373	0.05	0.06	0.19	0.29	0.29	0.21	0.05	0.01	0.00	0.00	0.00	0.00	0.00	0.00	0.00	0.00	0.00	0.00	0.00	0.00	0.00	0.00	0.00	0.00	0.00
JPC-27	373	0.59	0.95	0.88	0.94	0.80	0.51	0.20	0.11	0.14	0.17	0.19	0.15	0.11	0.07	0.05	0.02	0.00	0.00	0.00	0.00	0.00	0.00	0.00	0.00	0.00
JPC-27	393	0.59	0.92	0.82	0.92	0.88	0.67	0.30	0.16	0.16	0.18	0.21	0.19	0.18	0.06	0.01	0.00	0.00	0.00	0.00	0.00	0.00	0.00	0.00	0.00	0.00
JPC-27	413	0.13	0.14	0.29	0.46	0.43	0.21	0.04	0.01	0.00	0.00	0.00	0.00	0.00	0.00	0.00	0.00	0.00	0.00	0.00	0.00	0.00	0.00	0.00	0.00	0.00
JPC-27	433	0.55	1.06	0.98	0.87	0.63	0.39	0.20	0.16	0.20	0.22	0.21	0.17	0.16	0.16	0.14	0.07	0.00	0.00	0.00	0.00	0.00	0.00	0.00	0.00	0.00
JPC-27	433	0.57	0.88	0.54	0.33	0.22	0.17	0.11	0.05	0.02	0.04	0.04	0.02	0.04	0.09	0.11	0.08	0.02	0.00	0.00	0.00	0.00	0.00	0.00	0.00	0.00
JPC-27	433	0.89	1.57	1.01	0.53	0.29	0.26	0.25	0.27	0.26	0.26	0.24	0.28	0.34	0.41	0.44	0.39	0.24	0.24	0.22	0.20	0.19	0.10	0.00	0.00	0.00
JPC-27	453	0.96	1.75	1.47	1.24	0.98	0.75	0.41	0.29	0.38	0.49	0.50	0.33	0.27	0.24	0.23	0.23	0.24	0.24	0.22	0.20	0.19	0.10	0.00	0.00	0.00
JPC-27	453	0.43	0.73	0.85	1.05	0.97	0.70	0.27	0.12	0.14	0.18	0.23	0.24	0.21	0.15	0.08	0.05	0.04	0.03	0.02	0.00	0.00	0.00	0.00	0.00	0.00
JPC-27	473	0.59	0.98	0.61	0.34	0.23	0.20	0.12	0.07	0.06	0.04	0.00	0.00	0.00	0.00	0.00	0.00	0.00	0.00	0.00	0.00	0.00	0.00	0.00	0.00	0.00
JPC-27	493	0.55	0.95	1.00	1.17	1.05	0.69	0.21	0.05	0.11	0.22	0.31	0.31	0.27	0.09	0.02	0.00	0.00	0.00	0.00	0.00	0.00	0.00	0.00	0.00	0.00

Table D.20 (continued)

JPC-27	513	0.88	1.51	0.99	0.56	0.33	0.30	0.19	0.11	0.10	0.13	0.16	0.14	0.10	0.02	0.00	0.00	0.00	0.00	0.00	0.00	0.00	0.00	0.00	0.00
JPC-27	513	0.35	0.49	0.50	0.65	0.60	0.27	0.01	0.00	0.00	0.00	0.00	0.00	0.00	0.00	0.00	0.00	0.00	0.00	0.00	0.00	0.00	0.00	0.00	0.00
JPC-27	533	0.44	0.70	0.74	0.87	0.77	0.52	0.20	0.09	0.09	0.12	0.12	0.09	0.08	0.06	0.02	0.00	0.00	0.00	0.00	0.00	0.00	0.00	0.00	0.00
JPC-27	533	0.19	0.31	0.43	0.54	0.47	0.27	0.06	0.01	0.00	0.00	0.00	0.00	0.00	0.00	0.00	0.00	0.00	0.00	0.00	0.00	0.00	0.00	0.00	0.00
JPC-27	553	0.74	1.27	1.08	1.04	0.96	0.85	0.50	0.32	0.32	0.32	0.31	0.27	0.26	0.26	0.28	0.29	0.28	0.25	0.24	0.28	0.36	0.38	0.17	0.00
JPC-27	553	0.14	0.21	0.41	0.60	0.55	0.32	0.02	0.00	0.00	0.00	0.00	0.00	0.00	0.00	0.00	0.00	0.00	0.00	0.00	0.00	0.00	0.00	0.00	0.00
JPC-27	573	1.43	2.76	2.20	1.61	1.18	1.01	0.75	0.61	0.64	0.62	0.54	0.38	0.32	0.28	0.24	0.22	0.16	0.03	0.00	0.00	0.00	0.00	0.00	0.00
JPC-27	573	0.99	1.92	1.66	1.29	0.86	0.56	0.34	0.34	0.51	0.59	0.49	0.27	0.23	0.44	0.88	1.05	0.77	0.45	0.24	0.02	0.00	0.00	0.00	0.00
JPC-27	593	0.86	1.59	1.39	1.25	1.04	0.82	0.42	0.22	0.19	0.18	0.14	0.06	0.01	0.00	0.00	0.00	0.00	0.00	0.00	0.00	0.00	0.00	0.00	0.00
JPC-27	593	0.59	1.06	0.98	0.99	0.83	0.51	0.13	0.00	0.05	0.13	0.18	0.13	0.05	0.00	0.00	0.00	0.00	0.00	0.00	0.00	0.00	0.00	0.00	0.00
JPC-27	613	0.78	1.45	1.23	1.05	0.90	0.77	0.41	0.25	0.28	0.31	0.29	0.20	0.13	0.11	0.15	0.22	0.29	0.28	0.17	0.03	0.00	0.00	0.00	0.00
JPC-27	633	0.25	0.34	0.38	0.50	0.42	0.26	0.11	0.07	0.10	0.15	0.19	0.19	0.20	0.19	0.19	0.20	0.17	0.09	0.01	0.00	0.00	0.00	0.00	0.00
JPC-27	653	1.16	2.08	1.87	1.78	1.53	1.21	0.65	0.37	0.33	0.35	0.35	0.30	0.27	0.26	0.26	0.25	0.24	0.23	0.26	0.27	0.30	0.12	0.00	0.00
JPC-27	653	0.75	1.40	1.31	1.26	1.00	0.54	0.17	0.08	0.12	0.15	0.13	0.04	0.00	0.00	0.00	0.00	0.00	0.00	0.00	0.00	0.00	0.00	0.00	0.00
JPC-27	673	0.50	0.78	0.74	0.87	0.82	0.62	0.13	0.02	0.00	0.00	0.00	0.00	0.00	0.00	0.00	0.00	0.00	0.00	0.00	0.00	0.00	0.00	0.00	0.00
JPC-27	673	0.81	1.43	1.01	0.64	0.39	0.28	0.11	0.04	0.06	0.09	0.08	0.04	0.02	0.05	0.08	0.09	0.05	0.00	0.00	0.00	0.00	0.00	0.00	0.00
JPC-27	693	0.65	1.06	0.97	1.04	0.92	0.64	0.04	0.00	0.00	0.00	0.00	0.00	0.00	0.00	0.00	0.00	0.00	0.00	0.00	0.00	0.00	0.00	0.00	0.00
JPC-27	693	0.20	0.28	0.47	0.77	0.74	0.40	0.07	0.01	0.00	0.00	0.00	0.00	0.00	0.00	0.00	0.00	0.00	0.00	0.00	0.00	0.00	0.00	0.00	0.00
JPC-27	713	0.54	0.90	0.73	0.47	0.13	0.01	0.00	0.00	0.00	0.00	0.00	0.00	0.00	0.00	0.00	0.00	0.00	0.00	0.00	0.00	0.00	0.00	0.00	0.00
JPC-27	713	0.38	0.63	0.66	0.76	0.64	0.33	0.02	0.00	0.00	0.00	0.00	0.00	0.00	0.00	0.00	0.00	0.00	0.00	0.00	0.00	0.00	0.00	0.00	0.00
JPC-27	713	0.98	1.86	1.53	1.16	0.81	0.53	0.26	0.20	0.26	0.29	0.31	0.25	0.19	0.11	0.05	0.01	0.02	0.07	0.10	0.03	0.00	0.00	0.00	0.00
JPC-27	733	0.94	1.71	1.45	1.30	1.13	0.96	0.63	0.50	0.52	0.48	0.42	0.30	0.29	0.40	0.56	0.63	0.36	0.00	0.00	0.00	0.00	0.00	0.00	0.00
JPC-27	733	0.27	0.33	0.32	0.46	0.47	0.38	0.19	0.10	0.10	0.11	0.09	0.04	0.00	0.00	0.00	0.00	0.00	0.00	0.00	0.00	0.00	0.00	0.00	0.00
JPC-27	733	0.83	1.51	1.20	0.91	0.62	0.40	0.17	0.09	0.11	0.12	0.11	0.06	0.04	0.07	0.13	0.20	0.27	0.28	0.24	0.03	0.00	0.00	0.00	0.00
JPC-27	753	0.54	0.91	0.69	0.50	0.28	0.12	0.02	0.00	0.00	0.00	0.00	0.00	0.00	0.00	0.00	0.00	0.00	0.00	0.00	0.00	0.00	0.00	0.00	0.00
JPC-27	753	0.31	0.46	0.36	0.37	0.29	0.12	0.05	0.01	0.00	0.00	0.00	0.00	0.00	0.00	0.00	0.00	0.00	0.00	0.00	0.00	0.00	0.00	0.00	0.00
JPC-27	773	0.94	1.73	1.48	1.25	0.96	0.72	0.49	0.39	0.36	0.30	0.21	0.13	0.14	0.17	0.15	0.11	0.03	0.00	0.00	0.00	0.00	0.00	0.00	0.00
JPC-27	793	0.45	0.73	0.77	0.91	0.79	0.47	0.16	0.09	0.13	0.14	0.11	0.03	0.00	0.00	0.00	0.00	0.00	0.00	0.00	0.00	0.00	0.00	0.00	0.00
JPC-27	813	0.00	0.00	0.00	0.00	0.00	0.00	0.00	0.00	0.00	0.00	0.00	0.00	0.00	0.00	0.00	0.00	0.00	0.00	0.00	0.00	0.00	0.00	0.00	0.00
JPC-27	813	0.55	0.88	0.66	0.54	0.38	0.18	0.07	0.04	0.07	0.11	0.11	0.07	0.04	0.01	0.00	0.00	0.00	0.00	0.00	0.00	0.00	0.00	0.00	0.00
JPC-27	813	0.60	1.01	0.74	0.54	0.39	0.27	0.09	0.02	0.03	0.05	0.07	0.07	0.05	0.01	0.00	0.00	0.00	0.00	0.00	0.00	0.00	0.00	0.00	0.00
JPC-27	833	0.56	0.93	0.75	0.69	0.57	0.41	0.21	0.16	0.19	0.20	0.13	0.05	0.00	0.00	0.00	0.00	0.00	0.00	0.00	0.00	0.00	0.00	0.00	0.00
JPC-27	838	0.46	0.86	1.07	1.32	1.16	0.70	0.22	0.05	0.05	0.14	0.25	0.27	0.17	0.04	0.00	0.00	0.00	0.00	0.00	0.00	0.00	0.00	0.00	0.00
JPC-27	843	0.84	1.48	1.40	1.44	1.27	0.93	0.24	0.05	0.00	0.00	0.00	0.00	0.00	0.00	0.00	0.00	0.00	0.00	0.00	0.00	0.00	0.00	0.00	0.00
JPC-27	843	0.36	0.60	0.80	1.01	0.80	0.36	0.12	0.08	0.09	0.14	0.18	0.20	0.25	0.17	0.07	0.00	0.00	0.00	0.00	0.00	0.00	0.00	0.00	0.00
JPC-27	848	0.67	1.16	1.05	0.98	0.70	0.30	0.09	0.05	0.06	0.11	0.13	0.09	0.05	0.01	0.00	0.00	0.00	0.00	0.00	0.00	0.00	0.00	0.00	0.00
JPC-27	848	0.36	0.59	0.48	0.47	0.42	0.31	0.12	0.07	0.10	0.11	0.10	0.04	0.00	0.00	0.00	0.00	0.00	0.00	0.00	0.00	0.00	0.00	0.00	0.00

Table D.20 (continued)

JPC-27	848	0.75	1.22	0.77	0.39	0.12	0.08	0.08	0.10	0.10	0.06	0.00	0.00	0.00	0.00	0.00	0.00	0.00	0.00	0.00	0.00	0.00	0.00	0.00	0.00
JPC-27	853	0.63	1.19	1.21	1.14	0.74	0.39	0.20	0.17	0.19	0.23	0.22	0.17	0.15	0.14	0.15	0.15	0.13	0.07	0.01	0.00	0.00	0.00	0.00	0.00
JPC-27	853	0.55	0.93	0.80	0.75	0.53	0.18	0.02	0.00	0.00	0.00	0.00	0.00	0.00	0.00	0.00	0.00	0.00	0.00	0.00	0.00	0.00	0.00	0.00	0.00
JPC-27	858	0.90	1.61	1.28	0.97	0.64	0.37	0.13	0.07	0.09	0.09	0.08	0.03	0.02	0.03	0.04	0.06	0.09	0.09	0.08	0.01	0.00	0.00	0.00	0.00
JPC-27	858	0.19	0.45	0.64	0.71	0.49	0.13	0.01	0.00	0.00	0.00	0.00	0.00	0.00	0.00	0.00	0.00	0.00	0.00	0.00	0.00	0.00	0.00	0.00	0.00
JPC-27	863	0.66	1.22	1.08	0.99	0.80	0.59	0.31	0.24	0.31	0.34	0.29	0.18	0.14	0.14	0.17	0.15	0.11	0.03	0.00	0.00	0.00	0.00	0.00	0.00
JPC-27	873	0.71	1.26	1.27	1.41	1.31	1.01	0.44	0.19	0.24	0.35	0.41	0.33	0.26	0.23	0.24	0.25	0.22	0.13	0.01	0.00	0.00	0.00	0.00	0.00
JPC-27	878	0.69	1.22	1.05	0.91	0.64	0.39	0.16	0.12	0.18	0.23	0.21	0.15	0.15	0.08	0.02	0.00	0.00	0.00	0.00	0.00	0.00	0.00	0.00	0.00
JPC-27	883	0.33	0.35	0.08	0.05	0.09	0.13	0.11	0.07	0.02	0.00	0.00	0.00	0.00	0.00	0.00	0.00	0.00	0.00	0.00	0.00	0.00	0.00	0.00	0.00
JPC-27	883	0.02	0.01	0.11	0.21	0.22	0.13	0.02	0.00	0.00	0.00	0.00	0.00	0.00	0.00	0.00	0.00	0.00	0.00	0.00	0.00	0.00	0.00	0.00	0.00
JPC-27	888	0.51	0.81	0.74	0.76	0.60	0.32	0.05	0.00	0.00	0.00	0.00	0.00	0.00	0.00	0.00	0.00	0.00	0.00	0.00	0.00	0.00	0.00	0.00	0.00
JPC-27	888	0.62	0.87	0.39	0.26	0.34	0.39	0.15	0.04	0.00	0.00	0.00	0.00	0.00	0.00	0.00	0.00	0.00	0.00	0.00	0.00	0.00	0.00	0.00	0.00
JPC-27	894	0.58	1.00	0.96	0.97	0.76	0.43	0.16	0.09	0.10	0.11	0.09	0.05	0.04	0.05	0.07	0.05	0.02	0.00	0.00	0.00	0.00	0.00	0.00	0.00
JPC-27	894	0.20	0.19	0.09	0.06	0.00	0.00	0.00	0.00	0.00	0.00	0.00	0.00	0.00	0.00	0.00	0.00	0.00	0.00	0.00	0.00	0.00	0.00	0.00	0.00
JPC-27	894	0.37	0.62	0.84	1.16	1.10	0.74	0.05	0.00	0.00	0.00	0.00	0.00	0.00	0.00	0.00	0.00	0.00	0.00	0.00	0.00	0.00	0.00	0.00	0.00
JPC-27	898	0.52	0.83	0.61	0.48	0.35	0.17	0.02	0.00	0.00	0.00	0.00	0.00	0.00	0.00	0.00	0.00	0.00	0.00	0.00	0.00	0.00	0.00	0.00	0.00
JPC-27	898	0.87	1.63	1.38	1.09	0.74	0.44	0.20	0.13	0.17	0.19	0.17	0.11	0.07	0.06	0.06	0.06	0.05	0.03	0.00	0.00	0.00	0.00	0.00	0.00
JPC-27	903	0.58	0.89	0.69	0.66	0.57	0.39	0.13	0.05	0.07	0.09	0.08	0.05	0.02	0.03	0.04	0.05	0.05	0.04	0.00	0.00	0.00	0.00	0.00	0.00
JPC-27	918	0.41	0.68	0.74	0.87	0.75	0.46	0.06	0.00	0.00	0.00	0.00	0.00	0.00	0.00	0.00	0.00	0.00	0.00	0.00	0.00	0.00	0.00	0.00	0.00
JPC-27	928	0.38	0.60	0.59	0.63	0.51	0.28	0.08	0.02	0.00	0.00	0.00	0.00	0.00	0.00	0.00	0.00	0.00	0.00	0.00	0.00	0.00	0.00	0.00	0.00
JPC-27	933	0.25	0.19	0.03	0.00	0.00	0.00	0.00	0.00	0.00	0.00	0.00	0.00	0.00	0.00	0.00	0.00	0.00	0.00	0.00	0.00	0.00	0.00	0.00	0.00
JPC-27	933	0.27	0.38	0.45	0.67	0.63	0.35	0.06	0.01	0.00	0.00	0.00	0.00	0.00	0.00	0.00	0.00	0.00	0.00	0.00	0.00	0.00	0.00	0.00	0.00
JPC-27	948	0.23	0.34	0.28	0.22	0.08	0.01	0.00	0.00	0.00	0.00	0.00	0.00	0.00	0.00	0.00	0.00	0.00	0.00	0.00	0.00	0.00	0.00	0.00	0.00
JPC-27	958	0.04	0.08	0.19	0.20	0.07	0.01	0.00	0.00	0.00	0.00	0.00	0.00	0.00	0.00	0.00	0.00	0.00	0.00	0.00	0.00	0.00	0.00	0.00	0.00
JPC-27	963	0.00	0.00	0.00	0.00	0.00	0.00	0.00	0.00	0.00	0.00	0.00	0.00	0.00	0.00	0.00	0.00	0.00	0.00	0.00	0.00	0.00	0.00	0.00	0.00
JPC-27	963	0.06	0.04	0.02	0.03	0.03	0.00	0.00	0.00	0.00	0.00	0.00	0.00	0.00	0.00	0.00	0.00	0.00	0.00	0.00	0.00	0.00	0.00	0.00	0.00
JPC-27	968	0.04	0.04	0.04	0.05	0.02	0.00	0.00	0.00	0.00	0.00	0.00	0.00	0.00	0.00	0.00	0.00	0.00	0.00	0.00	0.00	0.00	0.00	0.00	0.00
JPC-27	973	0.05	0.04	0.07	0.10	0.11	0.06	0.00	0.00	0.00	0.00	0.00	0.00	0.00	0.00	0.00	0.00	0.00	0.00	0.00	0.00	0.00	0.00	0.00	0.00
JPC-27	973	0.03	0.00	0.00	0.00	0.00	0.00	0.00	0.00	0.00	0.00	0.00	0.00	0.00	0.00	0.00	0.00	0.00	0.00	0.00	0.00	0.00	0.00	0.00	0.00
JPC-27	978	0.00	0.00	0.00	0.00	0.00	0.00	0.00	0.00	0.00	0.00	0.00	0.00	0.00	0.00	0.00	0.00	0.00	0.00	0.00	0.00	0.00	0.00	0.00	0.00
JPC-27	983	0.30	0.46	0.34	0.32	0.29	0.25	0.08	0.02	0.00	0.00	0.00	0.00	0.00	0.00	0.00	0.00	0.00	0.00	0.00	0.00	0.00	0.00	0.00	0.00
JPC-27	983	0.18	0.27	0.36	0.49	0.41	0.22	0.08	0.04	0.04	0.06	0.08	0.08	0.07	0.01	0.00	0.00	0.00	0.00	0.00	0.00	0.00	0.00	0.00	0.00
JPC-27	993	0.02	0.01	0.00	0.00	0.00	0.00	0.00	0.00	0.00	0.00	0.00	0.00	0.00	0.00	0.00	0.00	0.00	0.00	0.00	0.00	0.00	0.00	0.00	0.00
JPC-27	998	0.23	0.36	0.32	0.35	0.28	0.08	0.01	0.00	0.00	0.00	0.00	0.00	0.00	0.00	0.00	0.00	0.00	0.00	0.00	0.00	0.00	0.00	0.00	0.00

Table D.21 Sortable silt data.

Core	Avg depth (cmd)	age	%<63	%10-63	SS%	log (%ss)	SSmean	log (SSmean)
MC-45	1.25	48.26255	94.981	50.667	53.344	1.727	25.421	1.405
MC-45	2.25	86.87259	97.201	57.554	59.211	1.772	26.274	1.420
MC-45	2.25	86.87259	95.847	58.714	61.257	1.787	27.408	1.438
MC-45	3.25	125.4826	96.289	53.684	55.753	1.746	25.076	1.399
MC-45	3.25	125.4826	96.931	48.838	50.384	1.702	23.935	1.379
MC-45	8.25	318.5328	95.567	52.485	54.920	1.740	24.975	1.398
MC-45	8.25	318.5328	98.784	50.057	50.673	1.705	23.444	1.370
MC-45	10.25	395.7529	99.371	50.872	51.194	1.709	23.716	1.375
MC-45	12.25	472.973	97.706	51.513	52.722	1.722	24.104	1.382
MC-45	14.25	550.1931	97.494	52.959	54.320	1.735	24.906	1.396
MC-45	16.25	627.4131	97.920	51.207	52.295	1.718	24.171	1.383
MC-45	18.25	704.6332	98.668	50.725	51.410	1.711	23.665	1.374
MC-45	21	810.8108	97.267	53.757	55.267	1.742	24.496	1.389
MC-45	25	965.251	98.571	48.784	49.491	1.695	23.158	1.365
MC-45	27	1042.471	96.499	57.659	59.751	1.776	24.886	1.396
MC-45	27	1042.471	94.279	57.631	61.128	1.786	25.482	1.406
MC-45	31	1196.911	94.987	55.482	58.410	1.766	25.903	1.413
MC-45	31	1196.911	94.540	56.072	59.311	1.773	26.656	1.426
MC-45	33	1254.826	96.473	55.813	57.853	1.762	25.547	1.407
MC-45	35	1254.826	99.547	52.929	53.169	1.726	24.024	1.381
MC-45	35	1274.131	95.317	54.732	57.421	1.759	25.781	1.411
KC-27B	32.5	1351.351	98.610	46.477	47.132	1.673	1.673	0.224
KC-27B	32.5	1351.351	92.641	47.849	51.650	1.713	1.713	0.234
KC-27B	36.5	1409.266	99.783	49.451	49.559	1.695	1.695	0.229
KC-27B	36.5	1409.266	98.576	48.879	49.585	1.695	1.695	0.229
KC-27B	42.5	1640.927	92.760	55.090	59.391	1.774	1.774	0.249
KC-27B	46.5	1795.367	95.839	51.848	54.099	1.733	1.733	0.239
KC-27B	46.5	1795.367	92.585	55.451	59.891	1.777	1.777	0.250
KC-27B	56.5	2181.467	96.214	55.867	58.066	1.764	1.764	0.246
KC-27B	56.9	2196.179	96.313	56.531	58.695	1.769	1.769	0.248
KC-27B	56.9	2196.179	94.838	57.401	60.525	1.782	1.782	0.251
KC-27B	62.5	2413.127	95.975	57.632	60.049	1.779	1.779	0.250
KC-27B	66.5	2567.568	97.210	52.547	54.055	1.733	1.733	0.239
KC-27B	66.5	2567.568	98.282	42.096	42.832	1.632	1.632	0.213
KC-27B	72.5	2799.228	99.406	48.428	48.717	1.688	1.688	0.227

Table D.21 (continued)

KC-27B	76.5	2953.668	96.590	59.146	61.234	1.787	1.787	0.252
JPC-27	82.0	3164.181	95.468	58.462	61.237	1.787	1.787	0.252
JPC-27	91.3	3526.231	96.712	53.258	55.069	1.741	1.741	0.241
JPC-27	100.5	3878.732	97.666	52.308	53.558	1.729	1.729	0.238
JPC-27	100.5	3878.732	97.483	54.057	55.453	1.744	1.744	0.242
JPC-27	107.8	4162.537	97.168	54.734	56.329	1.751	1.751	0.243
JPC-27	107.8	4162.537	97.936	47.767	48.773	1.688	1.688	0.227
JPC-27	114.2	4409.465	98.478	51.005	51.794	1.714	1.714	0.234
JPC-27	119.5	4613.366	95.152	53.468	56.192	1.750	1.750	0.243
JPC-27	131.3	5070.612	97.100	51.791	53.339	1.727	1.727	0.237
JPC-27	134.4	5187.346	98.879	51.570	52.154	1.717	1.717	0.235
JPC-27	137.8	5253.925	97.137	51.444	52.960	1.724	1.724	0.237
JPC-27	137.8	5253.925	97.990	49.330	50.342	1.702	1.702	0.231
JPC-27	163	5570.05	98.244	50.557	51.460	1.711	1.711	0.233
JPC-27	173	5695.363	98.588	55.669	56.466	1.752	1.752	0.243
JPC-27	183	5820.677	98.807	48.231	48.813	1.689	1.689	0.228
JPC-27	193	5945.99	98.323	49.876	50.727	1.705	1.705	0.232
JPC-27	213	6196.617	99.319	47.555	47.881	1.680	1.680	0.225
JPC-27	253	6697.87	96.166	54.011	56.165	1.749	1.749	0.243
JPC-27	273	6948.496	94.267	45.090	47.832	1.680	1.680	0.225
JPC-27	293	7199.123	99.909	40.325	40.362	1.606	1.606	0.206
JPC-27	313	7449.749	98.696	45.331	45.930	1.662	1.662	0.221
JPC-27	353	7951.003	98.537	39.783	40.373	1.606	1.606	0.206
JPC-27	353	7951.003	94.434	55.136	58.385	1.766	1.766	0.247
JPC-27	353	8201.629	98.670	39.067	39.593	1.598	1.598	0.203
JPC-27	373	8201.629	93.216	50.222	53.877	1.731	1.731	0.238
JPC-27	373	8452.256	92.861	45.445	48.939	1.690	1.690	0.228
JPC-27	393	8702.882	97.976	41.513	42.370	1.627	1.627	0.211
JPC-27	413	8953.509	93.123	35.172	37.770	1.577	1.577	0.198
JPC-27	433	8953.509	95.894	42.920	44.757	1.651	1.651	0.218
JPC-27	433	8953.509	90.641	41.544	45.833	1.661	1.661	0.220
JPC-27	433	9067.362	87.055	46.994	53.982	1.732	1.732	0.239
JPC-27	453	9067.362	92.869	41.416	44.596	1.649	1.649	0.217
JPC-27	453	9162.239	96.016	44.319	46.157	1.664	1.664	0.221
JPC-27	473	9257.116	92.201	43.569	47.255	1.674	1.674	0.224
JPC-27	493	9351.992	93.407	41.477	44.404	1.647	1.647	0.217
JPC-27	513	9351.992	96.571	45.496	47.111	1.673	1.673	0.224

Table D.21 (continued)

JPC-27	513	9446.869	94.411	41.829	44.305	1.646	1.646	0.217
JPC-27	533	9446.869	97.350	41.332	42.457	1.628	1.628	0.212
JPC-27	533	9541.746	88.011	46.418	52.741	1.722	1.722	0.236
JPC-27	553	9541.746	97.434	44.359	45.528	1.658	1.658	0.220
JPC-27	553	9636.622	83.379	44.961	53.924	1.732	1.732	0.238
JPC-27	573	9636.622	84.905	44.824	52.794	1.723	1.723	0.236
JPC-27	573	9731.499	90.767	39.339	43.341	1.637	1.637	0.214
JPC-27	593	9731.499	93.580	37.086	39.630	1.598	1.598	0.204
JPC-27	593	9826.376	89.726	41.269	45.994	1.663	1.663	0.221
JPC-27	613	9921.252	95.587	35.653	37.299	1.572	1.572	0.196
JPC-27	633	10016.13	84.074	50.863	60.498	1.782	1.782	0.251
JPC-27	653	10016.13	92.097	46.499	50.489	1.703	1.703	0.231
JPC-27	653	10111.01	94.755	43.472	45.878	1.662	1.662	0.221
JPC-27	673	10111.01	93.706	43.220	46.123	1.664	1.664	0.221
JPC-27	673	10205.88	93.737	46.836	49.966	1.699	1.699	0.230
JPC-27	693	10205.88	96.687	42.236	43.683	1.640	1.640	0.215
JPC-27	693	10300.76	96.495	47.613	49.343	1.693	1.693	0.229
JPC-27	713	10300.76	96.012	43.299	45.098	1.654	1.654	0.219
JPC-27	713	10300.76	89.804	44.884	49.980	1.699	1.699	0.230
JPC-27	713	10395.64	86.246	38.667	44.833	1.652	1.652	0.218
JPC-27	733	10395.64	96.649	39.566	40.938	1.612	1.612	0.207
JPC-27	733	10395.64	91.572	44.601	48.706	1.688	1.688	0.227
JPC-27	733	10490.51	96.232	40.446	42.030	1.624	1.624	0.210
JPC-27	753	10490.51	97.568	38.612	39.575	1.597	1.597	0.203
JPC-27	753	10585.39	89.268	44.335	49.665	1.696	1.696	0.229
JPC-27	773	10680.27	94.523	46.125	48.798	1.688	1.688	0.227
JPC-27	793	10775.14	99.962	31.842	31.854	1.503	1.503	0.177
JPC-27	813	10775.14	95.540	40.338	42.221	1.626	1.626	0.211
JPC-27	813	10775.14	95.278	42.144	44.233	1.646	1.646	0.216
JPC-27	813	10870.02	94.398	41.654	44.126	1.645	1.645	0.216
JPC-27	833	10893.74	92.575	44.784	48.375	1.685	1.685	0.227
JPC-27	838	10917.46	91.215	52.417	57.466	1.759	1.759	0.245
JPC-27	843	10917.46	94.174	45.132	47.924	1.681	1.681	0.225
JPC-27	843	10941.18	93.622	47.857	51.117	1.709	1.709	0.233
JPC-27	848	10941.18	96.350	29.372	30.485	1.484	1.484	0.171
JPC-27	848	10941.18	95.346	48.795	51.177	1.709	1.709	0.233
JPC-27	848	10964.9	91.868	45.340	49.354	1.693	1.693	0.229

Table D.21 (continued)

JPC-27	853	10964.9	95.479	43.872	45.949	1.662	1.662	0.221
JPC-27	853	10988.61	92.182	47.963	52.031	1.716	1.716	0.235
JPC-27	858	10988.61	97.096	29.228	30.102	1.479	1.479	0.170
JPC-27	858	11012.33	91.418	40.183	43.955	1.643	1.643	0.216
JPC-27	863	11059.77	88.768	44.905	50.587	1.704	1.704	0.231
JPC-27	873	11083.49	92.879	42.640	45.909	1.662	1.662	0.221
JPC-27	878	11107.21	98.267	37.558	38.220	1.582	1.582	0.199
JPC-27	883	11107.21	99.090	42.585	42.976	1.633	1.633	0.213
JPC-27	883	11488.46	95.445	44.155	46.262	1.665	1.665	0.221
JPC-27	888	11488.46	96.101	37.495	39.016	1.591	1.591	0.202
JPC-27	888	11776.92	93.632	44.507	47.534	1.677	1.677	0.225
JPC-27	894	11776.92	99.082	41.271	41.653	1.620	1.620	0.209
JPC-27	894	11776.92	94.529	45.868	48.522	1.686	1.686	0.227
JPC-27	894	11969.23	96.307	50.654	52.597	1.721	1.721	0.236
JPC-27	898	11969.23	91.471	50.510	55.220	1.742	1.742	0.241
JPC-27	898	12209.62	94.698	44.932	47.448	1.676	1.676	0.224
JPC-27	903	12930.77	95.402	45.158	47.335	1.675	1.675	0.224
JPC-27	918	13411.54	96.348	42.099	43.694	1.640	1.640	0.215
JPC-27	928	13550	99.141	38.788	39.124	1.592	1.592	0.202
JPC-27	933	13550	96.703	42.129	43.565	1.639	1.639	0.215
JPC-27	933	14300	98.469	40.164	40.788	1.611	1.611	0.207
JPC-27	948	14800	99.314	35.892	36.140	1.558	1.558	0.193
JPC-27	958	15050	99.977	36.471	36.480	1.562	1.562	0.194
JPC-27	963	15050	99.699	33.836	33.938	1.531	1.531	0.185
JPC-27	963	15300	99.701	26.112	26.191	1.418	1.418	0.152
JPC-27	968	15550	99.420	45.957	46.225	1.665	1.665	0.221
JPC-27	973	15550	99.850	45.856	45.925	1.662	1.662	0.221
JPC-27	973	15800	99.957	31.391	31.405	1.497	1.497	0.175
JPC-27	978	16050	97.500	38.765	39.759	1.599	1.599	0.204
JPC-27	983	16050	97.264	37.246	38.293	1.583	1.583	0.200
JPC-27	983	16550	99.887	31.659	31.694	1.501	1.501	0.176
JPC-27	993		98.042	37.628	38.379	1.584	1.584	0.200
JPC-27	998		78.883	41.137	52.150	1.717	1.717	0.235

APPENDIX E:

PERMISSIONS AND COPYRIGHT INFORMATION

Copyright information for Figure 1 (left panel) from “Extensive dynamic thinning on the margins of the Greenland and Antarctic ice sheets” by Pritchard et al. (2009), *Nature*, 461, 971-975.

SPRINGER NATURE LICENSE TERMS AND CONDITIONS

May 25, 2021

This Agreement between University of South Florida -- Kara Vadman ("You") and Springer Nature ("Springer Nature") consists of your license details and the terms and conditions provided by Springer Nature and Copyright Clearance Center.

License Number	5076041183093
License date	May 25, 2021
Licensed Content Publisher	Springer Nature
Licensed Content Publication	Nature
Licensed Content Title	Extensive dynamic thinning on the margins of the Greenland and Antarctic ice sheets
Licensed Content Author	Hamish D. Pritchard et al
Licensed Content Date	Sep 23, 2009
Type of Use	Thesis/Dissertation
Requestor type	academic/university or research institute
Format	electronic
Portion	figures/tables/illustrations
Number of figures/tables/illustrations	1
High-res required	no
Will you be translating?	no
Circulation/distribution	1 - 29
Author of this Springer Nature content	no

Title	Kara Vadman
Institution name	University of South Florida
Expected presentation date	May 2021
Portions	Figure 2: Rate of change of surface elevation for Antarctica and Greenland. University of South Florida 140 7th Ave S
Requestor Location	SAINT PETERSBURG, FL 33701 United States Attn: University of South Florida
Total	0.00 USD
Terms and Conditions	

Springer Nature Customer Service Centre GmbH Terms and Conditions

This agreement sets out the terms and conditions of the licence (the **Licence**) between you and **Springer Nature Customer Service Centre GmbH** (the **Licensor**). By clicking 'accept' and completing the transaction for the material (**Licensed Material**), you also confirm your acceptance of these terms and conditions.

1. Grant of Licence

1. The Licensor grants you a personal, non-exclusive, non-transferable, world-wide licence to reproduce the Licensed Material for the purpose specified in your order only. Licences are granted for the specific use requested in the order and for no other use, subject to the conditions below.
2. The Licensor warrants that it has, to the best of its knowledge, the rights to license reuse of the Licensed Material. However, you should ensure that the material you are requesting is original to the Licensor and does not carry the copyright of another entity (as credited in the published version).
3. If the credit line on any part of the material you have requested indicates that it was reprinted or adapted with permission from another source, then you should also seek permission from that source to reuse the material.

2. Scope of Licence

1. You may only use the Licensed Content in the manner and to the extent permitted by these Ts&Cs and any applicable laws.

2. A separate licence may be required for any additional use of the Licensed Material, e.g. where a licence has been purchased for print only use, separate permission must be obtained for electronic re-use. Similarly, a licence is only valid in the language selected and does not apply for editions in other languages unless additional translation rights have been granted separately in the licence. Any content owned by third parties are expressly excluded from the licence.
3. Similarly, rights for additional components such as custom editions and derivatives require additional permission and may be subject to an additional fee. Please apply to Journalpermissions@springernature.com/bookpermissions@springernature.com for these rights.
4. Where permission has been granted **free of charge** for material in print, permission may also be granted for any electronic version of that work, provided that the material is incidental to your work as a whole and that the electronic version is essentially equivalent to, or substitutes for, the print version.
5. An alternative scope of licence may apply to signatories of the [STM Permissions Guidelines](#), as amended from time to time.

- **Duration of Licence**

1. A licence for is valid from the date of purchase ('Licence Date') at the end of the relevant period in the below table:

Scope of Licence	Duration of Licence
Post on a website	12 months
Presentations	12 months
Books and journals	Lifetime of the edition in the language purchased

- **Acknowledgement**

1. The Licensor's permission must be acknowledged next to the Licenced Material in print. In electronic form, this acknowledgement must be visible at the same time as the figures/tables/illustrations or abstract, and must be hyperlinked to the journal/book's homepage. Our required acknowledgement format is in the Appendix below.

- **Restrictions on use**

1. Use of the Licensed Material may be permitted for incidental promotional use and minor editing privileges e.g. minor adaptations of single figures, changes of format, colour and/or style where the adaptation is credited as set out in Appendix 1 below. Any other changes including but not limited to, cropping, adapting, omitting material that affect the meaning, intention or moral rights of the author are strictly prohibited.

2. You must not use any Licensed Material as part of any design or trademark.
3. Licensed Material may be used in Open Access Publications (OAP) before publication by Springer Nature, but any Licensed Material must be removed from OAP sites prior to final publication.

- **Ownership of Rights**

1. Licensed Material remains the property of either Licensor or the relevant third party and any rights not explicitly granted herein are expressly reserved.

- **Warranty**

IN NO EVENT SHALL LICENSOR BE LIABLE TO YOU OR ANY OTHER PARTY OR ANY OTHER PERSON OR FOR ANY SPECIAL, CONSEQUENTIAL, INCIDENTAL OR INDIRECT DAMAGES, HOWEVER CAUSED, ARISING OUT OF OR IN CONNECTION WITH THE DOWNLOADING, VIEWING OR USE OF THE MATERIALS REGARDLESS OF THE FORM OF ACTION, WHETHER FOR BREACH OF CONTRACT, BREACH OF WARRANTY, TORT, NEGLIGENCE, INFRINGEMENT OR OTHERWISE (INCLUDING, WITHOUT LIMITATION, DAMAGES BASED ON LOSS OF PROFITS, DATA, FILES, USE, BUSINESS OPPORTUNITY OR CLAIMS OF THIRD PARTIES), AND WHETHER OR NOT THE PARTY HAS BEEN ADVISED OF THE POSSIBILITY OF SUCH DAMAGES. THIS LIMITATION SHALL APPLY NOTWITHSTANDING ANY FAILURE OF ESSENTIAL PURPOSE OF ANY LIMITED REMEDY PROVIDED HEREIN.

- **Limitations**

1. ***BOOKS ONLY:*** Where 'reuse in a dissertation/thesis' has been selected the following terms apply: Print rights of the final author's accepted manuscript (for clarity, NOT the published version) for up to 100 copies, electronic rights for use only on a personal website or institutional repository as defined by the Sherpa guideline (www.sherpa.ac.uk/romeo/).
2. For content reuse requests that qualify for permission under the [STM Permissions Guidelines](#), which may be updated from time to time, the STM Permissions Guidelines supersede the terms and conditions contained in this licence.

- **Termination and Cancellation**

1. Licences will expire after the period shown in Clause 3 (above).
2. Licensee reserves the right to terminate the Licence in the event that payment is not received in full or if there has been a breach of this agreement by you.

Appendix 1 — Acknowledgements:

For Journal Content:

Reprinted by permission from [**the Licensor**]: [**Journal Publisher** (e.g. Nature/Springer/Palgrave)] [**JOURNAL NAME**] [**REFERENCE CITATION** (Article name, Author(s) Name), [**COPYRIGHT**] (year of publication)

For Advance Online Publication papers:

Reprinted by permission from [**the Licensor**]: [**Journal Publisher** (e.g. Nature/Springer/Palgrave)] [**JOURNAL NAME**] [**REFERENCE CITATION** (Article name, Author(s) Name), [**COPYRIGHT**] (year of publication), advance online publication, day month year (doi: 10.1038/sj.[**JOURNAL ACRONYM**].)

For Adaptations/Translations:

Adapted/Translated by permission from [**the Licensor**]: [**Journal Publisher** (e.g. Nature/Springer/Palgrave)] [**JOURNAL NAME**] [**REFERENCE CITATION** (Article name, Author(s) Name), [**COPYRIGHT**] (year of publication)

Note: For any republication from the British Journal of Cancer, the following credit line style applies:

Reprinted/adapted/translated by permission from [**the Licensor**]: on behalf of Cancer Research UK: : [**Journal Publisher** (e.g. Nature/Springer/Palgrave)] [**JOURNAL NAME**] [**REFERENCE CITATION** (Article name, Author(s) Name), [**COPYRIGHT**] (year of publication)

For Advance Online Publication papers:

Reprinted by permission from The [**the Licensor**]: on behalf of Cancer Research UK: [**Journal Publisher** (e.g. Nature/Springer/Palgrave)] [**JOURNAL NAME**] [**REFERENCE CITATION** (Article name, Author(s) Name), [**COPYRIGHT**] (year of publication), advance online publication, day month year (doi: 10.1038/sj.[**JOURNAL ACRONYM**])

For Book content:

Reprinted/adapted by permission from [**the Licensor**]: [**Book Publisher** (e.g. Palgrave Macmillan, Springer etc)] [**Book Title**] by [**Book author(s)**] [**COPYRIGHT**] (year of publication)

Other Conditions:

Version 1.3

Questions? customercare@copyright.com or +1-855-239-3415 (toll free in the US) or +1-978-646-2777.

Copyright information for Figure 1 (right panel) from “Ice-shelf melting around Antarctica,” by Rignot et al. (2013), *Science*, 341(6143), 66-270.

THE AMERICAN ASSOCIATION FOR THE ADVANCEMENT OF SCIENCE LICENSE

TERMS AND CONDITIONS

May 25, 2021

This Agreement between University of South Florida -- Kara Vadman ("You") and The American Association for the Advancement of Science ("The American Association for the Advancement of Science") consists of your license details and the terms and conditions provided by The American Association for the Advancement of Science and Copyright Clearance Center.

License Number	5076020635502
License date	May 25, 2021
Licensed Content Publisher	The American Association for the Advancement of Science
Licensed Content Publication	Science
Licensed Content Title	Ice-Shelf Melting Around Antarctica
Licensed Content Author	E. Rignot,S. Jacobs,J. Mouginot,B. Scheuchl
Licensed Content Date	Jul 19, 2013
Licensed Content Volume	341
Licensed Content Issue	6143
Volume number	341
Issue number	6143
Type of Use	Thesis / Dissertation
Requestor type	Scientist/individual at a research institution
Format	Electronic
Portion	Text Excerpt
Number of pages requested	1
Title	Kara Vadman
Institution name	University of South Florida
Expected presentation date	May 2021
Portions	Fig. 1 Basal melt rates of Antarctic ice shelves. University of South Florida 140 7th Ave S
Requestor Location	

SAINT PETERSBURG, FL 33701
United States
Attn: University of South Florida

Total 0.00 USD

Terms and Conditions

American Association for the Advancement of Science TERMS AND CONDITIONS

Regarding your request, we are pleased to grant you non-exclusive, non-transferable permission, to republish the AAAS material identified above in your work identified above, subject to the terms and conditions herein. We must be contacted for permission for any uses other than those specifically identified in your request above.

The following credit line must be printed along with the AAAS material: "From [Full Reference Citation]. Reprinted with permission from AAAS."

All required credit lines and notices must be visible any time a user accesses any part of the AAAS material and must appear on any printed copies and authorized user might make.

This permission does not apply to figures / photos / artwork or any other content or materials included in your work that are credited to non-AAAS sources. If the requested material is sourced to or references non-AAAS sources, you must obtain authorization from that source as well before using that material. You agree to hold harmless and indemnify AAAS against any claims arising from your use of any content in your work that is credited to non-AAAS sources.

If the AAAS material covered by this permission was published in Science during the years 1974 - 1994, you must also obtain permission from the author, who may grant or withhold permission, and who may or may not charge a fee if permission is granted. See original article for author's address. This condition does not apply to news articles.

The AAAS material may not be modified or altered except that figures and tables may be modified with permission from the author. Author permission for any such changes must be secured prior to your use.

Whenever possible, we ask that electronic uses of the AAAS material permitted herein include a hyperlink to the original work on AAAS's website (hyperlink may be embedded in the reference citation).

AAAS material reproduced in your work identified herein must not account for more than 30% of the total contents of that work.

AAAS must publish the full paper prior to use of any text.

AAAS material must not imply any endorsement by the American Association for the Advancement of Science.

This permission is not valid for the use of the AAAS and/or Science logos.

AAAS makes no representations or warranties as to the accuracy of any information contained in the AAAS material covered by this permission, including any warranties of

merchantability or fitness for a particular purpose.

If permission fees for this use are waived, please note that AAAS reserves the right to charge for reproduction of this material in the future.

Permission is not valid unless payment is received within sixty (60) days of the issuance of this permission. If payment is not received within this time period then all rights granted herein shall be revoked and this permission will be considered null and void.

In the event of breach of any of the terms and conditions herein or any of CCC's Billing and Payment terms and conditions, all rights granted herein shall be revoked and this permission will be considered null and void.

AAAS reserves the right to terminate this permission and all rights granted herein at its discretion, for any purpose, at any time. In the event that AAAS elects to terminate this permission, you will have no further right to publish, publicly perform, publicly display, distribute or otherwise use any matter in which the AAAS content had been included, and all fees paid hereunder shall be fully refunded to you. Notification of termination will be sent to the contact information as supplied by you during the request process and termination shall be immediate upon sending the notice. Neither AAAS nor CCC shall be liable for any costs, expenses, or damages you may incur as a result of the termination of this permission, beyond the refund noted above.

This Permission may not be amended except by written document signed by both parties.

The terms above are applicable to all permissions granted for the use of AAAS material. Below you will find additional conditions that apply to your particular type of use.

FOR A THESIS OR DISSERTATION

If you are using figure(s)/table(s), permission is granted for use in print and electronic versions of your dissertation or thesis. A full text article may be used in print versions only of a dissertation or thesis.

Permission covers the distribution of your dissertation or thesis on demand by ProQuest / UMI, provided the AAAS material covered by this permission remains in situ.

If you are an Original Author on the AAAS article being reproduced, please refer to your License to Publish for rules on reproducing your paper in a dissertation or thesis.

FOR JOURNALS:

Permission covers both print and electronic versions of your journal article, however the AAAS material may not be used in any manner other than within the context of your article.

FOR BOOKS/TEXTBOOKS:

If this license is to reuse figures/tables, then permission is granted for non-exclusive world rights in all languages in both print and electronic formats (electronic formats are defined below).

If this license is to reuse a text excerpt or a full text article, then permission is granted for non-exclusive world rights in English only. You have the option of securing either print or electronic rights or both, but electronic rights are not automatically granted and do garner additional fees. Permission for translations of text excerpts or full text articles into other languages must be obtained separately.

Licenses granted for use of AAAS material in electronic format books/textbooks are valid only in cases where the electronic version is equivalent to or substitutes for the print version of the book/textbook. The AAAS material reproduced as permitted herein must remain in situ and must not be exploited separately (for example, if permission covers the use of a full text article, the article may not be offered for access or for purchase as a stand-alone unit), except in the case of permitted textbook companions as noted below.

You must include the following notice in any electronic versions, either adjacent to the reprinted AAAS material or in the terms and conditions for use of your electronic products: "Readers may view, browse, and/or download material for temporary copying purposes only, provided these uses are for noncommercial personal purposes. Except as provided by law, this material may not be further reproduced, distributed, transmitted, modified, adapted, performed, displayed, published, or sold in whole or in part, without prior written permission from the publisher."

If your book is an academic textbook, permission covers the following companions to your textbook, provided such companions are distributed only in conjunction with your textbook at no additional cost to the user:

- Password-protected website
- Instructor's image CD/DVD and/or PowerPoint resource
- Student CD/DVD

All companions must contain instructions to users that the AAAS material may be used for non-commercial, classroom purposes only. Any other uses require the prior written permission from AAAS.

If your license is for the use of AAAS Figures/Tables, then the electronic rights granted herein permit use of the Licensed Material in any Custom Databases that you distribute the electronic versions of your textbook through, so long as the Licensed Material remains within the context of a chapter of the title identified in your request and cannot be downloaded by a user as an independent image file.

Rights also extend to copies/files of your Work (as described above) that you are required to provide for use by the visually and/or print disabled in compliance with state and federal laws.

This permission only covers a single edition of your work as identified in your request.

FOR NEWSLETTERS:

Permission covers print and/or electronic versions, provided the AAAS material reproduced as permitted herein remains in situ and is not exploited separately (for example, if permission covers the use of a full text article, the article may not be offered for access or for purchase as a stand-alone unit)

FOR ANNUAL REPORTS:

Permission covers print and electronic versions provided the AAAS material reproduced as permitted herein remains in situ and is not exploited separately (for example, if permission covers the use of a full text article, the article may not be offered for access or for purchase as a stand-alone unit)

FOR PROMOTIONAL/MARKETING USES:

Permission covers the use of AAAS material in promotional or marketing pieces such as information packets, media kits, product slide kits, brochures, or flyers limited to a single print run. The AAAS Material may not be used in any manner which implies endorsement or promotion by the American Association for the Advancement of Science (AAAS) or Science of any product or service. AAAS does not permit the reproduction of its name, logo or text on promotional literature.

If permission to use a full text article is permitted, The Science article covered by this permission must not be altered in any way. No additional printing may be set onto an article copy other than the copyright credit line required above. Any alterations must be approved in advance and in writing by AAAS. This includes, but is not limited to, the placement of sponsorship identifiers, trademarks, logos, rubber stamping or self-adhesive stickers onto the article copies.

Additionally, article copies must be a freestanding part of any information package (i.e. media kit) into which they are inserted. They may not be physically attached to anything, such as an advertising insert, or have anything attached to them, such as a sample product. Article copies must be easily removable from any kits or informational packages in which they are used. The only exception is that article copies may be inserted into three-ring binders.

FOR CORPORATE INTERNAL USE:

The AAAS material covered by this permission may not be altered in any way. No additional

printing may be set onto an article copy other than the required credit line. Any alterations must be approved in advance and in writing by AAAS. This includes, but is not limited to the placement of sponsorship identifiers, trademarks, logos, rubber stamping or self-adhesive stickers onto article copies.

If you are making article copies, copies are restricted to the number indicated in your request and must be distributed only to internal employees for internal use.

If you are using AAAS Material in Presentation Slides, the required credit line must be visible on the slide where the AAAS material will be reprinted

If you are using AAAS Material on a CD, DVD, Flash Drive, or the World Wide Web, you must include the following notice in any electronic versions, either adjacent to the reprinted AAAS material or in the terms and conditions for use of your electronic products: "Readers may view, browse, and/or download material for temporary copying purposes only, provided these uses are for noncommercial personal purposes. Except as provided by law, this material may not be further reproduced, distributed, transmitted, modified, adapted, performed, displayed, published, or sold in whole or in part, without prior written permission from the publisher." Access to any such CD, DVD, Flash Drive or Web page must be restricted to your organization's employees only.

FOR CME COURSE and SCIENTIFIC SOCIETY MEETINGS:

Permission is restricted to the particular Course, Seminar, Conference, or Meeting indicated in your request. If this license covers a text excerpt or a Full Text Article, access to the reprinted AAAS material must be restricted to attendees of your event only (if you have been granted electronic rights for use of a full text article on your website, your website must be password protected, or access restricted so that only attendees can access the content on your site).

If you are using AAAS Material on a CD, DVD, Flash Drive, or the World Wide Web, you must include the following notice in any electronic versions, either adjacent to the reprinted AAAS material or in the terms and conditions for use of your electronic products: "Readers may view, browse, and/or download material for temporary copying purposes only, provided these uses are for noncommercial personal purposes. Except as provided by law, this material may not be further reproduced, distributed, transmitted, modified, adapted, performed, displayed, published, or sold in whole or in part, without prior written permission from the publisher."

FOR POLICY REPORTS:

These rights are granted only to non-profit organizations and/or government agencies. Permission covers print and electronic versions of a report, provided the required credit line appears in both versions and provided the AAAS material reproduced as permitted herein remains in situ and is not exploited separately.

FOR CLASSROOM PHOTOCOPIES:

Permission covers distribution in print copy format only. Article copies must be freestanding

and not part of a course pack. They may not be physically attached to anything or have anything attached to them.

FOR COURSEPACKS OR COURSE WEBSITES:

These rights cover use of the AAAS material in one class at one institution. Permission is valid only for a single semester after which the AAAS material must be removed from the Electronic Course website, unless new permission is obtained for an additional semester. If the material is to be distributed online, access must be restricted to students and instructors enrolled in that particular course by some means of password or access control.

FOR WEBSITES:

You must include the following notice in any electronic versions, either adjacent to the reprinted AAAS material or in the terms and conditions for use of your electronic products: "Readers may view, browse, and/or download material for temporary copying purposes only, provided these uses are for noncommercial personal purposes. Except as provided by law, this material may not be further reproduced, distributed, transmitted, modified, adapted, performed, displayed, published, or sold in whole or in part, without prior written permission from the publisher."

Permissions for the use of Full Text articles on third party websites are granted on a case by case basis and only in cases where access to the AAAS Material is restricted by some means of password or access control. Alternately, an E-Print may be purchased through our reprints department (brocheleau@rockwaterinc.com).

REGARDING FULL TEXT ARTICLE USE ON THE WORLD WIDE WEB IF YOU ARE AN 'ORIGINAL AUTHOR' OF A SCIENCE PAPER

If you chose "Original Author" as the Requestor Type, you are warranting that you are one of authors listed on the License Agreement as a "Licensed content author" or that you are acting on that author's behalf to use the Licensed content in a new work that one of the authors listed on the License Agreement as a "Licensed content author" has written.

Original Authors may post the 'Accepted Version' of their full text article on their personal or on their University website and not on any other website. The 'Accepted Version' is the version of the paper accepted for publication by AAAS including changes resulting from peer review but prior to AAAS's copy editing and production (in other words not the AAAS published version).

FOR MOVIES / FILM / TELEVISION:

Permission is granted to use, record, film, photograph, and/or tape the AAAS material in connection with your program/film and in any medium your program/film may be shown or heard, including but not limited to broadcast and cable television, radio, print, world wide web, and videocassette.

The required credit line should run in the program/film's end credits.

FOR MUSEUM EXHIBITIONS:

Permission is granted to use the AAAS material as part of a single exhibition for the duration of that exhibit. Permission for use of the material in promotional materials for the exhibit must be cleared separately with AAAS (please contact us at permissions@aaas.org).

FOR TRANSLATIONS:

Translation rights apply only to the language identified in your request summary above.

The following disclaimer must appear with your translation, on the first page of the article, after the credit line: "This translation is not an official translation by AAAS staff, nor is it endorsed by AAAS as accurate. In crucial matters, please refer to the official English-language version originally published by AAAS."

FOR USE ON A COVER:

Permission is granted to use the AAAS material on the cover of a journal issue, newsletter issue, book, textbook, or annual report in print and electronic formats provided the AAAS material reproduced as permitted herein remains in situ and is not exploited separately

By using the AAAS Material identified in your request, you agree to abide by all the terms and conditions herein.

Questions about these terms can be directed to the AAAS Permissions department permissions@aaas.org.

Other Terms and Conditions:

v 2

Questions? customercare@copyright.com or +1-855-239-3415 (toll free in the US) or +1-978-646-2777.

Copyright information for Figure 2 from “Pliocene and Eocene provide best analogs for near-future climates” by Burke et al. (2018), *PNAS*, 115(52), 13288-13293.

Permission is not required to use original figures or tables for noncommercial and educational use (i.e., in a review article, in a book that is not for sale) if the article published under the exclusive PNAS License to Publish.

Article Information

vol. 115 no. 52 13288-13293

DOI: <https://doi.org/10.1073/pnas.1809600115>

PubMed: [30530685](https://pubmed.ncbi.nlm.nih.gov/30530685/)

Published By: [National Academy of Sciences](#)

Print ISSN: [0027-8424](#)

Online ISSN: [1091-6490](#)

History: Published in issue December 26, 2018.

Published first December 10, 2018.

Article Versions

- [Previous version \(December 10, 2018 - 11:46\)](#).
- You are viewing the most recent version of this article.



Copyright & Usage: © 2018 Published under the [PNAS license](#).

Copyright information for Figure 3 modified from “Bedmap2: improved ice bed, surface and thickness datasets for Antarctica” by Fretwell et al. (2013), *The Cryosphere*, 7, 375–393.


The Cryosphere permissions guidelines:

Creative Commons Attribution 4.0 License

You are free to:

-  **Share** — copy and redistribute the material in any medium or format
-  **Adapt** — remix, transform, and build upon the material for any purpose, even commercially.

Under the following conditions:

-  **Attribution** — You must give appropriate credit, provide a link to the licence, and indicate if changes were made. You may do so in any reasonable manner, but not in any way that suggests the licensor endorses you or your use.

No additional restrictions — You may not apply legal terms or technological measures that legally restrict others from doing anything the licence permits.

Reproduction request ▶

All articles and preprints posted by Copernicus Publications have been licenced under the Creative Commons Attribution 4.0 License since 6 June 2017 or under its former version 3.0 since 10 December 2007. Under these licences the authors retain the copyright. There is no need from the publisher's side to allow/confirm a reproduction. We suggest contacting the authors to inform them about the further usage of the material. In any case, the authors must be given credit. If articles contain figures, maps, or other objects cited by the authors, the individual copyrights and distribution licences must be clarified individually.

Copyright information for Figure 4a from “Initiation and long-term instability of the East Antarctic Ice Sheet” by Gulick, Shevenell et al. (2017). *Nature*, 552, 225–229.

SPRINGER NATURE LICENSE
TERMS AND CONDITIONS

May 25, 2021

This Agreement between University of South Florida -- Kara Vadman ("You") and Springer Nature ("Springer Nature") consists of your license details and the terms and conditions provided by Springer Nature and Copyright Clearance Center.

License Number	5076051473468
License date	May 25, 2021
Licensed Content Publisher	Springer Nature
Licensed Content Publication	Nature
Licensed Content Title	Initiation and long-term instability of the East Antarctic Ice Sheet
Licensed Content Author	Sean P. S. Gulick et al
Licensed Content Date	Dec 14, 2017
Type of Use	Thesis/Dissertation
Requestor type	academic/university or research institute
Format	electronic
Portion	figures/tables/illustrations
Number of figures/tables/illustrations	1
High-res required	no
Will you be translating?	no
Circulation/distribution	1 - 29
Author of this Springer Nature content	no
Title	Kara Vadman
Institution name	University of South Florida
Expected presentation date	May 2021
Portions	Figure 1a: ASB elevations and Sabrina Coast bathymetry. University of South Florida 140 7th Ave S
Requestor Location	

SAINT PETERSBURG, FL 33701

Total
Terms and Conditions

United States
Attn: University of South Florida
0.00 USD

Springer Nature Customer Service Centre GmbH Terms and Conditions

This agreement sets out the terms and conditions of the licence (the **Licence**) between you and **Springer Nature Customer Service Centre GmbH** (the **Licensor**). By clicking 'accept' and completing the transaction for the material (**Licensed Material**), you also confirm your acceptance of these terms and conditions.

1. Grant of License

1. The Licensor grants you a personal, non-exclusive, non-transferable, world-wide licence to reproduce the Licensed Material for the purpose specified in your order only. Licences are granted for the specific use requested in the order and for no other use, subject to the conditions below.
2. The Licensor warrants that it has, to the best of its knowledge, the rights to license reuse of the Licensed Material. However, you should ensure that the material you are requesting is original to the Licensor and does not carry the copyright of another entity (as credited in the published version).
3. If the credit line on any part of the material you have requested indicates that it was reprinted or adapted with permission from another source, then you should also seek permission from that source to reuse the material.

2. Scope of Licence

1. You may only use the Licensed Content in the manner and to the extent permitted by these Ts&Cs and any applicable laws.
2. A separate licence may be required for any additional use of the Licensed Material, e.g. where a licence has been purchased for print only use, separate permission must be obtained for electronic re-use. Similarly, a licence is only valid in the language selected and does not apply for editions in other languages unless additional translation rights have been granted separately in the licence. Any content owned by third parties are expressly excluded from the licence.
3. Similarly, rights for additional components such as custom editions and derivatives require additional permission and may be subject to an additional fee. Please apply to

Journalpermissions@springernature.com/bookpermissions@springernature.com for these rights.

4. Where permission has been granted **free of charge** for material in print, permission may also be granted for any electronic version of that work, provided that the material is incidental to your work as a whole and that the electronic version is essentially equivalent to, or substitutes for, the print version.
5. An alternative scope of licence may apply to signatories of the [STM Permissions Guidelines](#), as amended from time to time.

- **Duration of Licence**

1. A licence for is valid from the date of purchase ('Licence Date') at the end of the relevant period in the below table:

Scope of Licence	Duration of Licence
Post on a website	12 months
Presentations	12 months
Books and journals	Lifetime of the edition in the language purchased

- **Acknowledgement**

1. The Licensor's permission must be acknowledged next to the Licenced Material in print. In electronic form, this acknowledgement must be visible at the same time as the figures/tables/illustrations or abstract, and must be hyperlinked to the journal/book's homepage. Our required acknowledgement format is in the Appendix below.

- **Restrictions on use**

1. Use of the Licensed Material may be permitted for incidental promotional use and minor editing privileges e.g. minor adaptations of single figures, changes of format, colour and/or style where the adaptation is credited as set out in Appendix 1 below. Any other changes including but not limited to, cropping, adapting, omitting material that affect the meaning, intention or moral rights of the author are strictly prohibited.
2. You must not use any Licensed Material as part of any design or trademark.
3. Licensed Material may be used in Open Access Publications (OAP) before publication by Springer Nature, but any Licensed Material must be removed from OAP sites prior to final publication.

- **Ownership of Rights**

1. Licensed Material remains the property of either Licensor or the relevant third party and any rights not explicitly granted herein are expressly reserved.

- **Warranty**

IN NO EVENT SHALL LICENSOR BE LIABLE TO YOU OR ANY OTHER PARTY OR ANY OTHER PERSON OR FOR ANY SPECIAL, CONSEQUENTIAL, INCIDENTAL OR INDIRECT DAMAGES, HOWEVER CAUSED, ARISING OUT OF OR IN CONNECTION WITH THE DOWNLOADING, VIEWING OR USE OF THE MATERIALS REGARDLESS OF THE FORM OF ACTION, WHETHER FOR BREACH OF CONTRACT, BREACH OF WARRANTY, TORT, NEGLIGENCE, INFRINGEMENT OR OTHERWISE (INCLUDING, WITHOUT LIMITATION, DAMAGES BASED ON LOSS OF PROFITS, DATA, FILES, USE, BUSINESS OPPORTUNITY OR CLAIMS OF THIRD PARTIES), AND WHETHER OR NOT THE PARTY HAS BEEN ADVISED OF THE POSSIBILITY OF SUCH DAMAGES. THIS LIMITATION SHALL APPLY NOTWITHSTANDING ANY FAILURE OF ESSENTIAL PURPOSE OF ANY LIMITED REMEDY PROVIDED HEREIN.

- **Limitations**

1. ***BOOKS ONLY:*** Where 'reuse in a dissertation/thesis' has been selected the following terms apply: Print rights of the final author's accepted manuscript (for clarity, NOT the published version) for up to 100 copies, electronic rights for use only on a personal website or institutional repository as defined by the Sherpa guideline (www.sherpa.ac.uk/romeo/).
2. For content reuse requests that qualify for permission under the [STM Permissions Guidelines](#), which may be updated from time to time, the STM Permissions Guidelines supersede the terms and conditions contained in this licence.

- **Termination and Cancellation**

1. Licences will expire after the period shown in Clause 3 (above).
2. Licensee reserves the right to terminate the Licence in the event that payment is not received in full or if there has been a breach of this agreement by you.

Appendix 1 — Acknowledgements:

For Journal Content:

Reprinted by permission from [the Licensor]: [Journal Publisher (e.g. Nature/Springer/Palgrave)] [JOURNAL NAME] [REFERENCE CITATION (Article name, Author(s) Name), [COPYRIGHT] (year of publication)

For Advance Online Publication papers:

Reprinted by permission from [the Licensor]: [Journal Publisher (e.g.

Nature/Springer/Palgrave)] [JOURNAL NAME] [REFERENCE CITATION (Article name, Author(s) Name), [COPYRIGHT] (year of publication), advance online publication, day month year (doi: 10.1038/sj.[JOURNAL ACRONYM].)

For Adaptations/Translations:

Adapted/Translated by permission from [the Licensor]: [Journal Publisher (e.g. Nature/Springer/Palgrave)] [JOURNAL NAME] [REFERENCE CITATION (Article name, Author(s) Name), [COPYRIGHT] (year of publication)

Note: For any republication from the British Journal of Cancer, the following credit line style applies:

Reprinted/adapted/translated by permission from [the Licensor]: on behalf of Cancer Research UK: : [Journal Publisher (e.g. Nature/Springer/Palgrave)] [JOURNAL NAME] [REFERENCE CITATION (Article name, Author(s) Name), [COPYRIGHT] (year of publication)

For **Advance Online Publication** papers:

Reprinted by permission from The [the Licensor]: on behalf of Cancer Research UK: [Journal Publisher (e.g. Nature/Springer/Palgrave)] [JOURNAL NAME] [REFERENCE CITATION (Article name, Author(s) Name), [COPYRIGHT] (year of publication), advance online publication, day month year (doi: 10.1038/sj.[JOURNAL ACRONYM])

For Book content:

Reprinted/adapted by permission from [the Licensor]: [Book Publisher (e.g. Palgrave Macmillan, Springer etc) [Book Title] by [Book author(s)] [COPYRIGHT] (year of publication)

Other Conditions:

Version 1.3

Questions? customercare@copyright.com or +1-855-239-3415 (toll free in the US) or +1-978-646-2777.

Copyright information for Figure 4b from “Repeated large-scale retreat and advance of Totten Glacier indicated by inland bed erosion” by Aitken et al. (2016). *Nature*, 533, 385-389.

SPRINGER NATURE LICENSE
TERMS AND CONDITIONS

May 25, 2021

This Agreement between University of South Florida -- Kara Vadman ("You") and Springer Nature ("Springer Nature") consists of your license details and the terms and conditions provided by Springer Nature and Copyright Clearance Center.

License Number	5076051077368
License date	May 25, 2021
Licensed Content Publisher	Springer Nature
Licensed Content Publication	Nature
Licensed Content Title	Repeated large-scale retreat and advance of Totten Glacier indicated by inland bed erosion
Licensed Content Author	A. R. A. Aitken et al
Licensed Content Date	May 18, 2016
Type of Use	Thesis/Dissertation
Requestor type	academic/university or research institute
Format	electronic
Portion	figures/tables/illustrations
Number of figures/tables/illustrations	1
High-res required	no
Will you be translating?	no
Circulation/distribution	1 - 29
Author of this Springer Nature content	no
Title	Kara Vadman
Institution name	University of South Florida
Expected presentation date	May 2021
Portions	Figure 1d: Interpretation of erosion in the Sabrina Subglacial Basin region. University of South Florida 140 7th Ave S
Requestor Location	

SAINT PETERSBURG, FL 33701
286

United States
Attn: University of South Florida

Total

0.00 USD

Terms and Conditions

Springer Nature Customer Service Centre GmbH Terms and Conditions

This agreement sets out the terms and conditions of the licence (the **Licence**) between you and **Springer Nature Customer Service Centre GmbH** (the **Licensor**). By clicking 'accept' and completing the transaction for the material (**Licensed Material**), you also confirm your acceptance of these terms and conditions.

1. Grant of License

1. The Licensor grants you a personal, non-exclusive, non-transferable, world-wide licence to reproduce the Licensed Material for the purpose specified in your order only. Licences are granted for the specific use requested in the order and for no other use, subject to the conditions below.
2. The Licensor warrants that it has, to the best of its knowledge, the rights to license reuse of the Licensed Material. However, you should ensure that the material you are requesting is original to the Licensor and does not carry the copyright of another entity (as credited in the published version).
3. If the credit line on any part of the material you have requested indicates that it was reprinted or adapted with permission from another source, then you should also seek permission from that source to reuse the material.

2. Scope of Licence

1. You may only use the Licensed Content in the manner and to the extent permitted by these Ts&Cs and any applicable laws.
2. A separate licence may be required for any additional use of the Licensed Material, e.g. where a licence has been purchased for print only use, separate permission must be obtained for electronic re-use. Similarly, a licence is only valid in the language selected and does not apply for editions in other languages unless additional translation rights have been granted separately in the licence. Any content owned by third parties are expressly excluded from the licence.
3. Similarly, rights for additional components such as custom editions and derivatives require additional permission and may be subject to an additional fee. Please apply to

Journalpermissions@springernature.com/bookpermissions@springernature.com for these rights.

4. Where permission has been granted **free of charge** for material in print, permission may also be granted for any electronic version of that work, provided that the material is incidental to your work as a whole and that the electronic version is essentially equivalent to, or substitutes for, the print version.
5. An alternative scope of licence may apply to signatories of the [STM Permissions Guidelines](#), as amended from time to time.

- **Duration of Licence**

1. A licence for is valid from the date of purchase ('Licence Date') at the end of the relevant period in the below table:

Scope of Licence	Duration of Licence
Post on a website	12 months
Presentations	12 months
Books and journals	Lifetime of the edition in the language purchased

- **Acknowledgement**

1. The Licensor's permission must be acknowledged next to the Licenced Material in print. In electronic form, this acknowledgement must be visible at the same time as the figures/tables/illustrations or abstract, and must be hyperlinked to the journal/book's homepage. Our required acknowledgement format is in the Appendix below.

- **Restrictions on use**

1. Use of the Licensed Material may be permitted for incidental promotional use and minor editing privileges e.g. minor adaptations of single figures, changes of format, colour and/or style where the adaptation is credited as set out in Appendix 1 below. Any other changes including but not limited to, cropping, adapting, omitting material that affect the meaning, intention or moral rights of the author are strictly prohibited.
2. You must not use any Licensed Material as part of any design or trademark.
3. Licensed Material may be used in Open Access Publications (OAP) before publication by Springer Nature, but any Licensed Material must be removed from OAP sites prior to final publication.

- **Ownership of Rights**

1. Licensed Material remains the property of either Licensor or the relevant third party and any rights not explicitly granted herein are expressly reserved.

- **Warranty**

IN NO EVENT SHALL LICENSOR BE LIABLE TO YOU OR ANY OTHER PARTY OR ANY OTHER PERSON OR FOR ANY SPECIAL, CONSEQUENTIAL, INCIDENTAL OR INDIRECT DAMAGES, HOWEVER CAUSED, ARISING OUT OF OR IN CONNECTION WITH THE DOWNLOADING, VIEWING OR USE OF THE MATERIALS REGARDLESS OF THE FORM OF ACTION, WHETHER FOR BREACH OF CONTRACT, BREACH OF WARRANTY, TORT, NEGLIGENCE, INFRINGEMENT OR OTHERWISE (INCLUDING, WITHOUT LIMITATION, DAMAGES BASED ON LOSS OF PROFITS, DATA, FILES, USE, BUSINESS OPPORTUNITY OR CLAIMS OF THIRD PARTIES), AND WHETHER OR NOT THE PARTY HAS BEEN ADVISED OF THE POSSIBILITY OF SUCH DAMAGES. THIS LIMITATION SHALL APPLY NOTWITHSTANDING ANY FAILURE OF ESSENTIAL PURPOSE OF ANY LIMITED REMEDY PROVIDED HEREIN.

- **Limitations**

1. **BOOKS ONLY**: Where 'reuse in a dissertation/thesis' has been selected the following terms apply: Print rights of the final author's accepted manuscript (for clarity, NOT the published version) for up to 100 copies, electronic rights for use only on a personal website or institutional repository as defined by the Sherpa guideline (www.sherpa.ac.uk/romeo/).
2. For content reuse requests that qualify for permission under the [STM Permissions Guidelines](#), which may be updated from time to time, the STM Permissions Guidelines supersede the terms and conditions contained in this licence.

- **Termination and Cancellation**

1. Licences will expire after the period shown in Clause 3 (above).
2. Licensee reserves the right to terminate the Licence in the event that payment is not received in full or if there has been a breach of this agreement by you.

Appendix 1 — Acknowledgements:

For Journal Content:

Reprinted by permission from [the Licensor]: [Journal Publisher (e.g. Nature/Springer/Palgrave)] [JOURNAL NAME] [REFERENCE CITATION (Article name, Author(s) Name), [COPYRIGHT] (year of publication)

For Advance Online Publication papers:

Reprinted by permission from [the Licensor]: [Journal Publisher (e.g. Nature/Springer/Palgrave)] [JOURNAL NAME] [REFERENCE CITATION (Article name, Author(s) Name), [COPYRIGHT] (year of publication), advance online publication, day month year (doi: 10.1038/sj.[JOURNAL ACRONYM].)]

For Adaptations/Translations:

Adapted/Translated by permission from [the Licensor]: [Journal Publisher (e.g. Nature/Springer/Palgrave)] [JOURNAL NAME] [REFERENCE CITATION (Article name, Author(s) Name), [COPYRIGHT] (year of publication)]

Note: For any republication from the British Journal of Cancer, the following credit line style applies:

Reprinted/adapted/translated by permission from [the Licensor]: on behalf of Cancer Research UK: : [Journal Publisher (e.g. Nature/Springer/Palgrave)] [JOURNAL NAME] [REFERENCE CITATION (Article name, Author(s) Name), [COPYRIGHT] (year of publication)]

For Advance Online Publication papers:

Reprinted by permission from The [the Licensor]: on behalf of Cancer Research UK: [Journal Publisher (e.g. Nature/Springer/Palgrave)] [JOURNAL NAME] [REFERENCE CITATION (Article name, Author(s) Name), [COPYRIGHT] (year of publication), advance online publication, day month year (doi: 10.1038/sj.[JOURNAL ACRONYM])]

For Book content:

Reprinted/adapted by permission from [the Licensor]: [Book Publisher (e.g. Palgrave Macmillan, Springer etc)] [Book Title] by [Book author(s)] [COPYRIGHT] (year of publication)

Other Conditions:

Version 1.3

Questions? customercare@copyright.com or +1-855-239-3415 (toll free in the US) or +1-978-646-2777.

Copyright information for Figure 5 from “Spatio-temporal variability of processes across Antarctic ice-bed–ocean interfaces” from Colleoni et al., (2018) *Nature Communications* 9, 2289.

SPRINGER NATURE	Spatio-temporal variability of processes across Antarctic ice-bed–ocean interfaces
	Author: Florence Colleoni et al Publication: Nature Communications Publisher: Springer Nature Date: Jun 18, 2018 Copyright © 2018, The Author(s)

Creative Commons
This is an open access article distributed under the terms of the Creative Commons CC BY license, which permits unrestricted use, distribution, and reproduction in any medium, provided the original work is properly cited. You are not required to obtain permission to reuse this article. To request permission for a type of use not listed, please contact Springer Nature

Copyright information for Figure 6b and 6c from “Past ice stream and ice sheet changes on the continental shelf off the Sabrina Coast, East Antarctica” by Fernandez et al. (2018), *Geomorphology*, 317, 20-22.

ELSEVIER LICENSE
TERMS AND CONDITIONS

May 25, 2021

This Agreement between University of South Florida -- Kara Vadman ("You") and Elsevier ("Elsevier") consists of your license details and the terms and conditions provided by Elsevier and Copyright Clearance Center.

License Number	5076060613106
License date	May 25, 2021
Licensed Content Publisher	Elsevier
Licensed Content Publication	Geomorphology
Licensed Content Title	Past ice stream and ice sheet changes on the continental shelf off the Sabrina Coast, East Antarctica
Licensed Content Author	R. Fernandez,S. Gulick,E. Domack,A. Montelli,A. Leventer,A. Shevenell,B. Frederick
Licensed Content Date	Sep 15, 2018
Licensed Content Volume	317
Licensed Content Issue	n/a
Licensed Content Pages	13
Start Page	10
End Page	22
Type of Use	reuse in a thesis/dissertation
Portion	figures/tables/illustrations
Number of figures/tables/illustrations	2
Format	electronic
Are you the author of this Elsevier article?	No
Will you be translating?	No
Title	Kara Vadman
Institution name	University of South Florida

Expected presentation date	May 2021
Portions	Figure 3 and Figure 6 University of South Florida 140 7th Ave S
Requestor Location	SAINT PETERSBURG, FL 33701 United States Attn: University of South Florida
Publisher Tax ID	98-0397604
Total	0.00 USD
Terms and Conditions	

INTRODUCTION

1. The publisher for this copyrighted material is Elsevier. By clicking "accept" in connection with completing this licensing transaction, you agree that the following terms and conditions apply to this transaction (along with the Billing and Payment terms and conditions established by Copyright Clearance Center, Inc. ("CCC"), at the time that you opened your Rightslink account and that are available at any time at <http://myaccount.copyright.com>).

GENERAL TERMS

2. Elsevier hereby grants you permission to reproduce the aforementioned material subject to the terms and conditions indicated.

3. Acknowledgement: If any part of the material to be used (for example, figures) has appeared in our publication with credit or acknowledgement to another source, permission must also be sought from that source. If such permission is not obtained then that material may not be included in your publication/copies. Suitable acknowledgement to the source must be made, either as a footnote or in a reference list at the end of your publication, as follows:

"Reprinted from Publication title, Vol /edition number, Author(s), Title of article / title of chapter, Pages No., Copyright (Year), with permission from Elsevier [OR APPLICABLE SOCIETY COPYRIGHT OWNER]." Also Lancet special credit - "Reprinted from The Lancet, Vol. number, Author(s), Title of article, Pages No., Copyright (Year), with permission from Elsevier."

4. Reproduction of this material is confined to the purpose and/or media for which permission is hereby given.

5. Altering/Modifying Material: Not Permitted. However figures and illustrations may be altered/adapted minimally to serve your work. Any other abbreviations, additions,

deletions and/or any other alterations shall be made only with prior written authorization of Elsevier Ltd. (Please contact Elsevier's permissions helpdesk [here](#)). No modifications can be made to any Lancet figures/tables and they must be reproduced in full.

6. If the permission fee for the requested use of our material is waived in this instance, please be advised that your future requests for Elsevier materials may attract a fee.

7. Reservation of Rights: Publisher reserves all rights not specifically granted in the combination of (i) the license details provided by you and accepted in the course of this licensing transaction, (ii) these terms and conditions and (iii) CCC's Billing and Payment terms and conditions.

8. License Contingent Upon Payment: While you may exercise the rights licensed immediately upon issuance of the license at the end of the licensing process for the transaction, provided that you have disclosed complete and accurate details of your proposed use, no license is finally effective unless and until full payment is received from you (either by publisher or by CCC) as provided in CCC's Billing and Payment terms and conditions. If full payment is not received on a timely basis, then any license preliminarily granted shall be deemed automatically revoked and shall be void as if never granted. Further, in the event that you breach any of these terms and conditions or any of CCC's Billing and Payment terms and conditions, the license is automatically revoked and shall be void as if never granted. Use of materials as described in a revoked license, as well as any use of the materials beyond the scope of an unrevoked license, may constitute copyright infringement and publisher reserves the right to take any and all action to protect its copyright in the materials.

9. Warranties: Publisher makes no representations or warranties with respect to the licensed material.

10. Indemnity: You hereby indemnify and agree to hold harmless publisher and CCC, and their respective officers, directors, employees and agents, from and against any and all claims arising out of your use of the licensed material other than as specifically authorized pursuant to this license.

11. No Transfer of License: This license is personal to you and may not be sublicensed, assigned, or transferred by you to any other person without publisher's written permission.

12. No Amendment Except in Writing: This license may not be amended except in a writing signed by both parties (or, in the case of publisher, by CCC on publisher's behalf).

13. Objection to Contrary Terms: Publisher hereby objects to any terms contained in any purchase order, acknowledgment, check endorsement or other writing prepared by you, which terms are inconsistent with these terms and conditions or CCC's Billing and Payment terms and conditions. These terms and conditions, together with CCC's Billing and Payment terms and conditions (which are incorporated herein), comprise the entire agreement between you and publisher (and CCC) concerning this licensing transaction. In

the event of any conflict between your obligations established by these terms and conditions and those established by CCC's Billing and Payment terms and conditions, these terms and conditions shall control.

14. **Revocation:** Elsevier or Copyright Clearance Center may deny the permissions described in this License at their sole discretion, for any reason or no reason, with a full refund payable to you. Notice of such denial will be made using the contact information provided by you. Failure to receive such notice will not alter or invalidate the denial. In no event will Elsevier or Copyright Clearance Center be responsible or liable for any costs, expenses or damage incurred by you as a result of a denial of your permission request, other than a refund of the amount(s) paid by you to Elsevier and/or Copyright Clearance Center for denied permissions.

LIMITED LICENSE

The following terms and conditions apply only to specific license types:

15. **Translation:** This permission is granted for non-exclusive world **English** rights only unless your license was granted for translation rights. If you licensed translation rights you may only translate this content into the languages you requested. A professional translator must perform all translations and reproduce the content word for word preserving the integrity of the article.

16. **Posting licensed content on any Website:** The following terms and conditions apply as follows: Licensing material from an Elsevier journal: All content posted to the web site must maintain the copyright information line on the bottom of each image; A hyper-text must be included to the Homepage of the journal from which you are licensing at <http://www.sciencedirect.com/science/journal/xxxxx> or the Elsevier homepage for books at <http://www.elsevier.com>; Central Storage: This license does not include permission for a scanned version of the material to be stored in a central repository such as that provided by Heron/XanEdu.

Licensing material from an Elsevier book: A hyper-text link must be included to the Elsevier homepage at <http://www.elsevier.com>. All content posted to the web site must maintain the copyright information line on the bottom of each image.

Posting licensed content on Electronic reserve: In addition to the above the following clauses are applicable: The web site must be password-protected and made available only to bona fide students registered on a relevant course. This permission is granted for 1 year only. You may obtain a new license for future website posting.

17. **For journal authors:** the following clauses are applicable in addition to the above:

Preprints:

A preprint is an author's own write-up of research results and analysis, it has not been peer-reviewed, nor has it had any other value added to it by a publisher (such as formatting, copyright, technical enhancement etc.).

Authors can share their preprints anywhere at any time. Preprints should not be added to or enhanced in any way in order to appear more like, or to substitute for, the final versions of articles however authors can update their preprints on arXiv or RePEc with their Accepted Author Manuscript (see below).

If accepted for publication, we encourage authors to link from the preprint to their formal publication via its DOI. Millions of researchers have access to the formal publications on ScienceDirect, and so links will help users to find, access, cite and use the best available version. Please note that Cell Press, The Lancet and some society-owned have different preprint policies. Information on these policies is available on the journal homepage.

Accepted Author Manuscripts: An accepted author manuscript is the manuscript of an article that has been accepted for publication and which typically includes author-incorporated changes suggested during submission, peer review and editor-author communications.

Authors can share their accepted author manuscript:

- immediately
 - via their non-commercial person homepage or blog
 - by updating a preprint in arXiv or RePEc with the accepted manuscript
 - via their research institute or institutional repository for internal institutional uses or as part of an invitation-only research collaboration work-group
 - directly by providing copies to their students or to research collaborators for their personal use
 - for private scholarly sharing as part of an invitation-only work group on commercial sites with which Elsevier has an agreement
- After the embargo period
 - via non-commercial hosting platforms such as their institutional repository
 - via commercial sites with which Elsevier has an agreement

In all cases accepted manuscripts should:

- link to the formal publication via its DOI
- bear a CC-BY-NC-ND license - this is easy to do
- if aggregated with other manuscripts, for example in a repository or other site, be shared in alignment with our hosting policy not be added to or enhanced in any way to appear more like, or to substitute for, the published journal article.

Published journal article (JPA): A published journal article (PJA) is the definitive final record of published research that appears or will appear in the journal and embodies all

value-adding publishing activities including peer review co-ordination, copy-editing, formatting, (if relevant) pagination and online enrichment.

Policies for sharing publishing journal articles differ for subscription and gold open access articles:

Subscription Articles: If you are an author, please share a link to your article rather than the full-text. Millions of researchers have access to the formal publications on ScienceDirect, and so links will help your users to find, access, cite, and use the best available version.

Theses and dissertations which contain embedded PJAs as part of the formal submission can be posted publicly by the awarding institution with DOI links back to the formal publications on ScienceDirect.

If you are affiliated with a library that subscribes to ScienceDirect you have additional private sharing rights for others' research accessed under that agreement. This includes use for classroom teaching and internal training at the institution (including use in course packs and courseware programs), and inclusion of the article for grant funding purposes.

Gold Open Access Articles: May be shared according to the author-selected end-user license and should contain a [CrossMark logo](#), the end user license, and a DOI link to the formal publication on ScienceDirect.

Please refer to Elsevier's [posting policy](#) for further information.

18. **For book authors** the following clauses are applicable in addition to the above: Authors are permitted to place a brief summary of their work online only. You are not allowed to download and post the published electronic version of your chapter, nor may you scan the printed edition to create an electronic version. **Posting to a repository:** Authors are permitted to post a summary of their chapter only in their institution's repository.

19. **Thesis/Dissertation:** If your license is for use in a thesis/dissertation your thesis may be submitted to your institution in either print or electronic form. Should your thesis be published commercially, please reapply for permission. These requirements include permission for the Library and Archives of Canada to supply single copies, on demand, of the complete thesis and include permission for Proquest/UMI to supply single copies, on demand, of the complete thesis. Should your thesis be published commercially, please reapply for permission. Theses and dissertations which contain embedded PJAs as part of the formal submission can be posted publicly by the awarding institution with DOI links back to the formal publications on ScienceDirect.

Elsevier Open Access Terms and Conditions

You can publish open access with Elsevier in hundreds of open access journals or in nearly 2000 established subscription journals that support open access publishing. Permitted third party re-use of these open access articles is defined by the author's choice of Creative Commons user license. See our [open access license policy](#) for more information.

Terms & Conditions applicable to all Open Access articles published with Elsevier:

Any reuse of the article must not represent the author as endorsing the adaptation of the article nor should the article be modified in such a way as to damage the author's honour or reputation. If any changes have been made, such changes must be clearly indicated.

The author(s) must be appropriately credited and we ask that you include the end user license and a DOI link to the formal publication on ScienceDirect.

If any part of the material to be used (for example, figures) has appeared in our publication with credit or acknowledgement to another source it is the responsibility of the user to ensure their reuse complies with the terms and conditions determined by the rights holder.

Additional Terms & Conditions applicable to each Creative Commons user license:

CC BY: The CC-BY license allows users to copy, to create extracts, abstracts and new works from the Article, to alter and revise the Article and to make commercial use of the Article (including reuse and/or resale of the Article by commercial entities), provided the user gives appropriate credit (with a link to the formal publication through the relevant DOI), provides a link to the license, indicates if changes were made and the licensor is not represented as endorsing the use made of the work. The full details of the license are available at <http://creativecommons.org/licenses/by/4.0>.

CC BY NC SA: The CC BY-NC-SA license allows users to copy, to create extracts, abstracts and new works from the Article, to alter and revise the Article, provided this is not done for commercial purposes, and that the user gives appropriate credit (with a link to the formal publication through the relevant DOI), provides a link to the license, indicates if changes were made and the licensor is not represented as endorsing the use made of the work. Further, any new works must be made available on the same conditions. The full details of the license are available at <http://creativecommons.org/licenses/by-nc-sa/4.0>.

CC BY NC ND: The CC BY-NC-ND license allows users to copy and distribute the Article, provided this is not done for commercial purposes and further does not permit distribution of the Article if it is changed or edited in any way, and provided the user gives appropriate credit (with a link to the formal publication through the relevant DOI), provides a link to the license, and that the licensor is not represented as endorsing the use made of the work. The full details of the license are available at <http://creativecommons.org/licenses/by-nc-nd/4.0>. Any commercial reuse of Open Access

articles published with a CC BY NC SA or CC BY NC ND license requires permission from Elsevier and will be subject to a fee.

Commercial reuse includes:

- Associating advertising with the full text of the Article
- Charging fees for document delivery or access
- Article aggregation
- Systematic distribution via e-mail lists or share buttons

Posting or linking by commercial companies for use by customers of those companies.

20. Other Conditions:

v1.10

Questions? customercare@copyright.com or +1-855-239-3415 (toll free in the US) or +1-978-646-2777.

Copyright information for Figure 7 from “Chapter 4 Circulation and Water Masses of the Southern Ocean: A Review,” by Carter et al. (2008), *Developments in Earth and Environmental Sciences*, 8, 85-114.

ELSEVIER LICENSE
TERMS AND CONDITIONS

May 25, 2021

This Agreement between University of South Florida -- Kara Vadman ("You") and Elsevier ("Elsevier") consists of your license details and the terms and conditions provided by Elsevier and Copyright Clearance Center.

License Number	5076060946503
License date	May 25, 2021
Licensed Content Publisher	Elsevier
Licensed Content Publication	Elsevier Books
Licensed Content Title	Developments in Earth and Environmental Sciences
Licensed Content Author	Lionel Carter,I.N. McCave,Michael J.M. Williams
Licensed Content Date	Jan 1, 2008
Licensed Content Pages	30
Start Page	85
End Page	114
Type of Use	reuse in a thesis/dissertation
Portion	figures/tables/illustrations
Number of figures/tables/illustrations	1
Format	electronic
Are you the author of this Elsevier chapter?	No
Will you be translating?	No
Title	Kara Vadman
Institution name	University of South Florida
Expected presentation date	May 2021
Portions	Figure 1
Requestor Location	University of South Florida 140 7th Ave S

SAINT PETERSBURG, FL 33701
United States
Attn: University of South Florida

Publisher Tax ID 98-0397604
Total 0.00 USD
Terms and Conditions

INTRODUCTION

1. The publisher for this copyrighted material is Elsevier. By clicking "accept" in connection with completing this licensing transaction, you agree that the following terms and conditions apply to this transaction (along with the Billing and Payment terms and conditions established by Copyright Clearance Center, Inc. ("CCC"), at the time that you opened your Rightslink account and that are available at any time at <http://myaccount.copyright.com>).

GENERAL TERMS

2. Elsevier hereby grants you permission to reproduce the aforementioned material subject to the terms and conditions indicated.

3. Acknowledgement: If any part of the material to be used (for example, figures) has appeared in our publication with credit or acknowledgement to another source, permission must also be sought from that source. If such permission is not obtained then that material may not be included in your publication/copies. Suitable acknowledgement to the source must be made, either as a footnote or in a reference list at the end of your publication, as follows:

"Reprinted from Publication title, Vol /edition number, Author(s), Title of article / title of chapter, Pages No., Copyright (Year), with permission from Elsevier [OR APPLICABLE SOCIETY COPYRIGHT OWNER]." Also Lancet special credit - "Reprinted from The Lancet, Vol. number, Author(s), Title of article, Pages No., Copyright (Year), with permission from Elsevier."

4. Reproduction of this material is confined to the purpose and/or media for which permission is hereby given.

5. Altering/Modifying Material: Not Permitted. However figures and illustrations may be altered/adapted minimally to serve your work. Any other abbreviations, additions, deletions and/or any other alterations shall be made only with prior written authorization of Elsevier Ltd. (Please contact Elsevier's permissions helpdesk [here](#)). No modifications can be made to any Lancet figures/tables and they must be reproduced in full.

6. If the permission fee for the requested use of our material is waived in this instance, please be advised that your future requests for Elsevier materials may attract a fee.

7. **Reservation of Rights:** Publisher reserves all rights not specifically granted in the combination of (i) the license details provided by you and accepted in the course of this licensing transaction, (ii) these terms and conditions and (iii) CCC's Billing and Payment terms and conditions.

8. **License Contingent Upon Payment:** While you may exercise the rights licensed immediately upon issuance of the license at the end of the licensing process for the transaction, provided that you have disclosed complete and accurate details of your proposed use, no license is finally effective unless and until full payment is received from you (either by publisher or by CCC) as provided in CCC's Billing and Payment terms and conditions. If full payment is not received on a timely basis, then any license preliminarily granted shall be deemed automatically revoked and shall be void as if never granted. Further, in the event that you breach any of these terms and conditions or any of CCC's Billing and Payment terms and conditions, the license is automatically revoked and shall be void as if never granted. Use of materials as described in a revoked license, as well as any use of the materials beyond the scope of an unrevoked license, may constitute copyright infringement and publisher reserves the right to take any and all action to protect its copyright in the materials.

9. **Warranties:** Publisher makes no representations or warranties with respect to the licensed material.

10. **Indemnity:** You hereby indemnify and agree to hold harmless publisher and CCC, and their respective officers, directors, employees and agents, from and against any and all claims arising out of your use of the licensed material other than as specifically authorized pursuant to this license.

11. **No Transfer of License:** This license is personal to you and may not be sublicensed, assigned, or transferred by you to any other person without publisher's written permission.

12. **No Amendment Except in Writing:** This license may not be amended except in a writing signed by both parties (or, in the case of publisher, by CCC on publisher's behalf).

13. **Objection to Contrary Terms:** Publisher hereby objects to any terms contained in any purchase order, acknowledgment, check endorsement or other writing prepared by you, which terms are inconsistent with these terms and conditions or CCC's Billing and Payment terms and conditions. These terms and conditions, together with CCC's Billing and Payment terms and conditions (which are incorporated herein), comprise the entire agreement between you and publisher (and CCC) concerning this licensing transaction. In the event of any conflict between your obligations established by these terms and conditions and those established by CCC's Billing and Payment terms and conditions, these terms and conditions shall control.

14. **Revocation:** Elsevier or Copyright Clearance Center may deny the permissions described in this License at their sole discretion, for any reason or no reason, with a full refund payable to you. Notice of such denial will be made using the contact information

provided by you. Failure to receive such notice will not alter or invalidate the denial. In no event will Elsevier or Copyright Clearance Center be responsible or liable for any costs, expenses or damage incurred by you as a result of a denial of your permission request, other than a refund of the amount(s) paid by you to Elsevier and/or Copyright Clearance Center for denied permissions.

LIMITED LICENSE

The following terms and conditions apply only to specific license types:

15. Translation: This permission is granted for non-exclusive world **English** rights only unless your license was granted for translation rights. If you licensed translation rights you may only translate this content into the languages you requested. A professional translator must perform all translations and reproduce the content word for word preserving the integrity of the article.

16. Posting licensed content on any Website: The following terms and conditions apply as follows: Licensing material from an Elsevier journal: All content posted to the web site must maintain the copyright information line on the bottom of each image; A hyper-text must be included to the Homepage of the journal from which you are licensing at <http://www.sciencedirect.com/science/journal/xxxxx> or the Elsevier homepage for books at <http://www.elsevier.com>; Central Storage: This license does not include permission for a scanned version of the material to be stored in a central repository such as that provided by Heron/XanEdu.

Licensing material from an Elsevier book: A hyper-text link must be included to the Elsevier homepage at <http://www.elsevier.com>. All content posted to the web site must maintain the copyright information line on the bottom of each image.

Posting licensed content on Electronic reserve: In addition to the above the following clauses are applicable: The web site must be password-protected and made available only to bona fide students registered on a relevant course. This permission is granted for 1 year only. You may obtain a new license for future website posting.

17. For journal authors: the following clauses are applicable in addition to the above:

Preprints:

A preprint is an author's own write-up of research results and analysis, it has not been peer-reviewed, nor has it had any other value added to it by a publisher (such as formatting, copyright, technical enhancement etc.).

Authors can share their preprints anywhere at any time. Preprints should not be added to or enhanced in any way in order to appear more like, or to substitute for, the final versions of

articles however authors can update their preprints on arXiv or RePEc with their Accepted Author Manuscript (see below).

If accepted for publication, we encourage authors to link from the preprint to their formal publication via its DOI. Millions of researchers have access to the formal publications on ScienceDirect, and so links will help users to find, access, cite and use the best available version. Please note that Cell Press, The Lancet and some society-owned have different preprint policies. Information on these policies is available on the journal homepage.

Accepted Author Manuscripts: An accepted author manuscript is the manuscript of an article that has been accepted for publication and which typically includes author-incorporated changes suggested during submission, peer review and editor-author communications.

Authors can share their accepted author manuscript:

- immediately
 - via their non-commercial person homepage or blog
 - by updating a preprint in arXiv or RePEc with the accepted manuscript
 - via their research institute or institutional repository for internal institutional uses or as part of an invitation-only research collaboration work-group
 - directly by providing copies to their students or to research collaborators for their personal use
 - for private scholarly sharing as part of an invitation-only work group on commercial sites with which Elsevier has an agreement
- After the embargo period
 - via non-commercial hosting platforms such as their institutional repository
 - via commercial sites with which Elsevier has an agreement

In all cases accepted manuscripts should:

- link to the formal publication via its DOI
- bear a CC-BY-NC-ND license - this is easy to do
- if aggregated with other manuscripts, for example in a repository or other site, be shared in alignment with our hosting policy not be added to or enhanced in any way to appear more like, or to substitute for, the published journal article.

Published journal article (JPA): A published journal article (PJA) is the definitive final record of published research that appears or will appear in the journal and embodies all value-adding publishing activities including peer review co-ordination, copy-editing, formatting, (if relevant) pagination and online enrichment.

Policies for sharing publishing journal articles differ for subscription and gold open access articles:

Subscription Articles: If you are an author, please share a link to your article rather than the full-text. Millions of researchers have access to the formal publications on ScienceDirect, and so links will help your users to find, access, cite, and use the best available version.

Theses and dissertations which contain embedded PJAs as part of the formal submission can be posted publicly by the awarding institution with DOI links back to the formal publications on ScienceDirect.

If you are affiliated with a library that subscribes to ScienceDirect you have additional private sharing rights for others' research accessed under that agreement. This includes use for classroom teaching and internal training at the institution (including use in course packs and courseware programs), and inclusion of the article for grant funding purposes.

Gold Open Access Articles: May be shared according to the author-selected end-user license and should contain a [CrossMark logo](#), the end user license, and a DOI link to the formal publication on ScienceDirect.

Please refer to Elsevier's [posting policy](#) for further information.

18. **For book authors** the following clauses are applicable in addition to the above: Authors are permitted to place a brief summary of their work online only. You are not allowed to download and post the published electronic version of your chapter, nor may you scan the printed edition to create an electronic version. **Posting to a repository:** Authors are permitted to post a summary of their chapter only in their institution's repository.

19. **Thesis/Dissertation:** If your license is for use in a thesis/dissertation your thesis may be submitted to your institution in either print or electronic form. Should your thesis be published commercially, please reapply for permission. These requirements include permission for the Library and Archives of Canada to supply single copies, on demand, of the complete thesis and include permission for Proquest/UMI to supply single copies, on demand, of the complete thesis. Should your thesis be published commercially, please reapply for permission. Theses and dissertations which contain embedded PJAs as part of the formal submission can be posted publicly by the awarding institution with DOI links back to the formal publications on ScienceDirect.

Elsevier Open Access Terms and Conditions

You can publish open access with Elsevier in hundreds of open access journals or in nearly 2000 established subscription journals that support open access publishing. Permitted third party re-use of these open access articles is defined by the author's choice

of Creative Commons user license. See our [open access license policy](#) for more information.

Terms & Conditions applicable to all Open Access articles published with Elsevier:

Any reuse of the article must not represent the author as endorsing the adaptation of the article nor should the article be modified in such a way as to damage the author's honour or reputation. If any changes have been made, such changes must be clearly indicated.

The author(s) must be appropriately credited and we ask that you include the end user license and a DOI link to the formal publication on ScienceDirect.

If any part of the material to be used (for example, figures) has appeared in our publication with credit or acknowledgement to another source it is the responsibility of the user to ensure their reuse complies with the terms and conditions determined by the rights holder.

Additional Terms & Conditions applicable to each Creative Commons user license:

CC BY: The CC-BY license allows users to copy, to create extracts, abstracts and new works from the Article, to alter and revise the Article and to make commercial use of the Article (including reuse and/or resale of the Article by commercial entities), provided the user gives appropriate credit (with a link to the formal publication through the relevant DOI), provides a link to the license, indicates if changes were made and the licensor is not represented as endorsing the use made of the work. The full details of the license are available at <http://creativecommons.org/licenses/by/4.0>.

CC BY NC SA: The CC BY-NC-SA license allows users to copy, to create extracts, abstracts and new works from the Article, to alter and revise the Article, provided this is not done for commercial purposes, and that the user gives appropriate credit (with a link to the formal publication through the relevant DOI), provides a link to the license, indicates if changes were made and the licensor is not represented as endorsing the use made of the work. Further, any new works must be made available on the same conditions. The full details of the license are available at <http://creativecommons.org/licenses/by-nc-sa/4.0>.

CC BY NC ND: The CC BY-NC-ND license allows users to copy and distribute the Article, provided this is not done for commercial purposes and further does not permit distribution of the Article if it is changed or edited in any way, and provided the user gives appropriate credit (with a link to the formal publication through the relevant DOI), provides a link to the license, and that the licensor is not represented as endorsing the use made of the work. The full details of the license are available at <http://creativecommons.org/licenses/by-nc-nd/4.0>. Any commercial reuse of Open Access articles published with a CC BY NC SA or CC BY NC ND license requires permission from Elsevier and will be subject to a fee.

Commercial reuse includes:

- Associating advertising with the full text of the Article
- Charging fees for document delivery or access
- Article aggregation
- Systematic distribution via e-mail lists or share buttons

Posting or linking by commercial companies for use by customers of those companies.

20. Other Conditions:

v1.10

Questions? customercare@copyright.com or +1-855-239-3415 (toll free in the US) or +1-978-646-2777.

Copyright information for Figure 8 from “Distribution of water masses and meltwater on the continental shelf near the Totten and Moscow University ice shelves” by Silvano et al. (2017), *JGR Oceans*, 122(3), 2050-2068.

JOHN WILEY AND SONS LICENSE
TERMS AND CONDITIONS

May 25, 2021

This Agreement between University of South Florida -- Kara Vadman ("You") and John Wiley and Sons ("John Wiley and Sons") consists of your license details and the terms and conditions provided by John Wiley and Sons and Copyright Clearance Center.

License Number	5076061266778
License date	May 25, 2021
Licensed Content Publisher	John Wiley and Sons
Licensed Content Publication	Journal of Geophysical Research: Oceans
Licensed Content Title	Distribution of water masses and meltwater on the continental shelf near the Totten and Moscow University ice shelves
Licensed Content Author	Alessandro Silvano, Stephen R. Rintoul, Beatriz Peña-Molino, et al
Licensed Content Date	Mar 16, 2017
Licensed Content Volume	122
Licensed Content Issue	3
Licensed Content Pages	19
Type of use	Dissertation/Thesis
Requestor type	University/Academic
Format	Electronic
Portion	Figure/table
Number of figures/tables	1
Will you be translating?	No
Title	Kara Vadman
Institution name	University of South Florida
Expected presentation date	May 2021
Portions	Figure 2

University of South Florida
140 7th Ave S

Requestor Location

SAINT PETERSBURG, FL 33701
United States
Attn: University of South Florida

Publisher Tax ID

EU826007151

Total

0.00 USD

Terms and Conditions

TERMS AND CONDITIONS

This copyrighted material is owned by or exclusively licensed to John Wiley & Sons, Inc. or one of its group companies (each a "Wiley Company") or handled on behalf of a society with which a Wiley Company has exclusive publishing rights in relation to a particular work (collectively "WILEY"). By clicking "accept" in connection with completing this licensing transaction, you agree that the following terms and conditions apply to this transaction (along with the billing and payment terms and conditions established by the Copyright Clearance Center Inc., ("CCC's Billing and Payment terms and conditions"), at the time that you opened your RightsLink account (these are available at any time at <http://myaccount.copyright.com>).

Terms and Conditions

- The materials you have requested permission to reproduce or reuse (the "Wiley Materials") are protected by copyright.
- You are hereby granted a personal, non-exclusive, non-sub licensable (on a stand-alone basis), non-transferable, worldwide, limited license to reproduce the Wiley Materials for the purpose specified in the licensing process. This license, **and any CONTENT (PDF or image file) purchased as part of your order**, is for a one-time use only and limited to any maximum distribution number specified in the license. The first instance of republication or reuse granted by this license must be completed within two years of the date of the grant of this license (although copies prepared before the end date may be distributed thereafter). The Wiley Materials shall not be used in any other manner or for any other purpose, beyond what is granted in the license. Permission is granted subject to an appropriate acknowledgement given to the author, title of the material/book/journal and the publisher. You shall also duplicate the copyright notice that appears in the Wiley publication in your use of the Wiley Material. Permission is also granted on the understanding that nowhere in the text is a previously published source acknowledged for all or part of this Wiley Material. Any third party content is expressly excluded from this permission.

- With respect to the Wiley Materials, all rights are reserved. Except as expressly granted by the terms of the license, no part of the Wiley Materials may be copied, modified, adapted (except for minor reformatting required by the new Publication), translated, reproduced, transferred or distributed, in any form or by any means, and no derivative works may be made based on the Wiley Materials without the prior permission of the respective copyright owner. **For STM Signatory Publishers clearing permission under the terms of the [STM Permissions Guidelines](#) only, the terms of the license are extended to include subsequent editions and for editions in other languages, provided such editions are for the work as a whole in situ and does not involve the separate exploitation of the permitted figures or extracts,** You may not alter, remove or suppress in any manner any copyright, trademark or other notices displayed by the Wiley Materials. You may not license, rent, sell, loan, lease, pledge, offer as security, transfer or assign the Wiley Materials on a stand-alone basis, or any of the rights granted to you hereunder to any other person.
- The Wiley Materials and all of the intellectual property rights therein shall at all times remain the exclusive property of John Wiley & Sons Inc, the Wiley Companies, or their respective licensors, and your interest therein is only that of having possession of and the right to reproduce the Wiley Materials pursuant to Section 2 herein during the continuance of this Agreement. You agree that you own no right, title or interest in or to the Wiley Materials or any of the intellectual property rights therein. You shall have no rights hereunder other than the license as provided for above in Section 2. No right, license or interest to any trademark, trade name, service mark or other branding ("Marks") of WILEY or its licensors is granted hereunder, and you agree that you shall not assert any such right, license or interest with respect thereto
- NEITHER WILEY NOR ITS LICENSORS MAKES ANY WARRANTY OR REPRESENTATION OF ANY KIND TO YOU OR ANY THIRD PARTY, EXPRESS, IMPLIED OR STATUTORY, WITH RESPECT TO THE MATERIALS OR THE ACCURACY OF ANY INFORMATION CONTAINED IN THE MATERIALS, INCLUDING, WITHOUT LIMITATION, ANY IMPLIED WARRANTY OF MERCHANTABILITY, ACCURACY, SATISFACTORY QUALITY, FITNESS FOR A PARTICULAR PURPOSE, USABILITY, INTEGRATION OR NON-INFRINGEMENT AND ALL SUCH WARRANTIES ARE HEREBY EXCLUDED BY WILEY AND ITS LICENSORS AND WAIVED BY YOU.
- WILEY shall have the right to terminate this Agreement immediately upon breach of this Agreement by you.
- You shall indemnify, defend and hold harmless WILEY, its Licensors and their respective directors, officers, agents and employees, from and against any actual or threatened claims, demands, causes of action or proceedings arising from any breach of this Agreement by you.

- IN NO EVENT SHALL WILEY OR ITS LICENSORS BE LIABLE TO YOU OR ANY OTHER PARTY OR ANY OTHER PERSON OR ENTITY FOR ANY SPECIAL, CONSEQUENTIAL, INCIDENTAL, INDIRECT, EXEMPLARY OR PUNITIVE DAMAGES, HOWEVER CAUSED, ARISING OUT OF OR IN CONNECTION WITH THE DOWNLOADING, PROVISIONING, VIEWING OR USE OF THE MATERIALS REGARDLESS OF THE FORM OF ACTION, WHETHER FOR BREACH OF CONTRACT, BREACH OF WARRANTY, TORT, NEGLIGENCE, INFRINGEMENT OR OTHERWISE (INCLUDING, WITHOUT LIMITATION, DAMAGES BASED ON LOSS OF PROFITS, DATA, FILES, USE, BUSINESS OPPORTUNITY OR CLAIMS OF THIRD PARTIES), AND WHETHER OR NOT THE PARTY HAS BEEN ADVISED OF THE POSSIBILITY OF SUCH DAMAGES. THIS LIMITATION SHALL APPLY NOTWITHSTANDING ANY FAILURE OF ESSENTIAL PURPOSE OF ANY LIMITED REMEDY PROVIDED HEREIN.
- Should any provision of this Agreement be held by a court of competent jurisdiction to be illegal, invalid, or unenforceable, that provision shall be deemed amended to achieve as nearly as possible the same economic effect as the original provision, and the legality, validity and enforceability of the remaining provisions of this Agreement shall not be affected or impaired thereby.
- The failure of either party to enforce any term or condition of this Agreement shall not constitute a waiver of either party's right to enforce each and every term and condition of this Agreement. No breach under this agreement shall be deemed waived or excused by either party unless such waiver or consent is in writing signed by the party granting such waiver or consent. The waiver by or consent of a party to a breach of any provision of this Agreement shall not operate or be construed as a waiver of or consent to any other or subsequent breach by such other party.
- This Agreement may not be assigned (including by operation of law or otherwise) by you without WILEY's prior written consent.
- Any fee required for this permission shall be non-refundable after thirty (30) days from receipt by the CCC.
- These terms and conditions together with CCC's Billing and Payment terms and conditions (which are incorporated herein) form the entire agreement between you and WILEY concerning this licensing transaction and (in the absence of fraud) supersedes all prior agreements and representations of the parties, oral or written. This Agreement may not be amended except in writing signed by both parties. This Agreement shall be binding upon and inure to the benefit of the parties' successors, legal representatives, and authorized assigns.

- In the event of any conflict between your obligations established by these terms and conditions and those established by CCC's Billing and Payment terms and conditions, these terms and conditions shall prevail.
- WILEY expressly reserves all rights not specifically granted in the combination of (i) the license details provided by you and accepted in the course of this licensing transaction, (ii) these terms and conditions and (iii) CCC's Billing and Payment terms and conditions.
- This Agreement will be void if the Type of Use, Format, Circulation, or Requestor Type was misrepresented during the licensing process.
- This Agreement shall be governed by and construed in accordance with the laws of the State of New York, USA, without regards to such state's conflict of law rules. Any legal action, suit or proceeding arising out of or relating to these Terms and Conditions or the breach thereof shall be instituted in a court of competent jurisdiction in New York County in the State of New York in the United States of America and each party hereby consents and submits to the personal jurisdiction of such court, waives any objection to venue in such court and consents to service of process by registered or certified mail, return receipt requested, at the last known address of such party.

WILEY OPEN ACCESS TERMS AND CONDITIONS

Wiley Publishes Open Access Articles in fully Open Access Journals and in Subscription journals offering Online Open. Although most of the fully Open Access journals publish open access articles under the terms of the Creative Commons Attribution (CC BY) License only, the subscription journals and a few of the Open Access Journals offer a choice of Creative Commons Licenses. The license type is clearly identified on the article.

The Creative Commons Attribution License

The [Creative Commons Attribution License \(CC-BY\)](#) allows users to copy, distribute and transmit an article, adapt the article and make commercial use of the article. The CC-BY license permits commercial and non-

Creative Commons Attribution Non-Commercial License

The [Creative Commons Attribution Non-Commercial \(CC-BY-NC\)License](#) permits use, distribution and reproduction in any medium, provided the original work is properly cited and is not used for commercial purposes.(see below)

Creative Commons Attribution-Non-Commercial-NoDerivs License

The [Creative Commons Attribution Non-Commercial-NoDerivs License](#) (CC-BY-NC-ND) permits use, distribution and reproduction in any medium, provided the original work

is properly cited, is not used for commercial purposes and no modifications or adaptations are made. (see below)

Use by commercial "for-profit" organizations

Use of Wiley Open Access articles for commercial, promotional, or marketing purposes requires further explicit permission from Wiley and will be subject to a fee.

Further details can be found on Wiley Online Library
<http://olabout.wiley.com/WileyCDA/Section/id-410895.html>

Other Terms and Conditions:

v1.10 Last updated September 2015

Questions? customercare@copyright.com or +1-855-239-3415 (toll free in the US) or +1-978-646-2777.

Copyright information for Figure 10 from “Freshening by glacial meltwater enhances melting of ice shelves and reduces formation of Antarctic Bottom Water” by Silvano et al. (2018), *Science Advances*, 4(4), eaap9467.

Article Information

vol. 4 no. 4

DOI: <https://doi.org/10.1126/sciadv.aap9467>

Published By: **American Association for the Advancement of Science**

Online ISSN: **2375-2548**

History: Received for publication September 16, 2017

Accepted for publication March 6, 2018

Copyright & Usage: Copyright © 2018 The Authors, some rights reserved; exclusive licensee American Association for the Advancement of Science. No claim to original U.S. Government Works. Distributed under a Creative Commons Attribution NonCommercial License 4.0 (CC BY-NC).

This is an open-access article distributed under the terms of the **Creative Commons Attribution-NonCommercial license**, which permits use, distribution, and reproduction in any medium, so long as the resultant use is **not** for commercial advantage and provided the original work is properly cited.

Copyright information for Figure 11 from “Wind-driven trends in Antarctic sea-ice drift” by Holland & Kwok (2012), *Nature Geoscience*, 5, 872-875.

SPRINGER NATURE LICENSE
TERMS AND CONDITIONS

May 25, 2021

This Agreement between University of South Florida -- Kara Vadman ("You") and Springer Nature ("Springer Nature") consists of your license details and the terms and conditions provided by Springer Nature and Copyright Clearance Center.

License Number	5076070651049
License date	May 25, 2021
Licensed Content Publisher	Springer Nature
Licensed Content Publication	Nature Geoscience
Licensed Content Title	Wind-driven trends in Antarctic sea-ice drift
Licensed Content Author	Paul R. Holland et al
Licensed Content Date	Nov 11, 2012
Type of Use	Thesis/Dissertation
Requestor type	academic/university or research institute
Format	electronic
Portion	figures/tables/illustrations
Number of figures/tables/illustrations	2
High-res required	no
Will you be translating?	no
Circulation/distribution	1 - 29
Author of this Springer Nature content	no
Title	Kara Vadman
Institution name	University of South Florida
Expected presentation date	May 2021
Portions	Figure 1 and Figure 2
Requestor Location	University of South Florida 140 7th Ave S

SAINT PETERSBURG, FL 33701

Total
Terms and Conditions

United States
Attn: University of South Florida
0.00 USD

Springer Nature Customer Service Centre GmbH Terms and Conditions

This agreement sets out the terms and conditions of the licence (the **Licence**) between you and **Springer Nature Customer Service Centre GmbH** (the **Licensor**). By clicking 'accept' and completing the transaction for the material (**Licensed Material**), you also confirm your acceptance of these terms and conditions.

1. Grant of Licence

1. The Licensor grants you a personal, non-exclusive, non-transferable, world-wide licence to reproduce the Licensed Material for the purpose specified in your order only. Licences are granted for the specific use requested in the order and for no other use, subject to the conditions below.
2. The Licensor warrants that it has, to the best of its knowledge, the rights to license reuse of the Licensed Material. However, you should ensure that the material you are requesting is original to the Licensor and does not carry the copyright of another entity (as credited in the published version).
3. If the credit line on any part of the material you have requested indicates that it was reprinted or adapted with permission from another source, then you should also seek permission from that source to reuse the material.

2. Scope of Licence

1. You may only use the Licensed Content in the manner and to the extent permitted by these Ts&Cs and any applicable laws.
2. A separate licence may be required for any additional use of the Licensed Material, e.g. where a licence has been purchased for print only use, separate permission must be obtained for electronic re-use. Similarly, a licence is only valid in the language selected and does not apply for editions in other languages unless additional translation rights have been granted separately in the licence. Any content owned by third parties are expressly excluded from the licence.
3. Similarly, rights for additional components such as custom editions and derivatives require additional permission and may be subject to an additional fee. Please apply to

Journalpermissions@springernature.com/bookpermissions@springernature.com for these rights.

4. Where permission has been granted **free of charge** for material in print, permission may also be granted for any electronic version of that work, provided that the material is incidental to your work as a whole and that the electronic version is essentially equivalent to, or substitutes for, the print version.
5. An alternative scope of licence may apply to signatories of the [STM Permissions Guidelines](#), as amended from time to time.

- **Duration of Licence**

1. A licence for is valid from the date of purchase ('Licence Date') at the end of the relevant period in the below table:

Scope of Licence	Duration of Licence
Post on a website	12 months
Presentations	12 months
Books and journals	Lifetime of the edition in the language purchased

- **Acknowledgement**

1. The Licensor's permission must be acknowledged next to the Licenced Material in print. In electronic form, this acknowledgement must be visible at the same time as the figures/tables/illustrations or abstract, and must be hyperlinked to the journal/book's homepage. Our required acknowledgement format is in the Appendix below.

- **Restrictions on use**

1. Use of the Licensed Material may be permitted for incidental promotional use and minor editing privileges e.g. minor adaptations of single figures, changes of format, colour and/or style where the adaptation is credited as set out in Appendix 1 below. Any other changes including but not limited to, cropping, adapting, omitting material that affect the meaning, intention or moral rights of the author are strictly prohibited.
2. You must not use any Licensed Material as part of any design or trademark.
3. Licensed Material may be used in Open Access Publications (OAP) before publication by Springer Nature, but any Licensed Material must be removed from OAP sites prior to final publication.

- **Ownership of Rights**

1. Licensed Material remains the property of either Licensor or the relevant third party and any rights not explicitly granted herein are expressly reserved.

- **Warranty**

IN NO EVENT SHALL LICENSOR BE LIABLE TO YOU OR ANY OTHER PARTY OR ANY OTHER PERSON OR FOR ANY SPECIAL, CONSEQUENTIAL, INCIDENTAL OR INDIRECT DAMAGES, HOWEVER CAUSED, ARISING OUT OF OR IN CONNECTION WITH THE DOWNLOADING, VIEWING OR USE OF THE MATERIALS REGARDLESS OF THE FORM OF ACTION, WHETHER FOR BREACH OF CONTRACT, BREACH OF WARRANTY, TORT, NEGLIGENCE, INFRINGEMENT OR OTHERWISE (INCLUDING, WITHOUT LIMITATION, DAMAGES BASED ON LOSS OF PROFITS, DATA, FILES, USE, BUSINESS OPPORTUNITY OR CLAIMS OF THIRD PARTIES), AND WHETHER OR NOT THE PARTY HAS BEEN ADVISED OF THE POSSIBILITY OF SUCH DAMAGES. THIS LIMITATION SHALL APPLY NOTWITHSTANDING ANY FAILURE OF ESSENTIAL PURPOSE OF ANY LIMITED REMEDY PROVIDED HEREIN.

- **Limitations**

1. **BOOKS ONLY**: Where 'reuse in a dissertation/thesis' has been selected the following terms apply: Print rights of the final author's accepted manuscript (for clarity, NOT the published version) for up to 100 copies, electronic rights for use only on a personal website or institutional repository as defined by the Sherpa guideline (www.sherpa.ac.uk/romeo/).
2. For content reuse requests that qualify for permission under the [STM Permissions Guidelines](#), which may be updated from time to time, the STM Permissions Guidelines supersede the terms and conditions contained in this licence.

- **Termination and Cancellation**

1. Licences will expire after the period shown in Clause 3 (above).
2. Licensee reserves the right to terminate the Licence in the event that payment is not received in full or if there has been a breach of this agreement by you.

Appendix 1 — Acknowledgements:

For Journal Content:

Reprinted by permission from [the Licensor]: [Journal Publisher (e.g. Nature/Springer/Palgrave)] [JOURNAL NAME] [REFERENCE CITATION (Article name, Author(s) Name), [COPYRIGHT] (year of publication)

For Advance Online Publication papers:

Reprinted by permission from [the Licensor]: [Journal Publisher (e.g. Nature/Springer/Palgrave)] [JOURNAL NAME] [REFERENCE CITATION (Article name, Author(s) Name), [COPYRIGHT] (year of publication), advance online publication, day month year (doi: 10.1038/sj.[JOURNAL ACRONYM].)]

For Adaptations/Translations:

Adapted/Translated by permission from [the Licensor]: [Journal Publisher (e.g. Nature/Springer/Palgrave)] [JOURNAL NAME] [REFERENCE CITATION (Article name, Author(s) Name), [COPYRIGHT] (year of publication)]

Note: For any republication from the British Journal of Cancer, the following credit line style applies:

Reprinted/adapted/translated by permission from [the Licensor]: on behalf of Cancer Research UK: : [Journal Publisher (e.g. Nature/Springer/Palgrave)] [JOURNAL NAME] [REFERENCE CITATION (Article name, Author(s) Name), [COPYRIGHT] (year of publication)]

For Advance Online Publication papers:

Reprinted by permission from The [the Licensor]: on behalf of Cancer Research UK: [Journal Publisher (e.g. Nature/Springer/Palgrave)] [JOURNAL NAME] [REFERENCE CITATION (Article name, Author(s) Name), [COPYRIGHT] (year of publication), advance online publication, day month year (doi: 10.1038/sj.[JOURNAL ACRONYM])]

For Book content:

Reprinted/adapted by permission from [the Licensor]: [Book Publisher (e.g. Palgrave Macmillan, Springer etc)] [Book Title] by [Book author(s)] [COPYRIGHT] (year of publication)

Other Conditions:

Version 1.3

Questions? customercare@copyright.com or +1-855-239-3415 (toll free in the US) or +1-978-646-2777.

Copyright information for Figure 12 from “Variation of Antarctic circumpolar current and its intensification in relation to the southern annular mode detected in the time-variable gravity signals by GRACE satellite” by Liao & Chao (2017), *Earth Planets Space*, 69, 93.

SPRINGER NATURE

Variation of Antarctic circumpolar current and its intensification in relation to the southern annular mode detected in the time-variable gravity signals by GRACE satellite

Author: Jen-Ru Liao et al

Publication: Earth, Planets and Space

Publisher: Springer Nature

Date: Jul 6, 2017

Copyright © 2017, The Author(s)

Creative Commons

This is an open access article distributed under the terms of the [Creative Commons CC BY](#) license, which permits unrestricted use, distribution, and reproduction in any medium, provided the original work is properly cited.

You are not required to obtain permission to reuse this article.

To request permission for a type of use not listed, please contact [Springer Nature](#)

Copyright information for Figure 13 from “The marine geological imprint of Antarctic ice shelves” by Smith et al. (2019), *Nature Communications*, 10, 5635.

SPRINGER NATURE

The marine geological imprint of Antarctic ice shelves

Author: James A. Smith et al

Publication: Nature Communications

Publisher: Springer Nature

Date: Dec 10, 2019

Copyright © 2019, Crown

Creative Commons

This is an open access article distributed under the terms of the [Creative Commons CC BY](#) license, which permits unrestricted use, distribution, and reproduction in any medium, provided the original work is properly cited.

You are not required to obtain permission to reuse this article.

To request permission for a type of use not listed, please contact [Springer Nature](#)